TEAM 2016

8th International Scientific and Expert Conference

TEAM 2016

Proceedings of the 8th International Scientific and Expert Conference

19th – 21st October 2016, Trnava, Slovakia

TEAM 2016, Proceedings of the 8th International Scientific and Expert Conference

19th – 21st October 2016, Trnava, Slovakia

Organizers International TEAM Society and Slovak University of Technology, Faculty of Materials Science and Technology in Trnava, Slovakia

All papers are reviewed.

Place of edition: Trnava
Editor: AlumniPress
Year of edition: 2016
Edition: 1st
Pages: 360
Reviewers:
Prof. Ing. Miloš Čambál, CSc.
Prof. Ing. Milan Marônek, CSc.
Assoc. prof. Ing. Mária Dománková, PhD.
Assoc. prof. Krunoslav Mirosavljevič, Dr. Sc.

ISBN 978 – 80 – 8096 – 237 – 1
EAN 9788080962371

Honorary Committee

Prof. dr. sc. Dražan Kozak	Croatia
Prof. dr. sc. Ivan Samardžić	Croatia
Prof. dr. sc. Antun Stoić	Croatia
mr. sc. Josip Jukić	Croatia
Prof. Dr. Lóránt Kovács	Hungary
Prof. Dr. Ing. Jozef Peterka	Slovakia
Prof. Ing. Jozef Zajac, CSc.	Slovakia
Prof. dr. sc.Vlado Guberac	Croatia
Prof. Dr. Radivoje Mitrović	Serbia
Prof. Dr. Aleksandar Sedmak	Serbia

Scientific Committee

Prof. Zoran Radakovic	Serbia
Dr. Vojislav Simonovic	Serbia
Dr. Zorana Golubovic	Serbia
Prof. Aleksandar Sedmak	Serbia
Dr. Nenad Mitrovic	Serbia
Dr. Milos Milosevic	Serbia
Dr. Sanja Petronic	Serbia
Dr. Katarina Colic	Serbia
Prof. Snezana Kirin	Serbia
Dr. Srdjan Tadic	Serbia
Dr. Zsolt Csaba Johanyák	Hungary
Dr. Lorant Kovács	Hungary
Dr. Erika Török	Hungary
Dr. Judit Pető	Hungary
Dr. Árpád Ferencz	Hungary
Prof. dr. sc. Ivan Samardžić	Croatia
Prof. dr. sc. Dražan Kozak	Croatia
Prof. dr. sc. Antun Stoić	Croatia
Prof. dr. sc. Željko Ivandić	Croatia
Prof. dr. sc. Goran Šimunović	Croatia
Prof. dr. sc. Vlado Guberac	Croatia
Prof. dr. sc. Sonja Marić	Croatia
Prof. dr. sc. Zvonko Antunović	Croatia
Prof. dr. sc. Darko Kiš	Croatia
Prof. dr. sc. Jasna Šoštarič	Croatia
mr.sc. Josip Jukič	Croatia
Assoc. prof. dr. sc. Krunoslav Mirosavljević	Croatia
dr. sc. Teuta Benković-Lačić	Croatia
dipl. Ing. Ivica Lacković	Croatia
Milan Stanić	Croatia
Prof. Ing. Milan Marônek, CSc.	Slovakia
Assoc prof. Ing. Mária Dománková, PhD.	Slovakia
Prof. Ing. Miloš Čambál, CSc.	Slovakia
Prof. Ing. Alexander Čaus, DrSc.	Slovakia
Prof. Ing. Maroš Soldán, PhD.	Slovakia

Prof. Ing. Jozef Zajac, CSc.	Slovakia
Assoc prof. Ing. Ján Piteľ, CSc.	Slovakia
Assoc prof. Ing. Peter Monka, PhD.	Slovakia
Prof. RNDr. Dušan Knežo, CSc.	Slovakia
Dr.hc. prof. Ing. Karol Vasilko, DrSc.	Slovakia
Prof. Ailer Piroska	Hungary
Prof. Nicolae Balc	Romania
Dr. Mislav Balković	Croatia
Dr. Jozef Bárta	Slovakia
Prof. Slađana Benković	Serbia
Prof. Pavel Beňo	Slovakia
Prof. Ivana Bilić	Croatia
Prof. Zlatan Car	Croatia
Prof. Somnath Chattopadhyaya	India
Prof. Robert Čep	Czech Republic
Prof. Ante Čikić	Croatia
Prof. Dražena Gašpar	Bosnia and Herzegovina
Prof. Nenad Gubeljak	Slovenia
Prof. Fuad Hadžikadunić	Bosnia and Herzegovina
Prof. Sergej Hloch	Slovakia
Prof. Grzegorz Królczyk	Poland
Prof. Leon Kukielka	Poland
Prof. Stanislaw Legutko	Poland
Prof. Marin Milković	Croatia
Prof. Mirjana Pejić Bach	Croatia
Prof. Marko Rakin	Serbia
Prof. Pero Raos	Croatia
Prof. Alessandro Ruggiero	Italia
Prof. Bahar Sennaroğlu	Turkey
Prof. Stevan Stankovski	Serbia
Prof. Mladen Šercer	Croatia
Prof. Udo Traussnigg	Austria
Prof. Vlado Tropša	Croatia
Prof. Nicolae Ungureanu	Romania
Prof. Jan Valíček	Czech Republic
Prof. Djordje Vukelić	Serbia

Organising Committee

Prof. Milan Marônek, PhD.
Ing. Jozef Bárta, PhD. (Chairperson)
Ing. Ivan Buranský, PhD.
Ing. Ingrid Kovaříková, PhD.
Ing. Beáta Šimeková, PhD.
Ing. Martin Bajčičák, PhD.
Assoc. Prof. Erika Hodúlová, PhD.
Prof. Koloman Ulrich, PhD.
PhDr. Kvetoslava Rešetová, PhD.
PaedDr. Dáša Zifčáková

CONTENT

TECHNICS SECTION

Using the Ant Colony Optimization method to find an optimal solution in drilling process

Danijela Pezer

Mechanical Engineering Faculty in Slavonski Brod, Trg I.B. Mazuranic 2, 35000 Slavonski Brod, Croatia, E-mail:dpezer@sfsb.hr

Abstract

The aim of each production process is to reduce the processing time, which ultimately leads to reduction of the total costs in production. Considering the stated objective, Ant Colony Optimization (ACO) method for searching of the optimal tool path in the process of drilling, was used in this paper. In this case the efficiency of production depends on the time required for drilling. ACO method is used to solve NP hard combinatorial optimization problems inspired by the behavior of different species of ants in searching for the shortest route. One of the most extensively studied combinatorial problem is the Traveling Salesman Problem (TSP). Analysis of this technological task is also based on this principle, and we consider an open tour in drilling process where at the end of the process of drilling, tool does not return to the starting point (which depends on the random selection of the proposed algorithm). With the proposed ACO algorithm, a satisfactory solution was achieved in a relatively short time, and the algorithm has shown that is reliable to use. The solution achieved with ACO algorithm was obtained by MATLAB program, and results are compared with the result obtained by manual programming. Simulation of drilling was performed by educational program EMCO WinNC for Sinumerik 840D Mill control unit.

Keywords: Ant Colony Optimization, Tool path planing, CNC programming, Drilling

1. INTRODUCTION

Today, many metaheuristic methods for solving combinatorial optimization problems are used. In this paper, for finding the shortest tool path in the process of holes drilling, the Ant Colony Optimization (ACO) metaheuristic method was used. The problem is based on the principle of a Traveling Salesman.

Traveling Salesman Problem (TSP) can be represented as a fully weighted undirected graph $G=(V,E)$ if it is symmetric, and fully weighted directed graph $G=(V,A)$ if it is asymmetric. The set $V=\{1,2,...n\}$ is the set of vertex, which represents the cities, $E=\{(i,j):i,j\in V,i<j\}$ represents the set of edges which connecting all vertices, while $A=\{(i,j):i,j\in V,i\neq j\}$ represents set of arcs. For each edge, or arc (i,j) is assigned a value d_{ij} which can indicate the distance, time, price or other interest factors associated with edges, respectively arcs. For standard TSP problem the assumption is that the square cost matrix, $D=\{d_{ij}:(i,j)\in V,i\neq j\}$ is symmetric $d_{ij}=d_{ji}$, respectively, distance is equal in both directions. Another standard assumption is that the distance matrix $D=(d_{ij})$ satisfies the triangle inequality in the case when $d_{ij}\leq d_{ik}+d_{kj}$, , za $\forall\, i,j,k\in V$.

The objective of the problem is to find a minimal Hamiltonian cycle, which closes the tour after each $n=|V|$ vertexes of G visited only once.

In many papers the possibility of applying ACO [1,2] and other algorithms, such as Particle Swarm Optimization [3], genetic algorithms [4], and more recently with the use of the bat algorithm [5], cuckoo search algorithm [6] etc., for the various production problems based on the principle of a Traveling Salesman described above are investigated.

2. ANT COLONY OPTIMIZATION METHOD

Ant Colony Optimization (ACO) is classified as swarm intelligence, inspired by the behaviour of different species (ants, bees, birds, fish, bats) during the search for food in nature.

Except the Ant Colony Optimization, the other algorithms that imitate the phenomenon of swarm intelligence, such as a Particle Swarm Optimization (PSO), bee algorithm, firefly algorithm, bat algorithm, etc. have been developed.

Ant Colony Algorithm imitate the movement of ants in the nature, during the search for the shortest route to the food, or finding the optimal solution for a given problem. Since ants haven't well-developed eyesight, their mutual communication is based on pheromone trails. The amount of pheromone on the ground determines the probability to be followed by other ants.

The basic algorithmic structure [7] of Ant Colony is presented by Algorithm 1.

Algorithm 1. General algorithm for ACO

```
Initialize the pheromone trails;
Repeat
  For each ant Do
    Solution construction using the
    pheromone trail;
    Update the pheromone trails:
      Evaporation;
      Reinforcement;
Until Stopping criteria
Output: Best solution(s) found
```

The steps of the algorithm work [7]:

- Initialize of pheromone trails (on each way is set the amount of pheromone that is equal to the reciprocal value of the path length found by using a greedy algorithm)
- Route selection - an ant selects the next hole from the group of holes that have not yet been drilled. Since that is a fully connected graph, from each hole it can be reached to any remaining hole with the probability:

$$P_{ij} = \frac{\tau_{ij}^{\alpha} \times \eta_{ij}^{\beta}}{\sum_{k \in N} \tau_{ik}^{\alpha} \times \eta_{ik}^{\beta}} \quad (1)$$

P_{ij} - the probability of path choosing from hole *i* to hole *j*

N - a set of holes that haven't been drilled yet

τ_{ij} - the intensity of the pheromone on the path from hole *i* to hole *j*

η_{ij} - the value of heuristic function on the path from hole *i* to hole *j*

α – constant (pheromone trail)

β – constant (visibility between holes).

For α=0 algorithm acts like Greedy algorithm.

For β=0 the search is based only on the pheromone trail.

- Updating the trails (occurs in two phases):
  - Evaporation phase

The pheromone trails are updated for all paths using relation

$$\tau_{ij} = (1-\rho)\tau_{ij}, \ \forall_i, j \in [1,n] \quad (2)$$

where is

ρ - evaporation constant, $\rho \in [0,1]$

Evaporation is possible to apply after each ant constructs a solution or after each iteration in which the solution constructed by all ants (as is the case in this paper).

  - Reinforcement phase

The pheromone trail is updated according to the last constructed solution and can be applied

after each step of the heuristics construction for each ant, after an each ant constructs a solution or after all ants construct a solution in which there are several strategies:

- reinforcement based on quality – the value of pheromone is updated according to the *k* best solutions (k=1:m; m – number of ants) with value proportional to the quality of solutions:

$$\tau_{i\pi^*(i)} = \tau_{i\pi^*(i)} + \Delta, \forall_i \in [1, n] \quad (3)$$

  where is $\Delta = 1/f(\pi)$.

- reinforcement based on the range – the *k* best solutions updating an appropriate components of trails to the amount which depends on their ranking
- reinforcement based on a worst solution – the worst found solution reduces the appropriate parameters of trails
- elitistic reinforcement – increasing the value of pheromone for the best solution found until then.

- By stopping the process, the best accomplished solution, or sequential represantation of possible order of execution of drilling, according to the assigned number of holes was displyed. Termination criterion is defined by the number of iterations.

3. EXPERIMENTAL PART

According to the given task (Fig. 1) the sequence of tool path holes drilling (156 holes) was optimized by ACO algorithm.

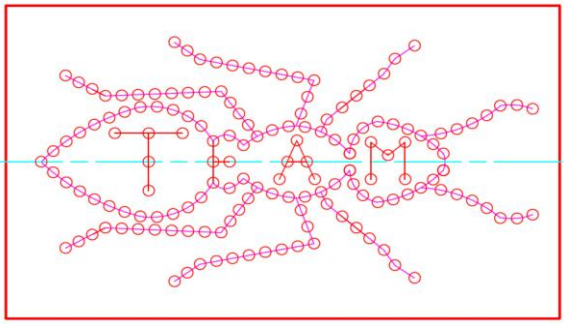

Fig. 1. Prismatic workpiece

The first hole from which starts drilling depends on the random selection of the algorithm, and when drilling operation is finished the tool doesn't return to the starting position. The results were compared with the results achieved by manual programming. For a given problem of the tool path optimization, minimizing the length of tool path was realized using the MATLAB software and the achieved software solution was simulated in EMCO WinNC program for Sinumerik 840D Mill control unit (Fig. 2).

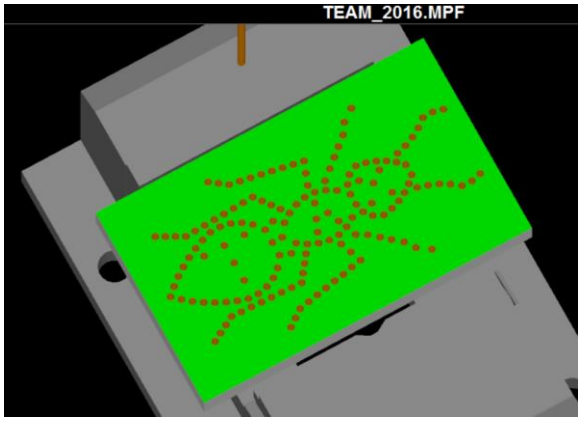

Fig. 2. Simulation of drilling in the Sinumerik 840D

The program was performed on a work station HP EliteBook 8560w, i72820 QM CPU, 2.3GHz, 16 GB of RAM.

The algorithm was started multiple (500 times) with different combinations of parameters α (the importance of the pheromone trail), β (the importance of visibility), ρ (evaporation factor) and *nAnt* (number of ants – population size). As the optimal parameters for a given problem are determineted the following parameters: α=1, β=4, ρ=0,45, *Q*=1, *nAnt*=70, maximal number of iteration *maxIter*=900, by which a minimal total tool path are achieved in the amount of 573,1939 mm (in 584 iteration).

The results of ACO algorithm were compared with results obtained by manual programming and total tool path length in the amount of 629,3353 mm was achieved, and the results are presented in the Table 1.

Table 1. The results achieved by ACO algorithm and manual programming

Method	Max. number of iteration	Num. of population	Best cost, mm	CPU time, s
Manual programming	---	---	629,3353	---
ACO algorithm	900	70	573,1939	738,9419

The optimal tool path achieved by ACO algorithm and manual programming is shown on Fig. 3.

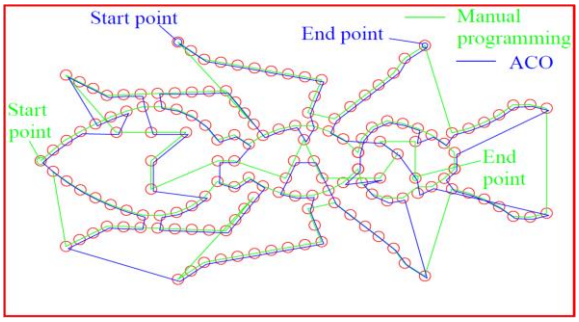

Fig. 3. Optimal tool path

The impact of the number of iteration in relation to the value of the minimum total tool path length is shown on Fig. 4.

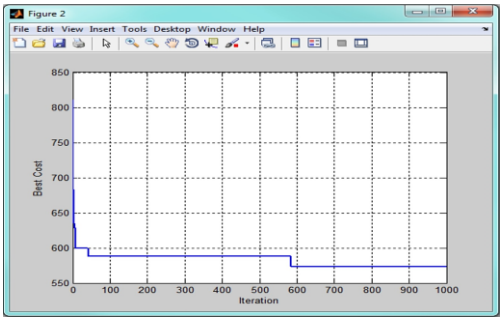

Fig. 4. Fitness function depending on the number of iteration

4. CONCLUSIONS

The aim of the optimization of the total tool path length is to reduce the total time, and thus the production costs. According to the technological task, by ACO algorithm was achieved suboptimal solution which is efficient in relation to the solution achieved by manual programming. The proposed algorithm certainly can have a greater use or efficiency at the problem with a larger number of holes (up to several thousand). The aim of this paper is to show that the proposed algorithm in a relatively short time finds (sub)optimal solution and that is reliable for use on the potential problems based on the principle of the TSP.

5. REFERENCES

[1] Z. Q. Li; X. Wang; Y. F. Dong, ACO-Based Holes Machining Path Optimization Using Helical Milling Operation. Advanced Materials Research, 834-836 (2014), pp.1386-1390

[2] X. Hong; L. Yuan; Z. Kaifu; Y. Jianfeng; L. Zhenxing; S. Jianbin, Multi-objective Optimization Method for Automatic Drilling and Riveting Sequence Planning. Chinese Journal of Aeronautics, 23(6) (2010), pp. 734-742

[3] W. Elloumia; H. El Abeda; A. Abrahama; A. M. Alimi, A comparative study of the improvement of performance using a PSO modified by ACO applied to TSP. Applied Soft Computing, 25 (2014), pp.234–241

[4] J. Abu Qudeiri, Optimization of Operation Sequence in CNC Machine Tools Using Genetic Algorithm. Journal of Advanced Mechanical Design, Systems and Manufacturing, 1(2) (2007), pp. 272-282

[5] E. Osaba; X.S. Yang; F. Diaz; P. Lopez-Garcia; R. Carballedo, An improved discrete bat algorithm for symmetric and asymmetric Traveling Salesman Problems. Engineering applications of artificial intelligence, 48 (2016), 59-71

[6] W. C. E. Lim; G. Kanagaraj; S.G. Ponnambalam, A hybrid cuckoo search-genetic algorithm for hole-making sequence optimization. Journal of intelligent manufacturing, 27(2) (2016), pp.417-429

[7] E.G. Talbi, Metaheuristics: from design to implementation. University of Lille – CNRS-INRIA, John Wiley & Sons Inc., Hoboken, New Jersey, (2009).

Numerical examination of a system model with a nonlinear component

Flóra Hajdu [a], Győző Molnárka[a]

[a] Széchenyi István University, Egyetem tér 1.,9026 Győr, Hungary, hajdfl@sze.hu

Abstract

This paper presents the numerical examination of a simple electrical circuit with a nonlinear Tunnel diode. The diode characteristics was implemented to the model by curve fitting.

This paper first introduces some model and simulation found in the literature, then describes the numerical analysis of the model. The effects of changing parameters on the behaviour of the system were examined based on time-dependent, phase-plane and bifurcation diagrams. The effects of the numerical solvers and the curve-fitting methods on the simulation are also described. The study concludes with the description of additional tests.

Keywords: nonlinear, system modelling, numerical simulation

1. INTRODUCTION

As computer science rapidly develops nowadays [1]. The system simulation is becoming faster and cheaper opening new opportunities. With numerical simulations the study and observation of complex, nonlinear systems became possible.

The examined model is a simple Tunnel diode circuit (Fig. 1). The parameter values including the diode characteristics was taken from [2].

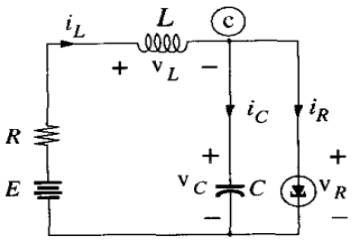

Fig. 1. : Examined Tunnel diode circuit

Tunnel diode is a semiconductor device with nonlinear I-V characteristics. It is used in a lot of applications like oscillators, memory, AD converters, logical circuits [3], microwave circuits like antennas [4 and 5], amplifiers [6] and military equipment [7]. Tunnel diode models can be even used for modelling of more complex systems, like superlattice [8]. Physical models are difficult to handle in numerical simulations because they require parameters, which are not easy to obtain. This is why they are not used in circuit simulators. There are some empirical models, which are based on measurements and curve fitting. They are easy to use, but a disadvantage is that there is no direct connection to the real physical reality and its exactness depends for example on the curve fitting methods. In some combined models some parameters are defined empirically [9]. In circuit simulators Tunnel diodes are modelled with single circuit elements like resistor, capacitor and inductance (Fig. 1.) [10], [11].

Our aim is not to understand exactly the physical process inside in a Tunnel diode but rather to construct a mathematical model of a circuit containing a nonlinear element and with this tool to examine the behavior of such systems. Moreover we shall examine the sensitivity of such nonlinear model from the used mathematical approximation tools such as the curve fitting method and the used system for the solution.

2. METHODS AND MATERIALS USED FOR RESEARCH

The model built was examined by Matlab, Simulink and Maple. Matlab and Maple uses scripts, which solve the state-space equations of the system [12]. The characteristics curve of the nonlinear element was implemented by curve fitting. The mathematical model of the circuit containing the Tunnel diode is [2]:

$$\dot{x}_1 = \frac{1}{C}[-h(x_1) + x_2] \quad (1)$$

$$\dot{x}_2 = \frac{1}{L}[-x_1 + Rx_2 + E] \quad (2)$$

where x_1 is the voltage across the capacitance (v_c), x_2 is the current through the inductance (i_L) and $h(x_1)$ is the Tunnel diode characteristics. The Simulink model can be seen on Fig 2. Here the characteristics curve was implemented by a lookup table.

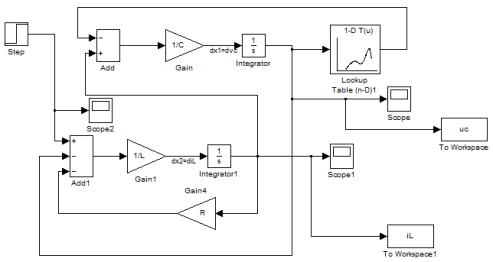

Fig. 2.: Simulink model of the Tunnel diode circuit

The behaviour of the system was examined by the calculation of time dependent, phase-plane [13] and bifurcation diagrams [14].

The setting time of the state variables and the sets of attraction depend on the parameters of the model. There are such parameters (called bifurcation parameters) from which the structure of the bifurcation diagram depends [14].

3. RESULTS

By the numerical solution of the equation 1-2 one can calculate the phase-plane diagram with fixed parameters. The result of the calculation is shown on Fig. 3. This figure is completed with the boundary of the sets of attraction [15] (see the bold magenta curve) and the characteristic curve of the Tunnel diode (red dashed curve).

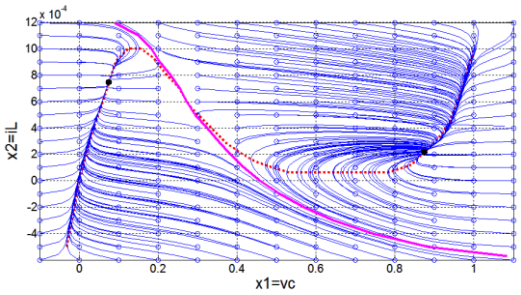

Fig. 3.: Phase plane diagram with boundary of the set of attraction

From Fig. 3 it can be observed that the system has 2 stable equilibrium points.

3.1.Effects detected by changing of parameters

We can observe that the number of equilibrium points doesn't depend on L and C (Fig. 1), but they effect on the boundary of the set of attraction and the setting time.

Increasing C or L increases the setting time, specially setting time of voltage. Decreasing them decreases the setting time. The changes of the different parameters can be seen on Fig 4.

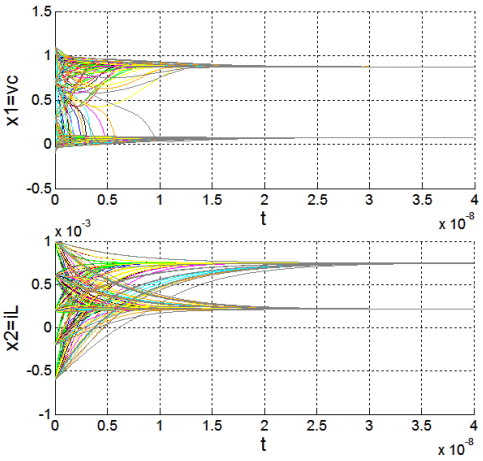

Fig 4.: Changes in setting time to the equilibrium states (blue: 0.5C- 0.5L, red: 0.5C- 1L, green: 0.5C- 2L, black: 1C- 0.5L, magenta: 1C- 1L, yellow: 1C- 2L, cyan: 2C- 0.5L, orange: 2C- 1L, grey: 2C- 2L)-see pdf version

On Fig. 5 one can see the parameter dependence on the boundary line of the sets of attraction. This information can be useful for designing Tunnel diode switching circuits [10].

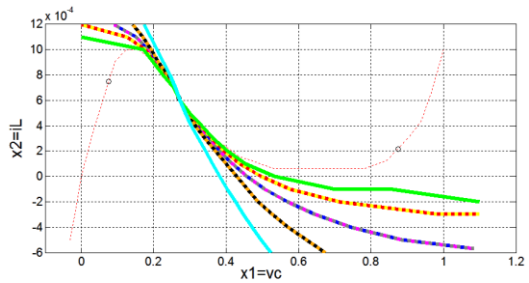

Fig. 5.: Changes in the boundary of the set of attraction (blue: 0.5C- 0.5L, red: 0.5C- 1L, green: 0.5C- 2L, black: 1C- 0.5L, magenta: 1C- 1L, yellow: 1C- 2L, cyan: 2C- 0.5L, orange: 2C- 1L, grey: 2C- 2L)-see pdf version

Resistance and input voltage are bifurcation parameters. From the bifurcation diagrams shown on Fig. 6 the influence of bifurcation parameters can be seen. Growing the parameter values (R and E) first there is only a single equilibrium point, then there will be 2 stable and a bistable points, then a stable and the bistable equilibrium points disappear and only a single equilibrium point remains.

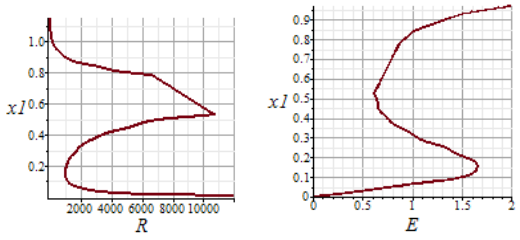

Fig. 6: Bifurcation diagrams (left: bifurcation diagram of R, right: bifurcation diagram of input E)

With more sophisticated calculation we can examine the 2 parametric bifurcation diagram shown on Fig. 7.

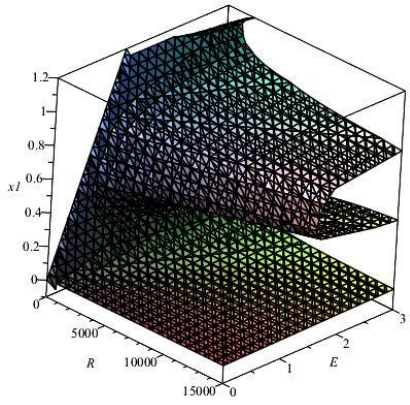

Fig. 7.: Bifurcation diagrams of both parameters

3.2. Influence of Spline function used for the simulation

The characteristics was implemented to the model by Spline function. In Matlab only the 3rd degree Spline function is properly included, so the examination was carried out in Maple. It was observed how the simulation is affected by the degree of the Spline function. The time dependent and phase-plane diagrams can be seen on Fig. 8. The degrees of the Splines are from 1 to 5. The simulation failed with 2nd degree Spline, because of singularity.

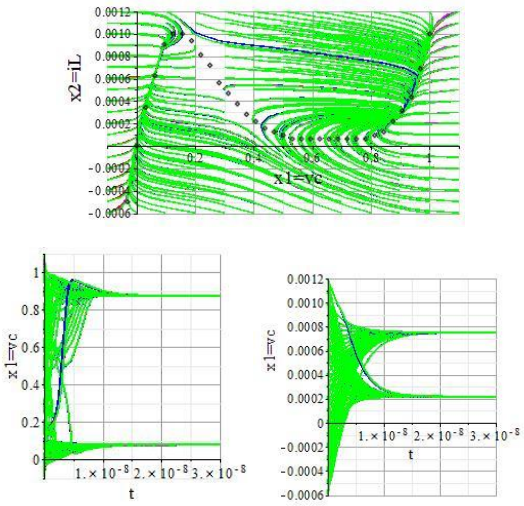

Fig. 8.: Phase plane (upper) and time dependent (bottom) diagrams in case of using different Splines (blue: 1st degree, red: 3rd degree, magenta: 4th degree, green: 5th degree) -see pdf version

It can be seen, that the degree of the Spline function does not significantly affect the simulation. There is small deviation at the edge of the test range. The 1st degree Spline gave the biggest difference. There are more significant differences at some points of the boundary of the set of attraction. As it can be seen on Fig 9. there were initial states, where degree of the Spline function led to a different equilibrium point.

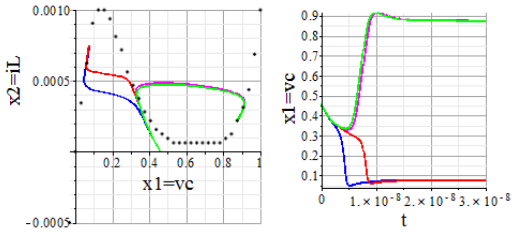

Fig. 9.: Example of different result at the boundary of the set of attraction

The calculation time was almost the same for all the 4 Spline used.

3.3. Comparing Matlab and Simulink solvers

By comparing the same solvers (ODE45) in Matlab and Simulink we got different results of simulation at the boundary of the set of attraction as it can be seen on Fig. 10. and Fig. 11. Simulink solver with variable step gave less exact trajectories, than fixed step or Matlab.

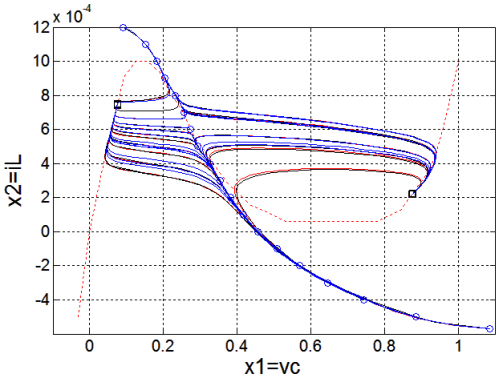

Fig 10.: Phase-plane diagram at the boundary of the set of attraction using Matlab and Simulink (blue: Matlab, black: Simulink variable step, red: Simulink fixed step)- see pdf version

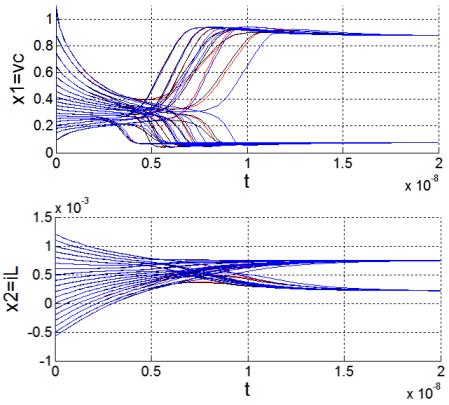

Fig. 11.: Time dependent (lower) diagrams at the boundary of the set of attraction using Matlab and Simulink (blue: Matlab, black: Simulink variable step, red: Simulink fixed step)- see pdf version

4. CONCLUSIONS

Detailed numerical examination of a system model with a nonlinear element was carried out. Changing parameters L and C influence the boundary of the set of attraction and the setting time. Different values of R and E can give different topology of the system, for example different number and values of the equilibrium points.

The effects of the degree of the fitted Spline function were also examined. Larger differences occurred at some points at the boundary of set of attraction.

One important observation of this examination is that the Matlab and the Simulink can give different simulation results using the same solvers (ODE45).

For rough simulation a common solver and a lower degree Spline function is satisfactory. For more exact simulation of systems the higher degree Spline and a more precise solver should be considered.

Forthcoming problem to solve is to generalize the simulation technique presented here to other nonlinear electrical, mechanical, hydraulic and mechatronic systems. Moreover it would be an interesting task to solve the calculation of the frequency spectrum map [16] of nonlinear oscillators.

5. REFERENCES

[1] Álló G., Bartolits I.: Unlimited bandwidth and computing power (in Hungarian), http://www.nhit-it3.hu/__ujsite2/images/tagandpublish/Files/it3-2-1-1-u.pdf

[2] Khalil H.K.: Nonlinear Systems, Prentice Hall,pp.7-8, 33-35., 1999

[3] Seabaugh A., Lake R.: Tunnel diodes, Encyclopedia of Applied Physics, Vol 22., (1998), pp. 335-359

[4] Matyi G.: Electrodynamics of Nano Antenna mom diode sensors (in Hungarian), dissertation, Pázmány Péter Catholic University, Doctoral School of Interdisciplinary Technical Science (2007), supervisor: Dr. Csurgay Á.

[5] Sharma P., Khan T.A., Vishwakarma B.R.: Tunnel Diode Loaded Rectangular Microstrip Antenna with Passive Components for Millimeter Range, International Journal of Innovative Technology and Exploring Engineering (IJITEE) ISSN: 2278-3075, Vol.4 Issue 3, (2014)

[6] Munstermann G.T.: Tunnel-Diode Microwave amplifiers, APL Technical Digest. Vol 4. (1965)

[7] Tunnel Diode and its Applications, http://www.electrical4u.com/tunnel-diode/

[8] Heinrich M., Dahms T., Flunkert V., Teitsworth S.W., Schöll E.: Symmetry-breaking transitions in networks of nonlinear circuit elements, New Journal of Physics, Volume 12, (2010)

[9] Pawlik D.: Development of tunnel diode devices and models for circuit design and characterization, Msc thesis, Rochester Institue of Technology, (2007)

[10] Lotfi M., Zohir D.: A Spice Behavioral Model of Tunnel Diode: Simulation and Application, International Conference on Automation, Control, Engineering and Computer Science (ACECS'14) Proceedings, pp.186-191

[11] Sellai A., Al-Hadhrami H., Al-Harthy S., Henini M.: Resonant tunneling diode circuits using Pspice, Microelectronics Journal 34, (2003), pp.741–745

[12] Bokor J., Gáspár P., Soumedilis A.: Control Engineering 2 (in Hungarian). Budapest University of Technology and Economics, lecture notes, pp. 20-34.

[13] Dynamical Systems, Budapest University of Technology and Economics, lecture notes (in Hungarian), http://www.fke.bme.hu/oktatas/meresek/7.pdf

[14] Simon L.P.: Differential Equations and Dynamical Systems (in Hungarian), Eötvös Loránd University, lecture notes, (2012), pp. 162-164. http://www.cs.elte.hu/~simonp/DinRJegyz/dinrendjegyzet.pdf

[15] Garay B.: Nonlinear Dynamical Systems (in Hungarian), Pázmány Péter Catholic University, lecture notes (2013), http://digitus.itk.ppke.hu/~garay/NDS_jegyzet/NDS_jegyzet_Garay_final_v4.pdf

[16] Billings S. A., Boaghe O.M.: The response spectrum map, a frequency domain equivalent to the bifurcation diagram, Research report No. 774, (2000)

Distributed congestion detection and classification method for the analysis of velocity

Krisztian Medgyes [a], Tamás Kovács [b]

[a] Pallasz Athéné University Kecskemét, Izsáki street 10., 6000 Hungary, Medgyes .Krisztian @gamf.kefo.hu

[b] [a] Pallasz Athéné University Kecskemét, Izsáki street 10., 6000 Hungary, Kovacs.Tamas@gamf.kefo.hu

Abstract

A centralized or distributed system of intelligent traffic management system is an important element of the congestion detection, achieved today using mostly external sensors. In this paper we propose a congestion detection and classification method that uses a mobile phone in vehicles GPS sensor data of the speed versus time for continuous recording and analysis of this function is to classify the traffic. The two important parameters, which will help you: characteristic parameters of the speed rate of progress and the prevailing traffic periodicity periodicity parameter, which the velocity autocorrelation about obtained. The method is known as traffic situations recorded data series mobile phones tested. The results obtained show that the proposed method can be made fully operational and additional measurements or algorithmic refinements, chances are applicable in the practice.

Keywords: transport optimization, traffic jam detection, classification, velocity.

1. INTRODUCTION

navigation systems in road vehicles is becoming a standard requirement to the moment of departure determines not only the optimal path, but can adapt on the fly to the dynamically changing traffic situation. More specifically, the move to be able to propose an alternative route instead of the route ahead, evolving or developing queues in heavy traffic, resulting in a small increase in train path, but a significant time savings.

The systems are available today only offer a navigation community to the possibility that users already jam indicate pressing a few keys to others, how much congestion if willing to do so. One problem is that this feedback makes a small percentage of users. Another shortcoming of this system is that it does not detect a possible cause of the congestion.

A number of publications were innovative transport area, which in-vehicle mobile phone GPS and other sensor data from records of the speed-time function and its analysis of the relevant information reaches some decisions. For example, Wang et al mobile applications harmfulness judge applied this method (Wang Yan, et al., 2013), Amin et al is a possible accident of a vehicle detects the speed-time function automatically and continuously evaluating (al Amin et. 2013). If the GPS sensor data are not precise enough for the task, it is possible to find a phone with accelerometer sensor fusion is (al Han et. 2014).

The speed of continuous monitoring allows the congestion detection well. A recently published solutions usually pay attention to one parameter, the driving pace, which is usually the speed versus time averaging and integrating determined (, Terroso-Sáenz et al. 2012, La inchua et al., 2013 Bingle et al., 2008) These can

be used in some vehicles detected congestion states and distributed across a larger environment information system functions well (Terroso-Sáenz et al. 2012, Bauza et al., 2013).

In the present research we are emphasis was placed, in ways that promote the flow of such information, which is not only suitable for congestion detection, but also give information to the question is that if congestion arose, then what kind. The causes of congestion can be anything from a traffic flow exceeds the capacity of traffic lights; difficulty getting out of the way with a child; a slow vehicle is causing an obstruction or even the queues formed due to a serious accident.

The first phase of our work, we developed a variety of reasons recorded in congested traffic situations were stuck in traffic on the vehicle speed as a function of time, and these functions by analyzing one of the methods published so far more sophisticated congestion detection and congestion sorting method we developed.

Further, this information is made up of cars from an ad-hoc network you would be able to spread, even without a mobile internet connection.

2. DATA COLLECTION

The speed time measurement data recording posted on an Android phone recording application has been developed, which can record the GPS data obtained from each sensor up to speeds of 100Hz. The mobile phone positioning accuracy of GPS satellites in addition to the increased use of GLONASS satellites, which inaccuracies in any case less than 1-1.5 meters reported. The device accelerometer sensors, we were able to distinguish between low-speed queues, data inaccuracies resulting from the satellites so-called "drift" from (drift). Various traffic situations nearly identical terms the repeated data acquisition.

The measurements were carried out in a residential area of Budapest (1757618 people) and Kecskemét (111 836 people). The traffic situations analyzed as follows:

- Due to limited permeability of the roundabout it caught about 800-850 meter range of car queues (8 pieces of measurement);

- Congestion situation caused by light intersection (11 pieces of measurement);

- Mandatory priority congestion caused by position (9 pieces of measurement) by broadcast or roundabouts;

- Normal progress, ie, congestion-free status (3 pieces of measurement).

Measurements are optimized per-second processing. The different measurement time window length, the resulting traffic jam as a function of the length of time (as short as 60 seconds, the longest was 1835 seconds). All measuring about 800 kilometers in scope, this represents little more than 34 hours of raw data in time.

3. GRADING METHOD FOR JAM

The fixed-rate time functions analysis of objective, therefore, is to determine the characteristics of the various properties, depending on congestion. On this basis, we are able to determine that congestion was emerging or developing any type of such. These studies suggest that in addition to this problem that the average speed of the other relevant parameters to measure the speed of short-term (i.e., in the range from 30 to 120 per second), the periodicity strength used periodicity of the speed as a function of the autocorrelation function, in which:

$$C(T) = \sum_{t} (v(t) - \langle v \rangle)\,(v(t+T) - \langle v \rangle))$$

using the formula was determined.

More information mean for us in the second autocorrelation function, i.e. auto-correlation function of the first autocorrelation function. This will help you decide how much of the

developed random or regular periodicity is caused by the traffic light congestion judging can be important. This means that road users in the traffic control equipment over time with a pre-programmed fixed period (traffic light) controls whether and removed from the front or not. In this work, the second autocorrelation function is not used. The other study characteristics were average speed, where an over-pass filter had to be applied for the speed, as if he has to run, makes a great speed in that time but in the meantime with anticipation, as if the speed is low, the same average speed arises. Using the High Pass Filter switch differentiate the phenomenon, if we go to traffic light step, or if the traffic control devices are not set according to the "green wave" and the traffic light can move at high speed, but because of the lamp incorrectly set to welcome a lot of new free signal. The high-pass filter threshold at 1 m / s selected. This eliminates the zero threshold values, but the slow progress (queues) leaves the reservoir levels.

Based on the average speed and the result of the autocorrelation we were divided into four classes of traffic congestion:

• Dynamically advanced, congestion-free

• lamp to lamp dynamic, but there is no green wave

• Traffic light congestion formed due

• Other developed due to congestion (priority broadcast, roundabout, technical defective vehicle, work on the road) congestion

3.1. Dynamically flow, congestion-free

In transport, the optimal condition when -close- the road can be safely allowed to move with maximum speed and neither traffic lights, level crossing, roundabout or other obstacles complicate.

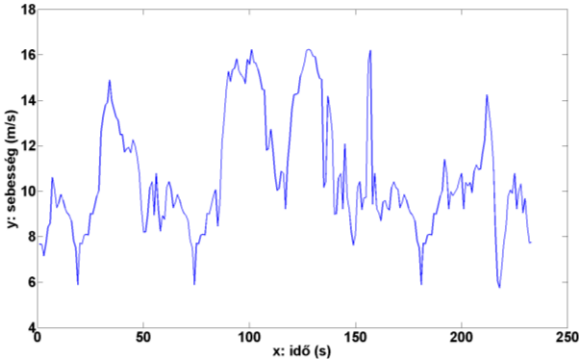

Fig. 1. One dynamically flow, congestion-free velocity and period

This state is divided into the traffic conditions when at least half of that route maximum speed is constantly moving, heavy and prolonged stoppages without slowing down (Figure 1).

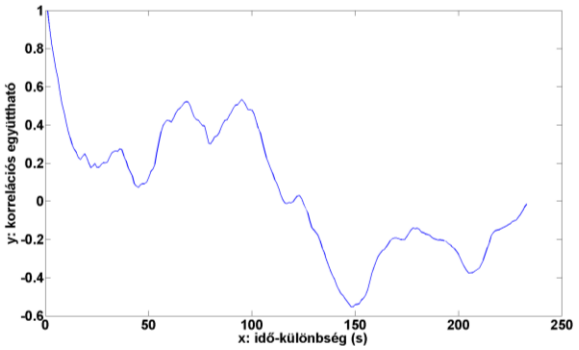

Fig. 2.A function of the previous figure autocorrelation

The horizontal axis is the time (seconds) and the vertical axis represents the current speed (m / sec) changes can be taken into account: Analysis of correlation unnecessary in this case because it does not carry us currently evaluable information but the autocorrelation curve shows anti-correlation (the second figure).

3.2 Dynamic from Lamp to Lamp without green wave

Large cities, if they can, transport organizers pay attention to the sweeping vehicle for guiding so-called "green wave" design, which can dynamically move a major traffic flow in at least one direction. In some cases, unfortunately, this is not feasible, and traffic compared to 45-50 km / h average speed is significantly lower than the average speed of around 25-30 km / h can only develop tailored green wave.

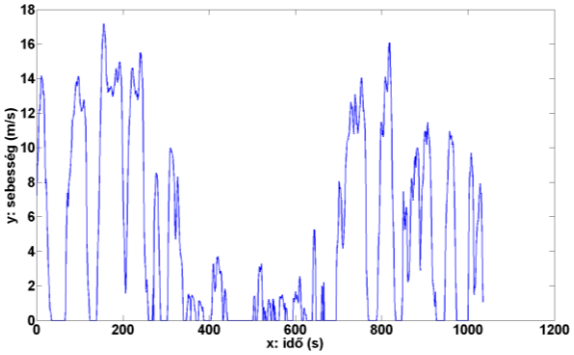

Fig. 3. A lamp to lamp dynamic and periodical driving

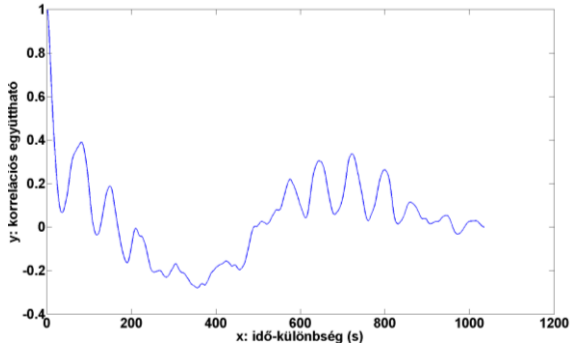

Fig. 4.A function of the previous figure autocorrelation

In this case, it observed the movement of vehicles is that between the two lamps plying the permitted rate of around 50 km / h, and the expectations comes the next traffic light, stress due to poorly designed traffic flow control. The speed-time development of the Figure 3 example. autocorrelation graph comprising the same for this measurement is shown in Figure 4. The maximum value of the correlation between the first local maximum at around 0.4, which requires a periodic movement.

3.3. Traffic light formed due to traffic jam

In many cases, if the permeability of light is located at the intersection traffic control equipment not sized for certain periods of increased traffic from one direction in accordance with the current, you can narrow significantly in the direction of the road permeability, which involves the formation of traffic jams during the periods in question. 5 illustrates stopped by a traffic light equipment járműsor speed of evolution. It can be observed that the evolution rate remains low (up to 5 m / s around), unlike the previous case, where there were over 13 m / s, this value.

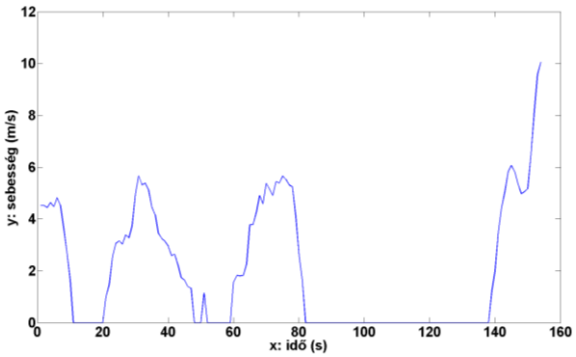

Fig. 5. Traffic light formed due to traffic jam

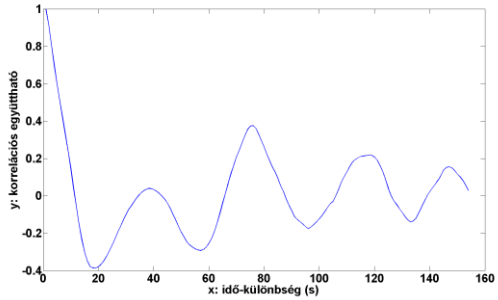

Fig. 6.A function of the previous figure autocorrelation

Correlation graph for measured data in Figure 5 (Figure 6) can be observed showing the presence of the periodic nature of a correlation value of about 80 seconds around 0.4, indicating a 80-second cycle, the second lamp local maxima.

3.4. Others congested traffic situation

Formed due to traffic conditions differ from past (STOP sign, broken-down vehicle stranded in the road, accidents, work on the road) traffic speed reduction is established that typically non-periodic, as in the previous case described examples. This correlation after the first and second phase of the curve rising up to its confirmation. In this case, 0.2 (or even 0.5 negative) value (Figure 8), clearly shows the absence period. A line of cars with low 3-4 m / s maximum speed (Figure 7) is clearly assumed queues. The corresponding correlation is shown in Figure 8:

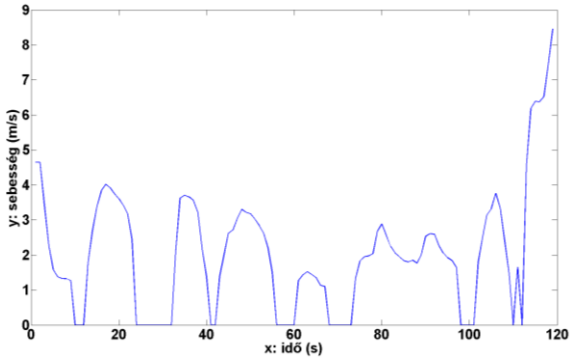

Fig. 7. A "STOP!" table Congestion function

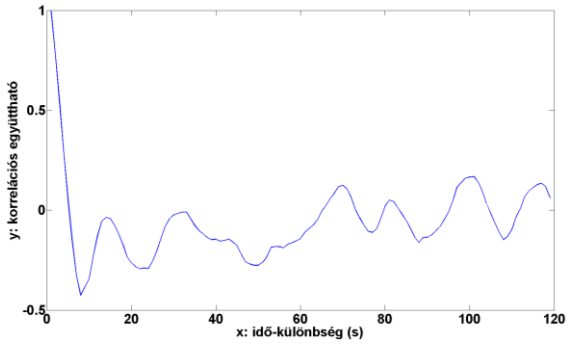

Fig. 8.A function of the previous figure autocorrelation

4. RESULTS

The fixed-rate time functions analysis of objective, therefore, is to determine the characteristics of the various properties, depending on congestion. On this basis, we are able to establish a classification algorithm that is able to autonomously classify and acceptable error is not yet known traffic conditions and congestion.

To do this, two parameters are selected on the basis of the above information. One parameter is the speed that the

$$V = \Phi\left(v(t)\right)$$

obtained using the formula where Φ an over-pass filter, in this case 1 m / s threshold value, the <> represents a window of a fixed length of time averaging reported. The time window length in this case was the length of the sample. The other parameters characterizing the periodicity, which was in this case, the autocorrelation function is the largest local maximum value when the 40 - 150 seconds ranged (based on values of the traffic light cycle).

9 is a 'speed parameter' - shown "periodicity is set to" plot the measured and known traffic situations. It can be seen that the four types of measurement situations are more or less separated from each other, and a periodicity of a speed threshold value, that is classified in the quadrant of the resulting four-aisle space. It gives us the opportunity to further refine the method is a reliable method for screening and detecting congestion to work out.

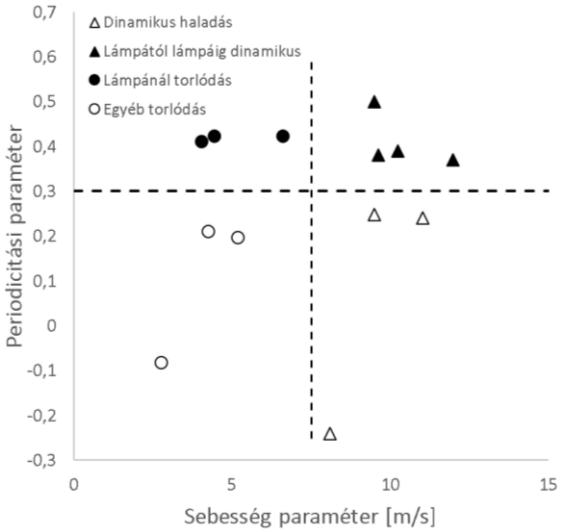

Fig. 9. The location of the speed measurement situations parameters - parameters periodicity phase space

5. CONCLUSION AND FURTHER WORK

Based on the average velocity parameters and periodicity parameters based on the speed of autocorrelation was tested using basic principles of a possible traffic jam sensor and sorting method. The results obtained show that the method can be used not only to determine the fact of the possibility of congestion, but also suggest that the congestion is caused by an overloaded traffic lights or some other non-periodic mode obstacle.

A reliable method for testing the number of measurement samples collected is not sufficient, further work is needed to test a wider variation traffic situation. Accordingly, not only for

accurate testing it is possible, but the method is more robust and make it more refining.

REFERENCES:

- Amin, Md Syedul, et al. "GPS and Map matching based vehicle accident detection system." Research and Development (SCOReD), 2013 IEEE Student Conference on. IEEE, 2013.
- Bauza, Ramon, and Javier Gozálvez. "Traffic congestion detection in large-scale scenarios using vehicle-to-vehicle communications." Journal of Network and Computer Applications 36.5 (2013): 1295-1307.
- Binglei, Xie, Hu Zheng, and Ma Hongwei. "Fuzzy-logic-based traffic incident detection algorithm for freeway." 2008 International Conference on Machine Learning and Cybernetics. Vol. 3. IEEE, 2008.
- Han, Haofu, et al. "Senspeed: Sensing driving conditions to estimate vehicle speed in urban environments." IEEE INFOCOM 2014-IEEE Conference on Computer Communications. IEEE, 2014.
- La-inchua, Jaraspat, Sorawat Chivapreecha, and Suttipong Thajchayapong. "A new system for traffic incident detection using fuzzy logic and majority voting." Electrical Engineering/Electronics, Computer, Telecommunications and Information Technology (ECTI-CON), 2013 10th International Conference on. IEEE, 2013.
- Terroso-Sáenz, Fernando, et al. "A cooperative approach to traffic congestion detection with complex event processing and VANET." IEEE Transactions on Intelligent Transportation Systems 13.2 (2012): 914-929.
- Wang, Yan, et al. "Sensing vehicle dynamics for determining driver phone use." Proceeding of the 11th annual international conference on Mobile systems, applications, and services. ACM, 2013

Development of the Lower Body of Assistive Humanoid Robot MARKO

M. Penčić [1], S. Savić [1], M. Čavić [1], B. Borovac [1], Z. Lu [2]

[1] Faculty of Technical Sciences, University of Novi Sad, Trg Dositeja Obradovića 6, 21000 Novi Sad, e-mail: {mpencic, savics, scomaja, borovac}@uns.ac.rs

[2] School of Electrical Engineering and Automation, Changshu Institute of Technology, Hushan Road 99, 215500 Changshu, P.R.China, e-mail: zhenlilu@cslg.cn

Abstract

As cerebral palsy is a complex neurological disorder and there are no two children with exactly the same manifestations, an individual approach to treatment is necessary. Rehabilitation/habilitation is based on the physical and kinesitherapeutic treatments that are tiresome and monotonous. Since the success of therapy depends directly on the time that a child spends exercising, it is necessary to find a way to motivate a child. The paper presents the development of the robot lower body – robot legs, which are intended to demonstrate the movements of gross motor function in therapeutic purposes. The research was conducted within the project which is developing humanoid robot *Marko* – an assistive tool in physical therapy for the children with cerebral palsy. Based on the set requirements a 3D model of the robot leg is formed. Dynamic simulation was performed and driving torques in joints are determined. The realized leg has 4 DOFs and enables movements of the upper leg in the direction of flexion 120°, extension 90° and abduction 90° (lateral movements) in hip joint, lower leg movements in the direction of flexion 80° and hyperextension 10° in the knee joint, and foot movements in the direction of dorsiflexion 30° and plantar flexion 30° (front and rear flexion) in the ankle joint.

Keywords: assistive robot, humanoid Marko, cerebral palsy, mechanical design, lower body, robot leg

1. INTRODUCTION

Children with non-progressive neuromuscular disorders, such as cerebral palsy [1], can have a significant deficit of motor functions and skills, body posture, as well as intellectual and emotional disorders [2]. The primary problem is a defect in the initiation and execution of the movement [3], considering that the motor activities represent the basis of human functioning.

In this paper the development of robot legs that are designed for demonstration of the movements in therapeutic purposes is presented. It should be noted that the robot is sitting on a pedestal in the form of the horse – Figure 1, and that the legs are intended only to demonstrate the movements during treatment and not for walking. The research was conducted within the project which is developing humanoid robot *Marko* that represents assistive tool in physical therapy for children with cerebral palsy. The conventional medical treatment involves exercises that are monotonous and exhausting for children, wherefore they rapidly lose interest for the work. Since the success of the therapy is directly proportional to the time that a child spends exercising, it is necessary to find a way to further motivate the child. The aim of the project is to offer a "partner" to children with whom they would be more interested to practice and who will be able to demonstrate the exercise that a child cannot perform. It is expected that the effects of the therapy will be increased through additional motivation and encouragement of patients to exercise as long as possible. The therapy is carried out in such a way that, at the beginning, a therapist asks the child to properly do an exercise. If the child is not able to do so because he does not understand what is required of him, then the therapist asks the robot to perform the exercise.

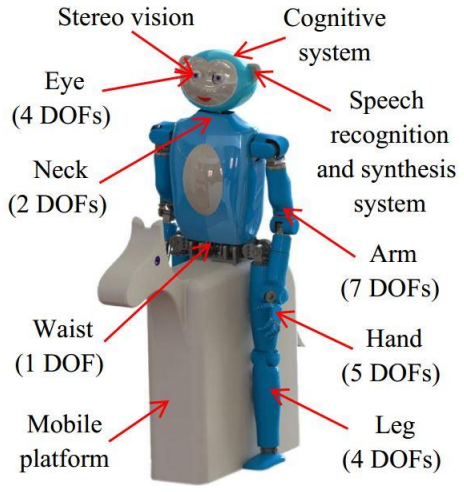

Fig. 1. Assistive humanoid robot Marko – CAD model

After the robot has performed the exercise (*e.g.*, touches the head with arm), the therapist then asks the child to repeat the exercise. When a child does the exercise correctly by itself, the robot will commend him.

1.1. Human lower body

The legs are moving parts of the human body which are attached to the pelvis [4]. Leg consists of six distinct sections: hip, upper leg, knee, lower leg, ankle and foot – Figure 2. Basic movements of the legs are flexion and extension – forward and backward movements, adduction and abduction – external and internal lateral movements and rotation movements. All these movements are performed by activating the hip joint. However, range of mobility is not the same for all joints. The most movable is the hip joint, then knee joint and the least is the ankle joint. Mobility range of the upper leg in the hip joint for the movements of flexion is approximately 140° and for the movements of extension is approximately 45°. Total lateral movement is approximately 70°, which is 25° for adduction movements and 45° for abduction movements. Mobility of the lower leg in the knee joint for the flexion movements it is approximately 140°, and for the hyperextension movements is approximately 10°. The total flexion of the foot in the ankle joint is approximately 75°, which is 55° for dorsiflexion movements and 20° for plantar flexion movements of [5], [6].

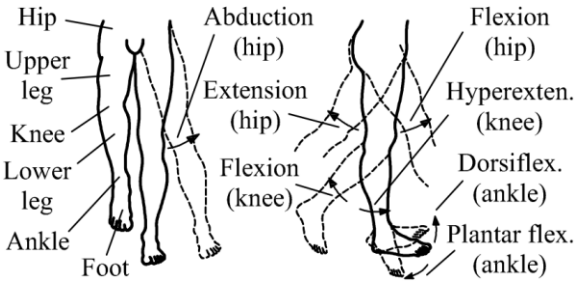

Fig. 2. Basic movements of human leg

1.2. State of the art

There are several robots that are used in physical therapy for children with cerebral palsy [7]. In [8] a social robot *KineTron* is shown that acts as a coach to encourage the patient. The therapy is based on the 9 scenarios in which robot demonstrates exercises and the child repeats them – three for the beginning of the session, three to encourage patients in the middle of training and three for the final part of the session. Each scenario is combined with voice and music. Evaluation of therapy is performed in a group of six children aged 4–9 years with 5–7 sessions lasting 20 minutes. Preliminary results indicate that there are benefits in using humanoid robots for motor training of patients with cerebral palsy – it appears that the robot motivates and actively encourages the child in the activities of rehabilitation. Some of the suggestions that have been proposed after the first experiences from working with the robot are that the robot needs to have different clothes, a greater assortment of movement scenarios, and different programs for girls and boys. *KineTron* has arms, each with 3 DOFs and legs, each with 6 DOFs, making a total of 18 DOFs. The height of the robot is 0.4 m and the mass is 1.7 kg. In [9] it is shown a robotic platform *Ursus* – friendly teddy bear. The therapy consists of two phase. In the first phase, patient mimics the movements that are displayed on the screen, and if he cannot, then in the second phase robot demonstrates the movements. During the session, the robot verbally and with gestures encourages the patient and records his movements – in this way the movements are compared and the success of therapy is monitored. Evaluation of therapy is performed with six pediatric patients aged 3–7 years who have upper limbs motor deficit. Preliminary results are encouraging and indicate that this type of therapy is more interesting than the conventional treatment. Advanced model of robot will be able to recognize facial expressions and body language that will simplify the communication and increase the success of therapy. *Ursus* has arms, each with 5 DOFs, the neck with 3 DOFs and an articulated mouth, making a total of 14 DOFs. The height of the robot is 1.4 m. In [10], [11] is shown *Nao* robot as assistive tool in physical therapy of children with cerebral palsy. The therapy is based on four interactive scenarios in which the robot demonstrates the movements, and the child repeats them. In the first scenario, a verbal communication is accomplished between the child and the robot – the first impression. The second scenario includes movements of the trunk and lower body – actions of stand up and sit down. The third scenario is based on the balance and the body posture – robot stands on one leg with arms spread out and balances. The fourth scenario should improve motor function of the child's leg – kicking ball. Evaluation of the therapy is performed with two patients aged 9 and 13 years, once a week for 8 weeks. Preliminary results indicate that the robot significantly motivates and encourages children to actively participate in the process of habilitation. *Nao* has a head with 2 DOFs, arms, each with 5 DOFs, pelvis with 1 DOF, legs, each with 5 DOFs and hands with 2 DOFs, making a total of 25 DOFs. The height of this robot is 0.57 m, and the mass is 4.5 kg [12]. In [13] it is shown a child-friendly space robot *CosmoBot* – motivating toy/friend which interacts with a child in the context of entertaining games. The child can control the robot's head, arms and mouth movements, and can activate a hidden set of wheels under his feet to drive him forward, backward, left and right. Evaluation of therapy is performed with six patients who have a motor deficit of upper extremities ages 4–10 years for a period of 16 weeks. Preliminary results indicate the positive aspects of the therapy as well as the significantly increased attention and interest of children during the therapy.

2. ROBOT LOWER BODY

Considering that the legs are intended to demonstrate the movements, the basic requirement is an adequate mobility of the leg in space – gross motor function: mobility of the upper leg in the hip joint – the movements of flexion, extension and abduction (lateral movement), mobility of the lower leg in the knee joint – movements of flexion and hyperextension, and the mobility of the foot in the ankle joint – movements of dorsiflexion and planar flexion (front and rear flexion of the foot). In order to minimize the driving torques in the joints it is necessary that the mass of segments are as small as possible, and their center of mass as close as possible to the pelvis. It is therefore advantageous that the actuators of the hip are placed in the pelvis – then the pedestal bears their mass, and the actuators for upper and lower leg should be placed as much as possible close to the hip. In addition, for forming the joints require reliable and simple mechanisms with small dimensions, low mass and low manufacturing cost. Although high positioning accuracy which enables high accuracy and repeatability of the movement of the secondary importance, it is important that the mechanisms have low backlash.

2.1. Forces and torques

The movements during the demonstration should be as natural as possible so it is adopted that their duration does not exceed 1 s, which has for a consequence certain dynamic effects. Therefore, based on the formed 3D model of the leg, dynamic simulation is performed. Torques in the joints which have been determined based on the simulation were used to dimension the drive units. Figure 3 shows the hip joint trajectory for the range of motion 60° and the knee

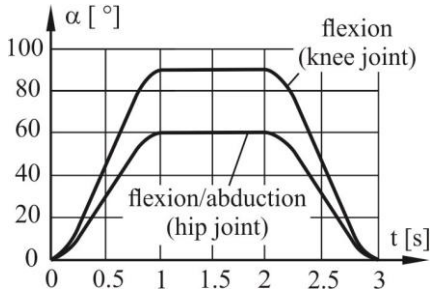

Fig. 3. Hip/knee joint trajectory

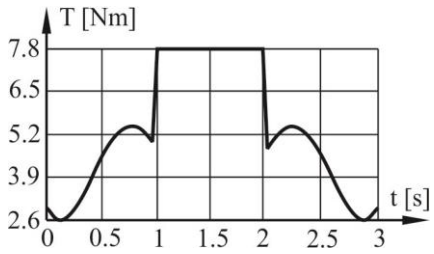

Fig. 4. Graph of the torque – flexion/abduction in the hip joint

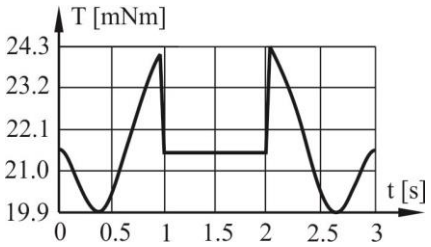

Fig. 5. Graph of the torque – flexion in the knee joint

joint trajectory for the range of motion 90°. The maximum value of the torque in the hip joint is 7.8 Nm – Figure 4, and the maximum value of the knee joint is 0.0243 Nm – Figure 5. A small value of torque in the knee joint is achieved by positioning the actuators in the upper leg wherefore, center of mass of the leg is moved closer to the hip. The use of carbon fiber for the manufacturing of the carrying structure, obtained a lightweight and strong construction.

2.2. Mechanical design

In Figure 6 it is shown a robot hip mechanism consisting of a base plate for attaching the legs to the mobile platform and two support plates between which there is a mechanism that enables the upper leg movements in the direction of flexion/extension. Mechanism consists of the two toothed gearings – the first one with the spiral bevel gears that enables the vertical position of the actuator within the mobile platform, and the second one with the helical gears – driven gear is designed as a hollow toothed shaft to enable the passage of electrical cables. The actuator is attached to the mounting plate and connected to the base plate. The driving bevel gear is directly placed on the gearhead shaft. Low backlash in gearing with the bevel gears is achieved by radial and/or axial moving of the actuator together with mounting plate – axial backlash adjustment is possible by inserting the shim washers between the mounting plate and the base plate or by placing them on the gearhead shaft. Low backlash in gearing with the helical gears is achieved by accurate manufacture of the support plates and the

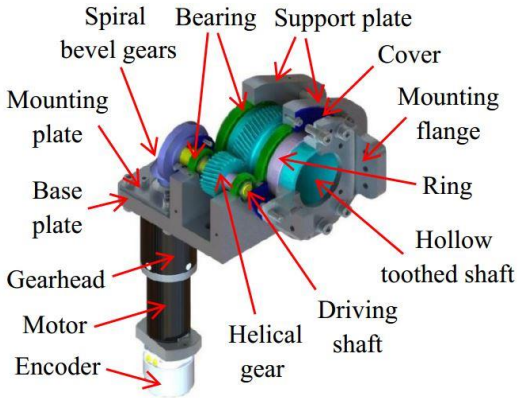

Fig. 6. Mechanical design of robot hip

preloading of the gears [14] – center distance is with negative tolerance. The total mass of the hip (gears, actuators and associated structural elements) is 2.9 kg.

Figure 7 presents the upper leg of the robot, which consists of carbon fiber tube with affixed mounting flanges on both ends. Within the carbon tubes two actuators are placed – the first one is attached to the upper mounting flange and enables the abduction movements of the upper leg – lateral movement, and the second one to the lower mounting flange and enables movements of flexion/hyperextension of the lower leg. Two support plates are attached to the upper mounting flange and a gearing with bevel gears is placed between them. Driven gear is immovable, because the shaft is fixed to the lateral flanges that are linked with the mounting plates. Movements of abduction are realized by using bevel gearing with straight teeth, while the lower leg movements by using the bevel gearing with spiral teeth. With increasing spiral angle of bevel gears, increases the overlap ratio of gears and therefore increases the carrying capacity. The greater overlap ratio effects positively on the reduction of backlash. On the other hand, with the increase of spiral angle of gears, the forces that are acting on the shaft of gearhead also increase – driving gears are directly attached to the shaft of gearhead whose bearings suffer relatively small value of radial and axial forces. Gearing for the abduction movements in the hip joint has a one-stage, and the gearing for movements of the flexion/extension in the hip joint has a two-stage – driving torques are the same for both movements, but the individual loads of tooth is much higher to the one-stage gearing. Therefore, for the movements of abduction a straight bevel gearing is adopted, and thus the axial forces were eliminated. Low backlash is achieved by axial and/or radial moving of the driven gears with use of the shim washers. The mass of the upper leg is 2.8 kg.

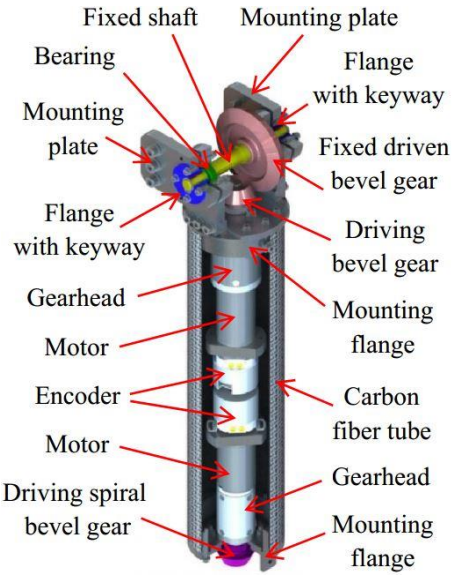

Fig. 7. Mechanical design of robot upper leg

Figure 8 shows lower leg of the robot, which consists of carbon fiber tube with mounting flanges affixed on both ends. Within carbon tube there is an empty space to accommodate electronics. Toothed gearing for movements of flexion/hyperextension of lower leg is designed in such a way that its driving gear is within the upper leg and driven gear is within the lower leg. A support plate is attached on the upper mounting flange together with the shaft and driven bevel gear. Bearings are placed at the ends of the shaft and on top of the support plates, *i.e.* mounting plates for fixing the lower leg with the upper leg. Low backlash is achieved by radial and/or axial moving of the actuator together with the mounting plate and/or axial moving of the driven gear with the use of the shim washers. The mass of the lower leg is 1kg.

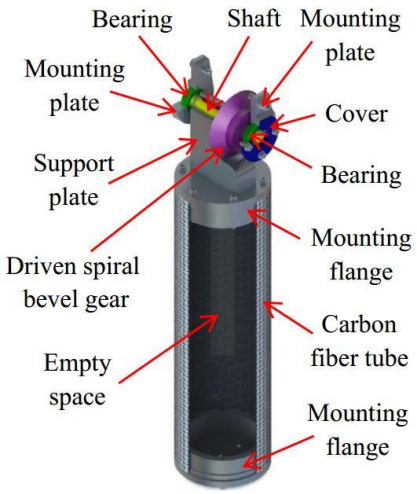

Fig. 8. Mechanical design of robot lower leg

On Figure 9 is shown the foot of the robot consisting of base plate and two support plates between which is placed an actuator – servo motor, which enables movements of the foot in the direction of dorsiflexion/plantar flexion. Servo motor is attached to the mounting plate and connected to the mounting flange of lower leg. At the opposite end of the motor in the direction of the output shaft, a pin is embedded on which the bearing is set. First support plate is attached to the motor shaft, and the other to the pin with bearing – thus enabling rotation of the foot. The mass of the foot is 0.3 kg.

The shafts and the gears of the mechanisms are made from carburising steel 16MnCr5 while all other parts are made from aluminium EN-W 6082. In Table 1 are shown the data of the mechanisms for each joint.

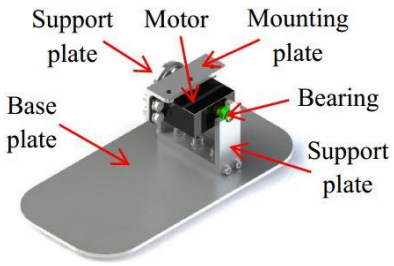

Fig. 9. Mechanical design of robot foot

Table 1. Mechanisms configuration

Flexion/Extension – hip joint		
dunker motor BG 32x20	power [W]	20
	torque [Ncm]	4.8
planetary gearhead PLG-42S	reduction	100
	torque [Ncm]	14
	efficiency [%]	73
encoder HENGSTLER ACURO-AD 36	counts per turn	2^{13}
	total counts	2^{25}
gearing with bevel gears	reduction	1.88
	module [mm]	1
	spiral angle [°]	38
gearing with helical gears	reduction	2
	module [mm]	1
	helix angle [°]	17
Abduction – hip joint		
dunker motor BG 32x20	power [W]	20
	torque [Ncm]	4.79
planetary gearhead PLG-42S	reduction	100
	torque [Ncm]	14
	efficiency [%]	73
encoder HENGSTLER ACURO-AD 36	counts per turn	2^{13}
	total counts	2^{25}
gearing with bevel gears	reduction	2.5
	module [mm]	1.5
Flexion/Hyperextension – knee joint		
dunker motor BG 32x10	power [W]	10
	torque [Ncm]	2.7
planetary gearhead PLG-32H	reduction	162
	torque [Ncm]	4
	efficiency [%]	73
encoder HENGSTLER ACURO-AD 36	counts per turn	2^{13}
	total counts	2^{25}
gearing with bevel gears	reduction	2
	module [mm]	1
	spiral angle [°]	38
Dorsiflexion/Plantar flexion – ankle joint		
servo motor MC-620 MG	power [W]	0.75
	torque [Nm]	0.7

3. RESULTS

In Figure 10 is shown a realized leg of the robot with 4 DOFs – three pitch joints and one roll joint. It consists of four subassemblies – the hip, the upper leg, the lower leg and the foot. It enables movements of the upper leg in the direction of flexion 120°, extension 90° and abduction 90° (lateral movement) and the hip joint, the lower leg movements in the direction of flexion 80° and hyperextension 10° in knee joint, and foot movements in the direction of dorsiflexion 30° and plantar flexion 30° (front and rear flexion) and ankle joint. Length of the leg from the hip joint to the ankle joint is 0.8 m, and the mass is 7 kg. The legs are covered with carbon fiber shell. Comparison between the human leg movements and the realized robot leg movements is shown in Table 2.

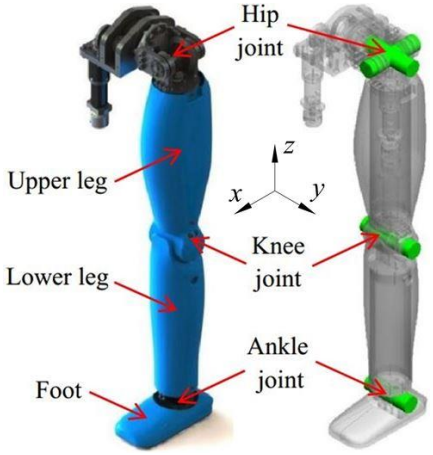

(a) *(b)*

Fig. 10. Leg of the assistive humanoid robot Marko: (a) mechanical design and (b) joints arrangement

Table 2. Range of human leg movements and realized leg of the robot Marko

Joint	Movement	Human leg	Robot leg
hip	flexion	140°	120°
	extension	45°	90°
	abduction	45°	90°
knee	flexion	140°	80°
	hyperextension	10°	10°
ankle	dorsiflexion	20°	30°
	plantar flexion	55°	30°

4. CONCLUSIONS

The development of the robot lower body – robot legs, which are intended to demonstrate the movements for the therapeutic purposes is presented in the paper. The research was conducted within

the project which is developing assistive humanoid robot *Marko*. Based on the set requirements a 3D model of the robot leg is formed. Dynamic simulation was performed and driving torques in the joints are determined. Realized leg has 4 DOFs and enables the upper leg movements in the direction of flexion 120°, extension 90° and abduction 90° (lateral movements) in the hip joint, lower leg movements in the direction of flexion 80° and hyperextension 10° in the knee joint, and foot movements in the direction of dorsiflexion 30° and plantar flexion 30° (front and rear flexion) of the ankle joint. The leg consists of the four subassemblies – the hip, the upper leg, the lower leg and the foot, and has the total mass of 7 kg. Length of the leg from the hip joint to the ankle joint is 0.8 m.

5. ACKNOWLEDGEMENTS

This work was funded by the Ministry of Education and Science of the Republic of Serbia under the contract III44008 and by the Provincial Secretariat for Science and Technological Development under the contract 114–451–2116/2011. The authors are grateful to Dunkermotoren for motors donation.

6. REFERENCES

[1] C. Bayon; R. Raya; S. Lerma-Lara; O. Ramirez; I. Serrano; E. Rocon, Robotic Therapies for Children with Cerebral Palsy: A Systematic Review. Translational Biomedicine 7(1) (2016), pp. 1–10, doi: 10.21767/2172-0479.100044

[2] F. Miler; M. Bolton; K. Capone; S. Travis, Physical Therapy of Cerebral Palsy. Springer, New York, (2007), doi: 10.1007/978-0-387-38305-7

[3] I. Novak; S. McIntyre; C. Morgan; L. Campbell; L. Dark; N. Morton; E. Stumbles; S.A. Wilson; S. Goldsmith, A Systematic Review of Interventions for Children with Cerebral Palsy: State of the evidence. Developmental Medicine & Child Neurology 55(1) (2013), pp. 1–26, doi: 10.1111/dmcn.12246

[4] S. Jovanović; P. Keros; A. Kargovska-Klisarova; I. Ruszkowski; S. Malobabić, Donji ekstremitet (Lower limb, in Serbian). Naučna knjiga, Belgrade, Serbia, (1989).

[5] D. Nikolić, Kineziologija (Kinesiology, in Serbian). College of Health Studies, Ćuprija, Serbia, (2007).

[6] P. Opavsky, Uvod u biomehaniku sporta (Introduction to Sports Biomechanics, in Serbian). Author's edition, Belgrade, Serbia, (1998).

[7] N. A. Malik; F. A. Hanapiah; R. A. A. Rahman; H. Yussof, Emergence of Socially Assistive Robotics in Rehabilitation for Children with Cerebral Palsy: A Review. International Journal of Advanced Robotic Systems 13(3) (2016), doi: 10.5772/64163

[8] V. Kozyavkin; O. Kachmar; I. Ablikova, Humanoid Social Robots in the Rehabilitation of Children with Cerebral Palsy. Proc. of the 8th Inter. Conf. on Pervasive Computing Technologies for Healthcare (2014), Oldenburg, Germany, pp. 430–431, doi: 10.4108/icst.pervasivehealth.2014.255323

[9] C. Suárez-Mejías; C. Echevarría; P. Nuñez; L. Manso; P. Bustos; S. Leal; C. Parra, Ursus: A Robotic Assistant for Training of Children with Motor Impairments. Converging Clinical and Engineering Research on Neurorehabilitation 1 (2013), pp. 249–253, doi: 10.1007/978-3-642-34546-3_39

[10] N.A. Malik; H. Yussof; F.A. Hanapiah; R. Adawiah; A. Rahman; H.H. Basri, Human-Robot Interaction for Children with Cerebral Palsy: Reflection and Suggestion for Interactive Scenario Design. Procedia Computer Science 76 (2015), pp. 388–393, doi: 10.1016/j.procs.2015.12.315

[11] R.A. Abdul-Rahman; F.A. Hanapiah; H.H. Basri; N.A. Malik; H.Yussof, Use of Humanoid Robot in Children with Cerebral Palsy: The Ups and Downs in Clinical Experience. Procedia Computer Science 76 (2015), pp. 394–399, doi: 10.1016/j.procs.2015.12.316

[12] D. Gouaillier; V. Hugel; P. Blazevic; C. Kilner; J. Monceaux; P. Lafourcade; B. Marnier; J. Serre; B. Maisonnier, Mechatronic Design of NAO Humanoid. Proc. of the Inter. Conf. on Robotics and Automation (2009), Kobe, Japan, pp. 769–774, doi: 10.1109/ROBOT.2009.5152516

[13] A.J. Brisben; C.S. Safos; A.D. Lockerd; J.M Vice; C.E. Lathan, The CosmoBot System: Evaluating its Usability in Therapy Sessions with Children Diagnosed with Cerebral Palsy, http://web.mit.edu/zoz/Public/AnthroTronix-ROMAN2005.pdf

[14] M. Penčić; M. Čavić; B. Borovac, Analysis of Mechanisms for Achieving Different Ways of Power Transmission and Motion of the Anthropomorphic Robots Upper Body. Proc. of the 5th BAPT Inter. Conf. on Power Transmission (2016), Ohrid, Macedonia.

Optimization of Planetary Gear Trains with Spur, Helical and Double Helical Gears

M. Penčić [1], M. Čavić [1], M. Rackov [1], B. Borovac [1], Z. Lu [2]

[1] Faculty of Technical Sciences, University of Novi Sad, Trg Dositeja Obradovića 6, 21000 Novi Sad, e-mail: {mpencic, scomaja, racmil, borovac}@uns.ac.rs

[2] School of Electrical Engineering and Automation, Changshu Institute of Technology, Hushan Road 99, 215500 Changshu, P.R.China, e-mail: zhenlilu@cslg.cn

Abstract

Planetary gear trains (PGTs) are used in humanoid robotics for increasing torque in the joints whereby mass of the gear reducer is from great importance, because it moves together with the segment. The optimization of PGTs with spur, helical and double helical gears which in size and power correspond to humanoid robots is shown in this paper. Based on the set requirements an objective function is formed – volume/mass minimization of the gear reducer. The constraints are defined and the optimization is performed by using the genetic algorithm method. All three types of PGTs have an equal number of planet gears and high efficiency, while other parameters are very similar. The optimal solution from the set of optimized variants of PGTs with helical gears has a volume that is 24.3% smaller than the volume of the PGT with spur gears, while the optimal solution from the set of optimized variants of PGTs with double helical gears has a volume that is 9.6% smaller than the volume of PGT with spur gears and 19.4% higher volume than the optimal solution of PGT with the helical gears.

Keywords: optimization, genetic algorithm, epicyclic gear train, planetary gear train, spur gear, helical gear, double helical gear

1. INTRODUCTION

Epicyclic gear trains (EGTs) or planetary-differential mechanisms – Figure 1a, are coaxial toothed gearings in which the axis of at least one of the gears is movable [1]. Gears with a movable axis of rotation are called planet gears (2), and gears with a fixed axis of rotation are called central gears (1,3). The element that gives the motion to the gear's axes is called a planet carrier (k). EGTs have two degree of freedom (DOFs) and are used for systems with multiple inputs/outputs [2]. Special type of EGTs are planetary gear trains (PGTs) – Figure 1b, in which one of the central gears is immovable [3]. Thanks to the higher number of planet gears, these mechanism enable the transmission of high powers. They can have a wide range of transmission ratios, but high efficiency is obtained only with rational gear ratios. They are reliable in different operating conditions and have a compact design. They are simple to produce and have a significantly lower mass compared to classical gear reducers, whose axes of gears rotation are immovable. Thanks to the technology that enables the production of high precision gears with small modules and low backlash, EGTs may have significant applications in humanoid robotics, especially for high-loaded joints, such as the torso joint or hip joint.

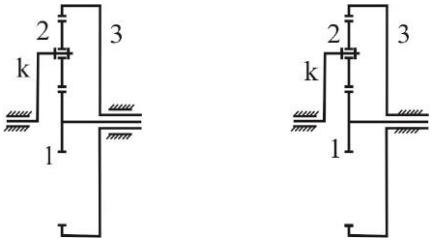

(a) *(b)*

Fig. 1. Scheme of epicyclic gear train (a) and scheme of planetary gear train (b): 1 – sun gear, 2 – planet gear, 3 – ring gear and k – carrier

1.1. PGTs in humanoid robotics

One of the ways to increase torque in joints of humanoids is by applying the PGTs [4]. There are numerous requirements that these mechanisms need to fulfil during dynamic activities of the robot. These are high carrying capacity and reliability, high efficiency, low backlash – provides high posi-

tioning accuracy that enables high accuracy and repeatability of movements which is essential for motion control, low vibrations, low mass moment of inertia, low noise, small mass and small dimensions. Considering that the gear reducer moves together with the segment (*e.g.* robot arm consists of several segments – shoulder, upper arm, elbow, lower arm, wrist and in each joint is embedded gear reducer) it is obvious that the mass of the gear reducer is very important. The scheme of a typical drive for robot joints is shown in Figure 2. It consists of an actuator, a gear reducer and a corresponding joint. The actuator is represented as a compact unit and consists of a sensor, motor and planetary gearhead. The function of the gear reducer, which is considered in this paper, is to increase the torque from the actuator to the joint with minimal power losses as well as to reduce the loss of motion – arc backlash, which is essential for motion control.

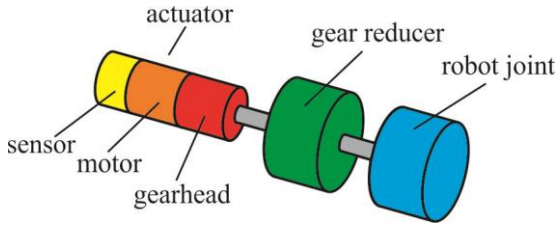

Fig. 2. Scheme of typical drive for robot joints

The optimization of PGTs with spur, helical and double helical gears which in size and power correspond to humanoid robots is shown in this paper.

1.2. State of the art

There are numerous papers in which the optimal synthesis of classical gear reducers is shown. In [5] is shown optimization of gear reducer mass by applying the method of modified directions. The optimization of gear reducers that is based on the Box simplex method and the branching method is shown in [6] – the number of gears teeth is treated as a continuously variable parameter. Particle swarm and simulated annealing algorithms are used for the optimization of gear reducer mass in [7]. In [8] is shown heuristic genetic approach for automatic design of gear reducers. Direct methods give solutions faster, but cannot involve non-continuous variable parameters. Since the optimization parameters of the gear reducer are of different character and can be continuous, discrete and integer variables, the heuristic method is more efficient. One of the features of the heuristic method is that it is able to find a global minimum of the problems.

The number of criteria needed for objective function forming is also a significant issue in the gear reducer optimization. In [5] and [7], the mass of the gear reducer is chosen for the objective function – single-criteria optimization. In [9], besides the mass, teeth flank strength is also chosen – multi-criteria optimization based on the weighted coefficients method. The optimization of gear reducers from the standpoint of vibration and noise is shown in [10]. A method for choosing the optimal conceptual solution of the gear reducer that is based on the so-called matrix of selection is presented in [11]. The optimization of multi-stage gear reducers with cylindrical gears is shown in [12]. In the first phase the optimal gear ratio is determined for each stage of the gear reducer. In the second phase, the parameters of optimization are volume/mass, efficiency, the safety factor, contact ratio and the centre distance. Multi-criteria optimization is performed by the method of stochastic optimization – the Monte-Carlo method. In [13], the evolutionary algorithm is used for the optimal design of a two-stage gear reducer with helical gears. The optimization is based on the mass and numerous design constraints such as dimensions of the housing shafts, bearings etc. In [14] is shown gear ratios optimization of the multi-stage gear reducer with spur gears in order to reduce arc backlash on the output shaft. Multi-criteria optimization can be complex and long-lasting, but gives quality solutions. Most authors choose the mass of the gear reducer as the only criteria – for single-criteria optimization, or as first one – for multi-criteria optimization.

The optimal synthesis of EGTs/PGTs is found less often in the literature. The analysis and design of an EGT with a high gear ratio is shown in [15], but the presented solution has a small carrying capacity and therefore limited use. The optimal design of an EGT from the standpoint of gear carrying capacity is shown in [16]. The procedure is based on varying the module depending on the defined power. In [17] and [18] is shown optimization of the PGT based on the multi-objective function that includes mass, volume, efficiency and manufacture cost – industrial PGTs with large modules. A nonlinear dynamic model of the PGT in which the tooth profile is modified in order to reduce vibration during the operation of the PGT is shown in [19].

2. OPTIMAL SYNTHESIS

Based on the set requirements discussed in section 1.1., a single-stage PGT type is adopted – structure A_{ha}^{b} (h – planet carrier, a – sun gear and b – immovable ring gear). For gear ratios from 3÷9, the PGT has a high efficiency of 97÷99%, small mass and small dimensions [20].

Optimization problem presents minimization of the objective function for the set constraints:

$$MIN\ f(x),\ x \in D \tag{1}$$

where: $x = (x_1, x_2, ..., x_m)$ – vector variables, $D = \{x \in R^n \,|\, g(x) \le 0 \wedge h(x) = 0\}$ – a set of solutions that fulfils the defined constraints, and $g(x) \le 0$ and $h(x) = 0$ – vectors constraints. During the dynamic activities of the robot, the gear reducer moves together with the segment so the mass of the gear reducer is of great importance. Therefore, the objective function is defined as the volume minimization of the gear reducer:

$$f(x) = V \tag{2}$$

respectively:

$$V = \frac{d_{f3}^2 \pi}{4} b \tag{3}$$

where:

– root diameter of ring gear:

$$d_{f3} = d_3 + 2h_p + 2x_3 m_n \tag{4}$$

– pitch diameter of ring gear:

$$d_3 = \frac{z_3 m_n}{\cos\beta} \tag{5}$$

– dedendum:

$$h_p = m_n + c_p \tag{6}$$

– bottom clearance:

$$c_p = 0.25 \cdot m_n \tag{7}$$

– total gear ratio:

$$i = 1 + \frac{z_3}{z_1} \tag{8}$$

– other parameters:

b – effective face width, $x_{1,2,3}$ – profile shift coefficient, m_n – normal module, β – helix angle, z_1 – number of teeth of the sun gear, z_2 – number of teeth of the planet gears and z_3 – number of teeth of the ring gear. By inserting eqs. (4) – (8) in (3), eq. (9) is obtained that defines the volume of PGT:

$$V = \frac{\pi b}{4}\left(\frac{z_1 (i-1) m_n}{\cos\beta} + 2.5 m_n + 2 x_3 m_n\right)^2 \tag{9}$$

For modules $m_n \le 1$ mm, the profile shift of the gears has a relatively small influence on carrying capacity and therefore it is ignored $x_{1,2,3} = 0$, so eq. (9) has the form:

$$V = \frac{m_n \pi b}{4}\left(z_1 \frac{i-1}{\cos\beta} + 2.5\right)^2 \tag{10}$$

The optimization variables are: module m_n – discrete variable that has standard values, total gear ratio i – continuously variable parameter, the number of teeth of the sun gear z_1, effective face width b and number of the planet gears n_w – integer parameters. Effective face width b of the planet gears must be sufficient for the bearings installation, it is adopted as constant and will not be a parameter of optimization. Therefore, the vector of variables is:

$$x = (x_1, x_2, x_3, x_4) = (i, z_1, m_n, n_w) \tag{11}$$

There are several functional constraints – conditions that PGTs must fulfil. These are assembly conditions – coaxiality, contiguity and gears meshing, geometry condition and strength condition. Coaxiality enables equality of all center distances of the meshed gears, *i.e.* overlapping of the central gears axis:

$$z_2 = \frac{z_3 - z_1}{2} = \frac{z_1}{2}(i-2) \tag{12}$$

Contiguity enables minimal distance (f) between the addendum circles of planet gears – Figure 3, in fact, it defines the maximum number of planet gears that can be incorporate in one plane of PGT:

$$n_w \le \frac{\pi}{\arcsin\left(\frac{z_2 + 2.5}{z_1 + z_2}\right)} \tag{13}$$

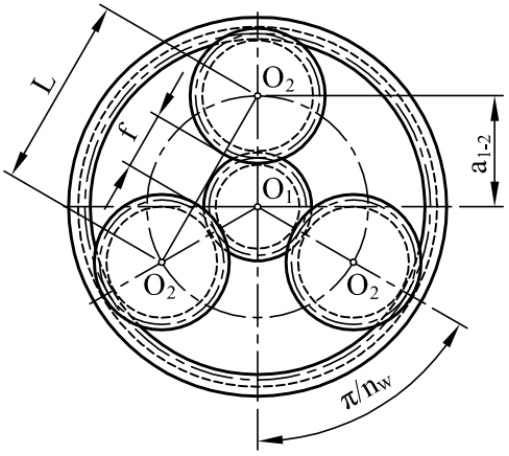

Fig. 3. Planet gears arrangement in plane of PGT

The meshing condition enables that the angles $2\pi / n_w$ between planet gears are equal, *i.e.* simultaneous meshing of planet gears with central gears. It is fulfilled if the sum of numbers of central gear teeth is fully divisible with the number of planet gears:

$$C = \frac{z_1 + z_3}{n_w} \tag{14}$$

By increasing the number of planet gears, the dimensions of the gear reducer are decreasing while the carrying capacity is increasing. Geometrical constraints include dimensions and gear tooth form, and are mostly fulfilled if the gear geometry is adopted according to the standards. However, to prevent interference – undercutting of the gears, the minimum number of teeth of the sung gear and the planet gears is limited:

$$z_{1,2} \geq 17 \tag{15}$$

Strength conditions ensure that the operating stresses are going to be less then the critical stresses and are expressed through safety factors whose values are for pitting $S_{\mathrm{H\,min}} = 1 \div 1.2$ and for bending failure $S_{\mathrm{F\,min}} = 1.25 \div 2.5$. Adopted safety factors are:

$$S_{H1,2,3} > S_{H\,\min} = 1.1 \tag{16}$$

$$S_{F1,2,3} > S_{F\,\min} = 1.25 \tag{17}$$

As the variables (i, z_1, m_n, n_w) have different characters, a genetic algorithm method is adopted for the optimization. Although this method has difficulties when working with problems with equality constraints, this situation can be easily solved – one equality constraint is redefined as a pair of inequality constraints. Optimization is performed in MATLAB software.

3. RESULTS

Parameters which do not change during optimization – constants are shown in Table 1a and Table 1b, while parameters that change during optimization – variables and their constraints are presented in Table 2.

Table 1a. Input parameters – constants

Output torque T_h [Nm]	Output speed n_h [rpm]	Addendum modification $x_{1,2,3}$	Accuracy grade IT
80	5	0	5

Table 1b. Input parameters – constants

Service life [h]	Face width b [mm]	Material for $m<1$	Material for $m\geq 1$
500	35	14CrMoV6.9	16MnCr5

Table 2. Optimization parameters – variables

Sun gear z_1	Gear ratio i	Module m [mm]	Planet gears n_w
18÷28	3÷9	0.5; 0.6; 0.7; 0.8; 0.9; 1	3÷5

The data for output torque and output number of revolutions – Table 1a, represent average values for the flexion movements of the robot in the torso joint, for the movement range of 90° and duration of 3 s – data are based on realized solutions. The adopted range of the helix angle β is 10÷20° for helical gears and 20÷30° for double helical gears. The gap for the double helical gears is 5 mm. In Table 3–5 the results of the optimization of the PGTs are shown. Comparing results from Tables 3-4, it can be concluded that the PGT with spur gears and variants of PGTs with helical gears have the equal numbers of teeth of the gears $z_1 = 28$, $z_2 = 27$, $z_3 = 82$, number of the planet gears total $n_w = 5$, gear ratio $i = 3.93$ and efficiency $\eta = 98.5\,\%$. All variants of PGTs with helical gears have equal module $m_n = 0.6$ mm that is smaller than the module of PGT with spur gears $m_n = 0.7$ mm. The optimal solution from the set of optimized variants of PGTs has a helix angle of 10° and volume that is 24.3% smaller than the volume of the PGT with spur gears. Comparing the results from Table 5, it can be concluded that all variants of the PGTs with double helical gears have the an equal number of planet gears $n_w = 5$, high efficiency, above $\eta = 98.5\,\%$ and a different module, which is $m_n = 0.7$ mm for $\beta = 20 \div 25°$ and $m_n = 0.6$ mm for $\beta = 26 \div 30°$. By increasing the helix angle, the module is decreased while the number of teeth, the volume and the carrying capacity are all increased. The other parameters are in intervals: $z_1 = 26 \div 28$, $z_2 = 24 \div 27$, $z_3 = 73 \div 82$, $i = 3.85 \div 3.93$. The optimal solution from the set of optimized variants of PGTs with double helical gears has helix angle of 26° and a volume that is 9.6% smaller than the volume of the PGT with spur gears and 19.4% higher volume than the optimal solution of the PGT with helical gears.

Table 3. PGT with spur gears – optimized parameters

Helix angle β [°]	Sun gear z_1	Module m [mm]	Planet gears n_w	Ring gear z_3	Gear ratio i	Volume V [mm^3]	Mass m [g]	Safety factor S_{H1}	Safety factor S_{H2}	Efficiency η [%]
0	28	0.7	5	82	3.9286	96176	769	1.1440	1.1348	98.52

Table 4. PGT with helical gears – optimized parameters

Helix angle β [°]	Sun gear z_1	Module m [mm]	Planet gears n_w	Ring gear z_3	Gear ratio i	Volume V [mm^3]	Mass m [g]	Safety factor S_{H1}	Safety factor S_{H2}	Efficiency η [%]
10	28	0.6	5	82	3.9286	72791	582	1.1132	1.1042	98.52
11	28	0.6	5	82	3.9286	73250	586	1.1162	1.1072	98.52
12	28	0.6	5	82	3.9286	73757	590	1.1195	1.1105	98.52
13	28	0.6	5	82	3.9286	74313	594	1.1230	1.1140	98.52
14	28	0.6	5	82	3.9286	74921	599	1.1269	1.1179	98.52
15	28	0.6	5	82	3.9286	75581	604	1.1311	1.1220	98.52
16	28	0.6	5	82	3.9286	76295	610	1.1357	1.1265	98.52
17	28	0.6	5	82	3.9286	77065	616	1.1405	1.1313	98.52
18	28	0.6	5	82	3.9286	77894	626	1.1457	1.1365	98.52
19	28	0.6	5	82	3.9286	78783	630	1.1512	1.1419	98.52
20	28	0.6	5	82	3.9286	79735	637	1.1570	1.1477	98.52

Table 5. PGT with double helical gears – optimized parameters

Helix angle β [°]	Sun gear z_1	Module m [mm]	Planet gears n_w	Ring gear z_3	Gear ratio i	Volume V [mm^3]	Mass m [g]	Safety factor S_{H1}	Safety factor S_{H2}	Efficiency η [%]
20	26	0.7	5	74	3.8462	88918	711	1.2357	1.1992	98.53
21	26	0.7	5	74	3.8462	90050	720	1.2422	1.2056	98.53
22	26	0.7	5	74	3.8462	91259	730	1.2491	1.2123	98.53
23	26	0.7	5	74	3.8462	92548	740	1.2564	1.2194	98.53
24	26	0.7	5	74	3.8462	93920	751	1.2641	1.2269	98.53
25	27	0.7	5	73	3.7037	92896	743	1.2752	1.1890	98.55
26	28	0.6	5	82	3.9286	86946	695	1.1997	1.1901	98.52
27	28	0.6	5	82	3.9286	88431	707	1.2082	1.1985	98.52
28	28	0.6	5	82	3.9286	90010	720	1.2170	1.2072	98.52
29	28	0.6	5	82	3.9286	91687	733	1.2263	1.2164	98.52
30	28	0.6	5	82	3.9286	93468	747	1.2360	1.2260	98.52

4. CONCLUSIONS

The optimization of PGTs with spur, helical and double helical gears which in size and power correspond to humanoid robots, is shown in this paper. Based on the set requirements, the objective function is formed – volume/mass minimization of gear reducer. Constraints are defined and optimization is performed using the method of genetic algorithm. All three PGTs type have five planet gears and high efficiency that is approximately 98.5%, while the other parameters are in the range of 0.6÷0.7 mm – module, 26÷28 – number of teeth of the sun gear, 23÷27 – number of teeth of the planet gears, 73÷82 – number of teeth of the ring gear and 3.70÷3.93 – total gear ratio. Optimal solution from the set of optimized variants of PGTs with helical gears has a helix angle of 10° and volume that is 24.3% smaller than the volume of the PGT with spur gears. The optimal solution from the set of the optimized variants of PGTs with double helical gears has a helix angle of 26° and volume that is 9.6% smaller than the volume of the PGT with spur gears and 19.4% higher volume than the optimal solution of the PGT with helical gears. Further research will include optimization of all three gear reducer types from the standpoint arc backlash on the output shaft, because low backlash provides high positioning accuracy that enables high accuracy and repeatability of movements, which is essential for motion control. In this manner, it will be determined which solution is most suitable for increasing the torque in the robot joints.

5. ACKNOWLEDGEMENTS

This work was funded by the Ministry of Education and Science of the Republic of Serbia under the contract III44008 and by the Provincial Secretariat for Science and Technological Development under the contract 114–451–2116/2011.

6. REFERENCES

[1] R. Mathis; Y. Remond, Kinematic and Dynamic Simulation of Epicyclic Gear Trains. Journal of Mechanism and Machine Theory 44(2) (2009), pp. 412–424, doi: 10.1016/j.mechmachtheory.2008.03.004

[2] V. Babin; C. Gosselin; J. F. Allan, A Dual-Motor Robot Joint Mechanism with Epicyclic Gear Train. Proc. of the IEEE-RSJ Inter. Conf. on Intelligent Robots and Systems (2014), Chicago, Illinois, pp. 472–477, doi: 10.1109/IROS.2014.6942601

[3] M. Raghavan, The Analysis of Planetary Gear Trains. Journal of Mechanisms and Robotics 2(2) (2010), doi: 10.1115/1.4001092

[4] M. Penčić; M. Čavić; B. Borovac, Analysis of Mechanisms for Achieving Different Ways of Power Transmission and Motion of the Anthropomorphic Robots Upper Body. Proc. of the 5th BAPT Inter. Conf. on Power Transmission (2016), Ohrid, Macedonia.

[5] M. Savage; S. B. Lattime; J. A. Kimmel; H. H. Coe, Optimal Design of Compact Spur Gear Reductions. Journal of Mechanical Design 116(3) (1994), pp. 690–696, doi: 10.1115/1.2919437

[6] N. Marjanovic, Optimizacija zupčastih prenosnika snage (Gear Trains Optimization, in Serbian). Faculty of Mechanical Engineering, Kragujevac, Serbia, (2007).

[7] V. Savsani; R.V. Rao; D. P. Vakharia, Optimal Weight Design of a Gear Train Using Particle Swarm Optimization and Simulated Annealing Algorithms. Journal of Mechanism and Machine Theory 45(3) (2010), pp. 531–541, doi: 10.1016 /j.mechmachtheory.2009.10.010

[8] C. Gologlu; M. Zeyveli, A Genetic Approach to Automate Preliminary Design of Gear Drives. Journal of Computers & Industrial Engineering 57(3) (2009), pp. 1043–1051, doi: 10.1016/j.cie.2009.04.006

[9] D. F. Thompson; S. Gupta; A. Shukla, Trade-off Analysis in Minimum Volume Design of Multi-Stage Spur Gear Reduction Units. Journal of Mechanism and Machine Theory 35(5) (2000), pp. 609–627, doi: 10.1016/S0094-114X(99)00036-1

[10] G. Bonori; M. Barbieri; F. Pellicano, Optimum Profile Modifications of Spur Gears by Means of Genetic Algorithms. Journal of Sound and Vibration 313(3–5) (2008), pp. 603–616, doi: 10.1016/j.jsv.2007.12.013

[11] N. Marjanovic; B. Isailovic; V. Marjanovic; Z. Milojevic; M. Blagojevic; M. Bojic, A Practical Approach to the Optimization of Gear Trains with Spur Gears. Journal of Mechanism and Machine Theory 53 (2012), pp. 1–6, doi: 10.1016/ j.mechmachtheory.2012.02.004

[12] B. Rosić, Multicriterion Optimization of Multistage Gear Train Transmission. Facta Universitatis, Series: Mechanical Engineering 1(8) (2001), pp. 1107–1115.

[13] O. Buiga; L. Tudose, Optimal Mass Minimization Design of a Two-Stage Coaxial Helical Speed Reducer with Genetic Algorithms. Journal of Advances in Engineering Software 68 (2014), pp. 25–32, doi: 10.1016/j.advengsoft.2013.11.002

[14] Y. L. Hsu; S. G. Wang, Minimizing Angular Backlash of a Multistage Gear Train. Proceedings of the Institution of Mechanical Engineers, Part B: Journal of Engineering Manufacture 216(4) (2002), pp. 565–569, doi: 10.1243/0954405021520256

[15] A. Kapelevich, High Gear Ratio Epicyclic Drives Analysis. The Journal of Gear Manufacturing (2014), pp. 61–67.

[16] S. I. Dilawer; A. R. Junadi; S. N. Mehdi, Design, Load Analysis and Optimization of Compound Epicyclic Gear Trains. American Journal of Engineering Research 2(10) (2013), pp. 146–153.

[17] J. Stefanović-Marinović; M. Petković; I. P. Stanimirović; M. Milovančević, A Model of Planetary Gear Multicriteria Optimization. Transactions of FAMENA 35(4) (2011), pp. 21–34.

[18] J. Stefanović-Marinović; M. Milovančević, The Optimization Possibilities at the Planetary Gear Trains. Journal of Mechanics Engineering and Automation 2 (2012), pp. 365–373.

[19] B. Cheon-Jae; R. G. Parker, Analytical Investigation of Tooth Profile Modification Effects on Planetary Gear Dynamics. Journal of Mechanism and Machine Theory, 70 (2013), pp. 298–319, doi: 10.1016/j.mechmachtheory.2013.07.018

[20] В. Н. Кудрявцев; Ю. А. Державец; Е. Г. Глухарев, Конструкции и расчет зубчатых редукторов (Design and calculation of gear reducers, in Russian). Машиностроение, Москва, (1971).

Optimal Synthesis of the Loader Bucket Mechanism

M. Čavić [a], M. Penčić [a], J. M. Djoković [b], M. Zlokolica [a]

[a] Faculty of Technical Sciences, University of Novi Sad, Trg Dositeja Obradovića 6, 21000 Novi Sad, e-mail: {scomaja, mpencic, mzlokolica}@uns.ac.rs

[b] Technical Faculty in Bor, University of Belgrade, Vojske Jugoslavije 12, 19210 Bor, e-mail: jelenamdjokovic@gmail.com

Abstract

There are two basic structures of the loader bucket mechanism. The first is based on the Z configuration mechanism, and the second on the Stephenson III complex structure mechanism. Both mechanisms enable arrow lifting and bucket rotation. With comparative analysis we determined that the Stephenson III mechanism requires approximately two times less force for driving the arrow and the bucket, than the corresponding Z configuration mechanism. In addition, the Stephenson III mechanism enables larger stability of the loader and better visibility for the operator. This paper presents an optimal synthesis of the Stephenson III loader bucket mechanism in order to minimize the forces in the cylinders. Based on the set requirements, kinematic-dynamic analysis was performed by applying the modular and kinetostatic approach. A dynamic model was formed and a dynamic simulation was performed. The optimized mechanism of the bucket requires 25% less force to drive the arrow and eliminates corrective motions of the loader, because the connection point of the bucket and arrow during the whole movement forms approximately rectilinear vertical trajectory – maximum misalignment is 70 mm. The dimensions of the constructive parameters are within the practical values, and the stroke length for the driving arrow is higher by 23%.

Keywords: optimal synthesis, loader bucket mechanism, Stephenson III mechanism, kinematic-dynamic analysis, dynamic simulation

1. INTRODUCTION

Loaders are transport machines that are used for loading bulk materials such as soil, sand, gravel, tailings, coal, rocks, mineral raw materials etc. They consist of a rigid or jointed chassis within which are placed the diesel engine, a cabin with the control system, transmission system and operating elements – bucket with the linkage mechanism and hydraulic system. The basic working element of the loader is the bucket which is connected with a revolute joint to the top of the lifting arrow. A lever mechanism enables positioning of the bucket and has a significant influence on the efficiency and stability of the loader. The bucket mechanism is a plane mechanism that performs two movements – arrow lifting and bucket rotation. All links are connected via rotational joints because they are reliable and have a simple design. The driving links are hydraulic cylinders. The loader working cycle consists of loading, lifting, transporting and emptying the bucket. It is therefore important that the connection point between the bucket and arrow forms approximately a vertical trajectory during the whole movement. This way, the corrective motions of the loader – distancing from the transport vehicle during the lifting of the bucket and approaching, so the bucket is in the correct position to eject the material into the transport vehicle, are eliminated. There are two basic structures of the loader bucket mechanism. The first is based on the Z configuration mechanism [1] – inverted slider-crank mechanism, in which the connection point between the bucket and arrow during the movement forms a circular trajectory – Figure 1. The second is based on the Stephenson III complex structure mechanism [2] – a third class kinematic group, in which the connection point between the bucket and arrow forms an approximately vertical trajectory during the whole movement – Figure 2. Connection point can also form any other trajectory, but it requires kinematic synthesis of the mechanism as a path generator.

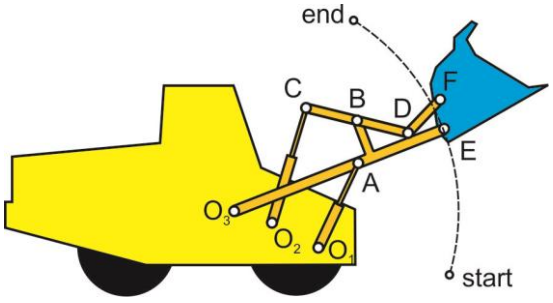

Fig. 1. Loader bucket mechanisms – Z mechanism

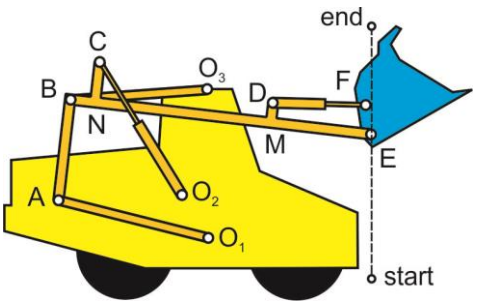

Fig. 2. Loader bucket mechanisms – type Stephenson III

The Z configuration mechanism is the one traditionally applied at the loaders. There are numerous papers in which the analysis and optimal synthesis of these mechanisms are shown. A simplified dynamic model of the loader with the analysis of the mechanism for bucket uplifting is shown in [3]. The software realization of the optimal geometry the Z mechanism needs to have to reduce the change of the bucket inclination angle during arrow lifting is shown in [4], and the optimization is based on four parameters. The optimal synthesis loader operating unit, where the delivery ratio, bucket swing angle and bucket reset are considered is shown in [5], the optimization consists of several schemes with numerous optimization parameters (8–22). The multi-objective optimization of the bucket mechanism which deals with translation bucket lifting, bucket rotating oil cylinder force and lifting oil cylinder output force is shown in [6]. In the patent [7], [8] the loader bucket mechanism – type Stephenson III is proposed. In [9], [10] the synthesis of the Stephenson III mechanism as a function generator is shown, and in [11] the dynamic optimization of an operating mechanism for the internal combustion engine which is based on the Stephenson III mechanism is presented. After reviewing the available literature, it has been concluded that there are no papers that show the analysis and optimal synthesis of a Stephenson III based loader bucket mechanism.

2. KINEMATIC-DYNAMIC ANALYSIS

Based on the set requirements (the first is that the inclination angle of the bucket during the whole movement is approximately constant, and the second that the connection point of the bucket and arrow during the whole movement forms an approximately rectilinear vertical trajectory, because then the corrective motions of the loader are eliminated – the approaching/distancing from the transport vehicle during lifting/emptying the bucket), a comparative analysis of the loader bucket mechanisms a Z configuration and the corresponding Stephenson III complex structure mechanism are performed. Mechanisms have 2 DOFs and consist of nine links. Based on the comparative analysis [12], it has been determined that the lifting heights of the bucket are equal in both cases and that the inclination angle of the bucket is approximately constant during the whole movement for both mechanisms. The Stephenson III mechanism requires approximately two times less force to drive the arrow and bucket then the Z configuration mechanism. During lifting of the load, the connection point between the arrow and the bucket in the Stephenson III mechanism forms an approximately the rectilinear vertical trajectory and thus eliminates the corrective motions of the loader. In addition, the Stephenson III mechanism enables larger stability of the loader and better visibility for the operator – the mechanism is out of the operator's field of vision. Within this paper, the optimal synthesis possibilities of the Stephenson III mechanism loader bucket are examined in order to reduce the forces in the cylinders for driving the arrow and the bucket.

The kinematic scheme of the nine-bar linkage loader bucket mechanism – type Stephenson III, is shown on Figure 3. The lever mechanism has 2 DOFs and consists of the arrow 4, the two links 5 and 6, the bucket 9 and two hydraulic cylinders both of which have two elements – the body of the cylinder and the piston. Links 2 and 3 represent the cylinder for driving the arrow, and links 7 and 8 the cylinder for driving the bucket. Links 3,4,5,6 form a third class kinematic group RR-RR-TR [13] – Figure 4, while links 7,8,9 form an inverted slider-crank mechanism [14] – Figure 5. The constructive parameters of the mechanism are the coordinates of immovable points O_1,O_2,O_3, the length of the links 5 and 6, the length and angles of the arrow 4 and the position of the bucket joints, i.e. the distance between the points E and F. The input parameters strokes of the cylinders, i.e. variable lengths O_2C and DF.

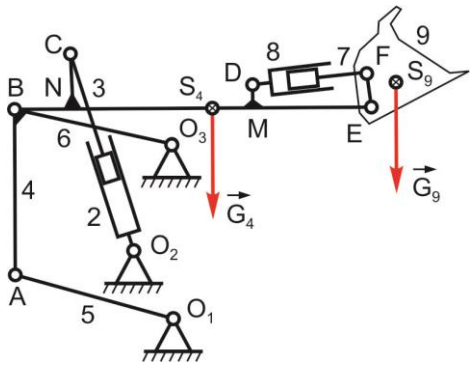

Fig. 3. Kinematic scheme of the nine-bar linkage loader bucket mechanism – type Stephenson III

By performing kinetostatic analysis [15], the equations are formed and forces in the cylinders are defined – force in the cylinder for driving the bucket:

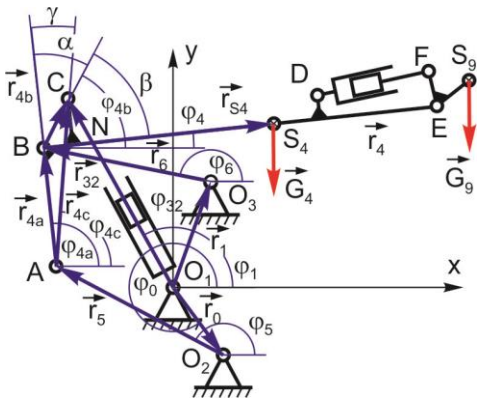

Fig. 4. Kinematic scheme of the mechanism for driving arrow – kinematic group of third class RR-RR-TR

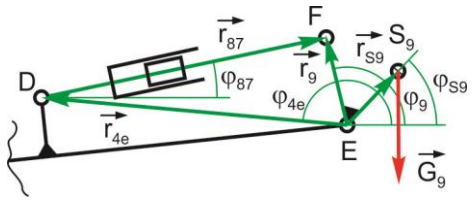

Fig. 5. Kinematic scheme of the mechanism for driving bucket – inverted slider-crank mechanism

$$F_{P1} = G_9 \frac{r_{S9}\cos\varphi_{S9}}{r_9 \sin\left(\varphi_{87} - \varphi_9\right)} \tag{1}$$

and force in the cylinder for driving the arrow:

$$F_{P2} = \frac{k_1 k_3 + k_5 k_6}{k_4 k_6 - k_2 k_3} \tag{2}$$

where:

$$k_1 = \left(\overline{AB}\cos\varphi_{4a} + \overline{BS_4}\cos\varphi_4\right)G_4 + \\ + \left(\overline{AB}\cos\varphi_{4a} + \overline{BE}\cos\varphi_4\right)G_9 + \\ + F_{P2}\,\overline{DE}\sin\left(\varphi_{87} - \varphi_{4e}\right) \tag{3}$$

$$k_2 = \left(\overline{AB}\cos\varphi_{4a} + \overline{BC}\cos\varphi_{4b}\right)\sin\varphi_{32} + \\ + \left(\overline{AB}\sin\varphi_{4a} + \overline{BC}\sin\varphi_{4b}\right)\cos\varphi_{32} \tag{4}$$

$$k_3 = \tan\varphi_6 - \tan\varphi_5 \tag{5}$$

$$k_4 = \cos\varphi_{32} - \sin\varphi_{32}\tan\varphi_5 \tag{6}$$

$$k_5 = G_4 + G_9 \tag{7}$$

$$k_6 = \overline{AB}\cos\varphi_{4a}\left(\tan\varphi_{4a} - \tan\varphi_6\right) \tag{8}$$

By applying the modular approach [16], a system of eqs. for high class kinematic group geometry is formed and the position angles of the mechanism links $(\varphi_4, \varphi_{4a}, \varphi_{4b}, \varphi_{4c}, \varphi_{4e}, \varphi_{32}, \varphi_5, \varphi_6)$ are defined. Eq. that defines angle φ_6:

$$\varphi_6 = \arctan\left(\frac{y_C - y_{O3}}{x_C - x_{O3}}\right) \pm \\ \pm \arccos\left(\frac{r_6^2 + \overline{CO_3}^2 - r_{4b}^2}{2r_6\overline{CO_3}}\right) \tag{9}$$

where:

$$x_C = r_{32}\cos\varphi_{32} \tag{10}$$

$$y_C = r_{32}\sin\varphi_{32} \tag{11}$$

$$\overline{CO_3} = \sqrt{\left(x_C - x_{O3}\right)^2 + \left(y_C - y_{O3}\right)^2} \tag{12}$$

$$r_{4b} = \sqrt{\overline{BN}^2 + \overline{NC}^2} \tag{13}$$

Eq. that defines angle φ_4 is:

$$\varphi_4 = \arctan\left(\frac{y_C - y_B}{x_C - x_B}\right) \tag{14}$$

where:

$$x_B = x_{O3} + r_6\cos\varphi_6 \tag{15}$$

$$y_B = y_{O3} + r_6\sin\varphi_6 \tag{16}$$

Eqs. that defines angles $\varphi_{4a}, \varphi_{4b}, \varphi_{4c}, \varphi_{4e}$ are:

$$\varphi_{4a} = \varphi_4 + \left(\alpha + \beta\right) \tag{17}$$

$$\varphi_{4b} = \varphi_4 + \beta \tag{18}$$

$$\varphi_{4c} = \varphi_4 + \left(\alpha + \beta\right) - \gamma \tag{19}$$

$$\varphi_{4e} = 180 - \arctan\frac{\overline{DM}}{\overline{DE}} + \varphi_4 \tag{20}$$

Eq. that defines angle φ_5 is:

$$\varphi_5 = \arctan\left(\frac{y_B - y_{O2}}{x_B - x_{O2}}\right) \pm \\ \pm \arccos\left(\frac{r_5^2 + \overline{BO_2}^2 - r_{4a}^2}{2r_5\overline{BO_2}}\right) \tag{21}$$

where:

$$\overline{BO_2} = \sqrt{\left(x_B - x_{O2}\right)^2 + \left(y_B - y_{O2}\right)^2} \tag{22}$$

Eq. that defines angle φ_{32} is:

$$\varphi_{32} = \arctan\left(\frac{y_{O1} - y_A}{x_{O1} - x_A}\right) \pm \\ \pm \left(\pi - \arccos\left(\frac{-r_{4c}^2 + \overline{AO_1}^2 + r_{32}^2}{2r_{32}\overline{AO_1}}\right)\right) \tag{23}$$

where:

$$x_A = x_{O2} + r_5 \cos\varphi_5 \tag{24}$$

$$y_A = y_{O2} + r_5 \sin\varphi_5 \tag{25}$$

$$\overline{AO_1} = \sqrt{\left(x_A - x_{O1}\right)^2 + \left(y_A - y_{O1}\right)^2} \tag{26}$$

$$r_{4c} = \sqrt{\left(x_A - x_C\right)^2 + \left(y_A - y_C\right)^2} \tag{27}$$

The symbol ± in the previous equations indicates that there are two possible solutions, i.e. two possible configurations that the observed dyad of the mechanism may take.

The coordinate of point E – a connection point between the bucket and arrow are:

$$x_E = r_{32} \cos\varphi_{32} + r_4 \cos\varphi_4 \tag{28}$$

$$y_E = r_{32} \sin\varphi_{32} + r_4 \sin\varphi_4 \tag{29}$$

The coordinates of point D – a connection point between the cylinder for rotation of the bucket and the arrow are:

$$x_D = x_E + r_{4e} \cos\varphi_{4e} \tag{30}$$

$$y_D = y_E + r_{4e} \cos\varphi_{4e} \tag{31}$$

Angle φ_9 that defines the position of the bucket is:

$$\varphi_9 = \varphi_{4e} - \arccos\left(\frac{r_{4e}^2 - \overline{DF}^2 + r_9^2}{2 r_{4e} r_9}\right) \tag{32}$$

Coordinates of the point F are:

$$x_F = x_E + r_9 \cos\varphi_9 \tag{33}$$

$$y_F = y_E + r_9 \cos\varphi_9 \tag{34}$$

Angle φ_{87} that defines position of the bucket cylinder is:

$$\varphi_{87} = \arctan\left(\frac{y_F - y_D}{x_F - x_D}\right) \tag{35}$$

The analysis of eq. (1), shows that the force in the cylinder that drives the bucket depends on r_{S9}, φ_{S9}, which directly depend on the geometry and dimensions of bucket. The parameters of the mechanism are φ_{87}, φ_9, whereby φ_9 also depends on the geometry of the bucket. The force in the cylinder will have a minimum value if the $\sin(\varphi_{87} - \varphi_9) = 1$, i.e. when the angle between the cylinder and the bucket is 90° during the whole movement. Therefore, the force in the cylinder that drives the bucket is not the subject of this optimization. The analysis of eq. (2) is not as obvious and therefore the force in the cylinder that drives the arrow is further considered.

3. DYNAMIC OPTIMIZATION

Optimization problem presents minimization of the objective function for the set constrains:

$$MIN\ f(x),\ x \in D \tag{36}$$

where: $x = (x_1, x_2, ..., x_m)$ - vector variables,

$D = \left\{ x \in R^n \,\middle|\, g(x) \le 0 \wedge h(x) = 0 \right\}$ - a set of solutions that fulfils the defined constraints, and

$g(x) \le 0$ and $h(x) = 0$ - vectors constraints.

The objective function – the force in the cylinder that drives the arrow, is formed:

$$f(x) = abs(F_{P2}) \tag{37}$$

The lifting height of the bucket is limited to 2 m, i.e.:

$$H = y_{E\,end} - y_{E\,start} = 2 \pm 0.1\ \text{m} \tag{38}$$

The prescribed constrains at the beginning and the end of the movement are:

$$0 < y_{E\,start} < -0.1\ \text{m} \tag{39}$$

$$1.8\ \text{m} < y_{E\,end} < 2\ \text{m} \tag{40}$$

i.e. vector of inequality constrains is:

$$g_1(x) = -y_{E\,start} \tag{41}$$

$$g_2(x) = y_{E\,start} - 0.1 \tag{42}$$

$$g_3(x) = 1.8 - y_{E\,end} \tag{43}$$

$$g_4(x) = y_{E\,end} - 2 \tag{44}$$

An additional condition is that the endpoint of the arrow (the connection point between the bucket and arrow) forms an approximately rectilinear vertical trajectory during the whole movement. Therefore, the maximum difference of the x-coordinate of point E in the current and initial positions be less than 80 mm during the whole movement, i.e.:

$$g_5(x) = \max\left(abs\left(x_{Ei} - x_{E\,start}\right)\right) - 0.08 \tag{45}$$

Parameters which do not change during optimization – constants are shown in Table 1a and Table 1b, while parameters that change during optimization – variables and their constraints are presented in Table 2.

Table 1a. Parameters of optimization – constants

x_{01} [m]	y_{01} [m]	x_{03} [m]	y_{03} [m]	$\overline{O_1A}$ [m]	$\overline{O_3B}$ [m]	$\overline{AB}$ [m]
0	0	0	0	1.8	1.6	1

Table 1b. Parameters of optimization – constants

$\overline{BE}$ [m]	$\overline{BS_4}$ [m]	$\overline{DM}$ [m]	$\overline{ME}$ [m]	$\overline{EF}$ [m]	$\overline{ES_9}$ [m]	$\varphi_9 - \varphi_{S9}$ [°]
3	1.5	0.25	0.5	0.4	$\overline{EF}\sqrt{2}/2$	60

Table 2. Parameters of optimization – variables

x_{02} [m]	y_{02} [m]	$\overline{BN}$ [m]	$\overline{CN}$ [m]
–0.5÷0.2	0÷0.4	0.3÷0.9	0÷0.5

4. RESULTS

The optimized Stephenson III loader bucket mechanism that retains the same bucket lifting height of 2 m, which is one of the requirements, is shown in Figure 6. A multi-stage telescopic cylinder is used to drive the arrow, because the installation space is less than the required working stroke of the cylinder. In Table 3 and Table 4 the parameters of the mechanism before and after optimization are shown. By comparing the results it is concluded that the dimensions of the constructive parameters are within the real range, and the stroke length is increased by 23%.

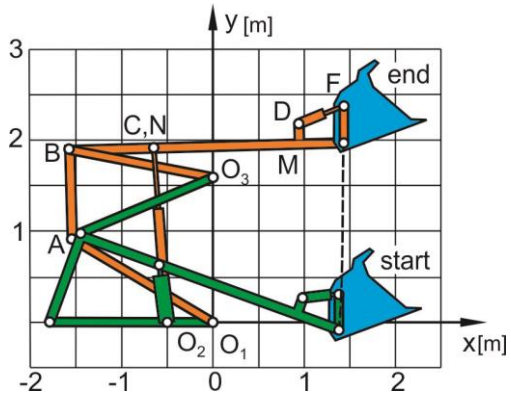

Fig. 6. Kinematic analysis of the loader bucket mechanism – type Stephenson III

Table 3. Parameters of non-optimized mechanism

x_{02} [m]	y_{02} [m]	$\overline{BN}$ [m]	$\overline{CN}$ [m]	stroke length [m]
0	0.2	0.5	0.25	1.05

Table 4. Parameters of optimized mechanism

x_{02} [m]	y_{02} [m]	$\overline{BN}$ [m]	$\overline{CN}$ [m]	stroke length [m]
–0.5	0	0.9	0	1.29

Figure 7 shows the force change in the cylinder for driving arrow, before and after optimization. The optimized mechanism requires 25% less force to drive the arrow. Figure 8 shows the change of the x-coordinates of point E during the whole movement. Point E allowance (maximum difference of the x-coordinates of point E in the current and initial position) is the largest for the initial and the end position, and has a value of 70 mm.

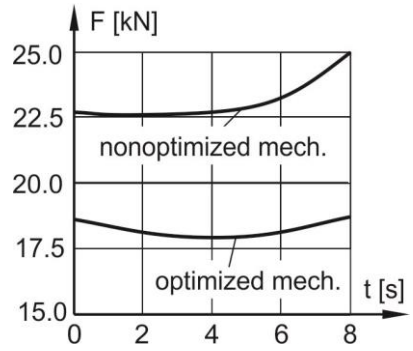

Fig. 7. Force change in the cylinder for arrow driving – before and after optimization

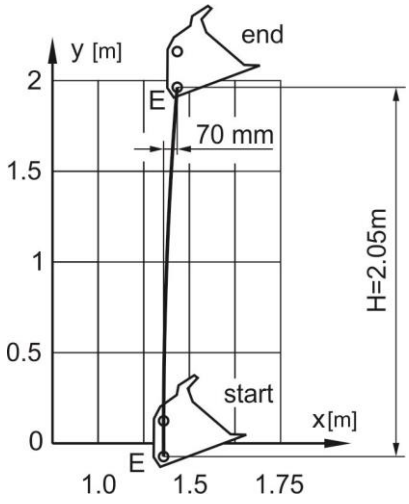

Fig. 8. Trajectory of the point E

5. CONCLUSIONS

This paper presents the optimal synthesis of a nine-bar lever loader bucket mechanism, which has 2 DOFs and contains two sets of mechanisms. The first group enables arrow driving – mechanism of the third class type RR-RR-TR (Stephenson III), and the second one that enables bucket driving – inverted slider-crank mechanism. Basic requirements for the realization are the minimization of forces in the cylinders for arrow and bucket driving, and that the connection point between the bucket and arrow forms an approximately rectilinear vertical trajectory during the whole movement, to eliminate the corrective motions of the loader. Based on the set require-

ments, the kinematic-dynamic analysis is performed by applying the modular and the kinetostatic approach. The force in the cylinder for bucket driving – eq. (1) directly depends on the geometry and dimensions of the bucket – the minimum value of the force is easily determined and is therefore not subjected to the optimization. The force in the cylinder for arrow driving eq. (2) is not as obvious, and is therefore further examined with the optimization. Aside from the basic requirements, an additional requirement is that the buckets lifting height remain the same. Based on the kinematic-dynamic analysis, a dynamic model is formed and a dynamic simulation is performed. The optimized loader bucket mechanism requires 25% less force to drive the arrow (working stroke of the bucket of 2 m is retained) and eliminates the corrective motions of the loader, because the connection point between the bucket and arrow forms approximately rectilinear vertical trajectory (maximum allowance is at the end of the movement, and is 70 mm). The dimensions of the constructive parameters are within the practical values. For driving the arrow, a multi-stage telescopic cylinder with 23% longer stroke length is used. Further research will examine the influence of other geometrical parameters on the forces in the cylinders with a wider range of variables optimization.

6. REFERENCES

[1] http://www.jcb.com/products/MachineOverview.aspx?RID=12, last time visited on Sep. 15th 2016.

[2] http://europe.construction.newholland.com/family.php, last time visited on Sep. 15th 2016.

[3] M. D. Worley; V. La Saponara, A Simplified Dynamic Model for Front-End Loader Design. Proceedings of the Institution of Mechanical Engineers, Part C: Journal of Mechanical Engineering Science 222(11) (2008), pp. 2231–2249, doi: 10.1243/09544062JMES688.

[4] J. Pavlović; M. Lj. Jovanović; A. Milojević, Optimal Synthesis of the Manipulator Using Two Competitive Methods. Facta Universitatis, Series: Mechanical Engineering, 12 (1) (2014), pp. 61–72.

[5] Y. Yu; M. L. Shen; M. Li, Optimum design of working device of wheel loader. Proc. of the IEEE-MACE Inter. Conf. on Mechanic Automation and Control Engineering (2010), Wuhan, China, pp. 461-465.

[6] Z. Yaohong; L. Ruiqin; W. Ailing, Kinematic Analysis and Optimization Design for Working Mechanism of Underground Load-Haul-Dump. Proc. of the 14th IFToMM World Congress (2015), pp. 1–7, doi: 10.6567/IFToMM.14TH.WC.OS3.014

[7] T. J. Roan; L. E. Albright, Folding Lift Arm Assembly for Skid Steer Loader. Patent (2004), WO 2004104304 A2.

[8] D. A. Ashcroft; R. R. Todd, Method of Lifting a Skid Steer Loader Bucket. Patent (1996), US 5542814 A.

[9] Čavić M; M. Kostić; M. Zlokolica, Design of the Door Opening Mechanism with Complex Structure. Journal of Trends in the Development of Machinery and Associated Technology 19 (1) (2015), pp. 165–168.

[10] M. M. Plecnik; J. M. McCarthy, Kinematic Synthesis of Stephenson III Six-bar Function Generators. Journal of Mechanism and Machine Theory 97 (2016), pp. 112–126, doi: 10.1016/j.mechmachtheory.2015.10.004

[11] A. Sullivan; J. D. van de ven; W. F. Northrop; K. McCabe, Integrated Mechanical and Thermodynamic Optimization of an Engine Linkage Using a Multi-Objective Genetic Algorithm. Journal of Mechanical Design 137 (2) (2015), doi: 10.1115/1.4029220

[12] M. Čavić; M. Penčić; J. M. Djoković; M. Zlokolica, Comparative Analysis of the Loader Bucket Mechanisms. Proc. of 48th Inter. October Conf. on Mining and Metallurgy (2016), Bor, Serbia.

[13] M. Čavić; M. Kostić; M. Zlokolica, Prenos snage i kretanja (Power and Motion Transmission, in Serbian). Faculty of Technical Sciences, Novi Sad, Serbia, (2014).

[14] C. H. Suh; C. W. Radcliffe, Kinematics and Mechanism Design. John Wiley & Sons, New York, (1987).

[15] M. Zlokolica; M. Čavić; M. Kostić, Mehanika mašina (Mechanics of Machinery, in Serbian). Faculty of Technical Sciences, Novi Sad, Serbia, (2013).

[16] M. Kostić; M. Čavić; M. Zlokolica, About Optimal Synthesis of Complex Planar Mechanism. Proc. of 12th IFToMM World Congress on Theory of Machines and Mechanisms (2007), Besançon, France, pp. 1–6.

Analysis of the Mechanism of Complex Structures with High Class Kinematic Group

M. Čavić, M. Penčić, M. Zlokolica

Faculty of Technical Sciences, University of Novi Sad, Trg Dositeja Obradovića 6, 21000 Novi Sad, Serbia, e-mail: {scomaja, mpencic, mzlokolica}@uns.ac.rs

Abstract

High class kinematic groups are commonly present as consisting components of contemporary complex industrial mechanisms. Their kinematic analysis cannot be done in a standard way. Due to the extensive practical use of computers, the development of efficient computational methods for kinematic analysis has gained importance. In this paper a new method for the analysis of this class of mechanisms is proposed. The basic idea of the method is to model the high class kinematic group using specific modules – dyads. A system of equations that describes the mechanism position is obtained from the kinematic structure of the linkage and the corresponding modules equations. The position of the mechanism is then obtained numerically. The presented method is very efficient and it quickly and accurately gives all possible solutions concerning the position of mechanism.

Keywords: complex mechanism, high class kinematic group, position analysis, assembly configuration

1. INTRODUCTION

In search of mechanisms that can fulfil certain tasks, it is interesting to examine those of high class kinematic groups because they can offer multiple solutions. The existence of multiple solutions means that the high class kinematic group and therefore, the whole mechanism, can be assembled in various configurations which can be further examined and optimized. As the position analysis is performed on the level of kinematic groups, the complexity of the problem depends on the structure of the mechanism being analysed, namely on the class of the kinematic groups it consists of. For the second class kinematic groups of different forms the analytical relations determining positions of the moving links have been derived in the explicit form [1]. The determination of the links positions in the higher class groups is more complex as the equations describing mechanism position are highly nonlinear. Numerical methods are commonly applied for solving this system of equations [2], [3]. However, the application of these methods has many problems:

- For the method convergence, the starting values of variables must be close to the exact solutions.
- Absence of convergence exists when the system is close to singular positions.
- Nonlinear equations always have multiple solutions, the number of which is unknown.

Another approach is based on obtaining the solution of the high class kinematic group position equations in a closed form [4], [5]. The expressions obtained are extremely long and complex, but main disadvantage here is the fact that equations derived are case dependant, *i.e.* they are applicable only for a specified linkage.

The basic idea of the method presented in this paper is to kinematic model the high class kinematic group using second class kinematic groups (dyads) – modules. By combining modules, any type of high class kinematic group can be formed. A system of equations is then obtained from the kinematic structure of the linkage and can be solved numerically. Way of forming and combining modules to a system ensures that all possible solutions for high class kinematic group position, *i.e.* all assembly configurations are found.

2. GENERAL CONCEPT OF KINEMATIC GROUP ANALYSIS

The position analysis of the high class kinematic group will be performed by using standard modules – groups of equations describing a par-

ticular type of dyad. The module form will be explained, especially its input and output parameters, which become very important when establishing the relationship between standard modules and a specific problem. The module equations are derived by following the principles presented in [1]. Two modules will be presented, each describing one typical second class kinematic group.

2.1. Kinematic analysis of the dyad

The general form of a dyad consisting of two links connected by a rotational joint is presented in Figure 1. All joints – external joints B_1 and B_2 and internal joint B_3 are of the rotational type, so this type of dyad is called an RRR type.

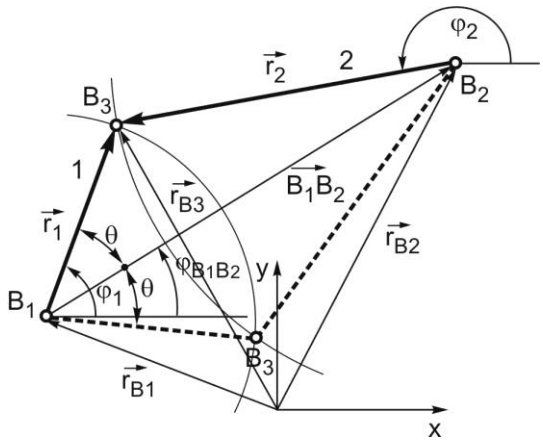

Fig. 1. Dyad – type RRR

The positions of the external joints B_1 and B_2, *i.e.* $\vec{r}_{B1}(x_{B1}, y_{B1})$ and $\vec{r}_{B2}(x_{B2}, y_{B2})$, and the lengths of links 1 and 2 are known (INPUT), while the position of the middle joint B_3, as well as the position angles of links 1 and 2 have to be determined (OUTPUT). The vector equation describing this dyad is:

$$\vec{r}_{B1} + \vec{r}_1 = \vec{r}_{B2} + \vec{r}_2 = \vec{r}_{B3} \tag{1}$$

After some transformations, the position angle of link 1 can be obtained as:

$$\varphi_1 = \varphi_{B1B2} \pm \theta \tag{2}$$

where:

$$\varphi_{B1B2} = \arctan\left(\frac{y_{B2} - y_{B1}}{x_{B2} - x_{B1}}\right) \tag{3}$$

$$\theta = \arccos\left(\frac{r_1^2 + \overline{B_1B_2}^2 - r_2^2}{2r_1\overline{B_1B_2}}\right) \tag{4}$$

The symbol ± represents the two possible configurations of dyad assembly (Figure 1 – full and dotted line). Now, with the position of join B_1 known, the position of joint B_3 is calculated as:

$$x_{B3} = x_{B1} + r_1\cos\varphi_1 \tag{5}$$

$$y_{B3} = y_{B1} + r_1\sin\varphi_1 \tag{6}$$

The position angle of link 2 is obtained in the following form:

$$\varphi_2 = \arctan\left(\frac{y_{B3} - y_{B2}}{x_{B3} - x_{B2}}\right) \tag{7}$$

The dyad presented in Figure 2 consists of two links connected by a rotational joint, the first link's end joint is rotational and second one's is translational – type RRT.

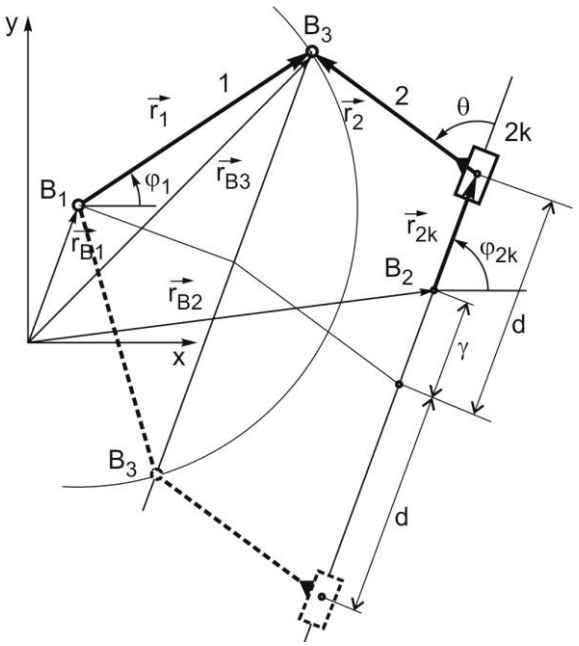

Fig. 2. Dyad – type RRT

The positions of external joints B_1 and B_2, *i.e.* $\vec{r}_{B1}(x_{B1}, y_{B1})$ and $\vec{r}_{B2}(x_{B2}, y_{B2})$, the lengths of links 1 and 2, the angular position of the guide 2k (φ_{2k}) and angle θ between the guide 2k and sliding link 2 are known (INPUT), while the position of middle joint B_3, the position angle of link 1 and the linear position of link 2 have to be determined (OUTPUT). The vector equation describing this dyad is:

$$\vec{r}_{B1} + \vec{r}_1 = \vec{r}_{B2} + \vec{r}_{2k} + \vec{r}_2 = \vec{r}_{B3} \tag{8}$$

The unknown distance r_{2k} can be calculated as:

$$r_{2k\,1/2} = -\gamma \pm d \tag{9}$$

where:

$$\alpha = (x_{B2} - x_{B1}) + r_2\cos(\varphi_{2k} + \theta) \tag{10}$$

$$\beta = (y_{B2} - y_{B1}) + r_2\sin(\varphi_{2k} + \theta) \tag{11}$$

$$\gamma = \alpha \cos\varphi_{2k} + \beta \sin\varphi_{2k} \tag{12}$$

$$d = \sqrt{\gamma^2 - \alpha^2 - \beta^2 + r_1^2} \tag{13}$$

The symbol ± represents the two possible dyad assembly configurations. Now, the position of joint B_3 can be obtained as:

$$x_{B3} = x_{B2} + r_{2k}\cos\varphi_{2k} + r_2\cos(\varphi_{2k} + \theta) \tag{14}$$

$$y_{B3} = y_{B2} + r_{2k}\sin\varphi_{2k} + r_2\sin(\varphi_{2k} + \theta) \tag{15}$$

The position angle of link 1 is:

$$\varphi_1 = \arctan\left(\frac{y_{B3} - y_{B1}}{x_{B3} - x_{B1}}\right) \tag{16}$$

2.2. Kinematic analysis of the third class kinematic group

General case of the third class kinematic group is presented in Figure 3.

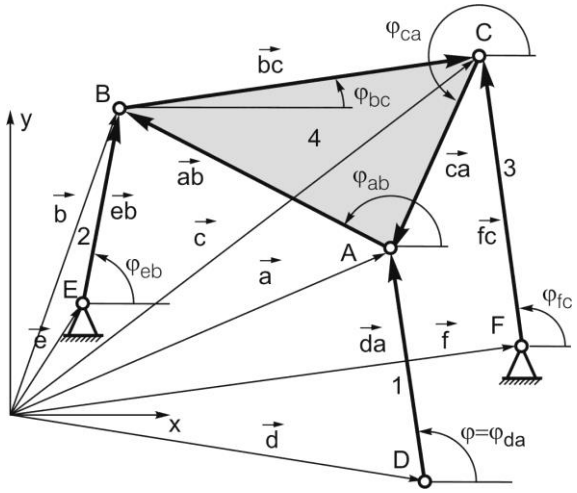

Fig. 3. RR-RR-RR type third class kinematic group

It is of the RR-RR-RR type – central link 4 is connected by rotational joints with binary links 1, 2 and 3, which are also connected to the rest of the mechanism by the rotational joints. Points A, B and C are called internal, and D, E and F external points. All link lengths as well as the positions of all external points are known (INPUT), while the positions of the internal points A, B and C have to be determined (OUTPUT).

The procedure begins by choosing one of the binary links as a "start" link. Its position parameter, for example it will be denoted as φ, will be the main variable of the model. The position of the corresponding internal point can then be expressed through φ and be considered as known. This enables one to treat the third class kinematic group as a combination of three modules – second class kinematic groups which can be described using equations from section 2.1. All equations, *i.e.* all other position parameters (changeable angles, lengths or vectors) are expressed in terms of φ and solving them for the given INPUT gives value for φ. With φ known, the OUTPUT is easily determined.

STEP 1 – *start, obtaining* $\vec{a}(\varphi)$

The procedure will start form link 1 and the angle $\varphi_{da} = \varphi$ will be adopted as a variable. The position of point A will be needed further in the process, so it is expressed in terms of φ as:

$$\vec{a}(\varphi) = \vec{d} + \overrightarrow{da}(\varphi) \tag{17}$$

STEP 2 – *forming first dyad, obtaining* $\varphi_{eb}(\varphi)$

Now, the positions of points E and A are known – $\vec{e}$ is given as INPUT. Links AB and BE form an RRR type dyad – section 2.1, where E corresponds to B_1, A to B_2 and B to B_3, link BE to link 1 and link AB to link 2. The vector equation describing this dyad is:

$$\vec{a} + \overrightarrow{ab} = \vec{e} + \overrightarrow{eb} = \vec{b} \tag{18}$$

This equation corresponds to eq. (1) in the module describing the RRR dyad. Using eq. (2), the angle is obtained in terms of:

$$\varphi_{eb} = \varphi_{eb}(\varphi) \tag{19}$$

With the expression for $\varphi_{eb}(\varphi)$ known, using eqs. (5) – (7), $\varphi_{ab}(\varphi)$ and the position of point B – vector $\vec{b}(\varphi)$ is obtained. Since angle $\varphi_{eb}(\varphi)$ can have two completely distinctive solutions (see eq. (2) – symbol ±), two expressions can be formed for both $\varphi_{ab}(\varphi)$ and $\vec{b}(\varphi)$. One symbol, *i.e.* one set of expressions $\left(\varphi_{eb}(\varphi), \varphi_{ab}(\varphi), \vec{b}(\varphi)\right)$ has to be chosen in order to continue.

STEP 3 – *forming second dyad, obtaining* $\varphi_{fc}(\varphi)$

The position of points B and F are now known – $\vec{f}$ is given as INPUT and for $\vec{b}(\varphi)$ is obtained in STEP 2. Links BC and CF form an RRR type dyad, where F corresponds to B_1, B to B_2 and C to B_3, link CF to link 1 and link BC to link 2. The vector equation describing this dyad is:

$$\vec{b} + \overrightarrow{bc} = \vec{f} + \overrightarrow{fc} = \vec{c} \tag{20}$$

Using eq. (2), angle φ_{fc} is obtained in terms of φ:

$$\varphi_{fc} = \varphi_{fc}(\varphi) \tag{21}$$

With $\varphi_{fc}(\varphi)$ known, using (5) – (7), expressions for $\varphi_{bc}(\varphi)$ and the position of point C – vector $\vec{c}(\varphi)$ is obtained. Again, φ_{fc} can have two distinctive solutions leading to two expressions for both $\varphi_{bc}(\varphi)$ and $\vec{c}(\varphi)$. One symbol, *i.e.* one set $\left(\varphi_{fc}(\varphi), \varphi_{bc}(\varphi), \vec{c}(\varphi)\right)$ has to be chosen in order to continue.

STEP 4 – *forming third dyad, obtaining* $\varphi_{da}(\varphi)$

Now, a dyad of the type RRR (links AC and AD) is formed:

$$\vec{c} + \overrightarrow{ca} = \vec{d} + \overrightarrow{da} = \vec{a} \tag{22}$$

The position of points C and D are known – $\vec{d}$ is given as INPUT and $\vec{c}(\varphi)$ is derived in STEP 3. Links AD and AC form an RRR type dyad, where D corresponds to B_1, C to B_2 and A to B_3, link AD to link 1 and link AC to link 2. Using eq. (2), angle φ_{da} is expressed in terms of:

$$\varphi_{da} = \varphi_{da}(\varphi) \tag{23}$$

Again, one equation for $\varphi_{da}(\varphi)$ has to be chosen. By solving equation (23) for the given INPUT $\left(\vec{d}, \vec{e}, \vec{f}, \overline{AB}, \overline{BC}, \overline{CA}, \overline{DA}, \overline{EB}, \overline{FC}\right)$, the value of angle φ_{da} is obtained, and further on, all other parameters describing the position of the third class kinematic group – OUTPUT $\vec{a}, \vec{b}, \vec{c}$.

All three dyads (eqs. (18), (20) and (22)), this third class kinematic group consist of, can have two solutions (assembly configurations), so there are, in total, 2^3=8 different cases, *i.e.* eq. (23) that can describe the mechanism position. Real solutions (complete mechanism assembly configurations), are found by examining, one by one, all of these eight cases. Keeping in mind that $\varphi_{da} = \varphi$, eq. (23) can be written in the following form:

$$\varphi = f(\varphi) \tag{24}$$

However, obtaining $f(\varphi)$ in its analytical form is not convenient because it leads to an extremely long and complicated expression. Eq. (24), whose form is well known in literature, will be solved using a numeric procedure such as the fixed point iteration method.

The starting equations for numerical method proposed in this paper – eqs. (19), (21) and (23), after transformations give:

$$G_0 \tan^6\frac{\varphi}{2} + G_1 \tan^5\frac{\varphi}{2} + G_2 \tan^4\frac{\varphi}{2} + G_3 \tan^3\frac{\varphi}{2} + \\ + G_4 \tan^2\frac{\varphi}{2} + G_5 \tan\frac{\varphi}{2} + G_6 = 0 \tag{25}$$

Coefficients G_i are functions of known geometric parameters of the mechanism. The solution leads to a maximum of six real solutions for φ, *i.e.* six possible assembly configurations of the third class kinematic group. This means that the proposed method recognizes all possible solutions for the position of the third class kinematic group, in this case six of them, which is consistent with similar researches papers [4], [5].

3. EXAMPLE – CALCULATIONS AND COMMENTS

In many machines, a four-member linkage is the most widespread solution. For example, the slider-crank mechanism was the first solution for a press mechanism. However, for many industrial solutions, the application of complex linkages is necessary as four-member linkages cannot fulfil either the prescribed task or the design limitations, so complex mechanisms have to be used – an eight-member linkage (Figure 4a) is commonly accepted as the structural mechanism for presses. Although better than the slider-crank mechanism, this mechanism still has a lot of limitations that can be significantly overcome by optimization [6],

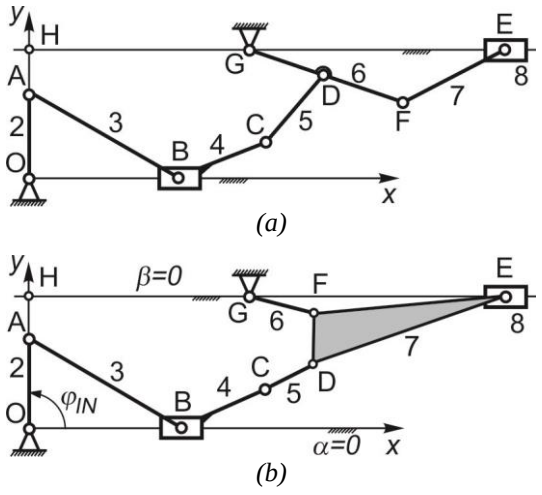

Fig. 4. Press structural mechanisms: (a) eight-bar linkage and (b) mechanism with third class kinematic group

[7]. Other researches [8] proposes, especially for heavy duty presses, the application of complex mechanisms which include high class kinematic groups – Figure 4b. The advantage are obvious, the output link can perform extremely complicated movement due only to only the mechanism structure, which can further allow more possibilities in the choice of kinematic functional parameters. Good kinematics can significantly improve the dynamic features of a machine. In order to fully examine the kinematic and dynamic properties of a mechanism, it is necessary to explore all possible configurations, *i.e.* it is important to know if there are any others except the one presented in Figure 4b. Data for the press mechanism from Figure 4b is given in Table 1a and Table 1b.

Table 1a. Constructive parameters of mechanism with third class kinematic group – Figure 4b

x_O [m]	y_O [m]	x_G [m]	y_G [m]	x_H [m]	y_H [m]	α [°]	β [°]	φ_{IN} [°]
0	0	2.5	1	0	0.7	0	0	60

Table 1b. Constructive parameters of mechanism with third class kinematic group – Figure 4b

$\overline{OA}$ [m]	$\overline{AB}$ [m]	$\overline{BC_X}$ [m]	$\overline{BC_Y}$ [m]	$\overline{CD}$ [m]	$\overline{DE}$ [m]	$\overline{DF}$ [m]	$\overline{EF}$ [m]	$\overline{FG}$ [m]
0.55	1.75	0.8	0.38	0.35	2	0.42	2.1	0.5

It consists of two parts: a slider crank mechanism to which, in point C, a third class kinematic group of the type RR-RR-RT is attached – Figure 5.

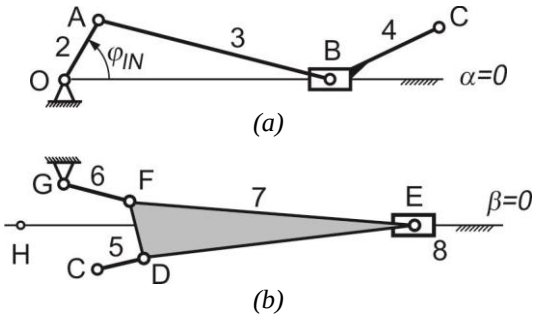

Fig. 5. Constitutive parts of press mechanism: (a) slider crank mechanism and (b) RR-RR-RT third class kinematic group

Position analysis is performed in the same order as mechanism assembly – first, the position of the slider crank mechanism will be calculated. The position of point A is:

$$x_A = \overline{OA}\cos\varphi_{IN} = 0.25 \text{ m}$$
$$y_A = \overline{OA}\sin\varphi_{IN} = 0.433 \text{ m}$$

Links 3 and 4 form an RRT dyad – section 2.2. Using eqs. (8) – (16) two possible configurations for the RRT dyad are obtained – Figure 6:

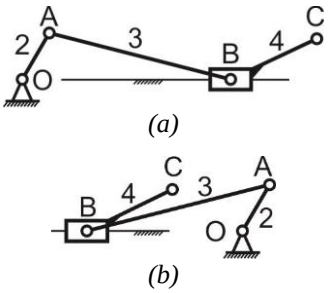

Fig. 6. Possible configurations of slider crank mechanism

– slider crank mechanism from Figure 6a:

$x_B = 1.946$ m; $y_B = 0$ m

– slider crank mechanism from Figure 6b:

$x_B = -1.446$ m; $y_B = 0$ m

Following the procedure described in section 2.2, position analysis of the third class kinematic group is performed. The positions of points C, H and G are known. The positions of internal joints D, E and F will be determined. The position angle φ_{gf} of link 6 is chosen as variable φ and the position of point F is expressed in terms of φ. The third class kinematic group is formed as a combination of the following three modules:

- First dyad – RRR type, where C corresponds to B_1, F to B_2 and D to B_3, link CD to link 1 and link FC to link 2,
- Second dyad – RRT type, where D corresponds to B_1, H to B_2 and E to B_3, link DE to link 1 and slider 8 to link 2, $\varphi_{2k} = 0°$, $\theta = 0°$ and $r_2 = 0$, and
- Third dyad – RRR type, where G corresponds to B_1, E to B_2 and F to B_3, link FG to link 1 and link EF to link 2.

These three dyads define function $f(\varphi)$. The procedure for solving $f(\varphi)$ has to be executed twice – the first time for the slider crank configuration from Figure 6a, and a second time for the slider crank configuration from Figure 6b. After calculations, the slider crank configuration from Figure 6b gives no real solutions, while the slider crank configuration from Figure 6a leads to two real solutions (assembly configurations) – Figure 7:

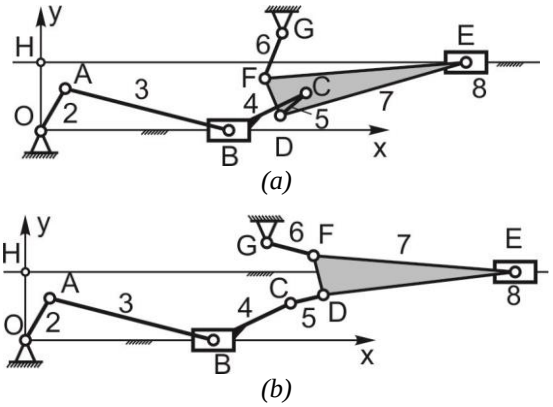

Fig. 7. Two possible configurations of press mechanism with third class kinematic group

After thorough kinematical and dynamical examination, the configuration presented on Figure 7b has been adopted and proposed for further research and optimization.

4. CONCLUSIONS

This paper proposes a method for the position analysis of the mechanisms with high class kinematic groups. A mechanism is presented as a combination of its constitutive parts – kinematic groups. Kinematic groups are, further, modeled using modules – set of equations used to calculate position. Each module corresponds to a particular type of dyad. High class kinematic groups are described as a combination of particular modules, three for third class kinematic groups, four for fourth class kinematic groups etc. A system of equations obtained this way is solved numerically through the fixed point iteration method. A procedure that allows easy recognition of real solutions and the choice of initial parameter values that ensures convergence of the fixed point iteration method is developed. Also, the proposed method recognizes all possible solutions for the position of the third class kinematic group, in this case six of them. The example presented in this paper contains a third class kinematic group, but this method is applicable for any high class kinematic group. The presented method is developed primarily for position analysis. Nevertheless, it can also be used for velocity and acceleration analysis – following the procedure described in section 2.1, but using expressions for velocity and acceleration kinematical parameters instead.

5. REFERENCES

[1] C. H. Suh; C. W. Radcliffe, Kinematics and Mechanism Design. John Wiley & Sons, New York, (1987).

[2] C. Radcliffe; M. Zlokolica; L. Cvetićanin, Kinematic Analysis of Assur Groups of the Third Class by Numerical Solution of Constraint Equations. Proc. of 7th IFToMM World Congress on Theory of Machines and Mechanisms (1987), Sevilla, Spain.

[3] T. Młynarski; K. Romaniak, The Methodization of Examination of the Mechanisms of High Structural Complexity. Journal of Mechanism and Machine Theory 36(6) (2001), pp. 709–715, doi: 10.1016/S0094-114X(01)00013-1

[4] S. Mitsi; K. D. Bouzakis; G. Mansour; I Popescu, Position Analysis in Polynomial form of Planar Mechanisms with Assur Groups of Class 3 Including Revolute and Prismatic Joints. Journal of Mechanism and Machine Theory 38(12) (2003), pp. 1325–1344, doi: 10.1016/S0094-114X(03)00090-9

[5] A.K. Dhingra; A.N. Almadi; D. Kohli, Closed-Form Displacement and Coupler Curve Analysis of Planar Multi-Loop Mechanisms Using Gröbner Bases. Journal of Mechanism and Machine Theory 36(2) (2001), pp. 273–298, doi: 10.1016/S0094-114X(00)00043-4

[6] C. Gosselin; J. Sefrioui; M. J. Richard, Solution polynomiale au problème de la cinématique directe des manipulateurs parallèles plans à 3 degrés de liberté. Journal of Mechanism and Machine Theory 27(2) (1992), pp. 107–119, doi: 10.1016/0094-114X(92)90001-X

[7] W. Chung, Position Analysis of Assur Kinematic Chain with Five Links. Journal of Mechanism and Machine Theory 40(9) (2005), pp. 1015–1029, doi: 10.1016/j.mechmachtheory.2004.12.016

[8] M. Kostić; M. Čavić; M. Zlokolica, About Optimal Synthesis of Complex Planar Mechanism. Proc. of 12th IFToMM World Congress on Theory of Machines and Mechanisms (2007), Besançon, France, pp. 1–6.

[9] H. Li; L. Fu; Y. Zhang, Optimum Design of a Hybrid-Driven Mechanical Press Based on Inverse Kinematics, Strojniški vestnik – Journal of Mechanical Engineering 56(5) (2010), pp. 301–106.

[10] A. A. Golovin, Comparison and Estimation Criteria for Complex Linkages. Proc. of 10th IFToMM World Congress on Theory of Machines and Mechanisms (1999), Oulu, Finland, pp. 310–316.

Investigation of Ultrasonic Assisted Milling of Nickel Alloy Monel

M. Kuruc [a], V. Šimna [b], T. Vopát [c], J. Peterka [d]

[a] Slovak University of Technology in Bratislava, Faculty of Materials Science and Technology in Trnava, Paulínska 16, 917 24, Slovak Republic, marcel.kuruc@stuba.sk

[b] Slovak University of Technology in Bratislava, Faculty of Materials Science and Technology in Trnava, Paulínska 16, 917 24, Slovak Republic, vladimir.simna@stuba.sk

[c] Slovak University of Technology in Bratislava, Faculty of Materials Science and Technology in Trnava, Paulínska 16, 917 24, Slovak Republic, tomas.vopat@stuba.sk

[d] Slovak University of Technology in Bratislava, Faculty of Materials Science and Technology in Trnava, Paulínska 16, 917 24, Slovak Republic, jozef.peterka@stuba.sk

Abstract

Rotary ultrasonic machining is a machining process designed for machining hard and brittle materials (such as ceramics and glass), utilising a tool of undefined geometry. Soft and tough materials, such as nickel alloys, are not suitable for this type of machining using a tool of undefined geometry. However, the milling of tough alloys is also possible with the assistance of ultrasound, using a tool of a defined geometry, which is called ultrasonic assisted milling. Nickel alloys are utilised especially in aerospace industry (due to their excellent creep and heat resistance) for components such as blades and frames, where is demand high quality of machined surface (high accuracy, low roughness, low residual stresses, etc.). In the experiment, there is investigated influence of machining parameters (feed rate and cutting speed) on resultant machined surface (namely roughness). Measurements were provided in direction of feed rate, as well as perpendicular to feed rate direction. Moreover, there is compared ultrasonic assisted milling with conventional milling. Obtained results could be applied at manufacturing of components in aviation and marine industry or in oil refining to increase surface quality and/or reduce machining time. This contribution investigates the surface quality parameters (Ra and Rz) achieved by the ultrasound assisted milling of Monel the nickel alloy.

Keywords: Ultrasonic assisted milling; Rotary ultrasonic machining; Conventional milling; Nickel alloys; Roughness.

1. INTRODUCTION

Ultrasonic assisted machining processes have many advantages. Application of ultrasound decreases cutting forces (enables machining thin-walled workpieces), decreases generation of process heat (enables machining heat sensitive materials) and increases tool life. Also, it enables machining hard and brittle materials, such as glass and ceramics. These effects also influence surface roughness. Rotary ultrasonic machining (RUM) can reach mean arithmetic surface roughness Ra 0.3 μm. However, RUM is usually used for the machining of brittle materials, and it utilises a tool with undefined geometry with diamond abrasive particles. Such tool, however, is not suitable for machining soft and tough materials, such as nickel alloys. Therefore the mill with defined geometry made of high speed steel (HSS) or sintered carbide and coated with TiCN is recommended for this kind of materials. Combination of the tool with defined geometry with ultrasonic vibration should positively affect the quality of surface and avoid to formation of build-up-edge (BUE) [1,2,3,4,5].

2. METHODS AND MATERIALS USED FOR RESEARCH

It is necessary to specify utilised machines, devices, materials and evaluation method at the beginning of the experiment, because they could affect each other. In following subchapters are described: workpiece material, machine tool, measuring device and evaluation method.

2.1. Material used for research

The current interest of aviation industry in the materials of high strength, high creep resistance and high heat resistance such as nickel alloys, keeps growing. Such materials are being increasingly used for their mechanical properties, as well as for their good corrosion resistance. Their main applications are in marine industry, aerospace and in oil industry especially for components which have to keep high strength at elevated temperatures, such as turbines. Nickel alloys (also known as superalloys) could be hardenable and they could achieve tensile strength up to 1800 MPa. One of the most utilised Ni alloy is Monel. Its chemical composition provided by microanalysis EDX is shown in Table 1. Its main mechanical properties are shown in Table 2. Table 3 shows its physical properties [6,7].

Table 1 Chemical composition of Monel 400.

Element	Ni	Cu	Fe	Mn	Si
wt. %	61.45	29.72	1.66	1.05	0.45

Table 2 Mechanical properties of Monel.

Hardness [HV10]	Elongation [%]	Yield strength [MPa]	Tensile strength [MPa]
215	20	510	690

Table 3 Physical properties of Monel.

Melting point [°C]	Density [kg/m^3]	Young´s modulus [GPa]	Thermal conductivity [W.m^{-1}.K^{-1}]
1350	8800	175	22

2.2. Machining equipment

Ultrasonic 20 linear, the machine tool made by DMG Mori Seiki was used in this experiment. It is a five-axis rotary ultrasonic and high speed cutting machine tool. Ultrasonic oscillation is provided by an ultrasonic generator with a piezo-ceramic convertor. High speed cutting is ensured by spindle, which can reach 42 000 rpm. Feed acceleration is over 2g. It has a 5-axis gantry construction with an integrated NC swivel rotary table. It has very high precision of positioning (± 2.5 μm). During the experiments, only four outer nozzles were used for cooling [8,9,10].

As a tool, a face mill with two cutting edges was used. The tool is made of carbide by SECO Company under the trade name 905XL020-MEGA-T. The main dimensions of the tool are presented in Table 4. Tool-holder bears a label HSK 32S-ER11 [11].

Table 4 Dimensions of the tool.

Diameter [mm]	Length of active part [mm]	Whole length [mm]	Number of teeth [-]
2	2.2	60	2

2.3. Description of the experiment

A plate by the dimensions 100 x 70 x 10 mm made of the above mentioned Monel Ni alloy was used for the experiment. On the biggest surface (100 x 70 mm) rectangular areas by the dimensions 20 x 14 mm were milled (25 areas at each side), as shown Figure 1.

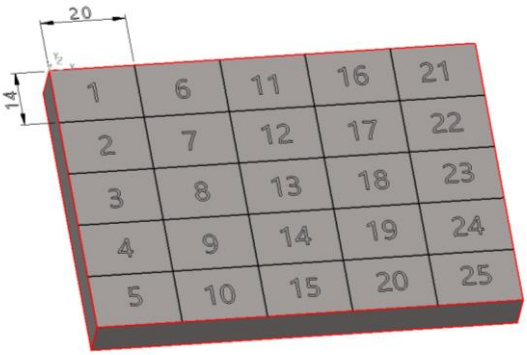

Fig. 1 Milled areas on the workpiece

Scheme of clamping and placement of workpiece in workplace of the machine tool is shown in Figure 2.

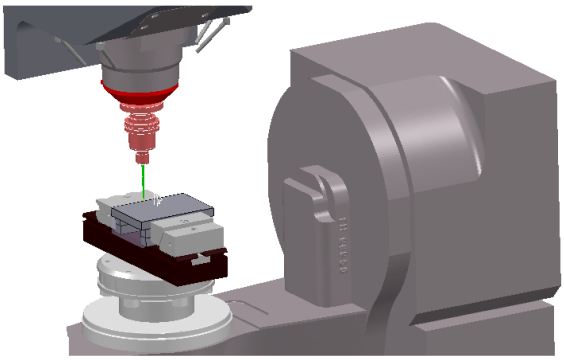

Fig. 2 Workpiece in machine tool

During the experiment, the speed of spindle changed in the horizontal direction (axis X) and the feed rate in vertical direction (axis Y). The spindle speed reached the values 5000 rpm (first column), 5500 rpm (second column), 6000 rpm (third column), 6500 rpm (fourth column) and 7000 rpm (fifth column). The feed rate reached the values 100 (first line), 200 (second line), 300 (third line), 400 (fourth line) and 500 mm.min^{-1} (last line). Depth of the cut was constant 0.1 mm. The workpiece was milled by ultrasound with frequency 21 467 Hz (harmonic frequency of tool – determined by FEM analysis) and amplitude 6 μm [12, 13, 14].

2.4. Evaluation of the experiment

Measurement was performed on Surtronic 3+, the measuring device made by Taylor Hobson Company [15]. Measured were the surface parameters, such as arithmetic roughness Ra and maximum height roughness Rz. Each measurement was repeated three times. The measurement was performed in the cross as well as longitudinal directions. It gives 600 results, including average values. Therefore, in this article, only the average values of Ra and Rz in cross direction will be presented. Generally, surface parameters in cross direction are much more important than surface parameters in longitudinal direction. Longitudinal roughness is usually much lower and therefore less significant, than cross roughness [16].

3. RESULTS AND ACHIEVEMENTS

Surface quality is one of the most important parameters of machined part. Increased surface quality is often related with productivity – if we are able to reach better quality and tool life at the same productivity (e.g. by ultrasonic assistance), we could often reach the same quality at higher productivity [17, 18].

3.1. List of results

The resultant surface roughness for conventional milling (CM) and ultrasound assisted milling (UAM) is shown in following tables. In Table 5 is summarized labelling of the machined areas obvious from Figure 1. In Table 6 is shown comparison of roughness parameter Ra between CM and UAM. And in Table 7 is shown comparison of roughness parameter Rz.

Table 5 Labelling of machined areas

No.		Feed rate	Spindle speed
CM	UAM	[mm/min]	[rpm]
1	26	100	5000
2	27	200	5000
3	28	300	5000
4	29	400	5000
5	30	500	5000
6	31	100	5500
7	32	200	5500
8	33	300	5500
9	34	400	5500
10	35	500	5500
11	36	100	6000
12	37	200	6000
13	38	300	6000
14	39	400	6000
15	40	500	6000
16	41	100	6500
17	42	200	6500
18	43	300	6500
19	44	400	6500
20	45	500	6500
21	46	100	7000
22	47	200	7000
23	48	300	7000
24	49	400	7000
25	50	500	7000

Average values of arithmetic roughness and maximum height roughness in cross direction are presented. Owing to the assistance of ultrasound, surface roughness is lower than the roughness measured in conventional milling in the most of cases.

Table 6 Comparison of achieved roughness Ra

No.		Ra_{CM}	Ra_{UAM}
CM	UAM	[µm]	[µm]
1	26	1.54	0.52
2	27	1.90	0.59
3	28	2.71	0.72
4	29	2.73	0.72
5	30	2.82	1.26
6	31	1.45	1.14
7	32	1.89	1.81
8	33	2.19	1.65
9	34	2.47	1.72
10	35	2.20	1.69
11	36	1.61	1.33
12	37	1.59	2.19
13	38	1.57	2.42
14	39	2.24	2.63
15	40	1.92	3.29
16	41	1.71	1.37
17	42	1.72	1.91
18	43	2.07	2.07
19	44	2.83	2.37
20	45	2.80	3.24
21	46	1.60	1.34
22	47	1.43	0.57
23	48	1.72	0.45
24	49	1.81	0.80
25	50	2.41	1.43

Surface roughness parameter Ra was decreased by 23 % when ultrasonic assistance was active, according Table 6. Similar relation as presented Table 6 for roughness parameter Ra can be shown in Table 7 for roughness parameter Rz as well. There was decreasing of surface roughness parameter Rz by 24 % when ultrasound was applied. Surface quality at conventional milling was better in cases, when spindle speed achieved value 6000 rpm and feed rate achieved value over 200 mm/min. At these machining parameters is positive effect of ultrasound negated.

Table 7 Comparison of achieved roughness Rz

No.		Rz_{CM}	Rz_{UAM}
CM	UAM	[µm]	[µm]
1	26	5.83	3.97
2	27	6.80	2.77
3	28	9.70	4.37
4	29	10.32	5.67
5	30	11.07	8.17
6	31	5.73	3.70
7	32	7.20	6.40
8	33	8.67	5.93
9	34	9.43	5.40
10	35	10.17	6.53
11	36	7.67	4.63
12	37	6.27	6.43
13	38	6.43	7.73
14	39	9.07	9.60
15	40	7.93	10.33
16	41	6.63	5.67
17	42	7.53	6.27
18	43	8.20	6.97
19	44	10.73	8.30
20	45	11.60	11.53
21	46	6.10	8.03
22	47	5.70	2,60
23	48	8.33	2.73
24	49	7.27	4.03
25	50	11.30	5.90

Obtained results could be presented also as graph. Results for both surface roughness parameters (Ra and Rz) are similar; therefore only graphical influence for Ra parameter is presented. Figure 3 shows influence of feed rate on roughness Ra, and Figure 4 shows influence of spindle speed on roughness Ra. Red line represent conventional milling and blue one represent ultrasonic assisted milling. These graphs are based on Table 6.

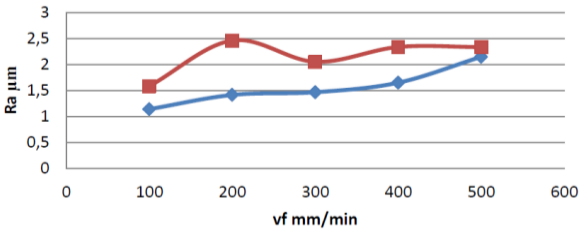

Fig. 3 Influence of feed rate on surface roughness parameter Ra

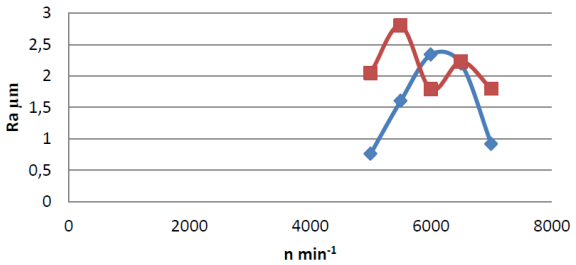

Fig. 4 Influence of spindle speed on surface roughness parameter Ra

4. CONCLUSIONS

Ultrasonic machining by a common tool for ultrasonic milling, i.e. of undefined geometry is not proper for soft materials. This is due to fine cutting teeth. However, the tool of defined geometry could have much larger teeth, and therefore active part of the tool could not be sealed by the soft material of workpiece. The experiment confirms the premise, that even soft and tough materials (in comparison with ceramics) such as Ni alloys can be machined with assistance of ultrasound, when using a tool of defined geometry. The best parameters of machined surface (Ra 0.45 µm) were achieved at the spindle speed 7000 rpm and feed rate 300 mm/min. The biggest difference (decreasing by 74 %) between CM and UAM (in favour of UAM) was at spindle speed 5000 rpm and feed rate 400 mm/min. Anyway, this fact could significantly decrease the production time and also improve the quality of machined surface. Therefore, in further research, influence of ultrasonic assistance on surface quality at machining of different alloys will be elaborated in detail (such as titanium and magnesia alloys).

5. ACKNOWLEDGEMENTS

This contribution is a part of the GA VEGA project of Ministry of Education, Science, Research and Sport of the Slovak Republic, No. 1/0477/14 “Research of influence of selected characteristics of machining process on achieved quality of machined surface and problem free assembly using high Technologies”.

This contribution is also supported by the Operational Project Research and Development of Centre of Excellence of Five Axis Machining, ITMS 26220120013, co-financed by the European Funds for Regional Development.

This contribution is supported by the Operational Project Research and Development of Centre of Excellence of Five Axis Machining, ITMS 26220120013, co-financed by European Founds for Regional Development.

Európska únia
Európsky fond regionálneho rozvoja

Operačný program VÝSKUM a VÝVOJ

We are supporting of research activities in Slovakia/ Project is co-financed by sources of ES

6. REFERENCES

[1] G. List et al.: Wear behaviour of cemented carbide tools in dry machining of aluminium alloy, Wear, Vol. 259 (2005), pp. 1177 – 1189.

[2] Z. J. Pei et al: Rotary ultrasonic machining of potassium dihydrogen phosphate (KDP) crystal: An experimental investigation on surface roughness, Journal of Manufacturing Processes, Vol. 11(2009), pp. 66-73.

[3] Z. J. Pei, P. M. Ferreira: Modeling of ductile-mode material removal in rotary ultrasonic machining, International Journal of Machine Tools & Manufacture, Vol. 38 (1998), pp. 1399-1418.

[4] G. Ya et al: Analysis of the rotary ultrasonic machining mechanism, Journal of Materials Processing Technology, Vol. 125 (2002), pp. 182-185.

[5] Z. J. Pei, P. M. Ferreira: An experimental investigation of rotary ultrasonic face milling, International Journal of Machine Tools &

Manufacture, Vol. 39 (1999), pp. 1327-1344.

[6] I. Hrivňák: Zváranie a zvariteľnosť materiálov. STU v Bratislave: 2009. ISBN 978-80-227-3167-6

[7] Nickel Institute. Available on internet 20th April 2015: https://www.nickelinstitute.org/NickelUseInSociety/MaterialsSelectionAndUse/Ni-ContainingMaterialsProperties/HighNickelAlloysAndSuperalloys.aspx

[8] Ultrasonic 20 linear. Available on internet 22nd April 2013:http://www.dmg.com/en,ultrasonic,ultrasonic20linear?opendocument

[9] M. Beňo, M. Zvončan, M. Kováč, J. Peterka: Circular interpolation and positioning accuracy deviation measurement on five axis machine tools with different structures. In: Tehnicki Vjesnik - Technical Gazette. - ISSN 1330-3651. - Vol. 20, No. 3 (2013), pp. 479-484.

[10] M. Zvončan, M. Kováč, M. Beňo, M. Košinár: Laser interferometry measurement of different structured five axis machine tools´ positioning accuracy. In: International Doctoral Seminar 2011: Proceeding. Smolenice Castle, SR, May 15-17, 2011. ISBN 978-80-8096-145.

[11] Seco tool catalog. Available on internet 24th April 2013, pp. 89: http://pdf.directindustry.com/pdf/seco-tools/seco-tools-catalog-jabro-tools/5699-26231-_89.html

[12] M. Kútny: Aplikácia ultrazvukových kmitov na nástroj s definovanou geometriou rezného klina – čelnú stopkovú frézu. Master thesis. STU 2013.

[13] M. Kuruc, M. Zvončan, J. Peterka: Comparison of conventional milling and milling assisted by ultrasound of aluminum alloy AW 5083. In IN-TECH 2013: Proceedings of International Conference on Innovative Technologies, Budapest, Hungary 10.-13.09.2013. Rijeka: Faculty of Engineering University of Rijeka, 2013, pp.177-180. ISBN 978-953-6326-88-4.

[14] M. Kuruc, M. Zvončan, J. Peterka: Investigation of ultrasonic assisted milling of aluminium alloy AlMg4.5Mn. In Annals of DAAAM and Proceedings of DAAAM Symposium: 24th DAAAM Zadar 2013-10-23/26, p.[6]. ISSN 2304-1382.

[15] Surtronic 3+. Rapid on the shopfloor Surface Texture Measurement. Available on internet 25th April 2013: http://www.zimmerman.com.tw/uploads/sur3005-salesbrochure.pdf

[16] Roughness (2D) parameter. Available on the Internet 16th March 2014: http://www.olympus-ims.com/en/knowledge/metrology/roughness/2d_parameter/

[17] T. Vopát, J. Peterka, V. Šimna, M. Kuruc: The influence of different types of copy milling on the surface roughness and tool life of end mills. In Annals of DAAAM and Proceedings of DAAAM Symposium. Vol. 25, No 1 & Collection of Working Papers for 25th DAAAM International Symposium (2014), 9 p. ISSN 2304-1382.

[18] A. Thakur, S. Gangopadhyay: State-of-the-art in surface integrity in machining of nickel-based super alloys. In International Journal of Machine Tools and Manufacture. Vol. 100, January 2016, pp. 25-54. ISSN 0890-6955. Available on the Internet: http://www.sciencedirect.com/science/article/pii/S0890695515300730

Influence of selected parameters on the machining of sintered carbide by WEDM

V. Šimna [a], M. Kuruc [b], P. Pokorný [c], T. Vopát [d]

[a] Slovak University of Technology in Bratislava, Faculty of Materials Science and Technology in Trnava, Paulínska 16, 917 24, Slovak Republic, vladimir.simna@stuba.sk

[b] Slovak University of Technology in Bratislava, Faculty of Materials Science and Technology in Trnava, Paulínska 16, 917 24, Slovak Republic, marcel.kuruc@stuba.sk

[c] Slovak University of Technology in Bratislava, Faculty of Materials Science and Technology in Trnava, Paulínska 16, 917 24, Slovak Republic, peter.pokorny@stuba.sk

[d] Slovak University of Technology in Bratislava, Faculty of Materials Science and Technology in Trnava, Paulínska 16, 917 24, Slovak Republic, tomas.vopat@stuba.sk

Abstract

WEDM (Wire Electric Discharge Machining) is very complex and difficult process. For the improvement it is necessary to study this process and identify the impacts of all input variables to output variables. The article deals with the issue of cutting of sintered carbide by WEDM. Many parameters are involved in the process and these parameters interact with each other. The aim was to clarify the impact of input parameters to the cutting process and to find those parameters to make the process as fast as possible and stable. Sintered carbide type K (PCG GMBH F10) was used as the sample. The experiment was performed on the machine Agie Charmilles Robofil 310. As input factors were selected pulse width, time between two pulses, servo voltage, pulse current, short pulse time and frequency. Due to the fact that it is necessary to assess the impact of a several input parameters, Taguchi experimental design was selected. L27 matrix was used. Screening experiment was used in the first part of the experiment. This experiment was necessary to perform because ANOVA cannot handle operate without measured parameters. It is necessary to avoid wire braking in each measurement of the value of MRR (Material Removal Rate). The rupture of the wire is of course also relevant results, and determining the area in which the wire rupture is at least as important as the detection of the impact of the MRR parameters, but the breakage of the wire cannot be expressed numerically. Setting levels of the variable factors in the screening experiment were elected to the extent possible the machine so that it could determine when a cutting process is stable. Parameters which were the highest influence on the stability of cutting process were able to determine after performing of the screening experiment. To evaluate the final experiment, ANOVA (Analysis of variance) was used.

Keywords: WEDM, electric erosion, material removal rate, dielectric, sintered carbide

1. INTRODUCTION

Material Removal Rate (MRR) is generally expressed as a proportion of the volume of removed material and time for which it has been taken. Sometimes it is expressed as a weight of removed material for a time. In the case of EDM wire cutting, for the calculation is most commonly used formula [1]:

$$MRR = v_c . B . H \, [mm^3 . min^{-1}] \quad (1)$$

Where:

v_c *-cutting speed [mm.min^{-1}],*

B *-width of the cut [mm],*

H *- height of the cut*

The basic parameters of wire EDM can be considered following: pulse on time, pulse off time, voltage, peak current, discharge current, flushing pressure of dielectric fluid, wire feed rate and wire tension. Each of these parameters (except wire tension and wire feed rate) has huge influence to cutting process, which is explained in detail in [2].

Research of the relationship between the cutting speed and input parameters has been described in [3]. The cemented carbide has been machined. It has been found that the increase of pulse duration leads to a higher cutting speed, greater duration of the pulse off time, the more cutting speed decreases and the voltage affects the cutting speed inversely and with increasing discharge current cutting speed increases.

It was found that the discharge current and the discharge pulse duration have a greater impact than other observed parameters on the MRR, surface roughness and wear wire [4].

In [5] has been proved, discharge frequency, voltage, pulse duration and wire feed rate has the greatest influence on the MRR.

S. R. NITHIN ARAVIND et al (2012) [6] presents the experimental study to select best suitable value of voltage, current, speed, pulse on/off time in order to get maximum metal removal rate (MRR) and minimum surface roughness (SR).

Relevant results can also be found in [7,8,9,10,11,12]

2. METHODS AND MATERIALS USED FOR RESEARCH

As workpiece material, sintered carbide PCG GMBH F10 was used. This is a cemented carbide with a fine structure where the main component is tungsten carbide in a cobalt matrix, and it is included in K group. The experiment was carried out on the Charmilles ROBOFIL 310 machine, which is a CNC machine for wire EDM. The diameter of the CuZn37 wire was 0.25 mm. Wire tensile strength R_e was 980 N.mm^{-2}. As dielectricum deionized water was used. Conductivity of the dielectricum was 5μS.

2.1. Experimental setup

For this experiment Taguchi experimental design was used. Six parameters were used at three levels, as can be seen in the Tab.1. It means L27 orthogonal array was used.

Table 1. Used parameters

Parameter	Unit	Level		
		L1	L2	L3
A	μs	0.4	0.5	0.6
B	μs	16	20	24
Aj	V	30	40	50
Ws	m.min^{-1}	5	10	15
TAC	μs	0.2	0.5	0.8
FF	%	50	75	100

Considering literature study and screening experiment, following parameters: pulse width (A), time between two pulses (B), Servo voltage (A_j), Wire speed (W_s), Short pulse time (TAC) and frequency were selected. Voltage between electrodes was set to 80V.

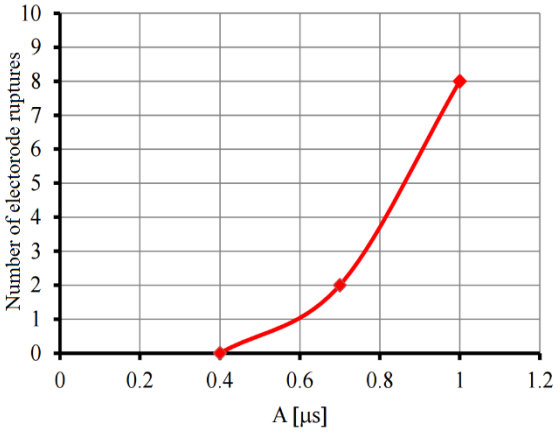

Fig. 1. Relation between pulse width and number of electrode ruptures

The result of the experiment was to find a stable cutting area. It was found that the greatest impact on the breakage of the electrode has a pulse width (A). Increasing the pulse width, the process becomes unstable, as can be seen in the Fig. 1.

3. RESULTS AND ACHIEVEMENTS

In the Table 1. Can be seen the experiment results. For each measurement the MRR value was recorded and the value of S/N ratio was calculated (2).

Table 2. Measured values and S/N ratios

	Parameters							
N	A	B	A_s	W_s	TAC	FF	MRR [mm^3/min]	SN Ratio [dB]
1	0.4	16	30	5	0.2	50	9.9	19.9127
2	0.4	16	30	5	0.3	75	14.9	23.4637
3	0.4	16	30	5	0.4	100	19.8	25.9333
4	0.4	20	40	10	0.2	50	7.8	17.8419
5	0.4	20	40	10	0.3	75	12.2	21.7272
6	0.4	20	40	10	0.4	100	15.0	23.5218
7	0.4	24	50	15	0.2	50	5.7	15.1175
8	0.4	24	50	15	0.3	75	7.8	17.8419
9	0.4	24	50	15	0.4	100	10.0	20.0000
10	0.5	16	30	5	0.2	50	14.2	23.0458
11	0.5	16	30	5	0.3	75	18.0	25.1055
12	0.5	16	30	5	0.4	100	11.9	21.5109
13	0.5	20	40	10	0.2	50	10.8	20.6685
14	0.5	20	40	10	0.3	75	13.6	22.6708
15	0.5	20	40	10	0.4	100	8.2	18.2763
16	0.5	24	50	15	0.2	50	12.0	21.5836
17	0.5	24	50	15	0.3	75	15.9	24.0279
18	0.5	24	50	15	0.4	100	10.4	20.3407
19	0.6	16	30	5	0.2	50	17.5	24.8608
20	0.6	16	30	5	0.3	75	11.8	21.4376
21	0.6	16	30	5	0.4	100	15.7	23.9180
22	0.6	20	40	10	0.2	50	18.0	25.1055
23	0.6	20	40	10	0.3	75	13.2	22.4115
24	0.6	20	40	10	0.4	100	19.0	25.5751
25	0.6	24	50	15	0.2	50	18.2	25.2014
26	0.6	24	50	15	0.3	75	10.7	20.5877
27	0.6	24	50	15	0.4	100	14.9	23.4637

$$S/N_{bigger} = -10log_{10}\left[\frac{\sum_{i=1}^{n}\left(\frac{1}{y_i}\right)^2}{n}\right] \quad (2)$$

Where:

n - *number of repetition,*

$\mathbf{y_i}$ - *is the measured value of the required characteristic*

Wire has not been interrupted when measured, that confirming the relevance of the screening experiment. ANOVA is a generalization of Student's t test for independent selections. using it shall examine the impact of factors on the observed response. The following table calculated ANOVA for individual impact of each factor on the MRR significance α= 0.05. If the *P* value less than 0.05, it is the statistical factor significant (significance level α). For the analysis of variation data set (ANOVA) needs to be examined if measured value and the signal / noise ratio meet normal probability division. In this case, measured values and S/N ratio values meets this requirement as can be seen in the Figure 2.

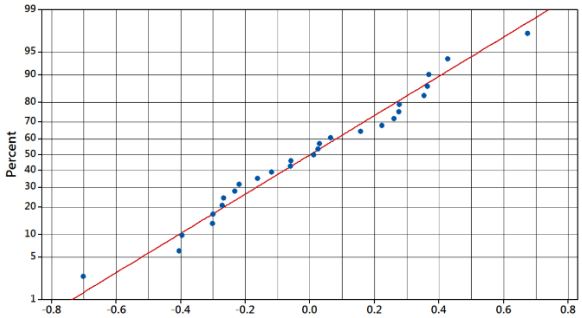

Figure 2. S/N ratio normal probability

Table 3. ANOVA for S/N Ratio

	DF	Seq SS	Adj SS	Adj MS	F	P
A	2	41.328	41.328	20.6638	110.48	0.000
B	2	24.613	24.613	12.3064	65.79	0.000
Aj	2	33.031	33.031	16.5155	88.30	0.000
Ws	2	1.235	1.235	0.6176	3.30	0.067
TAC	2	4.837	4.837	2.4183	12.93	0.001
FF	2	85.863	85.863	42.9313	229.53	0.000

In the Table 3. can be seen the results from analysis of variance. Statistically significant parameters related to measured data (significance level $\alpha = 0.05$) are the parameters A, B, A_j, TAC and FF. W_s parameter appears to be not statistically significant because of the value of P=0.067, and this is more than 0.05.

Table 4. Response table for S/N ratio

Level	A	B	Aj	Ws	TAC	FF
1	20.60	23.24	23.15	22.24	21.48	19.72
2	21.91	21.98	22.45	22.14	22.14	22.37
3	23.62	20.91	20.53	21.75	22.50	24.05
Delta	3.02	2.34	2.62	0.50	1.02	4.33
Rank	2	4	3	6	5	1

The biggest impact on material removal rate was observed at the frequency (FF) after followed by parameters in order pulse width (A), servo mean voltage (A_j), time between the two pulses (B), short pulse time (TAC) and finally unwinding speed of the wire (Ws). To determine the effects of the response is used Main Effects Plot (Fig. 3). These charts explain whether the given parameters and feedback direct or indirect dependence.

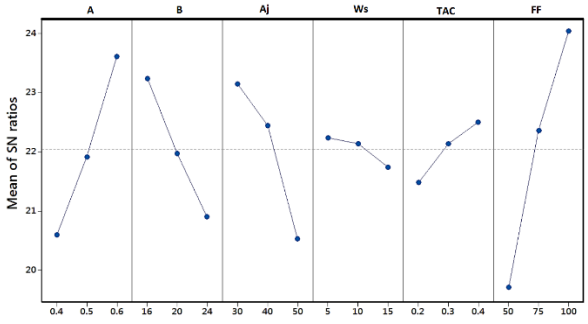

Figure 3. Dependence between S/N Ratio and input factors levels

The object of this experiment is to maximize the MRR. From the Fig.3 is clear, that the highest material removal rate in the measured range for given conditions in the following optimal settings of factors: A = 0.6 µs (level 3), B = 16 µs (level 1), A_j = 30 V (level 1), W_s = 5 m.min^{-1} (level 1), TAC = 0.4 µs (level 3), FF = 100 % (level 3).

4. CONCLUSION

Performing screening experiment, the stable area for final experiment was established. Influence of each parameter on the MRR was observed from the final experiment. A pulse width had a significant effect on the MRR and affect the response was 20% i.e. the second highest. This result is in line with the findings published by [3] SHAYAN, A. V, AFZA, R. A. a TEIMOURI, R. Increasing the pulse width (A) increases the MRR. The optimal value for this parameter is 0.6 µs.

The time between two pulses B does not quite correspond with [1] SHARMA, N., KHANNA, R. a GUPTA, R., because the level of impact is approximately one half smaller than the period between two pulses B. Has been confirmed that this parameter has a statistically significant effect on the MRR, and the increase of this parameter material removal rate decreases. It also has interaction with the pulse width, servo mean voltage and the speed unwinding wire. Its optimal value in this condition is 16 µs.

Servo mean voltage (A_j) has a significant influence on the MRR, which has the third biggest impact. Its increasing material removal rate decreases. The optimal value is 30V.

As expected, the rate unwinding the wire Ws has proved as statistically insignificant. Its degree of influence on the material removal rate reached 1%. However, the rate unwinding the wire had interactions with pulse width (A), time between two pulses (B) and servo mean voltage (A_j).

Short pulse time TAC had a statistically significance, but the degree of its impact reached only 2.5%, the second lowest after the Ws.

The biggest impact on the intensity of the material removal rate has frequency FF. Its share of the overall result is up 44.37%. Increasing the frequency leads to a significant increase material removal rate. Frequency does not interact with any other parameter except TAC.

5. ACKNOWLEDGEMENTS

The article was written within the project VEGA 1/0477/14. Research of influence of selected characteristics of machining process on achieved quality of machined surface and problem free assembly using high Technologies.

6. REFERENCES

[1] SHARMA, N., KHANNA, R. a GUPTA, R. 2013. Multi Quality Characteristics of WEDM Process Parameters with RSM. Procedia Engineering. 64.710-719. ISSN 1877- 7058.

[2] SINGH, H. a GARG, R. 2009. Effects of process parameters on material removal rate in WEDM. Journal of Achievements in Materials and Manufacturing Engineering. 32(1). 70-74. ISSN 1734-8412.

[3] SHAYAN, A. V, AFZA, R. A. a TEIMOURI, R. 2013. Parametric study along with selection of optimal solutions in dry wire cut machining of cemented tungsten carbide (WC-Co). Journal of Manufacturing Processes. 15(4). 644-658. ISSN 1526-6125.

[4] RAMAKRISHNAN, R. a KARUNAMOORTHY, L. 2006. Multi response optimization of wire EDM operations. The International Journal of Advanced Manufacturing Technology. 29(1-2).105-112. ISSN 1433-3015.

[5] LIAO, Y. S., HUANG, J. T. a SU, H. C. 1996. A study on the machining-parameters optimization of wire electrical discharge machining. Journal of Materials Processing Technology. 487-793. ISSN 0924-0136.

[6] S. R. NITHIN ARAVIND, S. SOWMYI and K. P. YUVARA 2012. Optimization of metal removal Rate and surface roughness on Wire EDM using taguchi method, IEEE-International Conference On Advances In Engineering, Science And Management (ICAESM -2012) March 30, 31.

[7] SANDEEP, Malik. 2014. OPTIMIZATION OF MACHINING PARAMETERS OF EN24 ALLOY STEEL ON WEDM USING RSM. International Journal of Advanced Research in IT and Engineering. 3(3). 9-20. ISSN 2278-6244.

[8] YUAN, J., WANG, K., YU, T. a FANG, M. 2008. Reliable multi-objective optimization of high-speed WEDM process based on Gaussian process regression. International Journal of Machine Tools & Manufacture. 48(1). 47-60. ISSN 0890-6955.

[9] JAHAN, M.P., RAHMAN, M. a WONG, Y.S. 2011. A review on the conventional and micro-electrodischarge machining of tungsten carbide. International Journal of Machine Tools & Manufacture. (51), 837–858. ISSN 0890-6955

[10] KOZAK, J., RAJURKAR, K. P. a CHANDARANA, N. 2004. Machining of low electrical conductive materials by wire electrical discharge machining (WEDM). Journal of Materials Processing Technology. (1149), 266–271. ISSN 0924-0136.

[11] KUMAR, A, KUMAR, V. a KUMAR, J. 2011. Effect of Machining Parameters on MRR during CNC WEDM of Pure Titanium. Gujarat: S.V. National Institute of Technology.

[12] LIAO, Y.S. a YU, Y. P. 2004. The energy aspect of material property in WEDM and its application. Journal of Materials Processing Technology. 77–82. ISSN 0924-0136.

Review of Anomaly-Based IDS Algorithms

László Göcs[a], Zsolt Csaba Johanyák[a], Szilveszter Kovács[b]

[a] Department of Information Technology, Pallas Athena University, GAMF Faculty of Engineering and Computer Science, Kecskemét, H-6001 Pf. 91, {gocs.laszlo, johanyak.csaba}@gamf.kefo.hu

[b] Department of Information Technology, University of Miskolc, Miskolc-Egyetemváros, Miskolc, H-3515, Hungary, szkovacs@iit.uni-miskolc.hu

Abstract

Intrusion detection systems (IDSs) can provide an effective solution for the information security needs of a company. Well configured IDSs are able to automatically recognize attacks that target either networks or hosts. IDSs can be categorized based on different aspects or properties. The intrusion detection approach is one of the most important properties of the IDS algorithms. Based on it one can identify signature based and behaviour based solutions. While the signature based approach tries to recognize attacks by using a database of known attack signatures, the behaviour based one first learns the normal behaviour of the supervised system and after finishing the learning process tries to identify anomalies, i.e. significant deviations from the normal behaviour.

In this paper, after presenting the main ideas of the functioning of behaviour based IDSs we do a survey on the currently most important anomaly detection types. Thus key features of statistical based, knowledge based, and computational intelligence based techniques are introduced. In the latter case methods applying fuzzy logic, neural networks, and clustering are described as well. Advantageous and disadvantageous features of the different approaches are also presented.

Keywords: information security, signature based IDS, behaviour based IDS, Anomaly-Based IDS, fuzzy logic, neural networks, clustering.

1. INTRODUCTION

An intrusion detection system (IDS) is a software or hardware solution that automates the monitoring and analysis of the network traffic and user activities to strengthen the security of an information system. The intrusion detection consists of two basic processes, i.e. monitoring the underlying system activities and analysing the resulting log data [1]. Generally, IDSs can be classified into two types based on the considered information source, i.e. Host based Intrusion Detection Systems (HIDS) and Network based Intrusion Detection Systems (NIDS) [2]. While members of the first group mainly work with local (operating system related) information IDSs belonging to the second group monitor network related events. This paper focuses on the latter type.

An NIDS contains one or more sensors connected to network interface cards that acquire information about network traffic volume, used protocols, source and destination IP addresses, service ports, etc. [7]. This IDS type usually is deployed in a segment or on the border of a network, and mainly investigates the network traffic. Usually it is capable to monitor and protect several systems and devices.

The type of the applied analysis is the most important aspect taken into consideration for the categorization of NIDSs. Conform to it one can

identify anomaly detection and signature detection based IDSs [3].

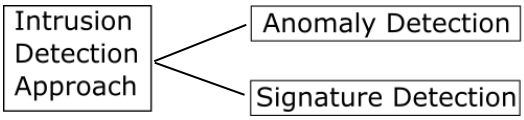

Fig. 1. Categorization of IDSs based on the applied analysis

While signature based IDS solutions look for the existence of known patterns or signatures the anomaly detection technics compare the actual behaviour of the system to its estimated "normal" behaviour. The advantage of the latter approach lies in the potential capability to recognize new intrusion types [7]. Being an intensively investigated and developing area our paper focuses on the anomaly detection based approaches.

The rest of this paper is organized as follows. Section 2 presents the main ideas of anomaly based IDSs as well as the three main subtypes. Section 3 is entirely dedicated to the computational intelligence based BIDSs.

2. ANOMALY DETECTION BASED IDSs

Although there are some differences between the anomaly detection based IDS (also called Behavior based IDSs - BIDS) subtypes but generally they can function on two different modes (see Fig. 2). In case of the training mode the system is fed with sensor data that describes the typical (normal) network and user behaviour. This input is transformed and formalized into the so called normal behaviour profiles by the parameterization module. Based on these profiles the training module creates a normal behavioural model for the network automatically, manually or in a combined way. Next, the BIDS is switched into the detection mode when it is used for its main purpose, i.e. the strengthening of the network security.

In the detection mode the actual sensor data is converted into actual profile by the parameterization module and the detection module compares it with the previously created model. Based on the acquired knowledge the detection module strives to determine whether the analysed activity is harmful to the system or not.

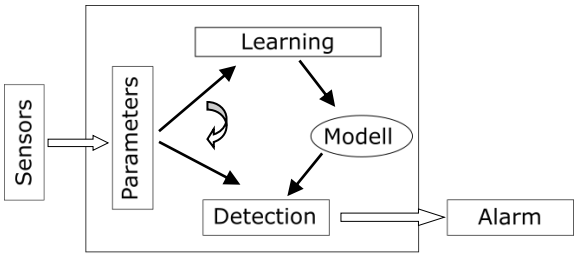

Fig. 2. BIDS functional architecture [7]

BIDSs create statistics for the logon time, the time a user was logged in, the usually accessed files, as well as for the frequency of the modification and movement of these files, etc. The advantage of the anomaly based approach is its fast and dynamic adaptation capability to unknown attack types.

The disadvantage of BIDSs is that they alert the administrator and take counter measures more often than knowledge-based IDSs due to their high rate of false alarms [9]. Additionally, a BIDS is less efficient in case of systems whose behaviour pattern is not static enough for the creation of statistics or in case of systems where user activity is not monotonous. One has to take extra precautions in course of the learning period to avoid the possibility of "learning" an actual intrusion as a normal behaviour [4].

BIDSs can be classified into three main categories based on the data processing mode, i.e. statistical based, knowledge based, and computational intelligence based. The following three subsections describe them briefly.

2.1. Statistical based BIDSs

Statistical based BIDSs monitor the network traffic, examine the communication speed, the used protocols and IP addresses focusing on the differences from the allowed values. It examines the current profile by comparing it to the normal profile. If an anomaly occurs in the network the anomaly measure is also calculated. If it exceeds a predefined threshold an alarm is activated.

This IDS type follows different activities and creates reports about malicious activities using statistical methods. Its shortcoming is its relative high rate of categorizing an attack occurring in course of the normal traffic as a normal activity [5].

2.2 Knowledge based BIDSs

Knowledge based BIDSs work with a database containing information about previous attacks. It is decided based on this samples whether the monitored activity is categorized as a hostile one or not. Actually this is the most used BIDS model. Its advantage is that it blacklists mistakenly significantly less traffic than the other approaches. Furthermore, in almost all of the cases it uses standard alerts that are easily understandable for system administrators. However, its demand on continuous update and maintenance of the sample database can be considered as a drawback. Moreover, this type of IDS cannot recognize new attack types. This shortcoming can result in whitelisting a new, previously unknown attack type and allowing it access to the system.

2.3 Computational Intelligence based BIDSs

Computational intelligence (CI) based BIDSs can recognize and define rules and regularities independently or with human help based on sample data. They not only learn samples but also became capable of making decisions on their own in case of previously unseen data. CI based BIDSs also use statistical analysis techniques to improve their performance. However, they usually require big computational resources owing to the huge amount of data to be processed.

3. COMPUTATIONAL INTELLIGENCE BASED BIDS APPROACHES

Computational Intelligence (CI) comprises a family of nature inspired heuristics methods that support various calculations related to artificial intelligence tasks [8]. Frequently used tools from this family are fuzzy logic, artificial neural networks as well as clustering and several optimization techniques. In this section, three CI based BIDS approaches are presented, namely artificial neural networks, fuzzy logic and clustering based BIDSs.

3.1 Artificial Neural Network

ANNs are the most commonly used soft computing technique in IDSs. An ANN is a processing system that is inspired by the biological nervous systems. It is composed of a large number of highly interconnected processing elements (called neurons) that are working together to solve specific problems. Each neuron is basically a summing element followed by an activation function.

Some IDS designers apply ANN as a pattern recognition technique [20]. Pattern recognition can be implemented for example by using a feed-forward neural network that has been trained with a sample data set. When the initial training process of the neural network is is finished the ANN identifies the current input pattern and it outputs the corresponding class. In case of the lack of an exact match the neural network gives an output, which corresponds to the known input pattern that is the least different one from the given pattern [17].

For example Kukiełka and Kotulski [18] proposed a distributed IDS system having three modules, i.e. the central module, the Net-LAN monitor and the H&N monitor. While the two monitors analize host log data and network data respectively, the central module is responsible for alerting the end user and retraining the system with new data vectors.

Ryan et al. presented anomaly neural network based intrusion detection system called NNID [21] of which presumption was that the user leaves a “print” when using a computer system. This “print” is described as a feature vector that contains among others the connections of a single user during a whole day and information

regarding the 100 most important commands they used. The vector can be learned by an ANN and so later the ANN can identify the current user. If the actual behaviour does not match the "print" a possible intrusion is in progress and the system administrator is alerted. NNID applied backpropagation ANN and achieved an accuracy of 96%

3.2 Fuzzy logic

Although on the surface there are always exact facts and numerical data the process of intrusion detection has to deal with vague boundaries between normal behaviour and anomalies. Besides being able to handle the inherent vagueness fuzzy logic based solutions also provide a self-explaining capability that can be a useful characteristic when analysing their functioning. Furthermore, they can easily incorporate human expert knowledge expressed in form of IF-THEN rules (see Fig. 4.).

IF unusual_connection_count is high AND destination_host_count is high AND observed_service_port_count is medium_low THEN service_scan_possibility is high

Fig. 4. Example rule for the detection of a host scan on a given port aiming the identification of a server [16]

There are several possible application areas for the fuzzy approach in the field of intrusion detection. For example Bridges et al. [12] proposed a system that in the training phase creates a fuzzy normal behaviour profile from intrusion free log data using data mining techniques and by creating fuzzy association rules. Later in the detection phase new association rules are created from the actual log data and the decision is made based on a similarity assessment. Anomaly detection can also be viewed as an outlier detection (exception mining) problem where the outlier points represent abnormal behaviour, i.e. a possible attack against the protected system.

Chimplee et al. [13] used fuzzy c-means clustering for the identification of intrusion attempts. They applied correlation analysis based feature selection in order to reduce the dimensionality of the problem. The fuzzy concept can find application at a higher level as well. Decision fusion can employ fuzzy logic (e.g. [14]) for making a final decision when more than one different techniques are used for intrusion identification purposes.

3.3 Clustering and identification of outliers

The goal of cluster analysis is to identify groups of objects in such a way that group members are more similar (close) to each other than to members of other groups. [11]. An outlier is an object that is distant from other objects and is not considered as member of any clusters. It can arise as a result of some kind of anomaly, which presents a potential applicability in intrusion system development.

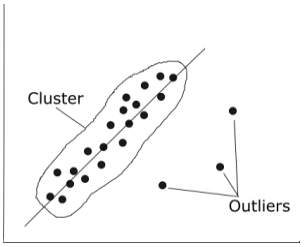

Fig. 5 Cluster and outliers

Scherer et al. [15] investigated the usage of Farthest First Traversal (FFT), K-means and COBWEB/CLASSIT algorithms for clustering and support vector machine (SVM) for classification. Taking into consideration different attack types K-means based clustering ensured the best average results.

4. CONCLUSIONS

Intrusion detection systems have become a very important component of the defence systems of individual computers and computer networks facing various threats of malicious activities. Although the IDS technology has a long history with several approaches and solutions this field is in continuous development.

This paper presented a survey on a main category of IDSs, i.e. anomaly based intrusion detection approaches. Depending on the applied data processing mode three main BIDS categories were identified. Beside the classical

solutions the computational intelligence based approach has gained more and more attention recently. Here fuzzy logic and artificial neural networks proved to be two straightforward options especially due to the proper hardware resource ensured by the current devices.

5. ACKNOWLEDGEMENTS

This research was supported by the Foundation for the Development of Automation in Machinery Industry.

6. REFERENCES

[1] Hazem M. El-Bakry, Nikos Mastorakis A, "Real-Time Intrusion Detection Algorithm for Network Security", WSEAS Transactions on communications, Issue 12, Volume 7, December 2008.

[2] Vishal Parande, Prof. Sharada Kori: "Host Based Intrusion Detection System", International Journal of Science and Research (IJSR) ISSN (Online): 2319-7064, Volume 4 Issue 4, April 2015. pp. 559-561

[3] LiberiosVokorokos, Anton BALÁŽ, Martin Chovanec: "Intrusion Detection System Usig Self Organizing Map", ActaElectrotechnica et Informatica No. 1, Vol. 6, 2006

[4] L. Göcs, Z. C. Johanyák: "Survey on Intrusion Detection Systems", Faculty of Mechanical Engineering, University of Belgrade, October 15-16, 2015, ISBN 978-86-7083-877-2, pp. 167-170.

[5] Davood Kheyri, Mojtaba Karami: "A Comprehensive Survey on Anomaly-Based Intrusion Detection in MANET", Published by Canadian Center of Science and Education, Computer and Information Science; Vol. 5, No. 4; 2012, ISSN 1913-8989 E-ISSN 1913-8997

[6] Roberto Di Pietro, Luigi V. Mancini: "Intrusion Detection Systems" ISBN: 978-0-387-77265-3, pp 4. 2008

[7] P. Garcıa-Teodoro, J. Diaz-Verdejo a , G. Macia-Fernandez, E. Vazquez, "Anomaly-based network intrusion detection: Techniques, systems and challenges," Computers & Security 28 (2009), pp. 18-28.

[8] Shelly Xiaonan Wu, Wolfgang Banzhaf: „The use of computational intelligence in intrusion detection systems: A review", Applied Soft Computing 10 (2010) pp. 1–35.

[9] LiberiosVokorokos, Anton BALÁŽ, Martin Chovanec: "Intrusion Detection System Usig Self Organizing Map", ActaElectrotechnica et Informatica No. 1, Vol. 6, 2006

[10] SANS Institute InfoSec Reading Room: „Application of Neural Networks to Intrusion Detection", SANS Institute, 2001

[11] Dr. Varga Beatrix, Szilágyi Roland: "Kvantitatív információképzési technikák" Nemzeti Tankönyvkiadó, 2011

[12] Bridges, Susan M., and Rayford M. Vaughn, "Fuzzy Data Mining and Genetic Algorithms Applied to Intrusion Detection," Proceedings of the Twenty-third National Information Systems Security Conference, Baltimore, MD, October 2000. http://web.cse.msstate.edu/~bridges/papers/nissc2000.pdf

[13] W. Chimphlee, A.H. Abdullah, M.N. Md Sap, S. Chimphlee, and S. Srinoy, "Unsupervised Clustering Methods for Identifying Rare Events in Anomaly Detection," World Academy of Science, Engineering and Technology International Journal of Computer, Electrical, Automation, Control and Information Engineering Vol:1, No:8, 2007, pp. 2562-2567 http://waset.org/publications/2474/unsupervised-clustering-methods-for-identifying-rare-events-in-anomaly-detection

[14] J. Tian, Y.Fu, Y. Xu,J. ling Wang, Intrusion detection combining multiple decision trees by fuzzy logic, in: Proceedings of the Sixth International Conference on Parallel and Distributed Computing, Applications and Technologies (PDCAT'05), 5–8 December 2005, IEEE Press, 2005, pp. 256–258.

[15] Peter Scherer, Martin Vicher, Pavla Drazdilova, Jan Martinovic, Jirí Dvorsky, and Vaclav Snasel: "Using SVM and Clustering Algorithms in IDS Systems" Dateso 2011, pp. 108-119, ISBN 978-80-248-2391-1.

[16] J.E. Dickerson, J. Juslin, O. Koukousoula, J.A. Dickerson, "Fuzzy Intrusion Detection", IFSA World Congress and 20th NAFIPS International Conference, 2001, Vol 3., DOI: 10.1109/NAFIPS.2001.943772, pp. 1506 – 1510.

[17] E.Kesavulu Reddy, Member IAENG: „Neural Networks for Intrusion Detection and Its Applications", Proceedings of the World Congress on Engineering 2013 Vol II,

[18] Przemysław Kukiełka, Zbigniew Kotulski: "Adaptation of the neural network-based IDS to new attacks detection", http://arxiv.org/abs/1009.2406, 2010, visited: 30.08.2016

[19] Mehdi Moradi And Mohammad Zulkernine: "A Neural Network Based System for Intrusion Detection and Classification of Attacks", Proceedings of the 2004 IEEE international conference on Advances in Intelligent Systems, 2004

[20] E.Kesavulu Reddy, Member IAENG: "Neural Networks for Intrusion Detection and Its Applications", Proceedings of the World Congress on Engineering 2013 Vol II.

[21] Ryan, Jake, Meng-Jang Lin, and Risto Miikkulainen. "Intrusion detection with neural networks." Advances in neural information processing systems (1998): 943-949.

Survey on SDN Programming Languages

Péter András Agg [a], Zsolt Csaba Johanyák [a], Szilveszter Kovács[b]

[a] Pallas Athena University, GAMF Faculty of Engineering and Computer Science, Kecskemét, Hungary, H-6001 Pf. 91, {agg.peter, johanyak.csaba}@gamf.kefo.hu

[b] University of Miskolc, Miskolc-Egyetemváros, Miskolc, H-3515, Hungary, szkovacs@iit.uni-miskolc.hu

Abstract

Software-Defined Networking (SDN) offers solutions for several difficulties of network configuration and control by separating the control logic of the network from the underlying hardware components and applying a logical centralization. Having software in focus the services and features offered by the used programming languages play a key role in the effective application development in this field.

These languages allow for users to determine different network configuration rules, for example the access control lists (ACLs). They can also provide specialized abstractions to cope with other management requirements, like monitoring. There are several available tools starting from low level languages up to high level languages. The former ones offer a framework to program computer networks through the Control to Data-Plane Interface (CDPI), which is similar to assembly languages and is not an easy way to control the network. On the contrary, high-level programming languages are easy-to-learn and can be powerful tools that ensure the quality of different important properties and functions of SDNs such as network-wide structures, modular composition, as well as virtualization.

Although at the moment there is no consensus on the programming technology to be applied, SDN will be the future for controlling computer networks. In this paper, we do a survey on the applicable languages starting from the low level ones like OpenFlow up to high level ones like Pyretic. The development of the available languages starting from 2009 is presented as well. Various programming problems and examples are also shown to compare the different levels of programing languages. Major features, application fields, advantages and disadvantages of the presented tools are discussed as well.

Keywords: SDN, Software-Defined Networks, SDN programming language, Networks, OpenFlow, Pyretic

1. INTRODUCTION

Software-Defined Networking (SDN) supports a centralized programming model for managing computer networks. SDN programming languages allows to the programmer to use simple programming language constructs to declare centralized algorithmic policies, which will be responsible for the behaviour of an entire network. These policies have to be translated into a language, which can be understood by the switches. SDN-compliant switches use a low-level interface. The controllers provide Application Programming Interfaces (APIs), which are also low-level tools. The high level languages support a good chance to program and control the network. There are many SDN programming languages that use different functionalities and focus on solving several network problems.

This paper is organized as follows. Section 2 reviews the main ideas of Software-Defined Networking. Section 3 gives a summary of the Low-level Programming, the API-based Programming and the Domain-Specific Language Programming. Section 4 presents eight SDN programming languages and shows some examples written in this languages as well.

2. SOFTWARE-DEFINED NETWORKING

Software-Defined Networking (SDN) allows the control over the functionality of a computer network, allowing its redefinition or modification. SDN is is based on an open architecture, which makes the network configuration and management flexible and programmable. The SDN architecture has three layers [1], i.e. the Data Plane, the Control Plane and the Application (Management) Plane (see Fig. 1).

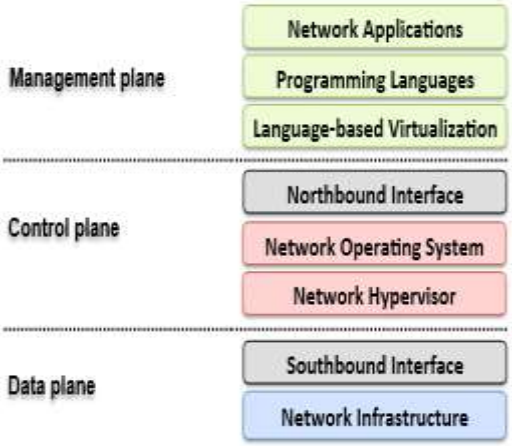

Fig. 1. SDN architecture [1]

The lowest layer of the SDN architecture is the Data Plane, which is also known as Forwarding Plane. This layer contains the forwarding physical devices like network devices, switches, etc. [1]. These hardware elements use a matching table to send the packets to the destination address. They implement a Control-Data-Plane Interface (CDPI) agent to communicate with the Control Plane layer.

The CDPI is often called Southbound Interface. This interface is defined between Data Plane and Control Plane layers and helps us by programmatic control of all sending operations. The most used CDPI is OpenFlow [2]. It was developed by researchers from the Berkeley and Stanford universities. OpenFlow makes possible overriding and modifying the network behavior.

There are many other available tools as well, like Network configuration protocol (NETCONF) [3], Protocol Oblivious Forwarding (POF) [4], New, and Open Policy Framework (OpFlex) [5].

The key part of the Control Plane layer is the controller. It allows SDN applications to exchange information with the Management Plane via the Northbound Interface (NBI). There are several controller solutions, like NOX [6], POX [7], or OpenDayLight [8].

The Northbound Interface connects the Control Plane and the Application Plane. It enables the specification of the network behaviour and requirements.

The Application (Management) Plane is the third and the uppermost level in the SDN architecture. This plane is responsible for the selection and use of one or more SDN Applications, which consist of Application Logic and NBI Drivers. These applications define the behaviour of the network and the network related requirements for the SDN controller using the NBIs.

3. SDN PROGRAMMING

When a network device receives a new packet, first it looks in its flow tables for an entry matching of the packet header fields, which may be the destination physical address (MAC address) or the logical address (IP address). If it finds a matching entry, the device tries to deliver the package. If no match is found, the packet will be sent to the controller. The controller manages the tables of the switch by adding, modifying, or removing some entries depending on the necessary task.

These applications can be programmed at three different levels: low-level programming, API-based programming, and Domain-Specific Language based programming [9].

In case of *Low-level Programming* the networks are programmed directly through CDPI. This approach can be considered as the assembly language of network programming. Using Low-level Programming one has to manipulate bit patterns in packets being careful with the shared rule-table space. The administrator has to program devices one by one, and the errors has to be handled manually. At this programming level, one has to use a

General-Purpose Language (GPL) (for example C/C++, Java, C#, Python, or shell script) to exchange CDPI messages on the switches.

In case of *API-based Programming* applications use the Application Programming Interfaces (APIs) exposed by the controllers at this programming level. These programs are translated by the controller into CDPI messages. Generally API-based Programming has the same problems as Low-level Programming. The controllers may use one of the two API types, i.e. *local* or *remote*.

SDN applications that use *local APIs* are implemented in the controller using classes, methods, and interfaces of the controller. The programmer usually writes these applications in the controller's own language, and they can run only on the given host (controller).

Remote APIs provide an abstraction layer between the two different environments. These allow for the different technologies to exchange information among each other, using either Extensible Markup Language (XML) or JavaScript Object Notation (JSON). Applications using this type of API can be written in any GPL and one can run them on a different host as well. The source code of remote APIs is cleaner than the local APIs based one [10].

A *Domain-Specific Language* (DSL) is a programming language that offers, through appropriate notations and abstractions, expressive power focused on, and usually restricted to, a particular problem domain [11]. DSLs have a compiler (or framework), which is responsible for translating high level instructions into a language that will be understood by a controller API. DSLs are usually declarative. DSLs ensure a high-level development tool by adding new abstractions for different programming aspects, such as monitoring, security, and virtualization. They also facilitate the optimization of network resource utilization.

While some DSLs are problem specific instruments, others provide more general abstractions, and can be used to create a broader range of network applications.

4. SDN PROGRAMMING LANGUAGES UNDER THE LOUPE

This section gives an overview of eight SDN programming languages presenting them in chronological order, and discussing their evolution and the relationships among them. We start with Flow-based Management Language (FML) [12], which was the first SDN programming language. Next, two branches of SDN programming languages are shown. The first one contains only two languages (Nettle [14] and Procera [16]) that are very useful, but not frequently used. The second branch is more commonly used and contains five languages (Frenetic [18], NetCore [19], Frenetic-OCaml [20], Pyretic [22], and NetKAT [24]). These languages are strongly related, they evolved from each other.

4.1. Flow-based Management Language

Flow-based Management Language (FML) is the first SDN programming language. FML is a language for specifying policies about flows. FML is based on non-recursive Datalog [13] with negation, where each statement represents a simple if-then relationship. FML is able to statically allow and/or deny specific flows depending on the actual task.

In the example presented below FML uses static policy to allow flows from TCP port 443 and IP source 10.1.1.1:

$$allow(Flow) \Leftarrow Prot = 443 \wedge H_s = 10.1.1.1$$

By using external information sources one can write policies as well. Although maximum values for jitter, bandwidth and latency can also be specified with parameters but the usage of this configuration type is not typical.

4.2. Nettle

Nettle [14] was the second SDN programming language. It makes possible programming OpenFlow networks in a declarative style. The programming paradigm of Nettle is based on the facts of Functional Reactive Programming (FRP)[15]. It supports

event-based operations and time-varying operations as well. Event-based operation allows that the OpenFlow switches can receive and send communication patterns upwards. The time-varying version allows the creation of dynamic policies for instance traffic engineering.

The Nettle code presented below is an example for flooding all network packets. The *packetIns* command filters the OpenFlow *PacketIn* messages (which are sent when there is no match in the switch table) from the incoming message stream. For each of them the *sendRcvdPacket* flood command instructs the switch to forward the packet on every port, except the incoming port.

```
floodPackets1 = proc evt → do
packetInEvt ← packetIns ≺ evt
return A ≺sendRcvdPacket flood packetInEvt
```

4.3. Procera

Procera [16] is based on FRP, just like Nettle and Frenetic. It uses ideas from Yampa [17] as well. This language was used in various prototype deployments in campus and home networks as well.

With Procera one can describe policies, like user authentications, time of day, bandwidth usage, or server load. Both Frenetic and Procera are able to use windowed event histories. While Frenetic can be applied only to network packets or flows, Procera allows windowed history to any event stream.

The following example uses event history abstraction and external events.

```
proc world → do
recent ← since(daysAgo 2) ≺ add(usageEvents
world)
usageTable ← group sum ≺ recent
return A ≺ usageTable
```

It collects the host usage logs every few seconds. The *UsageEvents* event filters the usage events from all existing events (world). After filtering a window of two days the result is used to create a device usage mapping. After the grouping operation the module returns a sum of all usage.

4.4. Frenetic

Frenetic [18] is one of the first SDN programming languages. Most of the existing SDN programming languages are derived from it. Frenetic contains a functional library for describing high-level packet-forwarding policies. It provides a declarative SQL-like query language for classifying and aggregating network traffic.

Frenetic has compositional constructs. It enables code reuse, and it is able to facilitate modular reasoning. This programming language ensures arbitrary wildcard and windowed history for grouping information by number of packets, by packet size or by time. Below is presented an example of host usage being collected (*GroupBy([script)]* every minute (*Every(60)*).

```
Select(bytes)
GroupBy([srcip])
Every(60)
```

4.5. Netcore

NetCore [19] had been developed as the replacement of Frenetic for defining forwarding policies. This language was the basis for the new version of Frenetic, written in OCaml, and also in Pyretic. NetCore was the first language, which presented formal semantics and proofs of correctness. The following NetCore example filters all HTTPs traffic (*DstPort = 110111011*) (443) and returns true if the total number of https packets sent is less than 1000 ($\sum s$), or if the packet *k* comes from a particular sender *(SrcAddr = 10.0.1.1).*

```
filterHttps = DstPort : 110111011
cond (∑, s, k) = cardinality ∑ 1000 ||
k.SrcAddr == 10.0.1.1
```

NetCore generates rules proactively instead of reactively. The compiler creates as many OpenFlow-level rules proactively as possible, otherwise it uses the reactive process.

4.6. Frenetic-OCaml

Frenetic-OCaml [20] is a new version of the Frenetic language, which is implemented in Objective Categorical Abstract Machine Language (OCaml)[21]. This language uses the

network query language from the Frenetic language. This query language gets information from the network about the topology changes and the traffic statistics as well. Frenetic-OCaml is able to decide which policy will be used during the packet update (the old one or the new one). This is the only language that avoids the use of both policies at the same time.

The example below shows how the monitor module and the repeater module work. The repeater applies the rules to forward the traffic, the monitor queries the amount of HTTPs traffic arriving on port 3. The main module just calls these modules in the program.

```
def monitor():
  z = (Select(bytes) *
      Where(inport = 3 & srcport = 443) *
      Every(20))
  z >> Print()
def repeater():
  rules = [Rule(inport : 1, [f wd(2)]),
           Rule(inport : 2, [f wd(1)])]
  register(rules)
def main():
repeater()
monitor()
```

4.7. Pyretic

Pyretic [22] is a language of the Frenetic Project. This language is the only SDN language provided with imperative programming.

The example below is a function that adds firewall rules in Pyretic. The program checks if the pair *mac_1* and *mac_2* (MAC Addresses) are contained in the *$self.firewall* list with true logical values. If the condition is fulfilled a message is printed ("The rule already exists") else, a new rule is added to the list. Pyretic contains *if* and *return* statements as well as variables and function definitions.

```
def AddRule (self, mac_1, mac_2) :
if (mac_1, mac_2) in self.firewall :
print "The rule already exists"
return
self.f irewall[(mac_1, mac_2)] = True
print "Adding new rule in %s : %s" % (mac_1,
mac_2)
self.update policy()
```

Pyretic specifies static and dynamic forwarding policies using NetCore [19]. The Pyretic language uses different policies with parallel and sequential operators. This language has a library for network topology abstraction, which can be used in virtualization. The policies of the virtualization can be used together with other policies, or they can serve as the base of another layer of virtualization.

4.8. NetKAT

NetKAT [24], is based on the Kleene algebra with Tests (KAT) [25]. This language uses KAT to specify and to program the networks. NetKAT was the first programming language to use normal phrases to specify the network forwarding paths from the source to the target. NetKAT is specifying and verifying network packet-processing functions. The language enables programmers to create significant, compositional network programs. The following example shows a firewall wrote in NetKAT. The firewall allows HTTPs traffic between hosts having IP addresses 10.1.1.1 and 10.1.1.2. The other traffic is dropped.

```
et f irewall : policy =
<: netkat <
if ( ( ip4Src = 10.1.1.1 && ip4Dst = 10.1.1.2
&& tcpSrcPort = 443 ) | |
( ip4Src = 10.1.1.2 && ip4Dst = 10.1.1.1 &&
tcpSrcPort = 443) )
then $forwarding
else drop
```

5. CONCLUSIONS

SDN provides a centralized approach for several network configuration related problems. Since the first appearance of this paradigm several software development supporting tools have been created in order to make possible or to facilitate the related programming tasks. In this paper, the main features of eight SDN programming languages are presented including their evolution process and some simple practical examples as well.

While the first language (FML) targeted mainly the specification of flow policies using a

simple syntax, later more and more functionality and services appeared like event based operations in Nettle, Windowed event histories for network packets in Frenetic and for event streams in Procera. The definition of forwarding policies was first offered by Netcore, which also introduced the usage of formal semantics. The OCaml based new version of Frenetic included the possibility to decide which policy was used during the packet update while NetKAT introduced the usage of normal phrases to specify the network forwarding paths from the source to the target.

Perhaps the most important milestone in this evolution is represented by Pyretic that introduced the imperative programming of SDN and contained a library for network topology abstraction and virtualization policy definition. This is why this language became one of the most widespread SDN languages. However, this field of SDN is developing very fast, therefore it is sure that new tools and languages are going to be released in the future as well.

6. REFERENCES

[1] Fernando M. V. Ramos, D. Kreutz, Paulo Verissimo: Software-defined networks: On the road to the softwarization of networking https://www.researchgate.net/publication/284922281_Software-defined_networks_On_the_road_to_the_softwarization_of_networking
Retrieved August 17, 2016

[2] A. Lara, A. Kolasani, and B. Ramamurthy, "Network innovation using OpenFlow: A survey," IEEE Communications Surveys & Tutorials, 2014, 16(1), pp. 493-512.

[3] R. Enns, M. Bjorklund, J. Schoenwaelder, and A. Bierman, "Network configuration protocol (netconf)," Internet Requests for Comments, RFC Editor, RFC 6241, June 2011.

[4] Protocol Oblivious Forwarding http://www.poforwarding.org/
Retrieved August 17, 2016

[5] What is Cisco OpFlex? https://www.sdxcentral.com/cisco/datacenter/definitions/cisco-opflex/
Retrieved August 27, 2016

[6] SDN Series Part Three: NOX, the Original OpenFlow Controller http://thenewstack.io/sdn-series-part-iii-nox-the-original-openflow-controller/
Retrieved July 17, 2016

[7] M. McCauley. (2015, December) About POX. [Online]. Available: http://www.noxrepo.org/pox/about-pox/

Retrieved July 19, 2016

[8] J. Medved, R. Varga, A. Tkacik, and K. Gray, "OpenDaylight: Towards a Model-Driven SDN Controller architecture," in 2014 IEEE 15th International Symposium on. IEEE, 2014, pp. 1–6.

[9] A. Van Deursen, P. Klint, and J. Visser, "Domain-specific languages: An annotated bibliography." Sigplan Notices, vol. 35, no. 6, 2000, pp. 26–36.

[10] Network Application Programming Interfaces (APIs) http://compnetworking.about.com/od/softwareapplicationstools/g/bldef_api.htm
Retrieved August 17, 2016

[11] M. Mernik, J. Heering, and A. M. Sloane, "When and how to develop domain-specific languages," ACM computing surveys (CSUR), vol. 37, no. 4, pp. 316–344, 2005.

[12] Timothy Hinrichs , Natasha Gude, Scott Shenker Expressing and Enforcing Flow-Based Network Security Policies, University of Chicago Technical report, 2008. https://www.cs.uic.edu/~hinrichs/papers/hinrichs2008design.pdf
Retrieved August 30, 2016

[13] N. Li and J. C. Mitchell, "Datalog with constraints: A foundation for trust management languages," in Practical Aspects of Declarative Languages. Springer, 2003, pp. 58–73.

[14] A. Voellmy, A. Agarwal, and P. Hudak, “Nettle: Functional reactive programming for openflow networks,” DTIC Document, Tech. Rep., 2010.

[15] What is Functional Reactive Programming https://www.quora.com/What-is-Functional-Reactive-Programming Retrieved August 12, 2016

[16] A. Voellmy, H. Kim, and N. Feamster, “Procera: a language for highlevel reactive network control,” in Proceedings of the first workshop on Hot topics in software defined networks. ACM, 2012, pp. 43–48.

[17] Courtney, H. Nilsson, and J. Peterson, “The yampa arcade,” in Proceedings of the 2003 ACM SIGPLAN workshop on Haskell. ACM, 2003, pp. 7–18.

[18] N. Foster, M. J. Freedman, R. Harrison, J. Rexford, M. L. Meola, and D. Walker, “Frenetic: a high-level language for OpenFlow networks,” in Proceedings of the Workshop on Programmable Routers for Extensible Services of Tomorrow. ACMA, 2010, p. 6.

[19] C. Monsanto, N. Foster, R. Harrison, and D. Walker, “A compiler and run-time system for network programming languages,” ACM SIGPLAN Notices, vol. 47, no. 1, 2012, pp. 217–230,

[20] N. Foster, A. Guha, M. Reitblatt, A. Story, M. J. Freedman, N. P. Katta, C.Monsanto, J.Reich, J.Rexford, C.Schlesinger et al.,“Languages for software-defined networks,” Communications Magazine, IEEE, vol. 51, no. 2, 2013, pp. 128–134.

[21] The Caml language, http://caml.inria.fr/about/history.en.html Retrieved August 02, 2016

[22] J. Reich, C. Monsanto, N. Foster, J. Rexford, and D. Walker, “Modular SDN programming with Pyretic,” Technical Report of USENIX, 2013.

[23] C. Monsanto, N. Foster, R. Harrison, and D. Walker, “A compiler and run-time system for network programming languages,” ACM SIGPLAN Notices vol. 47, no. 1, pp. 217–230, 2012..

[24] C. J. Anderson, N. Foster, A. Guha, J.-B. Jeannin, D. Kozen, C. Schlesinger, and D. Walker, “NetKAT: Semantic foundations for networks,” ACM SIGPLAN Notices, vol. 49, no. 1, 2014, pp. 113–126.

[25] D. Kozen, “Kleene algebra with tests,” ACM Transactions on Programming Languages and Systems (TOPLAS), vol. 19, no. 3, 1997, pp. 427–443.

Chip formation mechanism during composite materials machining

J. Líska [a]

[a] Pallasz Athéné University, Kecskemét Izsáki út 10, 6000, Hungary, liska.janos@gamf.kefo.hu

Abstract

The present article aims to investigate the chip separation process in order to derive the chip formation characteristics during cutting of GFRP (Glass Fibre Reinforced Plastic), CFRP (Carbon Fibre Reinforced Plastic). Composite materials are materials, which have very good material properties. Machining of these types of material are note easy, but not too hard. Typical problem at composite machining is chip formation. It affect chip braking, chip flowing speed, etc. The experiments are designed on the base of DOE (Design of Experiments) method. During the experiments – so called chiselling technology (free cutting) – we change two cutting parameters (depth of cut, cutting speed). The chip characteristics are measured by a high speed camera. The camera is connected with PC for recording and controlling the experimental procedure in real-time. After that we get informations about shape and size of chip, its motion after the tool.

Keywords: Composite, Chip formation, Machining process, Design of experiment

1. INTRODUCTION

The composite materials, or the composites, are the construction materials made of two or more components with significantly different physical and chemical properties. Combinating this two components we create a new material with unique properties that cannot be reached by none of these components separately neither by simply summarization [1].

As a composite it can be understood such a material that meets following conditions:

- Was made artificially,
- Consists of at least two chemically different components,
- The components have homogenous distribution throughout the volume from the macroscopic point of view,
- Consequential properties of composite are different from the properties of the individual components

These conditions exclude the natural materials (eg: wood as associated material to lignin matrix, reinforced by celluloid fibres, further bamboos, bones, etc.)

At present time the composite materials can be divided by a type of matrix and by a production method [1].

Division by a type of matrix is following:

- Polymers,
- Metallic,
- Ceramic [1].

Physical properties of basic material and fibre are completely different. Physical properties and fibre orientation determine cutting power and machining conditions of composite material [1].

Machining of glass-reinforced composite with tool made from material, which is under polycrystalline diamond in the Moh's hardness

scale (e.g. cemented carbide, carbide of silicon, boron carbide), wears more intensively.

It is possible to machine glass-reinforced composite on standard machine tool for metal or wood. Machining conditions don't require cooling but siphon off powder and chip 1].

Since composites' heat resistant is low (100 - 300 °C), cutting conditions should be determined not to reach the critical temperature [1].

At machining the conductive is not the chip, but the machining tool. Therefore heat is conducted by the tool, which leads to tool wear.

It is advised to use cemented carbide tools with high quality coat or diamond (PCD).

2. METHODS AND MATERIALS

The aim of the research is to better understand the mechanism of stock removal at composite materials. This mechanism is well-known (even more models can be found for this mechanism in literature), but at composite materials can be found only few. This is due to anisotropic character of material.

Full factorial experimental method was used during experiments. I used five different technological settings, applying the following formula:

$$n = 2^k + 1 \quad (1)$$

where n is the number of measurements and k presents the settings. The cutting speed (v) and depth of cut (ap) was changed.
I analyzed two different materials (Glass Fibre Reinforced Plastic Composite, Carbon Fibre Reinforced Plastic Composite), to get more comprehensive results about the mechanism of stock removal. At measurements I used the high-speed camera.

Fig. 1. Camera with equipment used at experiments [2]

Figure 2. and figure 3. presents the experimental settings.

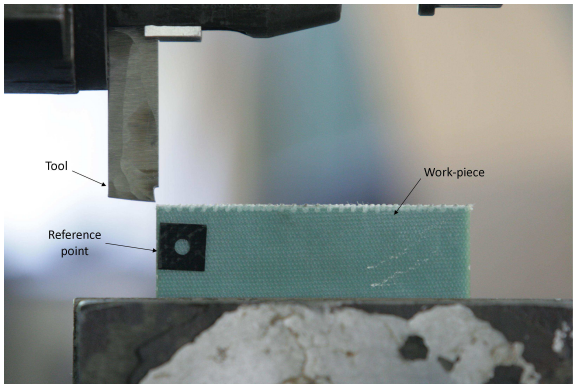

Fig. 2. Tool and work-piece experimental setup

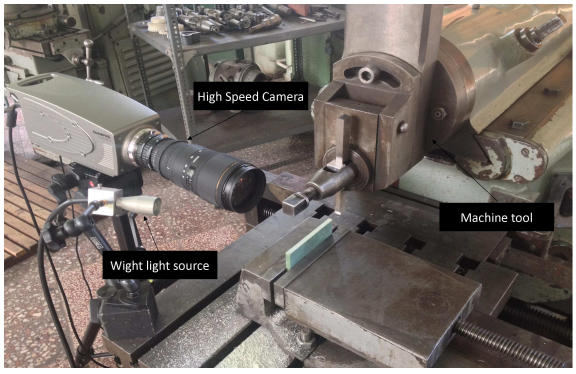

Fig. 3. Experimental setup of high-speed camera

At beginning of every measurement is also important the investigation of tool geometry, next to definition of technological parameters (Table 1.) Investigation of chisel-tool geometry

was made by the help of Mitutoyo Formtracer Contour measuring machine (Figure 4.)

Figure 4. Measuring machine Mitutoyo Formtracer CV 3100 [3]

Can be seen, that the rake angle of tool is big, therefore the cutting edge radius is small. For example, plastic materials are well machinable with this geometry. The material of tool is high speed steel.

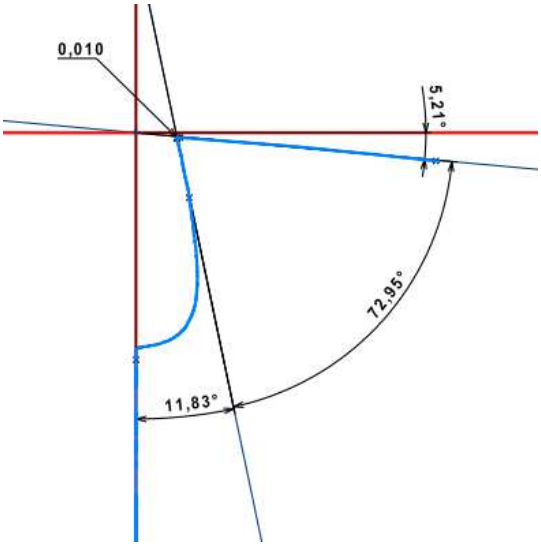

Fig. 5. Tool geometry

Table 1. Technological parameters

Cutting speed	Theorethical chip thickness	Work-piece lenght	Override and overrun	Machinig lenght	Strokes of ram per minute	Chip widht
v [m/min]	h [mm]	L_w [mm]	l_r [mm]	L [mm]	n_k	b [mm]
16,8	1,5	100	140	240	35	4
26,9	1,5	100	140	240	56	4
16,8	2,5	100	140	240	35	4
26,9	2,5	100	140	240	56	4
19,2	2	100	140	240	40	4

3. RESULTS

The primary concern at measuerments was to measure the chip ratio. The other values of measurements (shear plane angle, chip speed, breaking speed) follow from this index number.

After several repetitions of experiments showed that factor of chip shape deformation at cutting of polymer-based composites cannot be calculated, or calculation is very difficult. This is because does not happen ductil cutting. It means, that process of chip removal happens without ductil shape deformation.

The shear plane angle was stated from fast camera recordings (Figure 6.), which shows that increasing of depth of cut and cutting speed will reduce the shear plane angle. This leads that tool have to slough of larger surface. It requires larger force and energy needs.

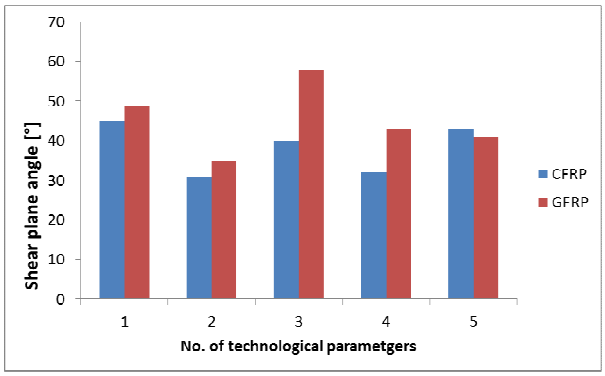

Fig. 6. Results of shear plane angles

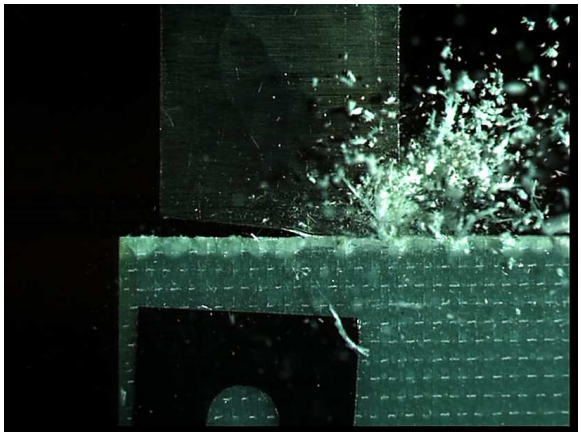

Fig. 7. GFRP high-speed camera image

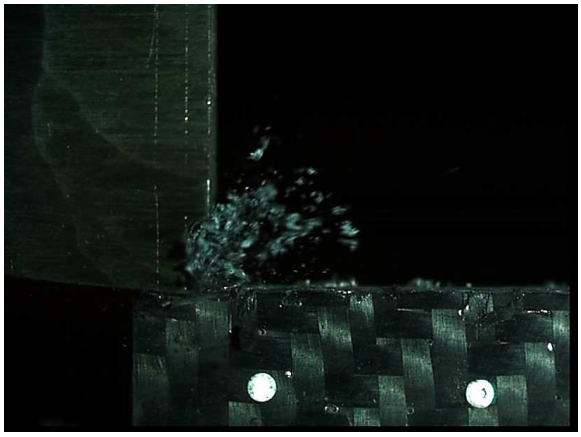

Fig. 8. CFRP high-speed camera image

4. CONCLUSIONS

At designing of experiments is never clean, which results are expected. This case is completely good example of that mechanism of stock removal at polimer based composite materials is very different compared to stock removal of metallic materials.

It is interesting from several aspects, because momentally do not exists model, which would accurately describe this process. During the experiments and at interpreting of results we can conclude, that in that case is no ductul cutting. It is clearly visible from both images (Figure 7. and figure 8.). The chip breaks in shear plane and there is no plastic surface deformation. It can be also observed that two machined material behaves differently. While at material GFRP shapes of chip are elongated, shapes of chip at materials CFRP are fragmented. This can be explained by fact, that modulus of elasticity of material GFRP is larger.

Furthermore, it was turned out also, that delamination as an accompanying phenomenon is present here as well. My conclusion at this experiment is, that depth of cut and grain direction influences most strongly the magnitude of this accompanying phenomenon.

5. REFERENCES

[1] TÁBORSKÝ, L., ŠEBO, P.: Konštrukčné materiály spevnené vláknami. Alfa 1982.

[2] Olympus i-speed III image, https://www.google.hu/search?q=olympus+i-speed+3&biw=1745&bih=930&tbm=isch&tbo=u&source=univ&sa=X&sqi=2&ved=0ahUKEwjV3sO5vafPAhUE0xQKHWMaAUEQsAQITA#imgrc=3r5QZW02dSaXyM%3A, last access 22/9/2016

[3] Mitutoyo Formtracer measuring machine image, http://ecatalog.mitutoyo.com/Contracer-C1149.aspx

Estimation of statistical parameters of electric appliances based on time of day information

Z. Domotor [a], L. Kovacs [b], R. Drenyovszki [c]

[a] Pallas Athene University, Izsaki ut 10, 6000 Kecskemet, Hungary, zeno.domotor@gamf.kefo.hu

[b] Pallas Athene University, Izsaki ut 10, 6000 Kecskemet, Hungary, lorant.kovacs@gamf.kefo.hu

[c] Pallas Athene University, Izsaki ut 10, 6000 Kecskemet, Hungary, rajmund.drenyovszki@gamf.kefo.hu

Abstract

Recently the Consumption Admission Control algorithm has been developed in the smart grid framework as a new concept for controlling the demand side by the means of automatically enabling/disabling electric appliances to make sure that the demand is in match with the available supplies. The new method is based on the statistical characterization of the need and it is sensitive to the accuracy of the estimation of the statistical descriptors and furthermore the statistics are generally not stationary and even depend on other parameters (such as presence of the owner, temperature, etc). Our paper introduces an RBF neural network based approximation method, which can be used to estimate the statistical parameters of the appliance load time-series. The estimated parameters can be fed into the Consumption Admission Control Algorithm. The capabilities of the approximation method are demonstrated by numerical analysis based on a publicly available dataset.

Keywords: consumption admission control, radial basis function neural networks

1. INTRODUCTION

One of the main tasks of electricity service providers is maintaining an almost perfect balance between supply and demand. Furthermore, there is a high social and political pressure to increase the percentage of renewable energy sources. The control of the supply side is difficult in many cases because of the large time constants of the base fossil and nuclear plants; the only solution is to use costly extra gas and oil generators. Hence, an alternative way to keep the balance is to control the demand side. This concept is referred to as Demand Side Management (DSM) [1] in the Smart Grid literature. There exist many DSM methods, for instance night-time heating with load switching, time-of-use pricing and direct load control. In general DSM covers all the activities or programs undertaken by service providers to influence the amount or timing of electricity use. The residential sector represents an important part of the electricity demand and contains flexible appliances in high number. The amount of consumption involved in direct control can eliminate the error between daily prediction based generation and actual demand. In this paper we are investigating appliance level statistical parameter estimation based on an RBF neural network as part of our previously proposed Consumption Admission Control algorithm [2,3]. Smart metering enable us to collect appliance level statistics, hence we can use this additional information in our method.

Appliance level statistical parameter estimation means the extraction of models describing how appliances are used by residents, given logged data of environmental/physical parameters and the consumption of electrical appliances. The aim of the paper is developing an RBF approximator which can estimate the current statistical descriptor of a given appliance based on environmental parameter acquisition. The focus of the paper is the time dependence of the statistics, however the method can be extended for other (and even multi-dimensional) parameters as well. Our concept is depicted by Figure 1.

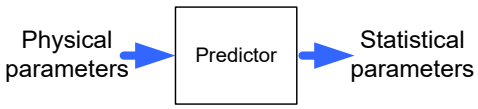

Fig. 1. The predictior structure

2. MATHEMATICAL MODEL

From a mathematical point of view there is an unknown mapping between some environmental parameters (such as time of days, day of week, temperature, humidity, light conditions, occupancy etc.) and the statistical descriptors of the corresponding power consumption time series model (e.g. probability distribution function, Markov state-transition matrix, etc). This unknown mapping can be interpreted as an unknown function which can be approximated by a proper tool. The approximator has to be optimized based on a training set $\tau^{(K)} := \{(\mathbf{u}_k, \mathbf{z}_k), k = 1,...,K\}$. The unknown function is denoted by $\Psi(\mathbf{u})$, where $\mathbf{z}_k = \Psi(\mathbf{u}_k)$. Here variable $\mathbf{u}$ represents the environmental parameter vector, whereas variable $\mathbf{z}$ corresponds to the statistical parameter vector. The underlying task is to develop an algorithm $F(\mathbf{u}, \mathbf{w})$, which is able to capture $\Psi(\mathbf{u})$ with a given level of accuracy. Here vector $\mathbf{w}$ represents the free parameters of the approximator which can be tuned to fit $F(\mathbf{u}, \mathbf{w})$ to $\Psi(\mathbf{u})$ over the training set $\tau^{(K)}$.

By using instead of $\Psi(\mathbf{u})$ one must make sure that it has the necessary (i) representation-, (ii) learning- and (iii) generalization capabilities needed to approximate $\Psi(\mathbf{u})$. In order to come to grips with the tasks listed above, the Radial Basis Function network implementations of $\mathbf{F}(\mathbf{u}, \mathbf{w})$ will be investigated (since the universal approximator property and off-line learning capability of this method).

2.1. Radial Basis Function

Radial Basis Function networks are one-hidden-layer neural networks. All the processing elements (neurons) of the first (hidden) layer get the whole input vector. The input vector is compared to the centre point of the given neuron, and a nonlinear function of this distance (in the Euclidean sense) gives the output. In the second layer only one processing element makes a weighted sum of the outputs of the hidden layer neurons.

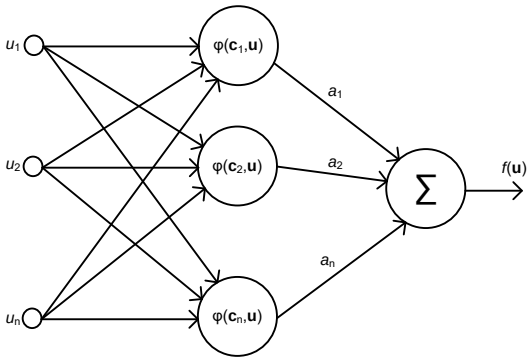

Fig. 2. The RBF structure

The formulae that describe the RBF network:

$$f(\mathbf{u}) = \sum_{i=1}^{K} a_i \varphi(\mathbf{c}_i, \mathbf{u}) \qquad (1)$$

$$\varphi(\mathbf{c}_i, \mathbf{u}) = exp\left(-\frac{\|\mathbf{c}_i - \mathbf{u}\|^2}{2\sigma_i^2} \right) \qquad (2)$$

where $\mathbf{u}$ is the input vector, K is the number of neurons in the hidden layer (the number of radial basis functions), $\varphi(.)$ is called the radial basis function, which is mostly the Gaussian function as indicated above, and σ is called the width parameter.

The complexity of the network

The complexity of the network is determined by the number of hidden layer neurons, i.e. the number of the basis functions of different centre points. The approximation is the weighted sum of the basis function values for a given input.

Setting the width parameters

The width parameters of the network can be different for all the basis functions, however they are mostly set to be equal. The approximation quality is not too highly dependent on the width parameters which are mainly set by the following empirical nearest-neighbor rule [Haykin]:

$$\sigma = \frac{1}{K}\sum_{i=1}^{K}\left\|\mathbf{c}_i - \mathbf{c}_j\right\| \qquad (3)$$

where c_j is the nearest neighbour of c_i in the Euclidean sense.

Training of the network

The training of the network is carried out based on a training set, i.e. some points of the function to be approximated are known. If the number of the known points is relatively small, then the known points are used to centre points of the basis function [5] as in our case as well. In this case the weights of the network can be calculated by solving a set of linear equations:

$$\mathbf{Ua} = \mathbf{d} \qquad (4)$$

where **U** is the so called interpolation matrix, and its elements are defined as

$$\mathbf{U}_{ij} = \varphi\left(\mathbf{u}_i - \mathbf{u}_j\right) \qquad (5)$$

and **d** is the desired response (i.e. the known function values). If **U** is almost singular, the $\mathbf{Ua} = \mathbf{d}$ equation can be solved using the regularization theory.

The benefits of RBF implementation are the following properties:

- Universal approximation in the L_2 space;
- Learning can be carried out analytically (solving a linear set of equations, if the number of neurons in the input layer is the same as the number of neurons);
- The complexity (and hence the approximation capability) of the network can be controlled by the dimensionality of the input vector;

3. NUMERICAL RESULTS

In the literature of power consumption time series modelling one can find different approaches such as applying Bernoulli *iid* (independent identically distributed) model (most simple) or different Markov models (MM) such as First Order MM, Semi-MM or Hidden MM [2,3]. In this paper we focus on approximating the ON-state probability of household appliances. In the case of Bernoulli *iid* modelling of power consumption time series of appliances there are two descriptors: the ON-state probability and the level of the ON-state. This latter is a constant, hence the only statistical parameter is the ON-state probability.

As an input we used a publicly available dataset, called as ECO Data Set [4]. The dataset consist of power consumption measurements of different appliances at different households with a sampling time of 1 s and with a span of 6 months. We applied the following pre-processing steps to extract the time-variability of the ON-state probability: (i) ON-OFF-ization by the rule: both expected value and peak value has to be the same as in the original measurement; (ii) consecutive days were averaged; (iii) working days and weekend days were handled separately; (iv) 15 minutes time segments were supposed to be stationary.

The RBF net was trained by equations (4) and (5). The performance was evaluated by cross validation and measured by the Mean Squared Error (MSE) and Mean Absolute Error (MAE).

In Figure 3. the time dependence of the ON-state probability of an entertainment device

(television) and the result of the cross validation are depicted. (Averaging of 24 weekend days were applied.) In each step one of the original function samples (black stars) was reserved for test, while all the other samples were used to train the net. After training the test element was approximated. The result is depicted by red circles. After going through all the data points by this manner, the MSE resulted to 5.98e-04, while MAE was 0.0189.

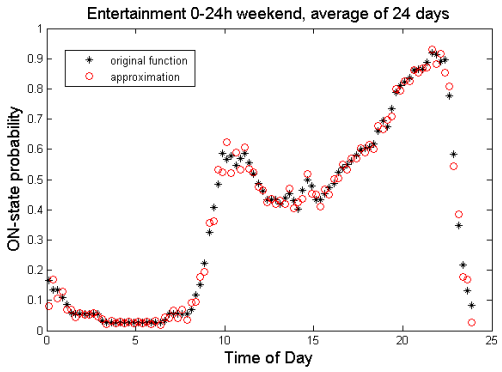

Fig. 3. Approximation of an entertainment device

In Figure 4. the results for a washing machine can be seen. 61 working days were averaged in order to get the ON-state probability as a function of the time. The performance metrics are of the same magnitude, namely MSE resulted to 1.97e-04, while MAE was 0.0096.

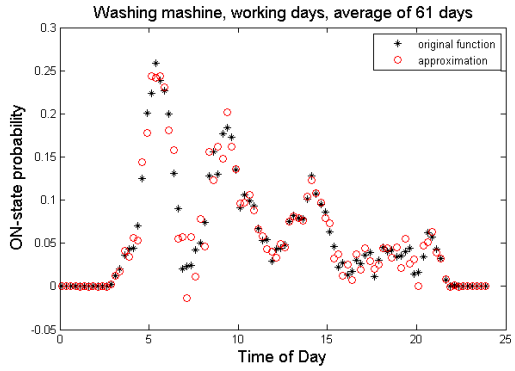

Fig. 4. The approximation of a washing mashine

4. CONCLUSION AND FUTURE WORK

In this paper Radial Basis Function Neural Network was used as a function approximator in order to learn the mapping between time of day and ON-state probability. The tool has been proven to be able to estimate the ON-state probability with a mean absolute error of about 0.01, which makes the tool suitable for plugging into Consumption Admission Control algorithms to deal with time dependence of statistical descriptors.

In the future work we try to extend the tool for multi-dimensional input, in this case other parameters, such as outdoor temperature, presence of the owner, etc. can be taken into account in order to enhance the performance of the approximator.

5. REFERENCES

[1] G. Strbac, Demand side management: Benefits and challenges, Energy Policy, vol. 36, Issue 12, pp. 4419-4426, Dec. 2008.

[2] L. Kovacs, J. Levendovszky, A. Olah, R. Drenyovszki, D. Tisza, K. Tornai and I. Pinter: A probabilistic approach for admission control of smart appliances in Smart Grids, TEAM 2013, pp. 18-21.

[3] L. Kovacs, R. Drenyovszki, A. Olah, J. Levendovszky, K. Tornai, I. Pinter: A probabilistic demand side management approach by consumption admission control, ArXiv eprintsarXiv: 1608.00546.

[4] Christian Beckel, Wilhelm Kleiminger, Romano Cicchetti, Thorsten Staake, Silvia Santini: The ECO Data Set and the Performance of Non-Intrusive Load Monitoring Algorithms, Proceedings of the 1st ACM International Conference on Embedded Systems for Energy-Efficient Buildings (BuildSys 2014). Memphis, TN, USA. ACM, pp. 80-89, November 2014

[5] S. Haykin, Neural Networks. A comprehensive foundation, Macmillan College Publishing, 2nd editon, New York, 2001.

Manufacturing of Twist-Free Surfaces by MAM Technologies

Zs. Kovács [a], Zs. Viharos [b], J. Kodácsy [c]

[a, b, c] Kecskemét Collage Faculty of Mechanical Engineering and Automation, Izsáki Street 10, Kecskemét H-6000, Hungary, kovacs.zsolt@gamf.kefo.hu

[b] Institute for Computer Science and Control of the Hungarian Academy of Sciences, Budapest, H-1111 Hungary

Abstract

Currently grinding is commonly used as the finishing operation to manufacture seal mating surfaces and bearing surfaces, especially in the automotive industry. It would lead to more resource-efficient production if the cost- and energy-intensive grinding process could be replaced by machining with magnetic polishing or magnetic roller burnishing. The machined surfaces by turning or grinding usually have twist structure on the surfaces, which can convey lubricants such as conveyor screw. To avoid this phenomenon have to use special kind of techniques or machine, for example, rotation turning, tangential turning, ultrasonic protection or special toll geometries. All of these solutions have a high cost and difficult usability. In this paper the authors describes a system and summarizes the results of the experimental research carried out by the authors mainly in the field of Magnetic Abrasive Polishing (MAP) and Magnetic Roller Burnishing (MRB). These technologies simple and also cheap while result the twist-free surfaces. During the tests C45 normalized steel was used as workpiece material which was machined by simple and Wiper geometrical turning inserts in a CNC turning lathe. After turning, the MAP and MRB technologies was used to reduce the twist structure. The evaluation was completed by advanced measuring and IT equipment.

Keywords: magnetism; twist-free; polishing; rolling

1. INTRODUCTION

The turning always creates a twisted surface, namely regardless of the machined material or whether that is hardened or not respectively. This surface has regular structures corresponding to a thread shaped structure (twisted) which, by the advance of the tool along the rotating workpiece are producing a screw pitch.

The reason for this phenomenon is that the feed motion of the tool will cause twist structures on counter faces for radial shaft seal rings can cause leakage. For example, the surface which is produced by turning with the typical kinematic roughness and spiral pattern creates a conveyor effect in the gap between the seal ring and the shaft. Depending on the direction of rotation leakage or dry running at the seal ring can occur which results in permanent leaking.

Plunge grinding is a tried and tested manufacturing technique for creating twist-free surfaces. However, it has been established in the meantime that in spite of twist, rolled surfaces do not create a conveyor effect. In fact a typical rolled surface does not show roughness peaks but wide plateaus which are interrupted by flat remaining valleys. This structure results in a high bearing line fraction. Substitution of grinding by hard turning and rolling can reduce costs for components of this type and shorten cycle times. [1, 2]

2. STRUCTURE OF TWIST SURFACE

Twist structures are characterized by microscopic structures which are comparable

with a thread structure on a shaft surface. The Fig 1 shows the surface of a turned shaft schematically. The parameters are described in the Mercedes-Benz standard MBN 31007-7 in 2009 [3, 4].

DP – period length (mm),
Dγ – twist angle (° ’ ”),
Dt – twist depth (μm),
DG – number of threads ( ),
DF – theoretical supply cross section (μm^2)

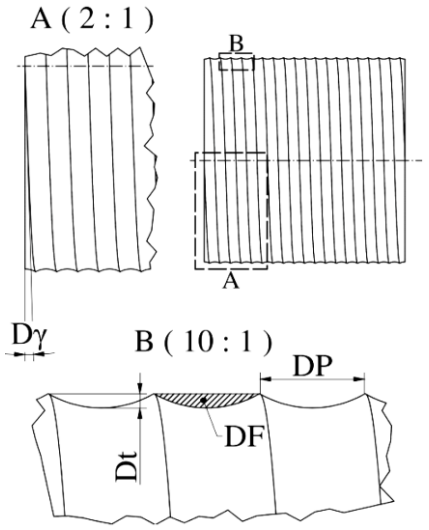

Fig. 1. Parameters of twist surface [5]

The parameters are dependent on process parameters (feed, nose radius etc.). During the rotation of a turned shaft, the liquid entrains in the circumferential direction and is deflected axially because of the twist structures [4].

The industry is currently looking for alternative manufacturing processes, for example hard turning, milling, burnishing or laser polishing. Besides these processes there are two similar technologies, the Magnetic Abrasive Polishing (MAP) and the Magnetic Assisted Roller Burnishing (MARB) which are also able to produce twist-free surface.

3. MAM TECHNOLOGIES [6]

Denomination Magnetism Aided Machining (MAM) comprises a number of relatively new industrial machining processes (mainly finishing and surface improving) developed presently, too.

The magnetic force makes these processes simpler and more productive. Machining force is generated by an adjustable electromagnetic field between two magnetic poles within the working area ensuring the necessary pressure and speed difference between the tools (abrasive grains, pellets or rollers) and the workpiece. [6]

3.1. Magnetic Abrasive Polishing (MAP) [7]

The polishing for decrease of surface roughness and increase of resistance against wear, corrosion and produce twist-free surface. Magnetic Abrasive Polishing is one such unconventional finishing process developed recently to produce efficiently and economically good quality finish. In this process, usually use ferromagnetic particles are sintered with fine abrasive particles (Al_2O_3, SiC, CBN or diamond. The MAP equipment for cylindrical surfaces was adapted to a universal engine lathe (Fig. 2.).

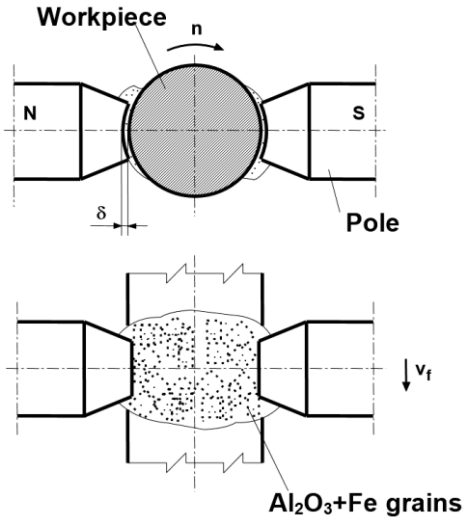

Fig. 1. MAP technology [7]

3.2. Magnetic Assisted Roller Burnishing (MARB) [7]

The main goal of roller burnishing is to achieve high-quality smooth surfaces or surfaces with pre-defined surface finish. One or more balls plastify and deform the surface layer of workpiece.

Almost all processes for the manufacturing of high-quality surfaces can be replaced by roller burnishing (e.g. fine turning, grinding,

superfinishing, lapgrinding). This proven process entails considerable technological and economic advantages for surfaces in the roughness area R_z <10 µm.

For roller burnishing was applying mechanical force to press the rolling ball onto the surfaces. To avoid the harmful deformation by mechanic pressing the necessary pressure and relative speed between the tools and the workpiece are ensured by the magnetic force.

The magnetic roller burnishing equipment for cylindrical surfaces was adapted to a universal engine lathe (Fig. 3.)

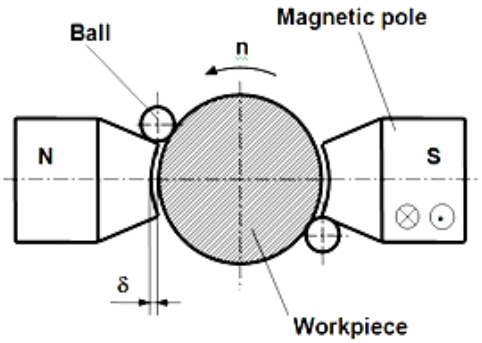

Fig. 2. MARB technology [7]

4. EXPERIMENTAL SETAP

In the performed investigations the shaft surfaces were manufactured purposefully by turning using different cutting tool. Then the surface was machined MAM technologies (MARB and MAP). Furthermore was made a grinded part as a reference to be able to compare the surfaces made by different technologies. During processing the workpieces C45-type steel with a diameter of 26 mm and a length of 100 mm were selected as processing elements. Cutting tool was inserts with wiper geometry (WNMG080404W-MF2, TP2501) and conventional inserts (WNMG080404-MF2, TP2501).

The MAM equipment is able to work as polishing and rolling function where the electromagnetic poles were fixed onto the slide of the lathe. In the tests the voltage (U = 40 V), current (I = 10 A) (direct current, adjustable) and the generating magnetic induction (B = 0,96 T) were the same under rolling and polishing too. The generated magnetic induction was reduced (B = 0,75 T) with polishing grain because of the applied Al_2O_3 shielding properties. The magnetic jaws (poles) surrounded the workpiece with a δ = 3 mm gap (clearance).

The turning, rolling and polishing technological parameters see the Table 1.

Table 1. Technical parameters of machining operations

Turning	
f (mm/min)	0,133
v_c *(m/min)*	117
a_p *(mm)*	1
Rolling	
f (mm/rev)	0,1
v_r *(m/min)*	22
Polishing	
t (min)	1,5
v_p *(m/min)*	62

5. EVALUTAION

After the manufacturing there are six different surfaces (grinded, turned by simple and Wiper insert). As first step were measured the surfaces roughens by MITUTOYO Formtracer SV-C3000 roughness tester. The measured results see in Table 2.

Table 2. Roughness values after machining

Technology	Ra (µm)	Rz (µm)
Grinded	0,54	3,43
Turned (simple)	1,2	6,09
Rolled	0,40	2,40
Polished	0,96	4,93
Turned (Wiper)	0,45	3,05
Rolled	0,27	1,92
Polished	0,38	2,79

Than was measured the twist surface by thread method. This method is a simple and fast method because it is consist of a thread and weight. The thread made from steel, plastic or wool (e.g.: fishing line or sewing thread). In this research were used steel thread where the steel

diameter of 0,04mm. The weight depends on the applied thread material and diameter so in this case is 50g [8].

5.1. Measuring procedure

During the measurement has to rotate the workpiece in horizontal position and superimpose the thread with the weight (Fig 4.)

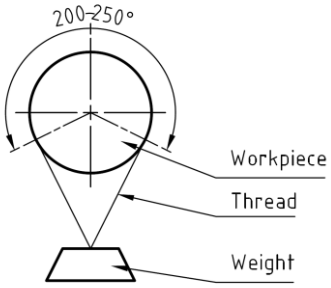

Fig. 4. Thread method [9]

The measuring takes one minute and during this time the workpiece peripheral speed 20 m/min. Then have to measure the displacement of thread (a_1) and must be performed the rotation the other direction and also have to measured it (a_2). The average of two values (1) is the characteristic number of twist surface (a_m). [9] The results are presented in Fig 5.

$$a_m = \frac{a_1 + a_2}{2} \text{ (mm)} \quad (1)$$

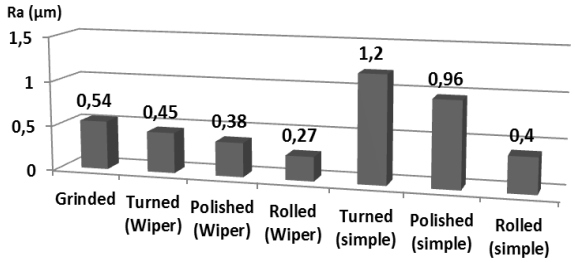

a)

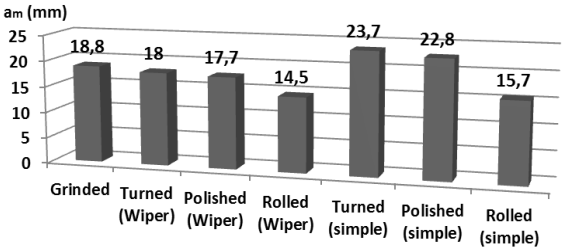

b)

Fig. 5. Measurement results of Ra roughness a) and characteristic number b) of twist surface

6. CONCLUSIONS

The research shows that MAM technologies are new manufacturing opportunity for surfaces to obtain desired functions such as surfaces with tribological function.

According to the expectations the Wiper insert produced a less than twisted surfaces compared to the simple one and as you see in the Fig 5. the grinded surface were worse than the rolled.

So that, instead of grinding can be machined with MAMRB which is faster, economical, easier and some case does not require workpiece transfer. Also there are negatives, like accuracy (size and position) which depends on the previous manufacturing. However, the MAP technology is not able to produce the expected surface.

7. ACKNOWLEDGEMENTS

The authors gratefully acknowledge the support of the SECO Company to provide the necessary cutting inserts.

8. REFERENCES

[1] S. Jung, W. Haas, Grundlehrang Dichtungstechnik. University of Stuttgart (2006)

[2] G. Lechner, H. Raab, Einfluss der Wellenlaufflache auf das Dichtverhalten von Radialwellendichtringen. Final report, BMWi/AiF Nr. 10670 (1998), pp.59-73.

[3] MBN 31007-7, 2002. Daimler AG, Stuttgard (2001), pp.312-316

[4] A. Schubert, R. Zhang, P. Steinert, Manufacturing of Twist-Free Surfaces by Hard Turning, Procedia CIRP (2013), pp.294

[5] J. Kundrák, I. Sztankovics, K. Gyáni, Analysis of the Theoritical Values of Several Characteristic Parameters of Surface Topography in Rotational Turning, World Academy of Science, Engineering and Technology International Journal of

Mechanical Aerospace, Industrial, Mechatronic and Manufacturing Engineering Vol:8, No:5, (2014), pp.908

[6] Kodácsy, J. Líska: Magnetic Assisted Roller Burnishing and Deburring of Flat Metal Surfaces. Advanced Materials Research Vol. TransTech 472-475 Publication Ltd, Zürich, 2012, pp. 908-911.

[7] J. Kodacsy, J. Danyi, A. Szabo, Gy. Fulop: Magnetic Aided Roller Burnishing Metal Parts. 7th International Conference on Deburring and Surface Finishing, UC Berkeley (USA), 2004, pp.375-378

[8] ZFN 5032:2013-10 (industrial standard)

[9] J. Kundrák, N. Nagy, Twisted surface machined by cutting (Forgácsolással megmunkált felületek sodrásossága), GYÁRTÁS 2015 Konferencia, 2015, November 20., Budapest, GépGyártás szakfolyóirat, INDEX: 25344, ISSN 0016-8580, pp.: 116-118.

Coefficient of friction in the design of non-metallic brittle interference fit parts

I. Abramov[a], P. Lekomtsev[a], A. Romanov[a], Y. Turygin[a], E. Sosnovich[a], P. Frankovsky[b]

[a] Kalashnikov Izhevsk State Technical University, ul. Studencheskaya 7, 426069 Izhevsk, Russia, lekomtsev@istu.ru

[b]Technical University of Kosice, Letná 9, 040 02 Košice, Slovakia

Abstract: Comparison of the results of determining the coefficient of friction for such combination of materials as alumina ceramics and quartz glass on the friction machine and, indirectly, by measuring the press-in and press-out forces of tapered interference fit are presented in the paper.

Keywords: coefficient of friction, brittle contact, tapered interference fit, alumina ceramics, quartz glass.

1. INTRODUCTION

When designing interference fits for parts with different properties of materials, it is important to calculate the friction forces under contact interaction of the parts in the process of forming and operating the fit. Interference fits of brittle non-metallic parts (fixtures of mixing devices in glass chemical reactors, ceramic bearings, impellers, gears, nozzles, etc.) distinct in improved wear- and corrosion-resistance, operated in broad temperature ranges are more and more widely applied in mechanical engineering. The coefficient of friction of such pair of materials as alumina ceramics and quartz glass, which can be used when evaluating the load capacity of tapered interference fit of parts from the foregoing materials is investigated in this paper.

Taking into account the difference in physical and mechanical properties, mainly the hardness, the process of relative sliding under the contact of rough bodies from such friction pair as alumina ceramics and quartz glass can be classified as scratching [1]. In [2] to describe the friction deformation model of such combination of materials, the dependence reflecting the properties of brittle materials and conforming well with previously conducted experiments on the friction machine was applied. The dependence obtained requires testing in actual fits.

2. METHODS AND MATERIALS USED FOR RESEARCH

The coefficient of friction of the pair of materials “alumina ceramics – quartz glass” was investigated in two ways:

- directly on the friction machine SRV–III Test System following the testing scheme “disc-indenter”;
- indirectly by measuring the press-in and press-out forces of the tapered interference fit.

The detailed description of experimental samples, machine and testing sequence used in the first way are given in [2].

In the second investigation way to evaluate the coefficient of friction in tapered interference fits, the following dependencies are applied [4]:

during pressing-in

$$f_{in} = \frac{F_{in}}{p_n S \cos\alpha} - tg\alpha\,, \qquad (1)$$

during pressing-out

$$f_{out} = \frac{F_{out}}{p_n S \cos\alpha} + tg\alpha\,, \qquad (2)$$

where p_n – average value of normal pressure in contact interface, MPa; S – nominal area of the contact surface, mm^2; F_{in} and F_{out} – press-in and press-out forces, respectively, N.

The results of measuring press-in and press-out forces, as well as the detailed description of the experiments in investigating the load capacity of the test tapered interference fit are given in [3,4]. The average value of the normal pressure in the conjugation for the test tapered interference fit was calculated by finite element method [5].

3. RESULTS AND ACHIEVEMENTS

This section presents the results of the measuring coefficient of friction of the pair of materials "alumina ceramics – quartz glass" on the friction machine SRV–III Test System and calculation result by measuring the press-in and press-out forces of the tapered interference fit.

3.1. Testing results on the friction machine

As a result of investigations on the friction machine, the curve of dependence of the coefficient of friction of the pair of materials "alumina ceramics – quartz glass" on the normal load was formed up (Fig. 1).

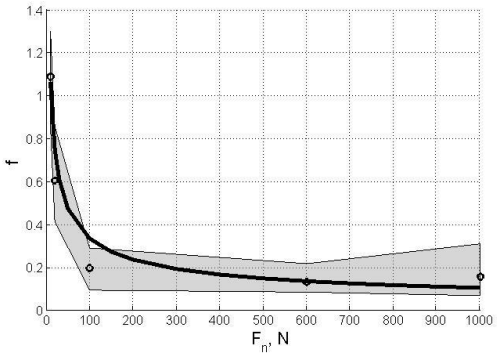

Fig. 1. Values of the coefficients of friction depending upon the normal load, confidential intervals ▭ with the probability of 0.95 obtained as a result of statistic processing of the experiment data

From the graphs in Fig. 1 it is seen that dependence f upon F_n repeats the general character of the dependence of the coefficient of friction upon the load at the elastic contact [6].

3.2. Calculation result by the indirect method

Fig. 2 demonstrates the dependencies of the coefficients of friction during pressing-out calculated by the formula (2) for tapered interference fits collected by thermal and mechanical methods.

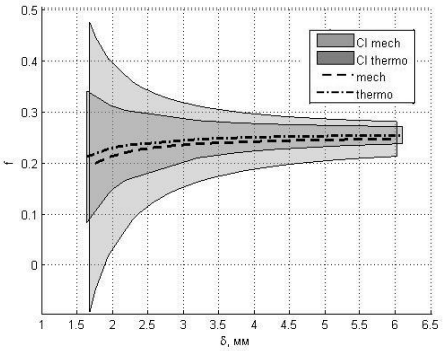

Fig. 2. Change in the coefficients of friction from the interference in the tapered fit: ▬ ▬ - during pressing-out of the press fit; ▬·▬·▬ - during pressing-out of the thermal press fit

The confidential intervals with the probability of 0.95 for the coefficients of friction during the pressing-out of tapered interference fits collected by mechanical and thermal

methods, respectively, are marked on the graph with light-grey and grey.

Fig. 3 demonstrates the dependence of the friction coefficient during pressing-in calculated by the formula (1). The confidential area with the probability of 0.95 is marked on the graph with light-grey.

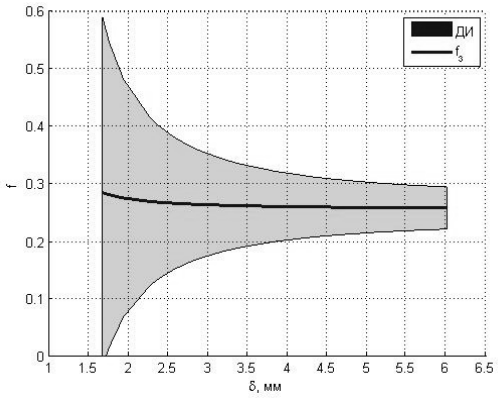

Fig. 3. Change in the coefficient of friction from the interference in the tapered fit during pressing-in

Fig. 4 demonstrates the graphs of the dependencies of the coefficients of friction during pressing-in, pressing out of the press fit and pressing out of the thermal interference fit.

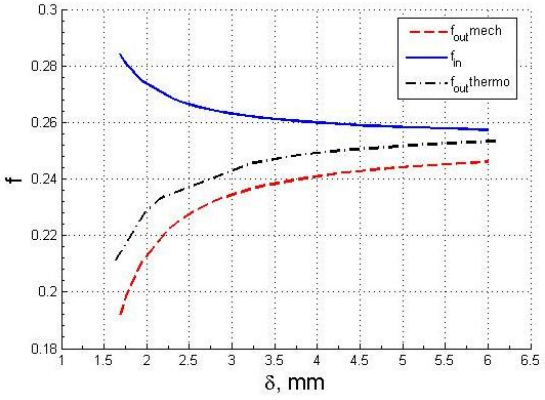

Fig. 4. Change in the coefficients of friction from the interference in the tapered fit: —— - during pressing-in; – – – - during pressing-out of the press fit; –·–·– - during pressing out of the thermal fit

From the graphs obtained it is seen that the coefficient of friction during pressing-in f_{in} somehow decreases with the interference increase, which is in compliance with the experimental results on the friction machine (Fig. 1) and general dependencies during the body friction in the elasticity area [5]. On the contrary, the coefficient of friction during pressing-out f_{out} (connection failure) increases with the growth of interference (contact pressures) number, which is explained by the increase in the actual contact area in the fit. However, the important and distinctive thing is that the coefficient of friction during pressing-out (friction at rest) is less than the coefficient of friction during pressing-in. This phenomenon is not characteristic for traditional fits of metal parts and can be explained by the availability of intermediate layer of abrasive particles, wear as a result of sliding of the contact surfaces during the formation of tapered interference fit, and the emergence of fissured (on microlevel) surface layer of the contact surface of the quartz pin at the penetration of harder projections of the female part of the tapered interference fit. The data obtained require additional investigations to search the options for increasing the load capacity and relative strength of such fits.

4. CONCLUSION

As a result of the investigations carried out on the friction machine it was found that the coefficient of friction of the pair of materials “alumina ceramics -quartz glass” changes from 0.2 to 0.16 when the normal force changes from 100 up to 1000 N. When assembling the trial tapered interference fit with the commensurate contact area, the coefficient of friction decreases from 0.28 to 0.26 when the press-in force changes from 800 up to 2400 N. Larger value of the coefficient of friction found by the indirect method is conditioned by edge effects in the actual tapered interference fit and geometrical errors of part production. The coefficient of friction during pressing-out (friction at rest) is less than the coefficient of friction during pressing-in. This phenomenon is not characteristic for traditional fits of metal parts and can be explained by the availability of intermediate layer of abrasive particles, wear as

a result of sliding of the contact surfaces during the formation of tapered interference fit, and the emergence of fissured (on microlevel) surface layer of the contact surface.

5. ACKNOWLEDGEMENTS

The reported study was funded by RFBR according to the research project No. 16-38-00719 “Investigation of brittle contact interaction interface of non-metallic interference fit parts”.

6. REFERENCES

[1] H. Czichos, K. H. Habig. Tribologie-Handbuch. Tribometrie, Tribomaterialien, Tribotechnik. Springer, (2010).

[2] P.V. Lekomtsev. EXPERIMENTAL INVESTIGATIONS OF DRY FRICTION OF THE PAIR OF MATERIALS “CORUNDUM CERAMICS-QUARTZ GLASS” // Young scientists – to the acceleration of scientific-technical progress in XXI century: electronic edition: proceedings of IV All-Russian scientific-technical conference of PhD and master students and young scientists with international participation, Izhevsk, 20-21 April, 2016. -Izhevsk: Kalashnikov ISTU, INNOVA, 2016. - P. 78-85. -ISBN 978-5-9906108-6-6.

[3] P. Lekomtsev, P. Božek, A. Romanov, A. Abramov, I. Abramov, Y. Nikitin, "Extracting Load Research of Taper Interference Fit Made of Glass and Ceramics Parts Using a Servo Press", Applied Mechanics and Materials, Vol. 816, pp. 461-468, 2015

[4] P.V. Lekomtsev, I.V. Abramov. Investigation of load capacity of tapered interference fit of parts from the pair of materials “technical ceramics-glass” // Young scientists – to the acceleration of scientific-technical progress in XXI century [Electronic source]: electronic scientific edition: proceedings of III All-Russian scientific-technical conference of PhD and master students and young scientists with international participation, Izhevsk, 22-23 April, 2015 / Kalashnikov ISTU. – Izhevsk: Kalashnikov ISTU, INNOVA, 2015. – P. 193-200. – ISBN 978-5-9906108-6-6.

[5] I.V. Abramov, P. V. Lekomtsev, N. A. Trefilov. Computer research of load-carrying capacity for tapered interference fit made of brittle nonmetallic parts // Intelligent Systems in Manufacturing, 2015. No. 2 (26). Pp. 44–51.

[6] V. Kragelsky. Friction and Wear. 2nd ed., revised and enlarged. – M.: Mashinostroenie, 1968. – 480 p.

Control system design of the parallel kinematics mechatronic press

I. Abramov[a], A. Abramov[a], A. Romanov[a]*,

Y. Nikitin[a], P. Lekomtsev[a], P. Božek[b]

[a] Department of Mechatronic System, Faculty of Quality Management, Kalashnikov Izhevsk State University, Studencheskaya 7, 426069 Izhevsk, Russia, ms_istu@mail.ru

[b] Institute of Applied Informatics, Automation and Mathematics, Faculty of Materials Science and Technology, Slovak University of Technology, Hajdóczyho 1, 917 24 Trnava, Slovakia

Abstract

The paper describes the development of mechatronic press with parallel axes. The fuzzy logic control system of mechatronic press are considered. The algorithm realized the control law of a swinging crosshead are presented. The experimental results of positioning accuracy research are given.

Keywords: fuzzy logic, control system, parallel kinematics, mechatronic press, positioning error.

1. INTRODUCTION

The advent of new type of multi-axis manufacturing equipment with synchronous controlled axes without rigid kinematic linkage was possible with the development of servo drives and emerges of control system with advanced features.

Closed kinematic route provides greater stiffness of whole construction, but it is achieved by redundant construction elements and equipment weighting. The alternative is equipment with control systems enabling to synchronize axis move by means of special mathematic control methods.

Servo drive and intellectual control system application makes it possible to achieve the high performance on a base of:

−high repeatability and positioning accuracy, full workflow parameters control for each controlled axis;

− high speed movements are caused by a lack of additional construction element and the reduction of moved masses.

Equipment with synchronously controlled axes are widely used in the technological processes, for example:

− assembling;

− machining (drilling, boring deployment);

− pressure processing (hole broaching, pressing, molding).

An analysis of electromechanical pressure equipment [2] are shown that the most applicable electric motors are permanent magnet synchronous motor (PMSM) [3], that's specified of the speed control necessity in a wide range with constant torque and ensure of a high transient performance and high overload capacity.

The analysis of linear motion gear [4] are shown that the ball screw compared with the roller screw gear has a lower performance and does not satisfy to the requirements for pressing equipment, in particular by a lifting capacity and maximum speed.

Taking into account the heavy loads, in terms of the experience of designing press equipment, the design map with parallel electromechanical drive elements was selected. This scheme allows for higher performance in terms of creating a considerable effort and compensating dynamic vibrations.

The kinematic diagram are sited in Figure 1.

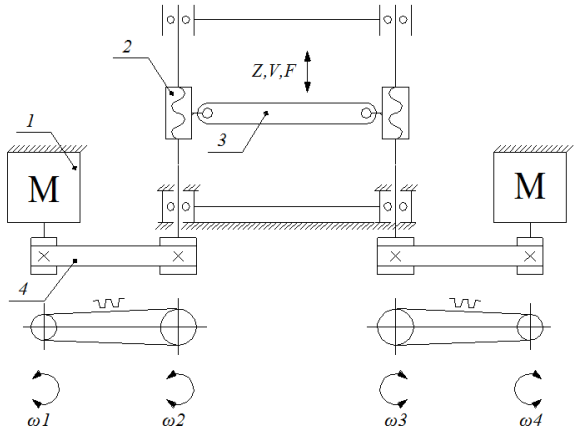

Fig. 1. Mechatronic press construction arrangement
1 – PMSM; 2 – roller screw gear;
3 – crosshead; 4 – belting

2. FUZZY LOGIC CONTROL SYSTEM OF MECHATRONIC PRESS

2.1 Parallel axes synchronization algorithm

The important problem of simultaneous multi-axis movement scheme is axes synchronization that requires the solution of specified problem number.

Synchronous servo drive control makes certain demands to “intellectuality” of control system and application possibility of special methods and algorithms to control synchronous axes movement with adaption of process variables.

The analysis of widely used synchronization algorithms [1] are revealed their specific disadvantages, that’s why modified synchronization algorithm on a base of master-slave method was proposed. The main idea consists in the change of master-slave function is occurred constantly as opposed to tradition approach (master is the motor with zero or minimal error). In according to the suggested method, slave motor is speeded up or speeded down by the controller depending on the lag of the lead from designated or master position.

The algorithm basis is a function of the condition change "master-slave", defined as (1):

$$\begin{cases} (Z_1 < Z_2)\ \&\ \&((Z_1 - Z_2) < \Delta Z_{MAX\_AXIS}); \\ (Z_2 < Z_1)\ \&\ \&((Z_2 - Z_1) < \Delta Z_{MAX\_AXIS}); \\ (Z_1 \neq Z_{SP})\ \&\ \&((Z_1 - Z_{SP}) < \Delta Z_{MAX}); \\ (Z_2 \neq Z_{SP})\ \&\ \&((Z_2 - Z_{SP}) < \Delta Z_{MAX}); \end{cases} \quad (1)$$

Z1 – axis 1 current position;

Z2– axis 2 current position;

Zsp – setpoint position;

ΔZmax_axis – maximum synchronization error between axes;

ΔZmax – maximum following error.

2.2 Fuzzy logic control system

In recent years, the fuzzy logic control algorithms are widely used in the theory of artificial intelligence and automatic control systems. Fuzzy controllers on the basis of fuzzy sets and fuzzy logic in the conditions of uncertainty disturbances provides a higher quality of transient performance compared to the conventional reach and robustness with a respect to various kinds of disturbances [5, p. 72], [6].

General view of fuzzy mechatronic press control system is shown in Figure 2.

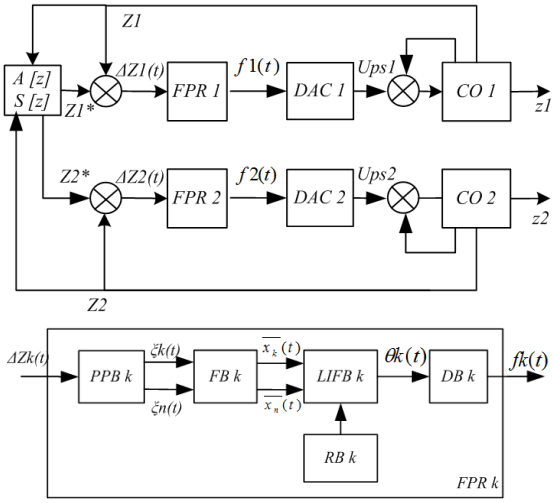

Fig. 2. Functional diagram of fuzzy mechatronic press control system

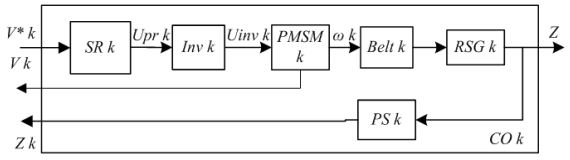

Fig. 2. Functional diagram of fuzzy mechatronic press control system (continuation)
A[z] - setpoint position and velocity; S(z) - synchronization controller; FPR1,2 - fuzzy position controllers of axes 1.2 respectively including:
PPB1,2 - parameters preparing blocks; FB1,2 - fuzzification blocks; LIFB1,2 - logical implication forming block; DB1,2 - defuzzification blocks; RB1,2 - rule base; DAC1,2 – digital-to-analog converter;
CO1,2 - control objects consisting of:
RS1,2 - speed regulators implemented in the inverter Inv; PMSM1,2 - permanent magnet synchronous motors; Belt1,2 – beltings; RSG1,2 - roller screw gears; PS1,2 - position sensors.

The driving position signal Z*(t) is compared with the signal of current crosshead position of the axis Z(t), obtained from the position sensor. Fuzzy controller consists of five blocks: preparation parameters block (PPB), fuzzification block (reduction to fuzziness) (FB), logical implication forming block (LIFB), rule base (RB) and defuzzification block (DB) [8].

The input parameters [ξ1 (t) ... ξn (t)] of fuzzy PID controller are: position error ΔZ, the first derivative of the error ΔZ' and the second derivative of the error ΔZ''. Fuzzy input variables have three triangle terms: negative (N), zero (Z) and positive (P).

The fuzzy variable with triangle terms: negative large (NL), negative medium (NM) negative small (NS), zero (Z), positive small (PS), positive medium (PM), positive large (PL) are used for the linguistic description of output variable.

The required value of output variable is calculated after the defuzzifacition.

When forming the rulebase, the assumption that the greater position mismatch must comply with higher control action was used, depending on the value of linguistic rules are formulated.

Fuzzy logic system is designed for Mamdani type. Rules are formed by type of IF ... AND ... AND THEN...

Here are some of them:
- if ΔZ = N and ΔZ' = Z and ΔZ''= N then *f* = PS;
- if ΔZ = P and ΔZ' = N and ΔZ''= P then *f* = OS.

3. RESULTS

The investigation of the developed mechatronic press and control systems was carried out with two types of master control at idle and under load.

The first type of control action sets with step speed excitation, that's allowed to estimate a limiting control quality modes (Table 1).

Table 1. Experimental results (control action type 1

No.	No. of section	L, mm	V, mm/sec	a, mm/sec^2	ΔZaxis, um	ΔZ, um
1	1	50	100	450	6,3	18,5
	2	100	200	400		
	3	70	70	340		
	4	80	50	250		
	5	60	30	70		
2	1	70	120	350	8,5	20,1
	2	60	170	400		
	3	50	90	300		
	4	100	60	200		
	5	80	40	50		
3	1	50	150	450	10	22
	2	100	200	250		
	3	70	100	340		
	4	80	80	250		
	5	60	20	70		

The experimental results are illustrated in Figure 3,4.

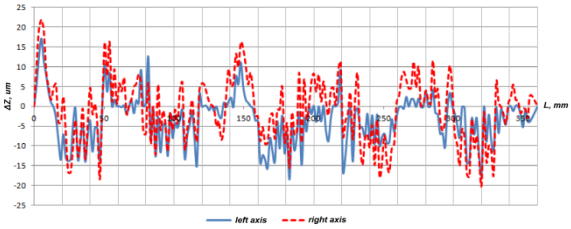

Fig. 3. Position error without load (experiment No. 3)

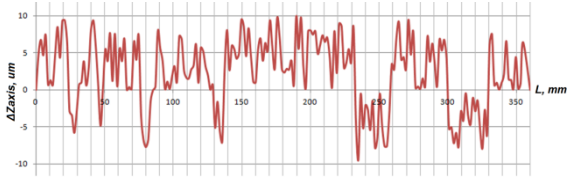

Fig. 4. Synchronization error without load (experiment No. 3)

The second type of reference variable forms a smooth movement of the press actuator that's

permitted to evaluate the work of control system in steady motion mode (Table 2).

Table 2. Experimental results (control action type 2)

No.	L, mm	V, mm/ sec	a, mm/ sec^2	F, kN	ΔZaxis, um	ΔZ, um
1	120	100	100	0	2,9	10,8
2				60	3,9	13,8
3			200	0	3,5	11,6
4				60	4,6	14,1
5		300	350	0	4,9	17,2
6				60	5,8	20,2
7			450	0	5,3	18,6
8				60	6,2	21,7
9	240	100	100	0	3,0	11,9
10			200	0	3,9	13,1
11		300	350	0	5,2	18,8
12			450	0	6,1	20,3
13	360	100	100	0	2,8	11,5
14			200	0	4,1	13,6
15		300	350	0	4,5	19,6
16			450	0	5,3	20,1

The experimental results are illustrated in Figure 5, 6.

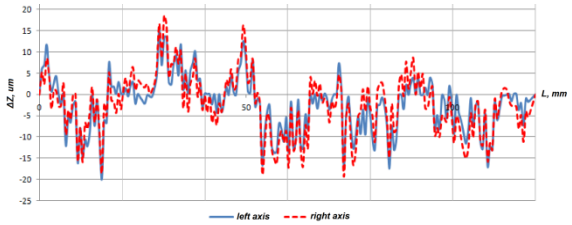

Fig. 5. Position error with load (L=120 mm, V=300 mm, a= 350 mm/sec^2)

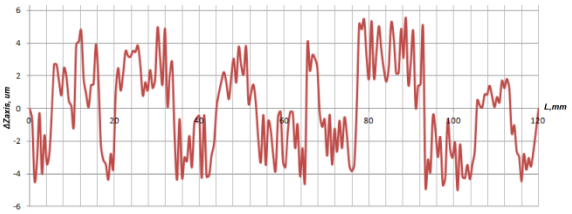

Fig. 6. Synchronization error with load (L=120 mm, V=300 mm, a= 350 mm/sec^2)

The analysis of experimental data is revealed that the proposed fuzzy logic control system of mechatronic press provides high quality control at idle and under load: in a step sets the largest axis mismatch does not exceed 22 um, the largest synchronization error at idle is 10 um; in steady state motion the largest axis mismatch is less than 21.7 um, the maximum idling synchronization error 5.3 um and 6.2 um under load.

4. CONCLUSION

The conducted full-scale experiment have proved the effectiveness of the developed mechatronic press control system with fuzzy output in transient and steady state modes. Fixed positioning accuracy of mechatronic press is sufficient for many tecnological operation, such as assembling; machining, pressure processing, etc.

5. REFERENCES

[1] Lorenz R. D., Schmidt P. B. Synchronized motion control for process automation // Proceedings of the IEEE Industry Applications Annual Meeting, vol. 2, pp. 1693-1698, 1989.

[2] Verbitckiy A. Inflexible rules. How don't be mistake with the choice of bender // Stanochniy park №6, 2014 pp. 32-34

[3] Gollandtcev Y. Comparison of the mechanical features of asynchronous and switched reluctance motors // Informatcionno-upravliaiushie sistemy №6, 2006. pp. 50-53

[4] Kozyrev V.V. Construction of the rollerscrew gears and the design methods / VLSU. Vladimir, 2004. 100 p.

[5] Kulenko M.S., Burenin S.V. Researching application of fuzzy controllers in technological processes control systems // Vestnik of ISPEU. Vol. 2 2010 y., pp. 72-76

[6] Leonenkov A. Y. Fuzzy simulation in Matlab and Fuzzytech. - S. - Ptb.: BKHV, 2003. 720 p.

[7] Chernetckii V.O., Chernetckaia I.V. Analysis and synthesis of fuzzy logic control system: - Chelyabinsk: SUSU, 2002.

Comparison of laser beam cutting and milling of plastics materials made from PMMA focusing on mechanical properties of the material

R. Nigrovič[a], J. Meško[a], R. R. Nikolić[b,c], V. Lazić[b], D. Arsić[b]

[a] University of Žilina, Faculty of Mechanical Engineering, Univerzitná 1, 01026 Žilina, Slovakia, E-mail: rastislav.nigrovic@fstroj.uniza.sk; jozef.mesko@fstroj.uniza.sk

[b] Faculty of Engineering, University of Kragujevac, Sestre Janijić 6, 34000 Kragujevac, Serbia, E-mail: vlazic@kg.ac.rs, dusan.arsic@fink.rs

[c] Research Center, University of Žilina, Univerzitná 1, 01026 Žilina, Slovakia, E-mail

Abstract

The characterization of influence of the laser cutting on material made from PMMA and comparison of laser beam cut samples to application of conventional method of milling for cutting the plastic materials are presented in this paper. The PMMA samples of 4 mm thickness were prepared and subjected to tensile test to establish their material strength after different types of cutting. Samples that were cut by the laser beam were also subjected to tempering to improve their mechanical properties. It was concluded that the way of cutting has the strong influence on those properties of the PMMA samples. The outcome of the experiment is a direct assessment of roughness of the cut samples, where the laser cutting demonstrates the lower values of surface roughness. However, for structural elements the more suitable would be application of the milling technology since it results in the higher mechanical properties of the cut sample.

Keywords: PMMA, laser cutting, milling, mechanical properties

1. INTRODUCTION

The principle of the laser cutting of metallic or non-metallic materials is based on the action of a focused laser beam on the material being cut. When cutting materials in technical practice, the surface is impacted by a focused circular beam of a diameter 0.1 to 0.4 mm, depending on the device construction and the thickness of the material to be cut. The laser beam of the above parameters, impacting the material being cut, will cause its rapid heating up. The material being cut is heated in milliseconds up to the melting or to the evaporation temperature, [1-2, 5-6, 8, 11].

When the laser beam hits the material being cut, there occurs an interaction between the material being cut and the laser beam. The subsequent processes, which take place during the cutting of the material, and the effect on the material properties following the focused beam impact, mainly depend on the chemical composition of the material being cut and on the quality of its surface, as well, [3-4, 6, 9, 10, 12].

In thermal cutting of metallic or non-metallic materials by a laser, it is always necessary first to create a hole in the processed material, from which the cutting would continue. Making the hole is based on the laser drilling principle and has slightly different characteristics of the course than that of the actual cutting. The impacting laser beam transmits the kinetic energy of the material photons, which is converted into heat that melts and partially evaporates the material being heated. The

surroundings of the laser beam inflammation site (in the material being cut) contain gases that become ionized instantaneously as the beam hits the material and change to plasma. The material being cut sublimates into a gaseous state, and is blown away from the material to the environment by the action of an assist gas under a relatively high pressure. The part of the material, which is not converted into a gaseous state, is blown in the liquid form by the flowing assist gas. The above-mentioned process causes formation of a pit in the material being cut, and the laser beam can penetrate continuously deeper, which results in depth melting of the material, [1, 7, 5, 12].

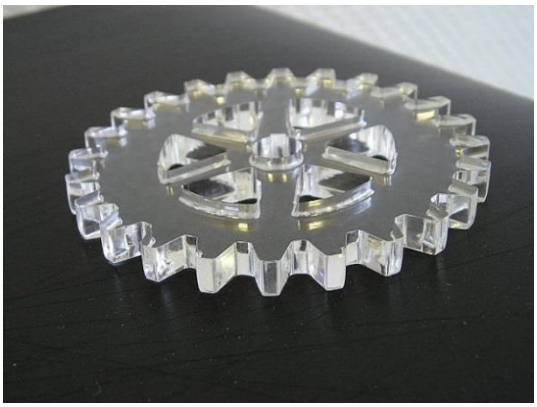

Fig. 1. Example of the PMMA product for laser cutting

The CO_2 lasers are particularly well suited to the cutting of PMMA. Applications of thermoplastic PMMA have grown considerably in many cases, for example, lenses, light pipes, outdoor signs, light covers, bathroom fittings, skylights, meter covers, baths and toys,[12].

2. EXPERIMENTAL CONDITIONS –MACHINES AND EQUIPMENT

The milling machine – GERBER Sabre 408 was used in experiments, with the following cutting parameters:

- tool diameter – ø 4 [mm]
- operating speed – 22 000 [RPM]
- milling speed – 36 [mms^{-1}].

The laser cutting and engraving machine – XL 1200 was used for the second type of cutting. The eurolaser offers the possibility to process extremely large samples on a comparatively small system. The processing area is 2270 mm x 1230 mm. With the optional camera recognition system, which is also available for other systems, the production flow can be automated, leading to an increased economy of the laser processing [14].

The laser beam cutting was done with the following parameters:

- power – 100 [W]
- cutting speed – 13 [mms^{-1}].

The PMMA milling schematics is shown in Figure 2 and the laser beam cutting in Figure 3.

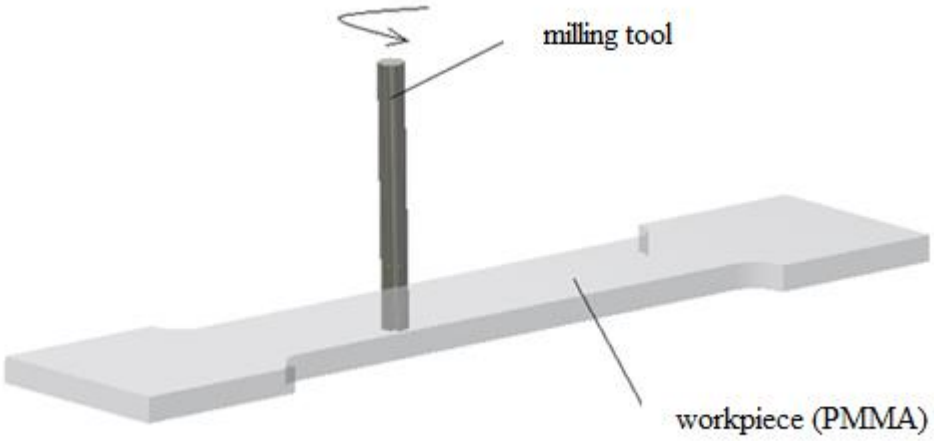

Fig. 2. Scheme of the PMMA milling

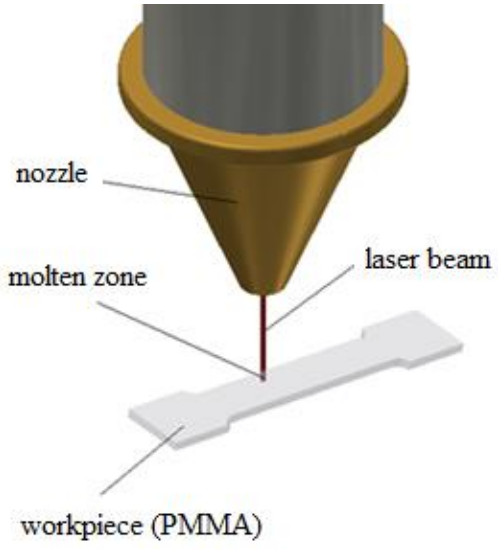

Fig. 3. Scheme of the PMMA laser cutting

3. EXPERIMENTAL CONDITIONS – MATERIAL

General Polymethacrylates are polymers of the esters of methacrylic acids. The most commonly used among them is polymethyl metacrylate - PMMA. Polymethyl metacrylate or polymethyl 2–methylpropenoate is the polymer of methyl methacrylate, with chemical formula $C_5H_8O_2$. It is a clear colorless polymer available on the market in both pellet and sheet form under the names Plexiglas, Acrylate, Perspex, Playcryl, Acylplast, Altuglas, Lucite etc. It is commonly called acrylic glass or simply acrylic, [13].

4. MAXIMUM STRENGTH MEASUREMENTS

In this experiment, the influence of the laser beam and the milling tool on the integrity and mechanical properties of the material was evaluated by measuring the strength of the PMMA. The samples were subjected to tensile test, to determine the impact of the character and integrity of the cutting edge after laser cutting and milling. Further, the laser cut samples were dried at 70 [° C] for 5 [h].

Table 1. The physical, mechanical and thermal properties of PMMA [13]

Density	1.15-1.19 [gcm^{-3}]
Water absorption	0.3 – 2 [%]
Hardness, Rockwell M	63 – 97
Tensile Strength, Ultimate	47-49 [MPa]
Tensile Modulus	2.2 – 3.8 [MPa]
Specific Heat Capacity	1.46 – 1.47 J/g ºC]
Thermal Conductivity	0.19-0.24 [W/mK]
Maximum Service Temperature , Air	41 – 103 [ºC]
Melting Point	130 [ºC]
Vicat Softening Point	47 – 117 [ºC]
Glass Temperature	100 – 105 [ºC]

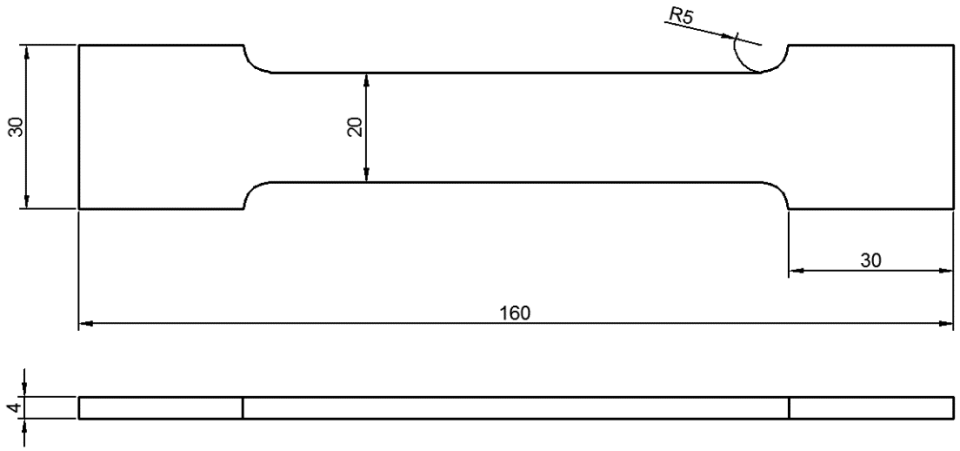

Fig. 4. Sketch of comparative samples for tensile test

The samples, which were milled had the average strength of 53.015 [MPa] and samples from laser cutting 35.405 [MPa], which means that the former samples (of 4 [mm] thickness and 20 [mm] width) had about 1.5 times higher tensile strength R_m than the latter, Table 2. These useful features make it ideal for use in demanding conditions. The laser cut samples were further additionally dried in a tempering oven at 70 [°C] for 5 [h]. However, that prolongs the time-consumption for production of parts cut by the laser beam, though it was almost 3 times faster (13 [mms^{-1}] compared to 36 [mms^{-1}] for milling. After the additional drying in tempering furnace, samples had the tensile strength of 40.57 [MPa].

Table 2. Tensile test for samples from PMMA [MPa]

Sample #	Laser cutting	Laser cutting – dried	Milling
1	35.65	42.86	57.12
2	39.04	38.42	49.97
3	34.44	41.52	43.99
4	32.5	39.5	60.98
average maximum strength Rm	35.4075	40.57	53.015

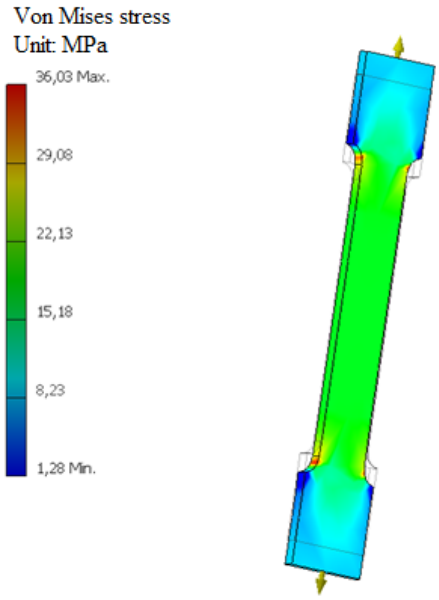

Fig. 5. Simulation tests of tensile strength

5. THE HAZ WIDTH MEASUREMENTS

During the laser beam cutting, the heat-affected zone (HAZ) appears in the PMMA samples. The measured values of the HAZ width are shown in Table 3, for both cases of the PMMA cutting, i.e. with and without additional drying. Appearance of the HAZ and the base material (BM) microstructures are shown in Figure 6 and 7, while in Figure 8 is presented the appearance of the surface after milling.

Table. 3. The PMMA HAZ width measurements [µm]

Sample #	Laser cutting	Laser cutting - dried	Milling
1	81.8	82.1	0
2	82.1	80.8	0
3	80.5	82.3	0
4	80.5	80.3	0
5	82.3	79.6	0
average	81.44	81.02	0

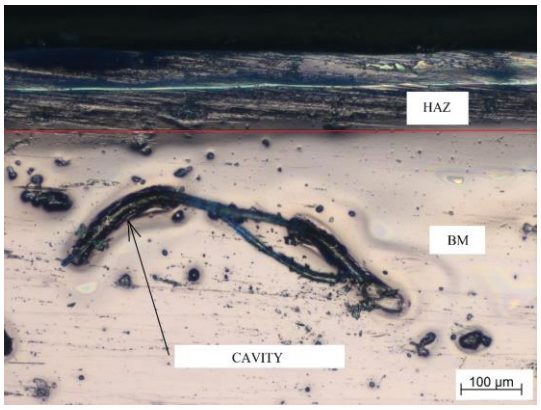

Fig. 6. HAZ and BM microstructures obtained by the laser cutting without drying

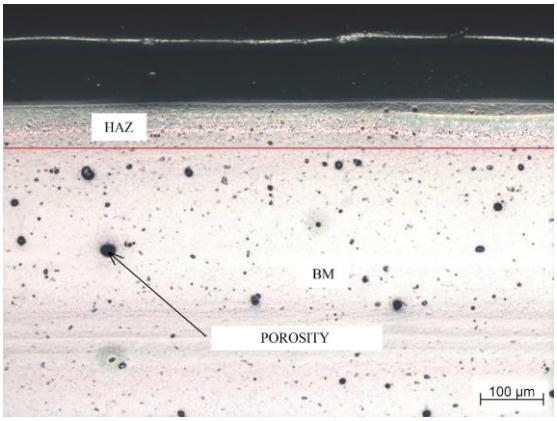

Fig. 7. HAZ and BM microstructures obtained by the laser cutting after drying

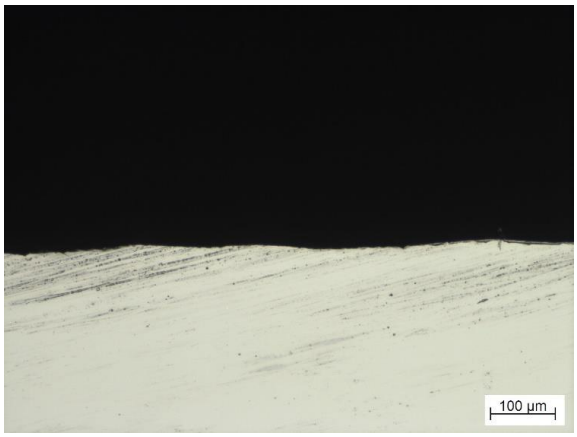

Fig. 8. Surface and microstructure after milling

From the measurements of the HAZ size and appearance of its microstructure, one can conclude that the tensile strength of the material was reduced due to appearance of cavities in the material just below the HAZ. On a small scale, those faults can be remedied by drying of the PMMA samples, what causes increase of the tensile strength, since the cavities sizes were reduced and the pores were regularly spaced. The width of the HAZ was not substantially changed after the samples drying. The heat-affected zone (HAZ) was not present in samples that were prepared by milling.

6. MEASUREMENT OF SURFACE ROUGHNESS EFFECT ON MAXIMUM TENSILE STRENGTH

The roughness of the cut surface was measured to establish if it imposes any influence on the material's maximum tensile strength. For the PMMA samples cut by milling the average surface roughness was R_z = 21.9 [µm], while for the laser-beam cut samples it was R_z = 1.1 [µm]. From those data, it can be easily concluded that the surface roughness has no effect on the material's maximum tensile strength; roughness was much bigger for the samples obtained by milling which had significantly higher maximum tensile strength. The only "influence' of the surface roughness is in optical appearance, since the surfaces obtained by the laser beam cutting looks smoother.

Images of the cut area surface geometry of experimental samples made of PMMA, obtained by laser cutting and by milling are shown in Figure 9 and 10, respectively.

7. CONCLUSION

The paper describes the principle of the laser cutting of plastics, in particular PMMA and the impact of the laser beam on the material and its ability to be cut. The PMMA is a specific type of plastic material that can be laser cut. Therefore, this type of material was considered from the viewpoint of its mechanical properties.

The PMMA samples were treated in three different ways – by milling and the laser beam cutting with and without drying. It was concluded that the type of cutting has the strong influence on material's mechanical properties, namely the tensile strength. It was significantly reduced for the samples cut by the laser beam than obtained by milling. It was also confirmed that this reduction in tensile strength is caused by appearance of cavities in the material just below the heat-affected zone, created due to heating during the laser cutting. The HAZ did not appear in samples obtained by milling.

The surface roughness of the cut surfaces did not impose any influence on the material's maximum tensile strength. It was significantly bigger for the PMMA samples obtained by milling, 21.1 [µm] (versus 1.1 [µm] for the samples obtained by laser cutting), which, on the other hand, had the maximum tensile strength significantly bigger, as well.

8. ACKNOWLEDGEMENT

This research presented in this paper was partially financially supported through realization of project VEGA no. 1/0186/09-(V-13-013-00) - responsible investigator: Jozef Meško and by the Ministry of Education, Science and Technological Development of Republic of Serbia through Grants TR35024 and ON174004 and Slovak state budget by the project "Research Centre of the University of Žilina" - ITMS 26220220183.

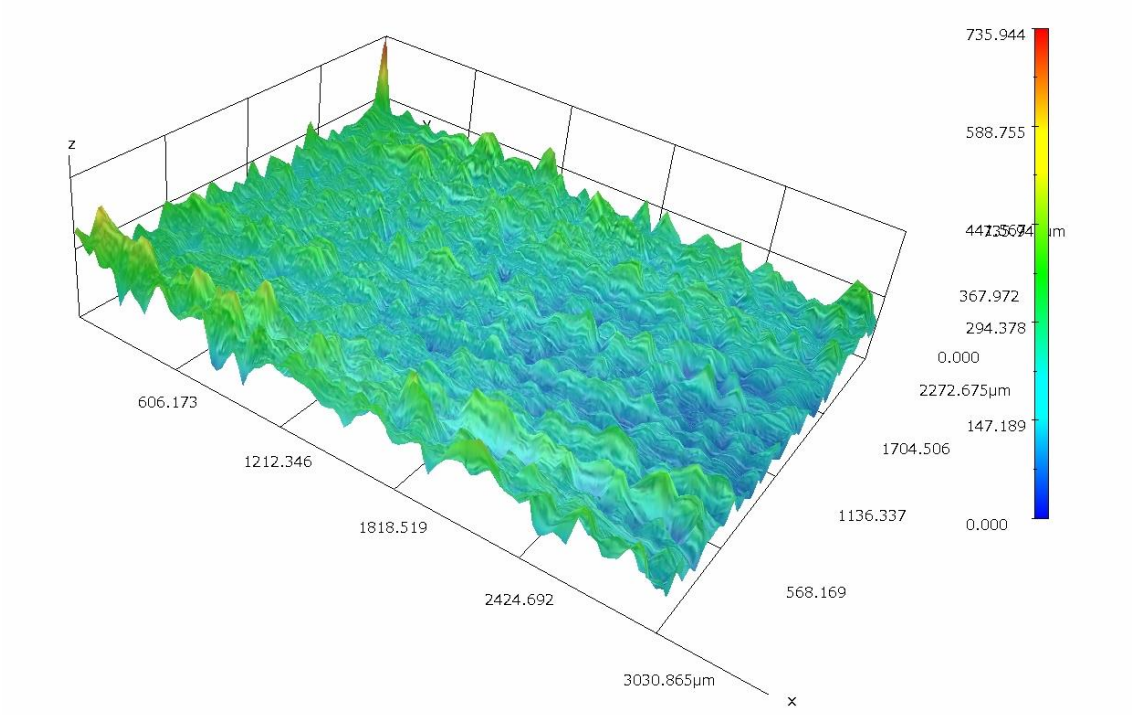

Fig. 9. Image of the cut area surface geometry of a PMMA sample obtained by laser cutting

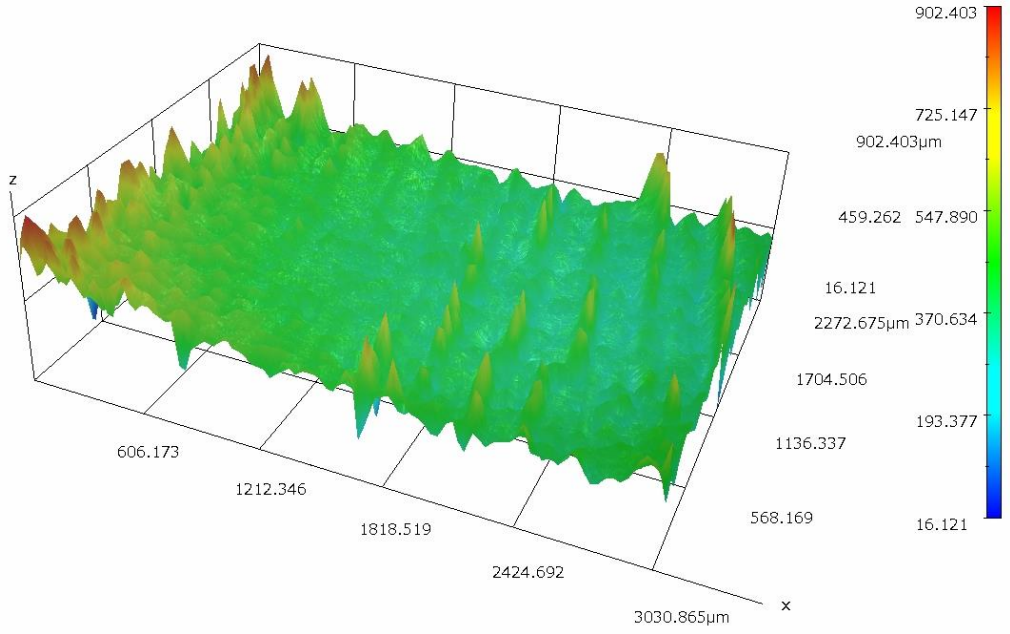

Fig. 109. Image of the cut area surface geometry of ae PMMA sample obtained by milling

9. REFERENCES

[1] Silvfast, W. T. (2004). Laser Fundamentals, Cambridge University Press, 666p. ISBN 0-521-83345-0.

[2] Caristan, L. C.(2004). Laser cutting guide for manufacturing. Dearborn, Michigan, USA: Society of Manufacturing Engineers, 452p.

[3] Žmindák, M., Meško, J., Pelagič, Z., Zrak, A. (2014) Finite element analysis of crack growth in pipelines. In: Manufacturing Technology: journal for science, research and production, Vol. 14, No. 1, s. 116-122.

[4] Sejc, P., Bielak, R., Svec, P., Rosko, M. (2006). Computer simulation of heat affected zone during MIG brazing of zinc-coated steel sheets. In: Kovové materiály. Metallic materials. Vol. 44, No. 4, pp. 225-234.

[5] Konar, R., Mician, M., Hlavaty, I. (2014). Defect detection in pipelines during operation using Magnetic Flux Leakage and Phased Array ultrasonic method. In: Manufacturing technology, Vol. 14, No. 3, pp. 337-341. J.E. Purkyne University, Ústi nad Labem.

[6] Konar, R., Mician, M. (2014). Non-destructive testing of welds in gas pipelines repairs with Phased Array ultrasonic technique. In: Manufacturing technology, Vol. 14, No. 1, pp. 42-47. J.E. Purkyne University, Ústi nad Labem.

[7] Mesko, J., Zrak, A., Mulczyk, K., Tofil, S. (2014). Microstructure analysis of welded joints after laser welding. In: Manufacturing technology, Vol. 14. No. 3, pp. 355-359. 341. J.E. Purkyne University, Ústi nad Labem.

[8] Radek, N., Mesko, J., Zrak, A. (2014). Technology of laser forming. In: Manufacturing technology, Vol. 14, No. 3, pp. 428-431. J.E. Purkyne University, Ústi nad Labem.

[9] Vrzgula, P., Faturik, M., Mician, M. (2014). New inspection technologies for identification of failure in the material and welded joints for area gas industry. In: Manufacturing technology, Vol. 14, No. 3, pp. 487-492. J.E. Purkyne University, Ústi nad Labem.

[10] Patek, M., Konar, R., Sladek, A., Radek, N. (2014). Non-destructive testing of split sleeve welds by the ultrasonic TOFD method. In: Manufacturing technology, Vol. 14, No. 3, pp. 403-407. J.E. Purkyne University, Ústi nad Labem.

[11] Lago, J., Bokuvka, O., NovY, F. (2015). The weld toe improvement of Domex 700 by laser remelting. In: 32nd Danubia-Adria symposium on advances in experimental mechanics, pp. 142-143. University of Žilina, Žilina.

[12] Huang, Y., Liu, S., Yang, W., Yu, Ch. (2010).Surface roughness analysis and improvement of PMMA-based microfluidic chip chambers by CO2 laser cutting. In: Applied surface science Vol. 256, pp. 1675–1678. Elsevier.

[13] Van Krevelen, D.W. (2009) Properties of polymers.

[14] EUROLASER. (2015). [online].2016, [accessed on 2016-02-01]. http://www.eurolaser.com/cz/products/laser-systems-for-acrylic/xl-1200-acrylic/>.

Statistical process control in the gear wheel manufacturing

M. Kučerová [a], H. Fidlerová [b], M. Homokyová[c]

[a,b,c] Faculty of Materials Science and Technology in Trnava, Slovak University of Technology in Bratislava, Jána Bottu 25, 917 24 Trnava, Slovakia, marta.kucerova@stuba.sk, helena.fidlerova@stuba.sk, maria.homokyova@stuba.sk

Abstract

Statistical process control (SPC) comprises very effective methods that use statistical tools to measure, monitor and control manufacturing process. The basic tool is a control chart; which is applied for specification of the process stability; thus if the process is under statistical control. Within SPC is assessed also the process capability. Capability is the ability of the process to produce products that meet customer's quality requirements.

This paper aims to present an application of the statistical process control in the manufacturing process of gear wheel. Based on a specification from a customer, it was necessary to improve the quality of products in company. Firstly, the teeth height was considered as an important quality parameter, primarily influenced by capability of the manufacturing process. Secondly, using control charts was detected a significant impact that caused the instability in the process. Corrective measures were subsequently proposed and implemented for a given process and the process capability was considered. Finally, the manufacturing process achieved a high level of capability, which provides conditions for manufacturing of products with the required quality. The proposed conceptual framework can help industrial engineers and managers in understanding application of SPC methods and tools for regulating and improving the manufacturing process in industrial company.

Keywords: Statistical process control (SPC); process capability; quality, case study; gear wheel

1. INTRODUCTION

Quality management is focused on quality planning, quality assurance, quality control and quality improvement. We agree with authors [1, 2] in compliance with mentioned quality components, it is necessary to carry out many corrective, preventive or proactive activities and measures.

Statistical Process Control (SPC) is a preventative approach to quality management. The aim of SPC is an early detection of deviations from the defined process level. The objective is to maintain a monitored process being at a desired and stable level, or the stable process further improved. It is realized by regular monitoring of regulated output. The result of this control is a confirmation, or non-confirmation that behaviour of the controlled variable is within the desired level. Maintaining the process stable depends on a comprehensive analysis of the process variability. It is necessary to monitor and analyse the process, its weaknesses, to find the causes and determine how to improve the process. Special developed processes are used for regulating the manufacturing process.

Objectives of the statistical process control are according Horálek [3]:

- More complex knowledge and information about monitored process;
- Control of this process to proceed in a desired manner;
- Elimination of the parameters variations of final product or process

improvement achieved by means of other approach.

Control charts are considered as an essential tool for regulating the manufacturing process. They are used for change of manufacturing process parameters, so that the amount of rejects does not exceed the permitted percentage. [4] Importance of control charts comprises in the quality management following activities:

- The process control: Control charts for variables are used to detect some changes in a mean and process variability, also to initiate a corrective action, thus to maintain the process stability;
- Analysis of the process capability: If the process is considered as stable, then the data from control chart should be used to calculate the capability indices and then the process capability is assessed;
- Analysis of the measurement system: Control chart demonstrates after assigning UCL, LCL if a measuring system is capable to ascertain the process or the product variability and also it is used to monitor the actual measuring system;
- Continuous improvement: through control charts can be monitored effectively the process performance, to predict its future status and to propose any necessary corrective action.

Aim of this paper is to present using SPC methods and tools for regulating and improving the manufacturing process in industrial company.

The structure of this paper is as follows: The first section considers a brief theoretical characteristic of the SPC and using of control charts. This section presents also a case study focused on the application of statistical methods and tools for the control of the moulding process. Within gear production is outlined a lack of quality in certain batch that had to be addressed. Furthermore, the main idea is to demonstrate a conducted process analysis and corrective measures to achieve a capable process as a prerequisite that the manufactured products have required quality and requirements of customer are met. Section 3 is devoted to the conclusions, whereby results and future recommendations are introduced for application of SPC methods.

2. METHODS AND MATERIALS USED IN CASE STUDY

In the quality management are used for improvement of products and process quality various methods, which are based on a standard procedure known as the Deming cycle PDCA. This technique is used by many methods, tools and techniques of quality management.

Methods and tools of statistical regulation were applied for the quality improvement of the wheel gears in this case study to monitor the current state of process, to analyze data, to test assumptions and to verify the proposed corrective measures.

Statistical process control is complex of methods that are based on statistical control and analysis of measured data.

The histogram was applied for a graphical presentation of data as well as a distribution and frequency analysis. Further, an inductive statistical method (Anderson -Darlingov test) was used for précising the normality valuation of the data distribution.

The Shewhart control chart was applied within analysis of the molding process in the gear wheel production.

The key method in statistical control is an evaluation of the process capability. Knowing the process capability is important for planning as well as for quality improvement. It provides an evidence for the producer and also the customer that the product is produced in stable

conditions, to ensure regular compliance with the prescribed criteria.

Assessment of the capability is based on statistical principles, using the capability indices as a quantitative form for expression a level of the quality for a given parameter or quality feature.

This includes the critical factor c_{pk} defined by Montgomery [5] as the measurement of the actual capability in the process. Index c_{pk} takes into account the process centering. In other words, c_{pk} deals with the case of a process with mean $\bar{x}$ that is not centered between the specification limits. The capability index c_{pk} can then be calculated as:

$$c_{pk} = \min\left\{\frac{USL - \bar{x}}{3\sigma}; \frac{\bar{x} - LSL}{3\sigma}\right\} \quad (1)$$

Where:
USL - upper specification limit
LSL - lower specification limit

It is important for precise evaluation a way of obtaining the data and compliance with restrictive conditions. Assessed process ought to be under statistical control and a distribution of the monitored quality characteristic ought to have a normal distribution [6].

2.1. Capability analysis of the manufacturing process

Presented case study was conducted in a manufacturing company in Slovakia. The main production program is focused on components produced for the automotive industry e.g. engines, gears, and wheel frames manufactured by means of the powder metallurgy. Core part of powder metallurgy is a compression moulding (stamping) of metal powder using heavy-duty presses. Powder metallurgy methods enable the production of structurally complex shaped products.

Determining characteristic, which is measured, monitored and controlled in most manufactured components – is a mass of the compact monitored immediately after the moulding process.

In certain cases, also other quality parameters are controlled such as a teeth height. Before assessment of a process capability it is necessary to assess the gauge, instrument and machine capability, as it is determined by standards, and the specifications and requirements of the customer.

Fig. 1. Component after a molding process

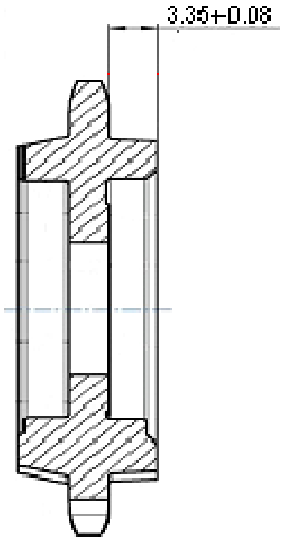

Fig. 2. Quality parameter according customers specification- teeth height of the gear wheel

Customer brought to attention the problem with the height parameter of a gear wheel in one batch (Figure 1). Produced pieces could not be calibrated and therefore had to be provided 100% control of all pieces in the company and defective pieces were discarded. From this reason the completion time was markedly increased and the amount of scrap was up to 2,354 units from production of 19,195 units.

During analysis the process capability was proven for the mass parameter, which is crucial for a powder metallurgy and then according customers' requirements was analyzed the teeth height parameter of gear wheel (Fig.2) which is presented in this study.

Measurement and determination of both parameters were carried out directly in three-shift operation in the production hall for the manufacturing of products.

Parameters were measured by several workers every hour, based on the set control intervals as well. The sample size was determined *n* is equal to 5 compacts, from a total amount produced per hour were randomly selected five items on which were controlled specified parameters.

The measured values were recorded to the prepared table. Software Minitab 14 was used for a data analysis, completing all the graphs and calculating statistical characteristics, UCL, LCL and capability indexes. For statistical process control was applied the Shewart control chart ($\bar{x}$, R) in the company.

The teeth height of gear wheel as a quality parameter defined by customer was measured by the digital dial indicator Mitutoyo. This parameter should be 3.35 mm with a tolerance of ± 0.08 mm according technical documentation.

During project required data were obtained after all 46 selections and the capability of molding process could be proceeded.

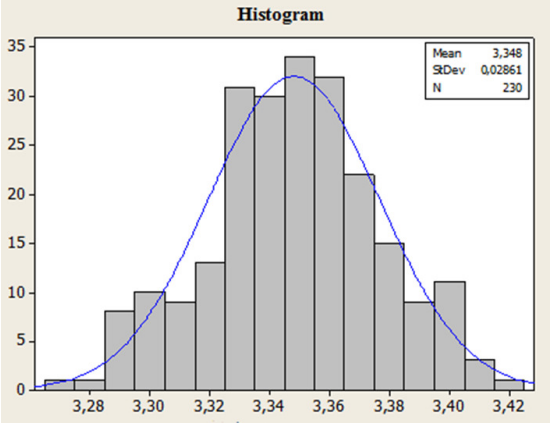

Fig. 3. Histogram [7]

Firstly, for verification of the normal distribution of collected data was used a graphical representation of the data set in the form of histogram. On the basis of a histogram (Figure 3), within the mean value 3.348 mm, it was not possible to confirm the assumption of a normal distribution.

Secondly, the data distribution normality was verified using Anderson - Darling test (Figure 4). According this one can consider a data distribution as normal if P-value ≥ 0.05. Otherwise (if P-value <0.05) assessed data set does not have a normal distribution. In our case, the P is equal to 0.541 and obtained frequency of distribution data can be considered as normal.

The next step of a project was determination whether the process is stable, so it is under statistical control using a Shewart control chart ($\bar{x}$, R) (Figure 5). Figure 5 describes a quality parameter assessment specified by customer from automotive industry – the teeth height of gear wheel. The large standard deviation of data and tighter USL and LSL illustrate the uncapable process. Graph for the process capability confirmed it and calculated capability indices c_p is equal to 0.94 and c_{pk} is equal to 0.92, which is less than 1, and therefore the process is considered as uncapable.

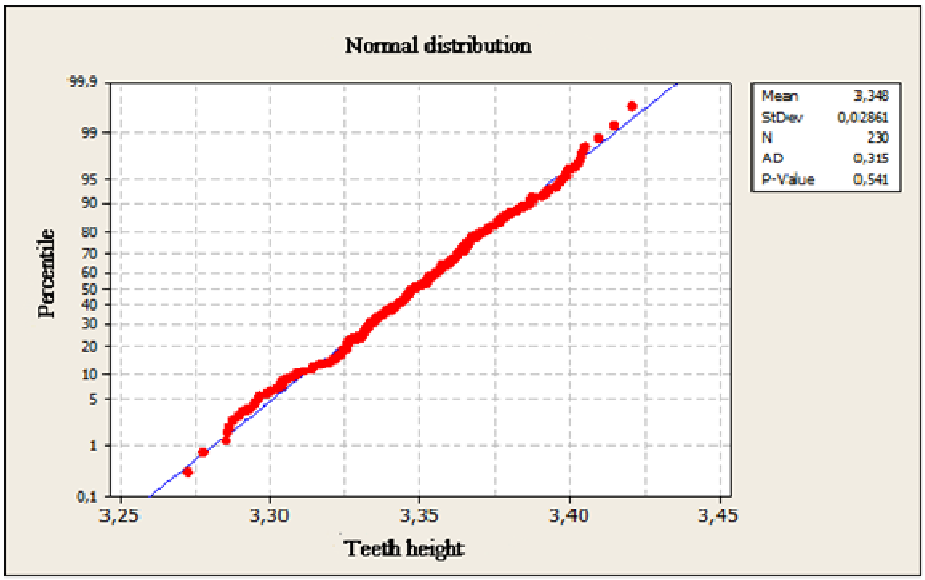

Fig. 4. Anderson - Darling test [7]

2.2. Capability analysis after the corrective measures in manufacturing process

In the previous part of project had not been confirmed the capability of molding process for the quality parameter – the teeth height of gear wheel. Important was primary to determine the cause of uncapable process and implement corrective action to eliminate it.

A frequent cause of uncapability of the manufacturing process is uncapability of the machine or equipment.

So it was necessary to solve the problem also in this case, to improve the quality and to propose some corrective measures in collaboration with experts from company.

It was noticed a significant influence in the manufacturing process and identified a root cause - setting of machine. The process capability was re-assessed after resetting the machine. Data were collected during more than 5 days.

The teeth height was measured again to achieve up to 610 data. Description of the data analysis is to find in the next part of contribution. The first step in the data analysis was also the same assessment if a set of received data corresponds to the normal distribution. After this condition was met, it could proceed the analysis of process stability by means of the Shewart control chart.

The capability index c_p for teeth height parameter of the gear was equal to 2.47 and a critical factor was 2.39. Based on the calculated indexes the manufacturing process could be considered after corrective measures as capable (c_p, $c_{pk} > 1.33$).

Improving the manufacturing process of gear wheel was confirmed by the company because from 11,484 units produced was neither discarded.

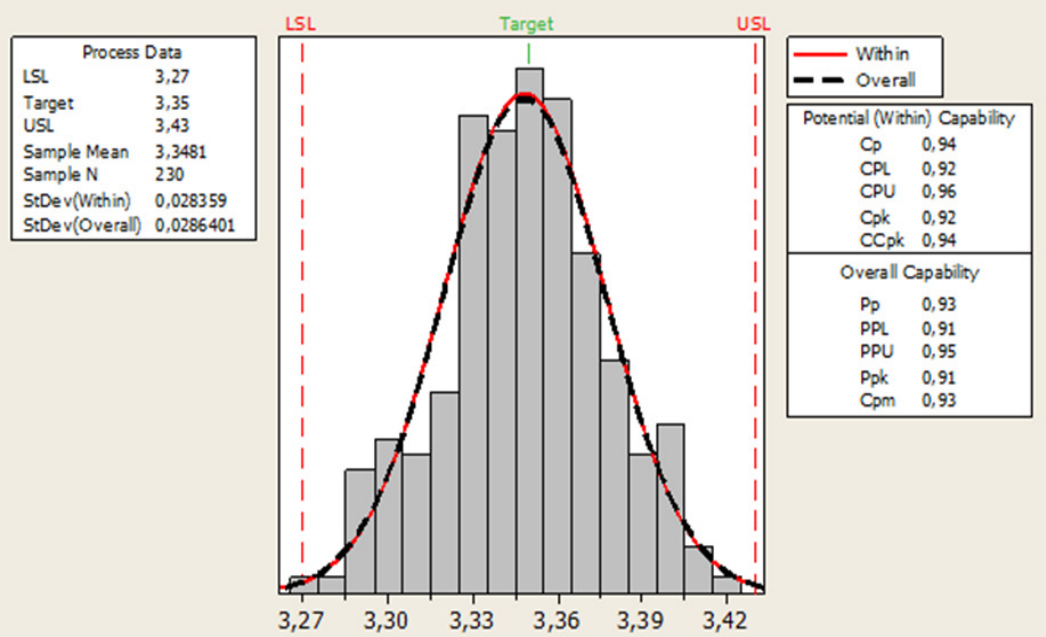

Fig. 5 Process capability for the quality parameter [7]

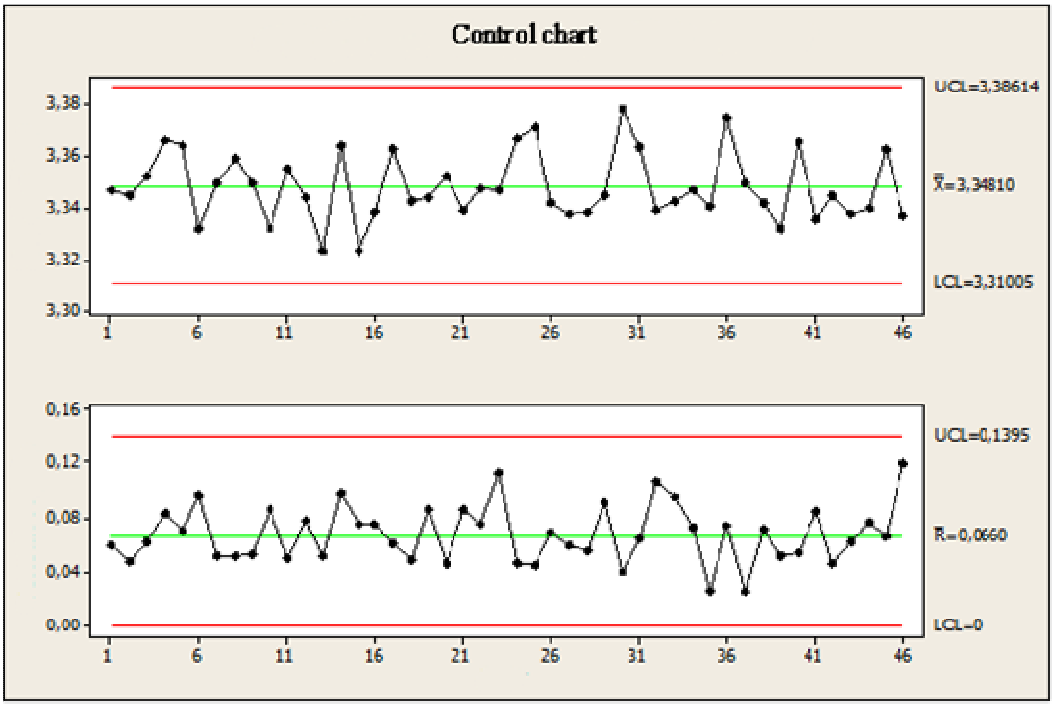

Fig. 6 Control chart for the quality parameter

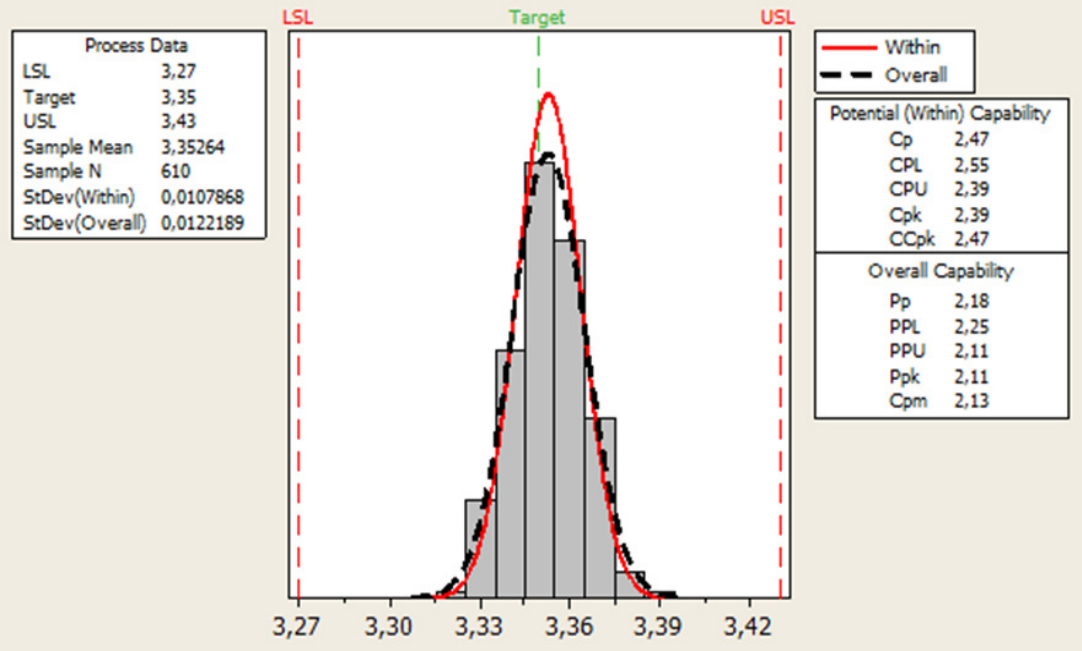

Fig. 7 Process capability for the quality parameter after corrective measures [7]

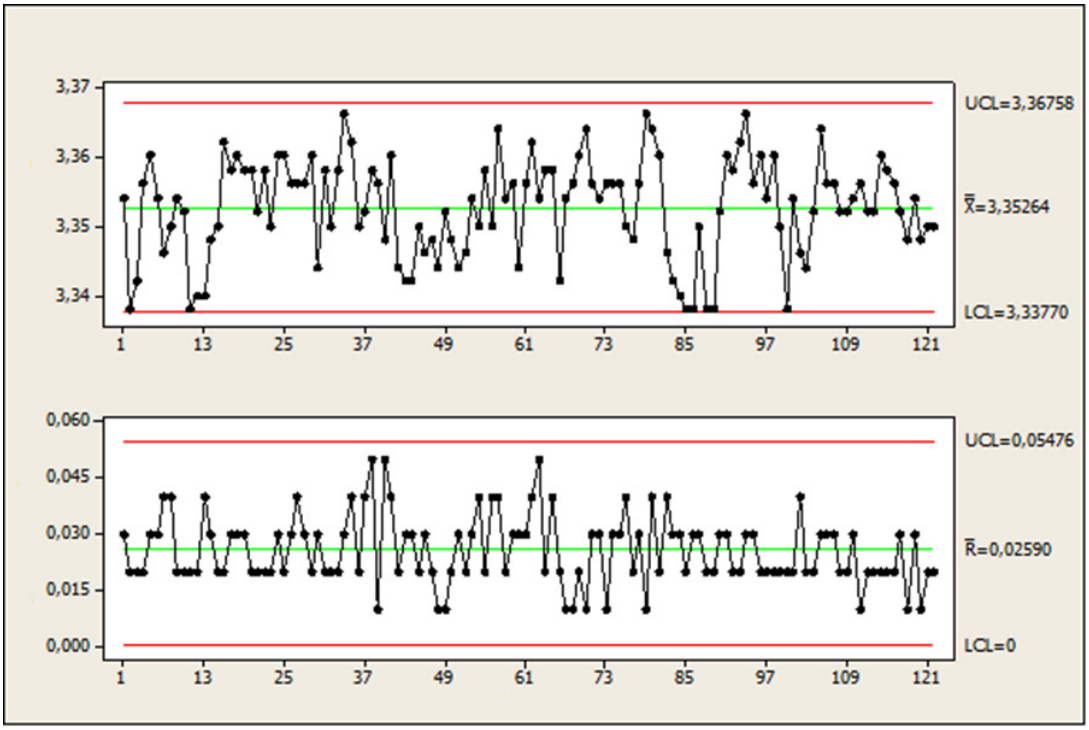

Fig. 8 Control chart for the quality parameter after corrective measures

3. CONCLUSIONS

The aim of introduced case study was to improve the molding process of gear wheels using the tools and methods of the SPC. In a production batch was identified a problem with the height parameter of products that did not comply with the specifications and it could not be calibrated and had to be discarded as a scrap. In addressing this issue, the important step was to determine why the process is incapable. It was subsequently performed as a measure the resetting of the machine. The problem was that prior to the identification of the process capability should be determined whether the production machine or equipment is capable. From conducted solution ensue specific measures for the application of SPC in the company in the production process of other products as well as general conclusions for monitoring, managing and improving production processes in manufacturing companies.

It is necessary before the capability assessment of the manufacturing process by the application of capability indexes to make first the capability assessment of the instrument, respectively Measurement System Analysis (MSA) and also assessment of the machine, respectively manufacturing facility, where the production process takes place. With determining MSA is evidence of the accuracy of the measured data, the correct use, and appropriate measuring device. Assessment of the production equipment capability helps to select for the process such a device which is able to produce the products with required parameters.
It is necessary based on requirements and specifications that given by customer in capabilities assessment of the instrument, machine and process. Fulfillment of customer requirements is one of the main principles of quality management.

We affirm from this case study and our research [8] that improving of processes and products is a permanent activity, in which can be applied to many statistical tools and methodology.

Each company aims to optimize the control and possible improvement of the processes that are directly related to customer specifications and requirements or processes that significantly influence the effectiveness of other processes.

As seen in introduced case study it is important that enterprise using statistical methods can convince its trading partners on the quality of production and products on the basis of facts obtained by the appropriate application of statistical methods and tools.

4. REFERENCES

[1] J. Nenadál et al., Moderní management jakosti: principy, postupy a metódy. Management Press, Praha (2008).

[2] M.Dekking, C. Kraaikamp, H.P. Lopuhaa, A modern introduction to probability and statistics, understanding why and how, Springer (2005).

[3] V. Horálek, Jednoduché nástroje řízení jakosti I, Národní informační středisko pro jakost, Praha (2004) , p.63-74

[4] M. Meloun, J. Militký, Kompendium statistického spracování dat. Karolinum, Praha (2012).

[5] D.C. Montgomery, Statistical Quality Control: A Modern Introduction. 6th ed. Hoboken: J. Wiley and Sons, 012. 768 p.

[6] S. Eldin., A. Hamza, Monitoring and controlling design process using control charts and process sigma, Business Process Management Journal, (2009), 15: 358–370.

[7] D. Maslíková, Measurement, monitoring and improvement of processes in an industrial enterprise. MTF STU Bratislava, (2014).

[8] M. Kučerová, H. Fidlerová, Improving the Quality of Manufacturing Process through Six Sigma Application in the Automotive Industry. In Applied Mechanics and Materials Vol. 693 (2014) pp. 147-152.

Cutting analysis of CFRP composites

Krisztián Kun [a]

[a] Pallas Athena University, GAMF
Izsáki st. 10, 6000, Kecskemét
kun.krisztian@gamf.kefo.hu

Abstract

This study shows the first step of a prospective research series. The composite materials form a heterogeneous system. These required much more complex examination, compared to conventional tasks. In this theme we search the answer how to analyze carbon fiber reinforced plastic (CFRP) pieces during cutting process. Orthogonal machining of carbon fiber reinforced polymer is simulated using finite element method.

Keywords: Analysis, CFRP, FEM, Composite, Cutting

1. INTRODUCTION

Carbon fiber reinforced polymer (CFRP) composites are widely used in various applications, due to their high specific strength and high specific stiffness. CFRPs can be expensive to produce but are commonly used wherever high strength-to-weight ratio and rigidity are required, such as aerospace, automotive, civil engineering, sports goods and an increasing number of other consumer and technical applications.

Most of the CFRP products are made to final shape, however material removal by machining is often carried out to meet dimensional requirements and assembly needs. The composite material forms a heterogeneous system so machining CFRP products is difficult due to their material discontinuity. Also various factors such as fiber pull-out, delamination, matrix burning and subsurface damage lead to undesired surface quality.

This study can be divided into two main parts: At first, with a computer-aided design application, Autodesk Inventor software we created the 3D digital prototype of the workpiece and the tool. The used method is relying on thoroughly recognised studies. The second part of the study aimed to analyze this model but to keep the process tractable it had some simplifications.

2. MODELLING OF COMPOSITE MATERIAL AND ITS TOOL [1,3,4,5]

Modelling of composite pieces can be accomplished in different ways. We operate with a model based technique to create the composite piece. In this case, we have to enter the thickness of the individual layers during the modelling.

Furthermore, to define material properties of each layer we made them separately. So there was a body of the carbon fibers and another one which was the matrix (epoxy). So we can say that the modeled piece is an equivalent homogeneous material. In orthogonal machining operation it will be probably the prime source of deviation between the further experimental and this numerical result.

2.1. Cutting tool design [2]

The simplest cutting operation is one in which a straight-edged tool moves with a constant velocity in the direction perpendicular to the cutting edge of the tool. This is known as the two-dimensional or orthogonal cutting process illustrated in figure 1. The cutting operation can

best be understood in terms of orthogonal cutting parameters.

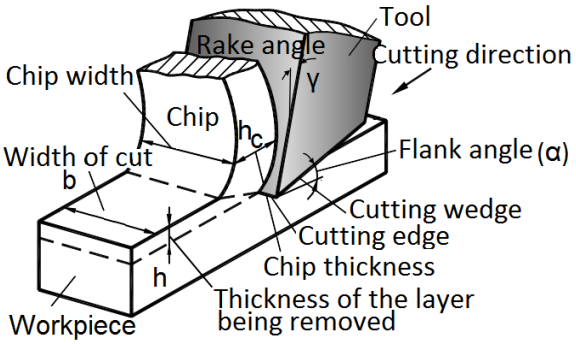

Fig. 1. Visualization of basic terms in orthogonal cutting [2]

We used a HSS planar tool for the experiment which is shown on the figure 2.

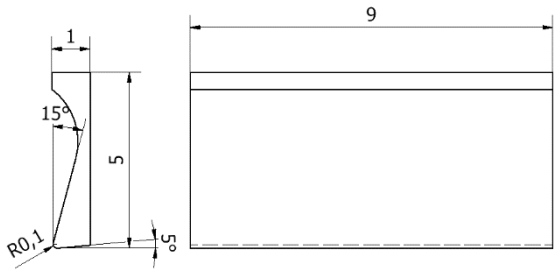

Fig. 2. The necessary detail of the planar tool for the analysis

As already mentioned earlier, there are some simplifications in the used model. As shown on the figure above only a detail of the tool has been designed. This modification facilitates the analysis.

2.2. Modelling of composite material [1]

There are some analytical as well as empirical models ([1,5]) proposed over the years to predict the occurring accompaniments. A small number of articles were presented in this area: work on cutting of CFRP composites [4,5]. In these studies, the machining characteristics were considered for only parallel fiber orientations.

Based on these articles, the model cited here presents the composite material as 0.05 mm thin layers. These forms 2 solid bodies: Fibers and Matrix. It is shown on figure 3.

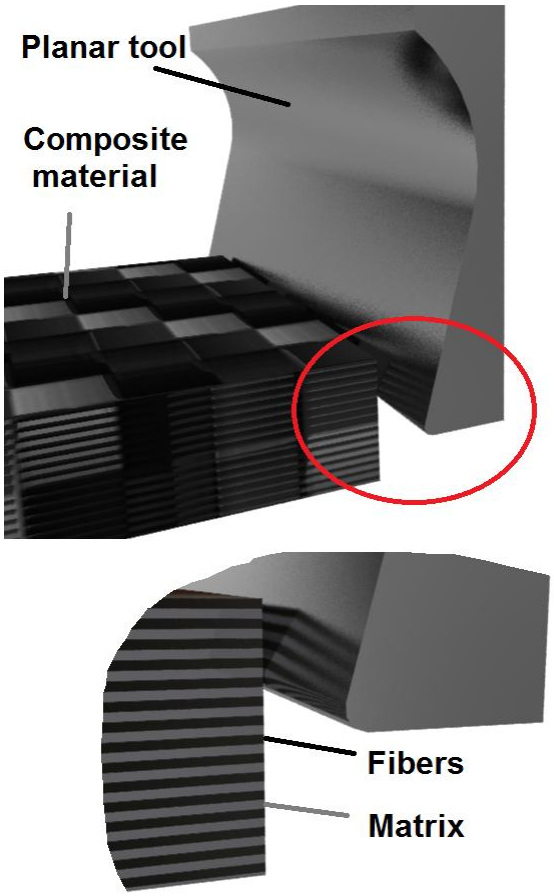

Fig. 3. The CFRP material's simplified composition: 0.05 mm thin fiber and epoxy layers

In the numerical model, to keep the problem tractable, only region of the work material is modelled. [1]

3. FINITE ELEMENT MODELLING

In the present study, a macro finite element model is developed to estimate the response of the machining process. Finite element method (FEM) is widely used to predict the machining parameters of metals. This technique has been extended to composites too.

Finite element analysis software tool ANSYS v14 was used for simulation of orthogonal machining. The explicit dynamics analysis used for machining the CFRP composites.

3.1. Material properties in Engineering data [1,5,6,7]

First of all, in ANSYS we have to set the right materials for each layers. In the general material

library, we cannot find CFRP so we have to create a fiber and an epoxy material as well.

The Young's modulus of carbon fiber in tension and compression in longitudinal direction is different (Table 1.).

Table 1. Mechanical properties of materials used in FE simulation [1]

No	Material	Properties	
1.	Carbon fiber	Young modulus (0°)	E = 14 GPa
		Tensile strength (0°)	R_m=350 MPa
		Comp. strength (0°)	f_c = 273
		Poisson's Ratio	υ = 0.2
2.	Matrix (epoxy)	Elastic constant	E = 3.1GPa
		Tensile strength	R_m = 70MPa
		Poisson's Ratio	υ = 0.3

Once we built these materials, we applied them on the correct pieces.

3.2. Finite element modelling

First of all, we have to know that the mesh is a sum of function plots that link every node in our FE model. Between nodes, the curves can be of 1st order, (line with no inflexion point) (fig. 4):

$$a \cdot x + b = 0, \qquad (1)$$

of 2nd order (quadratic with one inflexion point)

$$a \cdot x^2 + b \cdot x + c = 0, \qquad (2)$$

or 3'd order (cubic with 2 inflexion points)

$$a \cdot x^3 + b \cdot x^2 + c \cdot x + d = 0 \qquad (3)$$

higher the order, higher the resolution and the precision of the result.

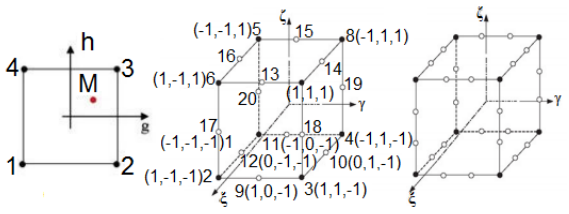

Fig. 4. From the first to the 3'd order

So a future improvement for this numerical result (to approach the experimental tests) is the mesh clarifications. In the Ansys explicit dinamics we use quadrilateral mesh for the composite material, which has 0,05 mm width, while the tool has a triangle mesh (Figure 5.).

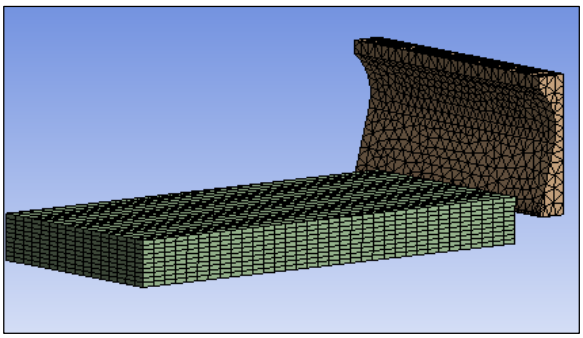

Fig. 5. The model represented by quadrilateral and triangle meshes

Thereafter we put fixed support on the composite workpiece and used 20 m/min (table 2.) velocity to the tool in the right direction as shown on figure 6.

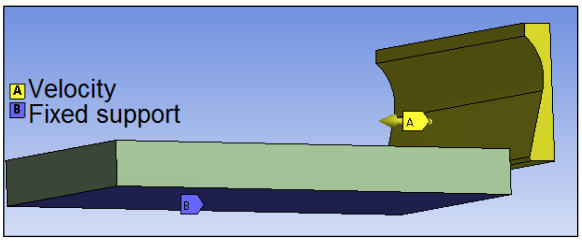

Fig. 6. 20m/min velocity tool and fixed workpiece

The table 2. contains all the important geometrical and technological parameters for the analysis.

Table 2. Mechanical properties of materials used in FE simulation

Cutting speed	v [m/min]	20
Theorethical chip thickness	h [mm]	0,5
Work-piece lenght	L_w [mm]	140
Chip widht	b [mm]	6
Rake angle	γ_n [deg]	15
Cutting edge radius	r_n [μm]	10
Temperature	T (°C)	22

4. RESULTS OF THE ANALYSIS

After analyzing we were interested in two results: First needed output was the shear plane angle and the other one was the equivalent (von Mises) stress.

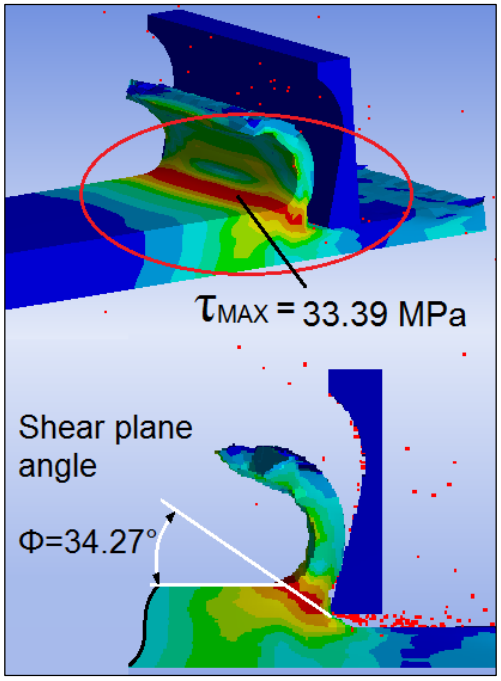

Fig. 7. Measure of the shear plane angle after the analysis

With these outputs we could use a simple 2D mechanistic model to find the shear force (fig 8.). We can proof this method with some simple calculations. [8]

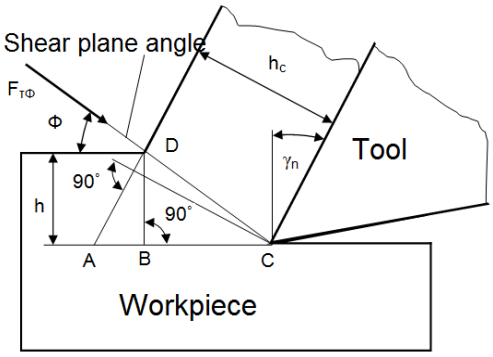

Fig. 8. 2D mechanistic model for shear force calculation [8]

$$F_{\tau\Phi} = A_{\Phi} \cdot \tau_{max} = (CD) \cdot b \cdot \tau_{max}$$

$$= \left(\frac{h}{sin\Phi}\right) \cdot b \cdot \tau_{max} \qquad (4)$$

$$F_{\tau\Phi} = \left(\frac{0.5}{sin34.27}\right) \cdot 6 \cdot 33.39 = \underline{353.24\ N}$$

5. CONCLUSION

The composite materials form a heterogeneous system, so these required much more complex examination, compared to conventional tasks. We had several simplifications in our model: We had simplification in the composite design as well as the analysis (mesh) to keep the problem tractable.

So future improvement for this numerical result needs several modifications, and further validations (experimental tests).

Considering the fact, this research is the first step in a prospective research series, further tests, useful advices and constructive criticism are necessary to improve the model.

6. REFERENCES

[1] G. Venu Gopala Rao, P. Mahajan, N. Bhatnagar. Micro-mechanical modeling of machining of FRP composites – Cutting force analysis (2006.) p.1-15.

[2] Viktor P. Astakhov. Basic Definitions and Cutting Tool Geometry, Single Point Cutting Tools (2010) p. 55-56

[3] Koplev A, Lystrup Aa, Vorm T. The cutting process, chips, and cutting forces in machining CFRP. Composites 1983;14(4):371–6.

[4] Caprino G, Santo L, Iorio I. Chip formation mechanisms in machining unidirectional carbon fiber reinforced plastics. In: Proceedings of the 3rd AITEM Congress, Salerno, Italy; 1997. p. 65–72

[5] Arola D, Ramulu M. Orthogonal cutting of fiber reinforced composites: a finite element analysis. Int J Mech Sci 1997;39(5): 597–613.

[6] Mahdi M, Zhang L. A finite element model for the orthogonal cutting of fiber-reinforced composite materials. 2001;113:373–7.

[7] Arola D, Sultan MB, Ramulu M. Finite element modeling of edge trimming fiber reinforced plastics. 2002;124:32–41.

[8] János Kodácsy, József Pintér. Forgácsolás és szerszámai (2010.) 3.1

Development of On-line monitoring system for monitoring main welding parameters

D. Marić [a], V. Starčević [a], M. Duspara [a], A. Stoic [a], I. Samardžić [a]

[a] Mechanical Engineering Faculty in Slavonski Brod, Trg Ivane Brlić Mažuranić 2, 35000 Slavonski Brod, Croatia, dmaric@sfsb.hr

Abstract

Paper describes development of application for on-line monitoring system for monitoring main welding parameters such as current and voltage. Main welding parameters (voltage and current) with other welding parameters (welding speed, arc length, stick – out, etc.) are very important for stability of welding process, and they will influence directly on quality of welding joint. In order to avoid poor quality of welded joint it`s important to monitor and control parameters of welding. Also, paper present some examples of successful applications of on-line monitoring system.

Keywords: On - line monitoring, main welding parameters, current, voltage, welding defects

1. INTRODUCTION

Measurement and recording of main welding parameters (electric current and voltage), with application of different temperature sensors, high speed cameras and weld defect detection system can be used to evaluate process stability. [1] Also, in order to deduce about stability of welding process from obtained data it is important to make acquisition of large number of data.

Welding process, i.e. main welding parameters can be recorded and monitored on different way (with ammeter, voltmeter, light sensors, sound sensors, with *on – line* monitoring system, with oscilloscope, with systems built – in welding devices (i.e. Welbee) etc.) [3]

Importance of monitoring and processing of main parameters is also shown by new trends in development of welding power supply with modules for evaluation of process stability built – in equipment. Moreover, welding parameters will strongly influence on mechanical property and microstructure of welded joint [4,5]. Monitoring of welding parameters and controlling is important for all welding processes [5,6,7,8], and all of the above requires development of new system for monitoring main welding parameters. Prior to the development of measuring device several requirements have been set. Some of requirements were flexibility (such as ability to connect on different welding power supply, simply data record, large amount of data which will be recorded, noise elimination from environment, ability of recording both AC and DC current, different temperature sensors ability, quality control, etc. Development of device will be shown in further work with one example of successful testing of device.

2. DEVELOPMENT OF EQUIPMENT FOR MAIN WELDING PARAMETERS MEASUREMENT

For measuring and control of main welding parameters UI MEASUREMENT BOX measurement device has been used. On Fig. 1 can be seen device for measuring electric current and voltage which is used for measurement

behaviour of electric current and voltage in experiments during the welding.

UI MEASUREMENT BOX is composed with following components:

- AC/DC current sensor, accuracy: 0,5%, range: +/- 500A
- Voltage sensor in range: +/- 100 V max, AC/DC
- ALU box
- Power supply, 85 - 264 V AC se +/- 12V
- Voltage, Power, USB connectors

Fig. 1. UI Measurement box

Specifications of NI USB-6212:

- 16 analog inputs (16-bit, 400kS/s)
- 2 analog outputs (16-bit, 250 kS/s); 32 digital I/O (24 for mass termination); two 32-bit counters
- Bus - powered USB for high mobility; built - in signal connectivity

Except sensors for electric current and voltage measurement built – in UI Measurement box for easier connection with welding device, also power sensor from Fig. 2 (Split-core DC current transducer hall effect current sensor HCT-0036-500, opening with ratings up to 500Amps) sensor from Fig. 3 (Split-core AC current sensor SCT-3000-2000, opening with ratings up to 2000 Amps) has been used. These two types of sensor were used because they have possibility to open and they are easier to connect with measuring spot on welding device.

Fig. 2. Sensor HCT-0036-500

Fig. 3. Sensor SCT-3000-2000

In order to ensure quality measurement, collecting and analysis of data it´s necessary to create software solution. In that purpose, two software's were created with software tool LabVIEW. First software is aimed for measurement and collecting data (Fig. 4). This software allows on – line data analysis too.

When data is recorded, it s possible to process them statistically in *off – line* mode and prepare for printing in other software (Fig. 5).

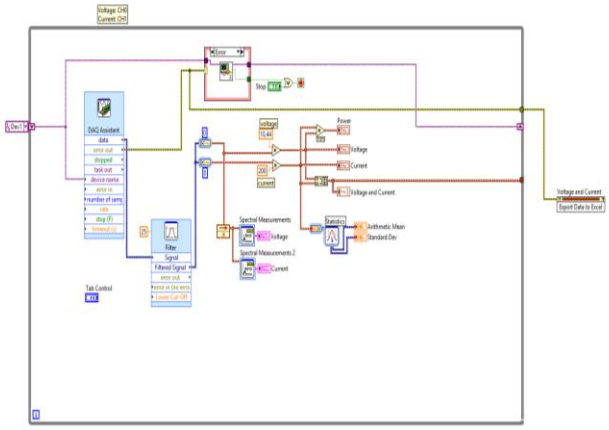

Fig. 4. Program block diagram of DAQ modular

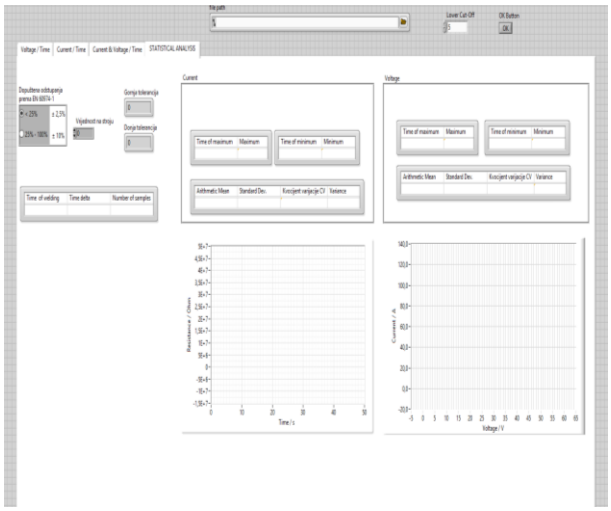

Fig. 5. Front panel of the LabVIEW statistical software

3. MEASURING, COLLECTING AND ANALYSIS OF DATA WITH CREATED EQUIPMENT

Experimental part of the work is conducted in laboratory conditions. For the purpose of experiment P265GH (1.0425) is used as a base material, dimensions 300 x 150 x 10mm. As a plan of experiment is used central composite design (CCD)

The aim of this work is, based on already well - known and controlled conditions during SMAW welding process to carry out testing of UI Measurement box equipment.

Since the SMAW process was chosen, selected parameters for this experiment were electric current and travel angle of electrode (according to recommendations from literature).

As a constant parameter were chosen: type of polarity (DC, plus (+) pole), type of electrode (Jadran S, L = 300 mm, Φ 2,5 mm), length of electric arc is trying to maintain as a diameter of electrode and horizontal welding position (P,H)

In table 1 review of welding parameters for each experiment for two variable (current and travel angle of electrode is shown. There are two repeating in central point, and total number of run in this experiment is ten.

Table 1. Experimental designs

Pokus	*I* [A]	*f* [°]
I	50	5
II	120	5
III	50	35
IV	120	35
V	135	25
VI	35	25
VII	85	0
VIII	85	40
IX	85	25
X	85	25

On Fig. 6 performance of experiment and proper determination of travel angle of electrode is shown.

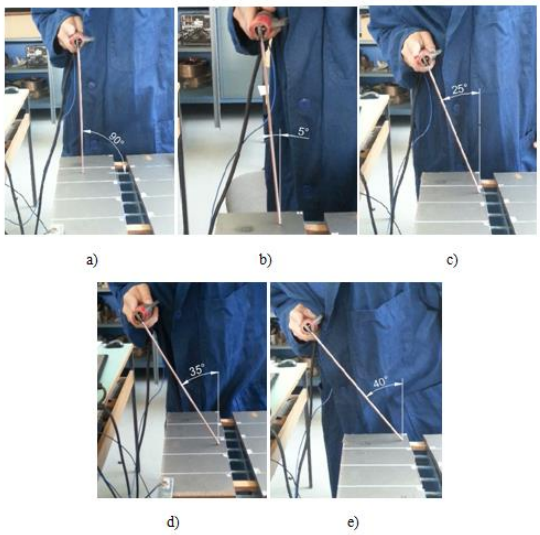

Fig. 6. Travel angle of electrode

(a - 0°, b - 5°, c - 25°, d - 35°, e - 40°)

In order to conduct measurement on a proper way, all equipment must be connected according to block scheme (diagram) shown in Fig. 7. Both sensors built – in UI MEASUREMEN BOX Current Transducer LF 305-S and sensor for current measuring were used (here).

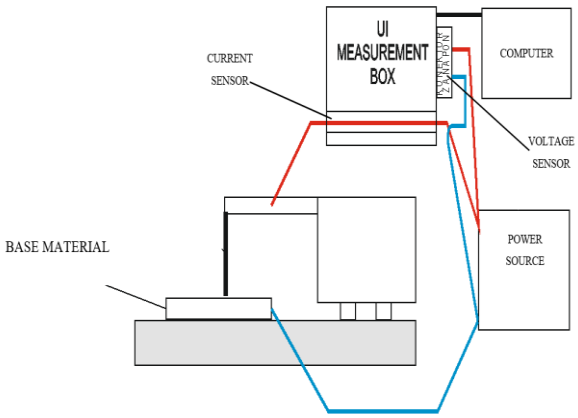

Fig. 7. Block scheme connection of UI Measurement box for main welding parameters measuring

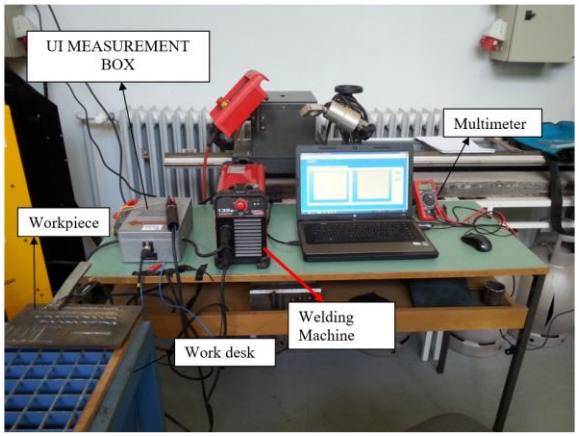

Fig. 8. Experimental setup

Equipment used for measurement of main welding parameters of SMAW welding is:

- **Welding power supply** (Lincoln Electric Invertec 135S)

- **Protecting mask**,

- **Protective equipment** (gloves, apron)

- **Universal measurement device**,

- **Computer**,

- **UI Measurement box.**

During the welding process universal measuring device UNI-T, UT132C and current clamp FLUKE, 376 True RMS also were used. These two measuring devices were used in order to compare and follow results obtained by UI Measurement box.

During the measurement, it´s possible to *on – line* monitor and record all data.

Since the large amount of data (100 000 data per second) is about, and time range from 40. to 120. second was considered, it was much easier to conduct after the welding process, with developed software. In table 2 recorded data of electric current and voltage for each experiment were shown.

Table 2. Measuring results

No	Welding parameters	Diagram of obtained values of electric current and voltage	Appearance of welding joint
1.	I= 50 A f= 5 °	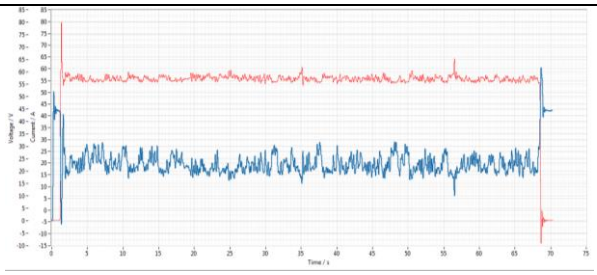	
2.	I= 120 A f= 5 °	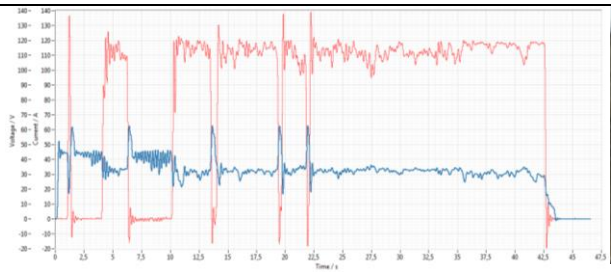	
3.	I= 50 A f= 35 °	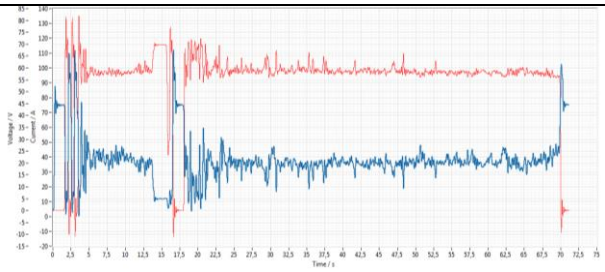	
4.	I= 120 A f= 35 °	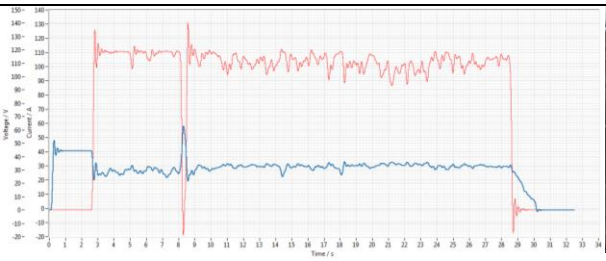	
5.	I= 135 A f= 25 °	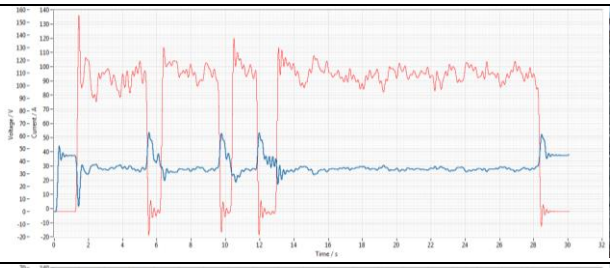	
6.	I= 35 A f= 25 °	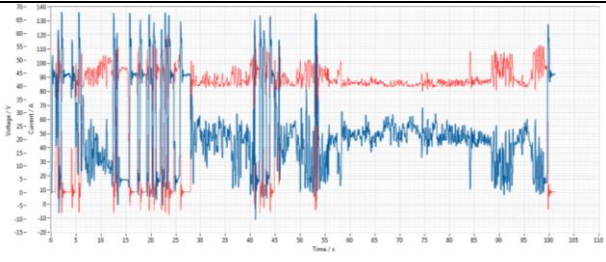	

7.	I= 85 A f= 0 °	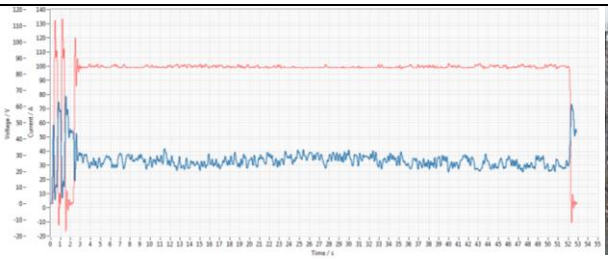	
8.	I= 85 A f= 40 °	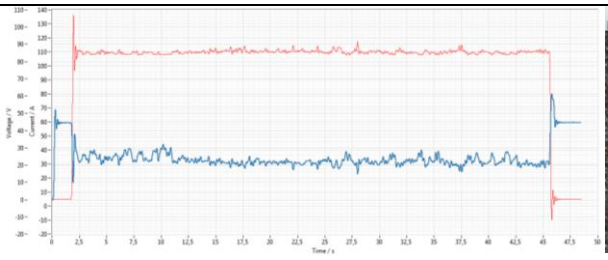	
9.	I= 85 A f= 25 °	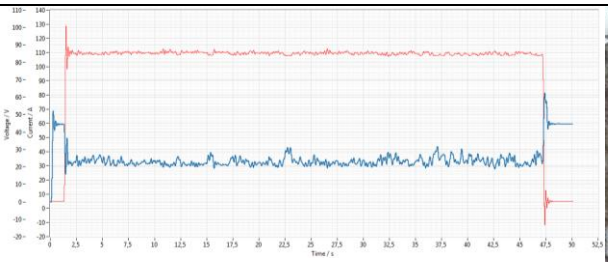	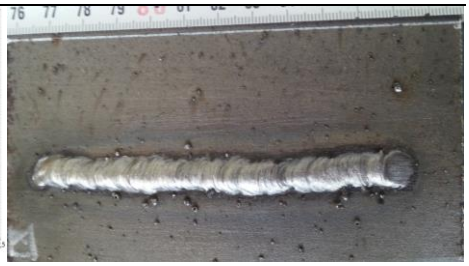
10.	I= 85 A f= 25 °	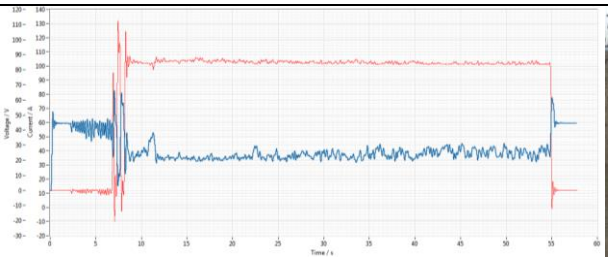	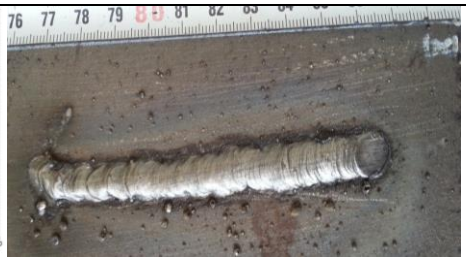

All data can be recorded in *.xslx format (Excel) but because of simplicity of processing were recorded in *.tdms format which can be easily load in LabVIEW statistical software solution.

On Fig. 9 was shown processing of signal in experiment no. 1. Besides the time of appearance of minimal and maximal values of current and voltage, some statistically important and necessary values for main welding parameters processing were given too.

Also, permissible deviations for current adjusted on welding power supply according to standard EN 60974-1 were given.

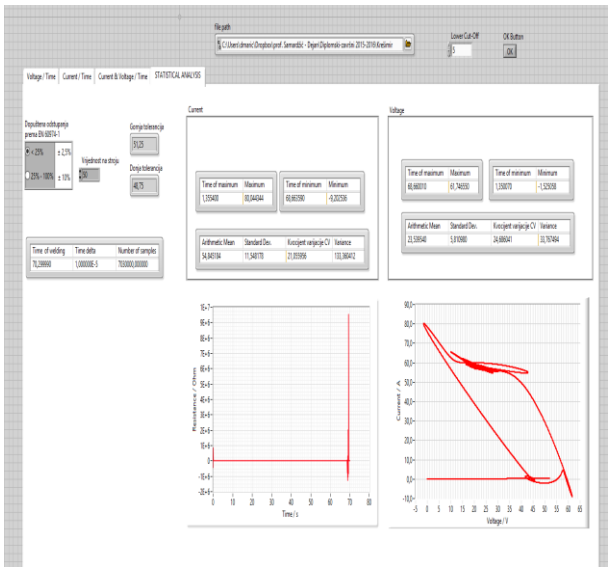

Fig. 9. The front panel of the LabVIEW statistical software with results of the experiment I

4. CONCLUSIONS

Control of main welding parameters (electric current and voltage) represents one very important based on maintaining quality of welding work.

In order to maintain quality of welding work and also stability of electric arc... it´s important to develop device which will be able to take and process large amount of data and make data analysis in *on – line* and in *off – line* mode.

UI Measurement box allows connecting new and advanced measuring equipment for control of welded joint, researching based on acoustic emission, etc.

Apart SMAW welding process, it´s possible to conduct experiment and make acquisition of data at almost all welding process, making sure that the sensors are in the border area of applied process.

5. REFERENCES

[1] K. Skrzyniecki; P. Kolodziejczak; P. Cegielski; A. Kolasa, Experimental studies onstability of power source – arcsystem of mag welding processes, Annals of the oradea university, Fascicle of Management and Technological Engineering, ISSUE #1, july (2013), pp. 359- 362.

[2] V. Kumar; N. Chandrasekhar; S.K. Albert; J. Jayapandian; M. Krishnamoorthy; G. Kempul Raj, Monitoring the learning of welding skill using high speed data acqusition system, Conference paper · december 2015

[3] D. Marić; M. Duspara; L. Maglić; A. Stoić; I. Samardžić, Monitoring of welding parameters with welding machine Welbee P500L. 7th International Scientific and Expert Conference TEAM 2015 Technique, Education, Agriculture & Management, Belgrad, October 15-16, (2015).

[4] I. Samardžić; M. Dunđer; V. Starčević; D. Marić; M. Horvat; V. Kondić, On-line monitoring system application for welding current and voltage measurement at welding, 41th CWS International conference, Opatija, Croatia, June,8-11. (2016), pp. 171-180.

[5] Siewert, Thomas; Samardžić, Ivan; Kolumbić, Zvonimir; Klarić, Štefanija: On-line monitoring system – an application for monitoring key welding parameters of different welding processes.Tehnički vjesnik 15, 2008, pp. 9-18

[6] W. Liu; S. Liu; J. Ma; R. Kovačević, Real-time monitoring of the laser hot-wire welding process, Optics & Laser Technology 57 (2014), pp. 66–76.

[7] O. Liskevych; A. Scotti, Determination of the gross heat input in arc welding, Journal of Materials Processing Technology 225 (2015), pp. 139–150

[8] I. Samardžić; P. Raos; Š. Klarić; M. Blažević, monitoring parametara elektrofuzijskog zavarivanja PE-HD cijevi. IV skup o prirodnom plinu, Osijek (2006).

Dilatometric testing of maraging steel

S. Kladaric [a], A. Milinovic [b], I. Kladaric [b]

[a] College of Slavonski Brod, Dr. Mile Budaka 1, 35000, Croatia, skladaric@vusb.hr

[b] Mechanical Engineering Faculty in Slavonski Brod, Trg Ivane Brlić Mažuranić 2, 35000, Croatia, apenava@sfsb.hr, ikladar@sfsb.hr

Abstract

Dilatometry is a method of measuring changes in volume, length, width or thickness of the material sample during the time, caused by temperature changes. Through dilatometric testing of materials, it is possible to determine the dilatation behaviour of the material during heating and cooling. The device used to conduct dilatometric tests is called dilatometer. Through dilatometric testing of metals it is possible to determine the coefficient of thermal expansion (dilatation) and the characteristic temperature of microstructure transformation during heating and cooling. In the experimental part of the work, the dilatogram of diffusion annealing of maraging steel X2NiCoMo18-9-5 was recorded. Transformation temperature was read from the dilatogram and corresponding dilatations and the values of the coefficient of thermal dilatation during heating and cooling of maraging steel X2NiCoMo18-9-5 were calculated. Knowing transformation temperatures is necessary to determine parameters of the heat treatment. Using the coefficient of thermal dilatation it is possible, within certain temperature intervals, to predict dimensional changes of steel.

Keywords: Dilatogram; Coefficient of thermal expansion; Transformation temperature; Maraging steel.

1. INTRODUCTION

The word "dilatation" comes from the Latin word "dilatatio" which means extension, expansion or enlargement.

Thermal dilatation is property of the matter to change the volume depending on the temperature. Heat excitation of bonded particles in solids is manifested in the form of oscillation of these particles (atoms, ions, molecules) around lattice points. Oscillation amplitudes of neighbour particles increase with temperature increase causing thermal expansion of rigid body [1].

Expansion and contraction of materials must be taken into account when designing large structural systems, parts of casting moulds in the foundries etc.

Thermal expansion must be also taken into account when designing different lap joints in various engineering applications.

Control of thermal expansion is very important when coating metallic materials. If base material and coating have different coefficients of thermal expansion, it may result in cracking and spall during coating.

2. DILATOMETRIC TESTING

Dilatometry is a method of measuring changes in volume, length, width or thickness of the material sample in time, caused by temperature changes.

Dilatometric methods are defined by many standards, like for example HRN EN 821-1, ASTM E 831 and ASTM E 228 [2].

Besides solid samples, powders, pastes and liquids in separate containers also can be dilatometric tested.

Device by which dilatometric tests are carried out is called dilatometer.

By dilatometric testing of metals it is possible to determine:

- coefficient of thermal expansion (dilatation)
- characteristic temperatures of microstructure transformations
- dilatation behaviour of the material during heating and during cooling.

2.1. Cofficient of thermal expansion

The coefficient of thermal expansion represents relative change in the size of the object with a temperature increase of 1 K.

Coefficient of thermal expansion is determined only for the temperature ranges in which there are no transformational changes or chemical reactions.

There are linear, area and volumetric thermal expansion coefficient [3].

The linear thermal expansion coefficient can be estimated by:

$$\alpha_{\mathrm{L}} = \frac{\Delta L}{L \cdot \Delta T};\ \frac{mm}{mm\,K};\ K^{-1} \tag{1}$$

The thermal expansion coefficient α_{L} is most often marked as α.

Using α_{L}, change in linear dimension can be calculated by:

$$\Delta L = \alpha_{\mathrm{L}} \cdot L \cdot \Delta T;\ mm \tag{2}$$

The area thermal expansion coefficient can be estimated by:

$$\alpha_{\mathrm{A}} = \frac{\Delta A}{A \cdot \Delta T};\ \frac{mm^2}{mm^2 K};\ K^{-1} \tag{3}$$

Using α_{A}, change in the area can be calculated by:

$$\Delta A = \alpha_{\mathrm{A}} \cdot A \cdot \Delta T;\ mm^2 \tag{4}$$

The volumetric thermal expansion coefficient can be estimated by:

$$\alpha_{\mathrm{V}} = \frac{\Delta V}{V \cdot \Delta T};\ \frac{mm^3}{mm^3 K};\ K^{-1} \tag{5}$$

The volumetric thermal expansion coefficient α_V is most often marked as β.

Using α_{V}, change in volume can be calculated by:

$$\Delta V = \alpha_{\mathrm{V}} \cdot V \cdot \Delta T;\ mm^3 \tag{6}$$

Materials with isotropic structure have the same values of linear coefficients of thermal expansion in different directions.

The area thermal expansion coefficient is two times the linear coefficient and the volumetric thermal expansion coefficient is three times the linear coefficient.

$$\alpha_A = 2\alpha_L \tag{7}$$

$$\alpha_V = 3\alpha_L \tag{8}$$

Materials with anisotropic structure have different linear coefficients of thermal expansion in different directions, and therefore change of volume in different directions is unequal for the same temperature change.

Table 1. The coefficient of thermal expansion for various materials

Material	α, at 20 °C (10^{-6}/°C)	β, at 20 °C (10^{-6}/°C)
Aluminium	23	69
Austenitic steel	17,3	51,9
Copper	17	51
Concrete	12	36
Steel*	10,8 - 13,0	33,0 - 39,0
Diamond	1	3
Quartz	0,59	1,77
Magnesium	26	78
Brass	19	57
Molybdenum	4,8	14,4
Nickel	13	39
Lead	29	87
Platinum	9	27
Glass	8,5	25,5
Tungsten	4,5	13,5
Water	69 (approximate)	207
Gold	14	42
Iron	11,1	33,3

* Depending on the composition

Some materials contract when heated within certain temperature ranges and this phenomena is called negative thermal expansion (contraction).

Orders of magnitude of the coefficient of thermal expansion for solids, liquids and gases are:

- solids $\alpha,\beta \approx 10^{-6}\ K^{-1}$
- liquids $\beta \approx 10^{-4}\ K^{-1}$
- gases $\beta \approx 10^{-2}\ K^{-1}$

Gases will expand most and solids least for the same temperature change.

The coefficient of thermal expansion is a characteristic of the material dependent on temperature range.

2.2. The temperature of microstructure transformations

Knowledge of the exact transformation temperatures of certain metals constitutes the basis of the entire heat treatment.

Alloys with polymorphic transformations have significant change of specific volume at transformation temperatures due to change of atom arrangement in crystal lattice which results in change of lattice density [4].

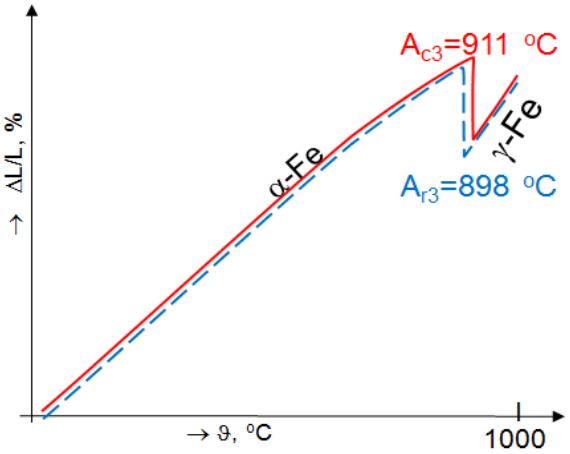

Fig. 2. The Expansion curve of pure iron

From room temperature to 911 °C iron has bcc lattice and is described as α-Fe.

Above the temperature of 911 °C iron has fcc lattice and is described as γ-Fe.

γ-Fe has a higher lattice density (atomic packing factor) and because of that smaller specific volume than α-Fe.

Therefore, significant contraction (≈ 25 %) at the turn of α-Fe in γ-Fe can be noted on the dilatation curve.

During cooling, transformation γ-Fe to α-Fe occurs at a slightly lower temperature of 898 °C.

Temperature difference between the transformation temperatures (911 °C-898 °C = 13 °C) during the heating and during the cooling is called the temperature hysteresis.

Using the expansion curves it is possible to differentiate certain types of steel.

Steels that contain perlite in the structure, exhibit significant contraction by transformation of bcc lattice into fcc lattice during heating.

Ferritic and austenitic steels exhibit no significant contractions because there are no structural transformations.

Ferrite steels have lower coefficient of elongation than austenitic steels, which is evident by lesser slope of the expansion curve of a ferrite steel compared to austenitic steel.

Transformation temperatures of steel depend significantly on the speed of heating into the austenite range and the speed of cooling from the austenite range.

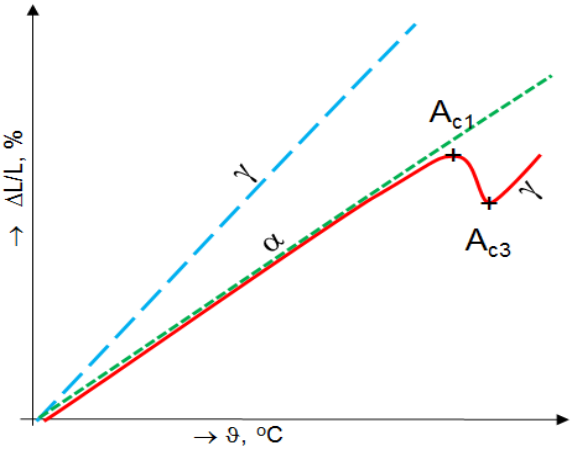

Fig. 3. Expansion curves of different steel types

Recording of expansion curves during austenitization of steel enables creation of TTS diagrams, while recording of expansion curves during the cooling of austenitized steel enables creation of TTT diagrams.

2.3. The expansion behaviour of the material during heating and cooling

Discontinuities noted on dilatation curve do not always indicate structural transformations or reactions of structural micro-constituents.

Residual stresses during the heating can cause expansion or contraction, depending on whether they are tensile or compressive stresses.

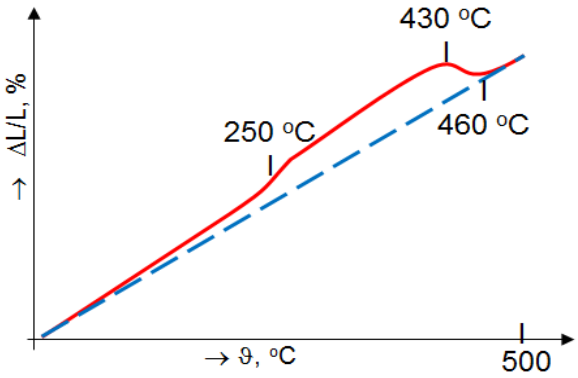

Fig. 4. Expansion curves of cast iron recorded after casting (solid line) and after annealing for reducing residual stresses (dashed line)

Expansion curve of cast iron recorded after casting shows that dilatation unevenly increases with temperature increase.

At the temperature of about 250 °C dilatation rapidly increases. From 430 °C the sample contracts again, and at the temperature of 460 °C it returns to its true size.

Expansion curve of cast iron that was previously annealed to remove residual stresses (3 h / 500 °C / air) is continuous.

Discontinuities of expansion curve recorded on the cast iron after casting can be attributed to the release of residual stresses induced by casting.

3. DILATOMETRIC TESTING OF MARAGING STEEL

In the experimental part of the work dilatometric testing of maraging steel X2NiCoMo18-9-5 were carried out with the aim of determining the temperature of structural transformation and the linear coefficient of thermal expansion of maraging steel.

The heat treatment of soluble annealing (ϑ_{SA}=820 °C, t_{SA}=0.5 h, cooling in the furnace) was conducted on the test sample ϕ6×50 mm in a Netzsch dilatometer 402 EP.

Fig. 5. Netzsch dilatometer 402 EP

Basic characteristics of Netzsch dilatometer 402 EP are:

- testing temperatures are in the range 20 °C to max. 1100 °C
- heating rate is adjustable in steps of 1 K/min
- cooling rate in the furnace is adjustable in steps of 1 K/min
- length of a sample is 25 mm to 50 mm
- diameter of a sample is 3 mm to 12 mm.

During the heat treatment dilatogram of soluble annealing of maraging steel X2NiCoMo18-9-5 was recorded.

From the dilatogram temperatures of structural transformations were read:

- temperature of the austenite formation beginning A_s = 635 °C
- temperature of the austenite formation ending A_f = 775 °C
- temperature of the nickel martensite formation beginning M_s = 150 °C

From the dilatogram of heat treatment of soluble annealing it is evident that maraging steel X2NiCoMo18-9-5 expands up to A_s temperature during heating. Above A_s temperature dilatometer curve declines, because the contraction of steel occurs up to A_f temperature. Within this temperature range contraction is caused by structural transformation of nickel martensite into austenite.

During cooling from temperature of the austenitization to the M_s temperature steel contraction occurs. After M_s temperature the steel expands again even though the temperature drop. Within this temperature range expansion is caused by structural transformation of austenite to nickel martensite.

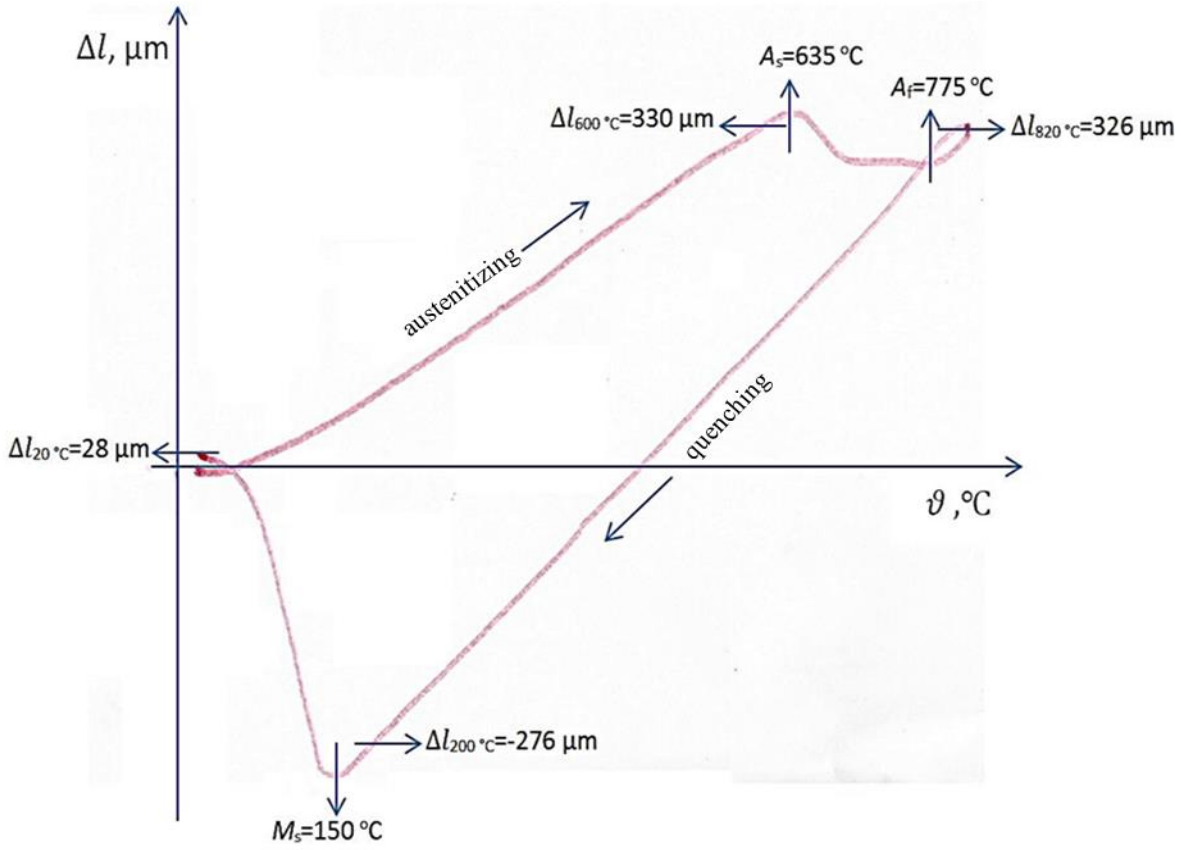

Fig. 6. Dilatogram of maraging steel X2NiCoMo18-9-5 solution annealed at 820 °C / 0.5 h

The linear thermal expansion coefficients of maraging steel X2NiCoMo18-9-5 during heating and cooling were estimated by:

$$\alpha(\vartheta_1,\vartheta_2)=\frac{\mathrm{L}(\vartheta_2)-\mathrm{L}(\vartheta_1)}{\mathrm{L}(\vartheta_1)}\cdot\frac{1}{\vartheta_2-\vartheta_1} \qquad (9)$$

where is:

- $\alpha(\vartheta_1,\vartheta_2)$ – linear thermal expansion coefficient for the temperature range between ϑ_1 and ϑ_2, K^{-1}
- $L(\vartheta_1)$ - length of the sample at the temperature ϑ_1, mm
- $L(\vartheta_2)$ - length of the sample at the temperature ϑ_2, mm
- ϑ_1, ϑ_2 - temperature of the sample, K

The linear thermal expansion coefficient of maraging steel X2NiCoMo18-9-5 during the heating was calculated for the temperature range from 20 °C to 600 °C (the range without structural transformations). Dilatation of the sample at 600 °C ($\Delta l_{600°C}$) in the amount of 330 µm was read from the dilatogram shown in Figure 6.

$$\alpha(20,600)=\frac{L(600)-L(20)}{L(20)}\cdot\frac{1}{600-20}$$

$$\alpha(20,600)=\frac{50{,}330-50}{50}\cdot\frac{1}{580}=11{,}38\cdot10^{-6}K^{-1}$$

The linear thermal expansion coefficient of maraging steel X2NiCoMo18-9-5 during the cooling was calculated for the temperature range from 820 °C to 200 °C (the range without structural transformations). Dilatation of the sample at 820 °C ($\Delta l_{820°C}$) in the amount of 326 µm, and dilatation of the sample at 200 °C ($\Delta l_{200°C}$) in the amount of -276 µm were read from the dilatogram shown in the Figure 6.

$$\alpha(820,200)=\frac{L(200)-L(820)}{L(820)}\cdot\frac{1}{820-200}$$

$$\alpha(820,200)=\frac{49{,}724-50{,}326}{50{,}326}\cdot\frac{1}{620}=-19{,}29\cdot10^{-6}K^{1}$$

Negative value of the linear thermal expansion coefficient indicates contraction of the material within observed temperature range.

4. CONCLUSIONS

The linear thermal expansion coefficient of maraging steel X2NiCoMo18-9-5 during heating in the temperature range 20 °C to 600 °C (structure of nickel martensite) is $11{,}38 \cdot 10^{-6}\,K^{-1}$, which is approximately the same as linear thermal expansion coefficient of unalloyed and low alloy steels.

Negative linear coefficient of thermal expansion of maraging steel X2NiCoMo18-9-5 during cooling in the temperature range 200 °C to 820 °C (austenite structure) is $19{,}29 \cdot 10^{-6}\ K^{-1}$, which is approximately the same as linear thermal expansion coefficient of austenite steel.

The main advantage of dilatometric testings is that structural changes can be determined exactly at the moment and at the temperature when they occur, which is not possible using other testings (e.g. metallographic), because the other testing give only the possibility of knowledge after of certain changes have occured.

5. REFERENCES

[1] J. R. Gordon; R. V. McGrew; R. A. Serway, Physics for Scientists and Engineers - Volume 1. Boston, (2010).

[2] Dilatometry - NETZSCH Thermal Academy, https://www.netzsch-thermal-academy.com/en/advanced-materials-testing/methods/dilatometry/, last access 01/09/2016

[3] Exercise in basic physics IV, http://www.phy.uniri.hr/~vlabinac/files/index/skripte/top_pregled.pdf, last access 01/09/2016

[4] H. Schumann, Metallography. Beograd, USA, (1989).

[5] I. Kladarić; D. Krumes; R. Marković, The Influence of Multiple-Solution Annealing on Kinetics of Structural Transformation of Maraging Steels. // Materials and Manufacturing Processes. 21 (2006), 783-785.

Design and calculation of cylindrical industrial air filter device with use of CFD analysis

M. Mandic [a], D. Kozak [b], I. Gelo [c], M. Holik [d]

[a] Mechanical Engineering Faculty in Slavonski Brod, J. J. Strossmayer University of Osijek, Trg Ivane Brlić Mažuranić 2, HR-35000 Slavonski Brod, Croatia, mmandic@sfsb.hr

[b] Mechanical Engineering Faculty in Slavonski Brod, J. J. Strossmayer University of Osijek, Trg Ivane Brlić Mažuranić 2, HR-35000 Slavonski Brod, Croatia, dkozak@sfsb.hr

[c] Mechanical Engineering Faculty in Slavonski Brod, J. J. Strossmayer University of Osijek, Trg Ivane Brlić Mažuranić 2, HR-35000 Slavonski Brod, Croatia, igelo@sfsb.hr

[d] Mechanical Engineering Faculty in Slavonski Brod, J. J. Strossmayer University of Osijek, Trg Ivane Brlić Mažuranić 2, HR-35000 Slavonski Brod, Croatia, mholik@sfsb.hr

Abstract

In order to reduce emissions and improve the quality of ambient air or air in the working space it is necessary to clean emission particles. Air purity is achieved by proper filtration process of emission particles. In this paper housing of cylindrical industrial air filter device was designed and optimized with the use of CFD analysis. Model of cylindrical filter device was made in the software SolidWorks Premium 2016. Several models of product were made until satisfactory design from the perspective of functional and technological feasibility was reached. Furthermore, multi physical analysis was conducted in software ANSYS Workbench. CFD analysis of fluid flow was carried out using software ANSYS CFX. Based on CFD analysis of fluid flow and distribution of pressure on filter device wall, analysis of strength was conducted in ANSYS Static Structural, and model optimization in ANSYS DesignXplorer. Optimized model serves as an orientation model for further analysis of critical loads (underpressure, overpressure). Optimized model strength analysis at working pressure with value of -1277.6 Pa show that maximum equivalent stress is 114.03 MPa. In the condition of high value of overpressure with value of 1059.43 Pa maximum equivalent stress is 378.09 MPa, and for high value of underpressure with value of -5936.6 Pa maximum equivalent stress is 534.91 MPa. Optimized model requires further work in order to reduce stresses in the case of critical loads. This paper presents a coupling of CAD and CAE technologies in process of new product development.

Keywords: Design, Filtering device, CFD analysis, Strength, Optimization

1. INTRODUCTION

1.1. Air pollution removal

The environmental as well as the ambient air is a subject to the contamination of solid or liquid particles that can be mineral or organic origin. The particle size range from is 0.0001 μm to 100 μm. Particles larger than the 10 μm are regularly deposited on the floor, while particles smaller than 1 μm, and particularly those less than 0.3 μm, remain floating in the air. The average concentration of these particles in the atmosphere over the European continent is measured in millions per 1 liter of air, and fall in to the categories:

- Dust – small solid particles
- Smoke – tiny solid particles
- Fog – small drops
- Haze – very small drops
- Steam – gaseous substance

Samples of formation of said particles have:

- Natural processes that take place on the surface of the Earth
- Flora on Earth
- The organisms that inhabit the Earth, including human beings
- Technological processes created by the man.

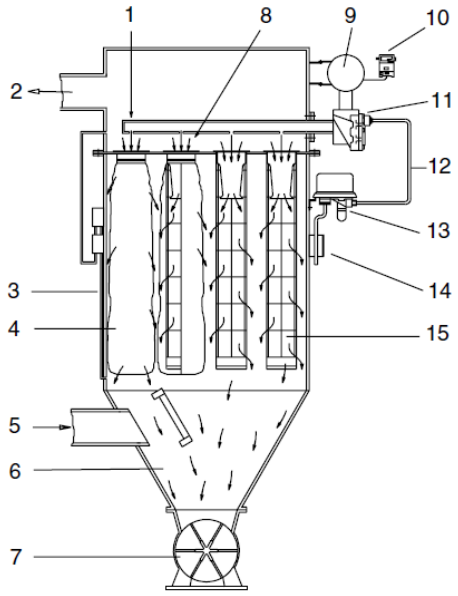

1) Compressed air jet
2) Clean air exhaust
3) Filter housing
4) Filter bag
5) Dirty air intake
6) Dust collector hopper
7) Dust lock
8) Secondary air
9) Supply air
10) Pressure switch
11) Dust collector valve
12) (Auxiliary) air control pipe
13) Valve block
14) Solid state sequential controller
15) Filter cage (shown without filter bag)

Fig. 1. Main components of the filter device

In addition to dust, environmental and ambient air contains viable, microbes, ferments, fungi, bacteria, viruses, etc. [1].

The most common method of meeting emission standards in industries that must control air pollution is by removal of the pollution.

Dry particulate matter is removed by:

- Filters – baghouse, fixed beds, or mats
- Electrostatic precipitators – plate – type, tube – type
- Inertial collectors – cyclones and baffles,
- Scrubbers – wet or dry

Liquid droplets and mists are controllable by:

- Filters – more loosely knit than for dry filters,
- Electrostatic precipitators – wetted wall type.
- Inertial collectors – cyclones and baffles,
- Venturi scrubbers [2].

The filter devices are consisting of one or more isolated sections comprising rows of the bags made of cloth which can be round, flat or shaped tubes; or pleated cartridge. Polluted air passes (usually) along with side of wall, rather than radially through the fabric. Contamination remaining in the fabric, and clean air comes out of the filter device. The filter devices collect particles with size of microns to several thousand micrometers in diameter with filtration efficiency of 99 % or 99.9 %. A dust cake, or dust deposited on the surface of the fabric is primarily responsible for such high efficiency. Accumulated dust is barrier with tortuous pores that capture particles as they pass through the sediment. Main components of the filter device are shown in Figure 1.

Filter devices can be divided:

- according to the method of cleaning bags (shaking, reverse air, pulse jet, sonic)
- according to the air flow direction through the bags (interior filtration, exterior filtration)
- according to the fan position in relation to the filter device (positive pressure, negative pressure)
- according to capacity (small, medium, big)

The use of filter devices:

- pharmaceutical industry
- food industry,
- wood industry,
- sinter plant,
- metal industry,
- foundries,
- textile industry,
- chemical industry etc. [3]

1.2. CAD/CAE integration

Computer Aided Design – CAD is technology that applies computers in engineering design and

preparation of technical documentation. By assembling primitive shapes using Boolean operations new body is formed. Boolean operations are union, subtraction and intersection [4]. CAD systems allow production of digital prototype in the early stage of the design process that can be used for testing and evaluation. A large number of users from different departments can share models, and express their opinions about the product at an early stage in order to complete the design in less time and with fewer errors. Most studies agree that with digital prototypes in the early stages makes it possible to spend more time in the defining stage of the design process than in redesigning an already completed design [5].

Computer Aided Engineering – CAE is a technology concerned with use of computer systems to analyze CAD geometry, allowing the designer to simulate and study how the product will behave so that the design can be refined and optimized [6]. The CAE approach to mechanical product development emphasizes system analytical modeling and analysis techniques at the earliest phase of design, that is, conceptual design. The process starts with an integrated set of total system simulations of the entire product. Each alternative product concept is mathematically modeled as an entire system. At this point, overall product designers have the flexibility of defining significantly varying concepts in order to minimize weight, reduce energy consumption and maximize performance for acceptable product concepts [7].

1.3. Requirements for design of filter air device

Based on many years of experience from the company "Tehno – filter" d.o.o. for design of cylindrical filter device following requirements are defined:

- cylindrical shape of housing,
- type of filter: cartridge filter,
- number of cartridge filters: 4,
- maximum air flow: 3600 m^3/h,
- sequences of cleaning: continuous sequence of cleaning,
- method of cleaning cartridges: pulse - jet,
- air flow direction through bags: external filtration,
- fan position in relation to the filter device: negative pressure,
- tangential entry of air through casing,
- cartridge replacement over the rotating upper turret,
- implement the existing system for the dust deposition,
- dust type: metal dust, grinding.

2. METHODS AND MATERIALS USED FOR RESEARCH

2.1. Design of air filter device model

The 3D model of industrial filter device according to the requirements of the company "Tehno – filter" d.o.o. was made using the software package SolidWorks 2016 Premium. SolidWorks is the CAD and CAE software package developed by Dassault System [8]. Development of the model is time consuming and exhaustive process where with iterative process required product model is achieved. The model was made in several versions; each version is better than the previous. First and second model version of air filter device is shown in Figure 2.

Fig. 2. Model version one (left) and model version two (right) of the filter air device

With further development final model version (Figure 3) meets design requirements for filter air device.

Fig. 3. Final model version of the filter air device

2.2. Operating principle of designed filter air device

Dirty air enters the filter device through a tube that is placed tangentially in a relation to the lower housing (Figure 4).

Air flows along the cylindrical wall and the larger dust particles are separating (due to gravity and friction along the wall) and falling through the hopper in dust deposition system. Furthermore, the air flows through the cartridge filter (located in centre of housing), and air is cleaned from the rest of dust (Figure 5).

Fig. 5. Cross – section of filter air device

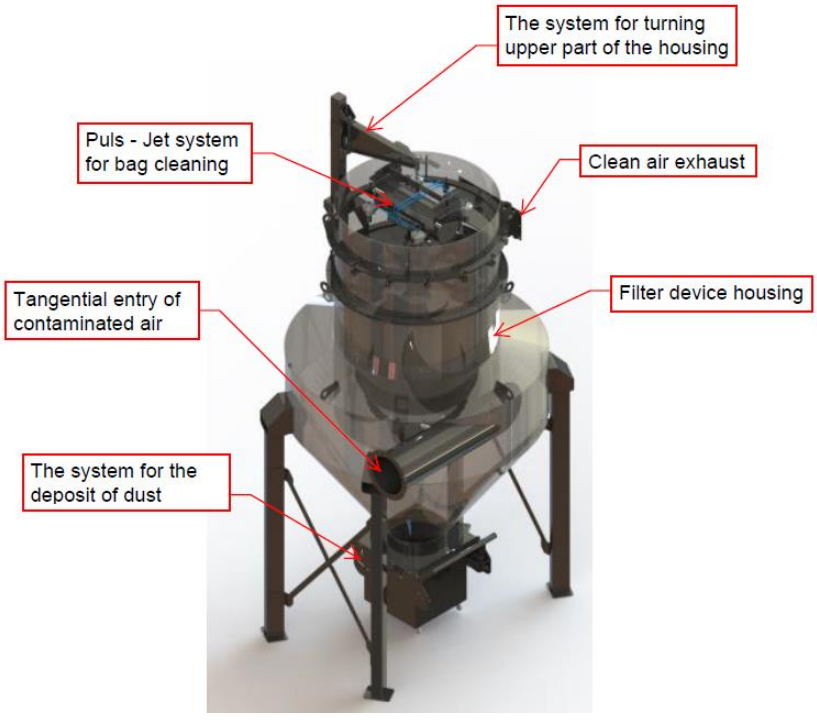

Fig. 4. Operating principle of designed filter air device

Clean air enters in the upper housing that is further taken in to the atmosphere or in the filtered room. In the process of air flow, cartridge filters are continuously cleaned with puls – jet system. In case of cartridge filter damage or wear, cartridges are replaced by rotating the top part of the housing to the side (Figure 6).

Fig. 6. System for turning upper part of the housing

Rotating to one side replacement of two cartridges are enabled (rotating to other side enables replacement for other two cartridges). Upper housing is raised by screwing the threaded rod at the end of cantilever beam (a few millimetres are necessary in order to avoid the friction between two flanges). Rotation of upper housing is limited with the limiters to protect the worker from uncontrolled rotation and possible injury. Furthermore, the entire construction is designed for easy assembly and disassembly and transport.

2.3. Optimization of filter air device housing construction

For optimization of filter air device housing construction multiphysics analysis was required. Multiphysics analysis was conducted in ANSYS Workbench platform, version 16. ANSYS Workbench [9] is product of ANSYS, Inc. CFD analysis was completed in ANSYS CFX [10], structural analysis in ANSYS Static Structural [11] and optimization with use of ANSYS DesignXplorer [12].

CFD analysis

The domain material is air at 25°C with increased density of air due the air contamination. Air density is set at $1.3\,\mathrm{kg/m^3}$. Turbulence model used was $k-\varepsilon$. Inlet boundary condition is relative pressure with value 0 Pa. Outlet boundary condition is mass flow with value 1.3 $\mathrm{kg/s}$. Geometry of filter air device was set as wall boundary condition (tangential fluid velocity equal to wall velocity, normal velocity component is set to be zero). Obtained pressure distribution is input load for structural analysis. Figure 7 show a distributed pressure on filter air device housing, it is visible that on housing wall is negative pressure as required.

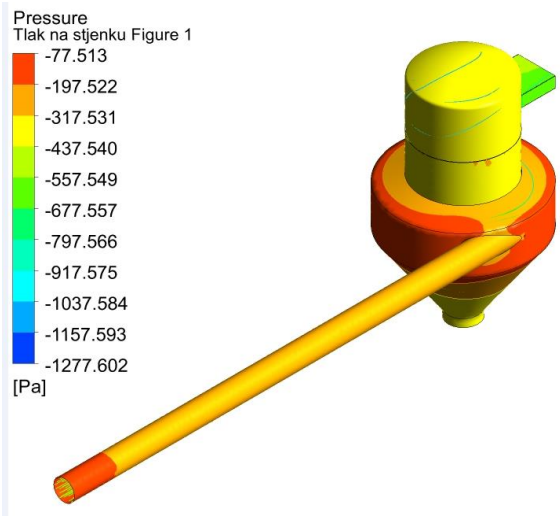

Fig. 7. Pressure distribution on the filter air device housing

Static structural analysis

Material for filter air device is construction steel S235. Applied finite element mesh is shown in Figure 8. Boundary conditions are shown in Figure 9. Standard earth gravity is set as load that affect whole construction (A). Furthermore, displacement was limited in direction of x, y, z axis ($u_x = u_y = u_z = 0$) on places were filter air device is connected with screws to foundation. Also, surface of a plate that contact foundation was limited in direction of y axis ($u_y = 0$), assuming that foundation is rigid body (C). Housing construction is loaded from inside with pressure. Pressure is imported from CFD analysis where pressure distribution was obtained.

Fig. 8. Applied finite element mesh

Considering that cartridge filters are not modelled, on cell plate mass of cartridges are defined (E).

Results of equivalent stress are presented in Figure 10. Maximal equivalent stress for conditions of working pressure is 59.1 MPa. Furthermore, based on results of equivalent stress, optimization of housing construction is conducted.

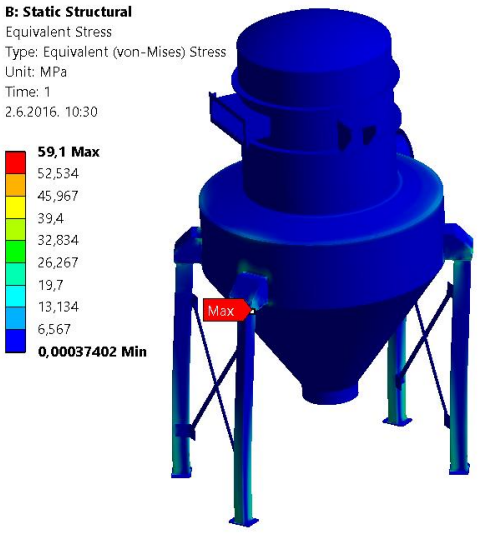

Fig. 10 Maximal equivalent stress for conditions of working pressure

Optimization of housing construction

After structural analysis for parameter optimization it is necessary to make design of experiment (DOE). DOE is made based on defined parameters in CAD model stated on preliminary structural analysis. Parameters are: P1 housing sheet thickness, P2 cell plate

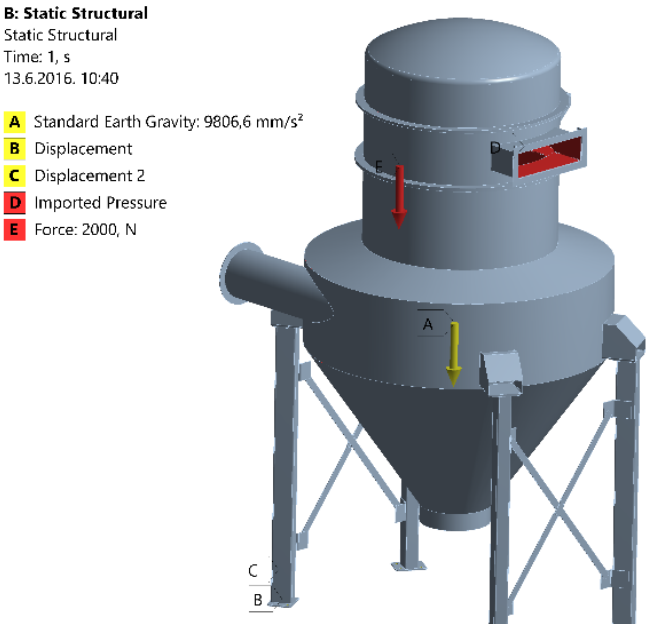

Fig. 9. Boundary condition in structural analysis on filter air device

thickness; P3, P4 and P5 profile dimension of supporting beam (width, length, thickness), P6 thickness of flange on housing. Furthermore, it is necessary to determine value of lower and upper bound of parameters that will define DOE. In table 1 lower and upper bound are shown. Based on that values in DOE 45 design points were generated with various combinations of parameter

Table 1. Lower and upper bound value.

Parameter	Value	Lower bound	Upper bound
P1-DS_P1	5	3	4
P2-DS_P2	5	3	4
P3-DS_P3	120	80	100
P4-DS_P4	80	60	88
P5-DS_P5	4	2	3
P6-DS_P6	8	4	6

Next step is defining an objectives and constrains. The objective is to minimize mass, while constrain is that the equivalent maximum stress is lower than 156 MPa.

$$\sigma_{dop} = \frac{\sigma_T}{S} = \frac{235}{1{,}5} \approx 156 \text{ MPa} \quad (1)$$

Where:

σ_{dop} – maximum allowable stress, MPa,

σ_T – yield strength, MPa,

S – safety factor.

3. RESULTS AND ACHIEVEMENTS

3.1. Results of housing construction optimization

After defining objectives and constrains, software will calculate and suggest potential solutions of optimization. Candidate point are shown in Figure 11. Candidate point 1 with combinations of parameters gives optimal solution with construction mass of 512.62 kg and maximal equivalent stress with value 115.94 MPa.

In the Tradeoff chart, the samples are ranked by non-dominated Pareto fronts, and you can view the tradeoffs that most interest you. To make sense of the true nature of the tradeoffs, the plots must be viewed with the output parameters as the axes. This approach shows which goals can be achieved and whether this entails sacrificing the goal attainment of other outputs. The best solution is showed with blue color, and worst solution is displayed with red color [12]. Tradeoff diagram is presented in Figure 12. It is visible that candidate point 1 is by far the best choice.

The sensitivities chart shows the global sensitivities of the output parameters with respect to the input parameters [12]. In Figure 13 sensitivities diagram is shown. It is evident that the parameter P1-DS_P1 has the greatest influence on mass construction, and parameter P5-DS_P5 on equivalent stress.

Table of Schematic D4: Optimization , Candidate Points

	A	B	I	J	K	L
1	Reference	Name	P10 - Geometry Mass (kg)		P11 - Equivalent Stress Maximum (MPa)	
2			Parameter Value	Variation from Reference	Parameter Value	Variation from Reference
3	◉	Candidate Point 1	512,73	0,00%	109,73	0,00%
4	○	Candidate Point 1 (verified)	512,62	-0,02%	115,94	5,66%
5	○	Candidate Point 2	549,65	7,20%	81,122	-26,07%
6	○	Candidate Point 3	564,89	10,17%	87,476	-20,28%
*		*New Custom Candidate Point*				

Fig. 11. Candidate points

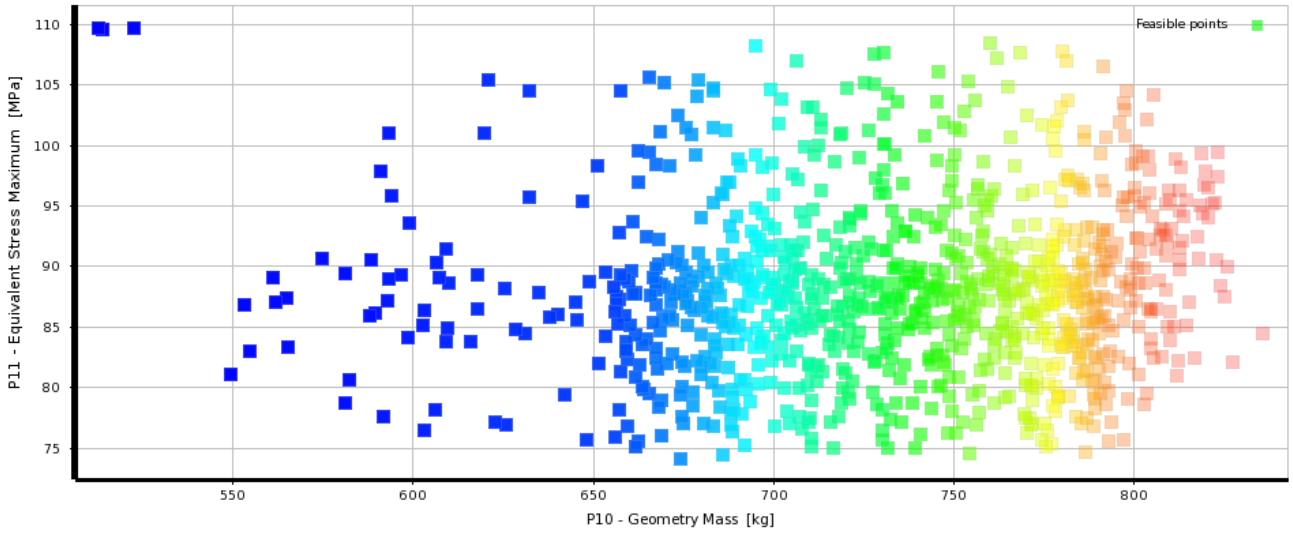

Fig. 12. Tradeoff diagram

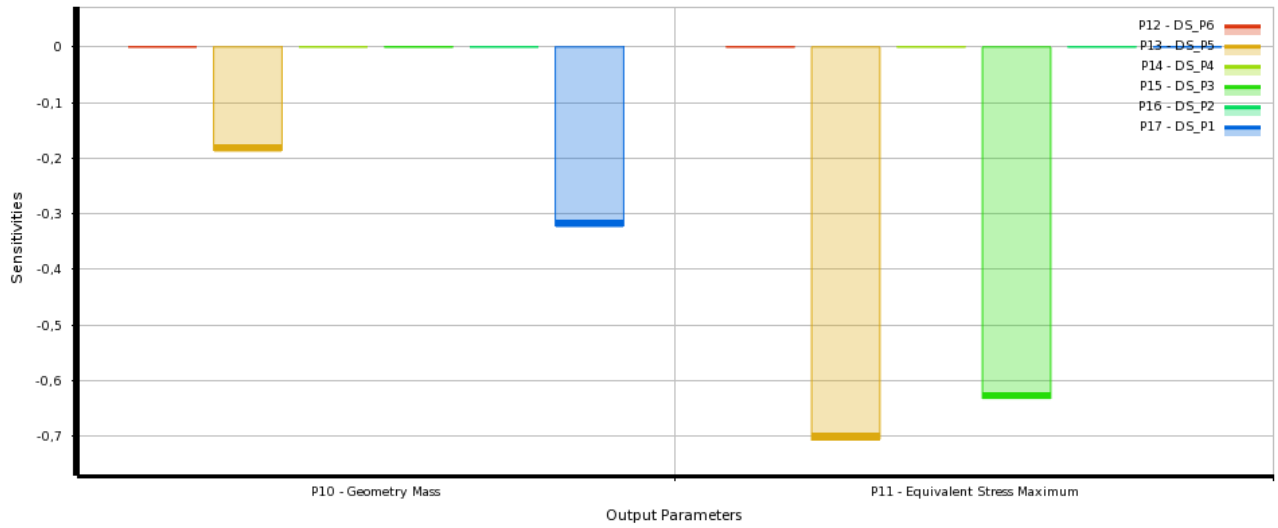

Fig. 13. Sensitivities diagram

Furthermore, table 2 shows value of input parameters before and after optimization. Comparison of the starting model and optimized model are presented in Figure 14. Different projections are shown, as the maximum equivalent stress occures in different positions on starting and optimized construction.

Table 2. Start value and optimized value of input parameters.

Parameter	P1-DS_P1	P1-DS_P1	P1-DS_P1	P1-DS_P1	P1-DS_P1	P1-DS_P1
Start value [mm]	5	5	120	80	4	8
Optimized value [mm]	3	3	80	50	2	4

The analysis of optimization results reveals that total weight was reduced from an initial value of 808.46 kg to 511.32 kg, which is 297.14 kg (≈36.75%) mass reduction. The maximum equivalent stress is increased from the initial 59.1 MPa to 114.03 MPa, an increase of 54.93 MPa (≈92.94%). Table 3 shows value of output parameters before and after optimization.

Table 3. Output parameters value before and after optimization

Initial mass value [kg]	808.46
Mass value after optimization [kg]	511.32
Initial maximum equivalent stress value [MPa]	59.1
Maximum equivalent stress value after optimization [MPa]	114.03

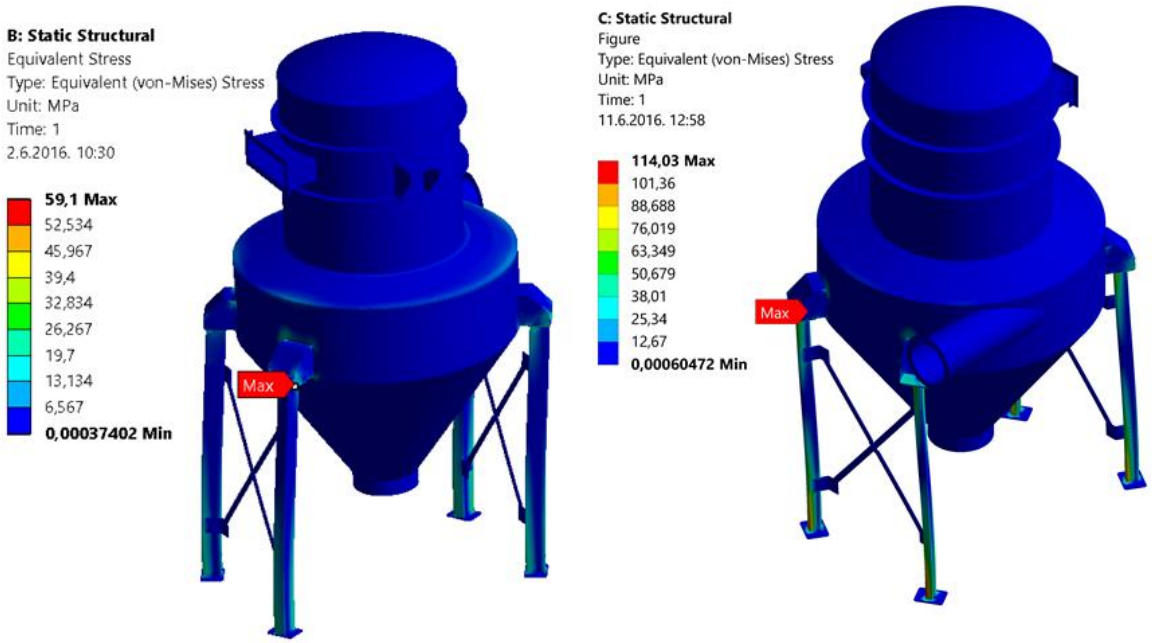

Fig. 14. Maximum equivalent stress on starting model (left) and optimized model (right)

3.2. Results of optimized construction strength calculation due critical loads

The critical loads of industrial air filter device mean the sudden changes in pressure inside of the housing of air filter device. Such loads rarely occur throughout the life cycle of the filter air device. The causes of critical loads can be different: the sudden termination of the fan, broken system for cartridge cleaning, dust explosion inside the housing, etc. and they are difficult to predict and simulate numerically. According to experience from the company "Tehno – filter" d.o.o. strength calculation will be carried out for overpressure value ≈1000 Pa and underpressure value ≈6000 Pa.

The first case of critical load is the sudden appearance of overpressure in the housing of filter air device. Pressure distribution for the first case is shown in Figure 15. Based on resulting pressure distribution strength calculation of optimized air filter device housing will be conducted.

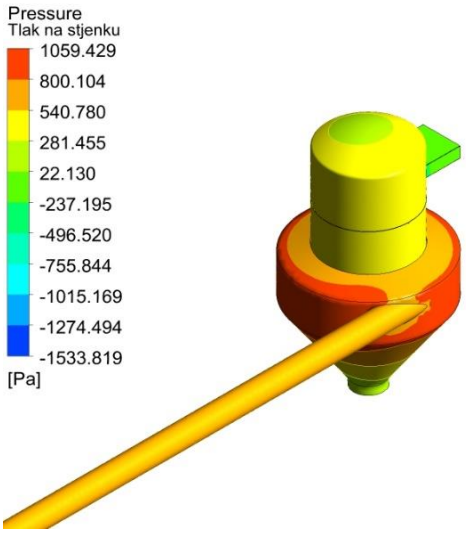

Fig. 15. Pressure distribution on the optimized filter air device housing for the first case of the critical load

The second case of critical load is the sudden appearance of underpressure in the housing of filter air device. Pressure distribution for the second case is shown in Figure 16. Based on resulting pressure distribution strength calculation of optimized air filter device housing will be conducted.

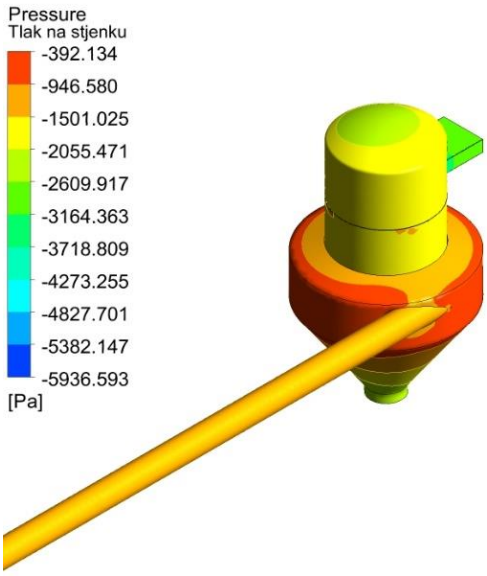

Fig. 16. Pressure distribution on the optimized filter air device housing for the second case of the critical load

Figure 17 shows a comparison of the equivalent stress results of optimized air filter device housing in case of overpressure and underpressure.

Furthermore, from analysis of the strength calculation results it is evident that both load cases are critical for construction. Since the condition for the high values of underpressure has higher value of maximum equivalent stress, second load case will be further analysed. From Figure 18 it is evident that on the leg support occurs a high stress concentration with value of 534.91 MPa. High value of equivalent stress continuous to the top of the leg. Since the foot is on the opposite side of tangential air inlet, assumption is that on that leg is occurring maximum bending moment (the largest distance). In order to minimize the stress on the leg support it is necessary to choose greater sheet thickness and form it with larger radius at the folding areas. This would provide a more regular force streamlines and prevent the occurrence of stress concentration. To reduce stress in legs of the filter device, it is necessary to choose the profile beams with larger cross-sectional area and higher section modulus. Since the legs are deformed in a Z-direction (in the direction of air flow through

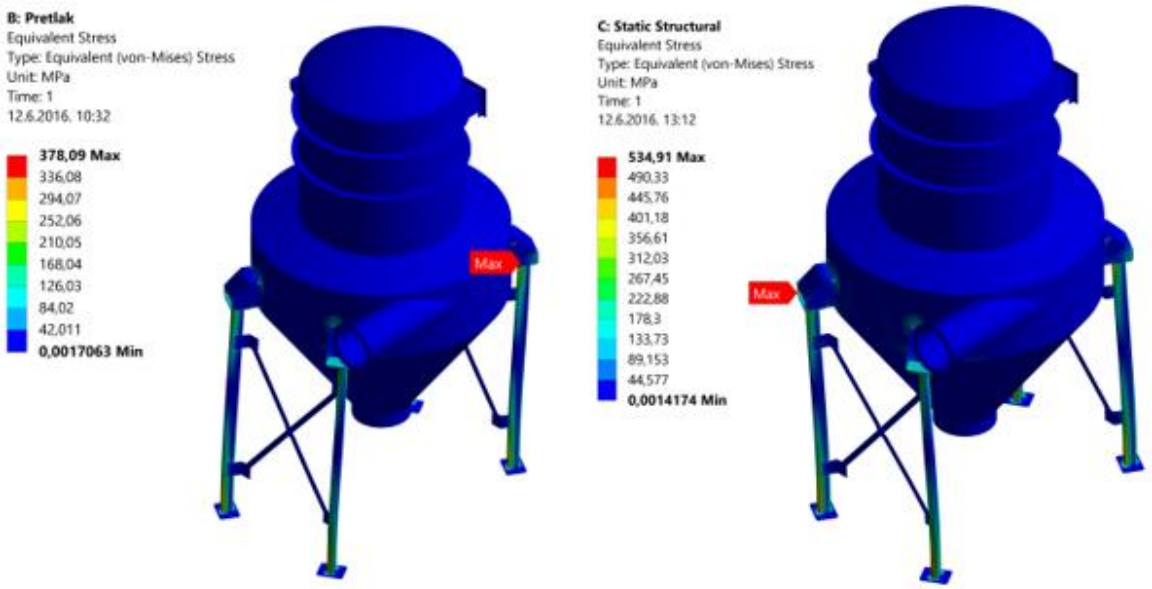

Fig. 17. Comparison of the equivalent stress results of optimized air filter device housing in case of overpressure (left) and underpressure (right)

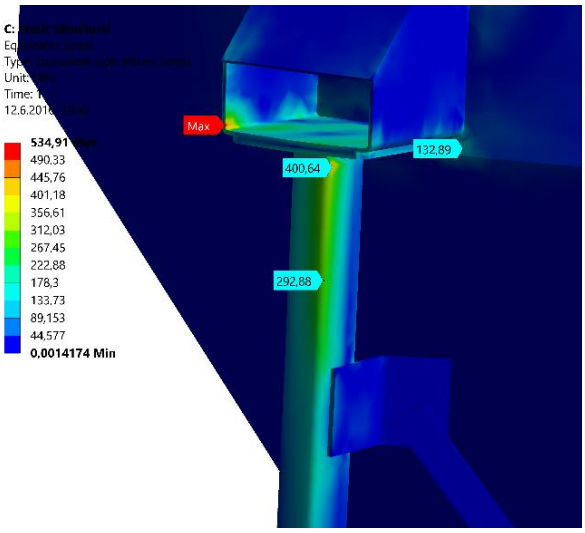

Fig. 18. Maximal equivalent stress in case of high underpressure

the tangential inlet) it is necessary to connect opposite pairs of legs, thereby ensuring that uncontrolled warping of each pair of legs for themselves won't occur.

4. CONCLUSIONS

In this paper, cylindrical air filter devic was designed and optimized based on CFD analyss. Initial construction weighted 808.46 kg wit maximum equivalent stress 59.1 MPa. Optimized construction weighted 511.32 kg and under working pressure value of maximum equivalent stress is 114.13 MPa. Since the allowable stress limit is 156 MPa, optimized construction of designed air filter device meets requirements of strength.

Furthermore, an analysis of optimized construction in cases of overpressure and underpressure was conducted. Both cases were critical for construction. In case of high overpressure maximum equivalent stress is 378.09 MPa, and in the case of high underpressure 534.91 MPa. Since the critical loads occur rarely in life cycle of air filter device explosion venting device can be added as deliberately weakened part of construction.

CAD/CAE technology has enabled faster process of designing and developing new products. While for the application of CAD technology sufficient basic technical knowledge, for the application of CAE technology requires knowledge from various scientific fields, it is necessary to know variety of methods, their advantages and disadvantages and application possibilities.

FURTHER WORK

- In future researches goal is to conduct an analysis of the construction with explosion venting device. Also, aim is to conduct analysis of stress in several steps of loads: in

first step air filter device would be loaded with working pressure, in second step with critical load (overpressure or underpressure), and in third step again with the working pressure. This would give us insight in how a sudden change of pressure effects on the stress increase and how the stop of high load effects on the construction relaxation. The analysis would be carried out with and without explosion venting device.

- Based on the optimization results and the impact of input parameters on the output parameters detailed optimization would be conducted.
- Depending on the availability of commercial licenses and with enough computing resource, analysis of construction with bolt joint would be conducted.

5. ACKNOWLEDGEMENTS

The authors would like to thank company "Tehno – filter" d.o.o." for helping with their experience and knowledge during writing of this paper. The work presented in this paper was financially supported by the Ministry of Science, Education and Sports, Republic of Croatia.

6. REFERENCES

[1] Cleanrooms - Turn key solution, Klimaoprema, http://www.klimaoprema.hr, last access 1.5.2016.

[2] Kreider, F., Jan; Rabl; Ari; Cook, E., Nevis; Cohen, Hewitt, R., Ronald; Illangasekare, Tissa; Zannetti, Paolo; Curtiss, S., Peter; Firor, John, The CRC Handbook of Mechanical Engineering. Boca Raton, Florida, CRC Press, 2004., pp. 2466

[3] Beachler, S., David; Joseph, Jerry; Pompelia, Mick, Fabric Filter Operation Review: Self-instructional Manual: APTI Course SI:412A. Industrial Extension Service, College of Engineering, North Carolina State University, 1995., pp. 156

[4] Kljajin, Milan; Karakašić, Mirko, Computer aided design (e.g. in Croatian). Mechanical faculty in Slavonski Brod, 2012., pp. 171

[5] Bilalis, N., Computer Aided Design – CAD. [Digital report from funded project of the European Commission], 2000. URL: http://www.adi.pt, last access 1.6.2016.

[6] Lee, K., Principles of CAD/CAM/CAE systems. Seoul, Addison Wesley Longman Inc., 1999., pp. 690

[7] Avallone, Eugene; Baumeister, Theodore; Sadegh, Ali: *Marks' Standard Handbook for Mechanical Engineers*, New York, The McGraw-Hill Companies Inc., 2007., 1800 str.

[8] SOLIDWORKS Premium, Dassault Systèmes SOLIDWORKS Corp., http://www.solidworks.com, last access 2.5.2016.

[9] ANSYS Workbench Platform. Ozen Engineering Inc., http://www.ozeninc.com, last access 3.5.2016.

[10] ANSYS CFX- Solver Theory Guide., ANSYS Inc., 2009., pp. 270

[11] ANSYS Mechanical APDL Structural Analysis Guide, ANSYS Inc., 2013., pp. 522

[12] ANSYS - Design Exploration User's Guide 2013., ANSYS Inc., pp. 296

Equalization of stress distribution on threaded connection optimizing pitch geometry

V. Šimunović [a], D. Kozak [b], Ž. Ivandić [c]

[a] Mechanical Engineering Faculty in Slavonski Brod, Trg Ivane Brlić Mažuranić 2, 35000 Slavonski Brod, Croatia, vsimunovic@sfsb.hr

[b] Mechanical Engineering Faculty in Slavonski Brod, Trg Ivane Brlić Mažuranić 2, 35000 Slavonski Brod, Croatia, dkozak@sfsb.hr

[c] Mechanical Engineering Faculty in Slavonski Brod, Trg Ivane Brlić Mažuranić 2, 35000 Slavonski Brod, Croatia, zivandic@sfsb.hr

Abstract

This paper presents an analysis and optimization of stress distribution on a screw connection with ISO metric thread. According to previous measurements, which were performed in the application, it was shown that the profile teeth at the joint are unequally burdened.

The task is to generally show screw connections, make a CAD parametric model of the joint, analyse the distribution of stresses and optimize it by changing or more precisely, increasing the pitch of the nut. Also it is necessary to compare the behaviour of the classical and optimized screw connection and create a table of optimized pitch solutions.

The performed FEM analysis presented the stress state of the classic screw connection on the selected example of thread M16. It shows and confirms the classic behaviour on bolted joints where the first profiles in contact transfers most of the load while other are much less burdened.

The assumption is that the increase of nut pitch or more specifically the existence of certain positive difference between the pitch of the nuts and bolt, the classical behaviour of bolted joints can be improved. This was done and it led to a reduction of the maximum von Mises stress for roughly 30%. In this way, stress distribution and fatigue life of bolted joints has improved.

By specifying the corrected pitch size for threads of general application, presented in the work in tables, it is to be concluded that the method is more appropriate for larger nominal diameter of the threads. Sizes of pitch difference, which are quite small, ascend with the increase in nominal diameter and thus acquire sizes that are easier and cheaper to implement.

Keywords: pitch optimizing, threaded connection, stress distribution

1. INTRODUCTION

It is known and proven that in threaded connections teeth in contact do not have the same load, but only the first two to three carry most of it.

Failures of bolted joint usually initiate at the root of the first bolt thread near the bearing surface of nut due to fatigue cycles, and this failure is encouraged by high stress concentration at the thread root. [1]

When tightening the screw and nut, axial stretching of screw and nut compression occurs, therefore, resulting in difference in pitch between the inner and outer coils that cause an uneven distribution of stresses through the screw connection. The assumption is that this can be improved by using threaded connection that in unloaded condition have differences in pitch.

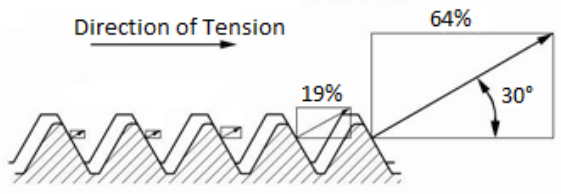

Fig. 1 Load distribution of standard threads [2]

2. METHODS AND MATERIALS USED FOR RESEARCH

Axisymmetric surface models are made with SolidWorks 2012 in accordance with the ISO metric profile and are analysed with Ansys 16.2.

2.1. Model

The model consists of a threaded part of the bolt, nut and the plate to which the nut rests. Unlike reality, the model is completely axisymmetric in order to continue the work analysing two-dimensional problems that is less computer demanding.

Bolt and nut measures (6g/6H) are used as the average value between the minimum and maximum according to ISO 965-1. The plate thickness will be equal to the length of the free part of the bolt, the inner diameter equal to the diameter of which is the root of the nut thread and the outside diameter will be increased from the inner to triple the amount of the length of contact between the nut and plate.

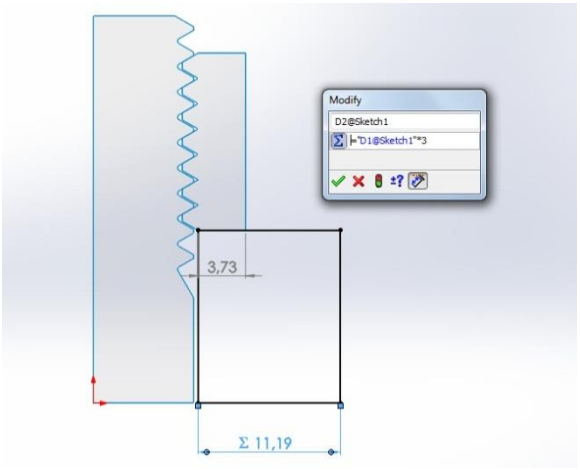

Fig. 2 Modelling the connection [3]

2.2. FEM Analysis

Allowed stress σ_{dop} for screws is determined usually depending on the yield strength: [4]

$$\sigma_{dop} \approx 0{,}3\, R_e \qquad (1)$$

For 10.9 class-strength bolts a frequently used material is 42CrMo4.

Table 1. 42CrMo4 Material data

Young's Modulus, *E*/GPa	210
Poisson's Ratio, *v*/-	0,3
Tensile Ultimate Strenght, R_m/MPa	1100
Tensile Yield Strenght, R_e/MPa	900

The force on the bolt is applied as an equivalent pressure to the bottom section of the bolt.

Friction factors are set as μ = 0,2 between the threads and μ_0 = 0,15 on the base plate.

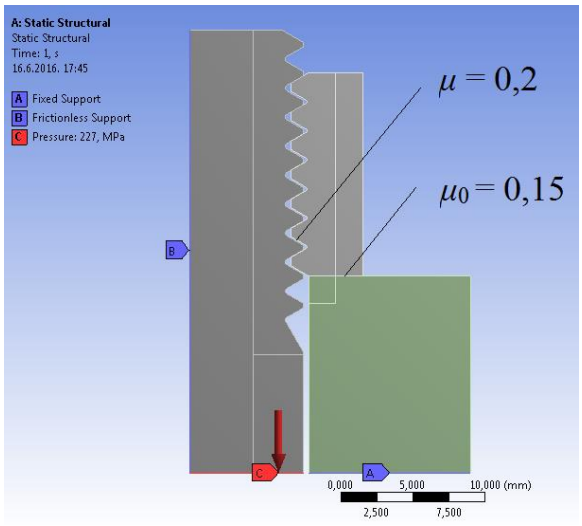

Fig. 3 Friction and boundary conditions [5]

Contact between the screw and nut is defined in such a way that the screw is set to be the contact, and the nut as the target body. Contact between the nut and the plate is defined so the nut is the contact body while the plate is the target.

Used finite elements:

- PLANE183
- SURF153
- CONTA172
- TARGE169

2.3. Pitch optimizing

In the Ansys Workbench project scheme, to an existing static analysis, the response surface optimization was added.

In the imported model of the nut, the pitch was named with the prefix DS to indicate this dimension as a design parameter within Ansys modules and allows its selection and modification. As an output parameter the maximum stress was selected.

The nut pitch is set to increase in small increments. Acquiring the overall results and stress values for each increment it can be observed how does the pitch increase affect the stress values and distribution on the threaded connection. With that data a optimal pitch value can be selected.

3. RESULTS AND ACHIEVEMENTS

On the pictures below is shown a comparative overview of stress and deformation solution for optimized, shown to the left, and the standard case that is shown in the right half on the example of thread M16. The distribution of colours is uniform so the display could easily be interpreted.

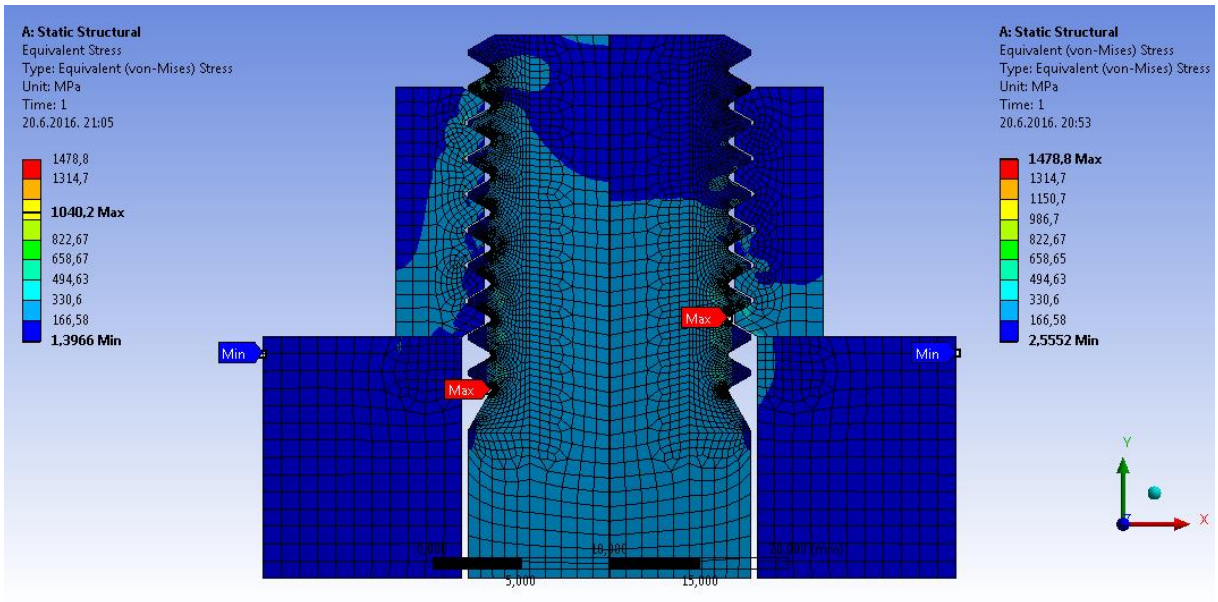

Fig. 4 Equivalent stress comparison of optimized and standard thread connection [4]

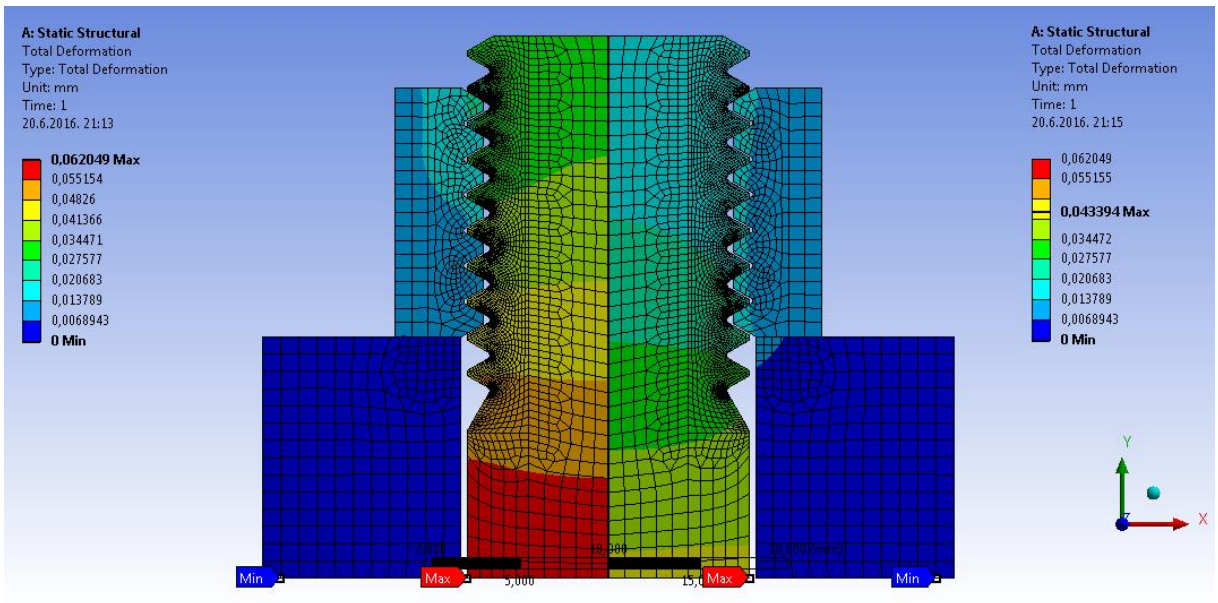

Fig. 5 Total deformation comparison of optimized and standard thread connection [4]

3.1. List of results

The stress distribution, by looking at the color image, takes place uniformly over all the thread profile in contact unlike the standard solution, where the first three profile are different from the other.

The stress on the nut rest plate is also improved, there is now less stress concentration on the bolt hole edge.

On the graph below it is visible that by increasing the pitch of the nut for the right amount the stress can decrease by up to 30%.

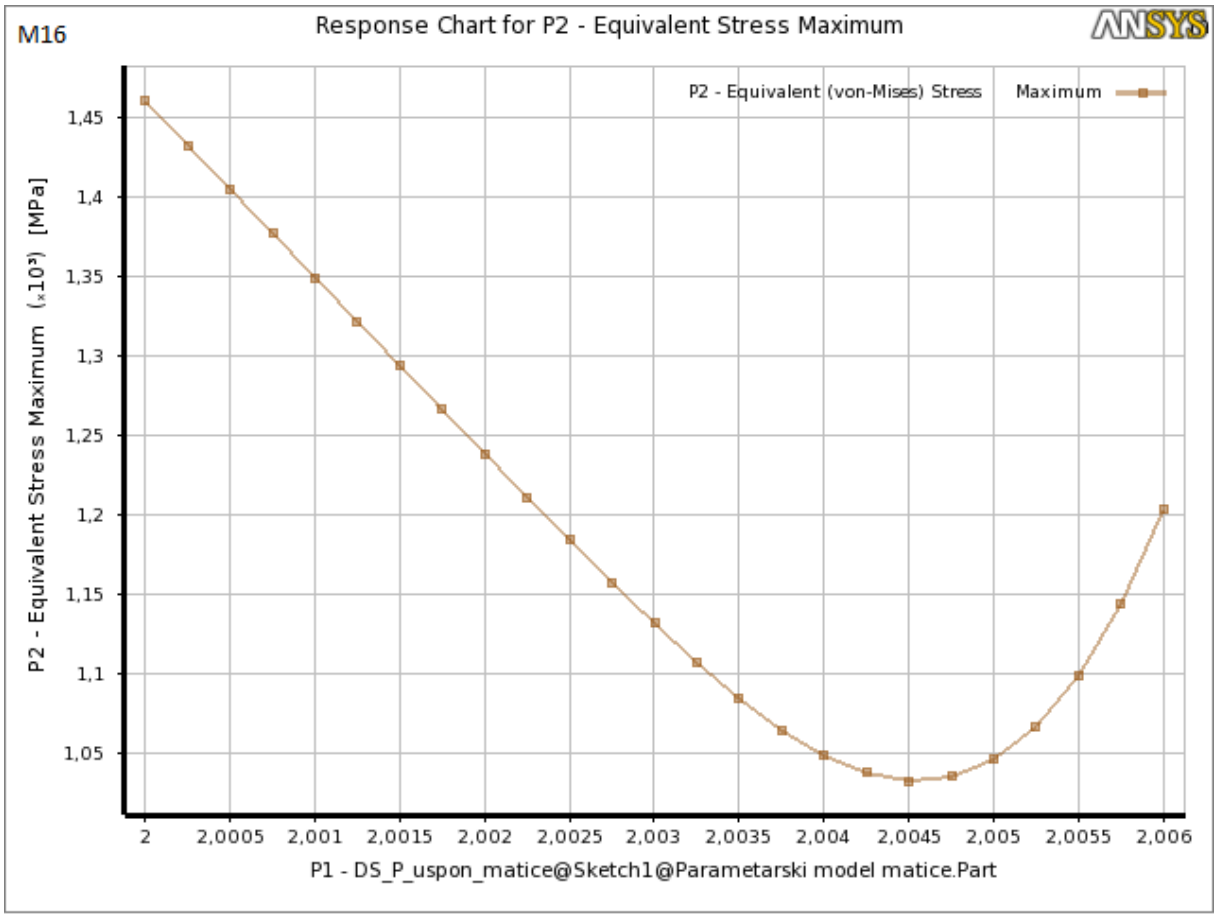

Fig. 6 Pitch - stress dependence [4]

Optimizing of all thread connection for selected ISO general purpose metric screw threads is performed and the proposed pitch increase amounts and maximum stress reduction are given in the table below.

Table 2 Nut pitch increase and stress reduction amounts

Thread	Nut pitch increase, a /µm	Maximum equivalent von Mises stress $\sigma_{maks,}$ /MPa		Stress reduction
		Standard thread	Optimized thread	
M8 x 1,25	2	1258,9	995,39	22,59%
M10 x 1,5	3	1293,7	983,7	23,96%
M12 x 1,75	3	1309,2	985,53	24,72%
M16 x 2	5	1478,8	1040,2	29,66%
M20 x 2,5	5	1386,5	989,15	28,66%
M24 x 3	7	1369,4	983,33	28,19%
M30 x 3,5	7	1398,7	992,58	29,04%
M36 x 4	8	1419,3	993,04	30,03%
M42 x 4,5	10	1478,6	1027,2	30,53%
M48 x 5	10	1477	1028,9	30,34%
M56 x 5,5	12	1493	1008,4	32,46%
M64 x 6	12	1514,5	1044,2	31,05%

Thread	Nut pitch increase, a /µm	Maximum equivalent von Mises stress $\sigma_{maks,}$/MPa		Stress reduction
		Standard thread	Optimized thread	
M8 x 1	2	1337,7	991,4	25,88%
M10 x 1,25	2	1348,5	999,92	25,85%
M12 x 1,5	3	1343,4	990,66	26,26%
M16 x 1,5	3	1476,3	992,92	32,74%
M20 x 2	4	1444,4	963,17	33,32%
M24 x 2	4	1526	1005,1	34,13%
M30 x 2	4	1637,1	1093,5	33,21%
M36 x 3	6	1540,8	1008,1	34,57%
M42 x 3	6	1627,1	1032,6	36,54%
M48 x 3	6	1687,2	1053,2	37,58%
M56 x 4	8	1631,8	1051,9	35,54%
M64 x 4	8	1834	1142,5	37,7%

4. CONCLUSIONS

Increasing nut pitch achieved significantly better stress distribution through the profile of the thread in contact and decreased the maximum stress in the amount of roughly 30%.

As the nut pitch increase amounts are relatively small, from 2 µm – 12 µm and are rising with the increase of the nominal diameter of the thread it is to be concluded that the method is more appropriate just for larger nominal diameter or for special applications such as threads on oil platform drilling pipes and similar.

Also, improving the distribution of stress and with it the fatigue life of threaded connections can be done by making build tolerances for bolt and nut manufacturing tools in accordance with the tolerance fields that allow the existence of certain positive difference between the pitch of screws and nuts.

Further work in this area could explore the impact of the material properties, the amount of load and friction factor between the threads and between the nut and rest plate on the principle of this method of improving stress distribution. Even though for special applications there is no alternative to a individual analysis, it would be useful to draw up charts of these influences and try to reach the analytical expression, which would link all the features that describe threaded connections, through which it would be easier to get to the correction of the pitch of the necessary pitch difference.

5. ACKNOWLEDGEMENTS

Special thanks to prof. dr. sc. Dražan Kozak and prof. dr. sc. Željko Ivandić on guidance and the assistance provided through analysing of these method.

6. REFERENCES

[1] Fukuoka, T., Evaluation of the Method for Lowering Stress Concentration at the Thread Root of Bolted Joints With Modifications of Nut Shape, Journal of pressure vessel technology, Vol. 119(1), 1997.

[2] Stanley Black & Decker, New Britain, SAD: Spiralock Load distribution, 2016., URL: http://www.stanleyengineeredfastening.com/brands/spiralock/technology/load-distribution (13.4.2016.)

[3] SolidWorks, 2012, Dassault Systèmes, 2011.

[4] Kraut, Bojan: Engineering manual. (in Croatian) Zagreb; Tehnička knjiga Zagreb, 1988.

[5] ANSYS, v16.2, Ansys Inc., 2015.

Influence of the mini - dental implants diameter on stress in the surrounding bone

M. Krisla [a], D. Kozak [b], A. Čelebić [c]

[a] Strojarski fakultet u Slavonskom Brodu, Trg Ivane Brlić Mažuranić 2, 35000 Slavonski Brod, Croatia, marin.krisla@gmail.com

[b] Strojarski fakultet u Slavonskom Brodu, Trg Ivane Brlić Mažuranić 2, 35000 Slavonski Brod, Croatia, dkozak@sfsb.hr

[c] Stomatološki fakultet, Gundulićeva 5, 10000 Zagreb, Croatia, celebic@sfzg.hr

Abstract

In this paper was analyzed impact of positioning the mini - dental implants on the bending stress in edentulous jaws, because edentulism is very often problem today. As a solution to edentulism those that stand out the most are removable dentures for three or four osseous implants. The implants are at present most commonly made of titanium and its alloys because it is the type of material which is biofunctional, biocompatible and it is not subject to biodegradation. Knowing mechanical properties of bone and material is very important to prevent rejection or fracture of the implant or bone.

Modeling toothless jaws and properly attributing the mechanical properties to bone is also a demanding job because from the mechanical point of view a bone is a composite material with different solid and liquid phases. Thus the structure of the bone tissue is complex, multi - phase, heterogeneous and anisotropic. In the solution of these problems Simpleware software was of great help.

Using Finite element method (FEM) was determined the equivalent stress in the bone surrounding the implant. Stresses in the bone around the implant threads do not exceed 10 MPa. The maximum stress in the bone (40-50 MPa) appear around the neck of the implant, due to occlusal forces that bend the implant and thus apply additional strain to the bone. The results of stress are satisfactory. The stress analysis of the implant with a changed position, it was concluded that the stress was approximately equal, which means that only the positioning of implants and their position in the bone does not play a significant role. Applying the stress analysis for the mini - dental implants larger in diameter, it was concluded that the stress in the surrounding bone was reduced, around threaded implants, as well as around the implant neck.

Keywords: Edentulous jaws, Mandible, Maxilla, Mini - dental implant, Bending stress

1. INTRODUCTION

Edentulousness is a condition in which the patient has lost some teeth, groups of teeth or all teeth of the upper (maxilla) and lower (mandible) jaw. The most common reasons for loss and tooth extraction are considered caries and periodontal disease. However, there are many other factors that lead to loss of teeth. Some of them are trauma, poor oral hygiene, irregular dental control, smoking, radiation, other systemic diseases, eg. diabetes, and insufficient education, cultural traditions, economy, system and access to health care and other psychosocial factors. Toothless patients due to disruption of function and aesthetics can develop psychosocial problems that manifest themselves as lack of security and withdrawal, poor socialization, general dissatisfaction with oneself and depression. In order to remediate these problems it is necessary to make the appropriate prosthesis, and thus implants. The main factors of acceptance of implants and dentures are: stability, retention, valve performance and the possibility of osseointegration of implants to bone. [1,2,3,4] This paper presents an attempt to optimize the

position of mini - implants in order to get lower bending stress and the impact of changes the diameter of the mini - implants on the stress in the surrounding bone.

2. METHODS AND MATERIALS USED FOR RESEARCH

The original premise for making this work consisted in the fact that it is possible to optimize the position of the mini - dentalnih implants and thus obtain better distribution of stress, and therefore longer lifetime of the implant in the bone. In the beginning it was necessary to make a CT (Computed Tomography) of the maxilla and mandible of the patient. The resulting images (CBCT) were transferred to the JPEG image format so that it could be imported into the software package Simpleware.

2.1. 3D of mandible and maxilla

Imported CBCT shots must be processed in the software in order to separate the jaws segmentation of background noise image. With this procedure it is possible to get a true 3D model of the observed body. Segmentation was done by using these options:

- Treshold
- Dilate
- Close
- Recursive Gaussian
- Shrink Wrap

Figure 1 shows the 3D model of the mandible.

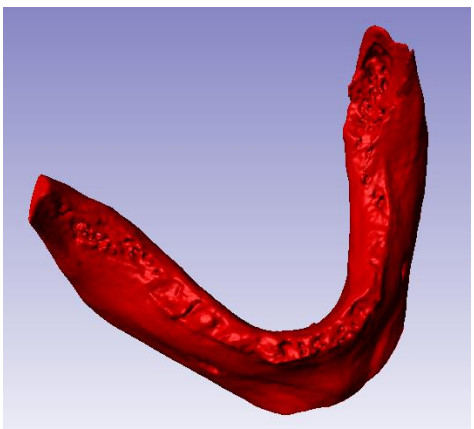

Figure 1. 3D model of the mandible

2.2. Implant material

To properly choose the implant material which will be used as a substitute in the oral cavity it is necessary to know the properties of the dental materials and their application technology. The implant, which is implemented in the oral environment must be biologically tolerable. Biocompatibility of dental materials is assessed through their [5] :

- biofunctionality
- biocompatibility
- biodegradation

The correct choice of dental material involves knowledge of several mechanical properties of materials, and they are [5]:

- stress
- Young's modulus of elasticity
- toughness
- impact energy
- fatigue strength of materials
- hardness

Young's modul of elasticity of the material should be close to the value of the module of elasticity of the surrounding material, in this case, tissue. Insufficient attention in the choice of materials can lead to structure failure in service. Fractures can be [5]:

- sudden breakage
- fracture occured fatigue material
- degradation
- depletion
- corrosion

The material and dimensions of the selected mini - dental implants are shown in table 1 and figure 2.

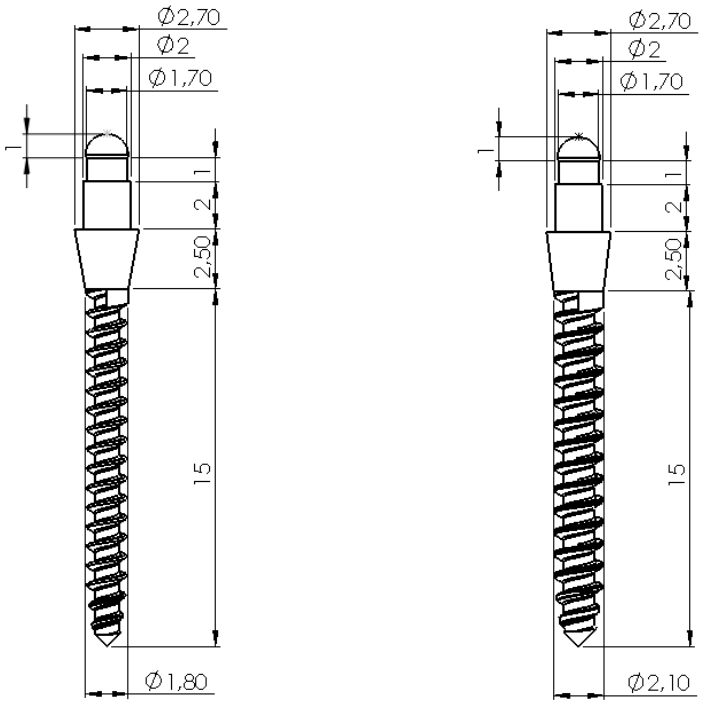

Figure 2. Geometry of two selected mini - dental implants

Table 1. Mecahnical properties of selected mini - dental implants

No	Material	Young's modulus of elasticity *E*/ GPa	Tensile strenght R_m/ MPa	Yield strenght $R_{p0,2}$/ MPa	Strain ε/ %	Alloy type
1.	TiNb29Ta1	65	911	864	13	β

2.3 Finite element analisys

The finite element method is an approximate numerical method [6], and in this paper it is used for discrediting the continuous complex system. Complex differential equations are replaced by simple algebraic equations because it would be impossible to reach the required results for such a complex system. It should be keped in mind that all the results obtained here are approximate, and the actual values would be able to reach only by a proper choice of calculation model and the correct choice of finite elements that are able to describe the real state of deformation [6].

In order to solve this problem a tetrahedral finite element for 3D analysis was chosen. The reason for using this and not heksahedral finite element or a combination of the two final elements is that the software package Simpleware module + FEGRID which is used to mesh with heksahedral finite element or combination heksahedral and tetrahedral finite elements does not allow users greater changes to the size of finite elements. The end result is an enormous number of finite elements (> 10 million), and with that requirements for your computer's performance grow. Module + FEFree allows meshing with only tetrahedral finite elements, but the user's possibility to change the size of the finite elements is much higher. In places where there is an expected stress concentration the mesh is denser, while in the areas between implants the mesh is tenuous. The number of finite elements and the number of nodes are shown in table 2, and the meshed model with tetrahedral elements is shown in figure number 3.

Table 2. Number of finite elements and number of nodes

No	Model	Number of finite elements	Number of nodes
1.	Mandible with three implants with a diameter of 1.8 mm	1 067 184	221 737
2.	Mandible with three implants with a diameter of 2.1 mm	756 202	154 396
3.	Mandible with four implants with a diameter of 1.8 mm	527 827	124 357
4.	Mandible with four implants with a diameter of 2.1 mm	591 994	138 443
5.	Maxilla with three implants with a diameter of 1.8 mm	1 025 809	251 410
6.	Maxilla with three implants with a diameter of 2.1 mm	985 764	203 352
7.	Maxilla with four implants with a diameter of 1.8 mm	1 082 542	264 102
8.	Maxilla with four implants with a diamete rof 2.1 mm	605 382	151 259

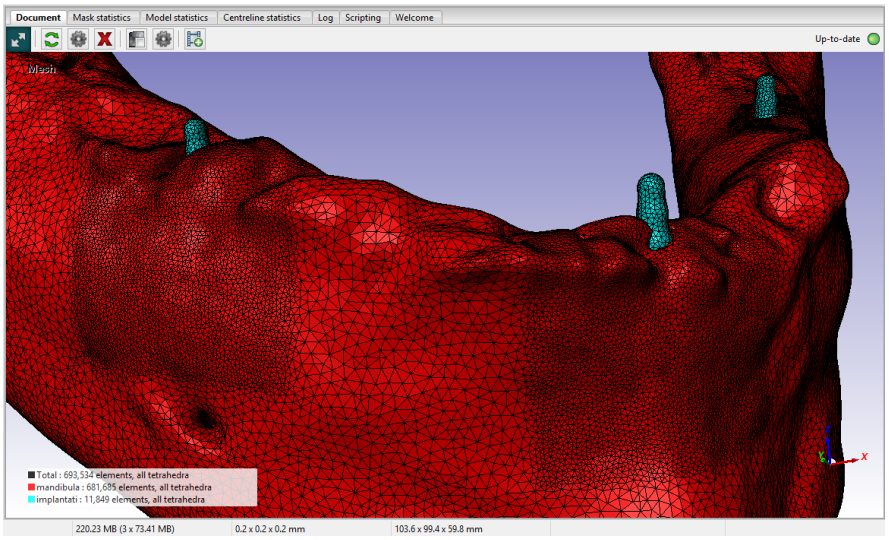

Figure 3. Meshed model of mandible

The basic tetrahedral element is the simplest finite element for three - dimensional analysis. It has twelve degrees of freedom (three in each node), and is shown in figure 4.

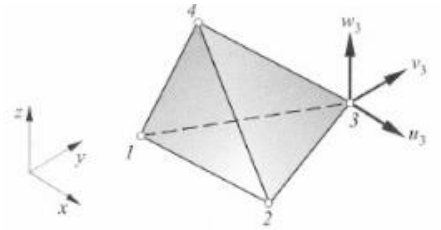

Figure 4. Basic tetrahedral element [6]

The unit consists of four nodes, each with three displacement components *u*, *v* and *w*, in the direction of the Cartesian coordinate axes. Degrees of freedom elements are components of the displacement in nodes. [6]

$$\mathbf{v}^T = \begin{bmatrix} u_1 & v_1 & w_1 & u_2 & v_2 & w_2 & u_3 & v_3 & w_3 & u_4 & v_4 & w_4 \end{bmatrix} \quad (1)$$

The distribution of displacement in the element is described in a complete polynomial of the first degree [6]:

$$\begin{aligned} u &= a_1 + a_2 \times x + a_3 \times y + a_4 \times z \\ v &= a_5 + a_6 \times x + a_7 \times y + a_8 \times z \\ w &= a_9 + a_{10} \times x + a_{11} \times y + a_{12} \times z \end{aligned} \quad (2)$$

The stiffness matrix is calculated using the formula [6]:

$$\mathbf{k} = \int_V \mathbf{B}^T \mathbf{D} \mathbf{B} \times \mathrm{d}V \quad (3)$$

Before the final resolution of the problem it is necessary to specify the boundary conditions so that the system defines maximally. Boundary conditions consist of placing the supports and effective force. The maxilla is fixed, while the mandible allows shifts. Due to the problem of assigning a shift in tomporomandibular joint which is not modeled as it is not seen on the CBCT images, the mandible is also fixed. This means that the resulting stresses will be higher in comparison with the case when the mandible was

fixed. The values of effective forces are shown in Table 3.

Table 3. The values of effective forces

No	Number of implants		Bite force/ N	Occlusal force/ N
1.	Three implants in jaw	Force on one implant	333	25
2.	Four implants in jaw	Force on one implant	250	25

3. RESULTS AND ACHIEVEMENTS

Results of numerical analysis were obtained using the software package Ansys Workbench.

3.1 List of results

As stated in the materials and methods of work, the original assumption consisted in the fact that it is possible to optimize the position of the mini - dental implants and thus obtain better distribution of stress, and therefore longer lifetime of the implant in the bone. By doing the research and obtaining solutions, it was found that changing the position affects very little or almost nothing to the resulting stress as shown below with table 4.

No	Jaw	Position	Stress/ MPa
1.	Mandible	Original	7
		Changed	6,8
2.	Maxilla	Original	7,2
		Changed	7,3

Also it was concluded that only the optimization does not make sense because the bone is of a different shape and it has different material properties with different people. What might be ideal for one patient might not be good at all for another. Therefore, an analysis of how changes in the diameter of the mini - implants affect the stress in the surrounding bone, was made. Using 1.8 mm diameter implant, the largest stress observed resulted 40 MPa, while using the 2.1 mm diameter implant in the same position reduced maximum stress to 30 MPa. Maximum results are shown in table 5.

Table 5. Maximum equivalent stress results

No	Jaw/ number of implants	Diameter of implants/ mm	Equivalent stress in surrounding bone/ MPa
1.	Mandible/ three	1.8	25
		2.1	21
2.	Mandible/ four	1.8	25
		2.1	21
3.	Maxilla/ three	1.8	40
		2.1	30
4.	Maxilla/ four	1.8	35
		2.1	30

The results are shown using the diagram in figure 5. This is a representative diagram which means that all other diagrams have the same shape, but different values of the resulting stress. This means that all the diagrams are in favor of increasing the diameter of the mini - implants which results in reduction of the resulting equivalent stress.

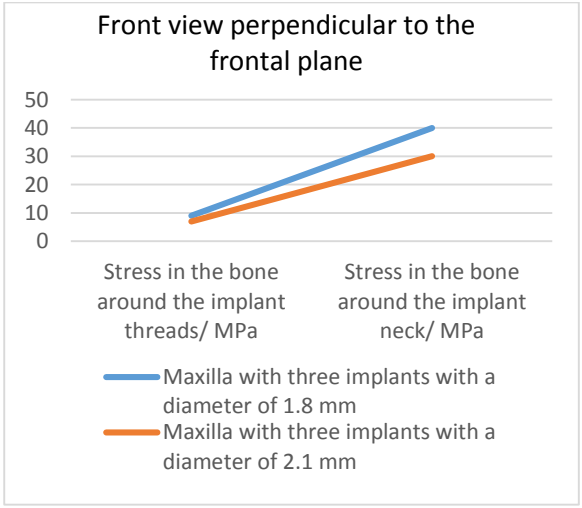

Figure 5. Representative diagram of results

As for the stress in the implant, the largest stresses occur on the neck of the implant (figure 6) because an occlusal force acts there in the amount of 25 N bending the implant around the bones. Changing the diameter of the mini - dental implant does not change the geometry of the head and neck of the implant, and since the largest stress was noticed there it does not make

sense to talk about reducing the resulting stress (figure 6).

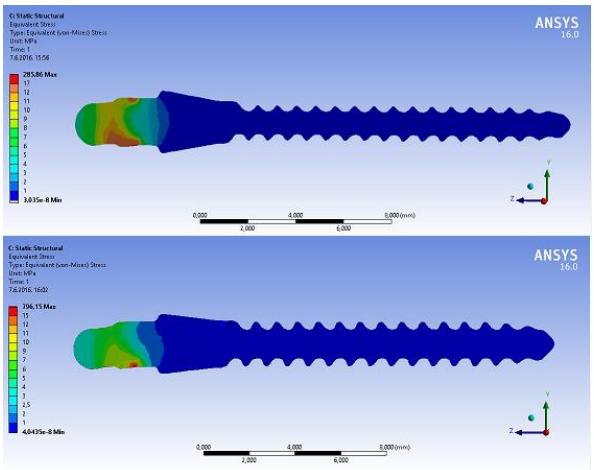

Figure 6. Equivalent stress results in implants (Ø 1.8 mm- up, Ø 2.1 mm down)

4. CONCLUSIONS

Dealing with the implants implies knowledge of many alloy materials used to produce implants, but also the mechanical properties of bone. Properties and the shape of the bone are individual for each person and it is impossible to make a pattern that would allow the implants being positioned so that it is the best solution for all people. The paper shows how the change of the diameter of the mini - dental implants affects on the equivalent stress in the surrounding bone. Using larger diameters results we got smaller equivalent stress than in those obtained by using smaller diameter. Also it is important to note that too large diameter implants can cause cleft alveolar portion of the jaw, so we also need to be careful when it comes to that. The larger diameter implant reduces the equivalent resultant stress in the surrounding bone, but if used in the jaw, which has a narrow alveolar ridge may cause its breakage.

In the dental practice World Health Organization (WHO) has recognized the treatment of edentulism by using removable dentures on four osseintegrated support. In this paper, finite element method (FEM) analyzed the stress in the case of four osseointegrated implants, and a contribution was given to the analysis of stress edentulous jaw with removable dentures in three osseointegrated implants. It is also made a comparison of stress when changing the diameter of the mini - implants. Treatment of loss of teeth in the future might be based on removable dentures resting on three osseointegrated implants, so in opinion for further development and progress in dental treatment of teeth loss should take that direction. Such treatment should be cheaper with the same quality.

5. ACKNOWLEDGEMENTS

First and foremost I would like to thank my mentour prof. dr. sc. Dražan Kozak whose generous advice and instructions helped me in doing this work.

I would like to thank my closest friends and family, my girlfriend for medical and dental interpretations and my sister who advized me when it came to translation. I also thank the Simpleware team on their generosity and assistance in the procurement of the software. Last but not least, I would like to thank dr. sc. Darko Damjanović who kindly helped me by lending me his work station for the purpose of carrying out this work.

6. REFERENCES

[1] Cooper, L.F., *The Current and Future Treatment of Edentulism*, J Prosth Dent. 2009., pp. 116-22.

[2] Carlsson, G.E., Omar, R. *The future of complete dentures in oral rehabilitation*, J Oral Rehabil, 2010., pp. 37, 56-143.

[3] Kraljević, Krešimir: *Potpune proteze*. Zagreb; Areagrafika, 2001., 26-130. str.

[4] Singh, Z., *The triumph of humanity-are we prepared to face the challenge?*, Indian J Public Health, 2012., Jul-Sep, 56(3), pp. 189-195.

[5] Jerolimov, Vjekoslav: *Osnove stomatoloških materijala.* Zagreb; Stomatološki fakultet, 2005., 2-22 str.

[6] Sorić, Jurica: *Metoda konačnih elemenata.* Zagreb; Golden marketing - Tehnička knjiga, 2004., 27, 276-279 str.

The impact of plasma cutting speed and pressure on surface quality

N. Blazinovic [a], A. Stoic [a], M. Stoic [b], I. Samardzic [a], M. Duspara [a], M. Culetic Condric [b]

[a] Mechanical Engineering Faculty in Slavonski Brod, J.J. Strossmayer University of Osijek, Trg I.B. Mazuranic 2, 35000 Slavonski Brod, Croatia

[b] College of Slavonski Brod, dr. M. Budaka 1, 35000 Slavonski Brod, Croatia, marija.stoic@vusb.hr

Abstract

This paper describes the effect of parameters: speed and pressure of cutting on the quality of the machined surface when cutting plasma. Working material is a general structural steel mark S355JR, 5 mm thick. In order to obtain optimum cutting conditions to give the best quality of cut for the selected working material in the experiment was varied cutting speed with a constant pressure of 5.5 bar, and in the second case the speed was constant, 1.2 m/min but the pressure was increased in steps of 0.5 bar. By analyzing the cut, it was noted that too small or too large cutting speed results in a very poor quality cut. Shiver which is formed from the excessive cutting speeds is difficult to remove, requiring grinding and that way increasing the overall cost of treatment.

Keywords: plasma, cutting speed, cutting pressure, roughnesss

1. INTRODUCTION

The production at the present time is set by many requirements, and in addition to price and delivery time a major role has the increase of quality parameters. When talking about cutting material one of these parameters is quality of the machined surface. For cutting structural steels, among other procedures such as laser cutting and gas cutting, plasma cutting is one of the often used procedure.

2. METHODS AND MATERIALS USED FOR RESEARCH

2.1. Plasma arc cutting

Plasma arc cutting is an non-conventional method appropriate for cutting high-alloy steels, carbon, copper, aluminum and other. It's an thermal removing process that consists in melting of material by very high temperatures. During the process an arc is established between a non fusing tungsten electrode that works as the catode and working piece – anode as shown in Figure 1[1].

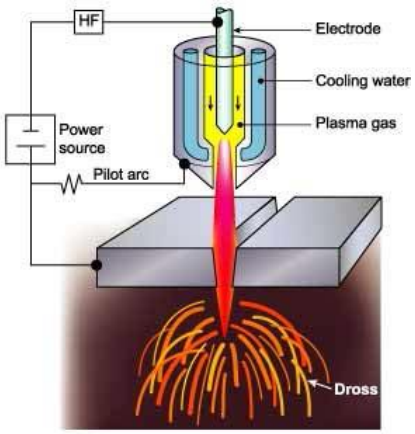

Fig. 1. The Plasma Arc Cutting Process [2]

Thin metal sheets up to 8 mm thick can be cut very precisely in "high definition" class, while the maximum cutting thickness is 20 mm. Plasma system uses the technical gases, oxygen, nitrogen, argon, hydrogen and mixtures thereof, which gives the optimal result for all metals. It

is also possible to use air. The source is designed with inverter technology and has unique capabilities to integrate with automated CNC systems. Management and control of the arc voltage and current cutting is performed automatically, which allows maintaining constant quality of cut. The source of current for high precision thermal cutting is PA-S25 W, Kjellberg [3]. Keeping the cutting head gas and plasma gun running triaxial CNC positioning system-table, DS-CUT is used, Figure 2.

High speed and dynamic characteristics of the table are managed by modern CNC control system that provides optimal technical parameters, as well as high accuracy, precision and dynamics when changing direction or speed cutting [3].

Fig. 2. CNC system-table DS-CUT [3]

2.2. Material

Working material is a construction steel S355JR. Construction steel is carbon steel (ordinary or stainless) by weight of carbon of less than 0.6% or alloy steel (mainly manganese, silicon, chromium, nickel, tungsten.) Steel S355JR of a group of non-alloy structural steel, and chemical composition of the steel shown in Table 1. One of the important technological properties of steel S355JR is good weldability, while from the other required properties to mention cold formability, suitability for bending, deep drawing, forging...

Table 1. The chemical composition of steel S355JR [3]

C	Si	Mn	P	S	N	Cu	CE
0,240	0,550	1,600	0,04	0,04	0,012	0,550	0,470

2.3. Experiment

The paper investigates the influence of cutting speed and pressure on surface roughness. For the experiment were used 5 mm thick plates as a working material. In the first case the speed cutting was varied, while the pressure stays the same, 4 and 5,5 bar. In the second case the speed remains constant, 20 mm/s, while the pressure increase pace of 0,5 bar. The surface roughness parameter measured during this study was Ra (μm) and Rz (μm). At each cutting surface there were made 5 mesuringes in order to get better results. Measuring of surface roughness was done at the device Mitutoyo SJ.301. The dimensions of the plate and sourface that the roughness were measured are shawn at Figure 3. and Figure 4.

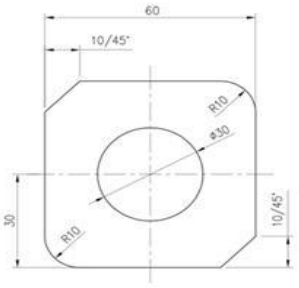

Fig. 3. Drawing of sample, 5 mm thick [3]

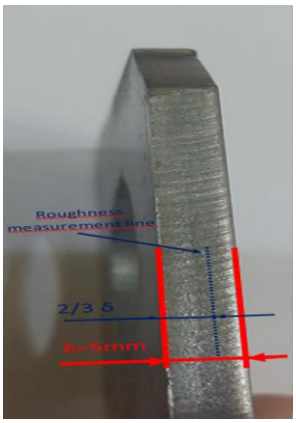

Fig. 4. Measured surface [2]

3. RESULTS

3.1. Surface roughness results

Table 2. shaws the results of surface roughness mesured by constant pressure of 4 bar and 5,5 bar and varied cutting speed from 13 mm/s till 35 mm/s.

Table 2. Results of surface roughness by constant cutting pressure

Cutting speed vc, mm/s	Ra, µm 4 bar	Rz µm 4 bar	Ra, µm 5,5 bar	Rz µm 5,5 bar
13	1,56	8,17	2,36	12,89
13	1,37	7,09	2,6	13,3
13	1,35	6,49	2,58	13,26
13	1,47	7,21	2,63	12,65
13	1,76	8,37	2,59	13,02
17	0,99	5,58	2,11	11,35
17	1	5,66	2,33	14,32
17	1	5,95	2,14	11,91
17	1,24	6,47	2,16	12,12
17	1,21	6,59	2,12	11,44
20	0,95	4,81	2,13	10,23
20	0,99	5,97	2,38	10,84
20	0,81	4,89	1,68	9,52
20	1,31	7,55	2,05	10,29
20	1,09	6,07	1,64	8,6
23	1,83	8,75	1,01	6,14
23	2,08	11,99	1,15	6,29
23	2,48	13,48	1,14	6,28
23	2,57	15,75	0,98	5,53
23	2,56	15,69	1,18	7
26	2,57	12,54	0,99	4,89
26	2,46	12,92	0,91	5,56
26	2,26	8,32	0,9	4,62
26	1,88	10,75	0,99	6,63
26	2,37	12,91	0,98	5,87
30	2,81	13,21	1,01	6,22
30	2,64	13,3	1,04	6,2
30	2,5	12,75	1,21	6,74
30	2,47	13,07	1,22	6,82
30	2,46	13,06	1,19	6,08
35	4,42	24,67	2,58	13,04
35	3,55	18,44	2,68	13,58
35	3,75	23,88	2,72	13,51
35	7,43	36,37	2,45	12,91
35	6,1	34,72	2,3	12,2

By analysing the results (Figures 6. and 7.) there can be seen that the best cutting speed by pressure of 4 bar is 17 mm/s and by 5,5 bar is 25 mm/s to get the minimum roughness. But increasing the cutting speed furtherly the roughness is rising.

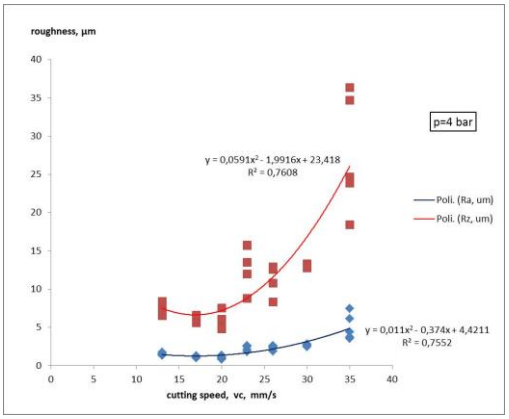

Fig. 6. Results by constant cutting pressure of 4 bar

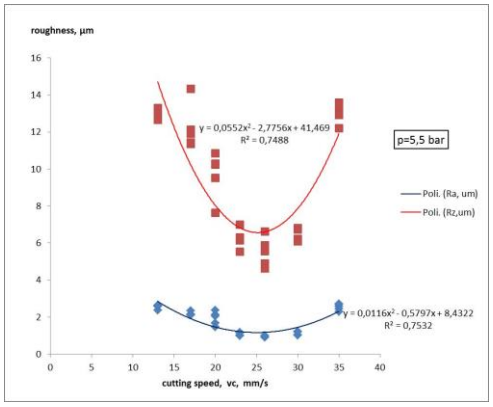

Fig. 7. Results by constant cutting pressure of 5,5 bar

Figure 8. shaws the results of surface roughness mesured by constant cutting speed of 20 mm/s while the pressure increase pace of 0,5 bar starting with 4 bar till 7 bar.

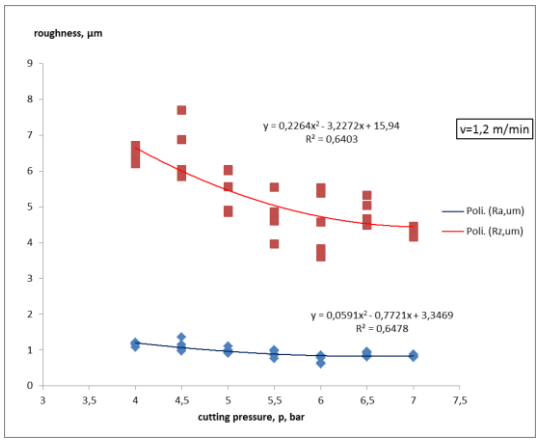

Fig. 8. Results by constant cutting speed of 20 mm/s

Figure 8. shows that the optimum cutting pressure at cutting speed of 20 mm/s is 6,5 bar to get the best roughness.

3.2. Impact on quality cut

The impact on quality cut is shawn in Figure 9.

V_c, mm/s	p, bar	picture of quolity cut
13	5,5	
17	5,5	
20	5,5	
23	5,5	
26	5,5	
30	5,5	
35	5,5	
40	5,5	

Fig. 9. Quality cut by cutting pressure of 5,5 bar and cutting speed from 13 till 40 mm/s

By lower or higher cutting speed from 20 mm/s there is a shiver on the bottom that has to be removed with some machinning process that increases the production time and costs.

Cutting with a constant speed of 20 mm/s and increasing the cutting pressure of 0,5 bar starting with 4 bar till 7 bar shaws that the optimum pressure for cutting to get a good quality cut is approximately 6 bar.

4. CONCLUSIONS

The aim of this paper was to determine the optimum cutting speed and cutting pressure to get as better surface roughnesss during plasma cutting for a given structural steel S355JR of 5 mm thickness.

The experiment was done in two ways: by changing the cutting speed while keeping the pressure constant at 4 bar and at 5,5 bar, and by changing the cutting pressure while the cutting speed was constant at 20 mm/s. The optimum result of sourface roughnesss was at the cutting speed of 20 mm/s and cutting pressure of 6,5 bar.

The analysis of the cut shows that too small or too large cutting speed results in a very poor quality cut. Shiver which is formed from the high cutting speeds it is difficult to remove and requires regrinding. If the cutting speed is too high this can lead to the fact that the plasma jet does not penetrate completely through the material. If the cutting speed is too small, the width of the cut will be higher, and the molten material will not be blown by gas but will accumulate at the bottom of the cut as a shiver that is easy to remove.

The best result of quality cat is at cutting speed of 20 mm/s and cutting pressure of 6 bar.

5. REFERENCES

[1] M. Harničárová, J. Zajac, A. Stoić, Comparison of different material cutting technologies in terms of their impact on the cutting quality of structural steel. Technical Gazette , 17, 3(2010) 371-376.

[2] A. Tsiolikas, J. Kechagias, K. Salonitis, N. Mastorakis, Optimization of cut surface quality during CNC Plasma Arc Cutting process. International journal of systems applications, engineering & development volume 10, 2016

[3] N. Blažinović, Sheet metal products by plasma arc cutting, Zavrsni rad, Strojarski fakultet u Slavonskom Brodu, 2016

[4] R. Bhuvenesh, M.H. Norizaman, M.S. Abdul Manan, Surface Roughnesss and MRR Effect on Manual Plasma Arc Cutting Machining. International Journal of Mechanical, Aerospace, Industrial, Mechatronic and Manufacturing Engineering Vol:6, No:2, 2012

[5] D. Begic, M. Kulenovic, A. Cekic, E. Dedic, Some experimental studies on plasma cutting quality of low alloy steel. Annals of DAAAM for 2012 & Proceedings of the 23rd International DAAAM Symposium, Volume 23, No.1, ISSN 2304-1382 ISBN 978-3-901509-91-9

Finite Elements Investigation of Laser Welding in a Keyhole Mode

S. Tadić [a*], J. Barta [b], S. Sedmak [a], S. Petronić [a], A. Sedmak [c]

[a] Innovation Centre of the Faculty of Mechanical Engineering, Kraljice Marije 16, Belgrade, Serbia, * srdjantadic26@gmail.com

[b] Faculty of Materials Science and Technology, Vazovova 5, Trnava, Slovakia

[c] Faculty of Mechanical Engineering, University of Belgrade, Serbia

Abstract

This paper reports 3D finite elements analysis of laser beam welding in a keyhole mode. Physically based constitutive equations were used in the heat source model. Total heat source, derived from the Gaussian shaped laser beam interaction, was partitioned into the volumetric heat source and the surface heat flux. This approach has shown to be stable and highly responsive to the laser welding variables. On such basis, two approaches were developed: first one – the standard model of heat distribution and, the second one – based on the analytically calculated keyhole profile and remapped into the FEM model. Both methods resulted in a close resemblance concerning keyhole profile and weld pool shape.

Keywords: Finite element method, laser welding, temperature distribution

1. INTRODUCTION

Laser beam welding is a contemporary joining technology with a lot of advantages if compared to conventional welding methods. Small heat affected zone with narrow weld bead, large welding speeds, low overall heat input are, among the others, the most prominent features of this technology. As well, laser welding requires concentrated, high power densities, ranging around 105 – 107 W/cm^2. At lower applied ranges, laser welding results in shallow weld penetration – conduction mode – with almost semi spherical weld bead. However, above some threshold value of power density, around 106 W/cm^2, starts, due to intense vaporization, formation of deep and narrow, vapor filled cavity – keyhole mode. It is characterized as highly efficient process, with deep welding propagation.

The first numerical models of laser beam welding dates back since the 'finite difference computation era' [1, 2]. These models established Gaussian beam intensity distribution which can be treated as surface and volumetric heat flux. It was supposed that energy absorption follows the Beer-Lambert's law, $I(z)=I(o)\exp(-\beta z)$, where I(0) and I(z) are laser beam intensities on the surface and at depth z, and β is the temperature-dependent absorption coefficient. While the law itself is more appropriate for semi-transparent materials, not for metals, it was capable to simulate physics of initiation and propagation of the keyhole. However, the mechanism of the penetration into the material is a much more complex phenomenon, involving aspects of light-metal interactions. Within the last two decades, numerous analytical and numerical models were published. The reader might be directed to the recent revives [3, 4] that cover finite elements modeling topics of keyhole welding. In order to facilitate extensive and long mathematical apparatus, in following segment will be given slight digest of the involved mathematics.

2. MATHEMATICAL MODEL

The intensity of the laser beam has Gaussian, bell-shaped distribution

$$I_{(x,y,z)} = I_{(r,z)} = I_0(t)\left(\frac{r_{fo}}{r_f}\right)^2 \exp\left(-\frac{2r^2}{r_f^2}\right) \quad (1)$$

where $I_0(t)$ is the time dependent beam intensity at the focal point, r_{fo} is the beam focal radius, r_f is the beam radius at depth z, and r is radial distance from the axis of the beam. The beam radius r_f at any z-depth plane is given by Eq.2, with r0 being the beam focal radius, z_o is the position of the focal plane relative to the plate top surface, and zr is so-called Reyleigh number, that depends on the focusing number, the wavelength of the beam and the beam quality.

$$r_f = r_0\left[1+\left(\frac{z-z_0}{z_r}\right)^2\right]^{1/2} \quad (2)$$

The peak intensity $I_0(t)$ is expressed as follows:

$$I_0(t) = \int_0^t \frac{2P}{\pi r_{fo}^2}\,dt \quad (3)$$

where P is total optical power of the laser beam and r_{fo} – beam focal radius.

Eqs (1-3**)** are schematically summarized, out of scale to enhance visualization, in Fig.1. Time dependent laser peak intensities, on the surface and any z-plane, were calculated according the Eq.3. while the spatial distributions were calculated from Eq.1. At some radial threshold distance from the beam axis, (when the beam intensity drops down to some critical value), keyhole surface wall is formed – that is the vapor-liquid front in the irradiated material and is shown as the yellow surface in Fig.1. Keyhole surface follows exponential decay according the Beer-Lambert law. Radially apart from the keyhole wall, (toward the red surface in the Fig.1) is the liquid, molten metal pool that finally encounters liquid-solid surface. But, it is still over-simplified approximation. In a real welding operations, the vector of welding speed involves distortions of the molten pool and vaporized keyhole. Traditionally, it may result in the so-called Goldak's double ellipsoidal pool, Fig. 2, which is, perhaps, the corner-stone in the analysis of conventional, arc-welding process. The asymmetric Gaussian distribution along the x-axis (i.e. along the welding direction), caused by welding speed, results in the elongated, double ellipsoidal molten pool (red surface) with the distorted keyhole around the beam axis (yellow surface). However, concerning the laser welding, it is believed that Goldak's approach results in a excessively shallow and wide molten weld pool. On this basis, and following above described mathematics, it seams that Fig's is more appropriate to describe weld pool behavior. It is calculated as asymmetric, double - ellipsoidal behavior accompanied with exponential decay in z-direction.

Further refinements of the model explicitly concerned the profile and the depth of the vaporized keyhole. Asymmetric keyhole profile was calculated point-by-point method on the front and back wall by iterative method to account for multiple Fressnel absorptions/ reflections and evaporative heat flux[5]. The purpose of this refinements was to numerically examine conditions for stable keyhole in terms of laser power, welding speed and thickness of welded plates. The model is straightforward but lengthy and hereafter only the essential steps will be described. The heat balance on the keyhole requires that heat flux absorbed into the keyhole (q_v) is balanced as (4):

$$q_v = I_0\,\alpha_{Fr}\tan(\Theta) = (T_{vap}-T_r)\lambda_{th}P_e\left(\cos(\phi)+\frac{K_1(P_e r)}{K_0(P_e r)}\right) \quad (4)$$

where I_0 is incoming laser beam intensity (from Eq.1), α_{Fr} is of multiple Fresnel's absorptions, θ is the angle of local keyhole inclination, T_{vap} and T_r are the evaporation and ambient temperatures; K_1 and K_0 are modified second kind Bessel functions of first and zeroth order; Pe is the modified Peclet number, $Pe=V_w/2k$ where V_w is welding speed and k is diffusivity. Substituting $\theta=\pi/4$ and $\phi=0$ and π for the front and rear keyhole wall in Eq.5, the radius r on the top of the keyhole can be calculated. In this manner, keyhole profile (and local heat flux) can be calculated from top surface, going downwards point-by-point at any z-plane until the front and rear keyhole wall crossed[6]. Procedure was iteratively repeated for additional Fresnel reflections. Calculated keyhole profile was remapped into the 3-D finite elements mesh for further examinations of the temperature distribution and weld pool shape in laser welding. Local heat flux was used as a boundary condition on the keyhole wall.

3. FINITE ELEMENT METHOD

Geometry of the model is the simple, half-width rectangle of the welded plates in a but-joint configuration. Dimensions of the plate was

20x5x2 mm. The material was supposed to be Ti6Al4V alloy with known thermal and physical temperature-dependent properties in solid and liquid phase. Melting temperature of this alloy is 1700K and the temperature of vaporization is 3300K. Non-uniform mesh was generated to be extremely fine along the path of the laser beam and swept coarser toward the lateral side of the plate, Fig.4.

Governing equation of the finite elements analysis is the fundamental heat-transfer partial differential equation

$$\rho c_p \frac{\partial T}{\partial t} - \nabla(k\nabla T) = Q \qquad (5)$$

where ρ is density of the material, c is specific heat, ∇ is 'nabla' differential spatial operator and Q is total heat input. The heat input distribution was computed according the Eqs.1-3. Total heat input was partitioned into the volumetric heat source and the surface heat flux on the top plane (z=0) of the plate. Transient, time dependent analysis was performed with reference to constant welding speed. Natural boundary conditions with Newtonian cooling were set at all boundaries, excepting the adiabatic condition on the symmetry plane. Due to extremely high temperatures on the top plane, radiation was combined with natural cooling.

Total laser power was 1500W, with 70% efficiency. Intentionally, high welding speed was chosen to be 50 cm/min. Focal beam radius was 0.5 mm with the focus point on top surface.

4. RESULTS

Temperature distribution of FEM analysis is shown in Fig. 5. Several features might deserve some attention: temperature within the keyhole is extremely high, which is in accordance with experimental and numerical reports [7,8] but exact values, due to lack of thermodynamic data in vapor state, should be consider as uncertain. However, the shape and dimension of the keyhole are in a good accordance with similar investigations [9]. The profile of the keyhole might be explained as a result of two mutually orthogonal issues – downward exponential decay of the laser beam intensity and the high vielding velocity. Apart the keyhole, the shape of the weld pool seems to be typical for this kind of welding [10]. In order to better resolve molten pool behavior, Fig. 6 depicts isothermal envelops within the weld pool. It follows distorted, double ellipsoidal behaviour that might be closely related to the Figs. 2, 3.

Results of second model, with analytically predetermined keyhole, is shown in Fig. 7. Although it might look to be more 'exact', due to the new boundary condition, careful examination resolved quite similar behaviour (in shape and penetration depth) that was shown in Fig.5. It is, however, somewhat slimmer - both keyhole and weld pool – within about the 15% in difference between the two models.

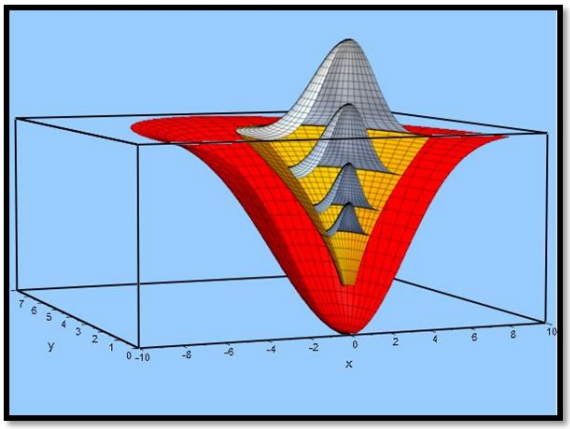

Fig.1. Schematics of laser beam propagation into the material

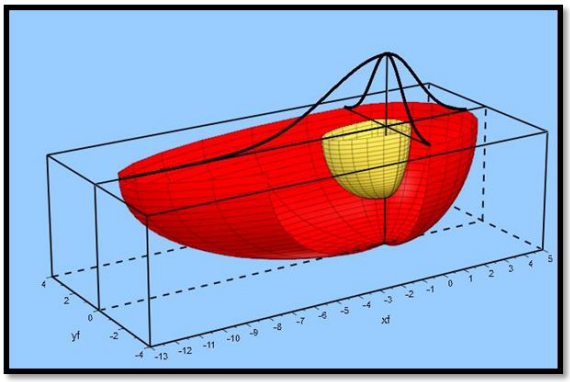

Fig.2. Goldak's double ellipsoidal weld pool with keyhole

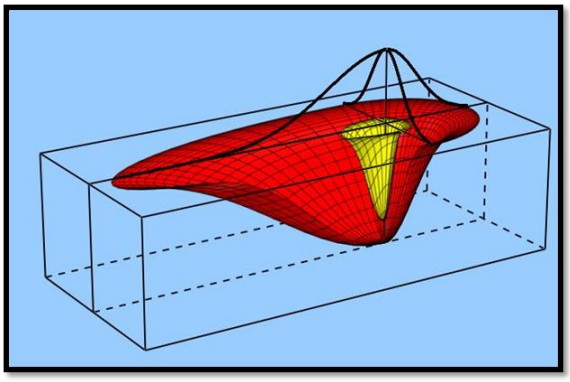

Fig.3. Double ellipsoidal pool and keyhole with Gaussian decay

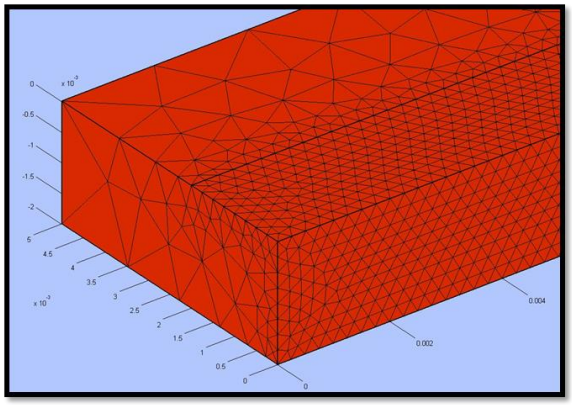

Fig.4 Mesh generated for the finite elements analysis

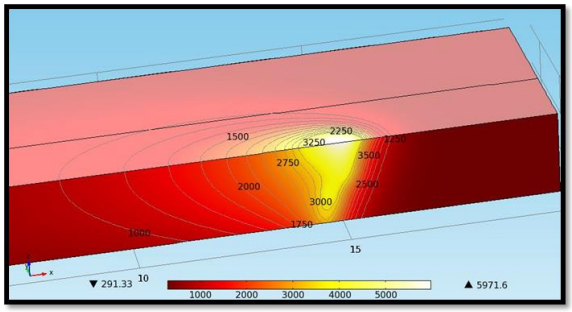

Fig.5 Temperature distribution of the laser beam welding analysis

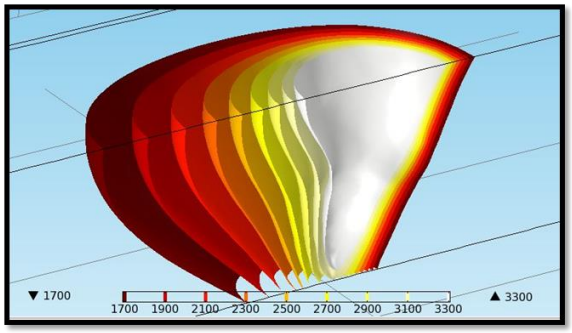

Fig.6 Isothermal envelopes of the weld pool and kethole (white)

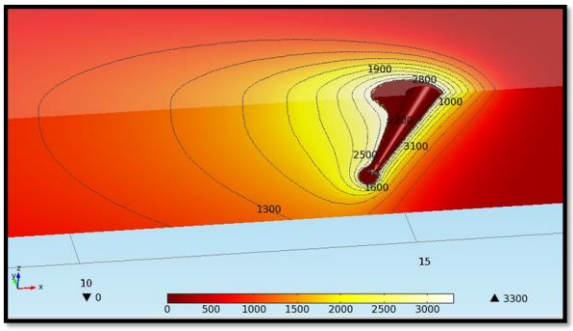

Fig.7. Temperature distribution around the pre-calculated keyhole

.

5. CONCLUSIONS

Finite elements analysis for laser keyhole-mode welding of thin Ti6Al4V alloy was performed. Concerning the keyhole geometry, two different models were applied. Both models were consequent from the firm physical backgrounds and result in a similar keyhole and weld pool behaviour. The mutual differences in isothermal outlines were estimated to be about 15%. Also, models have shown strong sensitivity on the processing variables. It is supposed that precise thermal analysis can be further used in mechanical analysis of laser welded joints.

6. REFERENCES

[1] J.Mazumder, W.Steen, *J.Appl.Phys.*, 1980, v.51, 941-947.

[2] T. Zaharia, S.David, J.Vitek, T.DebRoy, Metall.Mater.Trans, 1989, v.20A, 957-967

[3] J.Svenungsson, I.Chouquet, A.Kaplan, Phys.Procedia, 2015, v.78, 182-191

[4] A.Oto, H.Koch, R.Vasquees, Phys. Procedia, 2011, v.12A, 11-20

[5] A.Kaplan, J. of Appl. Phys., D:Appl.Phys., 1994, v.27, 1805-1814

[6] H.A.Kazzaz, *Mat.Chem.and Phys*., 2008, 109, 61-76.

[7] A.Kaplan, J. of Laser Appl, 2011, v.23, 042005

[8] S.Pang, I.Chen, J.Zhou, J.Yin, Y.Chen, J. of Phys.,D:Appl.Phys., 2007, v.44, 025301

[9] R.Fabrro, K.Chouf, J. of Appl. Phys., D:Appl.Phys., 2000, v.87, 4075-4083

[10] H.Ki, P.Mohonty, J.Mazumder, *Met.and Mat.Trans*., 2002, v.33A, 1817-1830

[11] G.Roy, J.Elmer, T.DebRoy, J.of App.Phys., 2006, v.100, 034903

A Study of Laser Sheet Bending with Finite Elements Method

S. Tadić[a], J. Barta[b], S. Sedmak [a], S. Petronić [a], A. Sedmak [c]

[a]Innovation Centre, Faculty of mechanical Engineering, Kraljice Marije 16, Belgrade, Serbia, *Srdjantadic26@gmail.com

[b]Faculty of Materials Science and Technology, Vazovova 5, Trnava, Slovakia

[c]Faculty of Mechanical Engineering, University of Belgrade, Serbia

Abstract

Laser-forming is a new, promising technology in a wide spectrum of laser technical applications. Instead of external forces, laser-forming uses defocused, low-power laser beam to induce heat and thermal stresses in sheet metal. This paper reports 3D, transient finite elements modelring of laser-bending mechanisms in Ti6Al4V sheets, 1.5 mm thickness. Simulations examined thermal expansion and stress field expansion during the bending of irradiated sheet.

Keywords: Laser-forming, laser technology, Finite element method.

1. INTRODUCTION

Laser forming is a non-traditional, non-contact forming technique that has been under substantial investigation over the last two decade [1]. Instead of traditional approach, sheet metal is formed by plastic deformation induced by thermal stresses resulted from rapid laser heating. Schematics of the laser forming process is shown in Fig.1 [2].

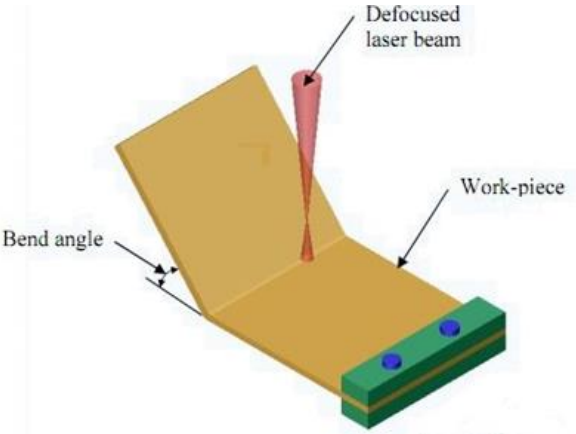

Fig.1. Schematic principle of laser forming, [2]

The laser beam irradiates the sheet surface along a predetermined path and moves with a scanning velocity. After the laser beam passes the target and the temperatures of the target return to ambient temperature, a permanent bending angle would be developed. So far, three laser forming mechanisms have been recognized: the temperature gradient mechanism (TGM), the buckling mechanism (BM), and the upsetting mechanism (UM),[3,4]

The temperature gradient mechanism (TGM) is the most widely reported [5]. Due to the rapid heating of the surface by the laser beam, a steep thermal gradient results in a differential thermal expansion through the thickness of the plate. As the material is heated, the thermal expansion on top, hot surface is much greater than that on the cold, bottom surface. As the material expands in the heated area, the material bends away from the beam - this is the period called 'counter-bending'. Once the thermal expansion stress reaches temperature-dependent flow stress of the material, any additional thermal expansion is converted into the plastic strain. To increase efficiency of the process, the more of the thermal expansion has to be converted into the plastic strain [6,7]. Once the laser beam surpass over the plate, starts the cooling period. During this period, the material contracts in the upper layer of the sheet so that the tensile stresses occurs in the upper region. This results in plastic bending toward the opposite side, typically resulting in a small bending angle, an order of 10. However, the whole process is fast (due to very high laser feed rates) and can be repeated multiple times. Without the spring-back, very accurate angles can be attained, up to 30 and more degrees, [8,9].

Regardless of intensive research, it seems that precise mechanism of the laser forming is not quite clear yet. In particular, the kinetics and driving force in heating period ('counter-bending') and rapid transition into the cooling, 'bending' phase, deserve to be more clarified. The purpose of this paper is developing finite elements numerical model that can analyze transient temperature and stress distribution in sheet metal during laser forming. The paper is focused in a 'counter-bending- phase' details of temperature and stress field spreading.

2. THE MATHEMATICAL BACKGROUND

The heating period of the laser forming was simulated by non-linear heat transfer equation:

$$\rho c_p \frac{\partial T}{\partial t} = \frac{\partial}{\partial x}\left(\lambda \frac{\partial T}{\partial x}\right) + \frac{\partial}{\partial y}\left(\lambda \frac{\partial T}{\partial y}\right) + \frac{\partial}{\partial z}\left(\lambda \frac{\partial T}{\partial z}\right) + \dot{q}(x,y,z,t)$$

where ρ is density of the material, c_p is specific heat, λ is thermal conductivity, t is time and q is the spatial and temporal heat rate flux generated be laser beam. Considering boundary conditions, temperature on top surface can be expressed.

$$-\lambda \frac{\partial T}{\partial z} = h\left(T - T_{ref}\right) + \sigma\varepsilon\left(T^4 - T_{ref}^4\right) - Q_{las}$$

where the first member on the right side refers to the natural convection and the second one to the radiation heat loses. All other surfaces are considered as natural convection boundaries. The third member is the laser beam generated energy that follows Gaussian distribution:

$$Q(x,y,t) = \frac{2\eta P}{\pi r_o^2} \exp - \left(\frac{r^2}{r_o^2}\right)$$

where the P is the total laser power, η is efficiency, r_o is the beam radius and r is radial coordinate of the laser beam depending on time and laser feed rate.

Total strain vector,

$$\varepsilon_{tot} = \varepsilon_{th} + \varepsilon_{el} + \varepsilon_{pl}$$

consists of thermal, elastic and plastic strain vectors. Thermal strain vector is expressed as

$$\varepsilon_{th} = \alpha\left(T - T_{ref}\right)$$

where α is temperature dependent coefficient of thermal expanssion, T is temperatureand T_{ref} is, commonly, room temperature.

Elastic strain vector is defined by elastic strain-stress relationship, whereas incremental plastic strain vectors are defined from Prandtl-Reuss rule.

$$\varepsilon_{pl} = \left[\frac{\partial F}{\partial \sigma}\right] d\lambda$$

where dλ is plastic multiplier (the amount of plastic straining) and F represent yield function which is, by Von Mises yield criterion, connected to temperature dependent yield stress.

3. FINITE ELEMENT METHOD

Geometry is the simple rectangular plate supposed to be Ti6Al4V alloy. Dimensions of the geometry was 10x20 mm with the thickness 1.5 mm. All material data was assumed to be temperature dependent. Special attention was paid to yield stress data, Fig.2. Beyond the yield strength level, work hardening flow stress was supposed in plasticity domain. Isotropic, linear work hardening was assumed. Coefficient of thermal expansion α is shown in Fig.3. In the numerical calculations, linear numerical interpolation of materials data were performed.

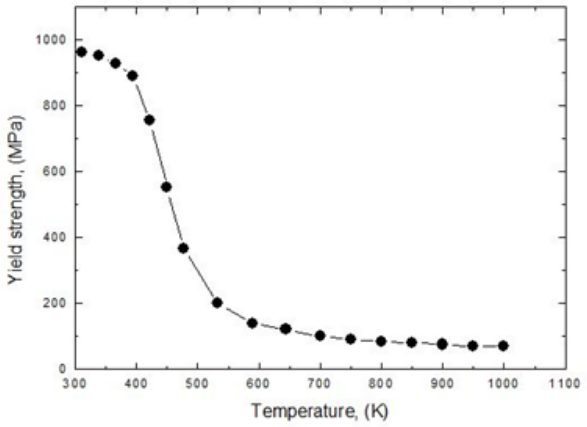

Fig.2. Temperature dependent yield strength [10]

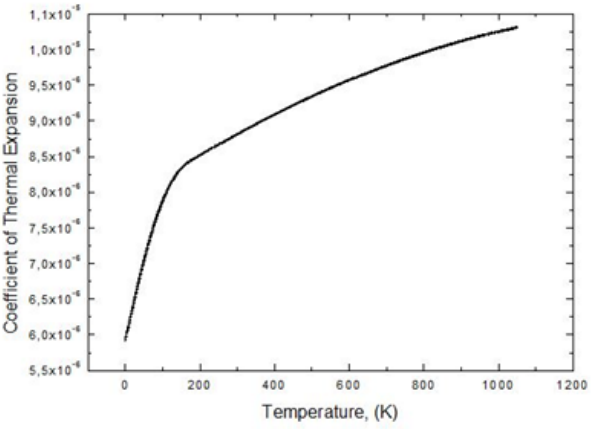

Fig.3. Thermal expansion coefficient [10]

A series of preparatory numerical investigations were performed to optimize laser power, laser beam radius and laser feed rate. The goal was to resolve optimal, low temperature regime – under the β' transition temperature (≈1000 ^{0}C) of the alloy. The chosen temperature field (700-800 ^{0}C) was at the lower end of the steep segment in Fig.2. Laser beam radius was 1 mm, feed rate was 10 mm/sec. and the laser power was 0.75kW and 1,0kW, with defocusing point far above the top surface. The finite elements mesh is shown in Fig.4. Extremely fine mesh (max. 0.1mm) is generated along the laser beam path and gradually enlarged apart. Right side of the plate was fixed, all other were set free.

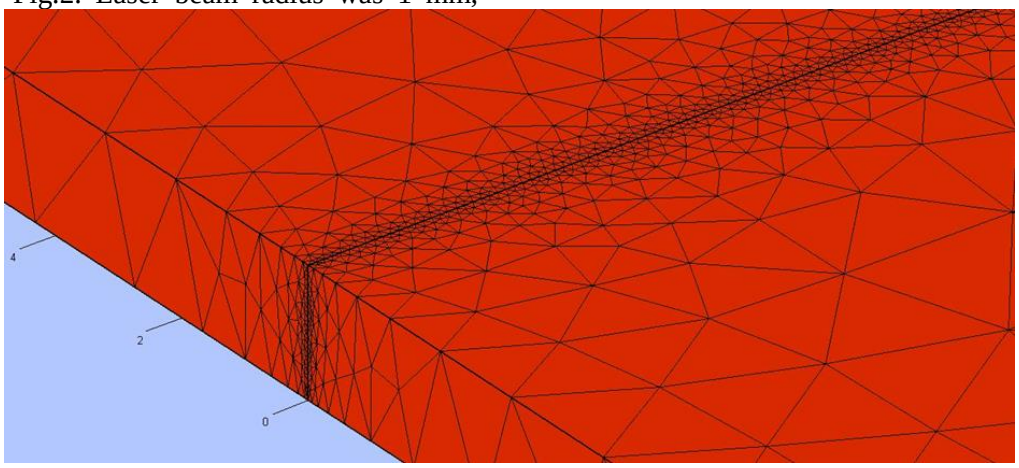

Fig.4. Mesh generated for the FEM analysis. Fine mesh is along the laser feed line

4. RESULTS AND DISCUSSION

First 0.5 seconds of the transient analysis, in steps of 0.1 sec., is shown in the left column in Fig.5. It might be noticed that maximum temperature slightly increases in every step, perhaps due to preheating. But, it is only a few degrees in every step, and the temperature is fair constant – about 700K. Von Mises stress field can be seen in the right column. Maximum stress level, in every step, is 177-191 MPa which is well above yield strength at 700 K, Fig.2. That are compressive stresses caused by thermal expansion. Negative magnitude of stress can be explained in a way that cold, surrounding material suppress otherwise positive plastic straining due to thermal expansion [11,12]. Careful examination reveals that maximal compressive stress is developed in front of heating area, (this is the dark blue area in figures), perhaps due to high thermal gradients that develops in front of laser beam. Much lower stresses are developed in a heating zone, (light blue and yellow area). Such behaviour strongly suggest that temperature gradient has important role in the generation of stress field. The same behaviour continuously repeats during the whole period of heating. But, at the end of the heating period, t=0.9sec, Fig.6, it might be noticed the absence of high stress field. It supports previous conclusion that temperature gradient has important role in the stress generation. The view from the advancing side is shown in Fig.7. High-stress field appears in a mid-thickness zone. However, it is due to bending moment of the plate and is concentrated in a cold area of material. It can be clarified referring to Fig.8 where the yield strength of the whole material field is shown. High-stresses were in a cold zone, far below the yield stress of material.

In order to check the responsiveness of the finite elements model, a series of examinations were performed varying laser power strength, feed rate and beam radius. An example of such investigations is show in Fig. 9a, where the laser power was 1,5kW, all other variables being the same as previous. Selected time is t=0.2 sec. It can be seen that temperature increased up to T_{max}=930K. Accordingly, the maximal compressive stress increased, up to about 200 MPa, Fig.9b. However, the mechanism of stress field developing has remained the same.

5. CONCLUSIONS

Finite elements model has been developed in order to simulate the process of laser bending. The model in details analyse the kinetics and mechanism of thermal expansion during the low-power, surface laser heating. It was revealed that temperature gradient has the governing role in a stress field generation.

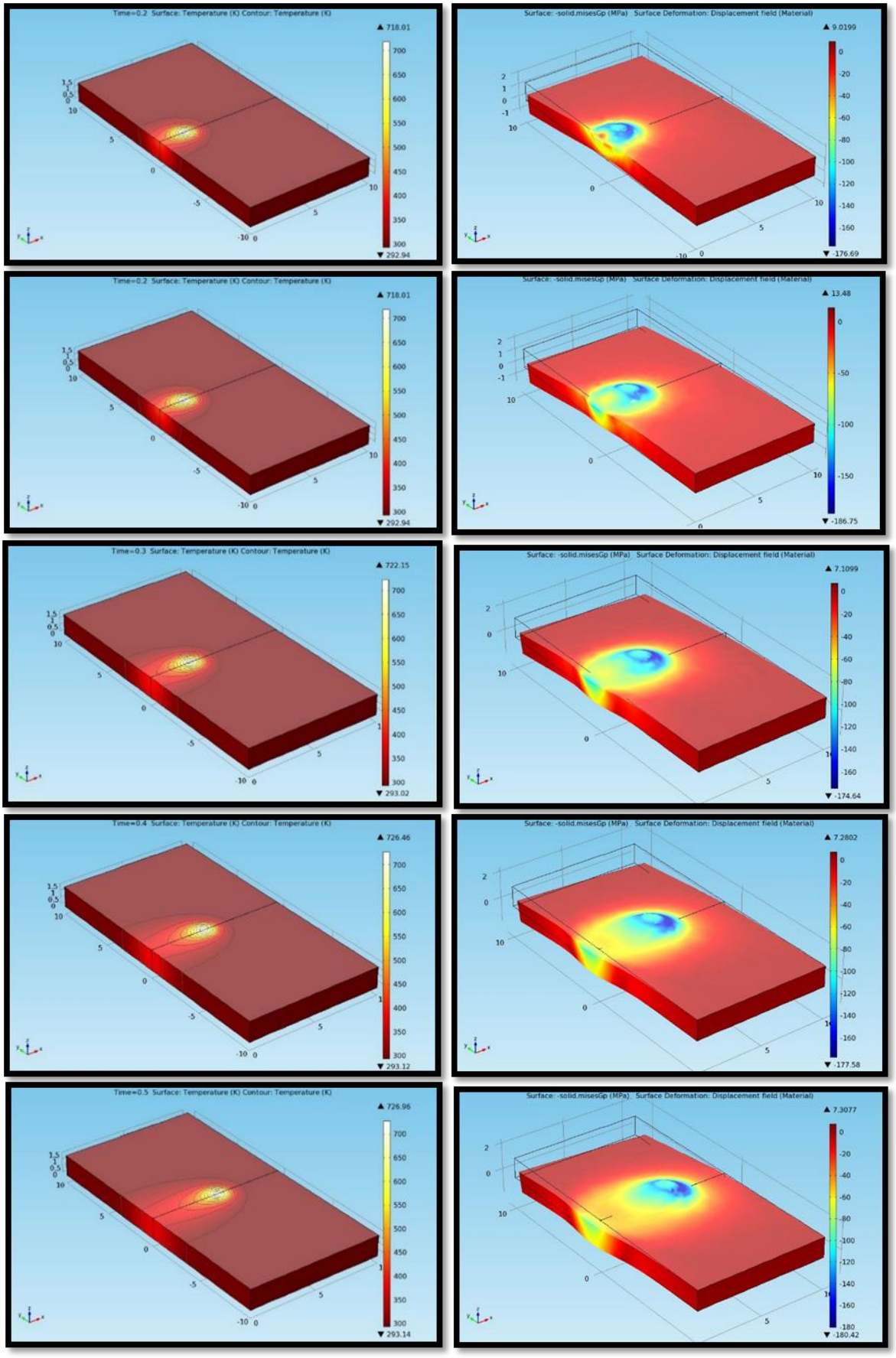

Fig.5. Temperature (left column) and Von-Misess stresses (right) obtained in FEM

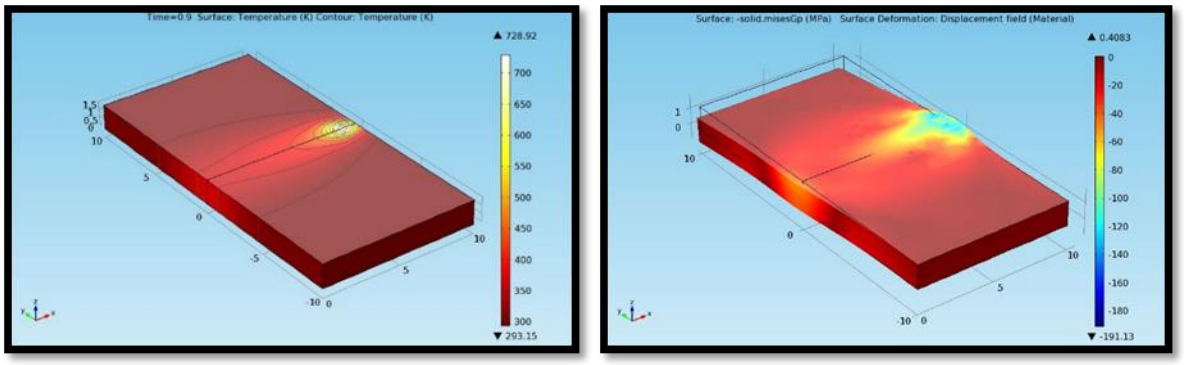

Fig.6. Temperature (left) and V-M stresses (right) obtained at the end (t=0,9 sec.) of heating

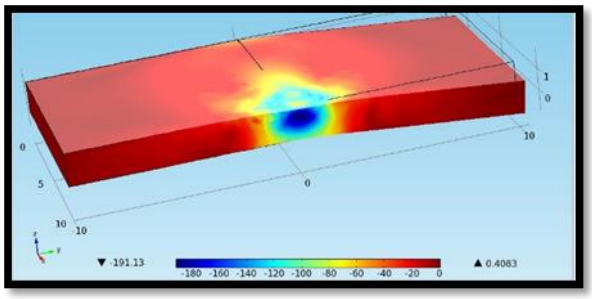

Fig.7. The same as Fig.6; advancing side view

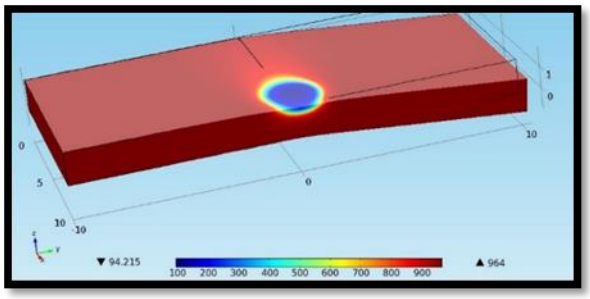

Fig.8. Yield strength levels of heated area

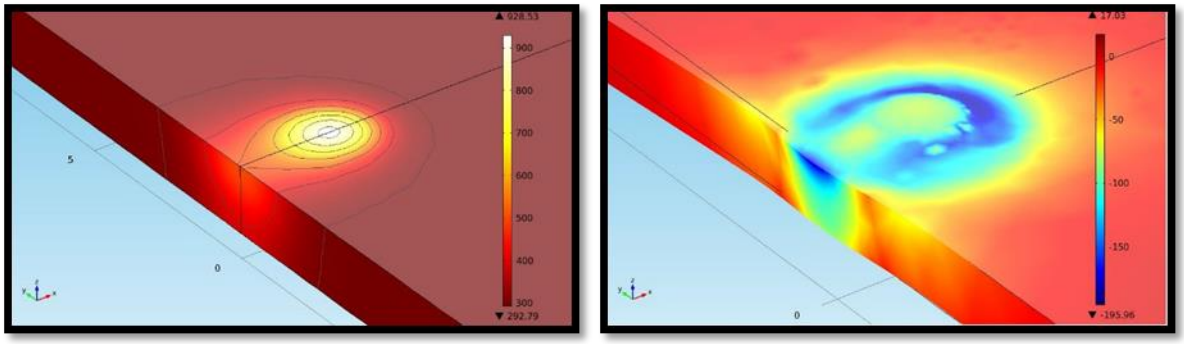

Fig.9 (a,b). Temperature field (a), and V-M stress field obtained after P=1,5kW, t=0.2sec

6. REFERENCES

[1] S.Edwardson, J.Griffits, G.Dearden, K.G. Watkins, *Phys.Procedia*, 2010, 5, 53-63

[2] H.C.Yung, PhD Thesys, U.of Canterbury, 2006.

[3] K.Venkadeshvaran, S.Das, D.Misra, *Int.J.of Eng.Sci and Tech*, 2010, 2, 163-175.

[4] D.Chen, S.Wu, M.Li, *J.of Mat.Proc.Tech.* 2004, 148, 30-44.

[5] W.Li, L.Yao, *Int.J.Adv.Manu.Techol*., 2001, 17, 196-203.

[6] R.McBride, R.Bardin, F.Gross, *J.of Phys D, Appl.Phys*, 2005, 38, 4027-4036.

[7] L.Yang, J.Tang, Y.Chen, *Appl.Surf.Sci*, 2010, 256, 7018-7026.

[8] K.Maji, K.Pratihar, A.Nath, *Opt.and Las.Tech*., 2013, 49, 18-27.

[9] L.Liu, A.Hirose, K.Kobayashi, *Acta.Mat*., 2002, 50, 1331-1347.

[10] P.Rangaswamy, H.Chao, M.Prime, Los Alamos Repport, LA-UR-00-5277, 2000.

[11] Q.Li, X.Wang, Y.Lin, *Acta Met.Sinica*., 2004, 17, 317-322.

[12] M. Hennige, T.Geiger, J.of Mat.Proc.Tech., 2001, 115, 159-165.

Structural Integrity Assessment of a Pressure Vessel

Aleksandar S. Sedmak[a], Aleksandar Milovanovic[b], Simon A. Sedmak[c]

[a] Faculty of Mechanical Engineering, Kraljice Marije 16, 11120 Belgrade, Serbia, asedmak@mas.bg.ac.rs

[b] D.Sc student at the Faculty of Mechanical Engineering, Kraljice Marije 16, 11120 Belgrade, Serbia,

[c] Innovation Centre of Faculty of Mechanical Engineering, Kraljice Marije 16, 11120 Belgrade, Serbia,

Abstract

Fracture mechanics parameters have been applied to assess structural integrity of a pressure vessel with unacceptable defect (lack of penetration) detected in welded joint. This defect has been modelled as a crack of equivalent dimensions, for which the stress intensity factor has been evaluated, for different sizes of plastic zone. These values have been compared with the critical value, i.e. with the fracture toughness, taken as the minimum value according to previous experimental research. Beside brittle fracture, plastic collapse has been considered, as well as their combination, given in the form of Failure Assessment Diagramme (FAD). In any case, this analysis has proved that pressure vessel is safe under given operating conditions.

Keywords: Structural integrity, pressure vessels, welded joint defects, Failure Assessment Diagram

1. INTRODUCTION

Shown in figure 1 is the comparison of classic design methods which apply strength theory vs the application of fracture mechanics.

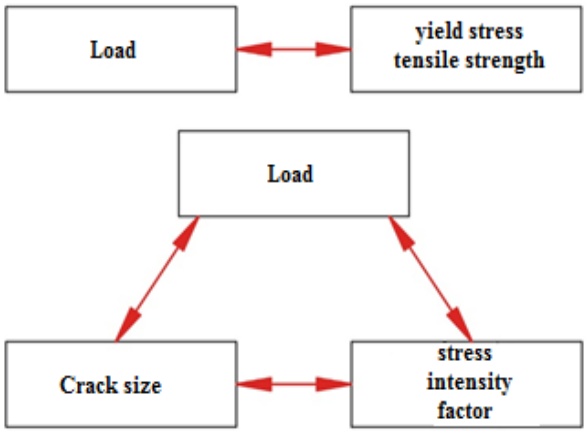

Figure 1. Design using: a) classic strength theory methods, b) fracture mechanics methods

In the case of design using classic strength theory, for given dimensions and loads, maximum stress is calculated and the material to be used is adopted in a way that ensures that it has a satisfying level of yield or tensile strength, or vice versa, maximum load is calculated for a given material. When applying fracture mechanics to design, there are three typical variables: structure load, damage magnitude (cracks) and stress intensity factor [1].

Shown in figure 2 is the classification of fracture mechanics depending on material behaviour. Linear elastic fracture mechanics assumes a linearly independent material behaviour under quasi-static load. For non-linear material behaviour and quasi-static loading, elastic-plastic fracture mechanics is applied. Dynamic, visco-elastic and visco-plastic fracture mechanics includes time as a variable, making material behaviour time-dependent [1].

As an example, let us analyse a membrane with a crack, loaded up to fracture, and let us give a schematic view of the relation between the load at fracture and the stress intensity factor.

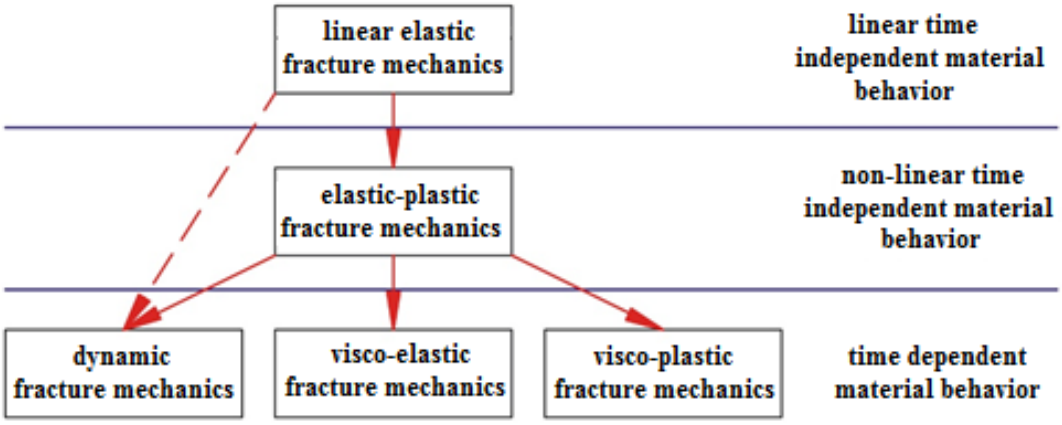

Figure 2. Fracture mechanics classification according to mechanical behaviour of the material

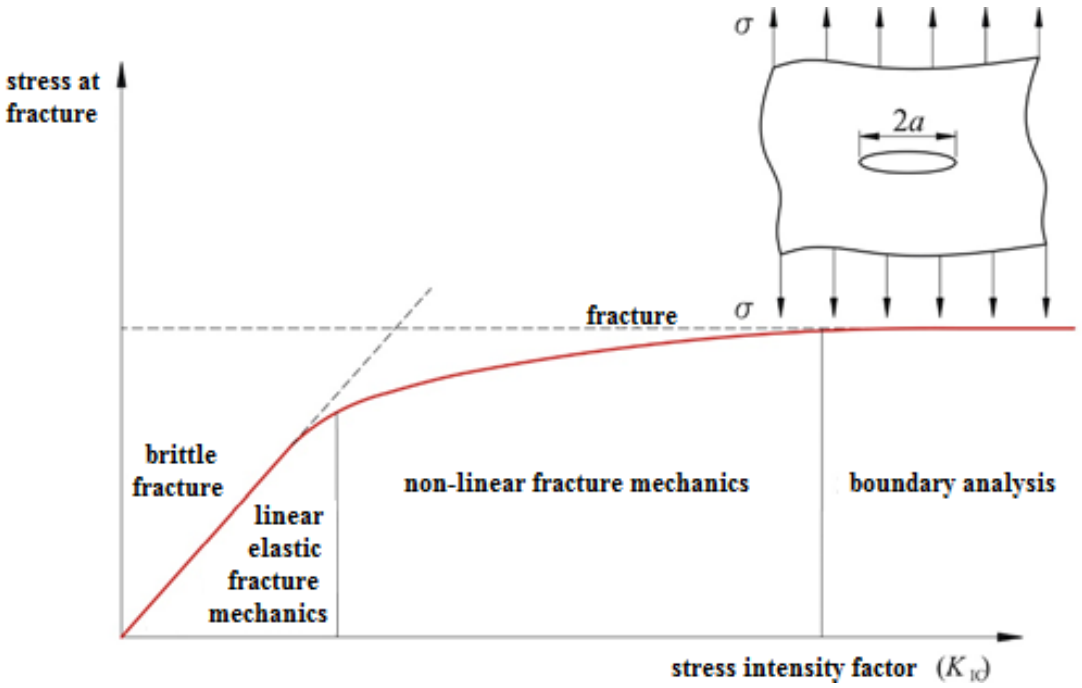

Figure 3. Influence of the stress intensity factor on structural failure mechanism

For materials with a low stress intensity factor, brittle fracture is the main fracture mode, and the critical load varies linearly with the stress intensity factor. For materials with a high stress intensity factor, linear fracture mechanics no longer apply and structural failure is typically related to the yield stress or tensile strength.

For materials with medium stress intensity factor values, there is a transition are between brittle and ductile fracture. Non-linear fracture mechanics related linear FM with plastic strain. From this, it can be concluded that linear elastic fracture mechanics is applied to problems which involve lower values of stress intensity factor. However, if the stress intensity factor is high, fracture mechanics is no longer relevant, since the load at fracture does not depend on toughness, and in these cases, boundary analysis is used [1].

- Derivation of expressions for determining of the stress intensity factor:

Based on the following expression (8): $K_I = \sigma \cdot \sqrt{\pi \cdot a}$, which defines the stress intensity factor for an infinite membrane subjected to tension, with a crack along its thickness (I crack opening mode), tensile stress σ is determined depending on the load to which a balance pipe of a turbine cover is subjected. Primary load acting on the analysed pipe is the internal pressure p. Let us observe figure 11.a)

and begin the analysis with basic Laplace equation for stresses that occur in cylindrical mantles or pipes:

$$\sigma_m/\rho_m + \sigma_t/\rho_t = p/s$$

$\rho_t = r$ - mantle or pipe radius

$\rho_m = \infty$

$\sigma_m = \frac{p \cdot r}{2 \cdot s}$ - stress along the generatrices

$\sigma_t = \frac{p \cdot r}{s}$ - stress in the circumferential direction

It was observed that the pipe was subjected to tensile stresses, thus the stress along the generatrix, σ_m was adopted as representative (figure 11.b)). Tensile stress was determined according to SRPS EN 13480-3 standard for pipeline calculation.

Stress intensity factor is increased by 12% since the edge crack opens more compared to a central crack, due to less geometric boundaries. In addition, it is also increased by the value of residual stress determined using a conservative procedure of reducing nominal analytical stress by 60%. All of these increases are on the safe side.

Expression for determining of stress intensity factor:

$$K_I \cong 1{,}12 \cdot (\sigma_m + 0{,}4 \cdot f) \cdot \sqrt{\pi \cdot a} \quad MPa\sqrt{mm}$$

2.1 Allowed stresses

Pipe material: STPG-38; Standard: JIS G 3454

Chemical composition in %:

Designation	C_{max}	Mn_{max}	Si_{max}	P_{max}	S_{max}
STPG-38	0,25	0,30 ÷ 0,90	0,35	0,04	0,04

Mechanical properties:

Designation	Yield stress MPa	Tensile strength MPa	Elongation % (min)
STPG-38	215	370	30

Allowed stress:

STANDARD	ALLOWED STRESS
EN 13480	$\min\left(\frac{R_m}{2,4}, \frac{R_{p0,2}}{1,5}\right)$

Element name	Material	p [bar]	Min σ [N/mm^2]	$\sigma_{allowed}$ [N/mm^2]
seamless pipe ϕ219,1 ×12.7mm	STPG-38 JIS G 3454	51,97	$R_m / 2,4$	154,16
			$R_{p0,2}/1,5$	143,33

2.2 Pipeline calculation according to SRPS EN 13480-3

$p = 51.97\ bar$ - Calculated pressure (bar)

$D_0 = 219.11\ mm$ - Outer pipe diameter (mm)

$e_n = 12.7\ mm$ - Nominal wall thickness (mm)

$R_m = 370\ MPa$ - Minimum tensile strength (MPa)

$R_{p0.2} = 215\ MPa$ - Yield stress for 0,2% (MPa)

$z = 1.0$ - Welded joint quality coefficient

$c_1 = 12.5\% \cdot e_n = 1.587\ mm$ - Negative tolerance value for nominal wall thickness (mm)

$c_2 = 1.0\ mm$ - Addition to corrosion and wear (mm)

$D_i = D_0 - 2 \cdot e_n = 193.7\ mm$ - Inner pipe diameter (mm)

$D_m = D - e_n = 206.4\ mm$ - Outer pipe diameter (mm)

Condition for application of the standard $D_0/D_i < 1.7$:

$$\frac{D_0}{D_i} = 1{,}13$$

Calculation of the nominal design stress f:

$$f = \left(\frac{R_m}{2,4}, \frac{R_{p0,2}}{1,5}\right) = 143{,}33 MPa$$

Minimum required pipe wall thickness without additions – for the inner pressure:

$$e = \frac{p \cdot D_i}{2 \cdot f \cdot z - p} = \frac{5,197MPa \cdot 193,7mm}{2 \cdot 143,33MPa \cdot 1,0 - 5,197MPa} = 3,58mm$$

Minimum adopted wall thickness without additions:

$$e_a = e_n - c_1 - c_2 = 10,11mm$$

Stress along the generatrix:

$$\sigma_m = \frac{p \cdot D_i + e \cdot p}{2 \cdot e_n \cdot z} =$$

$$= \frac{5,197MPa \cdot 193,7mm + 3,58mm \cdot 5,197MPa}{2 \cdot 10,11mm \cdot 1,0} =$$

$$= 40,36MPa$$

Stress along the generatrix increased by the value of residual stress:

$$\sigma_u = 1,12 \cdot (\sigma_m + 0,4 \cdot f) =$$

$$= 1,12(40,36 + 0,4 \cdot 143,33) = 109,42MPa$$

Stress intensity factor:

Defects	L (mm)	a(mm)
Incomplete penetration	200	2

$$K_I \cong 1,12(\sigma_m + 0,4 \cdot f) \cdot \sqrt{\pi a} \left[MPa\sqrt{mm} \right]$$

$$a = 2mm \rightarrow K_I = 274,27MPa\sqrt{mm}$$

Critical stress intensity factor value for material STPG-38:

$$K_{Ic} = 1580MPa\sqrt{mm}$$

Since $K_I = 274,27MPa\sqrt{mm}$, which represents 17% of the critical value $K_{Ic} = 1580MPa\sqrt{mm}$, structural integrity is not compromised.

In order to determine the final critical crack length a for which structural failure could occur, it is of great importance to predict its growth.

Based on the Irwin model for crack tip opening displacement, the correction factor r_y can be determined, and treated as the crack length increase factor ($a + r_y$). Correction factor r_y can be determined using the following expression:

$$r_y = \frac{\frac{1}{\pi} \cdot \left(\frac{K_I}{R_e} \right)^2}{2}$$ - for plane stress state

$$r_y = \frac{\frac{1}{\pi} \cdot \left(\frac{274,27}{215} \right)^2}{2} = 0,259mm \cong 0,3mm$$

Table T.1: Influence of crack length increase on the stress intensity factor

Crack length $a_n = 2 + n \cdot r_y$ [mm]		Stress intensity factor $K_{I(n)} \cong 1,12(\sigma_m + 0,4 \cdot f) \cdot \sqrt{\pi a_n}$ $\left[MPa\sqrt{mm} \right]$
n = (1,2,3, …,15)	a_n [mm]	
1	2,3	294,13
2	2,6	312,72
3	2,9	330,27
4	3,2	346,93
5	3,5	362,93
6	3,8	378,06
7	4,1	392,70
8	4,4	406,82
9	4,7	420,45
10	5,0	433,66
11	5,3	446,48
12	5,6	458,08
13	5,9	471,08

14	6,2	482,91
15	6,5	494,45
for a_n = 9 *mm*		581,83
for a_n = 12 *mm*		671,83
for $a_n = 2 \cdot e_n$ = 25.4 *mm*		977,44

2. RESULT ANALYSIS AND CONCLUSION

Crack length which is less than the double value of thickness will not cause catastrophic failure of the structure. Since $K_I = 977,44 MPa\sqrt{mm}$, which is 61.8% of the critical value $K_{Ic} = 1580 MPa\sqrt{mm}$, structural integrity is not compromised.

Conditions for prevention of structural failure are fulfilled in the case that the crack continues to grow.

3. ACKNOWLEDGEMENT

The authors of the paper would like to thank the Department of Science and Technological Development for their support of the TR 35040 project.

4. REFERENCES

[1] T.L. Anderson, Fracture Mechanics: Fundamentals and Applications, CRC Press, Boca Raton, 1995.

[2] E.E. Gdoutos, C. A. Rodopoulos, J. R. Yates, Problems of Fracture Mechanics and Fatigue: A Solution Guide, Kluwer Academic Publishers, Dordrecht, 2003.

[3] ABAQUS, Abaqus Documentation, Version 6.9, Dassault Systemes Simulia Corp., Providence, RI, USA, 2009.

[4] ABAQUS, Abaqus Software, Version 6.9, Dassault Systemes Simulia Corp., Providence, RI, USA, 2009.

[5] R.W.Hertzberg, Deformation and Fracture Mechanics of Engineering Materials, John Wiley & Sons, New York, 1996

[6] F.M.Burdekin, M.G.Dawes, Practical Use of Linear Elastic and Yielding Fracture Mechanics with Particular Reference in Pressure Vessels, Proc. of the Institute of Mechanical Engineering Conference, London, 1971, p. 28-37

Risk Based Management of Pressure Equipment Safety

Igor Martic[a], Aleksandar Sedmak[a], Snezana Kirin[b]

[a] Faculty of Mechanical Engineering, Kraljice Marije 16, 11120 Belgrade, Serbia, asedmak@mas.bg.ac.rs

[b] Innovation Centre of Faculty of Mechanical Engineering, Kraljice Marije 16, 11120 Belgrade, Serbia,

Abstract

Risk based management of pressure equipment safety has been presented as the combination of PED, API 581 and structural integrity assessment procedures. Pressure Equipment Directive (PED) 2014/68/EU and American Petroleum Institute (API) 581 procedures have been presented from the safety point in the case when defects in a pressure vessel are detected. These procedure are then analysed in combination of structural integrity assessment, based on fracture mechanics parameters evaluation. An example has been provided to illustrate this comprehensive approach, which is defined here as the risk based management.

Keywords: Risk management, pressure equipment, structural integrity, conformity

1. INTRODUCTION

Risk based management of pressure equipment safety as the represents multi complex approach and synergy combination of PED 2014/68/EU, API 581 and structural integrity assessment.

2. PRESSURE EQUIPMENT DIRECTIVE

The aim of the Directive are to remove barriers to trade of pressure equipment between European's countries. They apply to the design, manufacture and conformity assessment of pressure equipment and assemblies of pressure equipment with a maximum allowable pressure greater than 0.5 bar. These regulations identify under the Essential Safety Requirements that 'Pressure equipment must be designed and constructed so that all necessary examinations to ensure safety can be carried out' and that 'means of determining the internal condition of the equipment must be available where this is necessary to ensure the continued safety of the equipment [1].

Pressure Equipment Directive has been established the vary first time at 1997. as PED 97/23. The new PED was published in the EU Official Journal on 27th June 2014 and entered into force 20 days later. The transposition deadline is 1 June 2015 for fluid classification and 19 June 2016 for all PED.

Two biggest differences between PEDs are with modules and fluid classification.

2.1 Conformity assessment module changes [2]

The designation of some conformity assessment modules have changed as below table.

Table 1. Conformity assessment module changes [2]

97/23/EC	2014/68/EU
A1	A2
B1	B (design type)
B	B (production type)
C1	C2

Table 2 Category & Modul [2]

Category	Module
Category I	Module A
Category II	Modules A2, D1, E1
Category III	Modules B (design type) + D, B (design type) + F, B (production type) + E, B (production type) + C2, H
Category IV	Modules B (production type) + D, B (production type) + F, G, H1

2.2 Fluid classification change [2]

The reason for this change is that the Dangerous Substances directive – 67/548/EEC – that the PED currently uses to classify fluids as Group 1 or 2 is being replaced by the Classification, Labelling and Packaging (CLP) Regulation (EC 1272/2008).

An impact assessment by the European Commission showed that very few substances would actually change groups in the PED because of this change. Nevertheless manufacturers and notified bodies will have to familiarise themselves with the new requirements so as to be able to apply them to new equipment being placed on the market after 1st June 2015.

The regulations also states that 'Other means of ensuring the safe condition of the pressure equipment may be applied where it is too small for physical internal access, where opening the pressure equipment would adversely affect the inside or where the substance contained has been shown not to be harmful to the material from which the pressure equipment is made and no other internal degradation mechanisms are reasonably foreseeable'.

There is also a requirement for 'instructions for the user' to be supplied with the pressure equipment. These instructions should contain all the necessary safety information relating to putting the equipment into service, its continued safe use and maintenance. If appropriate, reference should be made to hazards arising from misuse.

The form that the conformity assessment takes is dependent on the classification of the pressure equipment. This classification is based on:

a) The type of equipment – vessel, piping or steam generator.

b) The state of the fluid contents – gas or liquid.

c) The fluid group of the contents – Group 1 (dangerous) or Group 2 (all others including steam).

d) The maximum allowable pressure.

e) The volume in litres or the nominal size as appropriate.

3. API 581 – RISK BASED INSPECTION

This is an industry specific document [3] designed to be applied to the petroleum and chemical process areas. It follows the same overall approach as the ASME document and recognizes that a RBI aims to [4]:

1) Define and measure the level of risk associated with an item.

2) Evaluate safety, environmental and business interruption risks.

3) Reduce risk of failure by the effective use of inspection resources.

The level of risk is assessed by following the same procedure as described in the ASME document i.e. a quantitative analysis is generally applied after an initial qualitative analysis has established those plant items for further analysis.

The qualitative approach assesses each plant item with a position in a 5 x 5 risk matrix. The likelihood of failure is determined from the sum of six weighted factors:

b) Damage mechanism.

c) Usefulness of inspection.

d) Current equipment condition.

e) Nature of process.

f) Safety design and mechanisms.

The consequence of failure is divided into only two factors:

a) Fire/Explosion.

b) Toxicity.

The general approach of the quantitative analysis is to first establish details on the process, the equipment and other pertinent information. Risk is then calculated as the product of each consequence and likelihood for each damage scenario, the total risk for an item being the sum of all the scenario risks:

risks = CS x FS

where:

S = Scenario

CS = Consequence of scenario

FS = Failure frequency of scenario

The inspection programme is then developed to reduce that risk. To do that one needs to establish:

1) What type of damage to look for.

2) Where to look for damage.

3) How to look for damage.

4) When to look for damage.

What and Where is established from reviewing the design data, process data and the equipment history, How to look for the damage is decided by reviewing the damage density and variability, inspection sample validity, sample size, detection capability of method and validity of future prediction based on past observations. When to look for damage is related to the estimated remaining life of the component. This document prescribes actual methods to use, with specific values that can be applied to given situations and conditions. There are also worked examples to obtain an idea of how to assess a system, what constitutes a failure and how to assess the resulting consequences. There are also several workbooks which can be utilised to assess a plant in terms of both qualitative and quantitative risk analysis. There are references made to known reliability data plus some details of specific reliability data available within the document itself.

4. RISK RANKING AND CATEGORISATION

Risk matrices are a useful means of graphically presenting the results from risk analyses of many items of equipment. Risk matrices should, however, not be taken too literally since the scale of the axes is only indicative. The simple matrix below is based on a linear scale of probability and consequence ranging from 1 to 5. The numbers in the cells are the product of the probability and consequence values as shown at Table 2. [4]

Table 3 Example of risk ranking and categorisation [4]

5	5	10	15	20	25
4	4	8	12	16	20
3	3	6	9	12	15
2	2	4	6	8	10
1	1	2	3	4	5
Probability/ Consequence	1	2	3	4	5

This matrix draws attention to risks where the probability and consequence are balanced and to risks where either the probability or the consequence is high. Often matrices will be sectored into regions covering different ranges of risk. As this example shows, the boundaries between regions depend on how the ranges are defined: changing the range of the red region from 21 to 25 to 20 to 25 could have a significant effect. For quantitative analyses risk may be presented as a point a probability/consequence plot. When the plot has logarithmic axes, straight lines represent lines of constant risk. If risk is evaluated numerically, then equipment may be ranked in order of risk.

From these processes of ranking, Duty Holders should be able to identify the items of equipment presenting the greatest risks of failure. For the purposes of inspection planning, equipment may be categorised according to the type of risk.

For example:

a) Equipment where there is a known active deterioration mechanism,

b) Equipment where there is a high frequency of failure but consequences are low, but the frequency of failure is low

c) Equipment where the consequences of failure are high

5. STRUCTURAL INTEGRITY ASSESSMENT

The Competent Person carrying out the examination of a system will evaluate the examination results and the condition of the equipment. Any changes in the condition from the design, since entry to service, and since the last inspection will be identified. From this and other information about the rate of deterioration, the Competent Person will assess whether the system is currently 'fit-for-service' and likely to remain so during the proposed interval to the next inspection. [4]

When faced with evidence of deterioration, the Duty Holder and Competent Person will need to assess the implications of the deterioration in more detail and decide what action should be taken. In making these assessments, risk based principles should apply. Initial considerations towards a decision to accept or reject the deterioration (i.e. corrosion, erosion or crack like defects etc) within the equipment will need to take into account the following:

- The type and magnitude of the deterioration, its cause and mechanism, and the accuracy of the NDT information available.

- The stress at the location which is affected, i.e. high stressed by areas are unlikely to tolerate the same degree of deterioration as other areas operating at lower levels of stress.

- The type of material, its strength and fracture properties over the range of operating temperature.

- The safe operating limits associated with each operating condition. These must be considered separately, e.g. a certain corrosion type defect may be acceptable under an operating condition where only pressure is considered. However, should a cyclic operating condition apply then the defect may not be acceptable. Care must be exercised when there are different operating conditions.

- Whether the deterioration has been present since entry to service, or has initiated during service (due to the contents, environment or operating conditions), and the rate at which it is proceeding.

- Whether the deterioration is within design allowances (e.g. for corrosion) or fabrication quality control levels (e.g. for defects).

Even if defects more severe than fabrication 'quality control levels' are revealed by an examination, rejection or repair of the equipment may not always be necessary. Quality control levels are, of necessity, both general and usually very conservative. A decision on whether to reject or accept equipment with defects may be made on the basis of an 'engineering critical assessment (ECA)' using fracture mechanics to assess the criticality of the defects. This may be carried out using before or after the examination. Many standards and recommended practice provides a 'Guide on methods for assessing the acceptability of flaws in metallic structures'. It is based on the concept of fitness-for-service and utilises a failure assessment diagram (FAD) derived from fracture mechanics. The assessment process positions the flaw within acceptable or unacceptable regions of the FAD.

The flaw lying within the acceptable region of the FAD does not by itself infer an easily quantifiable margin of safety or probability of failure. Conservative input data to the fracture mechanics calculations are necessary to place reliance on the result. If key data are unavailable, (e.g. fracture toughness properties of the weld and parent material), then conservative assumptions should be made. Sensitivity studies are recommended so that the effect of each assumption can be tested. Flaw assessment is a process to which risk based principles may apply. Degrees of uncertainty in the input data (e.g. flaw dimensions, stress, fracture toughness) may be handled in a lower bound deterministic calculation or by

probabilistic fracture mechanics if statistical distributions can be determined. The application of partial safety factors is an alternative approach to manage the variability in the input data without being overly conservative. The consequences of flaw growth and the possibility of leakage or catastrophic failure may also be factors to consider.

For refinery equipment designed to ASME codes, the American Petroleum Institute has published a recommended practice on fitness for service assessment, API 579 [5], which provided guidance on methods for assessing the acceptability of flaws in fusion welded structures. API 579 is in accordance to API 581 [3].

At the other side, PED regulations in Europe gives instruction in accordance to standard ISO 31000 [6]. This International Standard provides principles and generic guidelines on risk management.

For other industries like nuclear, ASME XI [7] should be fallowed for the assessment of results from in-service inspection of nuclear plant designed to ASME codes.

If deterioration is found in equipment, the best course of action for the Duty Holder will depend on the circumstances. Equipment that has deteriorated to a condition assessed to be unacceptable requires immediate action before it can re-enter service. Where equipment has deteriorated but has not reached unacceptable limits, monitoring or shorter inspection intervals or other action may be required depending on the rate at which the deterioration is proceeding, and the confidence with which this rate is known. Detail inspection's procedures are given at API 510 [8] for pressure vessels and API 570 [9] for piping.

Whilst there are many mechanisms of deterioration and modes of failure associated with pressure systems and other containment structures, they can be roughly broken down into the following classes in accordance to API 579 [10]:

- Corrosion/erosion (general, local, pitting),
- Creep and high temperature damage,
- Fatigue cracking,
- Stress corrosion cracking,
- Embrittlement,
- Hydrogen blistering/stepwise cracking,
- Brittle fracture,
- Buckling.

In practice, the Duty Holder will normally choose the most economical course of action, whilst maintaining the integrity and safety of the equipment. Duty Holders often prefer to return equipment to service and plan repairs or replacements for scheduled outages. Various alternatives can be considered:

- Changes to the operating conditions that reduce the rate of deterioration and increase margins of safety, e.g. lower pressures, temperatures.
- On-line monitoring of deterioration.
- Shortening the interval between subsequent inspections.
- Removal of defects or damage only (e.g. grinding).
- Removal of defects or damage and making a repair (e.g. over-welding).

6. CONCLUSION

RBI is a systematic analysis method for planning inspection intervals of static mechanical equipment used in the process industries. Risk of failures of the relevant system items is assessed in order to identify and determine suitable intervals. Over the years, RBI has gained reputation for being a successful method, but also for having some shortcomings. One of these is traced to the limited assessment of uncertainties.

Risk based management of pressure equipment safety is combination of PED, API 581 and structural integrity assessment. This is

the main reason why a team rather than one person should perform RBI.

Many plant in the World have been establishing RBI last decade, yet many more are in the progress of establishing. RBI is a continuous process like quality management system ISO 9001 [11], which means maintenance and upgrade after establishment.

7. ACKNOWLEDGEMENT

The authors of the paper would like to thank the Department of Science and Technological Development for their support of the TR 35040 project.

8. REFERENCES

[1] Cowan A., Picker C., Some considerations of overpressure test/limiting defect size arguments for ferritic pressure vessels, Int. J. Pressure Vessels and Piping, 15, 105-123, 1984.,

[2] http://www.lr.org/en/news-and-insight/articles/revising-the-pressure-equipment-directive.aspx,

[3] API 581,

[4] Wintle J.B., Kenzie B.W., Amphlett G.J., S Smalley S., Best practice for risk based inspection as a part of plant integrity management,

[5] API 579,

[6] ISO 31000,

[7] ASME XI,

[8] API 510,

[9] API 570,

[10] API 579,

[11] ISO 9001.

Procedures and evaluation of the stress strain fields on the Locking Compression Plates

Uros Tatic[a], Katarina Colic[a], Aleksandar Sedmak[b], Zarko Miskovic[b], Ana Petrovic[b]

a Innovation center of Faculty of Mechanical Engineering, Belgrade, Serbia

b Faculty of Mechanical Engineering, University of Belgrade, Serbia

Abstract

Locking Compression Plates (LCP) have found great application in the orthopedic healing process in the modern medicine nowadays. Their design is specifically modified depending on the bone and the loading a specific bone is subjected to. Dimensions of LCP as well as mechanical characteristics provide greater structural resistance than the bone itself, but as a consequence of continues application as well as cyclic loading, practice has shown that fails and breaks accrue. Defining of the testing approaches and procedures used for the evaluation of the stress and location of the potentially risk geometrical areas represent the aim of this paper. Results obtained in this paper apply modern experimental as well as numerical simulations on the modified and simplified LCP geometry with an aim to locate stress and strain fields, as well as areas with a stress concentration that can result in the appearance of the cracks during the cyclic loading.

Keywords: Locking-Compression-Plates, FEM fracture mechanics, testing methods, stress strain evaluation.

1.INTRODUCTION

Bone fractures (lat. Fracture) are mechanical injury, which consists of fractures of bone as well as soft tissue damage, which surround it. These injuries occur due to external forces and load whose intensities exceed the level of elasticity of the bone itself, thus, causing its damage. Depending on age, and global physical condition of the persons, breaks can globally be divided into:

- fractures occurred as a result of injury (excessive load)
- fractures caused by diseases (changes in the structure of the bone tissue).

The metal alloys a have found wide application in medicine in terms of stabilizing the injury outwards orthopedics duo to their mechanical properties. In today's medicine, biomedical implants and orthopedic elements found use in injuries and broken bones, joints, spine, etc. as a substitute for bones. Depending on the purpose metal implants can be divided into:

- Fixation implants for the reconstructive orthopedics bone processes (plates, intramedullary nail, screws, external fracture fixation ...)
- Prostheses for joint replacement (partial and total hip, knee and elbow ...)
- Spinal fixation implants.

2.BIOMATERIALS

Biomaterials are used in medical equipment that are implanted into the human body, due to the replacement of damaged or diseased body parts.

Biomaterials must be non-toxic, must not corrode, or in any other way react in contact with surrounding tissue, due to the fact that they are introduced in to organic environment. Any material that is exposed to interaction with living biological systems in their work environment can be considered biomaterials. Basically, every biomaterial must be negative for carcinogenicity tests, cytotoxicity, must possess good chemical stability, ie. corrosion resistance, and adequate mechanical properties, primarily dynamic strength. Orthopedic biomaterials are above all limited to those materials that are used to produce parts with cyclic loading. Ideal metallic biomaterials should possess:

- Resistance to fatigue,
- High levels of yield strength
- High levels of tensile strength
- Corrosion resistance

Over the years metal biomaterials have shown adequate and required properties for use in orthopedics in terms of, high strength, toughness, fracture resistance, hardness, corrosion resistance, biocompatibility and above all the ability to be easily processed, designed and developed. These characteristics are of great importance in the development of fixating implants which are most often subjected to cyclic loading [1-4] .

As the main function of bones in extremities is to carry the load, wherein the task of orthopaedic plates is to provide support to bones with reduced integrity, the choice for initial material for development of plates were metals. Biomaterial strength and stiffness significantly exceed those of the bone to which they are connected, and to which it provides additional support. Three biometal alloys [5-9] most commonly used for implants include:

- stainless steels
- Co-Cr alloys
- titanium alloys

During the 1950s, 316L steel [10] was developed, wherein the carbon percentage was reduced from 0.08% (in the case of previously used 316 steel [11]) to 0.03%. Reduction of carbon percentage significantly improved corrosion resistance. In addition to carbon, steels 316 and 316L were made with 18% chrome and 8% nickel.

Advantages of stainless steels are primarily reflected in low percentage of impurities, which makes them ideal for use in vivo conditions. Their significant disadvantage compared to other superalloys is reflected in lower dynamic strength and vulnerability to erosion of the material itself, which, in case of developing of orthopaedic plates may have significant influence to their integrity and life. Cobalt based alloys are characterized by increased resistance to corrosion, fatigue, wear and fracture, compared to iron alloys, however their major flaw is the elasticity modulus.

Stainless steel alloys have been improved and nowadays, orthopaedic plates made of stainless steels with enhanced mechanical properties can be seen in practical application. Such plates are most typically applied in the case of older patients, due to their lower expected physical activity and life.

In addition to alloys the aforementioned 316L and Co-Cr alloys, titanium and its alloy, Ti-6Al-4V (so-called aviation alloy) are also widely applied in orthopaedic plate manufacturing.

Titanium alloys, Ti-6Al-4V and Ti-6Al-7Nb in particular, represent materials with currently most suitable mechanical properties, and are registered in ASTM standard as biomaterials [5,

12-13]. Ti-6Al-4V alloy is made of 90% titanium, 6% aluminium and 4% vanadium. Such chemical composition is characterized by an extremely high corrosion resistance, high durability, favourable ratio between strength and weight (4.43g/cm^3[1]). Titanium is very resistant to corrosion due to a solid oxide layer (the only stable product of the reaction) which is formed in vivo conditions.

The main disadvantage of titanium alloys as biomaterials is the fact that it has a very high friction coefficient, which can lead to particle separation due to wear in the case of developing orthopaedic components meant for direct contact.

Depending on the chemical composition, nowadays numerous different titanium alloys are available, and each of them is characterized by individual properties that make it suitable for specific work conditions and modes. However, one should always take into account that improving one property could lead to degradation of others. One of the mentioned titanium alloys with a changed chemical composition which had found application in biomedicine is the Ti-6Al-7Nb, containing 7% niobium instead of vanadium. Due to the presence of niobium instead of vanadium, this alloy has increased corrosion resistance in comparison to Ti-6Al-4V.

Table 1. Mechanical parameters of biomaterials and bones

Material	Elasticity modulus [GPa]	Tensile strength [GPa]	Compressive strength [GPa]
Bone			
(humid at lower load)	15.2	0.090	0.15
(humid at higher load)	40.7	-	0.27-0.40
316 L	193	0.54	
Ti			
0% porosity	110	0.40	
40% porosity	24*	0.076	
Ti-6Al-4V			
0% porosity	124	0.94	
40% porosity	27*	0.14	

* Calculated with respect to $E^* = E(1-\nu)^3$

3.IN VIVO EXPERIENCE

Experience from modern medical practice has shown that LCP can be used with high reliability and success rate. However, in certain cases, failure occurs in form of plate fracture, or loosening of screws and breaking of the rigid contact between plate and bone. This case of plate failure during exploitation was observed in cooperation with doctors from AMA clinic in Belgrade. The case involved failure of LCP Metaphyseal Plate for distal medial tibia, manufactured by DePuy Synthes Company of Johnson and Johnson.

This plate was meant to fix the tibia during the bone healing period, and as such was subjected to cyclic load in normal exploitation, during the patient's walking period. This load resulted in the occurrence of an initial crack at the location of contact between the plate and screw, which has, during later stages of recovery lead to plate fracture. Examples of plate positioning provided by the manufacturer [14] as well as the view of a broken plate extracted from the patient are shown in figure 1.

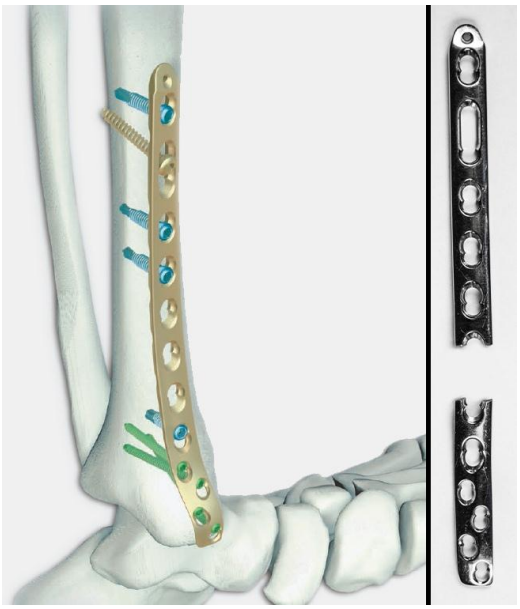

Fig. 1. Schematic example of LCP plate placed on the bone (left) broken extracted LCP plate (right)

4.TESTING METHOD

For the purpose of determining displacement and strain fields, GOM equipment was used (GOM, Braunschweig, Germany) for three-dimensional strain measuring, along with the ARAMIS system. A 3D non-contact optical system for calculation and analysis of displacement and strain does not depend on the type of the material and load, but is based on digital image correlation (DIC). Experimentally obtained data for each of the examined surface specimens were approximated by analytical expressions of satisfying accuracy. This system is based on two independent cameras, calibrated to record an identical surface, whose strain and displacement are observed, under different angles. In this way, it is possible to achieve special 3d measuring (whereas use of only one camera provides measure within plane). Strain field is determined based on the change in mutual distance between predefined pixels on the measured specimen's surface. By applying spatial digital image correlation, non-contact measuring is achieved, which provides reliability and repeatability of the experiment, reduces the risk of the effects of measuring equipment on the results and increases the number of measured parameters per test to spatial strain while using a single piece of equipment.

One of the main factors in the factors related to the surface area being measured is preparation of the surface. In order to achieve best definition of the separate pixels while recording measuring surface should be prepared with some high contrast. In order to achieve this surface is painted in a bright white colour with a black dots spreading pattern over it (*fig 3. bottom*). Depending on the size and density of the black pattern different volumes can be measured with a use of GOM system. In order to obtain a most of the deformation possible, since it is expected that during the experimental loading no significant deformation will be present, a measuring volume of 20mm x 20mm x 10mm was chosen. This volume allows a measuring volume of an area between only two adjacent bolts.

4.1. Numerical simulation

Finite element method (FEM) represents a numerical technique for determining of an approximate value of a problem solution by using a system of partial differential equations [15,16]. Numerical simulation was performed using finite element method (FEM). FEM represents the discretization of a physical model, i.e. its division into a finite number of smaller elements with their own initial volume, boundary conditions defined as displacements and/or loads, with simpler geometry. Displacements in nodes, i.e. points in which elements are connected, are calculated for each element individually. Based on these displacements, and by applying the parameters for the numerically simulated material, strain and stress fields are determined. Application of FEM typically involves the introduction of certain approximations in form of geometrical reductions in zones subjected to lower levels of stress and strain, which do not have significant effect on the global stress and strain field.

4.1. Fracture mechanics history

The presence of cracks in mechanical structures or its individual parts or elements can

significantly affect its behaviour during exploitation, especially in terms of durability and life.

During crack propagation, it is possible to distinguish two basic forms of fracture:

Plane fracture - fracture along a planar surface.

Slanted fracture - fracture along a surface under an angle.

Crack growth along a flat surface corresponds to the case where the crack surface is mostly perpendicular to the load direction, whereas in case of crack growth along a slanted surface, the angle occurs in the plane perpendicular to the crack propagation plane, and these cases are typically characterized by larger strain [17].

By examining the crack surface, smooth areas of this surface corresponding to fatigue fracture and crack growth can be observed, along with grainy areas which correspond to sudden brittle fracture.

In addition to crack growth surface and shape, three basic types of crack opening are distinguished (*fig 2*):

Cleaving - symmetrical crack surface opening, due to tensile stress σ.

Sliding - crack surfaces lie in the same plane, due to shear stress τ.

Shear - crack surface lie in different planes, due to shear stress τ.

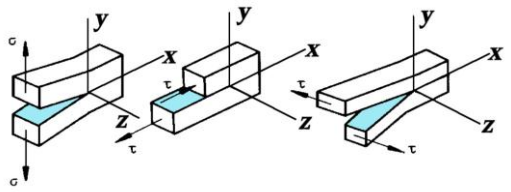

Fig. 2. Types of crack opening (right) [18]

In the case of cleaving, i.e. first crack opening mode, the force (σ) acts perpendicularly to the crack plane and separates its surfaces. In the case of shear and sliding crack opening mode, the surface slide along each other, whereas the force acts in form of shear on the crack plane (τ). Fractures caused by cleaving (force acting perpendicularly to the crack growth plane under the effect of tensile stress represent the most dangerous case of crack growth in fracture mechanics.

Procedures and evaluation of the stress strain fields on the Locking Compression Plates is based on the case of tensile load that can be present in cases of arm fracture in general, as well as in some special cases of loading of other bones. During the exploitation period of the LCP plates initial cracks are expected to form in the contact area of the screw and LCP. Cracks that are formed this way will be positioned normally to the longitude direction of the plate, and thereby they can be observed as cleaving in a case of a tensile loading.

5.EXPERIMENTAL SETUP

Evaluation process was based in two main stages. Frist stage was designed just to test the stress strain distribution throughout the model In case of tensile loading, while in the second phase a crack was to be added in the area of the biggest stress concentration in order to form a worst case scenario.

In order to eliminate any influence of the small geometrical modifications in the design of the plate it was determine to create a new plate made out of a Ti-6Al-4V with a geometry seen on the figure 3. The plate was cut using the water jet technique to prevent development of potential cracks caused by the machining.

Testing is planned to be performed on the pig bones, but do to the fact that they need special storing conditions as well as preservation and preparation, the tests were first performed on the wood specimens in order to adjust equipment and to define measuring parameters.

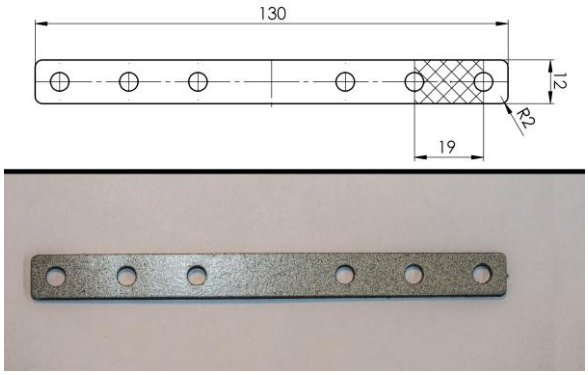

Fig. 3. Blueprint of the test plate with emphasized measuring area (up) test plate prepared for measuring (bottom)

Experimental setup can be seen on the figure 4. Plate was positioned on two separate wood pipes. Each pipe was connected via tree bolts to a LCP plate. Using this configuration, bone breakage was simulated in the middle of the LCP. This setup was chosen to provide adequate and equal stress strain field on the both sides of the LCP.

Fig. 4. Enlarged experimental setup with only specimen (left) whole experimental setup with lightning, tensile testing machine and cameras (right).

Load from the wood pipes was translated to the tensile machine via the metal plates positioned on the end of the pipes. During the initial testing phase it was determine that these plates should be positioned in the same plane as the LCP instead of the middle plane of the pipes in order to prevent bending in the middle of the LCP (directly above the simulated brakeage).

5.1. Loading

Although the pipes were connected with edge plate used for translating load via only one bolt, and with the plates with a tree separate bolts, this had a local character which was not of great importance for the experimental results. Results of a this setup would have a larger stress concentration on the outer edge of the pipe, but it would not have any influence on the mutual stress strain influence of the LCP and a pipe due to a fact that a equal loading would be transmitted to a tree bolts as a loading on the one top bolt. Load was gradually increased to a maximum value of 1500 N. Values of the stress and displacement on the tensile testing machine (edges to edge, including the deformation of the pipes, LCP and edge plates) can be seen on the figure 5.

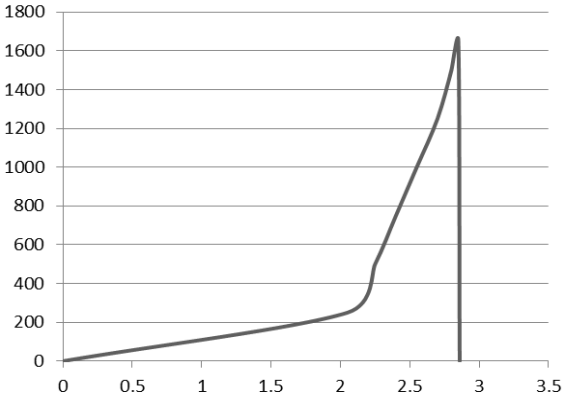

Fig. 5. Stress strain diagram for a tensile testing machine (whole specimen, LCP pipes and edge plates)

Maximal loading was measured at 1621.833N while the speed of deformation was defined as a 2 mm/min. Non linearity at the beginning of the diagram is caused by positioning of the bolts and plates in a same plane, wedging of the edge plates and tensile testing machine… and in general could be neglected. Loading for this experiment was stop before the breakage of the pipes appeared.

5.2. Digital image correlation DIC

Stress strain filed on the surface of the model was measured using digital image correlation based GOM measuring system [19-22].

In order to increase a measuring field, reduce light reflections and to provide more uniform light distribution throughout measured are two separate light sources positioned on each side of the measured specimen, at the same height as a cameras were used (figure 4 right). Furthermore size of the bolts head was made with reduced thickness mostly to reduce presence of the shadows (figure 4 left).

Measuring of the stress strain field was separately performed in the areas between the bolts one and two as well as bolts two and tree. Size of the measuring area between bolts 2 and 3 can be observed as hatched area at the figure 3.

Obtained results with DIC technology parallel to numerical models can be seen on the figure 5.

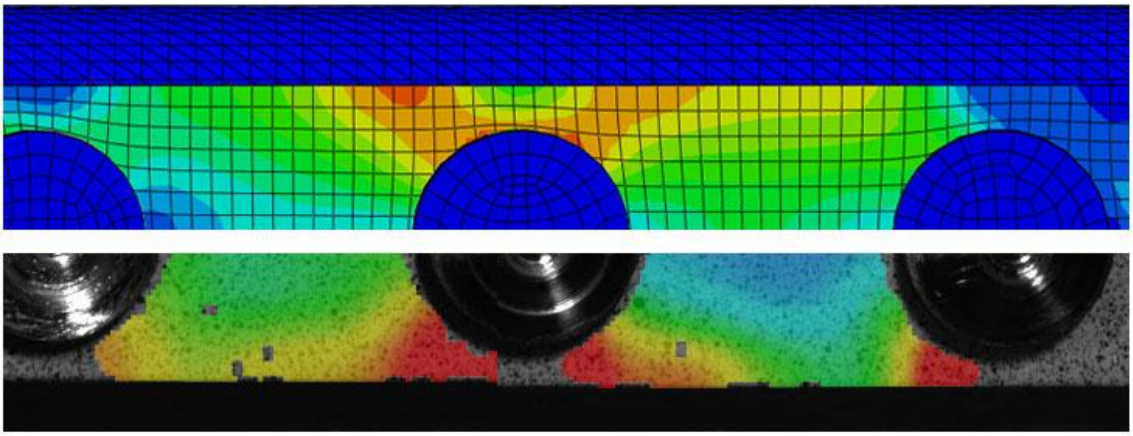

Fig. 5. Deformation field obtained in numerical model (up) parallel to the results obtained with DIC (bottom).

It can be seen that a deformation filed for real experiment as well as the numerical simulation has a similar distribution. Maximal deformation values are located around the bolts.

6.DISCUSION

Procedure for the evaluation of the stress strain field shown in this paper represents collaboration of different engineering tolls and techniques used to provide insight in the behaviour of the medical equipment during different stages of the loading. Loading conditions used represent the worst case scenario to which one LCP plate can be subjected.

Experimental setup is designed with focus on the mutual influence of the bone and LCP, stress transfer between them and measuring of the differences between separate areas of the LCP as well as the bolts. Preparation of the LCP specimen is made with aim to reduce any additional influence of the geometry that can be present on the real life LCP. Preparation of the experiment can be performed with ease in cases of artificial bone replacement materials that can be used, while the measurements on the real bones can be performed afterwards.

Replacement of the bone with an artificial material as it was a case of wood can provide basic insight in the stress strain behaviour and concentrations. Module of elasticity for the oak wood used throughout testing phase was around 11.000 MPa. It must be noted that testing with any organic material requires additional testing and evaluation of a material duo to the non-homogeneity of the materials used.

During the testing phase it was noticed that do to the relatively small area of the LCP observed in comparison to a whole specimen (LCP, simulated bones, end plates) local displacement would be much higher at area of the a plate connected to the moving jaws of the tensile machine. All specimens should be positioned in the way that measured areas are as close as possible to the stationary jaws, due to a fact that further you go away from a fix end global displacement of whole model becomes greater compared to a local displacement of the LCP since the high difference in the modulus of elasticity between different materials used.

Different models of test specimens should be made in order to define influence of geometrical changes present in the models. Geometry of the holes as well as outer geometry can have a major role on stress concentration that can lead to a appearance of a fatigue cracks during the cyclic loading present in the healing process.

7.CONCLUSION

With a use of the shown evaluation principle and methodology a stress strain filed for a local area of LCP can be obtained. Adequate preparation of the specimen has a major role in later experiment. Observed areas can be prepared with ether smaller spread patent used for a larger DIC area measurements, or with a smaller in order to insure more precise local values. Main disadvantage of the use of DIC method is that all data is gathered only at the surface of the specimen, which represents a reason for a further use of the numerally verified and comparable models with experimental results in order to gain insight in a complete behaviour of the model. Experimental setup can be used to replicate different geometries of the LCP as well as different bone material. This can have a major advantage in the further experimental process with real bones do to a fact that a specimen as well as the experimental setup can be prepared before the experiment, which allows for a fast performing of the experiment.

Further experiments with the same setup should be performed on ether human or the pig bones in order to simulate better load translation from a bone to a plate.

Numerical simulation and obtained experimental DIC values have shown similar results in an area of the deformation filed. Maximal values are located around the bolts, with a present difference between separate bolts. Obtained results have shown that procedures and evaluation techniques for the stress strain fields on the Locking Compression Plates shown in this paper can be used to provide insight in its behaviour. In order to obtain adequate results for the real behaviour of LCP experiments should be performed with different LCP geometries as well as with a real bone in order to have a better insight in to load distribution between bone and a plate.

8.ACKNOWLEDGEMENTS

The study was carried out within Project TR – 35040, financed by the Ministry of Education, Science and Technological Development, Republic of Serbia.

9.REFERENCES

[1] B.D.Ratner, A.S.Hoffman, F.J.Schoen et al., Biomaterials Science An Introduction to Materials in Medicine, San Diego: Academic Press, 1996.

[2] D. Raković, D. Uskoković, I. Balać et al., “Biomaterijali,” Društvo za istraživanje materijala, 2010.

[3] I. Milne, R. O. Ritchie, and B. Karihaloo, Comprehensive Structural Integrity, Oxford: Elsevier Ltd, 2003.

[4] J. B. Park, and R. S. Lakes, Biomaterials An Introduction, New York: Plenum Press, 1992.

[5] "ASTM F136-11 Standard Specification for Wrought Titanium 6Aluminum 4Vanadium

ELI (Extra Low Interstitial) Alloy for Surgical Implant Applications " (UNS R56401).

[6] "ASTM F139-08 Standard Specification for Wrought 18Chromium 14Nickel 2.5Molybdenum Stainless Steel Sheet and Strip for Surgical Implants," (UNS S31673).

[7] "ASTM F75-12 Standard Specification for Cobalt 28 Chromium 6 Molybdenum Alloy Castings and Casting Alloy for Surgical Implants " (UNS R30075).

[8] "ASTM F90- 09 Standard Specification for Wrought Cobalt 20Chromium 15 Tungsten 10 Nickel Alloy for Surgical Implant Applications," (UNS R30605).

[9] "ASTM F562-07 Standard Specification for Wrought 35Cobalt 35Nickel 20Chromium 10Molybdenum Alloy for Surgical Implant Applications " (UNS R30035).

[10] M. F. Montemor, M. G. S. Ferreira, N. E. Hakiki et al., "Chemical composition and electronic structure of the oxide flms formed on 316L stainless steel and nickel based alloys in high temperature aqueous environments," Corrosion Science, vol. 42, pp. 1635-1650, 2000.

[11] A. Y. El-Etre, "Khillah extract as inhibitor for acid corrosion of SX 316 steel," Applied Surface Science, vol. 252, no. 24, pp. 8521–8525, 2006.

[12] "ASTM F1108-04(2009) Standard Specification for Titanium 6Aluminum 4Vanadium Alloy Castings for Surgical Implants (UNSR56406)."

[13] ASTM F1295-11 Standard Specification for Wrought Titanium 6 Aluminum 7 Niobium Alloy for Surgical Implant Applications (UNSR56700).

[14] www.depuysynthes.com, Synthes GmbH Eimattstrasse 3 4436 Oberdorf, Switzerland

[15] R. W. Clough, "The Finite Element Method in Plane Stress Analysis."

[16] O. C. Zienkiewicz, Y. K. Cheung, The Finite Element Method in Continuum and Structural Mechanics: McGraw Hill, 1967.

[17] S. Kršćanski, ANALIZA UVJETA NASTANKA PUKOTINA I MODEL PROCJENE VIJEKA TRAJANJA KONSTRUKCIJA, Rijeka, 2013.

[18] A. Sedmak, Primena mehanike loma na integritet konstrukcija (monografija), Belgrade: Mašinski fakultet, 2003.

[19] WH Peters, WF Ranson, "Digital imaging techniques in experimental stress analysis". ," Optical Engineering, 1982;21:427-31.

[20] MY Fard, Y Liu, A Chattopadhyay, "Characterization of Epoxy Resin Including Strain Rate Effects Using Digital Image Correlation System.," J Aerospace Eng., vol. 2, pp. 308-319, 2012.

[21] S Hertelé, W De Waele, R Denys, " Investigation of strain measurements in (curved) wide plate specimens using digital image correlation and finite element analysis," J Strain Anal Eng. , pp. 276-288., 2012.

[22] N. Mitrovic. A. Sedmak M.Milosevic, A. Petrovic, T. Manevski., " Digital image correlation in experimental mechanical analysis," Structural Integrity and Life, vol. 1, pp. 39–42, 2012.

HARDNESS AND METALLOGRAPHIC TESTS OF REPAIRED VESSEL IN THERMAL POWER PLANT

L. Jeremić [a*], U. Tatić [b], A. Sedmak [a], B. Djordjevic [b], M. Aranđelović [b]

[a] Faculty of Mechanical Engineering, Kraljice Marije 16, 11120 Belgrade, Serbia,
[*]laki991@hotmail.com

[b] Innovation center of Faculty of Mechanical Engineering, Kraljice Marije 16, 11120 Belgrade, Serbia

Abstract

Shown in this paper are general characteristics of high-strength low-alloyed steel 15 NiCuMoNb5 (WB 36) including its chemical composition, usage in the pressure vessel facilities, as well as repairing technology with results of hardness measuring and microstructure analysis. Repair welding procedure is performed on starting vessels made of above mentioned steel used in thermal power plant TENT B (Serbia). Results of metallographic and hardness tests provide the information about welded joint characteristics. Analysis of performed welding repair procedure along with influences caused by welding procedure and influences that can lead to the cracks occurrence are presented and discussed.

Keywords: welded joint, high strength steel, hardness, metallography and starting vessels.

1. INTRODUCTION

Pressure vessels are most usually of circular-cylindrical shape, with a ring shaped cross-section, and have the following applications:

- for transport of gases, liquids and loose or grainy material
- in tanks (gas, liquid)
- in boilers
- in vessels used in processing industry
- as cylinders in pistons.

Pressure vessels can be subjected to inner and external pressure. They are also widely applied in thermal power plants. Basic elements of a boiler include parts in which processes related to transformation and transfer of heat from transmitter to the receiver take place: furnace, water heaters, evaporators, vapor overheaters and air heaters. In addition to these elements, auxiliary equipment can also be considered under the category of pressure vessels, including vapor coolers, vapor separators, etc.

A schematic view of the system in TPP TENT B, where vapor and moisture are separated, is shown in figure 1. Moist vapor exits the vaporizer and is transported to the vertical vapor separator (or starting vessel) wherein the remaining vapor is extracted. Such a separator functions according to the Sulzer circulating boiler principle.

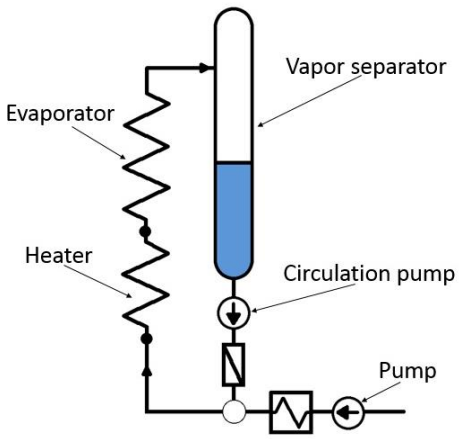

Fig. 1. Vapor separator (starting vessel) with other circulating boiler parts

The most commonly encountered problem in case of pressure vessels is the initiation of cracks in the heat affecteed zone (HAZ) during the manufacturing of the vessel or its repair [1]. Yet another reason for occurring of cracks can lie in the change in stress state in the vessel during exploitation, as well as the change in structural and mechanical properties in the material itself [2, 3]. Welded joints represent the most suitable locations for crack initiation and structural changes in pressure vessels, which lead to changes in mechanical properties.

Shown in the following section is the welding technology used for repairing of a starting vessel in exploitation in thermal power plant TENT-B, which was performed in order to remove a crack which was initiated in a welded joint after 220,000 work hours. In addition, results of hardness testing for the parent material, heat affected zone and weld metal are shown, before and after repairing. Repairing was performed using a probe for the purpose of determining and checking of compliance with standards. In addition, results of micro-structure testing using the zone replicating method for all zones within the repaired welded joint are presented. Shown in figure 2 is the model of the starting vessel.

2. THE REPAIR TECHNOLOGY FOR THE STARTING VESSEL

Starting vessel in TENT B in Obrenovac was made from steel 15 NiCuMoNb 5 (WB 36). The aforementioned steel belongs to the group of high strength low-alloyed steel, hence due to its high strength at elevated temperatures it is used for manufacturing of pipelines and pressure vessels. WB36 is a Ni-Mo steel, wherein its main alloying elements include copper and niobium. Since its basic micro-structure is ferrite-bainite, it is most commonly used for structures subjected to temperatures up to 450 ºC. Designation 15 NiCuMoNb 5 is in accordance with DIN standard, whereas according to ASTM standard, the steel is denoted by WB36.

Shown in tables 1 and 2 are the chemical composition and mechanical properties of steel 15 NiCuMoNb 5, [4].

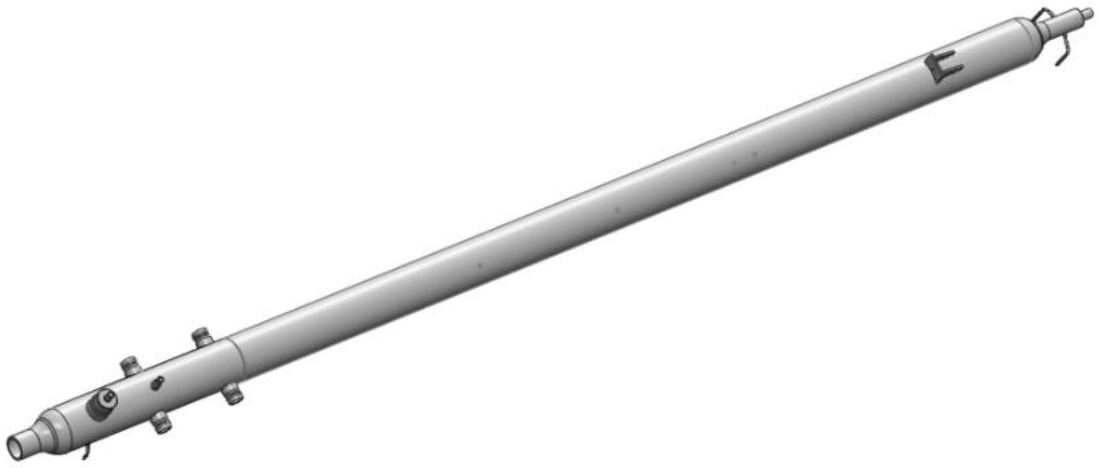

Fig. 2. Appearance of the three-dimensional model of the starting vessel

Table 1. Chemical composition of steel 15 NiCuMoNb 5

Element	C	Si	Mn	Cr	Mo	Ni	Nb	Cu	V	S	P
Percentage [%]	≤0,17	0,25 -0,5	0,8- 1,2	≤0,3	0,25- 0,4	1-1,3	0,2	0,5-0,8	≤0,006	≤0,014	≤0,014

Table 2. Mechanical properties of steel 15 NiCuMoNb 5

Mechanical properties	Yield stress R_e(MPa)		Tensile strength R_m(MPa) - 22ºC	Elongation (%)
	22 ºC	350ºC		
Values	≥430	≥353	610-760	≥16

During the inspection, in starting vessel narrowing zone, a crack was detected in one of the weld, located along the weld metal-heat affected zone area, and it was decided to perform repair welding in order to remove it. In Fig. 3 dimensions of crack are shown.

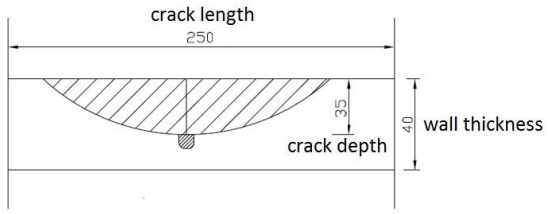

Fig. 3. Crack dimensions on one weld in the vessel

Vessel wall thickness at crack location was 40 mm, whereas the outer diameter of the vessel at this location was Ø350mm. During the first step, the damaged surface was ground, and a U groove was formed, and following this, repair welding and additional thermal treatment were performed. Grinding produced U groove whose depth was 40 mm, i.e. along the whole vessel wall thickness. The U groove was selected in order to reduce stress concentration.

The appearance of the groove is shown in figure 4a, whereas the filling plan during welding is shown in figure 4b.

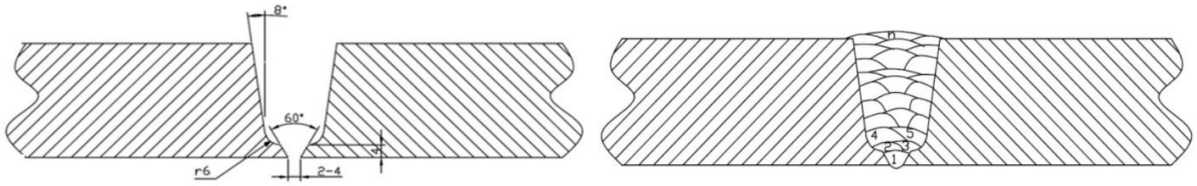

Fig. 4. a) Welding groove geometry b) filling plan during welding procedure

For the purpose of repairing the starting vessel, manual arc welding procedure with a coated wire was selected (Manual arc welding procedure or MAW), both for root and filling passes. A low-alloyed basic electrode manufactured by Böhler, 1NiMo.B, was selected, and its chemical composition is shown in table 3 [4].

Table 3. Chemical composition of the used electrode

Element	C	Si	Mn	Cr	Mo	Ni	Nb	Cu	V	S	P
Percentage [%]	0,06	0,3	1,2	0,1	0,4	1	0,2	0,05	0,01	<0,01	<0,01

Shown in table 4 are the repair welding parameters and the dimensions of the electrode. In the case of the root pass, as well as for first 2 filling layers, electrodes with a smaller diameter of 2.5 mm were used, whereas for the remaining later, larger electrodes with a diameter of 3.2 mm were used.

Table 4. Welding parameters

Weld	Welding procedure	Additional material diameter	Amperage (A)	Voltage (V)	Currency type /polarity
1	MAW	2.5mm	90-110	11-12	DC/+
2,3	MAW	2.5mm	70-100	16-18	DC/+
4-n	MAW	3.2mm	100-140	17-22	DC/+

Shown in figure 5 is the welded joint after repair. Once repair welding was completed, additional thermal treatment was performed. Selected temperature for additional thermal treatment via annealing was 600°C, wherein preheating and interpass temperatures were 250°C. Cooling rate after thermal treatment was completed was slower, below 300°C (figure 6). Preheating process and thermal treatment was performed in order to avoid the reoccurring of cracks during the repair.

Fig. 5. Appearance of the welded joint upon repairing procedure

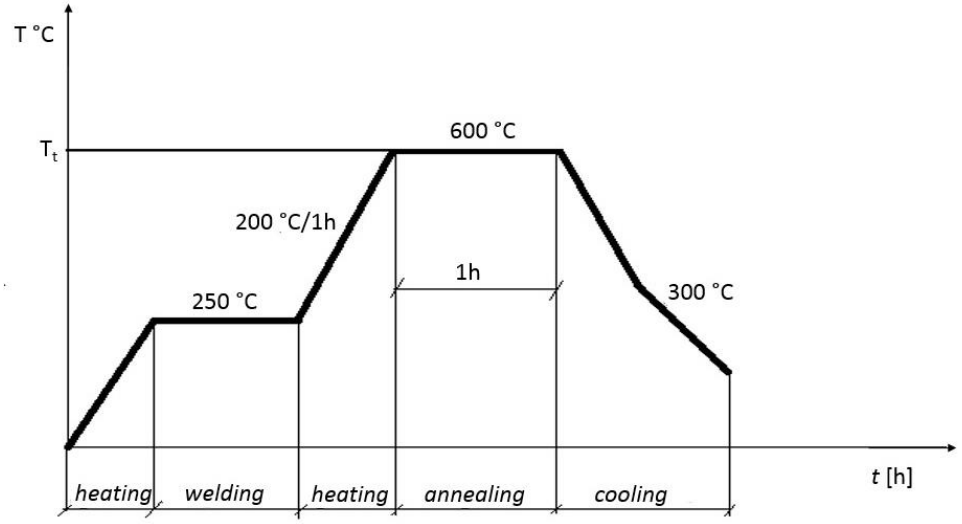

Fig. 6. Thermal treatment during repairing process

3. RESULTS

Hardness test was performed in locations where metallographic tests were also performed, using a probe, for the parent metal, heat affected zone and the welded joint itself. Shown in table 5 are hardness test results before and after repair for PM, WM and HAZ.

Table 5. Hardness testing results

Measuring location	Hardness before repair [HB]	Hardness after repair [HB]
Parent material	188	156
Weld metal	225	208
Heat affected zone	170	162

Since measured values of hardness deviate up to 5% from their limits according to standards for this material (for 15NiCuMoNb5: 190-240 HV10 or 181-228 HB), it is considered that the hardness was satisfying according to standard VGB R508L.

Using the replicating method, micro-structure was examined in all zones of the welded joint (parent metal, heat affected zone and welded joint). Seen in table 6 are the micro-structures of all zones of a repaired starting vessel after the welding process.

Table 6. Metallography test results

Parent material	Heat affected zone	Weld metal
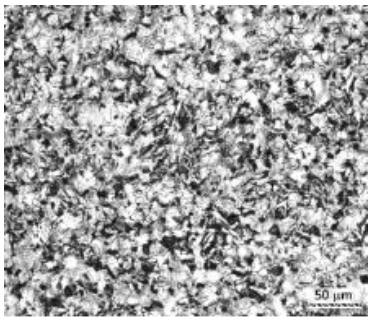	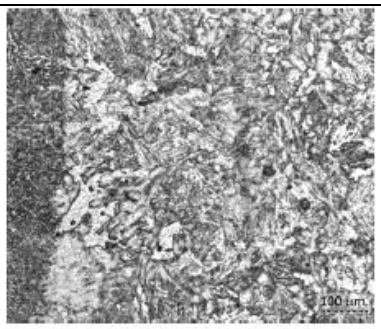	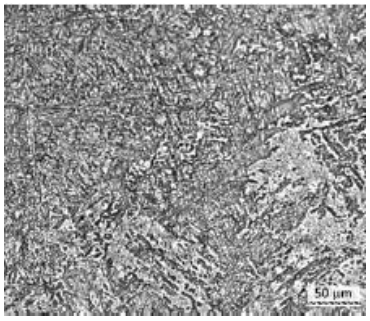
Microstructure of the parent material is a non-homogeneous bainite-ferrite-pearlite	HAZ microstructure is coarse-grained bainite-ferrite-pearlite	Weld metal microstructure is cast bainite-ferrite-pearlite

Microstructure of the parent material is bainite-ferrite-pearlite, whereas the heat affected zone was coarse grain bainite-ferrite-pearlite, and the micro-structure of the weld metal was cast bainite-ferrite-pearlite. In addition to these structures, the presence of a spheroid pearlite was observed in certain zones with the parent material, as a consequence of exploitation conditions to which the starting vessel was subjected.

4. DISCUSSION AND CONSLUSION

Metallography analysis of all zones of a welded joint in a repaired starting vessel did not reveal significant irregularities. The presence of a spheroid pearlite was observed in certain zones with the parent material, due to the exploitation conditions to which the starting vessel was subjected, however these structures did not affect the forming of cracks.

Since the hardness did not deviate by more than 5% from limit values defined by standards (for 15NiCuMoNb5: 190-240 HV10 or 181-228 HB), the hadrness was considered to be at a satisfying level. Based on the perfomed tests, obtained results have shown that the crack that had formed in the welded joint did not occur due to a change in hardness and micro-structure during exploitation, but was probably caused by the residual stresses due to previously used welding technology. Thus, during welding, i.e. the manufacturing of a starting vessel, and during repairing, better control is recommended, both during and after the welding. Additional recommendation involves the control of starting vessels after a period shorter than 220 000 work hours, in order to avoid major failure.

ACKNOWLEDGEMENT

The authors of this paper acknowledge the support from Serbian Ministry of Education, Science and Technological Development for projects TR35040 and TR35011.

5. REFERENCES

[1] Stojan Sedmak, Eksplatacione prsline u posudama pod pritiskom i rezervoarima, Beograd, 1994

[2] Adžiev Todor, Adžiev Gjorgji, Sedmak Aleksandar: Analysis Of The Haz Fracture Resistance Of Hsla Steel Weldments. Zavarivanje i zavarene konstrukcije vol. 54 (2009), pp 3-8

[3] Vencislav Golubović, Ivo Blačić, Aleksandar Radović, Stojan Sedmak: Toughness and ductility of high-strength steels welded joints. Structural Integrity And Life, Vol. 8, No 3(2008), pp. 181–190

[4] Böhler welding by Voestalpine. Filler Metals Bestseller for Joining Application, www.voestalpine.com/welding

The effects of electron beam welding process to the properties of superduplex stainless steel S32507 welds

B. Šimeková[a1], I. Kovaříková[a2], E. Hodúlová[a3], J. Bárta[a4]

[a] Slovak University of Technology in Bratislava, Faculty of Materials Science and Technology in Trnava, Institute of Production Technologies, J. Bottu 23, 917 24 Trnava, Slovak Republic

[1]beata.simekova@stuba.sk, [2]ingrid.kovarikova@stuba.sk, [3]erika.hodulova@stuba.sk, [4]jozef.barta@stuba.sk

Abstract

Stainless steel has a wide range of applications, including welded constructions. Commonly arc welding has disadvantages because has low speed and higher heat input and these realities can be cause the significant residual stresses and strains. The alternative to arc welding is laser welding that allows elimination of these negative effects. This paper investigates the weldability, metallurgical and mechanical properties of 5 mm thickness plate of superduplex stainless steel S32507 welds by electron beam welding (EBW) process. Experiment was performed to investigate the effects of process parameters on the microstructural and mechanical properties of the welds, and the process parameters were optimized. Welding experiments were done using universal electron beam welder PZ – EZ – ZH3 with accelerating voltage 60 kV and power 9 kW. Each joint was obtained by electron beam welding and their individual sub-regions through thickness were characterised by optical microscopy. Microstructure of both weld metal and heat affected zone are influenced by heat input which is a function of welding process and it can have impact on the transformation of grains. On the particular samples was observed microhardness and was performed tensile strength testing. This work describes the possibilities how to achieve the weld joints of high quality by using the optimal welding parameters.

Keywords: Please do provide up to five keywords which corresponds to the section topics of the paper. First keyword must be selected from the chosen set of the section titles.

1. INTRODUCTION

Super duplex stainless steels (SDSS) are high corrosion resistant alloys which offer better strength and toughness. It was reported that the greatest difficulty during welding operations is to obtain austenite amounts close to 50% and to avoid the formation of deleterious phases on cooling and reheating passes. As reported by Hsieh et al. [1], the presence of lower contents of austenite (<25%) is not usually acceptable in most of the industrial applications. Similarly to accept weld joints employed in welding and piping inspection, it is necessary to have a minimum austenite content of 30% in the last bead and root pass as necessary value [2]. To obtain the favourable microstructures, the heat input must be well controlled. It was reported that very low heat inputs lead to high ferrite contents and intense chromium nitride precipitation. Similarly high heat inputs and/or long exposure to temperatures in the 1000 –600 ^{o}C range may cause precipitation of brittle intermetallic phases such as σ (Sigma) or χ (Chi) which are assumed to deteriorate the weld

properties. The authors reported that the σ phase is considered to be the most dangerous phase because of its negative influence on weld toughness and its corrosion resistance [3,4]. Chi (χ) is a phase which forms before σ phase. It was also reported that the phases such as χ and σ provoke similar effects on the weld properties, but are not well distinguished by optical microscopy [5].

The authors addressed that fusion-welding processes destroy the favourable microstructure of this super duplex stainless steel and also contribute for the formation of detrimental inter-metallic phases. Also the fusion welds generally result in higher ferrite content and the formation of coarse grains which tend to decrease both the corrosion resistance and the mechanical properties of welded joints [10,11].

Electron beam welding (EBW) is well suited for thicker sections and enjoys the various advantages such as greater productivity, absence of secondary phases, a higher depth to width ratio, reduced residual stress and distortion and the possibility of automation. On employing EBW for SDSS, one of the serious problems addressed by Bonnefois [12] was that the ferrite–austenite ratio could be adversely affected as a result of the fast rate of cooling and also the loss of nitrogen during welding. However the rapid cooling in EBW will be beneficial in suppressing the formation of intermetallic precipitates. It was proposed that low heat input in EBW results in lower austenite content in the weld metal [13]. As claimed by various researchers, with the use of optimal process parameters in EBW, it could be possible to achieve the welds with sound toughness in spite of higher ferrite content [14]. As evident from the open literature sources, the EB welding has many advantageous aspects compared to other welding techniques.

2. EXPERIMENTAL PROGRAM

The investigated material is a type UNS S32507 steel (SDSS) in the form of 5 mm thickness plate. Super duplex stainless steel presents an attractive combination of mechanical properties and high corrosion resistance due the presence of two phases (δ and γ) in its microstructure. Welding experiments were done using electron beam with max. accelerating voltage 60 kV and power 9 kW. For the keyhole welds was used welding current in the range of 53 - 75 mA with welding speeds from 5 to 15 mm.s-1 and beam deflection was in three different schema without preheat. Welding parameters and heat input of the welds are presented in table 1. Welds were made on 5x50x100mm size plates. The heat input of electron beam welding was calculated using constant welding voltage 55 mV.

Table 1. Electron beam welding parameters of SDSS 5 mm thickness plates

Sample number	Power parameters				Deflection of electron beam					Physical parameters		
	Welding voltage U_{av} [mV]	Welding current I_{av} [mA]	Welding focus I_f [mA]	Welding defocus I_{def} [mA]	$V_{pp\ A}$ [mV]	$V_{pp\ B}$ [mV]	Deflection schema	f_A [Hz]	f_B [Hz]	v_{av} [mm/s]	Distance cannon h [mm]	Heat input [kJ/mm]
3A	55	53	855	0	450	80		513	513	15	254	0,175
5A	55	66	855	0	750	300		513	513	10	254	0,326
5B	55	60	855	0	750	300	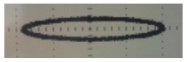	513	513	10	254	0,297
6A	55	76	855	0	750	300		513	513	15	254	0,251
6B	55	70	855	0	750	300		513	513	15	254	0,231
8C	55	60	855	0	1100	450	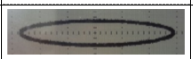	513	513	10	254	0,297
10A	55	73	855	0	600	600		513	513	5	254	0,723
10B	55	75	855	0	1100	450		513	513	5	254	0,743
11B	55	73	855	0	2000	400		513	513	10	254	0,361
11C	55	75	855	0	2000	400		513	513	10	254	0,371

3. RESULTS

Cross-section of macrostructure showed the fusion of base metals achieved by EBW (fig. 1). Welded joints made by changing the beam deflection are typical with barrel shape. The details of microstructure show the epitaxial and columnar grain growth is observed at the top region of the welds whereas the bottom end of the welds is showed like an equiaxed grains.

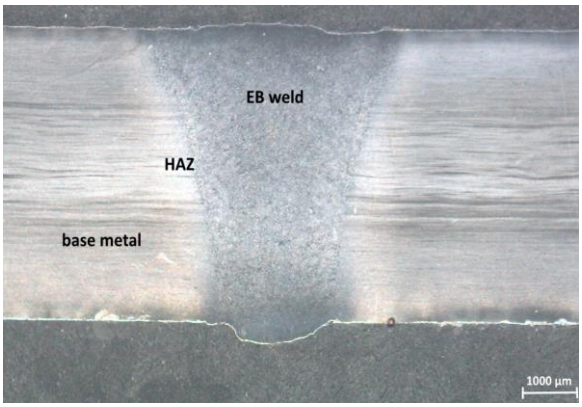

Fig. 1. Macrostructure of cross-sectional view of the EBW joint with 15 mm.s^{-1} welding speed and welding current 53 mA

The microstructure of the heat affected zone (HAZ) of SDSS is similar to that of the base metal, with the presence of elongated α (ferrite) and γ (austenite) phases (fig.2,3). There is no observed a atypical microstructural changes of HAZ. Proportions of the two phases are not equal. Austenite excluded in the grain boundary presented in the fusion zone which is acquainted to the faster cooling rates in the EBW process.

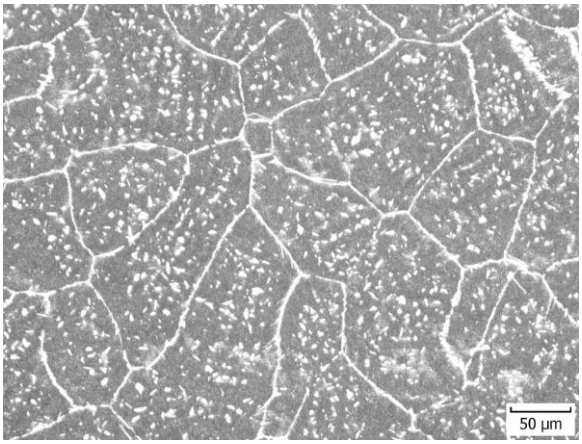

Fig. 2. Microstructure of cross-sectional view of the EB weld

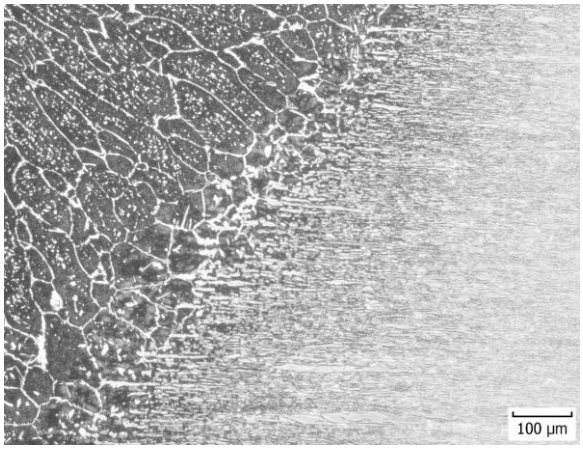

Fig. 3. Microstructure transition of HAZ and EB weld

Austenite content of the welded joints (tab.2) show that heat input and the cooling rate, together, decide the austenite content. In comparison with EBW process using higher welding current and smaller welding speed it can be argued that austenite content is higher in WM, but EBW process using smaller welding current and higher welding speed is closer to that small austenite content in WM. This is related to higher heat input in the case of EBW process and faster cooling rate through the temperature transformation range.

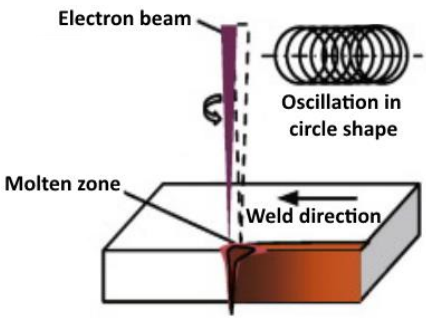

Fig. 4. Beam oscillation in EBW process

Oscillating the electron beam is an effective method to improve welding fusion and solidification, and increases the diameter of the keyhole. Beam oscillation prevents the molten envelopes from collapsing, and reduces the root spiking of the welds. Furthermore, beam oscillation increases the width of the fusion zone, and allows gas porosity to rise and escape from the weld pool [11].

The amplitude of beam oscillation was from 1 mm to 3 mm, and the oscillating frequency

was more than 200 Hz, which were optimum to weld by EBW. The functions of beam oscillation were circle illustrated in figure 4.

Table 2. Austenite content of the welded joints using EBW

Sample number	Welding voltage U_{zv} [mV]	Welding current I_{zv} [mA]	Welding speed v_{zv} [mm/s]	Heat input [kJ/mm]	Content of austenit [%]
3A	55	53	15	0,175	5,10
5A	55	66	10	0,326	12,92
5B	55	60	10	0,297	9,05
6A	55	76	15	0,251	8,25
6B	55	70	15	0,231	6,14
8C	55	60	10	0,297	9,56
10A	55	73	5	0,723	19,01
10B	55	75	5	0,743	19,50
11B	55	73	10	0,361	13,04
11C	55	75	10	0,371	15,37

Based on the results of the proportion of austenite microstructure analysis of the weld metal it was possible to predict the test results of corrosion resistance. According to ASTM A 923-06, the corrosion rate should not exceed 10 mdd (tab.3). The degree of corrosion for all the studied samples exceeds a given value, which can be welded joints considered defective.

Table 3. The values of corrosion resistance testing in accordance with ASTM A 923-01

Sample number	Sample weight (g)		Weight loss (mg)	Surface of samples (dm^2)	The degree of corrosion (mdd)
	before the test	after the test			
3A	46,046	46,026	20	0,1625	123,07
5A	45,112	45,098	14	0,1624	86,21
5B	45,885	45,868	17	0,1655	102,71
6A	44,980	44,962	18	0,1643	109,56
6B	46,481	46,462	19	0,1623	117,07
8C	51,277	51,117	16	0,1826	87,14
10A	45,774	45,764	10	0,1613	61,99
10B	45,867	45,858	9	0,1625	55,38
11B	45,516	45,505	11	0,1654	66,51
11C	45,299	45,179	12	0,1632	73,53

Hardness measurements showed the weld hardness was slightly increased compared to the base metals. The hardness measurements at the transverse sections indicated that the average hardness at the transition zone BM-HAZ-WM was observed with slightly upward trend.

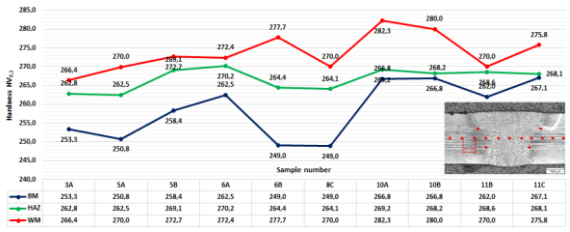

Fig. 4. Profile of average hardness across the welds

The highest tensile strength of the EB welds is observed at 898,4 MPa. The results clearly consider that the strength of the EB welds is higher than that of the base metal.

Table 4. Tensile properties of the SDSS samples

Rod	a [mm]	b [mm]	S0 [mm^2]	Fm [kN]	Rm [MPa]	Facture zone
5B.1	5,06	14,80	74,89	65,72	866,2	fracture in WM/HAZ
5B.2	5,03	14,80	74,44	64,92	860,7	fracture in WM/HAZ
6B.1	5,02	14,83	74,45	64,53	855,5	fracture in WM/HAZ
6B.2	5,02	15,02	75,40	65,62	859,0	fracture in WM/HAZ
10A.1	5,02	14,60	73,29	66,71	898,4	fracture in BM
10A.2	5,08	14,60	74,17	64,30	895,7	fracture in BM
10B.1	4,90	14,90	73,01	59,30	878,7	fracture in BM
10B.2	4,80	14,70	70,56	58,50	875,3	fracture in BM

4. CONCLUSIONS

The microstructure of the EB weld metal is characterized by large ferrite grains with intra- and inter- granular austenite. The austenite phase exhibits a needle like structure and it is formed from ferrite in the solid state.

Austenite content studies are showed that the ferrite–austenite balance ratio is not maintained in the weld metal similar to base metal.

Results of corrosion resistance confirms that the degree of corrosion is unsatisfactory.

The results clearly consider the strength of the EB welds which is higher than the base metal. Also the tensile results greatly support and are in line with the hardness data.

5. ACKNOWLEDGEMENTS

This research was supported by project Grant No. APPV-0248-12 funded by the by Slovak Research and Development Agency and Grant No. VEGA 1/0481/14 founded by the Ministry of Education of Slovak Research Agency.

6. REFERENCES

[1] Hsieh RI, Liou HY, Pan YT. Effects of cooling time and alloying elements on themicrostructure of the Gleeble-simulated heat affected zone of 22% Cr

duplexstainless steels. J Mater Sci Perform 2001;10(5):526–36.

[2] Norsok Standard M601. Welding and inspection of piping. 5th ed. Lysaker,Norway: Standards Norway; 2008.

[3] Lopez N, Cid M, Puiggali M. Influence of _-phase on mechanical properties andcorrosion resistance of duplex stainless steel. Corros Sci 1999;41:1615–31.

[4] Nilsson JO, Kangas P, Karlsson T, Wilson A. Mechanical properties, micro-structural stability and kinetics of _ phase formation in 29Cr–6Ni–2Mo–0.38Nsuperduplex stainless steel. Metall Mater Trans A 2000;31A:35–45.

[5] Domínguez-Aguilar MA, Newman RC. Detection of deleterious phases in duplexstainless steel by weak galvanostatic polarization in alkaline solution. CorrosSci 2006;48:2560–76.

[6] Sato YS, Nelson TW, Sterling CJ, Steel RK, Pettersson CO. Microstructure andmechanical properties of friction stir welded SAF 2507 super duplex stainlesssteel. Mater Sci Eng A 2005;397:376–84.

[7] Sato YS, Kokawa H, Kuwana T. Effect of nitrogen on transformation in duplexstainless steel weld metal. Sci Technol Weld Join 1999;4:41–9.

[8] Bonnefois B, Soulignac A, Charles J.Proceedings of the conference on duplexstainless steels ‘91, vol. 1. 1991. p. 469–78.

[9] Ku JS, Ho NJ, Tjong SC. Properties of electron beam welded SAF 2205 duplexstainless steel. J Mater Process Technol 1997;63(1-3):770–5.

[10] Muthupandi V, Bala Srinivasan P, Seshadri SK, Sundaresan S. Effect of weldmetal chemistry and heat input on the structure and properties of duplexstainless steel welds. Mater Sci Eng A 2003;358:9–16.

[11] H. Schultz. Electron beam welding (4rd ed.) Elsevier, Cambridge (2003).

WIZARDRY OF WATER – RAM PUMP

Zlatko Pavić* and Ivan Raguž student

Mechanical Engineering Faculty in Slavonski Brod, J. J. Strossmayer University of Osijek, Croatia
*Corresponding author e-mail: zpavic@sfsb.hr

Abstract

This article presents measurements and analysis of one homemade ram pump. From this analysis we got interesting knowledge, such as corelations between delivery height and flow rate of water, usefulness of whole system which all depends about system parameters.

Keywords:homemade ram pump, water flow, delivery water height

1. Introduction

Almost all pumps, which are known for us, need an external source of energy for the water to be shipped, especially if we are talking about higher altitude. The ram pump does not need any additional external power source other than the kinetic energy of water, but anyway can deliver water to the higher altitude. Only one assumption is really needed: pump must be located lower than water source. A ram pump can not transfer all the water from the starting point, because one part of water flows out of the pump giving its potential energy, with which pump will deliver rest of the water to the higher point.

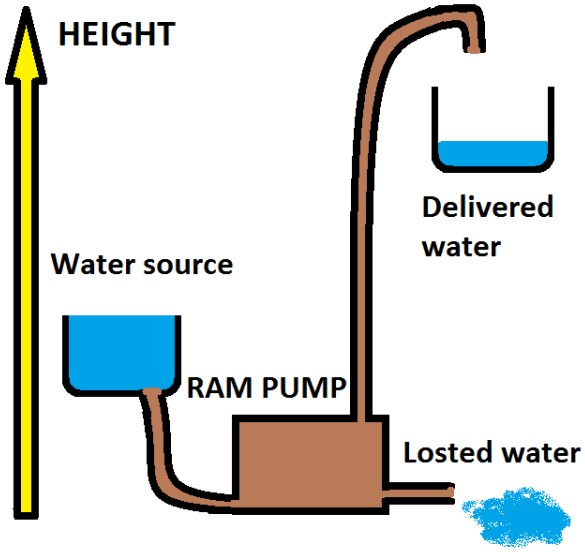

Figure 1. Position of ram pump in system

For purpose of research we have made a one homemade ram pump, which will be described into details.

Physical parameters, which were measuredare height, time and volume. On them are based all next analysis.

2. Theoretical operation of ram pumps

What happens to a car frame during crash into a strong barrier?Due to the large dynamic burden the frame bends and breaks.Likewise, when water is in move, the water has a certain kinetic energy. And then, during sudden stopping due high deacceleration pressure is rising rapidly.

The following figure shows the basic parts of the ram pump.

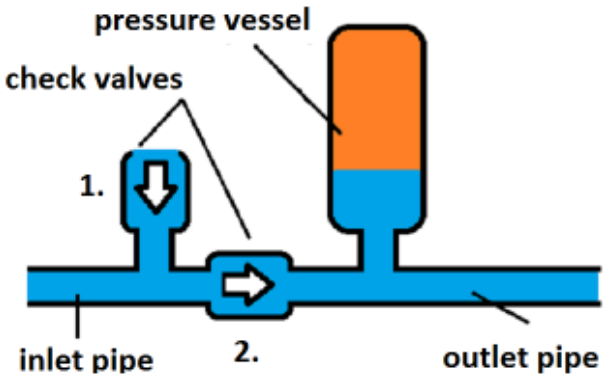

Figure 2. ram pump sketch

The inlet pipe brings water from the source to the pump. In order to raise the efficiency of the pump performance, the inlet hose must not be elastic. The check valve is marked with the number 1 in the foreign literature also referred to the valve for waste, because of it spilling a large amount of water from the system. The second check valve is used to pass the water next, immediately after a large increase of pressure, which is caused due to the sudden stop. Water passes through it, and comes to the pressure vessel in which it oppresses the air. After the fall of the pressure, the valve closes and does not allow water to return back.

In all drawings in the work of the arrow on the valve indicates the direction in which the valve allows the passage of water, if the arrow is painted green it means that the valve is open, and if the arrow is painted red it means that the valve is closed. Yellow indicates the direction of water movement. Important to say is that valve number 1

is inverted in opposite direction, but at the beginning is opened by a weight, which is not marked on the sketch. The mass of the weight we have determined experimentaly at our ram pump.

The description of the ram pump performance is partitioned down into three phases:

Step 1

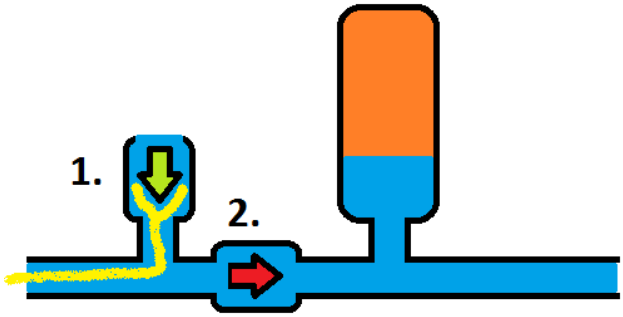

Figure 3. step 1

The first check valve is open; through it the water leaks, comes out of the pump and increases its speed. The valve with the help of weights is set to be closed when water reach certain speed. The second check valve is closed because the pressure in pressure vessel is bigger.

Step 2

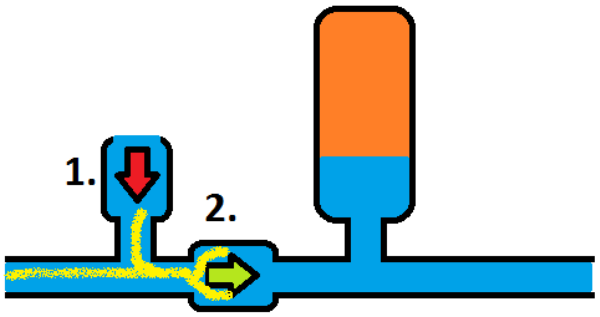

Figure 4. step 2

Pressure has increased, the first check valve is closed, and since the pressure is greater than the pressure in the pressure vessel, the second check valve opens and the water continues to the pressure vessels and then to the destination. Water will flow through the valve until the pressure is below a certain value.

Step 3

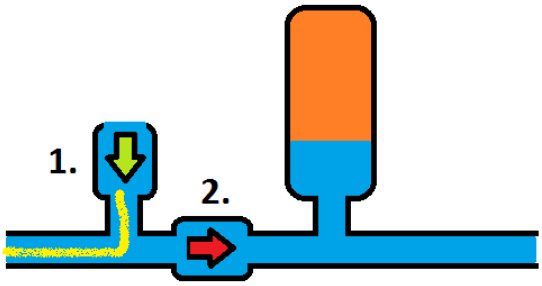

Figure 5. step 3

Once the pressure is reduced, the second check valve closes and the first re-opens. In the new cycle, the water is again passing through the first check valve, slowly speeding up and preparing for the resurgence of pressure, to repeat all the steps.

2. Description of our ram pump

On the picture below are marked every part of the ram pump.

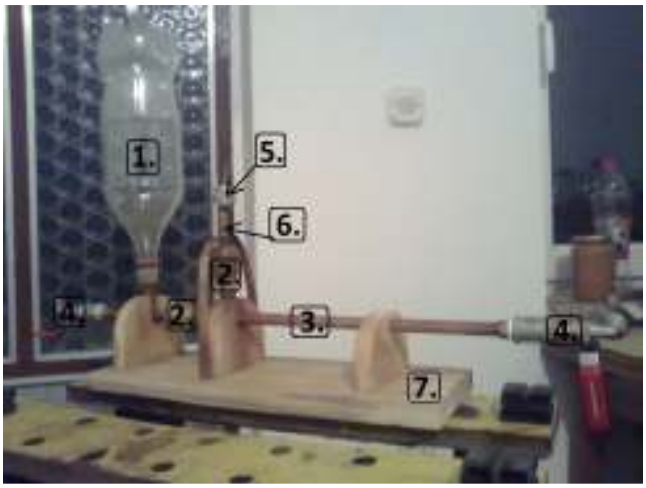

Figure 6. Our ram pump

Table 1. Parts of the ram pump

N:	Name:	Made of:	Assignment:
1.	Pressure vessel	PVC bottle with a volume of2l	System pressure regulation
2.	Check valves	Original	Allowing the water flow in only one direction
3.	Pipes	Copper pipes	Water flow
4.	Taps (a.k.a. faucets)	Original	Closing/opening the flow
5.	Weight	Iron	Check valve regulation
6.	Supporter of the weight	Copper	Supporting/holding the weight
7.	Stand	Wood	The base on which all other parts are fixed

We will say few facts about making:

- The pump has been made by tools which can be found in small home workshop;
- Pipes which were used are normal pipes for central heating systems with outer diameter 15 mm;
- our check valves are normaly used for plumbing systems, 1/2 cols in diameter;
- Pipes connections were connected with the soldering method and check valves on pipes using special brass extensions which at one end have a thread of ½ inch (for connection to the valve), and on the other side is where the copper pipe is soldered;
- In order to regulate the non-return valve which releases water we put weight and made a convenient holder for it;
- Weight is necessary for the operation of the pump as it regulates the openness of the valve;
- Mass of the weight required to drive the pump is determined in practice and is not discussed in detail in the analysis;

3. Measurements

Measurement of height and length we did with an ordinary tape meter, and in order to more accurately determine height difference, we used the device which is among the people known as "Inflatable balance device": hose set as U-tube is used to determine the gradient and thus achieves accurate measurement. Volumes are measured with a measuring cup. Since the measurement scale on the container in which we raise the water was in milliliters, before entering into a table, we immediately recalculated the measurements into m^3 which is consistent with the SI system of units.To measure time, I used a stopwatch. Stopwatch in these measurements was a sufficiently precise instrument, since the time that are measured are quite long.

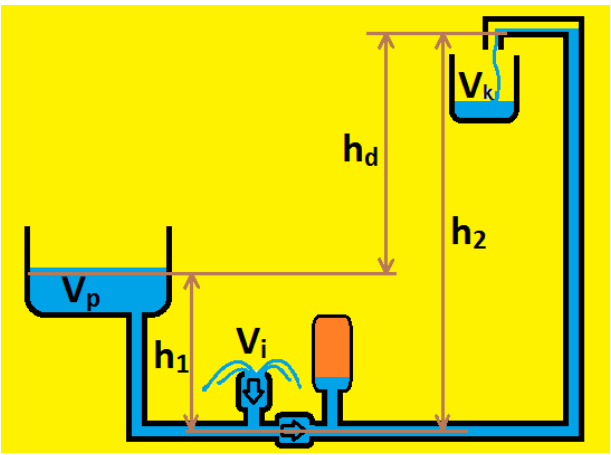

Figure 7. System sketch during measurements

We doneted the starting water volume with V_p, the water volume that was poured into the system. That volume will later be disbursed during the work of the pump. V_i denotes the lost water volume, and V_k denotes the useful water volume, the volume that was raised to a greater height than in the start.

Variables for heights are also very important. h_1 denotates the height between the middle of the inlet pipe and the middle of the water column when the vessel is full.; h_2 denotates the height between the middle of the inlet pipe and the highest level on which the pump raises the water; h_d is the height difference (h_2 and h_1),what we determined by calculation.

3.1.Measuring of the useful volume and the flow time

In these measurements, we measured the amount of useful volume and the time required for that measurement. Measurement of the time is needed so that we could later calculate the flow rate of the pump. Measurement results will be shown later in the table together with analysis. Every measurement we repeated three times in the same conditions.

3.2.Measuring of strokes in a minute

During this measurement we used a stopwatch so that we can exactly know how much time has passed, and we counted the strokes manually. This measurement will later be necessary to determine the volume that the pump supplies in one tact.

4. Analysis of measurement results

4.1. Analysis of measurements of the useful volume and the flow time

Table 2.Measurement resuts for the useful volume and the flow time

Measurement number	h_1/m	h_2/m	h_d/m	V_k/m^3	t/s	Q/m^{3}s^{-1} *10^{-6}	$\bar{Q}$/m^{3}s^{-1} *10^{-6}
I.	0.91	2.22	1.31	0.0029	473	6.13	6.37
				0.003	466	6.44	
				0.0031	474	6.54	
II.	0.81	3.04	2.23	0.0015	486	3.09	3.10
				0.00153	482	3.17	
				0.00148	489	3.03	
III.	0.81	4.16	3.35	0.00133	560	2.38	2.37
				0.00131	555	2.36	
				0.00132	557	2.37	
IV.	0.81	5.31	4.50	0.0009	521	1.73	1.70
				0.00085	510	1.67	
				0.00088	516	1.71	

V_p =0.015/ m^3– starting water volume
h_1 – seesketch
h_2 – seesketch
h_d – differencebetween $h_2$and h_1
V_k – useful water volume
t – measuringduration
Q – water flow
$\bar{Q}$ - average water flow

$h_d = h_2 – h_1$, [m]

$Q = V_k / t$, [m^{3}s^{-1}]

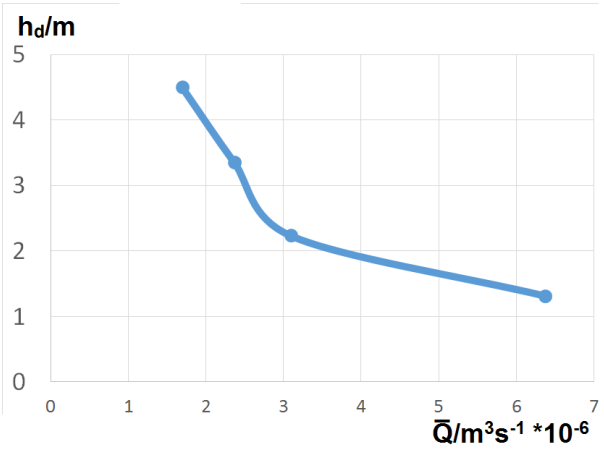

Figure 8. Dependence of delivery height and flow rate

From these analysis you can see that flow rate, decreases rapidly with increasing of delivery head.

4. 2. Analysis of the measurements of the tacts in a minute

Table 3.Measurement results of the number of tacts in a minute

Measurement number	h_1/m	h_2/m	h_d/m	tacts	tacts / s^{-1}	Tacts in a second/ tact s^{-1}
I.	0.91	2.22	1.31	97	1.62	1.58
				95	1.58	
				93	1.55	
II.	0.81	3.04	2.23	104	1.73	1.7
				100	1.67	
				102	1.70	
III.	0.81	4.16	3.35	107	1.78	1.75
				108	1.8	
				107	1.78	
IV.	0.81	5.31	4.50	103	1.72	1.72
				103	1.72	
				103	1.72	

h_1 – see sketch
h_2 – see sketch
h_d – difference between h_2 and h_1
t = 60 s - measuring duration
tacts – number of tacts measured in the time of measuring

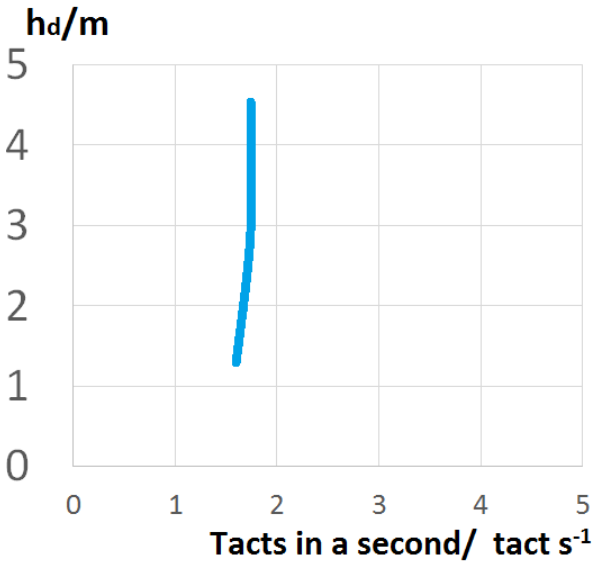

Figure 9 Dependence between tacts per second and delivery height

This analysis shows that the pump has a quiet uniform work at the different delivery heights

4. 3. Usefulness of the device

Table 4.Analysis of the usefulness of the ram pump

Measurement number	h_1/m	h_2/m	h_d/m	V_k/m^3	$\bar{V}_k$/m^3	η
I.	0.91	1.82	0.91	0.003 0.0029 0.0031	0.003	40.00%
II.	0.91	2.22	1.31	0.0029 0.003 0.0031	0.003	48.79%
III.	0.81	3.04	2.23	0.0015 0.00153 0.00148	0.0015	37.53%
IV.	0.81	4.16	3.35	0.00133 0.00131 0.00132	0.00132	45.20%
V.	0.81	5.31	4.50	0.0009 0.00085 0.00088	0.00088	38.46%

V_p= 0,015 m^3 – starting water volume
h_1 – see sketch
h_2 – see sketch
h_d – difference between h_2 and h_1

$\rho = m/V$, [kgm^{-3}]

$$\eta = \frac{V_k * \cancel{\rho * g} * h_2}{V_p * \cancel{\rho * g} * h_1} * 100\%$$

$$\eta = \frac{V_k * h_2}{V_p * h_1} * 100\%$$

As we can see, we can say that pump is equal useful at different delivery head. Energy being losed mostly at friction during flow through a pipe.

4. 4. Comparison of the useful and the lost water volume

Table 4.Comparison of the useful and the total volume

Measurement number	h_1/m	h_2/m	h_d/m	V_k/m^3	$\bar{V}_k$/m^3	Percentage V_k
I.	0.91	2.22	1.31	0.0029 0.003 0.0031	0.003	20.00%
II.	0.81	3.04	2.23	0.0015 0.00153 0.00148	0.0015	10.00%
III.	0.81	4.16	3.35	0.00133 0.00131 0.00132	0.00132	8.80%
IV.	0.81	5.31	4.50	0.0009 0.00085 0.00088	0.00088	5.87%

5. Conclusion

In this paper we shown one very simple device, which for its work doesn't require any energy source except good position in system.

The ram pump as a rule has only two moving parts and because of that, it brokes down very rare.

Presented facts makes it very useful in mountain regions for everything what needs water delivery.

Some simple systems can be homemade produced without any special efforts and it is quite cheap, what makes this device very good also from economical view.

7. References

[1] F. Matejiček, *Kinematika sa zbirkom zadataka*, Strojarski fakultet u Slavonskom Brodu, Slavonski Brod, Croatia, 2010.

[2] F. Matejiček, *Kinetika sa zbirkom zadataka*, Strojarski fakultet u Slavonskom Brodu, Slavonski Brod, Croatia, 2010.

[3] B. Kraut, Krautov strojarski priručnik, Axiom, Zagreb, Croatia, 2008.

[4] S. Landeka, *Motori i traktori*, Rotograf d.o.o., Vinkovci, Croatia, 2006.

DEVELOPMENT AND CONSTRUCTION OF MACHINE FOR FUSED DEPOSITION MODELING

I. Kocić[1*], Ž. Ivandić[2], D. Kozak[2], T. Baškarić[2] and K. Jelić[3]
[1]Faculty of Mechanical Engineering in Slavonski Brod, J. J. Strossmayer University of Osijek, Croatia
[2]Department of Mechanical Design, Faculty of Mechanical Engineering in Slavonski Brod, J. J. Strossmayer University of Osijek, Croatia
[3]Maritime Department, University of Zadar, Croatia
Corresponding author e-mail: i.k.kocic@gmail.com

Abstract

Understanding the basics of theoretical and practical issues that need to be solved, lead towards more understandable definition for developing process of the technical system. The structural and functional features of the fused deposition modeling machine are shown through the product requirement list (list of demands), morphological matrix and functional structure of the selected solution. Cause many different parts are involved, that should interact and seamlessly work together, it is prescribed quite long list of basic requirements that a product must fulfill. Describing the product with its function, enabled to view solutions regardless of its form. In accordance with the above, during the research were observed disadvantages of existing machines and then set a framework system that would bring some new operating principles of characteristic details in developed machine.

Keywords:

Fused deposition modeling; 3D printing; Product development; Design process; Product requirements (List of demands); Morphological matrix

1. Introduction

Fused deposition modeling is one of the additive manufacturing processes that are becoming a valuable and powerful personal „tool“. The process that goes from an idea to a plastic object is the future of limited production. The complexity and quality of printer designs, as far as finished products, varies from one to another. Although there are many different types of machines, there is still much space for further progress. This fact led to the development and construction of fused deposition modeling machine.

Once the problem is defined, decision making process can begin. It includes carefully planned synthesis of relatively well-known elements into a unique, previously unknown entity. [1]
Methodical design will be used for elaboration a concept of a machine for fused deposition modeling. Gathering useful informations as a first step, could help for better understanding earlier defined problem. Considering problems and successes associated with existing solutions may also provide easier establishing design requirements. In the design process a list of requirements represents an „input“ because it includes the needs and required terms about the machine, and the „output“ is observed as the final solution.
The problem-solving process requires solutions which are capable for realisation in practice. In addition, those solutions must be found for all the required functions.
Fused deposition modeling machine, as technical system can be modelled in terms of the flows and conversions of material, energy and information (signals). [2]
Each product function contains several possible solutions which can be expressed through morphological chart. [3]

2. Requirement list

Requirement list is defined as the specification of the construction [4] and represents a series of demands and wishes defined by the customer or the author. Such an approach enables the identification of the real problem and its limitation to a specific area of research. Distribution on demands and wishes also simplifies selection and results evaluation. Requirements are the features of the product that must be fulfilled under all conditions, so if they don't satisfy, the solution is not acceptable. They can be distributed according to a partial, functional and built-in groups or by the main features.
Most important requirements in developing process of FDM machine are: simplicity and stability of the frame; boundaries of working area; cooling system

for the main components; integrated screen for direct management and the ability of navigation through personal computer; as many as possible components made of plastic in order to achieve minimum making costs. Full requirement list for the FDM machine is shown in the table 1.

Table 1. Requirement list for FDM machine

Requirement or wish	Requirements	Requirement or wish	Requirements
	GEOMETRY		ERGONOMICS AND SAFETY
R	Max. height, width and length 500 mm	R	Warnings on extremely hot components
R	Max. working area 1×10^7 mm^2	R	Safety of electric shock
R	Separability of parts of the frame structure	R	Forbidden approach to extremely hot parts
	KINEMATICS	R	Protection from moving parts
R	Regulation speed 1-200 mm/s	W	Closed housing
R	Translational motion of the extruder in the horizontal plane	R	Easy access to the heatbed after finishing the work
R	Movement of the heatbed by height	W	Ventilation of working chamber
	FORCES	W	Transparent housing
R	Max. heatbed load 5 kg		PRODUCTION
R	Stability of the frame structure	R	Standard parts using
W	Max. weight of the frame 7 kg	W	As many as possbile components made of plastic
W	Min. deformation of heatbed	R	Separable connections of parts
	ENERGY	W	Adjustment of components inside the frame
R	Electrical running of machine	W	Min. costs of making
R	Cooling the main drive		INSTALLATION AND TRANSPORT
R	Cooling the system power	R	Easy installation
W	Heating heatbed up to 130 °C	W	Ease of connecting electronics
R	Max. power 500 W	W	Installation with standard tools
W	Continuation of work in case of power failure	W	Quick replacement of components in case of failure
R	Max. temperature of nozzle 250 °C		OPERATION AND MAINTENANCE
	MATERIAL	W	Quiet and smooth operation of the machine (small vibrations)
W	Using standard profiles	W	Small maintenance costs
W	Corrosion resistance	W	Easy control of machine
R	Decorative paint	W	Clean remaining plastic
R	Conductive material of heatbed	R	Lubrication of mechanic parts
W	Different material of partial machine systems	R	Simple replacement of consumable material
R	Temperature resistant support of heatbed		RECYCLING
R	Used material for printing – plastic	W	Provide recycling of material (components)
	SIGNALS	R	Reduce the variety of materials
R	Ability of navigation through personal computer	W	The use of biodegradable materials for printing
W	Integrated screen for direct management		
W	Easy feedback reading		
W	Visual supervision of work		
R	Safety button		

3. Functional structure diagram

Overall function is defined by gradual abstraction of requirement list, dropping out wishes and requirements that doesn't have direct influence on the function. Function structure is some kind of a graphical „review“ of the functions that a product performs on its inputs and outputs. Mentioned overall function is broken down to sub-functions which are connected with a flows. As first, creating black box model of future product can help in understanding product's basic function. Input flows for synthesizing three-dimensional objects would be polymer as material, signal as information and electrical energy. Desired output is formed polymer as the final solution. To get formed polymer, unwanted flows occur in a way of bad smell and waste of energy (heat).

The full black box diagram is shown in fig. 1.

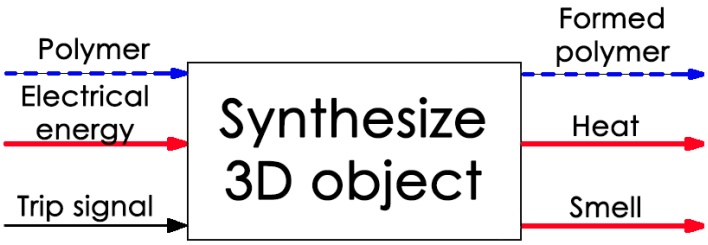

Fig. 1. The full black box diagram

Tracing of the input flows through the product should bring out the final function structure diagram. In order to get formed polymer, input flow must go through certain stages, starting with his acception inside of product.

After that, the polymer could be extruded with the help of some kind of energy. The same thing has been done for other two flows and all together assembled and combined. The result is shown in fig. 2.

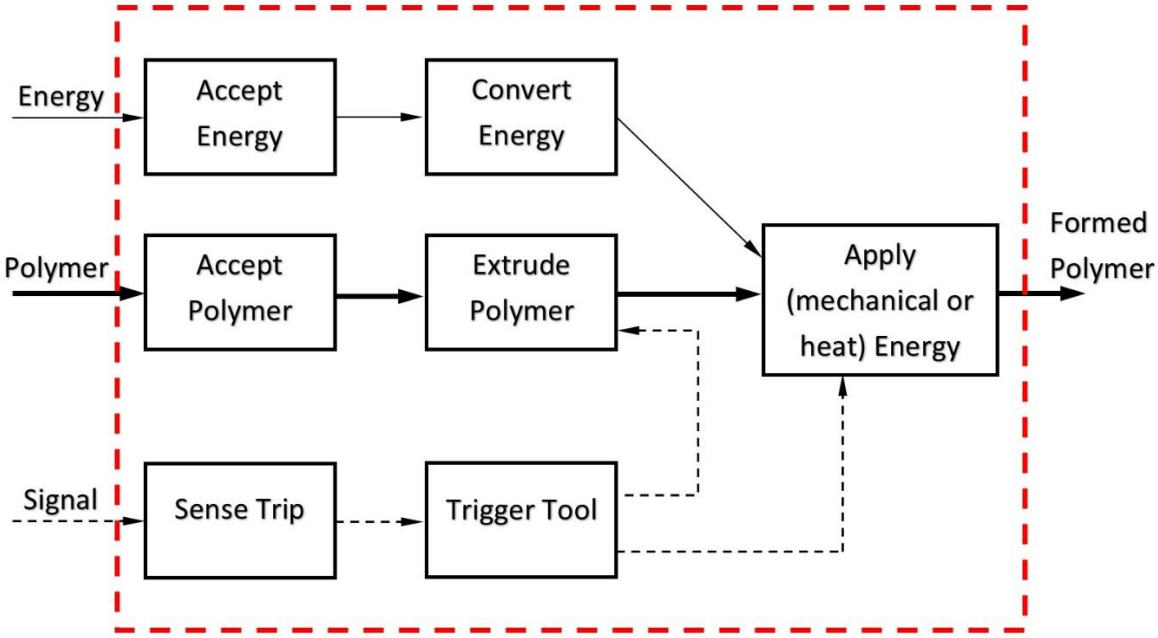

Fig. 2. The final function structure diagram

4. Morphological matrix

Morphological matrix is the principle of forming a conceptual solution by specifying a larger number of partial functions. [5] Description and formulation of problem are initial steps in developing this matrix. Different variants of solutions are formed by connecting individual partial functions and design solutions. So, a certain number of matrix are used for joining and showing the relationship between the properties of products and activities in the production process.

By identifying the most important parameters are made preliminary matrix and selected the one that provides the most information, and options are verified and completed. Choosing the best matrix begins the process of reviewing all of its fields and selecting those which are most useful for further consideration.

Table 2. Morphological matrix (■ - the best variant)

PARTIAL FUNCTIONS		SOLUTION PRINCIPLES		
		V1	V2	V3
1.	Power and torque produce	Electric motor	Servomotor	Stepper motor
2.	Power and torque transfer	Gear transmission	Chain transmission	Belt transmission
3.	Calibrate the machine (height adjust)	Counternut	Spring	
4.	Vertical movement allow	Threaded spindle	Rack and pinion	Worm gear
5.	Movement (per axis) stop	Mechanical switch	Sensor	Lever mechanism
6.	Locate shafts	Tapered bearing	Ball bearing	Roller bearing
7.	Construction frame accomplish	Steel profiles	Aluminium profiles	Plastic profiles
8.	Housing perform	Welding	Screw connections	Combination of welding and screws
9.	Stability of the „machine head“ provide	Screw connections	Shape of carrier	Positioning and centering of carrier
10.	Switching „on“ and „off“ enable	Switch	Classic switch	Sensor
11.	Enable cleaning	By opening the door	By optional tray	
12.	User protect from injuries	Locking door during operation	Cover moving parts	Sensors
13.	Reduce vibrations	Damping elements	„Isolation“	Lubrication
14.	Reading data	Integrated screen	Personal computer	Indicator lights
15.	Ensure from electric shock	Sound signal	Grounding	Warning light (Visual inspection)
16.	Regulate the amount of the deposit	The diametar of the nozzle	Speed of pulling through	Speed of movement of head unit
17.	Corrosion resistance achieve	Stainless materials	Protective coatings	
18.	Stability of the frame achieve	Adjustable foots	Wheels	Connection to another construction

5. Overview of the main components

The frame represents a support structure which is used for upgrading all the other elements of the machine. The role of frame is not only to keep all the pieces "together", but also to maintain the axis aligned all the time due to constant movement and vibration. It must resist to the forces and inertia that occur as a result of moving parts and sudden changes of their directions and speed. The most important feature of the frame is rigidity. To satisfy this requirement, decision was to apply weldment joints which will also directly contribute to better print quality and stability of the device.

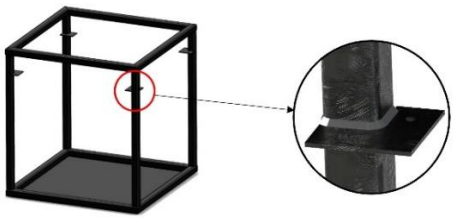

Fig. 3. The frame design

Extrusion is the process which is used to ensure a continuous flow of melted polymer in the nozzle. Therefore, it is the most important part of the process of three-dimensional printing. The extruder is divided into two main parts; housing and the print head. On that way is provided easy access and replacement of components in case of malfunctions or failures.

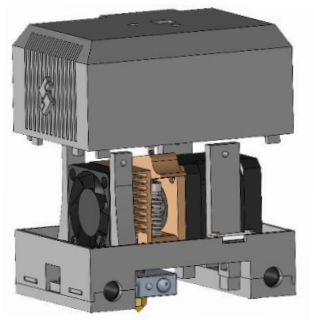

Fig. 4. Housing and print head of extruder

Controlling of the x-axis is performed by a timing belt transmission connected through a stepper motor to extruder. More complex form of carrier allows easy assembling and disassembling of the entire x-axis subsystem. Over the y-axis is ensured main relation of the entire system with a frame of machine. In the each corner of the frame, the carriers are fixed on lugs with screw connection. A stepping motor which performs a change of y-axis position is located on the housing.

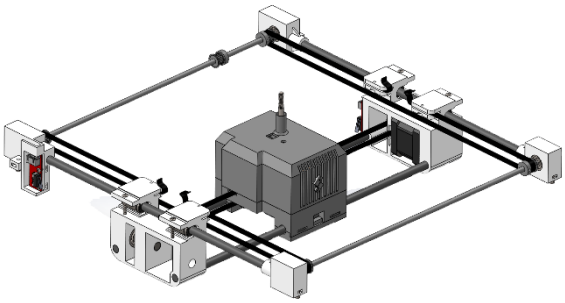

Fig. 5. X-axis and Y-axis subsystem

Positioning in height allows the machine stacking layers and upgrade models. The accuracy must be very high in order to avoid unequally applied layers. Depending on the level of machine calibration, the height of the layer can be up to 0.1 mm. The motion is achieved by a threaded rod. To better fit the rod profile, there were set two nuts compressed with the spring in the middle.

Fig. 6. Z-axis subsystem

Heatbed represents the area on which is made subject during printing. It defines the maximum dimensions of the object. In order to overcome the large temperature difference between extruded deposit and the heatbed, it is necessary to heat the surface at a certain temperature. The springs below the heatbed are intended to leveling before printing, so that the accuracy of the first extruded layer could be better.

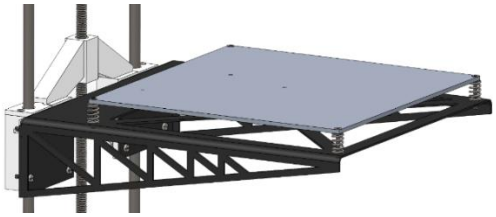

Fig. 7. Heatbed on Z-axis subsystem

Working principle of a plastic thread is based on leading from the wheel to the machine head, and then squeezed (melted) through the nozzle. Delivery of the plastic thread is realized by a chain guide, which is connected to the machine head.

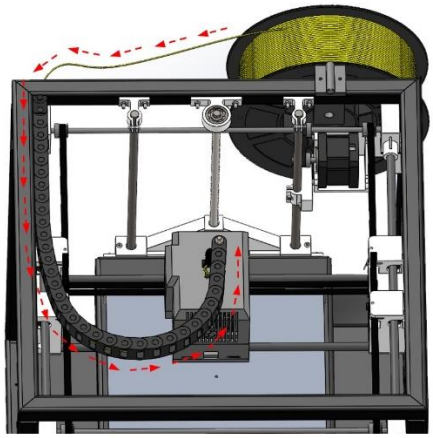

Fig. 8. Delivery of the plastic thread

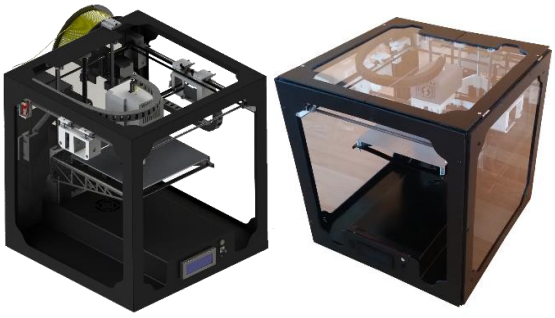

a) *b)*

Fig. 9. The final machine design
a) 3D model; b) Produced machine

The print quality was tested by making the standard type of „bolt and nut“. It has been done with PLA plastic and precision of 0,1 mm.

a) *b)*

Fig. 10. Printed „bolt and nut“
a) Bolt with wing nut;
b) M8 bolt with standard steel nut

5. Conclusion

Due to described requirement list, functional structure and best conceptual solution chosen from morphological matrix, the machine is designed and created. The main subsystem (extruder) performs the movement in the plane, and stacking layers is determined by heatbed movement in the vertical direction. It has been shown that such an embodiment does not affect the accuracy of the printing, moreover, inertial forces have influence only on a main subsystem while the heatbed is being stationary. Thus is created the possibility of easier access during the operations, especially from the standpoint of rigidity and stability.
The implementation of the vertical axis is significantly simplified because almost all of its components can be made by additive manufacturing processes.
By researching and creating this machine all foundations can help for further development of fused deposition modeling machine. The continuation should be directed toward improvements in terms of stability of the vertical subsystem with the ultimate aim of increasing the speed and mass of printed model.

6. References

[1] Hubka, V.; Eder, W. E.: *Theory of Technical Systems*. Berlin; Springer – Verlag, 1988.

[2] Wallace, Ken; Clarkson John: *An introduction to design process.* United Kingdom; University of Cambridge, 1999.

[3] Boeijen, A.; Daalhuisen, J.; Zijsltra, J.; Schoor, R.: *Delft design guide*. Delft; Delft University of Technology, 2014.

[4] Topčić, Alan; Tufekčić, Džemo; Cerjaković, Edin: *Product development (Razvoj proizvoda).* Tuzla; Univerzitet u Tuzli, 2012.

[5] Olević, Sato; Lemeš, Samir: *Basics of design (Osnovi konstruiranja).* Zenica; Univerzitet u Sarajevu, 1998.

Numerical simulation of metal cutting using the software DEFORM 2D

I. Milos [a], D. Kozak [b], M. Katinić [c]

[a] Mechanical Engineering Faculty in Slavonski Brod, J. J. Strossmayer University of Osijek, Trg I. B. Mažuranić 2, Slavonski Brod, Croatia, imilos@sfsb.hr

[b] Mechanical Engineering Faculty in Slavonski Brod, J. J. Strossmayer University of Osijek, Trg I. B. Mažuranić 2, Slavonski Brod, Croatia, dkozak@sfsb.hr

[c] College of Slavonski Brod, Dr. M. Budaka 1, Slavonski Brod, Croatia, marko.katinic@vusb.hr

Abstract

Machining is one of the jobs that are widespread due to a number of advantages. The goal of each company, whose activity is associated with machining, is separation of particles in optimum working conditions. Optimum working conditions, minimal production costs and the tool wear can be reached due to experiments which are very expensive or determined with computer programs based on the finite element method. In this work the numerical simulation of orthogonal turning of AISI 1025 steel is made in the software DEFORM 2D. The goal of making the numerical simulation of machining is to define the conditions of processing with a minimum temperature of the cutting part of the tool. With regard to the Taguchi plan experiment, statistical analysis was carried out of the output data "the temperature of the cutting parts of the tool" by using analysis of variance. Based on the regression equation it was concluded what parameter has the biggest impact on the observed output value.

Keywords: Numerical simulation, Metal cutting, DEFORM 2D, Finite Element Analysis, Tool wear

1. INTRODUCTION

Machining is one of the most used processing procedures in the industry for a number of its benefits [1]. The basic shape of the tool which is used in processing is called a wedge. While processing, there comes to a change of dimensions and the surface conditions of the workpiece for the purpose of making the items in predefined dimensions [1]. One processing procedure with the widest range and most commonly used machining processes is the separation of particles with turning. With regard to the position of the cutting part of the tool, there differ orthogonal and formal turning [2]. Orthogonal turning uses the following assumptions: the cutting speed is perpendicular to the main cutting blade as well as on the feeding speed, the cutting blade is wider than the width of processing, on the back surface of the tool is no friction, shearing occurs in a plane. [3] The market today sets the increasing demands on manufacturers with regard to the quality of the product which is reflected in the organization of production, optimization of existing technologies of production, costs. [4] In order to meet the requirements of the market with regard to product quality, special attention should be paid to the cutting tool, in turning that tool is the lathing knife [4]. Based on experimental research the optimum geometry and parameters for turning processes are defined [4]. The processing parameters for turning are: cutting speed, feed rate and depth of cut. Whereas experimental research is expensive and

requires a certain time interval, today's computer support, based on the finite element method, is one of the main tools that is used for modelling and simulation of turning processes [3]. In this article a numeric simulation of orthogonal turning will be displayed with a defined temperature of the cutting part of the tool. Numerical simulation was carried out in the software DEFORM 2D. Based on the input data, by using the Taguchi method, a plan of the experiment is defined which was used for the ANOVA analysis. Using the ANOVA analysis, the extent of the processing parameters influence on the heating of the cutting part of the tool was defined.

2. METHODS AND MATERIALS USED FOR RESEARCH

DEFORM 2D Version 8.1 is a computer software of the company Scientific Forming Technologies, based on the finite element method, which enables the analysis of procedures: material processing (processing of materials by deforming, processing of materials by separating particles) and heat treatment. [5] While in simulation in the 2D view, the observation is limited to the body of an axisymmetric model geometry and condition of a plane strain deformation. [5] With this computer program a numerical simulation of orthogonal turning is made for AISI 1025 steel, assuming the status of plane strain deformation, whereby the material of the cutting part of the tool is WC.

2.1. Numerical Simulation in DEFORM 2D

DEFORM 2D is using an implicit integration method [3]. For the formulation of a model, it uses the updated Lagrangian formulation [6]. In places with large deformations, while the formation of the separating of particles occurs, DEFORM 2D creates automatically a higher density mesh. Creation of the numerical simulation in the computer software DEFORM 2D is divided into three sections: Preprocessor, Processor ("Simulation Engine") and Postprocessor. Preprocessor covers the first phase of elaboration of the numerical simulation. It is intended to provide data required for numerical simulation, finite element mesh generation and setting up boundary conditions [5]. It represents the most important part of making the simulation. Processor, the central phase of production of the numerical simulation, is referred to as a Simulation Engine. It is intended for: numerical calculations that are required during the analysis process, the recording of the results in the database. Postprocessor represents the final stage of making the numerical simulation, and is used to review the results of the simulation. [5]

While creating a numerical simulation of orthogonal turning, the plane shown in figure 1. is observed.

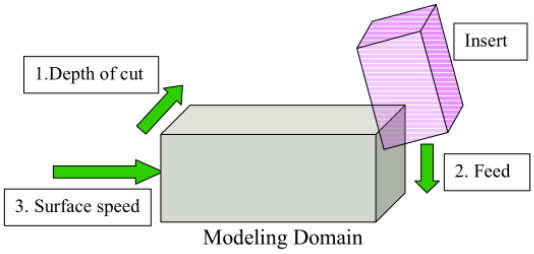

Figure 1. Modelled plane of orthogonal turning

Parameters for processing by turning, which are required by the software, are presented in figure 2.

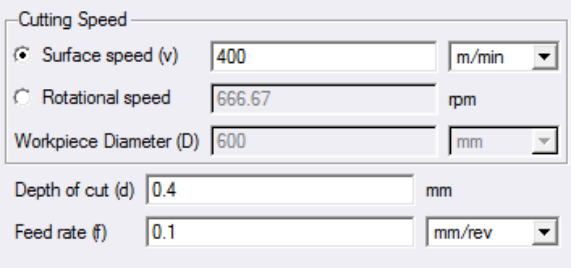

Figure 2. Processing parameters for turning

Besides the parameters of processing, it is essential to define the conditions in which the processing is proposed. Under the terms of processing these are implied: the temperature of the environment, a factor of shear friction and coefficient of heat transfer. Processing conditions are shown in table 1.

Table 1. Process Conditions

Environment Temperature	22°C
Shear friction factor	0,6
Heat transfer coefficient	100000 W/(m^{2}K)

When creating a numerical simulation, it is assumed that the cutting part of the tool will be rigid.

The dimensions of the cutting part of the tool are used to produce the numerical simulation shown in figure 3.

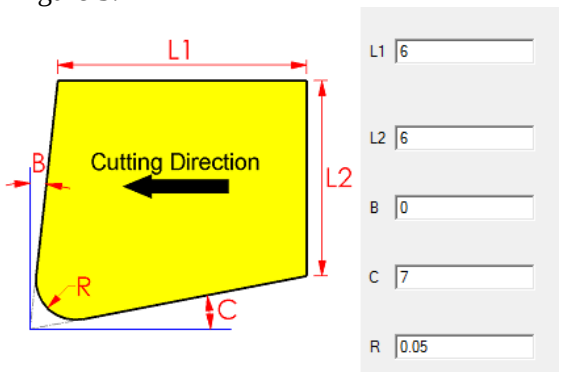

Figure 3. Dimensions of the cutting part of the tool

DEFORM 2D contains its own library of materials, so that the materials of the cutting part of the tool and the material of the workpiece are selected from the library's materials.
The selected material of the cutting part of the tool is tungsten carbide (WC).

Boundary conditions for the cutting part of the tool are the following: on the part of A-B, D-A the heat exchange with the environment (by convection) is defined. Convection coefficient for the air is 20 W/(m^{2}K). On the part of B-C, C-D a constant temperature of the tool is defined at 22 ºC.
Edges along which the boundary conditions are defined are shown in figure 4.

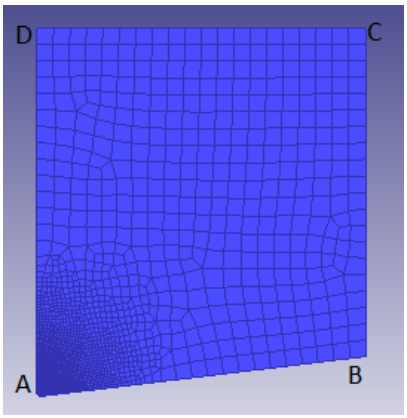

Figure 4. The boundary conditions of the cutting part of the tool

The dimensions of the work item used in the numeric simulation are shown in figure 5.

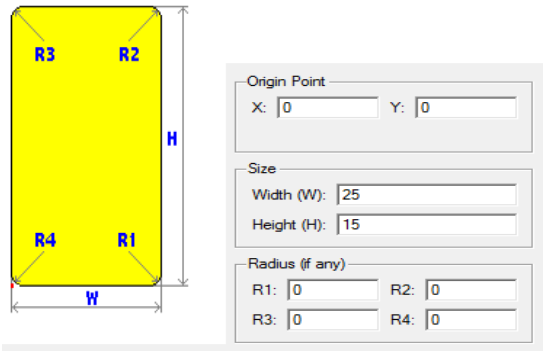

Figure 5. Dimensions of work item

The selected material of the work item is AISI 1025 steel. Properties of AISI 1025 steel are shown in table 2.

Table 2. Properties of AISI 1025 Steel

Density	7,85 g/cm^3
Hardness	145 Knoop
Elastic Modulus	190-210 GPa
Poisson ration	0,27-0,3
Thermal Conductivity	51,9
Tensile Strength	440 MPa
Yield Strength	370 MPa

The behavior of the material of the work piece is defined by Oxley's material model which includes two zones of deformation. The primary zone of deformation is parallel to the plane of shear. After the material reaches the plastic deformation in that area it continues the plastic deformation in a secondary zone, which is located between the front surface of the cutting part of the tool and the workpiece [7]. Oxley's material model, with simplified deformation zones, is shown in figure 6.

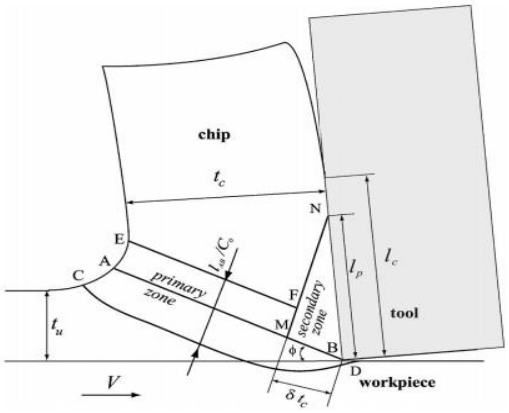

Figure 6. Oxley's material model

Boundary conditions for a workpiece are defined along the edges A-B, D-A where the temperature of the tool is defined as constant 22 ^{o} C. Along the edges B-C, C-D, the heat transfer is defined by convection. Apart from the boundary conditions that are related to temperature, the displacement boundary conditions are also defined. Along the edge A-B the speed of motion in the direction of the x axis is defined and a shift in the direction of the y axis is disabled. Boundary conditions which are defined for a workpiece are shown in figure 7.

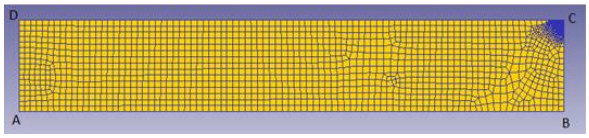

Figure 7. *Boundary conditions of the workpiece*

When generating the finite element mesh, DEFORM 2D uses iso-parametric rectangular two-dimensional finite elements [8]. In general, it is characteristically for iso-parametric finite elements to make a mapping of fixed finite elements, from the local coordinate system to different irregular final elements in the global coordinate system [9]. In places where large deformations are expected, a denser mesh is automatically generated. The finite element mesh model is shown in figure 8.

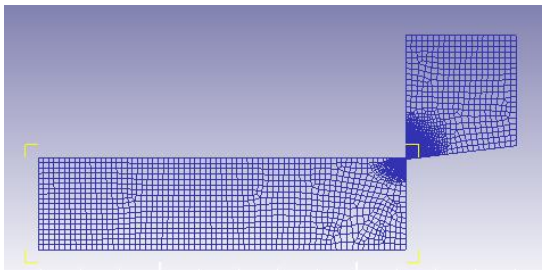

Figure 8. The finite element mesh

2.2. Design of Experiments

The experiments that are conducted in different engineering branches prove the different engineering assumptions and enrich the knowledge of engineers in certain areas. Therefore, the results of the experiments have great influence on the properties of the new products as well as the optimization of the processes with large investments of time and money. Today, by using different methods of planning the experiment, one can significantly increase the efficiency of it and come to essential conclusions in shorter time periods [10]. In this article the Taguchi method of the experiment plan was used which is based on the orthogonal array. It is therefore necessary to define the input variables (factors) and the level at which the input variables are observed. It is presented in table 3.

Table 3. Input variables (factors) and their levels

Factor/ Level	Cutting Speed (m/min)	Feed Rate (mm/rev)	Depth of a cut (mm)
Low	350	0,08	0,2
Medium	415	0,1	0,85
High	480	0,15	1,5

Preparation of the Taguchi orthogonal array was performed in software Minitab 17.1.0.0. and it is displayed in the table 4.

Table 4. Taguchi orthogonal array

Number of numerical simulation	Cutting Speed (m/min)	Feed Rate (mm/rev)	Depth of a cut (mm)
01	350	0,08	0,2
02	350	0,1	0,85
03	350	0,15	1,5
04	415	0,08	0,85
05	415	0,1	1,5
06	415	0,15	0,2
07	480	0,08	1,5
08	480	0,1	0,2
09	480	0,15	0,85

Using the ANOVA analysis in Minitab software 17.1.0.0 the impact of observed input variables to the output value is defined.

3. RESULTS AND ACHIEVEMENTS

This section presents the results of numerical simulations of the default processing parameters. Based on Taguchi orthogonal matrix, a number of numerical simulations were carried out, where the observed value of the cutting part of the tool was temperature.

3.1. Result of numerical simulation

Numerical simulation was carried out through 500 time steps. Damage factor is used for the prediction of ductile fracture in the material of the workpiece and increases as the material is deformed. When the damage factor reaches its critical value, a fracture occurs, ie. the formation of separate particles. The critical value of damage factors must be determined by an experiment. an experiment. During the numerical simulation, the value factors of damage are estimated for each element of the work item, at each time step. The occurrence of fracture, when turning on a lathe in software DEFORM 2D, is based on deleting elements that have reached the critical value of damage factors. To limit the loss of volume, it is necessary to define a dense network of finite elements in the area where the fracture is expected. Continuous deletion of critical elements achieves the initiation and propagation of cracks. [5] The accumulation of damage is presented on figure 9.

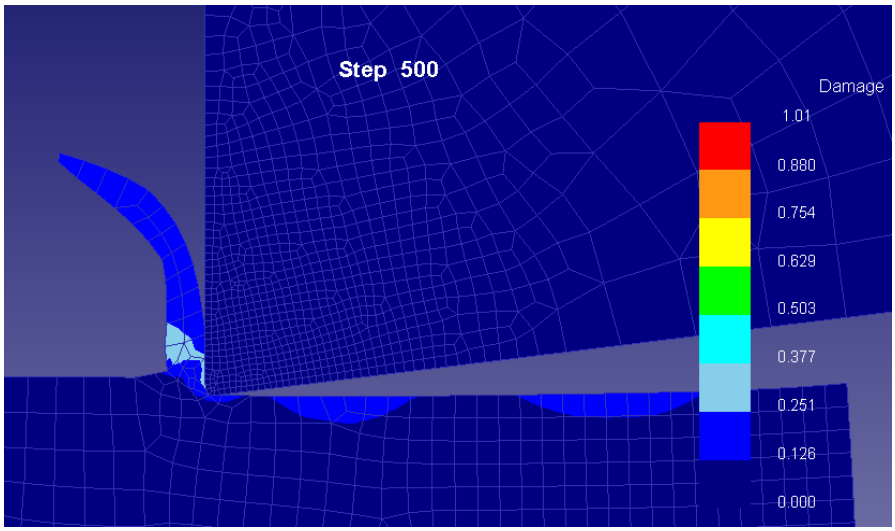

Figure 9. The accumulation of damage

Equivalent stress in DEFROM 2D is based on strength theory HMH [5]:

$$\bar{\sigma} = \frac{1}{\sqrt{2}} \times \sqrt{(\sigma_1 - \sigma_2)^2 + (\sigma_2 - \sigma_3)^2 + (\sigma_3 - \sigma_1)^2} \quad (1)$$

The maximum stress is expected in the processed shear zone and it is shown on figure 10. The value of maximum stress is 1390 MPa.

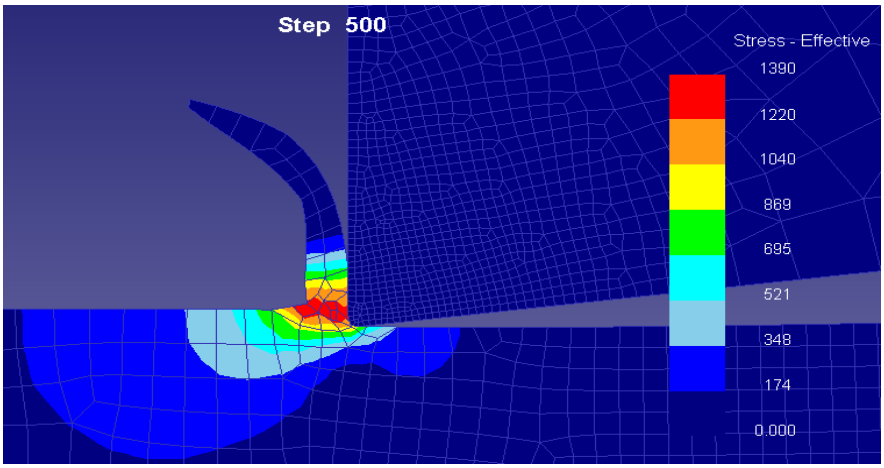

Figure 10. Stress in the system tool-workpiece

The pressure occurs due to contact of the work item and tool, expressed in MPa. For pressure can be said that it represents a force that acts on the unit area which connects the bodies in contact. The maximum pressure calculated in the numerical simulation is 1 MPa and it is presented on figure 11.

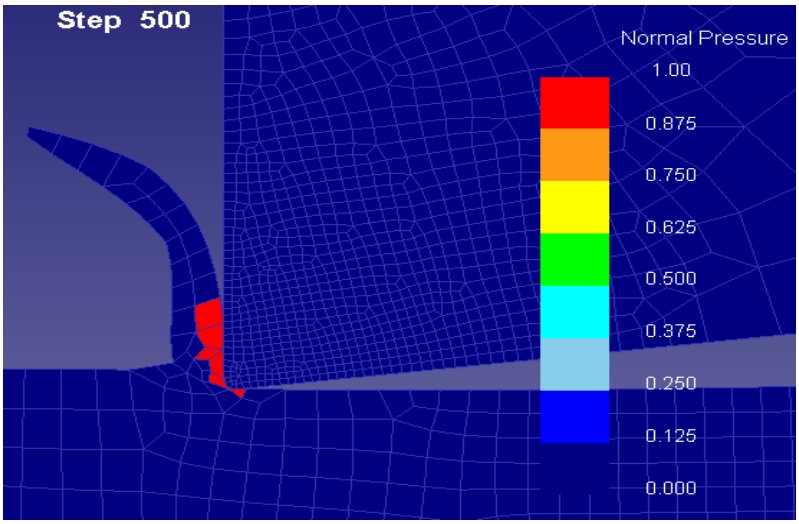

Figure 11. The pressure in the system tool-workpiece

Maximum temperatures that occur when processing on a lathe are to be found in the contact zone between the tool and the workpiece as shown in figure 12. Temperatures are expressed according to the SI system, and are in ° C.

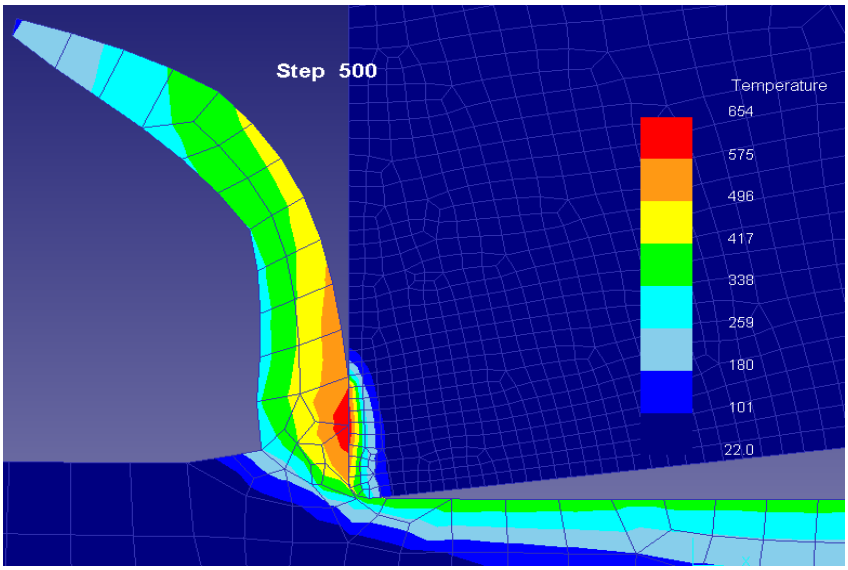

Figure 12. Temperature in system tool-workpiece

It is useful to display the temperature also with the use of isotherms. Assuming that the maximum spending will be on the site of maximum temperatures, zones of wear of the tool can be assumed also. The distribution of the temperature displayed by using isotherms on the cutting part of the tool is shown in figure 13.

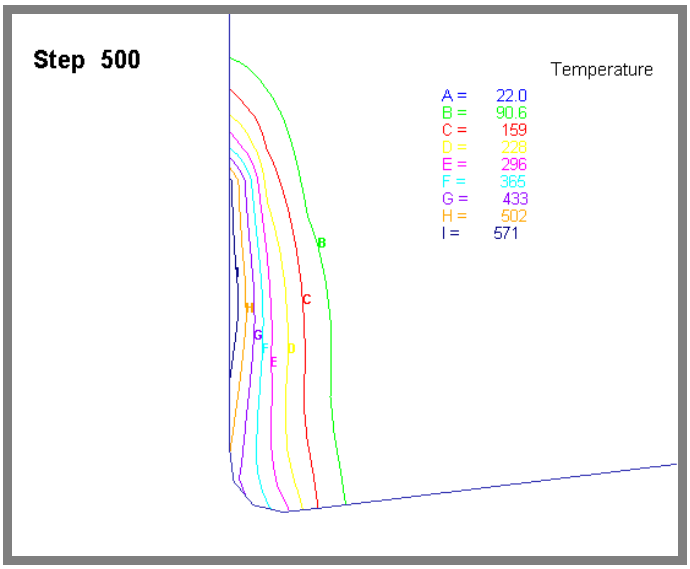

Figure 13. The distribution of temperature on the cutting part of the tool

3.2. Result of design of experiment

With regard to the Taguchi plan experiment, numerical simulation were performed in DEFORM 2D. Since the observed output value is the temperature of the cutting part of the tool in a contact zone, the results obtained by numerical simulations are shown in the table. Observed output value was calculated with different number of finite elements and showed in table 5. Temperature T_1^* is the temperature on the cutting part of the tool with a mesh of 1500 finite elements, temperature T_2^* is the temperature on the cutting part of the tool with a mesh of 1700 finite elements, temperature T_3^* is the temperature on the cutting part of the tool with a mesh of 1900 finite elements.

Table 5. Temperature on the cutting part of the tool

Number of numerical simulation	Input Factors			Output Factors		
	Cutting Speed (m/min)	Feed Rate (mm/rev)	Depth of a cut (mm)	Temperature T_1^* (°C)	Temperature T_2^* (°C)	Temperature T_3^* (°C)
01	350	0,08	0,2	530	531	514
02	350	0,1	0,85	566	543	540
03	350	0,15	1,5	604	620	599
04	415	0,08	0,85	577	565	555
05	415	0,1	1,5	581	586	606
06	415	0,15	0,2	649	656	647
07	480	0,08	1,5	554	570	543
08	480	0,1	0,2	584	584	605
09	480	0,15	0,85	667	667	680

Taguchi plan of experiments allows the analysis of the impact of changes in input variables on their levels on the response of the process, and it is defined by using a signal-to-

noise ratio (S/N) [10]. Since the goal is trying to achieve a minimum heating of tools, the signal-to-noise ratio is defined as Less is better. The minimum temperature of the cutting part of the tool, ultimately means less wear of the tool which saves money for the manufacturer and extends the service life of the tool.

It is necessary to determine the middle values for S/N ratios for each input variable, on the corresponding levels. The middle values for S/N ratios for each input variable on certain levels are shown in the table 6. The highest middle value of S/N ratios are for the cutting speed $350\ m/min$, feed rate 0,08 mm/revolution, the cutting depth 1,5 mm.

Table 6. The mean values for S/N ratios

Level	Cutting Speed	Feed Rate	Depth of a cut
1	-54,96	-54,78	-55,37
2	-55,58	-55,22	-55,47
3	-55,62	-56,16	-55,34
Delta	0,66	1,38	0,13
Rank	2	1	3

This means that those are the parameters which will ensure the minimum temperature of the cutting part of the tool, ie. these are the optimal parameters of processing. The specified cutting speed of $350\ m/min$, feed rate of 0,08 mm/revolution are present in the first numeric simulation defined according to Taguchi's plan of an experiment, while the cutting depth for the first numeric simulation is somewhat different from the optimum values of the cutting depth.

The graphic in figure 14 shows the mean values of S/N ratios for input variables and their levels.

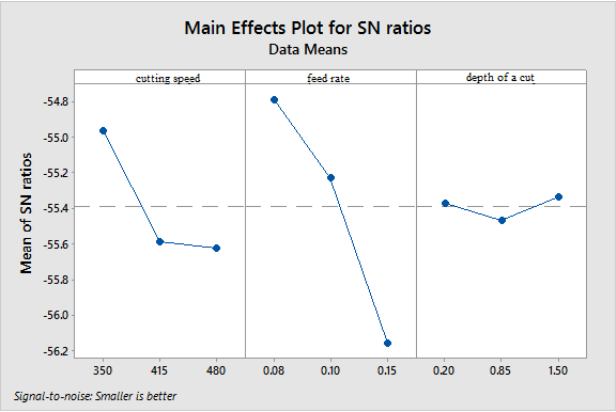

Figure 14. The mean values for S/N ratios

To prove optimal conditions of processing, it is necessary to make a numerical simulation with optimal processing parameters, which, in this case, represents the so-called "the attempt of certificate" and it is presented in table 7.

Table 7. The attempt of the certificate

Cutting speed	350 m/min
Feed Rate	0,08 mm/rev
Depth of a cut	1,5 mm
Temperature T_1^*	511 °C
Temperature T_2^*	531 °C
Temperature T_3^*	514 °C

Using analysis of variance in the Minitab17 computer program, a linear regression model is analyzed that shows the influence of the input variables on the temperature of the cutting part of the tool, based on the plan of experiments L27. It is necessary to explain the concept of variance, a variance is the sum of the average square deviation of individual values from the arithmetic middle [11]. A particular regression model is used to define the relationship between the input and output variables [11]. It is important to mention the coefficient of determination (R^2) that should be as close to 100%. Given the coefficient of determination, one can determine the correlation coefficient (R) which should be contained in the interval $-1 \le R \le 1$. High values of the coefficient of determination are pointing to a strong connection between the input and output variables (response). Results of analysis of variance are given in table 8.

Table 8. Results of analysis of variance

Source	DF	Adj SS	Adj MS	F-value	P-value
Regression	3	51521,2	17173,7	72,96	0,000
Cutting speed	1	9202,7	9202,7	39,10	0,000
Feed rate	1	42242,5	42242,5	179,46	0,000
Depth of the cut	1	76,1	76,1	0,32	0,575
Error	23	5413,9	235,4		
Total	26	56935,2			

Based on the above mentioned values, it can be seen that the feed rate affects the temperature of the cutting part of the tool to the fullest extent, then the cutting speed, and at least the cutting depth.

The influence of input variables to the output variable can be presented by the equation:

$$\text{Temperature} = 300{,}3 + 0{,}3479 \times \text{Cutting Speed} + 1344 \times \text{Feed Rate} - 3{,}16 \times \text{Depth of a cut} \quad (2)$$

It is necessary to say that the input parameter depth of a cut, which is required by the software, doesn't have any significant influence on the orthogonal turning with plain strain settings. Because of orthogonal turning, depth of a cut can be considered as a constant and its influence is negligible.

4. CONCLUSION

This article shows the numerical simulation of orthogonal turning on the assumption of the status of plane strain deformation in a computer program DEFORM 2D. The presented model, as a result of the numerical simulation can define stresses, temperatures that are generated during the simulation, the pressure in the contact area of the tool and the workpiece and many other significant output values.

The geometry of the model can be made in another computer program, but it must be saved as *.dxf format, so the format could be used in the software DEFORM 2D. While defining the mesh of the finite element method, the length of the final edge of the element for the defined mesh of the workpiece depends largely on the value of feeding. When creating a simulation, it is observed that the value of the length of the final edge of the element needs to be about one half the feed value or less. For the defined parameters of processing, output values are calculated with the numerical simulation and are observed in the sequel.

The maximum stress occurs in the shear zone of the workpiece in the amount of 1390 MPa. Pressure that occurs on the contact surfaces between the cutting part of the tool and the work piece is 1 MPa. The maximum temperature in the contact zone is 654 ºC. On a separated particle from the workpiece high temperatures can be seen (330 ° C – 500 ° C) which allows a big heat exhaust into the environment, and therefore less wear of the tool.

Special attention is paid to the temperature of the cutting part of the tool, as it largely affects the wear of the tool. Given that, Taguchi plan experiment is defined for the parameters of the processing, and is defined by an orthogonal matrix with respect to the output value of the temperature of the cutting part of the tool calculated by the numerical simulation. Using the ANOVA analysis the influence of processing parameters on the temperature of the cutting part of the tool is defined.

Therefore, a numerical simulation is made, which confirms optimal conditions of processing: cutting speed of 350 m/min, feed rate of 0,08 mm/revolution and depth of a cut in value of 1,5 mm.

Using analysis of variance, based on the P-values, the significance of the influence of processing parameters is defined. Regression model shows the influence of processing parameters on the temperature of the cutting part

of the tool in the form of the equations from which it is evident that the greatest influence on the temperature of the cutting blade has a feed rate, then cutting speed and finally cutting depth.

5. REFERENCES

[1] A.Pavić,Technology-Machining. College of Karlovac, Karlovac, (2013). (e.g. in Croatian)

[2] P. De Vos; J.E. Stahl. Applied metal cutting physics – best practice. Fagersta, Sweden, (2016).

[3] C. Constantin; S.M., Croitoru; E.Strajescu. Fem tools for cutting process modelling and simulation. Journal Scientific Bulletin (2012), pp. 150-162.

[4] M. Skvaža; Z. Botak. Alati za obradu kod visokobrzinskih obrada. Technical Journal (2010), pp. 32. - 36. (e.g. in Croatian)

[5] J.Fluhrer. DEFORM TM 2D Version 8.1. User Manual. Columbus, Ohio, (2004).

[6] J. P. Davim. Machining of Hard Materials. London, Springer (2011).

[7] T.Ozel; E. Zeren. A Methodology to Determine Work Material Flow Stress and Tool-Chip Interfacial Friction Properties by Using Analysis of Machining. Journal of Manufacturing Science and Engineering (2006), pp. 119.-129.

[8] B. Sing: Modelling and simulation of metal cutting by finite element method. International journal of scientific processes research and application (2015), pp. 23.-31.

[9] J. Sorić. Finite element method . Zagreb, (2004). (e.g. in Croatian)

[10] M. Ukrainczyk. Planing Experiments in the Industry. Hrvatski časopis za prehrambenu tehnologiju, biotehnologiju i nutricionizam (2010), pp. 96.-105. (e.g. in Croatian)

[11] M.Šilj. Introduction in modern bussines statistic. Ekonomski fakultet u Mostaru, Mostar. (1998). (e.g. in Croatian)

Kerf Variation Analysing After Cutting With Abrasive Water Jet of a Steel Part

A. P. Basarman [a], D. Damjanovic [b], D. Kozak [c], M. Lobonțiu [d], N. Medan [e]

[a,d,e] Technical University Cluj Napoca, North University Center Baia Mare,

Dr. Victor Babeș Street 62A, 430083 Baia Mare, Romania

[b,c] Josip Juraj Strossmayer University in Osijek, Mechanical Engineering Faculty in Slavonski Brod, Croatia

Corresponding author: adrian.basarman@cunbm.utcluj.ro

Abstract:

The method of cutting materials using water jet is a method that is in full ascension regarding the level of usability in production. In order to have the adequate setup for water jet cutting on a certain system, the surface quality, the kerf aspect, the shape and respectively the form of the obtained part have to be researched and analyzed.This paper presents the results obtained after cutting one square shaped part, made of 1C45 material. In the study was analised both the inside and the outside of the cut, the kerf width, the aspect of the taper and the profile deviation.

Keywords: Abrasive Water Jet, Surface Quality, Surface Aspect, Kerf, Taper

1. INTRODUCTION

The water jet cutting method is a modern method for cutting materials. There is no relevant literature that specifies a formula for calculation of the stock left for machining for metallic parts. The cutting with abrasive water jet is like cutting with a bandsaw that uses a blade consisting of a continuous band of toothed metal rotating on opposing wheels to cut material. The only difference is that here, it has high pressure water with particles inside, instead of the metal cutting band.

This paper presents a continuation of a study started with the first steel piece cutted in the same principles but at different cutting speed. The first one was cut at 45 mm/min cutting speed [1], the present study was made at higher speed but same material and thickness.

In the process of cutting the materials using abrasive water jet, the surface resulted can be very rough or very fine, the difference between this would be the combination of the next variables:

-thickness of the steel part,

-hardness of the material,

-the water pressure used for cutting,

-the mixture between the water and the abrasive material,

-the type and quality of the abrasive particles,

-the cutting speed.

Researches in this field, regarding the water jet, have been made, by authors like Fowler [2] for the purpose of milling the surface of metal parts using this technology. Hloch et. al. [3], Hlaváček et. al. [4] and Valíček et.al. [5] researched the way of turning materials using abrasive water jet cutting method.

2. EXPERIMENTAL SETUP

2.1 The abrasive water jet (AWJ) cutting machine

The experiments were conducted using an abrasive water jet (AWJ) cutting machine - Bystronic ByJet Pro L - presented in Figure 1.

The advantage in using this method is that the cutting element is the abrasive water jet, not like the conventional cutting methods where there is contact of the tool with parts that needs to be cut, like the bandsaw.

Fig. 1. Bystronic ByJet Pro L

Another advantage of this method is that, during the cutting process the material is cooled down by the water, acting like a coolant liquid.

The abrasive water jet (AWJ) cutting machine has several components which are presented in Figure 2.

Fig. 2. Elements of the abrasive water jet machine

The components of the abrasive water jet (AWJ) machine are:

1) The catch tank,

2) The workpiece,

3) The cutting head,

4) Abrasive delivery system,

5) The motion system

6) Grill for supporting the parts

This abrasive water jet (AWJ) cutting machine is computer numerical controlled machine (CNC).

2.2 Preparation for experiments

In order to take notice of how the surface has modified after cutting, we had to analyse both, the interior and the exterior of the kerf, as presented in Figure 3. Furthermore, on that way, by measuring the kerf width, we can experimentally determine the stock left for machining, needed in order to have a correct and more accurate cut.

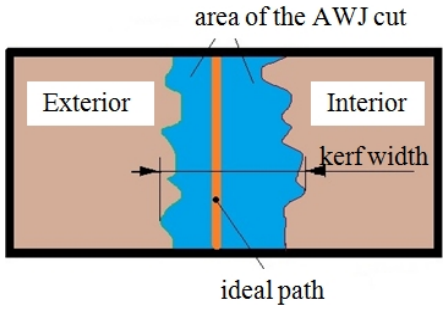

Fig. 3. The general aspect of the abrasive water jet cut

These experiments were performed on a 1C45 material plate with 20 mm of thickness. Figure 4 shows the dimensions of the part which is going to be cut out as well as the cutting plan.

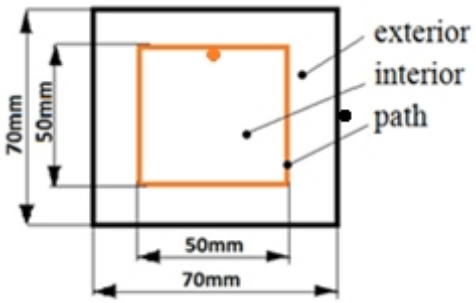

Fig 4. The design for cutting

From the list of cutting regimes offered by the machine, regarding the speed of cut, it was selected the next one after the one used in the previous study [1]. In present study the cutting speed was doubled.The selected parameters for cutting are presented in the Table1.

Table 1. The parameters used for the cutting regime

Parameters	Value selected
Breakthrough time	13 s
Breakthrough pressure	3600 bar
Abrasive material used	GMA Garnet 80 Mesh (300-150 micron)
Quantity of abrasive material	342 g/min
Cutting pressure	3600 bar
Cutting speed	95 mm/min
Interior sapphire nozzle	0,28 mm
Exterior nozzle	0,8 mm

2.3 Performing the experiments

The first step in performing the experiments is putting the steel part on the machine's grill support and fixing it down, using the machine's clamping system.

After this step, the program of cut is loaded in the software of the machine and the next step is selecting the regime of cutting, presented in Table 1.

After this, the part is being cut. The part that has been cut is presented right after cutting, still on the machine's grill support, in Figure 5, and after taking out of the base plate, in Figure 6.

Fig. 5. The part after cutting it with abrasive water jet (AWJ)

Fig. 6. The 1C45 steel part cut with abrasive water jet (AWJ)

2.4 Measuring the profile deviations of the part cutted using abrasive water jet (AWJ)

After cutting the steel part, for both parts resulted, as one can observe in Figure 6, each surface was measured separately and analysed one with each other, both for the interior and for the exterior of the cut.

Being a square part, that meant having four exterior surfaces (E1-4) and four interior surfaces (I1-4) which were analysed together (example- exterior E1 with interior I1), as shown on the Figure 7.

To determine the exact aspect of the surfaces, the surface was divided in three rows and measured using a 3D measuring arm, as presented in Figure 8. They were performed 10 measurements on each row, having a total of 30 points measured on a surface. Those values were set to be measured from the ideal path of cut, specified in the Figures 4 and 7.

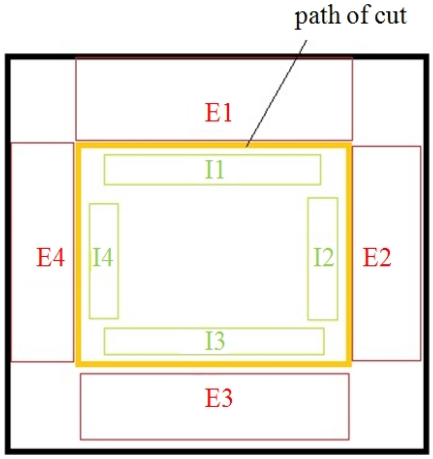

Fig. 7. The surfaces analysed after cutting

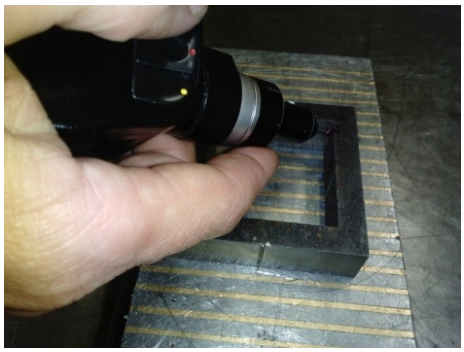

Fig. 8. Measuring the exterior surface cut by abrasive water jet

Table 2. Values measured on every surface on the steel part cutted using abrasive water jet (AWJ)

Area	*Part*	*Row*	*M 1*	*M 2*	*M 3*	*M 4*	*M 5*	*M 6*	*M 7*	*M 8*	*M 9*	*M 10*
I	Int	Up	0.885	0.905	0.915	0.922	0.946	0.880	0.866	0.873	0.877	0.892
		Mid.	0.809	0.804	0.804	0.804	0.849	0.795	0.766	0.764	0.766	0.781
		Down	0.707	0.675	0.677	0.687	0.761	0.673	0.651	0.662	0.565	0.678
	Ext	Up	-0.010	0.019	0.024	0.020	-0.001	-0.023	0.001	-0.001	0.001	-0.034
		Mid.	0.000	0.063	0.073	0.091	-0.004	-0.005	0.035	0.052	0.056	-0.022
		Down	0.015	0.089	0.100	0.132	-0.031	-0.006	0.064	0.052	0.115	-0.040
II	Int	Up	0.900	0.877	0.894	0.885	0.884	0.877	0.907	0.874	0.877	0.900
		Mid.	0.875	0.815	0.807	0.820	0.814	0.829	0.807	0.822	0.814	0.883
		Down	0.893	0.781	0.768	0.824	0.774	0.823	0.821	0.821	0.783	0.844
	Ext	Up	0.005	-0.003	-0.010	-0.027	-0.020	-0.028	-0.023	-0.005	0.013	-0.015
		Mid.	0.088	0.163	0.112	0.128	0.121	0.139	0.133	0.107	0.131	0.088
		Down	0.201	0.264	0.254	0.242	0.258	0.241	0.246	0.240	0.251	0.224
III	Int	Up	0.860	0.834	0.832	0.832	0.826	0.829	0.829	0.831	0.846	0.876
		Mid.	0.927	0.883	0.866	0.853	0.865	0.864	0.860	0.857	0.883	0.933
		Down	0.996	0.924	0.947	0.921	0.948	0.919	0.923	0.908	0.908	0.995
	Ext	Up	-0.088	0.004	-0.015	-0.026	-0.047	-0.029	-0.051	-0.003	-0.050	-0.033
		Mid.	0.086	0.200	0.190	0.200	0.202	0.182	0.170	0.198	0.166	0.131
		Down	0.316	0.387	0.443	0.390	0.362	0.362	0.419	0.412	0.403	0.369
IV	Int	Up	0.801	0.802	0.751	0.787	0.798	0.761	0.778	0.781	0.781	0.778
		Mid.	0.626	0.587	0.562	0.576	0.559	0.547	0.554	0.559	0.524	0.604
		Down	0.418	0.352	0.359	0.378	0.345	0.304	0.351	0.365	0.313	0.431
	Ext	Up	-0.096	-0.064	-0.066	-0.071	-0.079	-0.069	-0.085	-0.089	-0.084	-0.123
		Mid.	-0.119	-0.099	-0.091	-0.086	-0.075	-0.080	-0.096	-0.087	-0.123	-0.160
		Down	-0.207	-0.209	-0.192	-0.171	-0.202	-0.175	-0.197	-0.201	-0.174	-0.273

3. ANALYSING THE RESULTS

After measuring every surface, the values were presented both, referring to the ideal path of cut, both on each side of the path in some cases, as presented in Table 2, some of the values resulted, were negative.

Regarding the kerf width, the values from each side of the ideal path were summed together, to form the resulted measurement of the kerf width and the values are presented in the Table 3.

The values presented in Table 3 are correspondent directly proportional with the kerf width. After analysing the values, one can observe that the *smallest kerf width* from all the surfaces analysed is *0,450 mm* and the *biggest kerf width* is *0,948 mm*.

4. ANALYSING THE ASPECT OF SURFACE

Because the part was cut with the same cutting parameters on every surface, the values should be approximately the same so we will only present two cases:

-*first one* - when the cutting head moved longitudinally

-*second one*- when the cutting head moved transversally.

In this case, regarding the order of cut presented in Figure 7, surface 1 and 2 are taken for analysis.

In Figure 9 it can be seen the aspect of the cut, and also of the surfaces, both for the interior of the cut and also for the exterior. One can see that the surface is not straight, presents a V shape taper which slides in one direction, towards the exterior and the lines have an irregular and very sharp aspect.

Putting the values together, it was generated the aspect of the width of cut, shown in the Figure 10.

Table 3. The value of the kerf width on every surface

Area	Row	M 1	M 2	M 3	M 4	M 5	M 6	M 7	M 8	M 9	M 10
I	Up	0.895	0.886	0.891	0.902	0.947	0.903	0.865	0.874	0.876	0.926
	Mid.	0.809	0.741	0.731	0.713	0.853	0.800	0.731	0.712	0.710	0.803
	Down	0.692	0.586	0.577	0.555	0.792	0.679	0.587	0.610	0.450	0.718
II	Up	0.895	0.880	0.904	0.912	0.904	0.905	0.930	0.879	0.864	0.915
	Mid.	0.787	0.652	0.695	0.692	0.693	0.690	0.674	0.715	0.683	0.795
	Down	0.692	0.517	0.514	0.582	0.516	0.582	0.575	0.581	0.532	0.620
III	Up	0.948	0.830	0.847	0.858	0.873	0.858	0.880	0.834	0.896	0.909
	Mid.	0.841	0.683	0.676	0.653	0.663	0.682	0.690	0.659	0.717	0.802
	Down	0.680	0.537	0.504	0.531	0.586	0.557	0.504	0.496	0.505	0.626
IV	Up	0.897	0.866	0.817	0.858	0.877	0.830	0.863	0.870	0.865	0.901
	Mid.	0.745	0.686	0.653	0.662	0.634	0.627	0.650	0.646	0.647	0.764
	Down	0.625	0.561	0.551	0.549	0.547	0.479	0.548	0.566	0.487	0.704

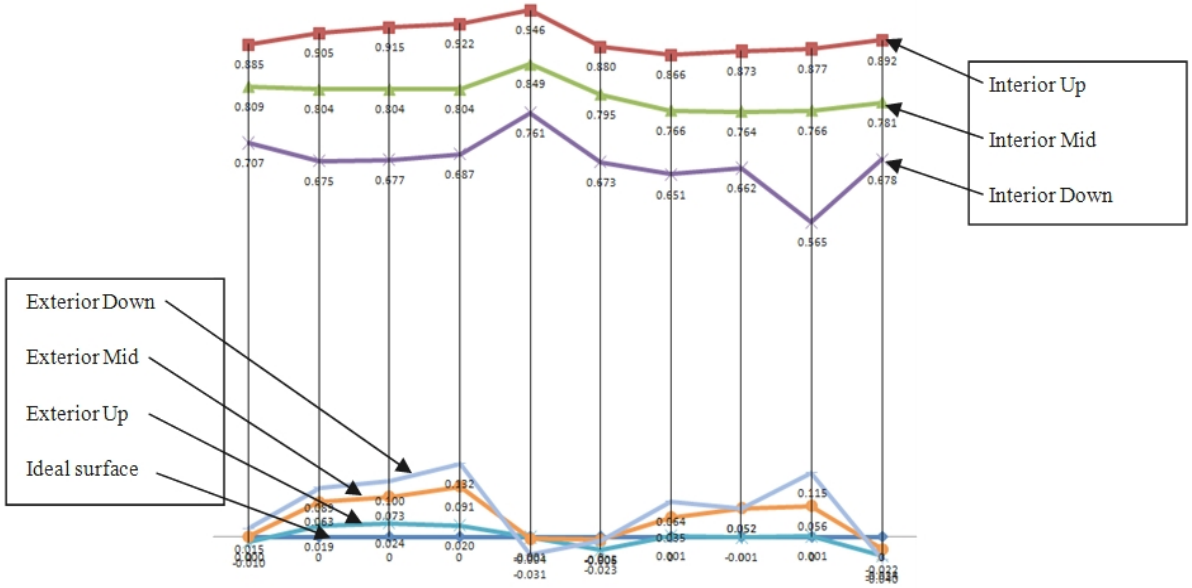

Fig. 9. Top view for the aspect of the surface I

As it can be observed in Figure 10, the bulging aspect of the surface is accentuated in the middle and even more up in the corners and the more different is measurement 9 which is opposite to measurement 5. The aspect from the corners may result because of the machine error while switching the movement direction from one axis to another. The *smallest kerf width* resulted here is *0,450mm* and the *biggest kerf width* is *0,947 mm.*

Analysing the next surface, presented in Figure 11, similar aspects can be seen, like in the ones in Figure 9.

As one can see, in Figure 11, it can be observed a little difference from the surface I. The exterior surface is more straight but presents also a V shaped taper, and in this case, the sliding is towards the interior. On Figure 12 one can observe the kerf width for the second surface.

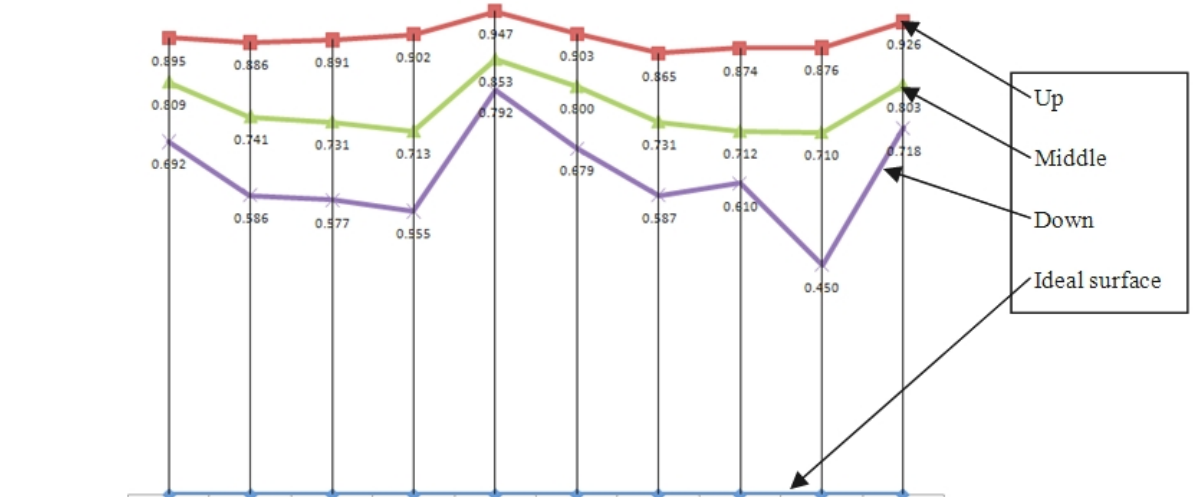

	1	2	3	4	5	6	7	8	9	10
Ideal surface	0	0	0	0	0	0	0	0	0	0
Up	0.895	0.886	0.891	0.902	0.947	0.903	0.865	0.874	0.876	0.926
Middle	0.809	0.741	0.731	0.713	0.853	0.800	0.731	0.712	0.710	0.803
Down	0.692	0.586	0.577	0.555	0.792	0.679	0.587	0.610	0.450	0.718

Fig. 10. The width of cut for surface I

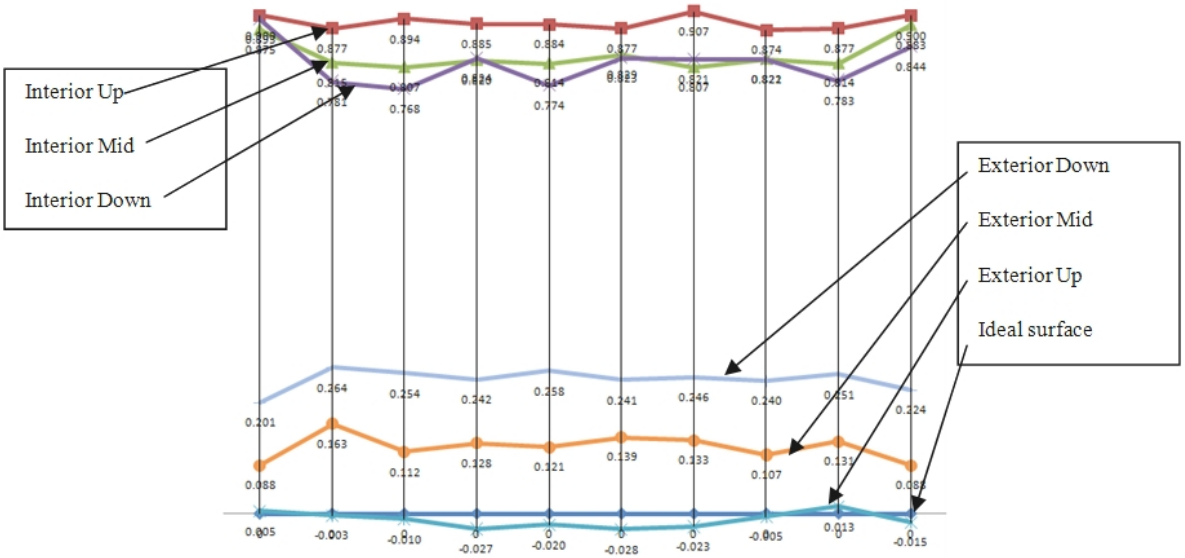

Fig 11. Top view for the aspect of the surface II

As it can be observed in Figure 12, the surface has the same bulging aspect in the middle and more up in the corners because the water jet kicked back, and also that the surface has the same irregular shape, but not as irregular as surface I. The *smallest kerf width* resulted here is *0,514 mm* and the *biggest kerf width* is *0,930 mm*.

This confirms that the error of the machine is the one causing this while it's switching the movement direction from one axis to another, but taking a look at the values of the kerf width on both surfaces analyzed, the difference between the values is not very big. In order to verify this hypothesis more experiments are required, with different speeds and different thicknesses.

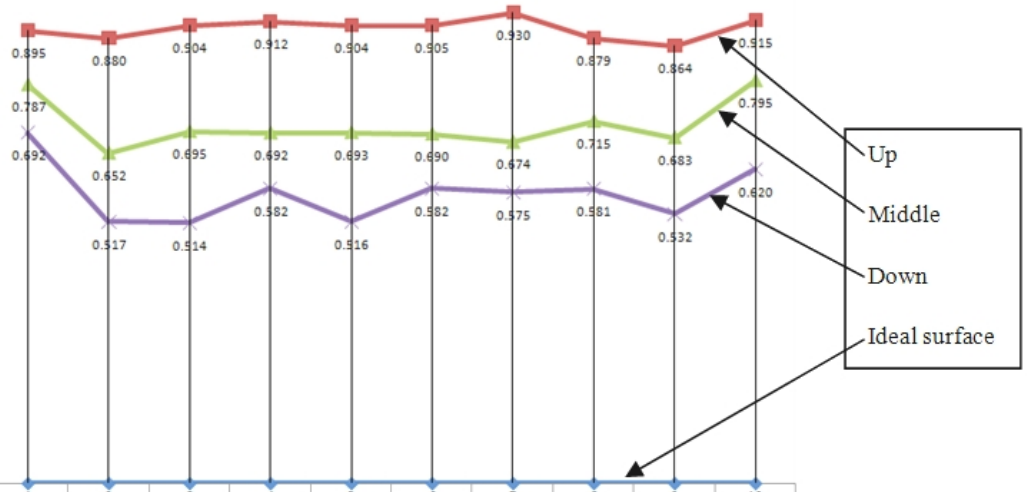

	1	2	3	4	5	6	7	8	9	10
Suprafata ideala	0	0	0	0	0	0	0	0	0	0
SUS	0.895	0.880	0.904	0.912	0.904	0.905	0.930	0.879	0.864	0.915
MIJLOC	0.787	0.652	0.695	0.692	0.693	0.690	0.674	0.715	0.683	0.795
JOS	0.692	0.517	0.514	0.582	0.516	0.582	0.575	0.581	0.532	0.620

Figure 12. The width of cut for surface II

5. CONCLUSIONS AND FUTURE DIRECTION OF RESEARCH

After analysing the results of the described experiments, it can be concluded:

1)The surface aspect has a slight deviation of profile because of the error of the machine, depending of the direction of moving,

2)The maximum stock needed to be left for machining with abrasive water jet (AWJ) is *0,948 mm* for a *20 mm* thickness steel *1C45* part, cutted at a speed of 95mm/min,

3)The aspect of the surface after cutting it with abrasive water jet (AWJ) has V-shape tapper that tends to narrow down as the speed increases, compared to the other study [1].

As direction of further research, the following can be considered:

1)Repeating the experiment for other materials or/and thicknesses,

2)Changing the cutting regimes and comparing the results,

3)Making a 3D version of the aspect of the surface out of all the points for better visualising the inclination of the surfaces.

6. REFERENCES

[1] A.P. Basarman, M. Lobontiu, Analyse of the kerf variation for abrasive water jet (AWJ) cutting of steel. Nonconventional Technologies Review, XX(2), (2016), pp.10-16

[2] G. Fowler, Abrasive water jet: controlled depth milling of titanium alloys, Phd. Thesis, University of Nottingham, (2003)

[3] S. Hloch, et al., Abrasive water jet (AWJ) titanium tangential turning evaluation, METALURGIJA, Vol.53, No.4, (2014), pp.537-540

[4] P. Hlaváček, et al., Sandstone Turning by Abrasive Water jet, Rock Mechanics and Rock Engineering, Vol. March, (2015), pp.1-5

[5] J. Valíček, et. al., Analogy between flexible abrasive water jet technology and traditional chip - Machining technology, Materialwissen-schaft und Werkstoff-technik, Vol.46, No.4-5,(2015), pp.401-413

Experimental determination of Tensile Strain-Hardening Exponent and Strength Coefficient of the S355J2+N steel grade

V. Milovanović [a], A. Dišić [b] G. Jovičić [c], M. Živković [d]

[a] Faculty of Engineering University of Kragujevac, Sestre janjić 6, 34000 Kragujevac, Serbia, vladicka@kg.ac.rs

[b] Faculty of Engineering University of Kragujevac, Sestre janjić 6, 34000 Kragujevac, Serbia, aleksandardisic@gmail.com

[c] Faculty of Engineering University of Kragujevac, Sestre janjić 6, 34000 Kragujevac, Serbia, gjovicic.kg.ac.rs@gmail.com

[d] Faculty of Engineering University of Kragujevac, Sestre janjić 6, 34000 Kragujevac, Serbia, miroslav.zivkovic@kg.ac.rs

Abstract

The purpose of this paper is to determine tensile strain-hardening exponent and strength coefficient of the S355J2+N steel grade utilizes stress-strain data obtained in a uniaxial tension test. Tensile data were obtained in continuous and rate-controlled manner via displacement control. Ramberg-Osgood relationship was used to describe the uniaxial tension behaviour of the S355J2+N steel grade. The tensile strain-hardening exponent and strength coefficient are determined from an empirical representation over the relation between the true-stress versus true-strain.

Keywords: strain-hardening exponent, strength coefficient, yield stress-strain

1. INTRODUCTION

It is well known that both the strain-hardening exponent and the strength coefficient are basic mechanical behaviour performance parameters of metallic materials. When the tensile properties of metallic materials are being evaluated, these two parameters must be known. The value of strain-hardening exponent gives measure of the material's work hardening behaviour and is usually between 0 and 0.5. Values of strength coefficient and strain-hardening exponent for some engineering alloys are given in [1].

There are many methods for determination strength coefficient and strain-hardening exponent. Theoretical calculation of the strain-hardening exponent and the strength coefficient of metallic materials were presented in [2]. Authors were obtained some theoretical results from the deduced expressions and compared with test data. Some authors investigated strain-hardening exponent with a new method named "Double Compression Test". The test was performed experimentally and the results were compared with those obtained by the conventional method [3]. Predicting work hardening exponent of engineering metals using

residual indentation profiles of nano-indentation were presented in [4].

Today steels represent the most used group of mechanical materials. Steels are used in various branches of industry for constructing bridges, buildings, ships, cars, rail vehicles, railways. There are several thousand types of steel obtained by an appropriate combination of carbon and alloying elements of different characteristics.

Because of good mechanical properties, good cutting, forming (forging, rolling, extrusion, pressing), good weldability and low prices, structural steels are widely used in industry. The most commonly used steel for producing carrying parts of structures, exposed to dynamic loads and low temperatures is medium-strength S355J2+N steel grade.

This paper presents determination of tensile strain-hardening exponent and strength coefficient of the S355J2+N steel grade utilizes stress-strain data obtained in a uniaxial tension test according to ASTM E646-00 [5].

2. THEORETICAL BASES

The uniaxial tension test is the most common method for determining the mechanical properties of materials, such as strength, ductility, toughness, elastic modulus, stress-strain behaviour and strain hardening capability. Uniaxial tension stress-strain properties are usually reported in handbooks and are used in many specifications. Stress-strain behaviour is obtained from uniaxial tension test where specimen with circular or rectangular cross section with the uniform gage length is subjected to increasing tensile force until it fractures.

When the load (force) is applied, the specimen elongates in proportion to the load, called linear elastic behaviour. If the load is removed, the specimen returns to its original length and shape.

As the load is increased, the specimen begins to undergo nonlinear elastic deformation at a stress called the proportional limit. At that point, the stress and strain are no longer proportional, as they were in the linear elastic region, but when unloaded, the specimen still returns to its original shape. Permanent (plastic) deformation occurs when the yield stress, of the material is reached.

Property of material that the increase of plastic deformation leads to an increase of yield strength is called work hardening. Knowledge of these property is very important to describe the behaviour of metals in the region of plasticity. In the plastic region, a commonly used relation to define the relation between stress and strain is given by equation:

$$\sigma = K\left(\varepsilon_p\right)^n, \tag{1}$$

where K is strength coefficient and n strain hardening coefficient.

According to equation (1) and relation that the total strain equals the sum of the elastic and plastic strain and in the region of elasticity Hooke's law is valid, equation for total strain can be derived. Equation (2) represents analytical true stress – true strain relationship, often referred to as the "Ramberg-Osgood relationship" [1], [6], [7], [8]:

$$\varepsilon = \frac{\sigma}{E} + \left(\frac{\sigma}{K}\right)^{\frac{1}{n}}. \tag{2}$$

In equations (1) and (2) σ and ε represent true stress and true strain. True strain is the natural logarithm of the ratio of instantaneous length, l, to the original gage length l_0 that is:

$$\varepsilon = ln\left(\frac{l}{l_0}\right) = \ln\left(1+e\right). \tag{3}$$

True stress is the instantaneous normal stress, calculated on the basis of the instantaneous cross-section area, A, that is:

$$\sigma = \frac{F}{A} = S\left(1+e\right). \tag{4}$$

In equation (3) e represent engineering strain – dimensionless value that is the change in length Δl per unit length of original linear dimension l_0 along the loading axis of specimen:

$$e=\frac{l-l_0}{l_0}=\frac{\Delta l}{l_0}. \quad (5)$$

In equation (4) S represent engineering stress – the normal stress, expressed in units of applied force, F, per unit of original cross-section area, A_0:

$$S=\frac{F}{A_0}. \quad (6)$$

3. EXPERIMENTAL PROCEDURE

Experimental determination of tensile strain-hardening exponent and strength coefficient of the S355J2+N steel grade, was done on SHIMADZU Servopulser EV101K3-070-0A [9] (Figure 1.).

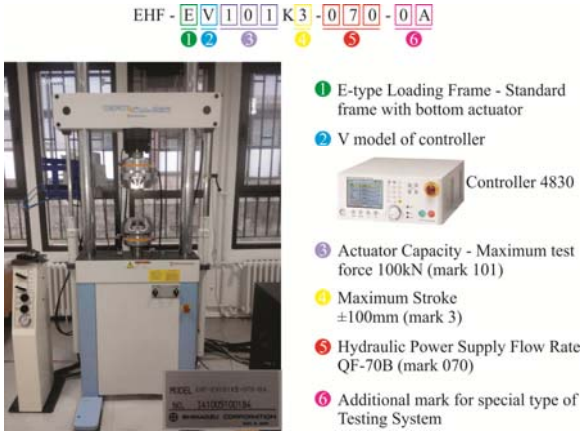

Fig. 1. SHIMADZU Srevopulser EHF-EV101K3-070-0A

Experimental determination of tensile strain-hardening exponent and strength coefficient of the S355J2+N steel grade was done at room temperature ambient (23±5ºC) under static loading conditions.

The shape and dimensions one of tested specimens are shown on Figure 2., in accordance with standard ASTM E646-00 [5].

In preparing the specimens, it is necessary to make a representative specimen, which is flat and the same thickness in all cross sections. Especially attention should be paid to prevent of appearance any possible residual stresses.

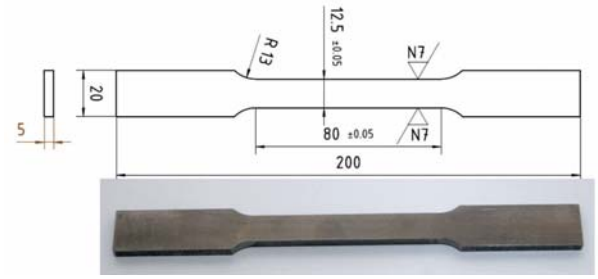

Fig. 2. Specimen for determining Tensile Strain-Hardening Exponent and Strength Coefficient

Testing of specimens for determining tensile strain-hardening exponent and strength coefficient were done at room temperature ambient in stroke control, without change speed of testing, during the strain interval over which n was determined (region of plasticity). Rate of speed load is 4mm/min.

For the purpose of measurement of elongation, on gage length (50mm), extensometer Mess & Feinwerktechnic GmbH MFA25 was used (Figure 3.).

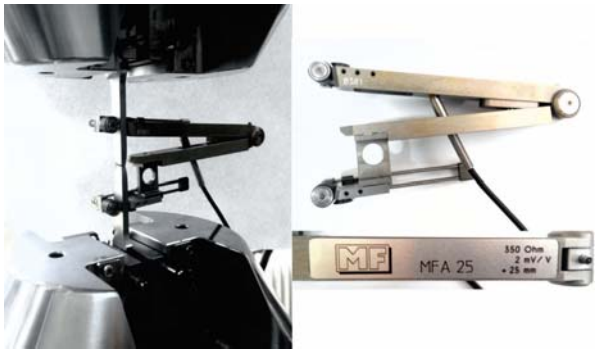

Fig. 3. Extensometer MFA25

4. RESULTS AND DISCUSSION

Load-engineering strain diagram, with data-pairs, for determination of tensile strain-hardening exponent and strength coefficient of the S355J2+N steel grade is shown on Figure 4. Measured values of force and corresponding values of engineering strain into nine equal intervals in the plastic region, obtained during the tests procedure are shown in Table 1.

All other parameters necessary for the further determination of tensile strain-hardening exponent and strength coefficient could be obtained based on the values of force and elongation. Values of engineering and true stress

and engineering and true strain can be determined from the equations (6), (4), (5) and (3), respectively.

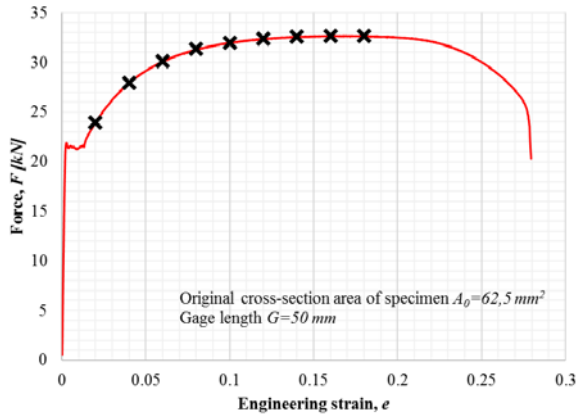

Fig. 4. Load-engineering strain diagram with data-pairs (S355J2+N)

For determination of tensile strain-hardening exponent n and strength coefficient K it necessary logarithmic form of the equation (1). Logarithmic form of the power curve representation of the true-stress versus true-strain curve within region of plasticity is given by:

$$\log\sigma = \log K + n\log\varepsilon\,. \tag{7}$$

According to selected data-pairs and calculated logarithm values of true-stress ($\log\sigma$) and true strain ($\log\varepsilon$), via linear regression analysis, tensile strain-hardening exponent n can be determined by

$$n = \frac{N\sum_{i=1}^{N}\left(\log\varepsilon_i \log\sigma_i\right) - \left(\sum_{i=1}^{N}\log\varepsilon_i \sum_{i=1}^{N}\log\sigma_i\right)}{N\left(\log\varepsilon_i\right)^2 - \left(\sum_{i=1}^{N}\log\varepsilon_i\right)^2}, \tag{8}$$

where N represents number of data-pairs.

Equation (8) are made convenient by symbolic representation for: $Y=\log\sigma$, $X=\log\varepsilon$ and $b=\log K$, as follows:

$$n = \frac{N\Sigma XY - \Sigma X\Sigma Y}{N\Sigma X^2 - \left(\Sigma X\right)^2}\,. \tag{9}$$

Strength coefficient K can be determined by:

$$K = 10^b\,, \tag{10}$$

where

$$b = \frac{\Sigma Y}{N} - n\frac{\Sigma X}{N}\,. \tag{11}$$

All test results for experimental determination of tensile strain-hardening exponent and strength coefficient of the S355J2+N steel grade are shown in Table 1. According to previously derived equations, experimentally obtained results of test and via linear regression analysis tensile strain-hardening exponent and strength coefficient were determined. Procedure of their determination were summarized in algorithm and given in Table 2.

Table 1 Determination of *the Strain Hardening Exponent and Strength Coefficient – Testing Results*

Data pair	Load [*kN*]	S [*MPa*]	σ [*MPa*]	Y $\log_{10}\sigma$	Y^2	Δl [*mm*]	e	ε	X $\log_{10}\varepsilon$	X^2	XY
1	23.972	383.52	391.22	2.592	6.721	1	0.02	0.012	-1.703	2.901	-4.416
2	27.965	447.44	465.34	2.668	7.117	2	0.04	0.039	-1.407	1.978	-3.752
3	30.121	481.94	510.85	2.708	7.335	3	0.06	0.058	-1.235	1.524	-3.344
4	31.355	501.68	541.81	2.734	7.474	4	0.08	0.077	-1.113	1.240	-3.045
5	31.995	511.92	563.11	2.751	7.566	5	0.10	0.095	-1.021	1.042	-2.808
6	32.434	518.94	581.22	2.764	7.642	6	0.12	0.113	-0.946	0.894	-2.614
7	32.628	522.05	595.13	2.775	7.699	7	0.14	0.131	-0.883	0.779	-2.449
8	32.671	522.74	606.37	2.782	7.744	8	0.16	0.148	-0.829	0.686	-2.306
9	32.694	523.10	617.26	2.791	7.787	9	0.18	0.166	-0.781	0.610	-2.180

Table 2 Algorithm and Worksheet for Calculating the Strain Hardening Exponent and Strength Coefficient of steel S355J2+N grade

Marks:

X=log ε

Y=log σ

n – strain hardening coefficient

b – log of the strength coefficient

All data were taken from Fig. 4 and evaluated in Table 1. The number of data pairs is N=9. All logarithms are base10.

A. Ordering data from Table 1.

$$\Sigma X = \Sigma\left(\log \varepsilon_i\right) = -9.9169$$

$$\overline{X} = \frac{\Sigma X}{N} = \frac{-9.9169}{9} = -1.1019$$

$$\Sigma X^2 = \Sigma\left(\log \varepsilon_i\right)^2 = 11.6560$$

$$\Sigma Y = \Sigma\left(\log \sigma_i\right) = 24.5651$$

$$\overline{Y} = \frac{\Sigma Y}{N} = \frac{18.0788}{9} = 2.7295$$

$$\Sigma Y^2 = \Sigma\left(\log \sigma_i\right)^2 = 67.0826$$

$$\Sigma\left(X \cdot Y\right) = \Sigma\left(\left(\log \varepsilon_i\right) \cdot \left(\log \sigma_i\right)\right) = -26.9125$$

B. Determination of strain hardening exponent n

Step 1 $$\frac{\Sigma X \cdot \Sigma Y}{N} = \frac{-9.9169 \cdot 24.5651}{9} = -27.0677$$

Step 2 $$S_{XY} = \Sigma\left(X \cdot Y\right) - \text{Step 1} = -26.9125 - \left(-27.0677\right) = 0.1552$$

Step 3 $$\frac{\left(\Sigma X\right)^2}{N} = \frac{\left(-9.9168\right)^2}{9} = 10.9272$$

Step 4 $$S_{XX} = \Sigma X^2 - \text{Step 3} = 11.6560 - 10.9272 = 0.7288$$

Step 5 $$n = \frac{S_{XY}}{S_{XX}} = \frac{\text{Step 2}}{\text{Step 4}} = \frac{0.1552}{0.7288} = 0.2129$$

C. Determination of strength coefficient K

Step 6 $$n\overline{X} = 0.2129 \cdot \left(-1.1019\right) = -0.2346$$

Step 7 $$b = \overline{Y} - n\overline{X} = \overline{Y} - \text{Step 6} = 2.7295 - \left(-0.2346\right) = 2.9640$$

Step 8 $$K = 10^b = 10^{2.9640} = 920.4955\,\text{MPa}$$

The red line of stress-strain diagram on Figure 5 shows that the power function with determined tensile strain-hardening exponent and strength coefficient is a good approximation of the plastic portion of the curve true-stress versus true-strain obtained by experiment.

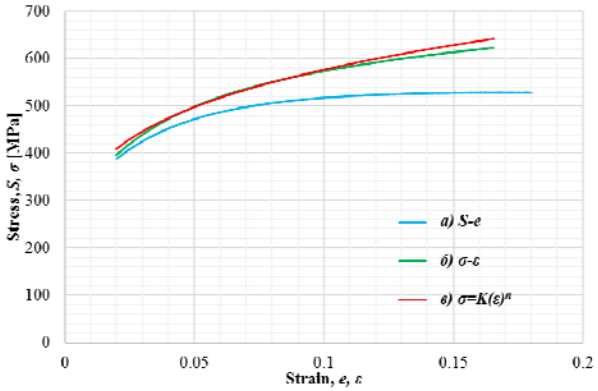

Fig. 5. Stress-strain diagram

5. CONCLUSIONS

This paper describes the determination of the tensile strain-hardening exponent and strength coefficient of the S355J2+N steel grade exhibiting a continuous stress-strain curve in the plastic region. The stress-strain data was obtained in a uniaxial tension test. The displacement was applied in a continuous and rate-controlled manner while the normal tensile load and strain are monitored. Based on obtained data and test results, true-stress and true-strain were calculated. According to ASTM E646-00 and calculated logarithm values of true-stress and true strain, via linear regression analysis, tensile strain-hardening exponent and strength coefficient were determined.

Results obtained by power function with determined tensile strain-hardening exponent and strength coefficient show good approximation of the plastic portion of the curve true-stress versus true-strain obtained by experiment. This results and their good matching give a good basis for further research and analysis.

6. ACKNOWLEDGEMENTS

The part of this research is supported by Ministry of Education, Science and Technological Development, Republic of Serbia, Grant TR32036.

7. REFERENCES

[1] R. Stephens, A. Fatemi, R. Stephens and H. Fuchs, Metal Fatigue in Engineering, New York: John Wiley & Sons Inc., (2001)

[2] Z. Zhang, Q. Sun, C. Li, and W. Zhao, Theoretical Calculation of the Strain-Hardening Exponent and the Strength Coefficient of Metallic Materials. Journal of Materials Engineering and Performance 15 (2006), pp 19-22

[3] R. Ebrahimi, N. Pardis, Determination of strain-hardening exponent using double compression test. Materials Science and Engineering A 518 (2009), pp. 56–60

[4] Byung-Min Kim, Chan-Joo Lee, and Jung-Min Lee, Estimations of work hardening exponents of engineering metals using residual indentation profiles of nano-indentation, Journal of Mechanical Science and Technology 24 (2010), pp.73-76

[5] ASTM: E646-00 Standard Test Method for Tensile Strain-Hardening Exponents (n-Values) of Methalic Sheet Materials, 2000.

[6] G. Jovičić, M. Živković and S. Vulović, Fracture and Fatigue Mechanics, Kragujevac: Faculty of Mechanical Engineering, University of Kragujevac, 2011. (in Serbian)

[7] O. H. Basquin, "The Exponential Law of Endurance Tests," *Proc. ASTM,* vol. 10, no. 11, p. 625, 1910.

[8] M. Živković, Nonlinear Analysis of Construction, Kragujevac: Faculty of Mechanical Engineering, University of Kragujevac, 2006. (in Serbian)

[9] SHIMADZU Servopulser Fatigue and Endurance Testing Systems

Specifics of the possible applications of polyester laminates considering mechanical properties

I. Opačak [a], I. Putnik [b], M. Samardžić [c], V. Marušić [d]

[a] Mechanical Engineering Faculty in Slavonski Brod, Trg I. B. Mažuranić 2, 35 000 Slavonski Brod, Croatia, iopacak@sfsb.hr

[b] Đuro Đaković Termoenergetska postrojenja d.o.o., Dr. Mile Budaka 1, 35 000, Slavonski Brod, Croatia, iputnik87@gmail.com

[c] Mechanical Engineering Faculty in Slavonski Brod, Trg I. B. Mažuranić 2, 35 000 Slavonski Brod, Croatia, msamardzic@sfsb.hr

[d] Mechanical Engineering Faculty in Slavonski Brod, Trg I. B. Mažuranić 2, 35 000 Slavonski Brod, Croatia, vmarusic@sfsb.hr

Abstract

This paper examines the possibility of applying polyester laminates with reinforced different layers of glass fibers concearning the mechanical properties. Test plates are made by impregnating reinforcing fibers with resin with the manual extrusion of air bubbles by rollers. Based on the results of strength test (interlayer, tensile and flexural), modulus of elasticity, toughness and share of inorganic matters, it was concluded that the mechanical properties of polyester laminates depend not only on the „composition“, but also cavities presenting themselves as no homogeneity in boundary matrix/reinforcement.

Keywords: polyester laminates, mechanical properties, glass fibers, porosity structure

1. INTRODUCTION

Polyester laminates are composites based on the unsaturated polyester resin reinforced with glass fibers. The application of glass fibers as reinforcement of composites enables production of composites having high specific strength [1]. These laminates are strong and rigid. By varying the number and arrangement of layers of reinforcing material, one can act on their mechanical properties.

Modifications with respect to number of layers of reinforcement as well as their redistribution and thickness create optimal conditions for achievement of highly improved properties [2, 3]. They are used in construction, food and the automotive industry, as well as in agriculture and production of vessel. In their application they are exposed to various strains, as well as to the impact of the environment. Research of the properties and damage of polyester laminates represents extremely complex and demanding field of study [4]. In the production of small number of pieces as a rule manual extrusion of air procedure applies, and for larger series more and more a new procedure (infusion under pressure lamination) called of injection pressing in vacuum („RTM procedure“ Resin Transfer Moulding) is used. In this paper we will examine the influence of the arrangement, type and number of reinforcing layers onto mechanical properties of polyester laminates produced by manual procedure of extrusion of air (by rollers).

These results should be helpfull in further research, conducted on laminates with the same reinforcement, but produced with RTM procedure.

2. COMPOSITION AND PREPARATION OF THE TEST PLATES FOR TESTING

For purpose testing seven polyester laminate plates is made. The dimensions of each plate were ~ 500x200 mm. Figure 1 schematically shows a system, or arrangement of reinforcing in a matrix the within plate cross section.

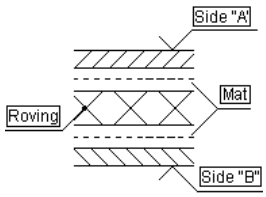

Fig. 1. Schematic representation of the arrangement reinforcement in the matrix per plates cross section

Extrusion of air was done manually, by rollers, Figure 2. There are two sides of plates: side „A“ which is rough and of polyester resin, and side „B“ which is smooth and shiny, and of polyester resin with additives („gel coat“) to achieve an aesthetic effect.

Fig. 2. The procedure of manual extrusion of air by rollers

Table 1. Standard tests and number of samples

No.	Norm	Properties	No. samples
1.	BS 2782 [5] Side „A“ and side „B“	Interlayer strength	5 + 5
2.	DIN 53453 [6] Side „A“ and side „B“	Testing toughness by Charpy 4 J, 4x6 mm	5 + 5
3.	DIN 53457 [7]	Tensile modulus of elasticity	3
4.	DIN 53455 [8]	Tensile strength	3
5.	DIN 53452 [9] Side „A“ and side „B“	Flexural strength	5 + 5
6.	DIN 52330 [10]	Content of inorganic matter	1

In order to check the influence of composition on the properties of the plates test samples are made. Properties and standard by which the test will be perfomed, and the number of test samples are shown in Table 1.

Composition of the test plates and their thicknesses are given in Table 2.

Table 2. The composition and thicknesses of the test plates of polyester

Composition of the plates					δ, mm
1 Resin	3x mat 450 g/m^2	2x mat 450 g/m^2	Gelcoat		3
2 Resin	2x mat 450 g/m^2	1x Roving 300 g/m^2	2x mat 450 g/m^2	G*	4
3 Resin	2x mat 300 g/m^2	Combimat	1x mat 450 g/m^2	G*	4
4 Resin	1x mat 450 g/m^2	2x Roving 300 g/m^2	1x mat 450 g/m^2	G*	3
5 Resin + calcite	3x mat 450 g/m^2	2x mat 450 g/m^2	Gelcoat		4
6 Resin + calcite	1x mat 450 g/m^2	2x Roving 300 g/m^2	2x mat 300 g/m^2	G*	4
7 SER**	2x mat 450 g/m^2	3x mat 450 g/m^2	Gelcoat		4

* Gelcoat; ** Self extinguishing resin

Figure 3.a shows the artificial boulder for climbing made of polyester laminates. Figure 3.b shows the horse trailer. These examples represent the products obtained by individual production. Due to the high cost of making the mold, it is most likely their production is more economical by application of a manual procedure of extrusion of air.

a) *b)*

Fig. 3. Boulder for climbing (a); horse trailer (b) [11]

Figure 4 shows the examples of polyester laminates for making the parts of the vehicle, exterior and interior. These examples represent the products obtained by serial production.

Within this type of production a new RTM procedure is being used increasingly.

a) *b)*

Fig. 4. Parts of the vehicle: a) exterior; b) interior [12]

An example in Figure 5.a shows tank made for use in the agriculture and food industry. An example of mechanically damaged tank successfully repaired by manual procedure is shown in Figure 5.b.

a) *b)*

Fig. 5. Repaired tank (a); detail of the repaired tank (b)

3. TEST RESULTS

After the samples are made from the plates, the two experiments in tests plan envisaged, were carried out as well as the structure cross section was captured.

Measurement of plates thicknesses and testing of share of inorganic materials (glass threads and fibers) in plates, was done previously, Table 3.

Table 3. Thickness of the plates and mass fraction of inorganic matter

No.	Content of inorganic matter, %	Thickness, mm
1.	49,49	3,8
2.	44,76	4,1
3.	42,06	4,2
4.	47,85	3,9
5.	51,49	4,2
6.	44,79	4,0
7.	44,65	4,8

3.1 Mechanical properties of the plates

After the tests were carried out calculated by the arithmetic mean of interlayer strength were shown in Table 4.

Table 4. The results of interlayer strength

No.	Interlayer strength, MPa	
	Side „A“	Side „B“
1.	21,9	23,7
2.	23,7	24,5
3.	16,8	19,8
4.	18,7	21,8
5.	24,9	25,1
6.	19,3	22,8
7.	15,0	18,2

Toughness test results are shown in Table 5.

Table 5. The results of toughness test

No.	Toughness, J/cm^2	
	Side „A“	Side „B“
1.	62	7,7
2.	76	9,2
3.	87	8,8
4.	77	11,5
5.	71	7,5
6.	77	8,9
7.	62	7,3

Test results of tensile strength and tensile modulus of elasticity examinations are shown in Table 6. The mean values have been obtained measured on the three samples.

The results of flexural strength tests are shown in Table 7. All tests were specifically carried out with respect to the side „A“, as well as the side „B“ of laminates.

Table 6. The arithmetic mean of the tensile strength and tensile modulus of elasticity

No.	Tensile strength, MPa	Tensile modulus of elasticity, MPa
1.	126,6	8803
2.	117,4	12073
3.	105,9	10916
4.	Without fracture	12791
5.	106,1	8734
6.	130,7	10101
7.	100,3	6083

Table 7. The results of flexural strength

No.	Flexural strength, MPa	
	Side „A“	Side „B“
1.	239,8	242,4
2.	251,1	239,5
3.	202,7	233,5
4.	247,1	291,0
5.	157,3	212,0
6.	209,0	175,2
7.	156,6	175,3

4. ANALYSIS OF THE RESULTS

In order to establish a relationship between the results of tests of mechanical properties and structure of laminate the recording of plates cross section has been carried out through use of light microscope under polarized light. These recordings should assist in the identification of defects in the structure or present irregularities at the reinforcement/matrix border which can indicate the reason for differences in mechanical properties among the plates.

Figure 6 shows slightly lower mechanical properties of the plate 3. The consequence is a smaller number of reinforcing layers, though the cross sectional structure shows the presence of the porosity in the form of cavities.

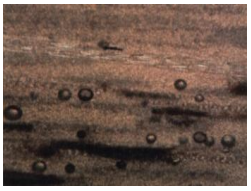

Fig. 6. The cross section of plate 3

The homogeneous structure shown in Figure 7.a, as well as the largest number of layers of fabric (two layers) in the center of the plate, have resulted in an average high ranking of the plate 4.

The mediocre ranking of the plate 6 can be explained through moderate cavity content, Figure 7.b, and the presence of two layers of fabric in the center.

a) *b)*

Fig. 7. The cross section of plate 4 (a); and plate 6 (b)

The advent of a significant share of the cavity results in a marked difference in the ranking of the plates 2 and 5 (which also have two layers of fabric in the center), Figures 8.a and 8.b.

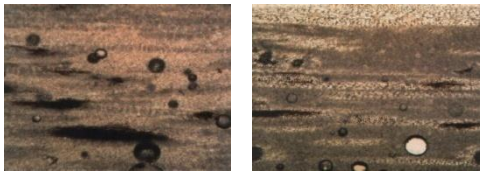

a) *b)*

Fig. 8. The cross section of plate 2 (a); and plate 5 (b)

Smaller content of reinforcing (no fabric) and inhomogeneous structure are reflected in a marked worsening in ranking of the plate 7 in relation to the plate 1, and especially in relation to other plates, Figures 9.a and 9.b.

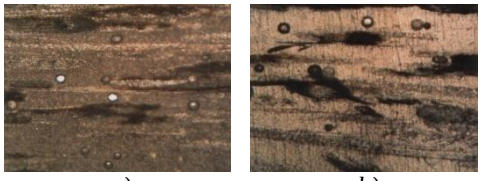

a) *b)*

Fig. 9. The cross section of plate 7 (a); and plate 1 (b)

5. CONCLUSION

By various factors influenced on the properties of polyester laminates. In addition to the type and share of reinforcing special attention should be paid to the state at the reinforcement/matrix interface. In production

by soaking, which is used in the production of test plates, it is very important to use appropriate technique (eg. by roller) to extract the air. The results are reflected in the reduction of the number of cavities present on the boundary surfaces. This procedure is generally applied where it is essential that only one side of the surface is smooth, meaning when you produce in small batches.

Clips of laminate structure help in spotting defects or irregularities that indicate possible opportunities for further damage to the laminate. Better properties of composite materials can be achieved by changing the layers of reinforcing their arrangement, but also by varying the thickness of the test plates.

The results of the study show a significant effect of porosity (residual air bubbles) on the properties of the laminates. Further research should be focused on the possibility of applying a RTM procedure in order to reduce the presence of air bubbles, and a more homogeneous structure. The result should be manifested in achieving the best possible mechanical properties, but also a smooth upper surface (side „A“), because for some applications it is important that both sides are of the aesthetically smooth.

6. ACKNOWLEDGEMENTS

The authors would like to thank the companies Plastex and Tehno Plastika from Slavonski Brod on help for making test samples.

7. REFERENCES

[1] G. C. Jacob, J. M. Starbuck, J. F. Fellers, S. Simunovic, Strain rate effects on the mechanical properties of polymer composite materials, Journal of Applied Polymer Science 94 (2004) 1, 296-301.

[2] S. Rassmann, R. Paskaramoorthy, R. G. Reid, Effect of resin system on the mechanical properties and water absorption of kenaf fibre reinforced laminates, Materials & Design 32 (2011) 3, 1399-1406.

[3] K. S. Ahmed, S. Vijayarangan, Experimental characterization of woven jute-fabric-reinforced isothalic polyester composites, Journal of Applied Polymer Science 104 (2007) 4, 2650-2662.

[4] I. M. De Rosa, C. Santulli, F. Sarasini, M. Valente, Post-impact damage characterization of hybrid configurations of jute/glass polyester laminates using acoustic emission and IR thermography, Composites Science and Technology 69 (2009) 7-8, 1142-1150.

[5] BS 2782: 1970 Methods of testing plastics.

[6] DIN 53453: 1975-05 Testing of Plastics; Impact Flexural Test.

[7] DIN 53457: 1968-05 Testing of Plastics; Determination of the Modulus of Elasticity by Tensile, Compression and Flexural Test.

[8] DIN 53455: 1981-08 Testing of plastics; Tensile Test.

[9] DIN 53452: 1977-04 Testing of Plastics; Flexural Test.

[10] DIN 52330: 1971-08 Testing of mineral fibres and products made from them; determination of content of organic substances.

[11] Tier-Inserate, Switzerland: *Steinsberger*. URL:http://www.tierinserate.ch/Pferdemarkt/Pferdeanhaenger-197354.aspx (18.08.2016.)

[12] CompositesWorld,Cincinnati:*Composites Technology*. URL:http://www.compositesworld.com/articles/car-seat-concept-scores-a-first (20.08.2016.)

Design, 3d model and calculation of pelleting machine

I. Lacković [a], N. Veljić [a] J. Matić [a]

[a] College of Slavonski Brod, Slavonski Brod, Croatia

Abstract

The task of this paper is design, model and calculation of pelleting machine, which will be competitive in the market. The first part of the paper discusses the pellets as a source of renewable energy, the pelleting process, analyses the economic use of pellets, gives an overview of European standard for pellets, describes and analyses the existing machines for the production of pellets. The second part deals with the design of the machine. List of demands and desires, morphological matrix, freeform drawings defined the concept of the machine and describes the functions and specifications of individual components and sub-assemblies are determined based on the analysis of existing solutions. The third part of the paper is the creation of a 3D model of the machine in the software package Autodesk Inventor Professional 2013 with images of components, sub-assemblies and assemblies. The fourth part is a calculation that includes a calculation of forces, moments and stresses on the components essential for the effective functioning of the machine.

Keywords: pellet, compressing, pelleting machine, pelleting mill, design

1. INTRODUCTION

In Croatia, a large amount of biomass that could be used as useful energy is not used and simply perish. The problem is that the energy density of biomass is small and therefore it is done processing into a form that is suitable for transport, storage and use. There are only a few processing plants in our country.

It seems that the most interesting is pelleting as one of the technologies for processing biomass with briquetting, baling and chopping. Automatic control in today's stoves and pellet boilers provides the same comfort as when using gas or fuel. The burner is automatically turned on, off, achieves, and maintains the set temperature with an automatic dosing which gives it an advantage over heating wood or briquettes.

The goal is to construct a machine that would allow biomass pellet, to a greater amount of biomass was used. The machine should be allowed to pelleting various types of biomass such as crop residues, waste wood processing companies and the like. It is easy to use, maintain, secure in the work and competitive in the market.

2. PELLETS

2.1. Generally the pellets

Manufacturing of pellets lasts more than a century, by using pressure and heat are formed a small cylinders – pellets and may be prepared from different materials for different purposes. During the oil crisis of the 1970s, some companies from Europe and the United States that used pellet presses for the production of animal feed start production of pellets as a fuel source, but as a cheaper and high-quality replacement fuel oil. Some countries in the 1990s begin to encourage the use of renewable energy sources thus the use of pellets as a source of energy is more increased.

The process of making pellets consists of several stages: Shredding biomass, drying, pressing - pelleting, cooling and packaging. In the pressing step, the mixture is heated because of friction and enhances the release of lignin.

Lignin acts as a natural resin, and denotes a group of macromolecular joints made by phenyl propane units and is the one of the natural ingredients of the biomass. The pellet is prepared from comminuted biomass compressed under high pressure. Large pressure and a lignin allow binding pellets. A large biomass is previously served, and dried in kilns to the moisture content down to 12 % to 15 %. Such pulverized biomass is the main raw material for the production of pellets. Figure 1.shows different phase of materials from biomass to pellets. Pellets are produced exclusively from biomass so it does not contain substances harmful to the environment. In the combustion produces significantly less emissions of NOx, SOx and CO of the permitted limit values. The density of the pellets is 800 kg / m3 to 1400 kg / m3 with a moisture content of less than 10 %. Energy value of pellets is approximately 18 MJ / kg (5 kW / h).

Figure 1. Wood chips, sawdust, pellets [1]

The most common use of pellets is in households as a source of heating energy. Heating with pellets is economically feasible compared to conventional energy sources. It is renewable and environmentally friendly due to neutral CO_2 emissions. Optimum and clean combustion is ensured by electronic regulation, which ultimately results in significantly lower emissions of harmful compounds. Heating systems in the pellets have a significant advantage in terms of environmental protection compared to conventional heating methods. Table 1 shows the price of the most common energy sources so it is obviously that the wood pellets are economically the most profitable. [2].

The shape and dimensions of the pellets determined is by the European standard for pellets EN 14961 -1 [Table 2.].

2.2. Machines for the production of pellets

By the analysis of the market and existing solutions it was found that two types of machines for the production of pellets are in the most common use due to the way the pressing. Machinery (pellet mill) with a flat matrix and machinery (pellet mill) with a ring die.

Table 1. price of the most common energy sources [2]

Energy sources	Moisture content	Energy value		Price per kWh	% price of heating oil
1 l heating oil	-	10,00 kWh/l	36,000 MJ/Kg	0,070 €/kWh	-
1 m^3 natural gas	-	10,28 kWh/m^3	37,008 MJ/Kg	0,078 €/kWh	111 %
1 kg wood pellets	-	4,90 kWh/kg	17,640 MJ/Kg	0,041 €/kWh	58 %
1 kg firewood	20 %	4,03 kWh/kg	14,508 MJ/Kg	0,052 €/kWh	74 %
1 kg wood chips	20 %	4,90 kWh/kg	17,640 MJ/Kg	0,044 €/kWh	63 %

Table 2. shows an overview of EN 14961-1.

Norma	ENplus A1
Diameter, mm	6 (+-1)
Length, mm	3,15 <=L <= 40
Density, kg/m³	600 <=
Energy value, MJ/kg	16,5 <=
Water content, %	10 >=
Small pieces, (<3,15 mm) %	1 >=
The rest of the ash after combustion, %	0,7 >=
Mechanical cohesiveness, %	97,5 <=
Melting ashes, °C	1200 <=
Content:	
Chlorine %	≤ 0,02
Sulfur %	≤ 0,05
Copper mg/kg	≤ 10
Chromium mg/kg	≤ 10
Arsenic mg/kg	≤ 1
Cadmium mg/kg	≤ 0,5
Mercury mg/kg	≤ 0,1
Lead mg/kg	≤ 10
Zinc mg/kg	≤ 100

2.2.1. Machines with a flat matrix

The principle of molding is based on the relative movement of the rollers in relation to the matrix, which rollers are pressed and the mixture forced through axial openings in the matrix, shown in Figure 2. There are two modes of operation. In the first case, the matrix turns and the rollers rotate about a fixed axis due to friction with the raw material. In the second case, matrix is stationary while the rollers rotate around its axis and move rotational in relation to the matrix. This design is simple, provides direct access to the chamber where the process of production of pellets. This principle is suitable for molding machines with a small production capacity.

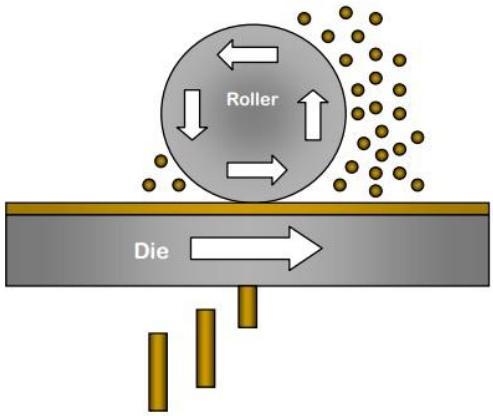

Figure 2. The principle of molding machines with flat matrix[3]

2.2.2. Machines with ring die

The principle of molding is based on the relative movement of the rollers relative to the ring die matrix, the raw material is *supplied* from above, via the rollers falls on the matrix, which rollers pressed and the mixture forced through the radial holes on the matrix shown in Figure 3. There are two modes of operation. In the first case the matrix is turned and the rollers rotate about the fixed axis due to friction with the raw material. In the second case, the matrix is fixed, and the rollers rotate around its axis and turn to the inner part of the matrix. This design is more complicated compared to the pellet mill with a flat matrix, so making a ring matrix is complicated and expensive, and for this reason it is used for the machines with a bigger production capacity.

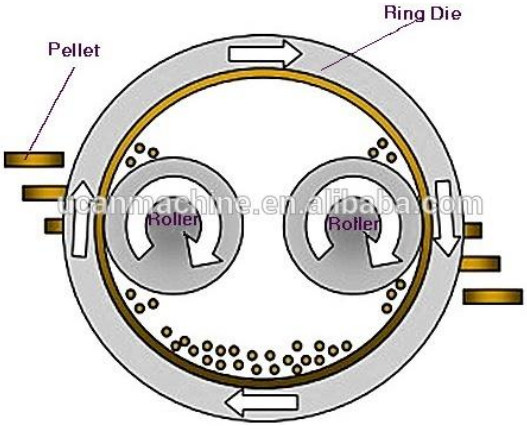

Figure 3. Principle molding machines with ring die[3]

3. CONSTRUCTION OF THE MACHINE

3.1. Comparison of machines for pelleting

Considering that there are two types of machines for pelleting, table 2 compares the characteristics of the machine with the flat and ring die matrix. Machine with improved features is assigned to the "+", and the machine with less successful "-".

Table 3. Comparison of machines for pelleting

	Machines with a flat matrix	Machines with ring die
Dimensions	+	-
Mass	+	-
Price	+	-
Simplicity of construction	+	-
Consumption of energy	-	+
Production of capacity	-	+

Pelleting machines with a flat matrix are due to its simpler structure smaller, and therefore less weight compared to the machines with a ring die. Creating a ring die matrix is much more expensive and complicated than making a flat matrix.

When the energy consumption is concerned, the problem of friction is observed which is caused by the rotation of the roller by raw material. For the machines with a ring die matrix, friction is less compared with the flat matrix machines, and thus the energy consumption is less. For the machines with a flat matrix, a roller rotate due to the difference in the peripheral speeds. Namely, when a drive engine drives the matrix and the rollers rotate due to the friction with a layer of the mixture, rollers slip due to the difference in the circumferential speed of the outer and inner edge of the matrix. The flow of raw materials is better for the machines with ring die, and less potential for accumulation of material that could cause stoppage of work at straight matrix. When comparing production capacity, machines with flat matrix are suitable for smaller production capacity due to its simpler and cheaper construction. Machines with a die ring matrix are applied for a large production capacity of 300 kg / h.

3.2. Concept

Based on the objectives it is formed the list of requirements and desires. The requirements represent the characteristics that construction must meet, and desires are the characteristics that construction does not necessarily satisfy. Based on the list of demands and wishes it is worked out the concept of freeform sketching. Figure 4 shows a freeform outline of the machine for the production of pellets.

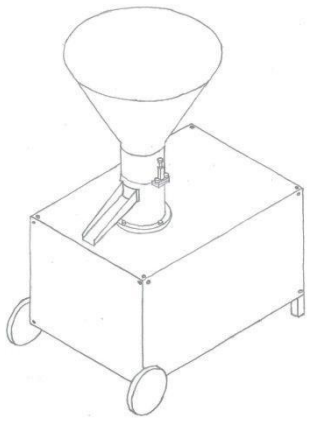

Figure 4. Freeform drawing machine for pelleting

Machine dimensions are: length of a = 1000 mm, width b = 600 mm, height h = 1427 mm and weight of the machine is m = 100.16 kg according to Autodesk Inventor Professional 2013 together with an electric motor. The supply of material is performed manually, adding the mixture into the tin funnel and a finished product removal from the machine is by rotating plate and a tin part mounted at front of the machine. The machine concept for the production of pellets is based on the principle of molding the raw material with a rotating flat matrix and rollers which rotate around an axis which is stationary, thus rollers compress material axially through the holes of the matrix and thus are formed the pellets.

Figure 5 shows a freeform outline sectional working part of the machine

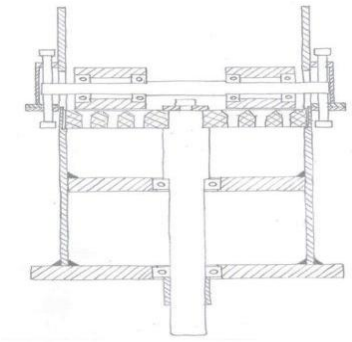

Figure 5. Freeform drawing section of the working part of the machine

Rollers rotate due to friction, and therefore the speed of rotation of the matrix and the rolls is equal to one part only, The rolls slippage in relation to the matrix which leads to a heating of the mixture it is beneficial to reduce pressure required for the molding of the mixture and quality of the final product, because it increases a durability of product.

As a drive engine is electric Wattdrive 3BW132M - 06G: power P = 4.5 kW, torque M = 45 Nm, and the speed n = 960 r / min is selected, which over the belt gear with V- belts and shafts runs matrix . Belt drive enables quiet and flexible operation, and in case of overload leads to belt slippage, by which are the mechanical parts are protected against overload. Shaft is supported by two closed bearings SFK 7206 BE placed in a cylindrical plates , welded pipe φ219,1 mm and wall thickness of 6.3 mm , length 230 mm . There is an opening on the tube 120 x 70 mm for remove pellets and around the opening is the welded sheet metal bracket for attaching a knife and sewer. The lower plate is φ279,1 mm and 25 mm thick , which also serves as the basis of a tool for fixing the base by four screws M12 . The top plate is φ 219,1 mm and a thickness of 25 mm, and the distance between the plates is 105 mm . At the top of the pipe are welded two lugs on which are fastened working chamber with rollers. On the shaft above the upper plate is fixed the rotating plate by three screws M6, and by centrifugal force remove the pellets from the machine. At the top of the shaft is a matrix that is used to create pellets by replacing the matrix with a matrix different shape hole by which is possible processing of biomass from different backgrounds. The matrix is connected with the shaft by cotter DIN 6888 8 x 9 and stabilized self-locking nut DIN 1804 M30. The working chamber is made of pipes φ219,1 mm and wall thickness of 6.3 mm , length 145 mm . On the ground floor, there are two welded lugs by which are the working chamber fastened by four screws M12 for the bearing. At the bottom of the pipe, two symmetrical openings are cut out and by which support the axis of the rollers. On the outside of the pipe welded the two cantilevers with 12 nuts and are used to adjust the distance of the rollers from the matrix by two screws M12. Rollers are φ60 mm and a length of 65 mm. Each of the rollers is mounted with two closed SKF bearings 7203 BE. Shaft roller is attached with two screws from above M12 and M12 the two screws on the bottom. Upper Bolts provide crimping force and the lower screws are used to lift the rollers of the matrix when the chamber does not have the raw material to avoid damage to the rollers or dies. The parts in contact with the biomass are of corrosion durable material, or coated or protected because the biomass is processed should have a 10 % to 15 % moisture content. The base is made of square pipe ISO 25 x 25 mm and a thickness of 2 mm, which are connected by welding. At the front of the pedestal welded the two branches (either side) on which are mounted wheels and secured with split pin. The entire base is covered by tin plates to rotating parts of the machine, an electric motor and belt transmission protected from contact. On the back of the engine at the tin plates are made open to allow easier removal of heat from the electric motor.

The system of pellets removal consists of an adjustable knife, rotating plate and sewer. Adjustable knife is attached with two screws M6 on tin support of sewer. It is possible to set the distance of the knife from the matrix, thus making it possible to change the length of the finished product. Cut (broken off) pellets fall on a rotating plate that the principle of spin -lead pellets from the machine to the discharge channel. The pellets still leave the machine by gravity.

4. 3D MODEL MACHINE

3D modeling is the process of creating a mathematical representation of any three-dimensional object. The result of 3D modeling is called a 3D model. It can be displayed as a 2D image through a process called rendering or used in a computer simulation of physical

phenomena. 3D model can also be physically created using 3D printers.

3D model of the machine, which is shown in Figure 6, is made in the software package Autodesk Inventor 2013. Working of 3D models is started by modeling component subassemblies. Some components, such as screws, nuts, washers , tubes , bearings , etc., are not necessary to model, because these parts are standard in Inventor catalog . After creating the components, the assemblage of sub-assemblies is followed, and after that, subassemblies to final assembly of the machine.

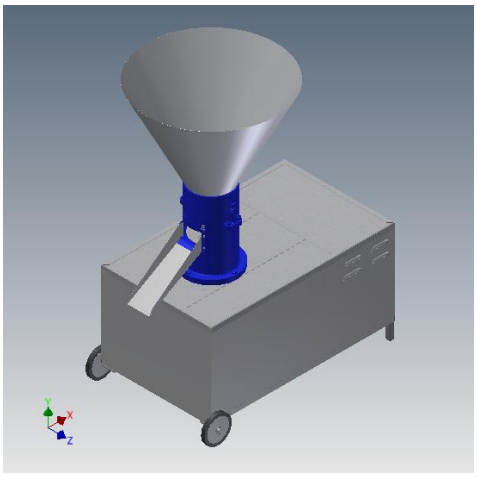

Figure 6. 3D model of the machine

Table 4. shows the 3D models of the components of the machine for the production of pellets .

The title of the parts	3D model
The tube housing	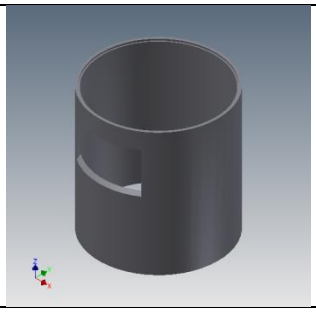
Subassembly housing with bearings	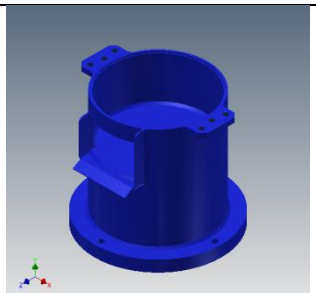
Subassembly of the working chamber	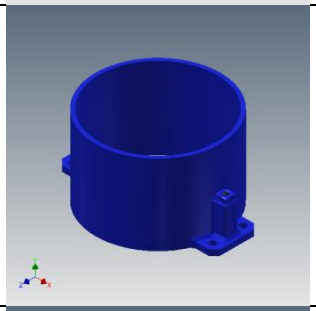
Shaft subassembly roller	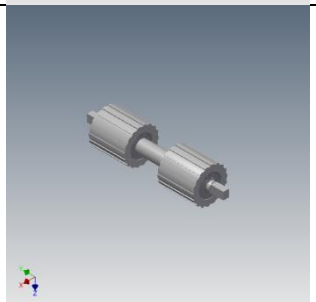
Subassembly stand	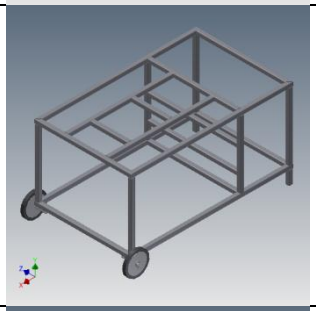
Machine assembly without the protective sheet	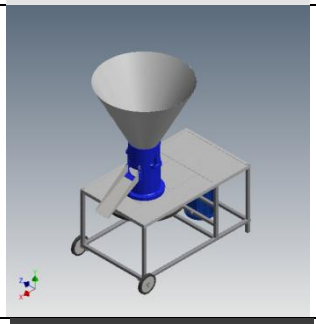
Axle with bearings	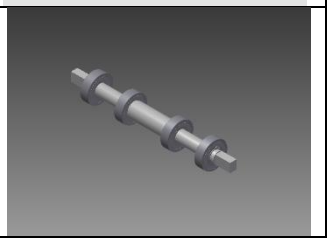

5. CALCULATION

5.1. Calculation of forces

Figure 7 shows the matrix and the shaft with rollers between which occur forces during the pressing process. Axial force is the force by which the pressing rollers suppress the raw material through the holes in the matrix. Tangential force is the force as a result of friction [4] .

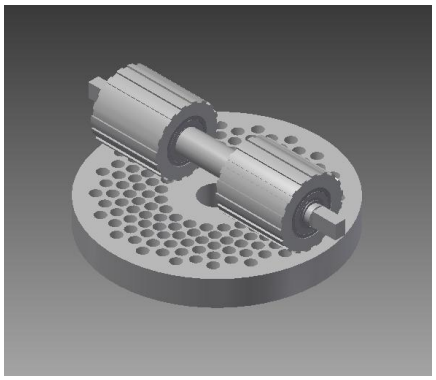

Figure 7. Matrix and axle with press rolls

5.2. Calculation of torque shaft

By rotating the matrix, due to friction, is caused the rotation of the rolls , but because here the rollers does not transfer power except to overcome friction in the bearings of rollers, it can be concluded that the overall power and torque of the matrix is spent on friction [4]. Figure 8 shows the shaft axis of the matrix and press rolls.

Figure 8. Shaft, matrix and axle with press rolls

5.3. Calculation stress in bending the shaft rollers

Stresses in the bending the roller axis are the resulting strain by the stresses in the vertical plane and the stresses in the horizontal plane . Figure 9. shows the shaft which is located in the working chamber .

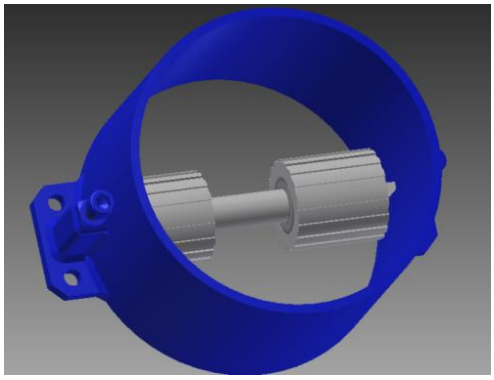

Figure 9. Working chamber with the shaft and press rolls

Bending stress of roller axis in a vertical plane, is calculated by first determination forces in the supports, then the amount of the maximum torque is calculated, because the greatest stress is at place of the maximum torque. Then it is calculated the axial torque for a given section [5]

5.4. Calculation of the belt drive

On the basis of the required torque on the shaft of the working machine M_2 = 278.77 Nm, gear ratio i = 7 and electric Watt drive 3BW132M - 06G : P = 4.5 kW ; n = 960 rev / min ; M = 45 Nm, are selected [6] . The drive pulley with standard dimensions D_1 = 80 mm is selected too.

Figure 10 shows the machine pulley and belt transmission that consists of a drive pulley, the driven pulley, and tensioning the V-belt pulley.

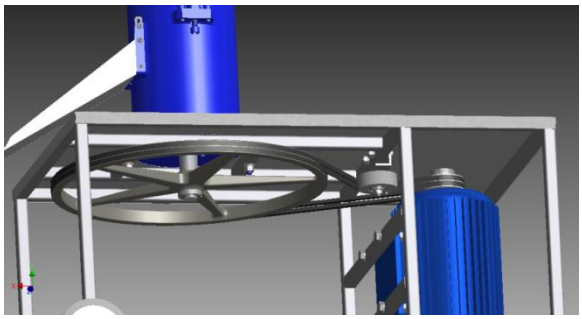

Figure 10. Belt transmission machine

For the mathematical detailed description of the calculation, you can contact the author of the work on contact mail.

6. CONCLUSIONS

This paper discusses the existing solutions of machines for the production of pellets. Based on the analysis, the list of requirements and desires are generated. Freeform drawings defined the concept of the machine and then creates a 3D model of the machine. For the modeling, the software package Autodesk Inventor 2013 is used.

Using computers and software packages as well as help for design, one can significantly save the time for developing new products or improving existing products and thereby reduce the possibility of error.

The design concept meets all its targets and provides improvement of existing solutions. By installing two screws that raise the rollers of matrix, is prevented damage rolls or matrix, when the chamber is without the raw material. However, in order to provide the best solution, it would be necessary to make several versions of the machine, and then access to techno economic evaluation and according to the results of technical and economic goodies, choose a variant of the machine nearest ideal variant.

7. REFERENCES

[1] http://www.drvnipelet.hr/

[2] http://www.peletgrupa.hr/

[3] The beginners guide to pellet production http://www.weedcenter.org/mrwc/docs/The_Beginners_Guide_To_Making_Pellets.pdf (11. April 2015.)

[4] B. Kraut (2006): Strojarski priručnik, Tehnička knjiga, Zagreb

[5] K. H. Decker (1982): Elementi strojeva, Tehnička knjiga, Zagreb

[6] D.Jelaska, S.Podrug: Proračun remenskih prijenosa, Fakultet elektrotehnike, strojarstva i brodogradnje , Split

https://bib.irb.hr/datoteka/321904.Remenski_pr.pdf, (11. April 2015.)

Selecting Image Feature Points Based on the Object Contour Curvature

I. Arkhipov [a], B. Yakimovich [a], K. Židek [b], M. Elantsev [a]

[a] Kalashnikov Izhevsk State Technical University, Studencheskaya 7, 426069, Izhevsk, Russia, aio1024@mail.ru

[b] Technical University of Kosice, Faculty of Manufacturing Technologies with a seat in Prešov, Bayerova1, 08001, Prešov, kamil.zidek@tuke.sk

Abstract

We propose a search method of feature points of the image area using the curvature of the characteristic contours of terrain objects. A feature point corresponds to the positive or negative curvature extreme loop characteristic of the object. Stationary and sufficiently large area objects (roads, water, buildings, large accumulations of vegetation) are used for that purpose. Small objects as well as moving objects (people, vehicles) are removed from the image at the pre-treatment stage. It results in an image marked up by feature points with positive and negative curvature. The proposed method can be used in solving problems of comparison of image feature points.

Keywords: Computer and information technologies, feature points, the curvature function, object contour mapping pictures.

1. INTRODUCTION

Search for the image characteristics is an important task of computer vision. Feature points can effectively accomplish the following tasks: stitching panoramas and aerial photographs (image stitching); 3D reconstruction; search and identification of objects, fingerprints verification [1], etc. A large number of works in this direction [2, 3, 4] testifies indirectly to the relevance of the problem of finding image feature points. Unfortunately, at present there is hardly any universal algorithm for generating an acceptable solution to the problem at hand in different subject areas. The reason is all sorts of distortions of recorded images such as affine and projective transformations are associated with the movement of the camera or objects in the scene, scene change illumination, occlusion and shadowing objects in the scene, etc. In this work, the task of finding the image feature points mage is solved in the context of a comparison of the current photograph area, made on board the aircraft, with the search field composed of aerial photographs or satellite images. Such comparisons will enable to position the aircraft.

2. FEATURE POINTS SEARCH ON THE TERRAIN IMAGE

The successful positioning of the aircraft needs detected feature points belonging to the objects that will be called stable area reference objects. Not all objects in the current image area can be classified as stable reference objects. In these images often moving or variable objects are present. People and vehicles should be classified in the class of moving objects. The objects, which are easily subjected to changes, such as single trees, paths, small single buildings, etc, are meant by variable objects. The presence of these objects in the image makes it difficult to find stable reference object. Fig. 1 shows the original image areas. In this image stable reference objects are roads,

buildings and clusters of trees. Cars, trails, single trees and bushes, hedges are easily changeable.

Fig. 1. The source image of terrain

To reduce the number of moving and changing objects in an image we use the median image filtering with the N × N pixel aperture, which allows to preserve the boundaries of the major objects in an image. [5]

Fig. 2. The result of median filtering (N=3)

The value of the aperture should be selected for the following considerations. The maximum aperture size of the median filter is dependent on the minimum width of the road. The minimum size of the median filter aperture is calculated from the condition of suppression of moving objects such as buses, passenger cars and trucks. Depending on the scale and resolution of the shooting aperture value typically ranges from 3 to 9 pixels.

Fig. 3. The result of median filtering (N=7)

Fig. 2 shows an image output from the median filter with N = 7 aperture. Median filtering suppressed all vehicles, narrow dirt roads, small elements of vegetation and small buildings. In addition, the image preserved road network, large buildings and groups of trees. It is necessary to emphasize the preservation of boundaries between the objects which remained on the image.

However, even if the boundary between the object area is close to the ideal, after sampling it becomes unsharp, which makes it more complicated to highlight the contours of objects further. To restore the boundaries the extreme filter is used [4]. When used extreme filter calculates the distance between the current brightness of the input image pixel brightness and extreme values in the neighborhood of (x, y).

$$\begin{cases} d_{\min}(x,y) = \left| b_1(x,y) - e^N_{\min}(x,y) \right| \\ d_{\max}(x,y) = \left| b_1(x,y) - e^N_{\max}(x,y) \right| \end{cases}, \quad (1)$$

where $e^N_{\min}(x,y)$, $e^N_{\max}(x,y)$ – the minimum and maximum extreme values of brightness in the N × N pixel vicinity of the current image.

The value of the extreme (maximum or minimum), closest to the brightness of the central pixel, is assigned to the current pixel of the output image

$$b_2(x,y) = \min\left(d_{\min}(x,y); d_{\max}(x,y)\right). \quad (2)$$

As a result, the boundary gets aggravated and actually becomes a step one (Fig. 4), which highly facilitates the construction of the circuit stable area landmarks.

Fig. 4. The result of extreme filtering

Extreme filter aperture size is set to the minimum value of 3×3. However, it is experimentally found out that slightly better results can be obtained by increasing the filter extreme aperture to median filter aperture size, while significantly increasing the cost of computational complexity.

Further, any available contour detector builds the contours of objects (Fig. 5). In this paper, we used Canny detector [6].

Further on, the curvature function for each circuit is calculated The choice of the curvature function as a basis for feature points is due to its invariance to the shift, rotation and lighting conditions. In addition, if we do not use the information about the value of curvature at the point of its extreme for the further comparison, and will only fix the coordinates of extreme points, the proposed method will have invariance and scale change.

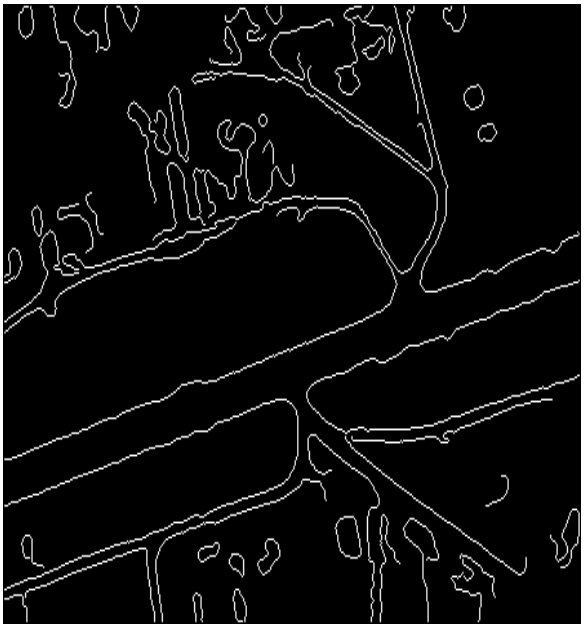

Fig. 5. The Contours of stable reference terrain objects

Curvature function is one-dimensional and requires unbranched circuit, but the description of complex objects may call for contour branching. In this case, the branching point becomes the anchor point and the outline of a complex object becomes an integral of multiple curvature functions. Positive and negative curvature function extreme exceed a predetermined threshold, the markers are marked on the original image. It results in an image of the current location frame marked up with feature points.

If the number of feature points is not enough to match the current frame with the search area image , or the comparison is made with a low reliability, the extreme threshold of curvature function is adaptively reduced and the extreme search is repeated. A large number of isolated feature points can significantly slow down the process of further comparison. In this case, raising the extreme search threshold is provided.

3. RESULTS AND ACHIEVEMENTS

Fig. 6 shows the original image, and areas marked thereon singular points found as described above.

Fig. 6. The source image labeled by feature points

Fig. 6 shows that all the major junctions and bends of the roads are marked by feature points. The rest of the feature points are located at the corners of buildings and in the bends of the outlines of large clusters of trees. At the same time, cars, small buildings, light fencing, single trees and bushes remained untagged.

4. CONCLUSIONS

The paper proposes the method of searching for feature points of the image area, adapted for use in automatic orientation systems of aircraft on visual images. The described method involves the selection of resistant targets areas with the further release of their contours. Analysis of the shape of stable terrain objects based on curvature function extreme search is performed. We justify the choice of aperture size of the median filter which is responsible for the selection of stable reference object area. Guidelines for choosing the extreme of the filter aperture, emphasizing the objects contours in the image are also given. The curvature function extreme search involves the adaptive nature of the threshold change. The proposed threshold adaptation procedure allows to obtain feature points in an amount sufficient for further comparison. The suggested method of searching for feature points has very important properties of invariance to the shift, rotation, scale change and changing light conditions (except for shading).

Acknowledgment

This work was supported by the Slovak Research and Development Agency under the contract No. APVV-15-0602.

5. REFERENCES

[1] E. Pivarčiová, P. Božek , A. Al Akkad, B. Yakimovich. Automated System of Image Verification. PA NOVA SA. Gliwice (2015) 227 p.

[2] C. Harris, M. Stephens. A Combined Corner and Edge Detector, Proceedings of 4-th Alvey Vision Conference (1988), p. 147-152

[3] X. Chen He, N. Yung. Corner detector based on global and local curvature. Opt. Eng. 47(5), 057008 (2008).

[4] S.C. Bae, I.S. Kweon, C.D. Yoo. COP: a new corner detector. Pattern Recogn. Lett. 23 (2002) pp. 1349-1360.

[5] T.S. Huang Two-Dimensional Digital Signal Processing II. Transform and Median Filters. Springer-Verlag Berlin Heidelberg New York (1981)

[6] J. A. Canny. Computational Approach to Edge Detection. IEEE Transaction on Pattern Analysis and Machine Intelligence. Vol. PAMI-8 No. 6 (1986) pp. 679-698.

[7] S. Y. Kim, S. S. Lee, K. Židek, V. Maxim, Navigation of Mobile Devices based on Embedded Image Processing with Support of GPS Systems and Sensors. Journal of Korean Society of Mechanical Technology. Vol. 15, no. 5 (2013), pp. 731-741.

Design of polymeric electrolyte membrane reformer

M. Milosevic [a*], G. Mladenovic [b], A. Sedmak [b], A. Plohar [c], B. Likozar [c] J. Lozanovic Sajic [a]

[a] Innovation Center of Faculty of Mechanical Engineering, Belgrade, Serbia,
* mmilosevic@mas.bg.ac.rs

[b] Faculty of Mechanical Engineering, Univesrity of Belgrade, Serbia

[c] Department of Catalysis and Chemical Reaction Engineering, National Institute of Chemistry, Ljubljana, Slovenia

Abstract

This paper describes the design and manufacturing aspects of polymeric electrolyte membrane (PEM) reformer from the beginning step of realization that includes modelling of main parts of the reformer, adopting changes in shape and dimensions, and manufacturing and development of the reformer. For these purposes, one model in SolidWorks software was developed, and based on that model manufacturing was performed. Adopted changes in the reformer are presented, along with detailed explanations. Beside the main subject of this paper, general data about proton exchange membrane fuel cell are shown in the introduction of this paper with short description and explanations of PEM function, method and purpose.

Keywords: PEM, reformer, design, manufacturing

1. INTRODUCTION

Proton exchange membrane fuel cells or PEMFC are also known as polymeric electrolyte membrane (PEM) [1]. These two terms have the same acronyms. PEM are based on a polymeric electrolyte which is proton conducting. Conventional PEMs usually employ water containing polymers as electrolyte that is responsible for proton conduction. These type of fuel cell that contains water have a high power density at low operating temperature, and due to the physical properties of water cannot be used above a temperature of 80 °C.

High temperature PEMs or HTPEM are based on polymers doped with phosphoric acid. High temperature PEMs, unlike conventional PEMs, can operate at temperatures up to 200° C. Higher temperatures causes faster chemical reactions, higher efficiencies and most important better tolerance to fuel impurities. HTPEMs can be started and shutdown relatively quickly and also have good fuel tolerance. Because of aforementioned characteristics they are most suitable for mobile applications (electric cars, boats). The material challenges encountered in HTPEMs are mainly related to the phosphoric acid which migrates under operation.

The best fuel for PEMFC is pure hydrogen and for all other type of fuel cells, but the storage of hydrogen and portability of hydrogen storage systems are problematic for small-size mobile applications. Highest efficiency is achieved by using pure hydrogen as fuel, since then the amount of pollutant byproducts is minimal (it would be ideal if there weren't any). As a substitution, hydrocarbons, especially methanol and methane is recognized as more practical choices as a fuel for PEMFCs [2, 3, 4, 5].

Presented in the following text are spects of design and production of reformers for high temperature PEMs. One model of reformer with its dimension and parts is presented in further text. Manufacturing is performed based on this model as well as studies related to dimension influences to reforming process with reformer dimension proposal and CFD analysis [6].

Addition to these tests, scientists all around the world have carried out numerous other test

in order to achieve efficiency increasing of reformer [7]. CFD analysis are more easiest way for performing simulation based on the further test will be or not be performed thus have a great role in fuel cell examinations [6].

2. PEM FUEL CELL SYSTEM

One system of polymeric electrolyte membrane fuel cell contain three main reactors. One is the reformer for methanol steam reforming (MSR). The second is the high temperature proton exchange membrane fuel cell stack (HT PEMFC). The third is the vaporizer.

Whole system is built from components that can be seen in Figure 1. From top to bottom the following components are:

- incoming and out coming connectors for fluids
- top metal plate with holes for compression bolts
- 10 mm inner insulation layer
- Vaporizer with metal cover plate
- 5 mm inner insulation layer
- HT PEMFC stack consisting of:
  - 2 membrane electrode assemblies (MEA)
  - 4 MEA gaskets
  - 3 graphite-composite bipolar plates
  - 2 copper current collectors
- methanol steam reformer (MSR)
- 15 mm inner insulation layer
- bottom metal plate with holes for compression bolts

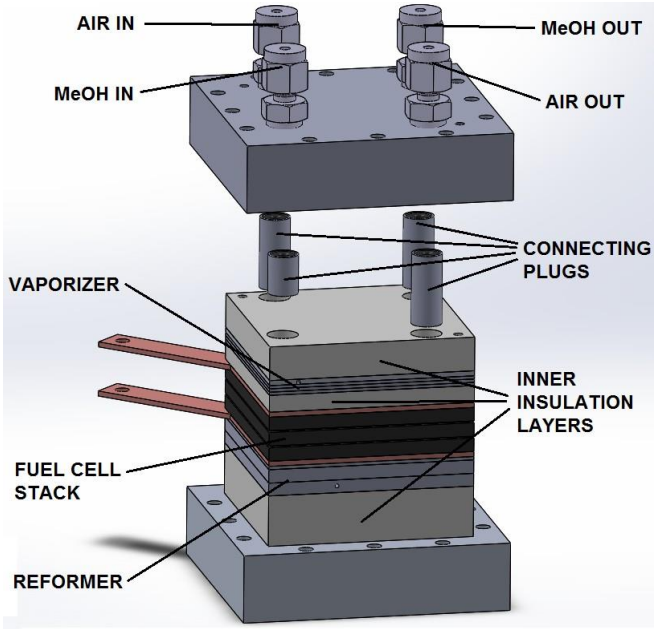

Figure 1. Design of the system with HTPEM fuel cell stack and integrated vaporizer and reformer

The inner insulation layers are used to obtain the desired temperature distribution within the system. The reactors are stacked in a planar way to enhance heat transfer from exothermal HT PEMFC stack to endothermal reformer and vaporizer. The fuel processing reactors are positioned in the system according to their operating temperature and they are connected via series of connecting plugs. The sealing of flowing fluids is achieved by using O-ring gaskets. Dimensions of all the parts constructing the system match the dimensions of actual model components with the exception of MEA and gaskets which are already drawn in a compressed state.

The bipolar plate flow fields also match the ones of an actual component. The only thing missing is the connection between the main entry channel (φ3 mm) and the main flow field distributing channel.

3. METHANOL STEAM REFORMING MODEL OR REFORMER

In Figure 2 left can be seen a SolidWorks assembly of parts that form the MSR or reformer. The middle part represents the reaction volume with incoming and out coming channels. The reaction volume is separated by two stainless steel mashes (after widening of the incoming channel and narrowing of the out coming chan-

nel) which are inserted into 0.5 wide grooves perpendicular to three-direction of flow. The external dimensions of the reformer, 60×60 mm are complementary with fuel stack dimensions. As can be seen in Figure 2 - right, it is composed of three plates,– upper and lower cover plates, with thickness of 3.8mm and 1mm respectively, and a middle plate, 4mm thick. The middle plate contains the reaction volume and inlet and outlet channel.

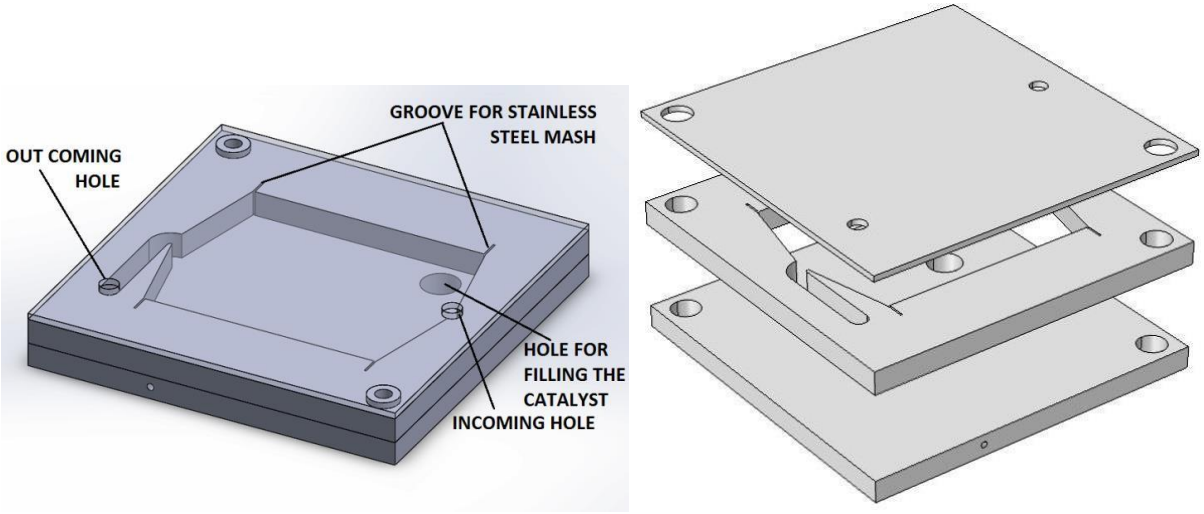

Figure 2. Left: Trigonometric view of the MSR with top plate in transparent mode, Right: Three plates of the methanol steam reformer stack

The initial geometry of the reaction volume with channels is shown in Figure 3 left. The reaction volume dimensions are 34 x 37.4 x 4 mm. The catalyst bed in the reaction volume should be separated from the channels with a stainless steel mesh, with the space of 3mmin front and behind of the reaction volume. Inlet and the outlet both have a diameter of 3 mm. The non-variable parts of the reformer geometry are designated by gray in Figure 3 right. In the variable part, there is a length of 3.5mm between the center of the inlet circle and the steel mesh, and a 5.5mm gap between the steel mesh and the center of the outlet circle.

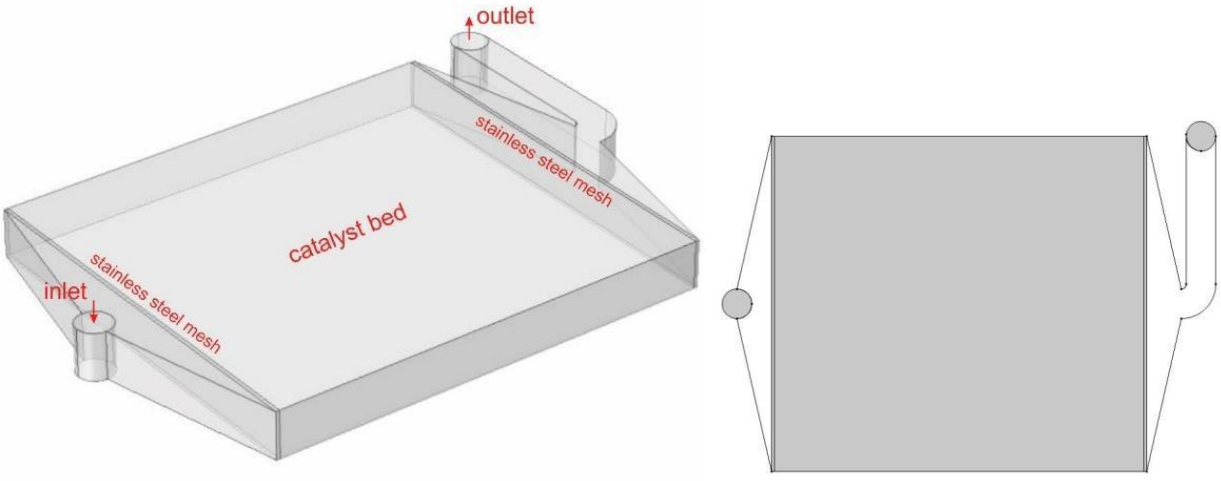

Figure 3. Left: The initial geometry of the reaction volume with inlet and outlet channels, Right: Cross section of the reaction volume with channels

Before examination test or reforming the following data are defined:

- ratio methanol-water mixture
- temperature in the reformer
- flow rate at the inlet channel
- catalist particle dimater
- bulk density
- catalyst density

4. MANUFACTURING AND DEVELOPMENT

For the purpose of development of the shown reformer, operations involving processing on a milling machine and EDM with a wire. Before designing the processing, an analysis of assembly parts was performed. Since the application of non-conventional processing methods increases manufacturing costs, shape and dimensions optimization of the reformer was performed. Since EDM processing requires the use of a wire with a diameter of 0.3 mm, the shape and dimensions of the middle plate opening was changed. Transversal hole on the reformer is meant for the placing of the thermocouple, thus the hole diameter was changed from 1 to 2 mm, whereas the depth remained the same.

5. CONCLUSION

The reformer is an integral part of the existing indirect internal reforming high temperature PEMFC and most of its geometry is already defined. Experiments based on the above mentioned reformer model prove that the changes in geometry have an influences in flow irregularities but do not have a large influence on the value of pressure at the entrance of the porous media or on the pressure drop in the porous media [6].

As mentioned before, application of non-convectional processing methods increases general costs, thus optimization of reformer shape and dimensions was performed in order to decrease the time needed for its production. One of the adopted change in reformer manufacturing is the change of the middle plate opening diameter (due to the fact that EDM processing wire has a diameter of 0.3 mm) from 1 to 2 mm.

6. ACKNOWLEDGEMENTS

This research was carried out under the NATO SPS Project EAP.SFPP 984738, and the Ministry of Education and Science of the Republic of Serbia projects TR35040 and III 43007. Slovenian Research Agency is gratefully acknowledged for supporting the Programme P2-0152, Chemical Reaction Engineering.

7. REFERENCES

[1] Fuel Cell Handbook, 7th edition, U.S. Dept. of Energy, Nov. 2004.

[2] J.R. Rostrup-Nielsen, Conversion of hydrocarbons and alcohols for fuel cells. Phys.Chem. Chem. Phys., 3 (2001) 283-288.

[3] J.O. Jensen, Q. Li, C. Pan, et al, High temperature PEMFC and the possible utilization of the excess heat for fuel processing. 32 (2007) 1567-1571.

[4] D. Palo, R.Dagle and J. Holladay, "Methanol steam reforming for hydrogen production," Chemical Reviews, vol. 107, p. 3992–4021, 2007.

[5] J. Agrell, H. Birgersson and M. Boutonnet, "Steam reforming of methanol over a Cu/ZnO/Al2O3 catalyst: a kinetic analysis and strategies for suppression of CO formation," Journal of Power Sources, vol. 106, p. 249–257, 2002.

[6] I. Ivanović, A. Sedmak and M. Milošević, "The Influence of Inlet Geometry on the Performance of a Micro Methanol Steam Reformer," in t*he 6th International Conference and Workshop, REMOO-2016*, Budva, Montenegro, 2016. Jing Su: Development of a Novel Compact Reformer for PEMFC, Doctoral Dissertation, University Of Florida, 2009.

[7] H. An, A. Angli, B. Agus, B. Sasmito, C. Jundika and A. Kurnia, "Computational fluid dynamics (CFD) analysis of micro-reactor performance: effect of various configurations," Chemical Engineering Science, vol. 75, p. 85–95, 2012.

Initial Sensitivity Analysis of Packed-bed Methanol Steam Reforming Reactor

Ivana Ivanović[a], Aleksandar Sedmak[b], Miloš Milošević[a], Sanja Petronic[a], Andrej Pohar[c], Blaž Likozar[c]

[a] Innovation Centre, Faculty of Mechanical Engineering, University of Belgrade, Kraljice Marije 16, 11120 Belgrade 35, Serbia

[b] Faculty of Mechanical Engineering, University of Belgrade, Kraljice Marije 16, 11120 Belgrade 35, Serbia

[c] Department of Catalysis and Chemical Reaction Engineering, National Institute of Chemistry, Hajdrihova ulica 19, 1000 Ljubljana, Slovenia

Abstract

A packed-bed steam reforming rector model is complex, involves several physical phenomena that need to be analysed simultaneously and includes large number of parameters difficult to validate. The aim of this study was to investigate to which level results of numerical analysis of specific reactor model are uncertain and to perform sensitivity analysis with respect to boundary parameters before an introduction of a chemical reaction model into simulations. As the necessity of sensitivity analysis was noticed, the model was built gradually and sensitivity analysis was performed using finite differences. First a steady laminar fluid flow through a reaction volume with inserted porous media was simulated, then the heat transfer model was added to the flow simulations through the reaction volume, finally the walls are added to geometry and a conjugate heat transfer model was built. The valuable results were obtained concerning an influence of inlet flow rate and boundary temperatures on the flow through a porous media of the reactor.

Keywords: steam reforming reactor, heterogeneous catalyst bed, laminar flow, CFD, heat transfer, sensitivity analysis

1. INTRODUCTION

The subject of this study is specific packed-bed methanol steam reforming reactor which is part of polymer electrolyte membrane – methanol steam reforming (PEM-MSR) fuel cell system or PEM indirect internal reforming fuel cell system. Since the methanol reforming process is endo-thermic, in the indirect internal reforming fuel cell system heat of the system is used for re-forming process, reactor exists as a separate part, it is placed in the fuel cell system stack with other devices necessary for the reforming process.

A good review of work related to fuel cell methanol steam reforming reactors is given in Refs. [1] and [2]. In Ref. [1] was specified that the first study analysing reforming in indirect internal reforming high temperature fuel cell system was the experimental study published in 2005 in Ref. [3]. Resulting performance was lower than in the case of the same fuel cell stack directly supplied with the mixture of H_2 and CO_2.

The way in which packed-bed methanol steam reforming reactors have been developed during last decade can be seen from experimental and numerical studies given in Refs. [4], [5], [6], [7], and [8]. In the work of Pattekar and Kothare from 2005 (see Ref. [4]) the radial micro rector with integrated vaporizer was presented. The reactor was packed with commercial $Cu/ZnO/Al_2O_3$ catalyst as in Ref. [3]. Experimental study and

numerical study were performed. It was demonstrated that that reactor produced hydrogen for up to 20W of power. The same type of the reactor was studied in Ref. [5]. Kinetics of the model and pressure drop are calculated. The goal was to produce hydrogen for 24W and 72W of power which was achieved. The analysis of carbon monoxide as by-product was also presented in Ref. [5].

Design, extensive experimental analysis, and 3D thermal analysis of real micro reactor are presented in Ref. [6]. Copper based catalyst was used again in the form of packed-bed. Special attention was paid to heat transfer and insulation of the reforming system. The study presented in Ref. [7] from 2015 is noteworthy since it gives an extensive experimental and CFD analysis of three packed-bed reactors with different geometry: multi-channel, radial as in Ref. [3], and tubular. Another comprehensive experimental and complete 3D CFD analysis of plate-type micro methanol steam reformer is given in Ref. [8].

Here, sensitivity analysis was initiated in order to obtain detailed information about numerical model, and to prepare the model for an experimental analysis, for proper chemical reaction model simulations, and, for a design optimization.

2. MODEL DESCRIPTION

Geometry of packed-bed methanol steam reforming reactor is illustrated in Figure 1. The reactor consists of three square plates of different thicknesses. The reaction volume is cut from the four-millimetre-thick middle plate. The reaction volume consists of inlet and outlet channel and inlet and outlet chamber. Central section of the reaction volume is filled with catalyst. The stainless steel mesh, that will hold catalyst in place, was not included in the current model. Diameters of the inlet and the outlet openings are 3 mm.

In the PEM-MSR system, the reforming reactor stack is placed between the fuel cell stack at the top and the thick insulation layer at the bottom. It is expected that the heat, necessary for the reforming process which is endothermic, will be supplied from exothermic fuel cell electrochemical reactions.

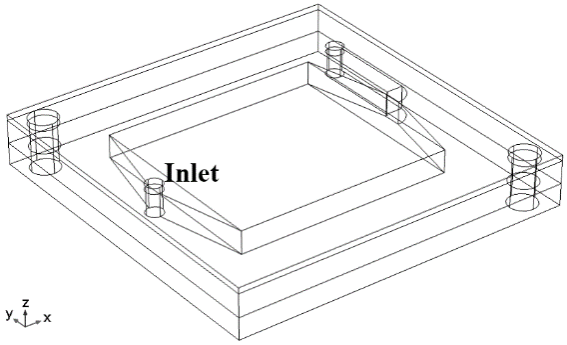

Figure 1. Geometry of the packed-bed methanol steam reforming reactor stack

3. NUMERICAL SOLUTION

The flow was modelled as steady, laminar, with inserted porous media. Free flow in the inlet and the outlet channel is given by incompressible continuity equation

$$\rho \nabla \boldsymbol{u} = 0$$

and Navier-Stokes equations

$$\rho(\boldsymbol{u} \cdot \nabla)\boldsymbol{u} = [-p\boldsymbol{I} + \mu(\nabla \boldsymbol{u} + (\nabla \boldsymbol{u})^T)]$$

Flow in porous media is given by Brinkman equation

$$\frac{\rho}{\epsilon_p}\left((\boldsymbol{u} \cdot \nabla)\frac{\boldsymbol{u}}{\epsilon_p}\right) = \left[-p\boldsymbol{I} + \frac{\mu}{\epsilon}(\nabla \boldsymbol{u} + (\nabla \boldsymbol{u})^T) - \frac{2\mu}{3\epsilon_p}(\nabla \cdot \boldsymbol{u})\boldsymbol{I}\right] - \frac{\mu}{k_p}\boldsymbol{u}$$

The heat in solid and fluid is simulated using heat transfer equation.Results and Discussion

Simulations were carried out on desktop PC with Intel Core i5-6400 CPU on 2.7GHz and 32GB RAM memory. First simulations were executed for the steady laminar fluid flow only through reaction volume with inserted porous media and without heat transfer. Three values of inlet flow rate are selected for flow simulations: 2.923, 1.949, and $0.974 \cdot 10^{-6} m^3/s$. The methanol-water mixture ratio was 1:1.3 and the fluid temperature was 180℃. The catalyst particle diameter was 300 μm, bulk density was 1.1g/mL, and catalyst density was 4.7g/mL.

These numerical results have already been presented in details in Refs. [9] and [10]. The main characteristic of the free flow is recirculation at the entrance of the inlet chamber, which, as expected, weakens with decreasing of the inlet flow rate (see Refs. [9] and [10]).

For the final model, with complete geometry and heat transfer included, the SS304 stainless steel was selected as the material for the plates. The constant temperature of 180℃ is applied at the top surface of the top plate, the insulation boundary condition is applied at the bottom of the bottom plate, and the heat flux to the surroundings is applied at the side boundaries. The heat transfer coefficient was set to constant value of 10W/m^2·K.

The fluid mixture, which is already preheated in the vaporizer, is also set to a temperature of 180℃. Although other options are taken into account for the fluid inlet temperature, it has been noticed that it reaches the temperature maximum shortly after entering the inlet chamber. All material parameters were set to be dependent on temperature and are recalculated during simulations.

Resulting temperature range, illustrated in Figure 2, is between 178.6 and 180℃.

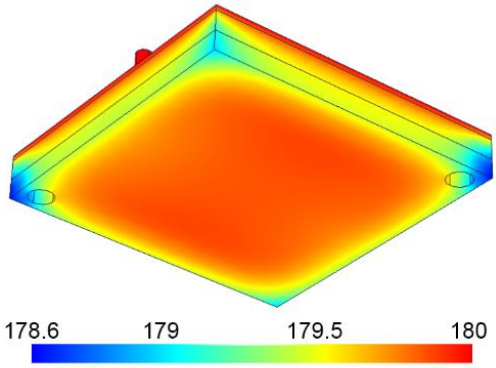

Figure 2 Temperature distribution for the final model in the case of the highest inlet flow rate

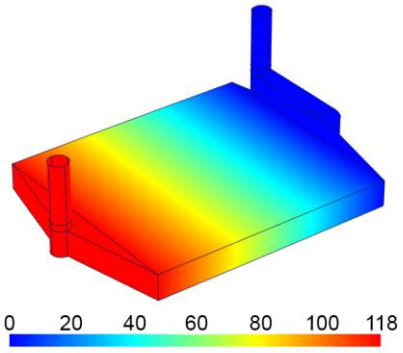

Figure 3 Pressure distribution in the reactor volume for the final model in the case of the highest inlet flow rate

The gage pressure for two solutions, without and with heat transfer and complete geometry, at the entrance region of the porous media is illustrated in Figure 4. Difference between gage pressures for two models is approximately 0.2Pa.

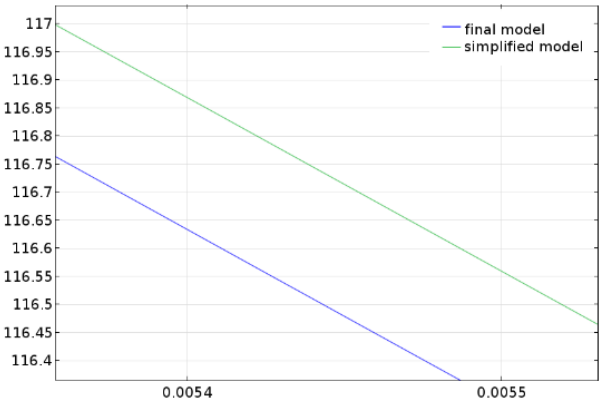

Figure 4 Gage pressure distribution at the entrance region of porous media presented for two solutions (simplified and final model)

4. SENSITIVITY ANALYSIS

The model named in this work as "final reforming reactor model" is already robust and packed with uncertain parameters. The flow parameters are: inlet flow rate, fluid density and viscosity and catalyst density and porosity. The heat transfer parameters are density, heat capacity, and conductivity for fluid, solid, and porous media, one or more boundary temperatures, and one or more heat transfer coefficients. Some of the parameters are imposed temporarily and planned to be changed in the future in accordance with experimental results, for example. In addition, there are two completely different types of flows – free flow and porous media flow. Because of large difference in values, they must be observed separately.

Sensitivity analysis is carried out using finite differences calculated from the flow solutions obtained for the above mentioned highest inlet flow rate.

Sensitivity of pressure with respect to inlet flow rate in the inlet part of the reactor is presented in Figure 5.

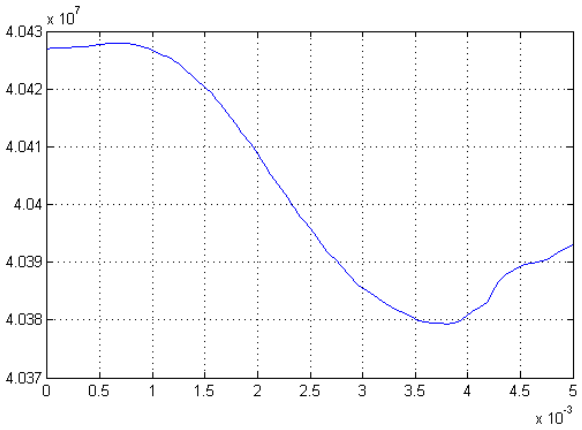

Figure 5 Sensitivity of pressure with respect to inlet flow rate presented at the mid-line lying in the symmetry plane of the inlet chamber

The form of the sensitivity curve has the form of the pressure curve ([9], [10]). The value of sensitivity decreases almost along the entire length of the chamber and has the positive value over the entire length.

Sensitivity of temperature with respect to inlet flow rate in the porous media is illustrated in Figure 6. The value of sensitivity rapidly decreases in the first few millimetres of the porous media. The value of temperature sensitivity is also positive over the entire length.

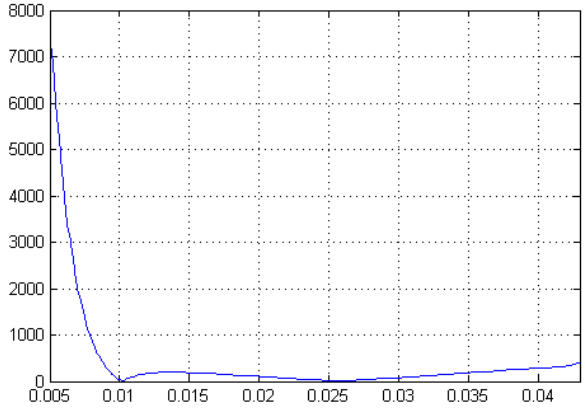

Figure 6 Sensitivity of temperature with respect to inlet flow rate presented along the axis of symmetry of the porous media

Temperature sensitivity at the cross section parallel to the bottom of the reaction volume is presented in Figure 7. It is even more clear from that figure that the sensitivity of temperature with respect to the inlet flow rate is highest at the inlet chamber and that it rapidly decreases in the central part of the entrance into the porous media.

Compared to other regions, a higher value of temperature sensitivity can be observed in the outlet chamber and channel (Figure 7).

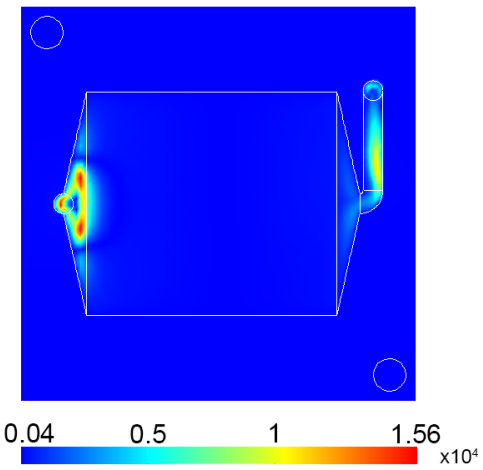

Figure 7 Sensitivity of temperature with respect to inlet flow rate presented at the cross section parallel to the bottom with distance of 2mm from the bottom of the reaction volume

The sensitivities with respect to temperature are important since almost all parameters of the model are temperature dependent. Here only sensitivities with respect to temperatures imposed at the boundaries will be presented.

From the results for the sensitivity of temperature with respect to temperature of the top boundary, illustrated at Figure 8, this sensitivity experiences minor change along the porous media. Despite the appearance of the curve, the order of magnitude of the change is 10^{-4}.

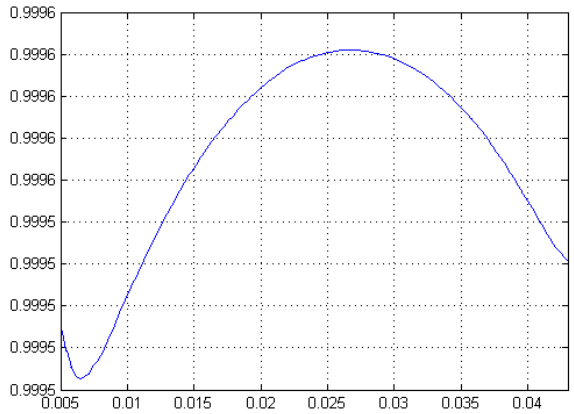

Figure 8 Sensitivity of temperature with respect to constant temperature boundary condition at the top of the top plate presented along the axis of symmetry of the porous media

In contrast to temperature sensitivity the pressure sensitivity with respect to this boundary temperature is not negligible, it has the positive value and linearly decrease through porous media (see Figure 9).

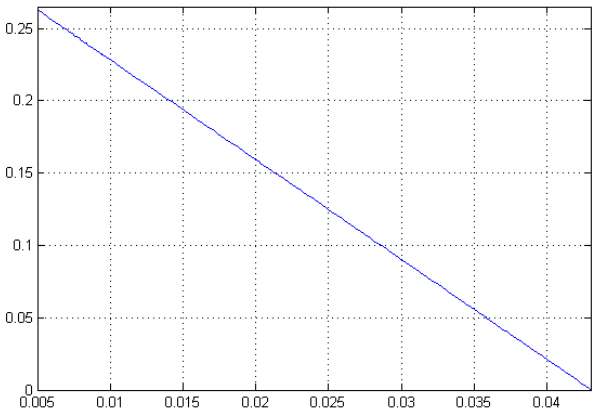

Figure 9 Sensitivity of pressure with respect to constant temperature boundary condition at the top of the top plate presented along the axis of symmetry of the porous media

In the previous calculations, the same value is imposed as the top boundary wall temperature and as the fluid inlet temperature. Distinct values are selected for fluid inlet temperature for sensitivity calculations.

The pressure sensitivity, illustrated in Figure 10, has completely different behaviour than in the previous case. It has much smaller value and is negative almost the entire length of the porous media.

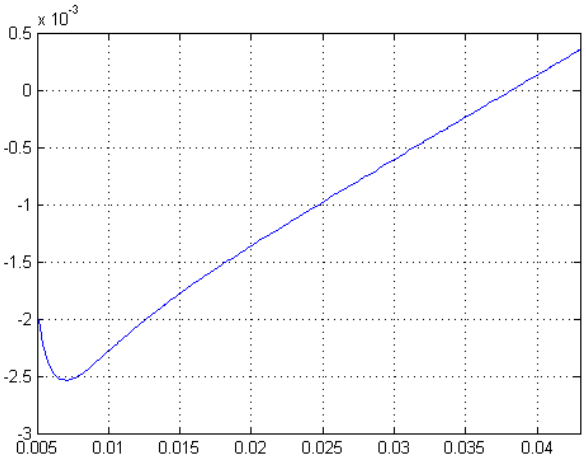

Figure 10 Sensitivity of pressure with respect to inlet flow temperature presented along the axis of symmetry of the porous media

The value of temperature sensitivity is positive as expected and rapidly decreases at the first part of the porous media (see Figure 11).

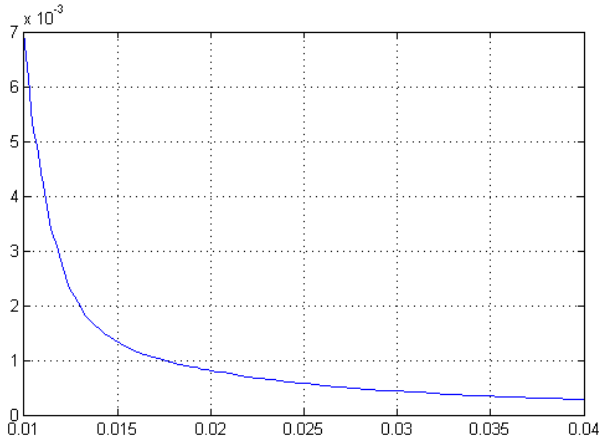

Figure 11 Sensitivity of temperature with respect to inlet flow temperature presented along the axis of symmetry of the porous media

5. CONCLUSIONS

Sensitivity analysis of this model is complex as well as the model. It is difficult to create the selection of all parameters and regions which are important. In this work, the boundary conditions are selected as sensitivity parameters, in the further work, more effective selection will be performed. Also, the sensitivity calculations must be tested for different values of inlet flow rate or other sensitivity analysis method must be applied.

Since the model was built gradually, it was interesting to compare the results obtained with, end without heat transfer model.

6. ACKNOWLEDGEMENTS

This research was carried out under the NATO Science for Peace Project EAP.SFPP 984738, and the Ministry of Education and Science of the Republic of Serbia projects TR35040 and III 43007. Slovenian Research Agency is gratefully acknowledged for supporting the Programme P2-0152, Chemical Reaction Engineering

7. REFERENCES

[1] A. Iulianellia, P. Ribeirinhab, A. Mendesb and A. Basilea, "Methanol steam reforming for hydrogen generation via conventional and membrane reactors: A review," *Renewable and Sustainable Energy Reviews,* vol. 29, p. pp 355–368, 2014.

[2] D. R. Palo, R. A. Dagle and J. D. Holladay, "Methanol Steam Reforming for Hydrogen Production," *Chemical reviews,* vol. 107, no. 10, p. pp 3992–4021, 2007.

[3] C. Pan, R. He, Q. Li, J. O. Jensen, N. J. Bjerrum, H. A. Hjulmand and A. B. Jensen, "Integration of high temperature PEM fuel cells with a methanol reformer," *Journal of Power Sources,* vol. 145, p. pp 392–398, 2005.

[4] A. V. Pattekar and M. V. Kothare, "A radial microfluidic fuel processor," *Journal of Power Sources,* vol. 147, p. pp 116–127, 2005.

[5] A. Pohar, D. Belavič, G. Dolanc and S. Hočevar, "Modeling of methanol decomposition on Pt/CeO2/ZrO2 catalyst in a packed bed microreactor," *Journal of Power Sources,* vol. 256, pp. 80-87, 2014.

[6] P. Ribeirinha, M. Boaventura, J. C. B. Lopes, J. M. Sousa and A. Mendes, "Study of different designs of methanol steam reformers: Experiment and modeling," *International journal of hydrogen energy,* vol. 39, pp. pp 19970-19981, 2014.

[7] K. Shah and R. Besser, "Understanding thermal integration issues and heat loss pathways in a planar microscale fuel processor: Demonstration of an integrated silicon microreactor-based methanol steam reformer," *Chemical Engineering Journal,* vol. 135S, p. pp S46–S56, 2008.

[8] J. C. Telotte, J. Kern and S. Palanki, "Miniaturized Methanol Reformer for Fuel Cell Powered Mobile Applications," *International journal of chemical reactor engineering,* vol. 6, no. 1, pp. pp 1542-6580, 2008.

[9] I. Ivanović, A. Sedmak and M. Milošević, "The Influence of Inlet Geometry on the Performance of a Micro Methanol Steam Reformer," in *The 6th International Conference and Workshop, REMOO-2016*, Budva, Montenegro, 2016.

[10] I. Ivanović, A. Sedmak, M. Milošević, I. Cvetković, A. Pohar and B. Likozar, "Influence of Geometry on Pressure and Velocity Distribution in Packed-bed Methanol Steam Reforming Reactor," in *14th International Conference on Numerical Analysis and Applied Mathematics, ICNAAM 2016*, Rhodes, Greece, 2016.

Structural Integrity Assessment of a Pressure Vessel

Aleksandar S. Sedmak[a], AleksandarMilovanovic[b], Simon A. Sedmak[c]

[a]Faculty of Mechanical Engineering, University of Belgrade, Serbia,
asedmak@mas.bg.ac.rs

[b]D.Sc student at the Faculty of Mechanical Engineering, University of Belgrade, Serbia,

[c]Innovation Centre of Faculty of the Mechanical Engineering, Belgrade, Serbia

Abstract

Fracture mechanics parameters have been applied to assess structural integrity of a pressure vessel with unacceptable defect (lack of penetration) detected in welded joint. This defect has been modelled as a crack of equivalent dimensions, for which the stress intensity factor has been evaluated, for different sizes of plastic zone. These values have been compared with the critical value, i.e. with the fracture toughness, taken as the minimum value according to previous experimental research. Beside brittle fracture, plastic collapse has been considered, as well as their combination, given in the form of Failure Assessment Diagramme (FAD). In any case, this analysis has proved that pressure vessel is safe under given operating conditions.

Keywords: Structural integrity, pressure vessels, welded joint defects

1. INTRODUCTION

Shown in figure 1 is the comparison of classic design methods which apply strength theory vs the application of fracture mechanics.

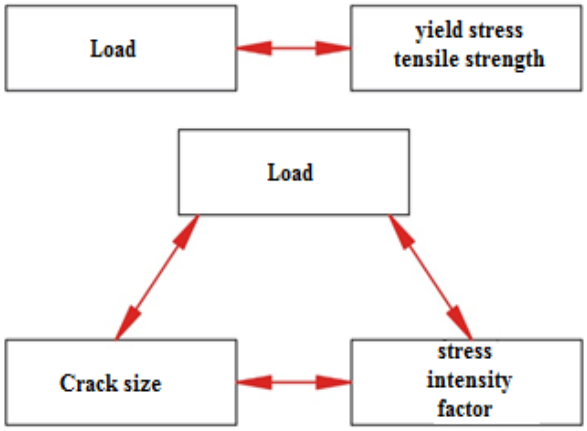

Figure 1. Design using: a) classic strength theory methods, b) fracture mechanics methods

In the case of design using classic strength theory, for given dimensions and loads, maximum stress is calculated and the material to be used is adopted in a way that ensures that it has a satisfying level of yield or tensile strength, or vice versa, maximum load is calculated for a given material. When applying fracture mechanics to design, there are three typical variables: structure load, damage magnitude (cracks) and stress intensity factor [1].

Shown in figure 2 is the classification of fracture mechanics depending on material behaviour. Linear elastic fracture mechanics assumes a linearly independent material behaviour under quasi-static load. For non-linear material behaviour and quasi-static loading, elastic-plastic fracture mechanics is applied. Dynamic, visco-elastic(plastic) fracture mechanics includes time as a variable, making material behaviour time-dependent [1].

As an example, let us analyse a membrane with a crack, loaded up to fracture, and let us give a schematic view of the relation between the load at fracture and the stress intensity factor.

For materials with a low stress intensity factor, brittle fracture is the main fracture mode, and the critical load varies linearly with the stress intensity factor. For materials with a high stress intensity factor, linear fracture mechanics no longer apply and structural failure is typically related to the yield stress or tensile strength.

For materials with medium stress intensity factor values, there is a transition are between brittle and ductile fracture. Non-linear fracture mechanics related linear FM with plastic strain. From this, it can be concluded that linear elastic fracture mechanics is applied to problems which involve lower values of stress intensity factor. However, if the stress intensity factor is high, fracture mechanics is no longer relevant, since the load at fracture does not depend on toughness, and in these cases, boundary analysis is used [1].

In this paper the linear elastic fracture mechanics concept is applied to assess structural integrity of a pressure vessel, i.e. a pipe in the hydro power plant Bajina Basta.

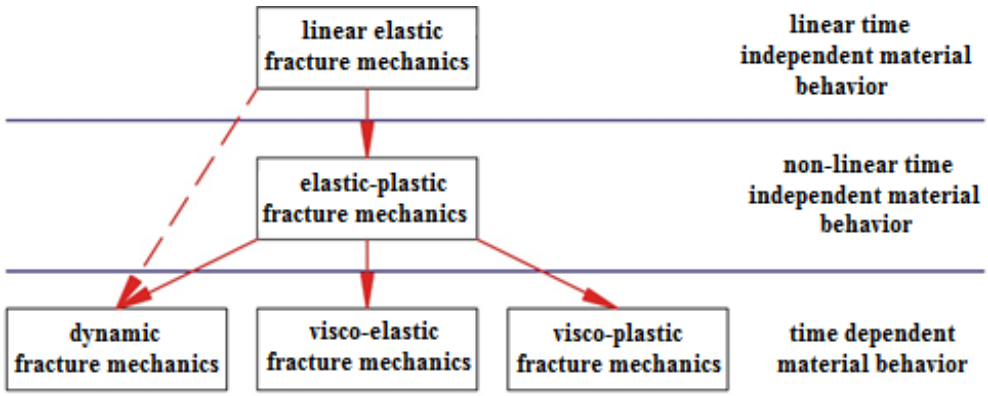

Figure 2. Fracture mechanics classification according to mechanical behaviour of the material, [1,2]

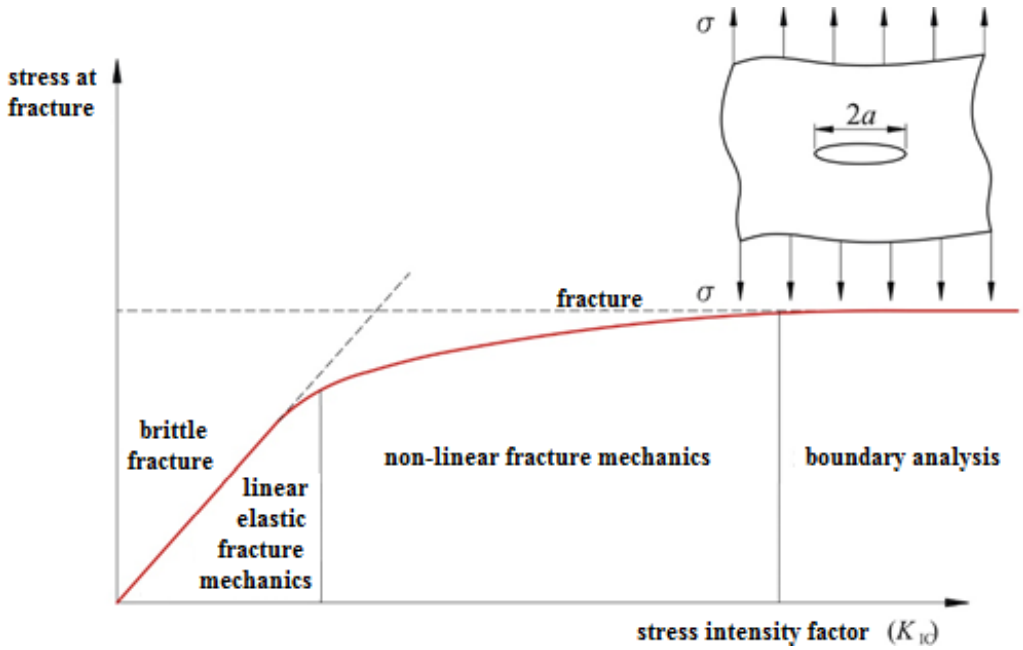

Figure 3. Influence of the stress intensity factor on structural failure mechanism, [1,2]

2. STRESS CALCULATION

Based on the expression $K_I = \sigma \cdot \sqrt{\pi \cdot a}$, i.e. the stress intensity factor for an infinite membrane in tension, with a central crack, tensile stress σ is determined. Primary load acting on the pipe is the internal pressure p, which is in balance with internal stresses in a cylindrical pipe:

$$\sigma_m / \rho_m + \sigma_t / \rho_t = p / s$$

$\rho_t = r$ - pipe radius,

$\rho_m = \infty$

$\sigma_m = \dfrac{p \cdot r}{2 \cdot s}$ - axial stress

$\sigma_t = \dfrac{p \cdot r}{s}$ - hoop stress

Stress intensity factor is increased by 12% since the edge crack opens more compared to a central crack, due to less geometric boundaries. In addition, it is also increased by the value of residual stress, *f*, determined using also conservative procedure. Expression for determining of stress intensity factor:

$$K_I \cong 1{,}12 \cdot (\sigma_m + 0{,}4 \cdot f) \cdot \sqrt{\pi \cdot a} \quad MPa\sqrt{mm}$$

2.1 Allowed stresses

Pipe material: STPG-38; Standard: JIS G 3454

Chemical composition in %:

Designation	C_{max}	Mn_{max}	Si_{max}	P_{max}	S_{max}
STPG-38	0,25	0,30÷0,90	0,35	0,04	0,04

Mechanical properties:

Designation	Yield stress MPa	Tensile strength MPa	Elon. %
STPG-38	215	370	30

Allowed stress:

STANDARD			ALLOWED STRESS	
EN 13480			$\min\left(\frac{R_m}{2,4}, \frac{R_{p0,2}}{1,5}\right)$	
Element name	Material	p [*bar*]	Min σ [N/mm^2]	$\sigma_{allowed}$ [N/mm^2]
seamless pipe ϕ219,1 ×12.7 mm	STPG-38	51,97	$R_m / 2,4$	154,16
	JIS G 3454		$R_{p0,2}/1,5$	143,33

2.2 Pipeline calculation according to SRPS EN 13480-3

$p = 51.97$ *bar* - Calculated pressure

$D_0 = 219.11$ *mm* - Outer pipe diameter

$e_n = 12.7$ *mm* - Nominal wall thickness

$R_m = 370$ *MPa* – Min. tensile strength

$R_{p0.2} = 215$ *MPa* - Yield stress for 0,2%

$z = 1.0$ - Welded joint quality coefficient

$c_1 = 12.5\% \cdot e_n = 1.587$ *mm* - Negative tolerance value for nominal wall thickness

$c_2 = 1.0$ *mm* - Addition to corrosion and wear

$D_i = D_0 - 2 \cdot e_n = 193.7$ *mm*- Inner pipe diameter

$D_m = D - e_n = 206.4$ *mm*- Outer pipe diameter

Condition for application of the standard $D_0/D_i < 1.7$:

$$\frac{D_0}{D_i} = 1{,}13$$

Calculation of the nominal design stress:

$$f = \left(\frac{R_m}{2,4}, \frac{R_{p0,2}}{1,5}\right) = 143{,}33 MPa$$

Minimum required pipe wall thickness without additions – for the inner pressure:

$$e = \frac{p \cdot D_i}{2 \cdot f \cdot z - p} = \frac{5{,}197 MPa \cdot 193{,}7 mm}{2 \cdot 143{,}33 MPa \cdot 1{,}0 - 5{,}197 MPa} = 3{,}58 mm$$

Minimum wall thickness without additions:

$$e_a = e_n - c_1 - c_2 = 10{,}11 mm$$

Stress along the generatrix:

$$\sigma_m = \frac{p \cdot D_i + e \cdot p}{2 \cdot e_n \cdot z} =$$

$$= \frac{5{,}197 MPa \cdot 193{,}7 mm + 3{,}58 mm \cdot 5{,}197 MPa}{2 \cdot 10{,}11 mm \cdot 1{,}0} =$$

$$= 40{,}36 MPa$$

Stress along the generatrix increased by the value of residual stress:

$$\sigma_u = 1{,}12 \cdot (\sigma_m + 0{,}4 \cdot f) =$$

$$= 1{,}12 (40{,}36 + 0{,}4 \cdot 143{,}33) = 109{,}42 MPa$$

Stress intensity factor:

Defects	L (mm)	a(mm)
Incomplete penetration	200	2

$$K_I \cong 1{,}12 (\sigma_m + 0{,}4 \cdot f) \cdot \sqrt{\pi a} \left[MPa\sqrt{mm} \right]$$

$$a = 2mm \rightarrow K_I = 274{,}27 MPa\sqrt{mm}$$

Critical stress intensity factor value for material STPG-38:

$$K_{Ic} = 1580 MPa\sqrt{mm}$$

Since $K_I = 274{,}27 MPa\sqrt{mm}$ is just 17% of the critical value $K_{Ic} = 1580 MPa\sqrt{mm}$, structural integrity is not compromised.

Plasticity is taken into account by applying Irwin model for crack tip opening displacement, the correction factor r_y can be determined, and treated as the crack length increase factor ($a + r_y$). Results are given in Table 1. Correction factor r_y is determined using the following expression:

$$r_y = \frac{\frac{1}{\pi}\cdot\left(\frac{K_I}{R_e}\right)^2}{2}$$ -for plane stress state

$$r_y = \frac{\frac{1}{\pi}\cdot\left(\frac{274,27}{215}\right)^2}{2} = 0,259mm \cong 0,3mm$$

Table 1: Influence of crack length increase on the stress intensity factor

Crack length $a_n = 2 + n \cdot r_y\ [mm]$		Stress intensity factor $K_{I(n)} \cong 1,12\left(\sigma_m + 0,4 \cdot f\right)\cdot\sqrt{\pi a_n}\ \left[MPa\sqrt{mm}\right]$
n = (1,2,3, …,15)	$a_n\,[mm]$	
1	2,3	294,13
2	2,6	312,72
3	2,9	330,27
4	3,2	346,93
5	3,5	362,93
6	3,8	378,06
7	4,1	392,70
8	4,4	406,82
9	4,7	420,45
10	5,0	433,66
11	5,3	446,48
12	5,6	458,08
13	5,9	471,08
14	6,2	482,91
15	6,5	494,45
For a_n = 9 *mm*		581,83
For a_n = 12 *mm*		671,83
For $a_n = 2 \cdot e_n$ = 25.4 *mm*		977,44

3. CONCLUSION

For all crack lengths considered in this paper (Table 1) the critical value of the stress intensity factor has not been reached, so the structural integrity of analysed pipe is not compromised.

4. ACKNOWLEDGEMENT

This research was supported by the Ministry of Education, Science and Technological Development, project TR 35040 project.

5. REFERENCES

[1] T.L. Anderson, Fracture Mechanics: Fundamentals and Applications, CRC Press, Boca Raton, 1995.

[2] E.E. Gdoutos, C. A. Rodopoulos, J. R. Yates, Problems of Fracture Mechanics and Fatigue: A Solution Guide, Kluwer Academic Publishers, Dordrecht, 2003.

Flat Die Sliding Model with Variable Contact Pressure in Deep Drawing Process

M. Djordjević[a], S. Aleksandrović[b], A. Sedmak[a], R. Nikolić[a], V. Lazić[b], D. Arsić[a],

Abstract

The influence of contact pressure in deep drawing processes is the current research subject related to sheet processing technology. Within this research, a tribological model was developed based on the flat die sliding process between contact surfaces under variable pressure during the process, and an original experimental computerized device was made for this purpose. A complex multi-factor experiment was performed, using an Al alloy and contact elements of varying roughness, various lubricants and variable contact pressure during the process. In addition to the description of the machinery, this paper also presents the way in which theoretical variable contact pressure dependencies were determined. Based on the predefined, theoretical pressure variations for each of the conditions mentioned here, real contact pressure was obtained. Based on this, it was possible to determine the effect of tribological factors on real pressure. Obtained real contact pressure shows the reliability of the experimental machinery, i.e. the degree of present deviations of theoretical pressure dependencies from the real ones.

Keywords: flat-die test, deep drawing, tribological model, variable contact pressure

1. INTRODUCTION

The possibilities of affecting the process of deep drawing during its duration are limited. They are reduced to the effects on the sheet edge, typically through contact pressure (holding force) and due to effects from tensile anchors of the support. Typically, in today's research, values of the holding force or support pressure were adopted as constant in the case of deep drawing tools. Continuous defining of variable pressure using predefined functions, during the sliding process and the development of the corresponding physical model represents the subject of this study, with the aim to include the influence of variable contact pressure during the deep drawing process, in addition to other corresponding effects (tool, contact conditions, material, etc.). The influence of variable contact pressure during the deep drawing process represents a current topic in the field of discovering the possibilities of management of this process. For this purpose, physical-tribological models are developed, wherein sheet strip sliding between two flat contact surfaces is typically applied, as can be seen from various relevant [1-5] papers. In the aforementioned papers, the issue of modelling a deep drawing process for sheet edges between flat contact surfaces of the support and the matrix was discussed. Tribological models were formed in a totally realistic environment, in terms of materials, tools, machinery, contact conditions, etc. Most of the research monitors the change in the friction coefficient and deformation (pulling) force by varying the above mentioned real conditions under which the process takes place. The contact conditions are, along with the state of tool contact surfaces, achieved by using multiple types of lubricants for deep drawing, as well as by using sheets with various coating (Al and steel sheets). In addition, it is possible to vary the sheet siding speed [6, 7]. The goal of these researches is to manage the output parameters of the deep drawing process with a tendency to obtain deformation force and friction coefficient values that are as low as possible. On the other hand, desired geometry without edge defects (ripples) should be achieved as well [8-10].

2. TRIBOLOGICAL MODEL AND EXPERIMENTAL SETUP

2.1 Tribological model

Deep drawing of parts with complex geometry is followed by a number of relevant parameters. Thus, this process is one of the most complex and demanding in plastic shaping technology. For better understanding of this process, the principle of physical modelling of characteristic zones of a complex part is applied (fig. 1a), which represents the basis for complete tribological modelling [11]. Sheet sliding (drawing) between flat support and matrix surfaces (model "A", fig. 1a) corresponds to zones which are not subjected to tangential compression, but only to radial tension.

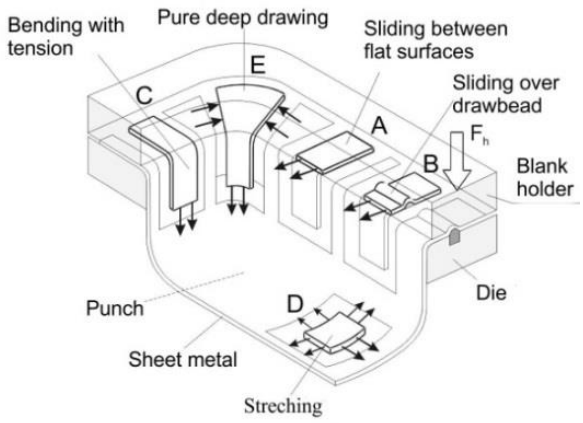

Fig. 1. a) The schematics of physical modelling of deep drawing of complex geometries; b) Schematics of testing of sliding between contact surfaces

Tensile force, caused by the drawer, is transferred to the zones under the support via a filleted matrix edge (fig. 1b).

Values of surface pressure during sliding are lower than the yield stress and correspond to values underneath the support. The sheet slides between the compressed surfaces and the deformation is elastic since the longitudinal stress does not exceed the yield stress. Changes in contact surfaces (wear, bonded particles, etc.) can interfere with the sliding process stability.

2.2 Experimental setup

Experimental setup, developed for the purpose of this research, represents a simulator for realization and studying of a physical model of an important segment of the deep drawing process in entirely realistic conditions. The device is basically made of: a laboratory triple effect press ERICHSEN 142/12, a hydraulic-mechanical module assembly, a separate hydraulic modul and an electro-electronic module. The hydraulic module consists of a hydraulic aggregate (pump, tank, filter, regulation valve and a three-stage manual distributor), which ensures sufficient pressure levels (fig. 2).

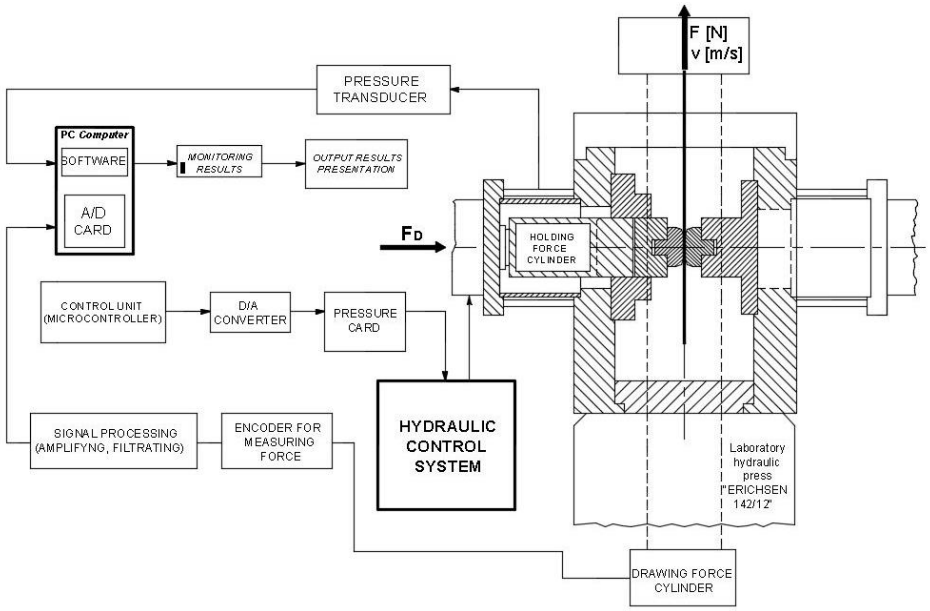

Fig. 2. Schematics of sheet strip drawing device with flat contact surfaces

3. EXPERIMENTAL PRESSURE FUNCTIONS

By using the experimental setup shown above, a complex multi-factor experiment with a large number of tribological contact conditions was performed. This involved different contact surface roughness of sliding elements, different types of sheets and lubricants [12, 13], along with simultaneous input of defined pressure values P1-P4. A large number of results conditioned by various combinations of these conditions was obtained. Shown in this paper is a part of those results, related to the analysis of achieved real pressure dependencies from stroke for an aluminium sheet AlMg4.5Mn0.7 (0.9 mm), for two types of lubricants (deep drawing oil, lubricating oil based on MoS_2) for given pressure functions P1-P4.

The focus was on checking the reliability of real obtained pressure dependencies for each of the analytically given functions (P1, P2, P3 and P4, defined in section 3 of the paper). Four types of sliding contact surface elements were used (ground surfaces, nitrated surfaces, polished surfaces and TiN coated surfaces), figs. 3-4.

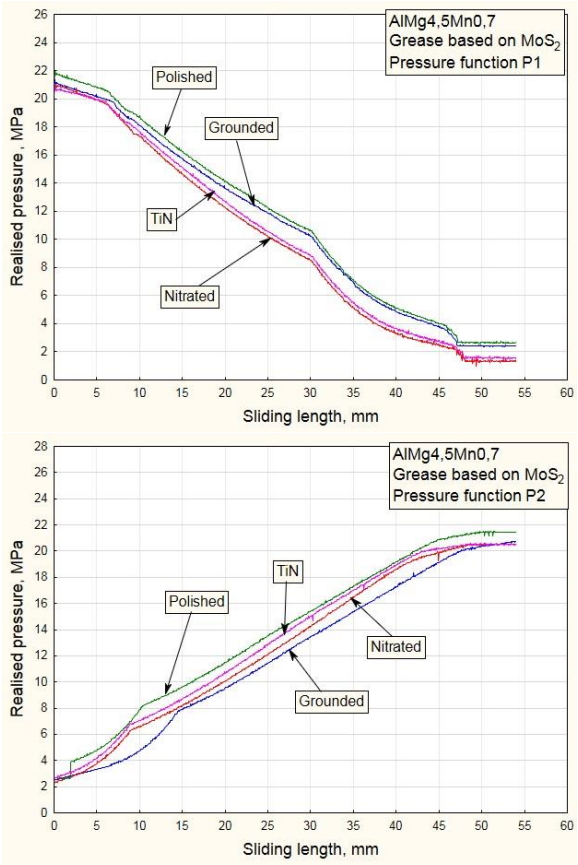

Fig. 3. Obtained values for pressures P1 (a) *P2* (b) *using MoS_2 based lubricant oil*

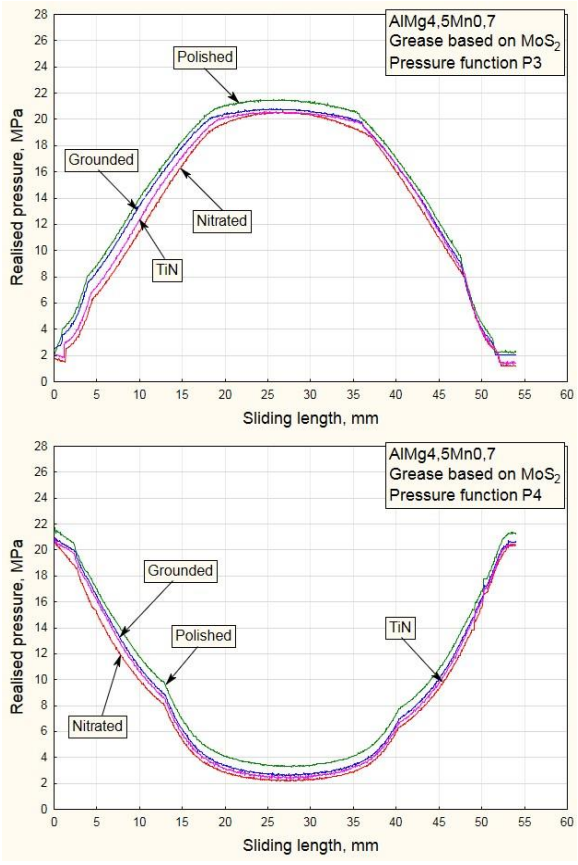

Fig. 4. Obtained values for pressures P3(a) P4 (b)using MoS2 based lubricant oil

In this way, it was possible to draw conclusions about the functioning of the setup, i.e. the measure of deviation of real pressure functions under the given conditions compared to theoretical pressure curves. In addition, it is possible to determine the effect of tribological conditions on the realistically achieved pressure.

4. CONCLUSION

Described in this paper was the original experimental setup developed for the realization of a physical model used for studying of the behaviour of sheet edges during deep drawing. Presented results confirm that by properly selecting the functional dependence between the contact pressure and tribological conditions, it is possible to positively affect the sliding of sheet edges, while minimising numerous problems that occur during this process in real manufacturing conditions. Conclusions from this research can be summed up as the following:

a) The setup is fully functional and very successful in realizing of given mathematical pressure functions, as shown in the real pressure dependence diagrams (figs. 3-4);

b) The effect of lubricant type and the state of contact surfaces on the real measured pressure is negligible. Varying of the aforementioned tribological conditions would lead to various dependencies between the pulling force and the friction coefficient, which opens more space for further research and application of such a setup;

c) Realization of this experimental setup and the results achieved by it have considerable significance as an alternative approach in the field of modern thin sheet shaping technology;

d) Further research should include the use of various materials, such as high strength steel sheets, stainless steel sheets, etc.

5. REFERENCES

[1] L. Fratini, S. L. Casto, E. L. Valvo: A technical note on an experimental device to measure friction coefficient in sheet metal forming, Journal of Materials Processing Technology, Vol. 172, No. 26 (2006), pp.16-21.

[2] E. D. Szakaly, J. G. Lenard: The effect of process and material parameters on the coefficient of friction in the flat-die test, Journal of Materials Processing Technology, Vol. 210, No. 30 (2010), pp. 868-876.

[3] L. Figueiredo, A. Ramalho, M. C. Oliveira, L. F. Menezes: Experimental study of friction in sheet metal forming, Wear, Vol. 271 (2011), pp. 1651-1657.

[4] J. Coello, V. Miguel, A. Martinez, F. J. Avellaneda, A. Calatayud: Friction behavior evaluation of an EBT zinc-coated trip 700 steel sheet through flat friction tests, Wear, Vol. 305 (2013), pp. 129-139.

[5] A. Yanagida, A. Azushima: Evaluation of coefficients of friction in hot stamping by hot flat drawing test, CIRP Annals-Manufacturing Technology, Vol. 58 (2009), pp. 247-250.

[6] A. V. Manoylov, M. J. Bryant, H. P. Evans: Dry elasto-plastic contact of nominally flat surfaces, Tribology International, Vol. 65, No. 21 (2013), pp. 248-258.

[7] J. Kondratiuk, P. Kuhn: Tribological investigation on friction and wear behaviour of coatings for hot sheet metal forming, Wear, Vol. 270 (2011), pp. 839-849.

[8] A. Ghiotti, S. Bruschi: Tribological behaviour of DLC coatings for sheet metal forming tools, Wear, Vol. 271 (2010), pp. 2454-2458.

[9] B. H. Lee, Y. T. Keum, R. H. Wagoner: Modeling of the friction caused by lubrication and surface roughness in sheet metal forming, Journal of Materials Processing Technology, Vol. 130-131 (2002), pp. 60-63.

[10] L. Kirkhorn, V. Bushlya, M. Andersson, J. E. Stahl: The influence of tool steel microstructure on friction in sheet metal forming, Wear, Vol. 302 (2013), pp. 1268-1278.

[11] S. Aleksandrović, M. Stefanović, D. Adamović, V.Lazić, M. Babić, R. Nikolic, T. Vujinovic: Variable tribological conditions on the flange and nonmonotonous forming in deep drawing of coated sheets, Journal of the Balkan Tribological Association, Vol.17, No.2 (2011) pp. 165-178.

[12] L. Peña-Parás D. Maldonado-Cortés, J. Taha-Tijerina P. García-Pineda, G. Tadeo Garza, M. Irigoyen, J. Gutiérrez, D. Sánchez: Extreme pressure properties of nanolubricants for metal-forming applications, Industrial Lubrication and Tribology, Vol. 68, No. 1 (2016), pp. 30-34.

[13] J. Mucha, J. Jaworski: The tool surface wear during the silicon steel sheets blanking process, EksploatacjaiNiezawodnosc – Maintenance and Reliability, Vol. 18, No. 3 (2016), pp. 332-342.

Thermal Analysis of Packed-bed Methanol Steam Reforming Reactor

Ivana Ivanović[a], Aleksandar Sedmak[b], Emina Džindo[a], Simon Sedmak[a], Andrej Pohar[c], Blaž Likozar[c]

[a] Innovation Centre, Faculty of Mechanical Engineering, University of Belgrade, Kraljice Marije 16, 11120 Belgrade 35, Serbia

[b] Faculty of Mechanical Engineering, University of Belgrade, Kraljice Marije 16, 11120 Belgrade 35, Serbia

[b] Department of Catalysis and Chemical Reaction Engineering, National Institute of Chemistry, Hajdrihova ulica 19, 1000 Ljubljana, Slovenia

Abstract

The efficiency of indirect internal reforming reactor depends, among other, on the temperature of the surrounding system. Since the temperature of the surroundings is difficult to control as it originates from an electro-chemical reaction in the neighboring fuel cell stack, the main goal of this study was to analyze the dependence, and the sensitivity of the system to the temperature changes. In addition to numerical simulations for different values of temperature, possible deformation of the plates was analyzed. As expected, for this values of temperature, and the stainless steel as components material, the deformation is negligible and it does not have significant influence on the system.

Keywords: steam reforming reactor, heterogeneous catalyst bed, laminar flow, CFD, heat transfer

1. INTRODUCTION

The idea of an indirect internal reforming fuel cell system is little more than a decade old. Upon review given in Ref. [1], first study dealing with this type of fuel cell system dates back to 2005, and is described in Ref. [2]. The indirect internal reforming means that the reforming reactor, with other supporting parts, is included in the fuel cell system as a separate stack. The operation of the system is based on thermal exchange between exothermic electro-chemical process, taking place in fuel cell stack, and endothermic reforming process, taking place in reforming reactor stack. The energy exchange is enabled through a contact surface between fuel cell and reforming reactor stacks.

Detailed analysis of similar plate-type reactor was presented in Ref. [3]. The numerical analysis of the geometry of this reactor is given in Refs. [4] and [5], simulations were performed for constant value of temperature.

In this work, the thermal analysis of the reforming reactor stack was performed. The heat transfer was included in the simulation.

2. MODEL DESCRIPTION

The external dimensions of the reformer 60×60mm correspond to the dimensions of the fuel cell stack. It is composed of three plates, illustrated in Fig.1(top). The middle plate contains reaction volume, inlet and outlet channels, and inlet and outlet chambers. The catalyst bed in the reaction volume is expected to be separated from the channels with stainless steel mesh, a space left for that purpose is 3mm in front and behind of the reaction volume.

Diameters of the inlet and the outlet are 3mm. The inlet and outlet and the reaction volume are colored in gray in Fig.1(bottom).

The rest of the data are - methanol-water mixture ratio 1:1.3, temperature at the top surface of the reformer stack 180-240℃, expected to be effective at the lowest possible temperature, and flow rate at the inlet of $2.923 \cdot 10^{-6} m^3/s$. The catalyst particle diameter is 250-500mm, bulk density is 1.1g/mL, and catalyst density is 4.7g/mL.

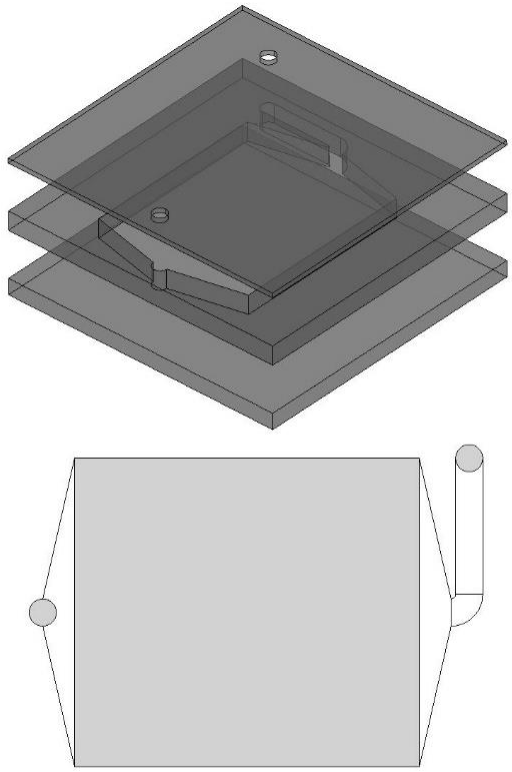

Figure 1 Methanol steam reformer stack (top) and the cross section of the reaction volume with channels and chambers (bottom)

3. NUMERICAL SOLUTION

Flow simulations were carried out following the procedure given in Ref. [6]. The steady incompressible Navier-Stokes equations are applied to free flow areas

$$\varrho\vec{u} \cdot \nabla\vec{u} = \nabla \cdot [-p + \mu(\nabla\vec{u} + (\nabla\vec{u})^T)]$$

$$\nabla\vec{u} = 0$$

and the Brinkman equation was used to simulate flow through porous media

$$\left(\frac{\mu}{k}\right)\nabla\vec{u} = \nabla \cdot \left[-p + \frac{\mu}{\varepsilon}(\nabla\vec{u} + (\nabla\vec{u})^T)\right]$$

$$\nabla\vec{u} = 0$$

where ε and k are porosity and permeability respectively. The heat in solid and fluid is simulated using heat transfer equation.

Mass transport equation, used for the simulation of chemical reaction

$$-\nabla \cdot \overrightarrow{N_\iota} + R_i = 0$$

Flux of species, $\overrightarrow{N_\iota}$, and rate of generation of species, R_i, are given with the following equations

$$\overrightarrow{N_\iota} = -D_i\nabla C_i + C_i\nabla\vec{u} \qquad R_i = \rho_{cat}(1-\varepsilon)\nu_i r_M$$

where D_i is effective diffusion coefficient of gas species, C_i is concentration of species, ν_i is stoichiometric coefficient of species for methanol, and r_M is rate of methanol steam reforming.

For the flow calculations, the flow rate was imposed as laminar inlet boundary condition, and the zero gage pressure was imposed at the outlet. The heat transfer boundary conditions were constant temperature at the top surface of the reactor stack, insulation at the bottom of the stack and heat flux at the side walls.

4. RESULTS AND DISCUSSION

Simulations were carried out on desktop PC with Intel Core i5-6400 CPU on 2.7GHz and 32GB RAM memory.

Initial calculations were executed for the inlet flow rate of $2.923 \cdot 10^{-6} m^3/s$ and top surface temperature of 180℃. With the insulation at the bottom, and the heat flux to the surroundings at the side walls with the value of heat transfer coefficient of $10 W/(m^2K)$, the temperature difference through the reactor is barely 0.25℃. This can be confirmed from the temperature distribution illustrated in Figure 1.

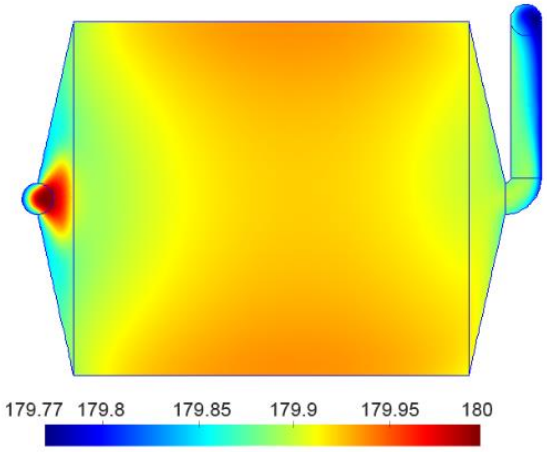

Figure 2 Temperature distribution at the cross section placed at the distance of 2mm from the bottom of the reaction volume of the reactor

With the increase of a top surface temperature the temperature difference through the rector increase but the value remains small. For the top boundary temperature of 240°C this value is 0.4°C.

The pressure distribution at the same cross section for the top boundary temperature of 180°C is presented in Figure 3. The maximal value of gage pressure obtained in the case of 240°C is 134Pa, 16Pa higher than in the case of 180°C.

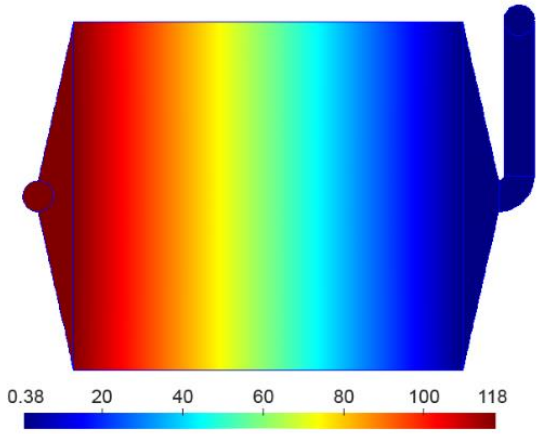

Figure 3 Pressure distribution at the cross section placed at the distance of 2mm from the bottom of the reaction volume of the reactor

The basic structural analysis of the model was performed. Only deformation due to thermal expansion was taken into account. Holes are extracted from the plates in two diagonal corners and fixed constraints were imposed at the surfaces of the holes. The same constraints were imposed to the top and the bottom surface. It is obvious from Figure 4 that the value of the total displacement is negligible even when compared with the value of reaction volume thickness which is small and has the value of 4mm.

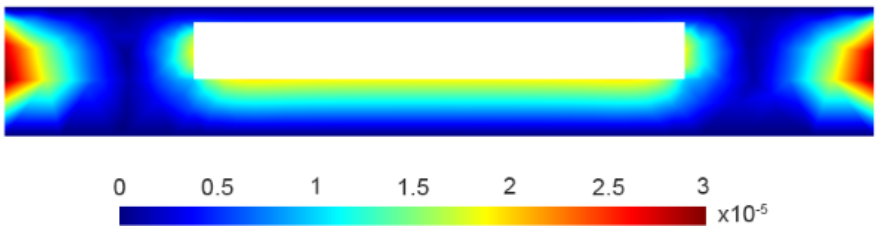

Figure 4 Total displacement presented in the cross section placed at the mid length of the reaction volume

Even the small deformation of the interior of the reactor may lead to a change of catalyst porosity. The decrease of porosity of 0.01 in the case of the top boundary temperature of 180°C resulted in larger increase in gage pressure than the above presented increase in the top boundary temperature to a value of 240°C. The difference in the maximal value of the gage pressure was approximately 2Pa.

5. ACKNOWLEDGEMENTS

This research was carried out under the NATO Science for Peace Project EAP.SFPP 984738, and the Ministry of Education and Science of the Republic of Serbia project III 43007. Slovenian Research Agency is gratefully acknowledged for supporting the Program P2-0152, Chemical Reaction Engineering

6. REFERENCES

[1] A. Iulianellia, P. Ribeirinhab, A. Mendesb and A. Basilea, "Methanol steam reforming for hydrogen generation via conventional and membrane reactors: A review," *Renewable and Sustainable Energy Reviews*, vol. 29, p. pp 355–368, 2014.

[2] C. Pan, R. He, Q. Li, J. O. Jensen, N. J. Bjerrum, H. A. Hjulmand and A. B. Jensen, "Integration of high temperature PEM fuel cells with a methanol reformer," *Journal of Power Sources*, vol. 145, p. pp 392–398, 2005.

[3] A. Pohar, D. Belavič, G. Dolanc and S. Hočevar, "Modeling of methanol decomposition on Pt/CeO2/ZrO2 catalyst in a packed bed microreactor," *Journal of Power Sources*, vol. 256, pp. 80-87, 2014.

[4] I. Ivanović, A. Sedmak and M. Milošević, "The Influence of Inlet Geometry on the Performance of a Micro Methanol Steam Reformer," in *The 6th International Conference and Workshop, REMOO-2016*, Budva, Montenegro, 2016.

[5] I. Ivanović, A. Sedmak, M. Milošević, I. Cvetković, A. Pohar and B. Likozar, "Influence of Geometry on Pressure and Velocity Distribution in Packed-bed Methanol Steam Reforming Reactor," in *14th International Conference on Numerical Analysis and Applied Mathematics, ICNAAM 2016*, Rhodes, Greece, 2016.

[6] R. Suwanwarangkul and S. Charojrochkul, "Modeling of Methanol Steam Reformer for Hydrogen Production in Fuel Cell Application," *Int. J. Sc. Tech.,Special Edition,* vol. 13, pp. 67-74, 2008.

The difference in somatotype between football and not football players

H. Sivrić [a], M. Erceg [b], B. Gilić [c]

[a] College of Slavonski Brod, Dr. Mile Budaka 1, 35000 Slavonski Brod, Croatia, Hrvoje.Sivric@vusb.hr

[b] University of Split, Faculty of Kinesiology, Teslina 6, 21000 Split, Croatia

[c] University of Split, Faculty of Kinesiology, Teslina 6, 21000 Split, Croatia

Abstract

The somatotype is a convenient shorthand descriptor of overall physique in terms of body shape and composition independent of body size. Because of its uniqueness, somatotyping has been used to study many aspects of exercise, sports sciences and human biology, which may be important in identifying talented young athletes for particular sports [1]. The aim of this research was to compare the somatotype of football players and not players aged 12-15. The somatotype data was gathered on a sample of 41 players from the clubs' NK Junak" Sinj, "NK Dugopolje" and "NK Omladinac" VRANJIC and 56 not players (non-athletes) from "PS Ante Starcevic" Dicmo. Average body height players is 166,98 ± 10,75, and the body weight of 52,88 ± 9,68. Not players the mean body height 166,23 ± 11,30, and body mass 56,59 ± 14,07. With the aim of calculating the somatotype (by Heath-Carter method), 10 anthropometric measures were measured: height and mass; triceps, subscapular, supraspinale and calf skinfolds; flexed arm and calf girth; humerus and femur breadth. The data was analyzed by computer software packages Somatotype and Statistica ver. 11.00. The somatotype means were 3,77-4,00-4,12 ± 0,85-1,32-1,14 for football players and 4,61-4,53-3,40 ± 1,07-1,98-1,42 for not players. The differences in somatotype of football players and not players were calculated by the analysis of variance. There were statistically significant differences with F=6,26 and the level of significance of p=0,014, but there was a tendency noticed. Therefore, further research is recommended on a larger subject sample.

Keywords: differences, morphological characteristics, football players, Heat-Carter

1. INTRODUCTION

Somatotype is an adequate descriptor of overall physique in terms of body type and composition regardless of body size. Due to its uniqueness, somatotype is used when conducting research on exercising, sport science and human biology. This type of research could be useful in identification of talented young athletes [1]. The usage of the new computer program Somatotype Ver 1.2.5 developed by Goulding [2], has made the research of somatotypes of different athletes and populations again attractive to scientists because it uses not only morphological measurements but also specific coefficients for age and sex. The method is applicable to both sexes and to all ages. There are three methods for determining the Heath-Carter Somatotype: the photoscopic method, the antrophometric method and the combination of the two. The antrophometric method is based on ten morphological antrophometric measurements: body height, body mass, upper arm, abdomen, back and lower leg skinfold, diameter of elbow and knee, amplitude of flexed and tensed upper arm and amplitude of lower leg when standing. The first (endomorph) component is a relative development of a body mass, the second component is mesomorph and the third

(ectomorph) measures the relative linearity of a body. The result is a three digit number which can be presented via graph as well. The endomorph component is valued from 0,5 to 16, mesomorph from 0,5 to 12 and ectomorph from 0,5 to 9. By combining here mentioned components we can get 13 somatotype categories. The main aim of this paper is to determine somatotype of young (between age 12 and 15) primary school football players and their peers who are not playing football, and to analyze differences. In accordance, the following hypothesis has been made:

H1: There is a statistically significant difference between somatotypes of football players and non- football players.

2. METHODS AND MATERIALS USED FOR RESEARCH

2.1. Examinee sample

The sample was defined with 97 examinees, aged 12-15 years. Examinees were divided on football players (41 footballer, mean age 13,64 years from clubs "NK" Sinj, "NK Dugopolje "and" NK "Vranjic" and not players (56 boys, mean age 13,15 years, from "Primary school Ante Starcevic" Dicmo).

2.2. Variable sample

The sample of variables represents a set of 10 anthropometric measures designed to calculate the somatotype according to Heat-Carter method (1990). The measurements of each variable are made in 3 replications. Measurements included the following measures:

Body height (anthropometer): the subject is standing on level ground. The shoulders is relaxed, heels closed and head into position so. frankfurt horizontal. Horizontal arm anthropometry descends to the crown of the head.

Body weight (balance): subject standing barefoot on the scale wearing as little clothing.

Forearm skin fold (caliper): the subject standing with his hands down at your sides. Left hand timekeeper lifted longitudinal skin fold on the back of the upper arm, accept it with tips of calipers and reed the value.

Skin fold back (caliper): the subject standing with relaxed shoulders. Forefinger and thumb of the left hand timekeeper lifted longitudinal skin fold just below the point of the shoulder. Skin folds can catch with caliper and read the value.

Abdominal skinfold (caliper): the subject standing with relaxed shoulders. Forefinger and thumb of the left hand timekeeper up longitudinal skin fold 1 cm above and 2 cm medial to the pelvic bone protrusions.

Skinfold shin (caliper): the subject standing. Fingers of his left hand held up the skin fold at its widest point shin on its rear.

Scope of flexed arm (centimeter): the subject standing with hand flexed at the elbow with a two-headed muscle contraction of the upper arm. The tape is placed horizontally at the widest part of the left upper arm in its upper half.

Scope of the lower leg (centimeter): the subject is in an upright position, with a little spaced equally burdened feet. Centimeter measure horizontal, the largest circumference of the lower leg.

Diameter - elbow: The subject standing and his arm is bent at the elbow at a right angle. The tips of sliding calipers are laid on the medial and lateral epicondyle of the humerus thereby compressing the soft tissue.

Diameter - knee: the subject is sitting so that his leg bent at the knee at a right angle, a foot placed on a flat surface. The tips of sliding calipers are placed on the most protruding part of the medial and lateral femoral condyle.

2.3. Methods of data processing

Methods of data processing: descriptive statistical indicators of ten morphological measures: central value (Median), arithmetic mean (AS), standard deviation (SD), and KS-Test. To determine the stability of significant differences between somatotype of football and non-football players SANOVA analysis of

differences was used. Data was analyzed with computer programs Somatotype and Statistica Ver.11.00.

3. RESULTS AND ACHIEVEMENTS

Table 1. shows results of descriptive statistics of morphological variables of football players, average age 13,64. The analysis of distribution parameters shows normal distribution of variables and no significant deviations from normal distribution. By comparing the results of this research with the results of research conducted by Gil and associates [3] it can be concluded that there is a partial overlapping between the results. Both results show that football players are taller than non-football players. But in terms of body weight, according to Gil and associates research football players weigh more than non- football players while according to this research football players weigh less than non- football players.

Table 1. Descriptive statistics of morphological variables of football players (N=41)

Variables	Median	AS	SD	max D
Body height	169,00	166,98	10,75	0,13
Body weight	54,00	52,88	9,68	0,10
Scope of flexed arm	25,10	25,26	2,69	0,08
Scope of the lower leg	32,10	32,73	2,85	0,16
Diameter - elbow	6,90	6,88	0,72	0,09
Diameter - knee	9,90	9,89	0,85	0,11
Forearm skin fold	12,60	12,94	2,37	0,16
Skin fold back	12,10	12,41	3,24	0,10
Abdominal skinfold	10,60	10,89	3,46	0,16
Skinfold shin	11,10	11,72	2,99	0,16

Median – central value, **AS –** arithmetic mean**, SD** – standard deviation, **max D** - the maximum distance between the theoretical cumulative relative frequency and relative cumulative empirical frequency

Table 2. shows results of descriptive statistics of morphological variables of non-football players, average age 13,15. The analysis of distribution parameters shows normal distribution of variables, except for abdomen skinfold, and no significant deviations from normal distribution.

Table 2. Descriptive statistics of morphological variables of non- football players (N=56)

Variables	Median	AS	SD	max D
Body height	164,50	166,23	11,30	0,11
Body weight	54,50	56,59	14,07	0,09
Scope of flexed arm	25,30	26,04	3,54	0,10
Scope of the lower leg	32,45	33,38	3,90	0,11
Diameter - elbow	6,90	6,92	1,03	0,11
Diameter - knee	9,90	10,17	1,36	0,15
Forearm skin fold	15,30	15,69	3,02	0,08
Skin fold back	15,75	15,48	4,69	0,06
Abdominal skinfold	12,15	14,02	5,24	0,15
Skinfold shin	12,60	12,90	2,86	0,11

Median – central value, **AS –** arithmetic mean**, SD** – standard deviation, **max D** - the maximum distance between the theoretical cumulative relative frequency and relative cumulative empirical frequency

By analyzing the results it can be concluded that on average football players are 5,50 cm taller than non-football players and that they weigh 0,50 kg less. On average amplitude of flexed upper arm is 0,20 cm larger in non-football players, while amplitude of lower leg is on average larger by 0,35. The results show that average diameter of elbow and knee is larger in non-football players by 0,04 apropos 0,28. Upper arm skinfold is larger in football players by 2,70, back skinfold is smaller in football players by 3.65, abdomen skinfold is smaller by 1.55 while lower leg skinfold is smaller by 1,50. Results further show that football players (mean age 12) are 154-155 cm tall and weigh 42-43 kg while non-football players are shorter (148-150) and weigh less (39-40 kg). At age 14, football players are 172-173 cm tall and weigh 57-59, while non-football players are 166 cm tall and weigh 53 kg. Professional football players are (at the age 18) 177 cm tall and weigh 70-71 kg.

The results of univarant analysis of variance (adapted for analysis of somatotypes (SANOVA) in computer program Somatotype) are shown in table 3. There is a statistically significant difference in somatotype of football players and non-football players on level p=0,014.

Table 3. Analysis of variance (SANOVA) of somatotypes football (N=41) and non-football players (N=56)

Examinee sample	AS	SD
Somatotypes – football players	3,76 - 4,05 - 4,13	0,86 - 1,24 - 1,14
Somatotypes – non-football players	4,61 - 4,53 - 3,40	1,07 - 1,98 - 1,42
SANOVA	**F=6,26**	**P=0,014**

AS – arithmetic mean, **SD** – standard deviation

Table 4. shows descriptive parameters of somatotype components, the value of variance analysis and the level of significance of the sample. Considering the value of somatotype components, it can be concluded that both football players and non-football players fall into central category.

Table 4. Descriptive parameters of somatotype components and value of variance analysis football and not football players

Components of somatotype	Football players (N=41)		Non-football players (N=56)			
	AS	SD	AS	SD	F	p
Endomorph	3,77	0,85	4,61	1,07	17,64	<0,001
Mesomorph	4,00	1,32	4,53	1,98	1,86	0,172
Ectomorph	4,12	1,14	3,40	1,42	7,32	0,008

AS – arithmetic mean**, SD** – standard deviation, **F –** the value of F-test, **p –** level of significance

Endomorph type can be characterized as round body type with larger weight, short and thick neck and wide torso with emphasis on abdomen and adipose tissue. Table 4. shows that non-football players are more endomorph types with an average value of 4,61 ± 1,07 than football players who have an average value of 3,77±0,85.

Mesomorph type can be characterized as with strong bone structure and developed and strong musculature. A neck is long and strong and chests are wide and bulged. In comparison to chest, abdomen is indent, and waist is narrow. Limbs are well developed and strong. In terms of mesomorph type, football players should be more developed and stronger, but the results of this research do not support this thesis.

According to this research, the average value of football players is 4,00±1,32, while non-football players have an average value of 4,53±1,98. We assume that this is because the research was conducted in rural region where children are always on the move.

Ectomorph type can be characterized as tall, slim, with wide forehead, small face and pointing nose. Neck is long and thin, and chests are narrow. Limbs are long and thin, with long and thin muscles. The results show that football players are more ectomorph types than non-football players with an average value of 4,12±1,14, while non-football players have an average value of 3,40±1,42.

The results are in correspondence with the research conducted by Vivian and associates (1993). Both research results show significant difference in endomorph and ectomorph components. The main difference is that Vivian and associates conducted a research on experienced football players and beginners while this research was conducted on football players and non-football players.

4. CONCLUSIONS

A body constitution is a specific set of structural morphological, physiological functional and psychological cognitive-conative characteristics that make a person different from all others. It is influenced by heritage but by environmental factors as well. It is used for assessment of readiness of examinees for overcoming physical and psychological effort, as well as a reaction to different environmental influences. Based on the results using biostatic methods the readiness of examinees can be expressed in numbers, norms and tables. The aim of this research was to compare somatotypes of 12-15 year old football players and non-football players. The data was based on sample of 41 football players from „NK Junak“ Sinj, „NK Dugopolje“ and „NK Omladinac“ Vranjic and on 56 non-football players from „OŠ Ante Starcevic“ Dicmo. Ten antrophometric measures were taken by Heat-Carter method with the purpose of measuring somatotypes. The main descriptive variable indicators and relative values of different somatotype categories have been calculated. By analyzing the variance (SANOVA) the differences between somatotypes of football players and non-football players have been calculated. The results confirm the hypothesis that there is a significant difference between football players and non- football players. In next research we plan to enlarge number of participants and to compare somatotypes of young athletes and non-athletes.

5. REFERENCES

[1] J.E.L. Carter; B. H. Heath, Somatotyping: Development and Applications, Cambridge University Press, New York (1990).

[2] M. Goulding, Somatotype – 1.2.5. Mitchell Park, SA: Sweattechnologies, (2010).

[3] S.M. Gil; J. Gil; F. Ruiz; A. Irazusta; J. Irazusta. Physiological and anthropometric characteristics of young soccer players according to their playing position: Relevance for the selection process. J. Strength Cond. Res. 21 (2), (2007), pp. 438–445

[4] F. Viviani; G. Casagrande; F. Toniutto, The morphotype in a group of peri-pubertal soccer players. J Sports Med Phys Fitness. (1993) pp.178-183

Effectiveness indicators and performance measurements in dual training

E. Török [a], Zs. Kovács [b]

[a] Pallasz Athéné University, 10. Izsáki street, 6000 Kecskemét, Hungary, torok.erika@gamf.kefo.hu

[b] Pallasz Athéné University, 10. Izsáki street, 6000 Kecskemét, Hungary. kovacs.zsuzsanna@gamf.kefo.hu

Abstract

Dual training is one among the forms of renewing higher education. The training reacts to the social, industrial and educational demands and gives an opportunity for real cooperation between industry and higher education institutions. The effectiveness of dual training is valued by how much the basic targets concerning institutional and social effectiveness are realized. The development of the training fitting into the given economic and social environment is based on ongoing reviews of the outcome indicators. The aim of our research is to reveal the necessary system of indicators leading to the effectiveness of dual training. These indicators are suitable for showing the extent of the realization of the objectives. Our research methods can be divided into two groups. On one hand, documents and regulations related to the training were analysed, on the other, performance data of the students taking part in the training was interpreted. Accordingly our target groups are the joining industrial partners as well as the dual students learning at our University. The developed indicators, firstly, refer to the prevalence of the dual training (through the number of companies and students involved), secondly, to the partnership (number and contentment of the companies), thirdly, to the contentment of the training (student contentment and extent of student drop-out). In addition indicators also show the quality performance (student learning results, employment data). As a result of our research, with the help of the developed system of indicators it can be seen whether local targets, primary company targets and primary student objectives were realized. The objectives of the training and its indicators play an important role in creating the strategic target map of dual training. The target map covers the most important practical knowledge required from industrial partners and the methods of ensuring labour supply of each region to provide flexible professional higher education training. The introduction of dual training in Hungary involves a number of tasks. With the research we wish to contribute to creating such a system which is able to assess, control and measure the quality performance of this training form which is significantly different from the traditional university training forms. In the future other higher education institutions will be able to use this system developed by us, to measure the effectiveness of their dual trainings.

Keywords: Dual training, higher education, effectiveness indicators

1. INTRODUCTION

Dual training model, which was a non-existing training form in the Hungarian higher education system, was launched in 2012 in the predecessor of Pallasz Athéné University. The idea of introducing dual training in Hungarian higher education emerged as a common demand from both our institution and two significant automotive companies with sites in our town (Mercedes-Benz Manufacturing Hungary Ltd, Knorr-Bremse Brake System Ltd). This pilot initiative played an important role in adding this type of training system in higher education to the National Act of Higher Education in 2014. In 2015 on national level 20 higher education institutions in 4 training fields (engineering, information technology, agriculture and economics) with 350 industrial partners joined dual training.

Concerning the training the Ministry of Education provided the following principles [1]:

- The dual training is a form of practice-oriented training in the Bachelor program where practical training can be conducted at professionally qualified companies.
- The student taking part in dual training accomplish the academic period together with the "traditional" full time students at the University (institutional period) then take part in the education and practice of the corporate section.
- Higher education institutions sign a cooperation agreement with industrial partners to take part in the training.
- The industrial partner and the student sign a student employment contract. The company is bound to allocate remuneration to the student for the total duration of the training, meaning both at the institutional period and the corporate section (the amount of fee is the 15% of the current minimum wage per week).

2. EFFECTIVENESS IN HIGHER EDUCATION - FRAMEWORKS OF INTERPRETATION

Competition is becoming more and more significant in the sphere of higher education whereas, as a result, qualitative aspects are brought into fore. Besides the traditional quality indicators of higher education diploma programs meeting the needs of the labour market play an important role as well. This means applying graduates who meet the requirements of their qualification plays a distinctive role among the possible indicators measuring quality within higher education. Knight and Yorke (2003) mention four main components of employability; expertise, skills, self-awareness and self-confidence moreover, mention susceptibility and competence towards a strategic way of thinking [2]. In order to measure efficiency the average duration of studies, the drop-out rate (the number of students dropping out compared to the total number of students admitted) and the graduation rate (the number of graduating students compared to the total number of admitted students) are examined in general. Another important group of the indicators are the indicators of students' contentment which are based on the fact that students are more content at an institution giving quality training than in the case of lower quality education. The rate of those graduates who have proved can be a significant indicator of the effectiveness of higher education. Concerning dual training this indicator cannot be measured yet due to the shortness of time from the introduction of the training.

3. INDICATORS IN DUAL TRAINING

Dual training is one among the forms of renewing higher education. The training reacts to the social, industrial and educational demands and gives an opportunity for real cooperation between industry and higher education institutions. One of the most important expectations of competitive industry is to fit tightly the knowledge acquired during the academic years in higher education to the demands of the constantly changing labour market. Dual training is a form of ensuring cooperation of practical training between higher education and industrial partners. Dual training presumes a tight, target-oriented cooperation between the three parties (industrial partners, higher education institution and students involved in the training). This practice-oriented training has gained popularity in many countries in Europe, though in several different types of system, all introduced and accomplished in an effective way.

With the acquisition of the international experience and German model (DHBW), then adapting it to the Hungarian higher education system following the successful introduction of the training at the former Kecskemét College (now Pallas Athene University), introducing dual training widespread in the country became

of the most important target of the Hungarian higher education.

There are several targets that dual training has to meet in order to be effective. In the course of dual training primarily industrial partners and higher education institutions are in cooperation, however, as third party students taking part in dual training also join in. Thus indicators should be measured through more but at least from three aspects. Besides the primary targets of the institutions, industrial partners and students, two very important indicators should be added to the strategic target map: local/regional targets and strategy of higher education.

3.1. Interlocking components for monitoring and evaluating

The effectiveness of dual training is valued by how much the basic targets concerning institutional and social effectiveness are realized. The development of the training fitting into the given economic and social environment is based on ongoing reviews of the outcome indicators.

One of the most important principal targets of the industrial partners is to increase the number of those students with a degree who can be more adaptable to the demands of the companies. As students spend three and half years at the chosen company it is able to produce a colleague formed to the needs and demands of the company. Secondly, companies find dual training a less expensive investment than retrain fresh graduates coming from the labour market.

From the institution's point of view the primary target is to increase the number of cooperation with industrial partners. Dual training enhances broadening the cooperation net between industry and higher education thus expanding R+D+I activity towards more training areas, moreover involving local partners in it have a great significance. It is of great importance to get industry involved into the system of higher education. In order to produce highly skilled professionals it is in the interest of the institution to get the academic sector to have an insight in the rapidly changing economic and industrial life. In addition higher education with dual training takes a social responsibility by satisfying the demands of the region. With the growing popularity of dual training higher education institutions gain more prestige as students are more motivated, ambitious and hard-working thus creating a more quality education.

The third party is the student who takes part in the practice-oriented training. These students seek a stable career model and/or a secure job and workplace. During the training financial independence is ensured, in addition, potentially, they have much better expectations in the labour market.

Targets should be considered from social and regional point of view as well. Among the targets improving regional labour supply with the process of training adequate number of professionals with appropriate competencies is one of the most immediate tasks. It has several benefits such as reducing labour migration from less developed regions in the country for this purpose partner companies are willing to take social contribution as well.

Lastly, among the targets of higher education a flexible quality education should be aimed and realized with dual training which adapts to the labour market needs and adjusts the offered trainings and majors of universities according to the economic demands.

3.2. The indicators of dual training efficiency

In order to measure the effectiveness of dual training a system of indicators is needed which is suitable for showing the extent of the realized targets. The table shows the indicators of effectiveness in dual training (Table 1) [3].

Table 1. Indicators of dual training

Popularity of the training	The number of trainings involved in dual training
	The number of

	students enrolled in training (per head)
Cooperation with partner companies	The number of partner companies in dual
	The contentment of the partner companies
Contentment with the training	The aggregate value of contentment
	The number of students dropping out (per head)
Quality education performance	Performance of dual students
	The rate of graduated students and employed

3.3. Popularity of the training – The number of trainings involved in dual training

During the pilot period in 2012 dual training was launched only among vehicle engineer undergraduates. In 2013 mechanical engineering and mechanical management majors joined the training system. At present dual type of training is available in 6 majors (vehicle engineering, mechanical engineering, information technology engineering, mechanical management, economy and management, logistical engineering) at the three faculties of Pallasz Athéné University. In addition to the initial training of technical areas there are students in the fields of information technology, agriculture, and economic sciences who take part in dual training (Fig. 1.).

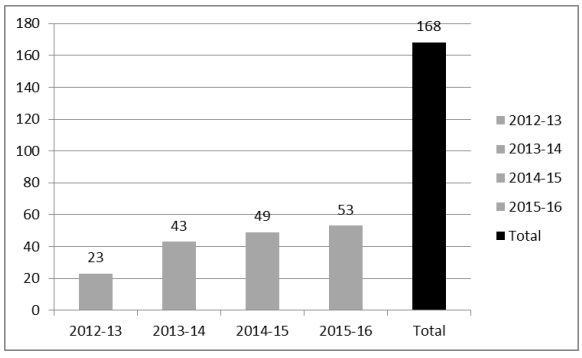

Fig. 1. The number of students enrolled in training (per head)

3.4. Cooperation with partner companies

The key indicator of business relationship is measured by the number of joining companies. Up till now 73 industrial companies have joined as partners. The following table shows the growing number of companies joining dual training each year (Table 2.).

Table 2. The number of partner companies in dual

Semester	Number of joining companies /year
2012-13	2
2013-14	13
2014-15	7
2015-16	19
2016-17	32

Currently 73 companies take part in the four faculties of the University, 12 multinational companies and 61 small- and medium-sized companies.

3.5. Contentment with the training

Among the indicators of dual training the contentment of students is of great importance. Contentment is measured with respect to several areas. .In our research with the help of questionnaires the following areas were covered concerning contentment: contentment with the practice at the company, contentment regarding university education, contentment with education management, contentment with one's own achievement and finally contentment concerning the community. Based on the answers of 116 dual students the received data can be seen in Fig. 2.

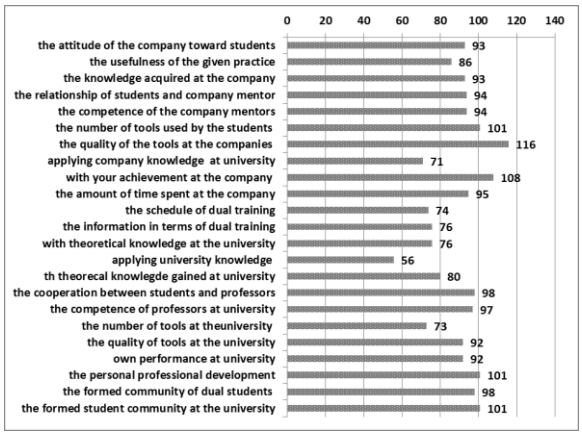

Fig. 2. References to contentment (per head)

Among the items only in one case were the numbers up to 60 satisfied with the given issue. In all other cases the major part of the questioned students (more than 90 people) gave positive assessment to the items. However, it can be noticed that the two lowest numbers are to be found within the application of academic knowledge in practice (56 people) and within the application of the practical knowledge in the academic sphere (71 people). These two lower values draw attention on the importance of transferring experience and knowledge within the frames of academic sphere and company environment. The relationships with professors and mentors show positive values as well as the contentment with the community, the self-evaluation, the usage of tools and in the case of their quality all give higher value than 90.

3.6. The number of students dropping out

The number of dropped out students also serves as an input concerning the quality of training. Between 2012 and 2016 about 10% of students in dual training dropped out or finished their studies in dual training. Among the most common reasons was studying which proved to be much of a burden in addition to company practice. Not choosing the suitable major or having problems with company integration also led to finishing dual training. It is very important to mention that these students are not removed from higher education in this case but continue their studies within the frame of traditional training.

3.7. Quality education performance

Assumptions on the extent of student progress in higher education can be made from the most recorded and performed number of credits. During the training each semester requires 30 credits from the model curriculum. With the help of fig. 3.the average of recorded and performed credits of the dual and non-dual students can be compared. It can be seen that though dual students need to perform on the practices of the company take more credits but more importantly significantly performed better in this respect.

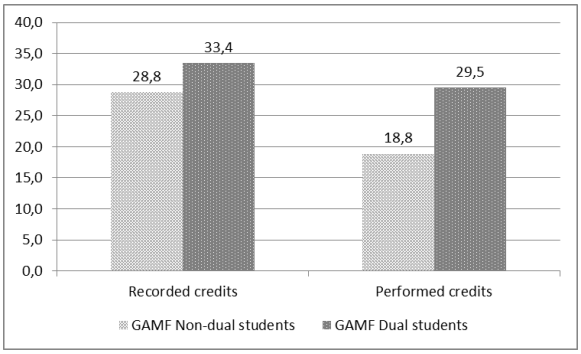

Fig. 3. Comparative chart on the basis of students' credits

Another measure of student success can be academic achievement. The standard average means an average over a given semester while accumulated average is included in the so far gained cumulative average of the student. Dual students perform better than those students who take part in traditional training (Fig. 4.).

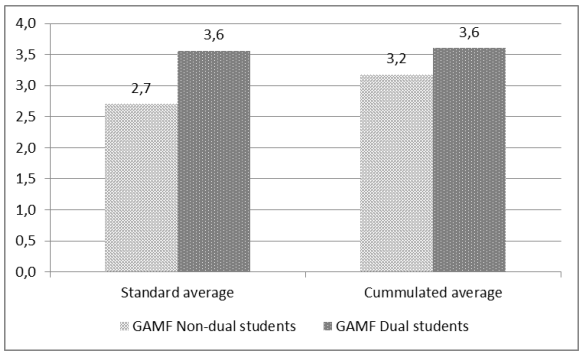

Fig. 4. Comparative chart on the basis of the students' averages

3.8. The rate of graduated students and employed

One of the most important way to measure the success of dual training is the rate of graduated and then employed students. As we have already noted down in the framework of interpretation for all three participants of dual training (company. institution, student) the indicator is to meet the requirements of the labour market of the acquired qualification.

The first 24 students finished their studies in dual training in 2016. 11 graduates remained at the company and work as engineer. The rest of the graduates work at other companies in their profession, or continued their studies in master courses. We expect that employment rate will be similar high on the labour market according to research data of those other countries where dual training has been a significant training form in higher education [4].

4. CONCLUSIONS

Based on the indicators objectives concerning meeting local targets, primary company targets or student primary targets can be demonstrated. In the case of institutions having cooperation with too many companies the way to harmonize curricula, get company feedback on students and supervise can be very difficult. Moreover, coordinating the schedules of students and carrying out administrative and professional communication between the companies and the institution also could make dual training difficult. It can be a fortunate case if a company takes more students even from more major as this situation can result a tighter and more continuous cooperation between partner companies and universities. It can be stated if a partner company takes a student from time to time professional cooperation is less based. Based on the above stated facts it can be seen that joining dual training requires taking an informed decision followed by responsible and diversified work for a partner company. Companies need to decide if it is worth to join the training strategically considering the number of students to take and the regularity (academic year to academic year or less). Multinational companies in the terms of their size are in a more advantageous situation than small-and medium-sized companies as they can promote professional development of students more and supply a wider range of personal and tool demands. The companies basically start this form of training because in cooperation with the university, at the same time in line with their needs would like to create their own professional supply base during the training. A company which takes more students within the frames of the training is much more able to choose from among their own trained students [5].

This system of indicators needs to be developed, thus determining indicators and their measures require regular supervision with specification based on the results.

5. REFERENCES

[1] Duális Képzési Tanács: The Principles of Dual Training in Higher Education (A duális felsőfokú képzés alapelvei). http://dualisdiploma.hu/documents/dualis-felsofoku-kepzes-alapelvei-a-dkt-meghatarozasaban.pdf 2015.10.

[2] Knight, P. & Yorke, M. (2003): Employability and Good Learning in Higher Education. Teaching in Higher Education, Vol. 8, No. 1.

[3] Dr. Kovács Lóránt, Dr. Török Erika, Dr.Lukács Pál, Kovács Zsuzsanna, Pomázi Gyula, Kisbej András, Ambrusné Magó Aranka, Dr. Ailer Piroska, Prof. Dr. Belina Károly: Dual Training in Higher Education (Felsőfokú duális képzés) – Institutional White Book (Intézményi Fehér Könyv); ForArea Gazdaságfejlesztő Kft, Kecskemét,

[4] Axel Göhringer (2002), University of Cooperative Education – Karlsruhe: The Dual System of Higher Education in Germany, Asia-Pacific Journal of Cooperative Education

[5] Kecskemét College (2015),“Dual Training System”,Kecskemét College, Kecskemét,http://kefoportal.kefo.hu/dual, (Accessed 26 April 2015)

FUNCTIONS ASSOCIATED WITH THE WEIGHTED MEAN AND MEDIAN

Zlatko Pavić* and Ivan Raguž[student]

Mechanical Engineering Faculty in Slavonski Brod, J. J. Strossmayer University of Osijek, Croatia
*Corresponding author e-mail: zpavic@sfsb.hr

Abstract

We investigate the application and generalization of the weighted mean and median by using continuous and convex functions. The paper offers a clear and systematic approach to the notion of weighted medians. As a useful result, essential characteristics of weighted medians are presented better, which facilitates their application.

Keywords: weighted mean, weighted median, global minimum

1. Introduction

Let $n \geq 2$ be an integer, let $x_1, \ldots, x_n \in \mathbb{R}$ be points, and let $w_1, \ldots, w_n \in [0,1]$ be coefficients satisfying $\sum_{i=1}^{n} w_i = 1$, as such are usually called weights.

An arithmetic mean of the given points is the inserted point

$$\bar{x} = \frac{1}{n} \sum_{i=1}^{n} x_i. \tag{1}$$

A weighted (arithmetic) mean of the given points respecting the given weights is the inserted point

$$\bar{x} = \sum_{i=1}^{n} w_i x_i. \tag{2}$$

If the points x_i are sorted from smaller to larger, we are able to observe medians. Suppose that $x_1 < \ldots < x_n$. If n is odd as $n = 2k+1$, then the middle point x_{k+1} is a median. If n is even as $n = 2k$, then the middle points x_k and x_{k+1} are a lower and upper median. Weighted medians can be defined as follows.

If for a weight w_k, where $k \in \{1, \ldots, n\}$, applies

$$\sum_{i=1}^{k} w_i > \frac{1}{2} \text{ and } \sum_{i=k}^{n} w_i > \frac{1}{2}, \tag{3}$$

then the point x_k is a weighted median. In this case, w_k is unique and positive.

If for weights w_k and w_l, where $k \in \{1, \ldots, n-1\}$ and $l \in \{k+1, \ldots, n\}$, apply

$$\sum_{i=1}^{k} w_i = \frac{1}{2} \text{ and } \sum_{i=l}^{n} w_i = \frac{1}{2} \tag{4}$$

with the integers k and l as the smallest and largest possible, then the points x_k and x_l are a lower and upper weighted median. In this case, w_k and w_l are unique and positive, and if $l \geq k+2$, then $w_{k+1} = \ldots = w_{l-1} = 0$.

The conditions in equation (3) and equation (4) exclude each other. If all weights are the same, $w_1 = \ldots = w_n = 1/n$, then the weighted arithmetic mean coincides with arithmetic mean, and the weighted medians coincide with medians.

2. Weighted mean and median as the minimum points

In this section, we employ a collection of functions defined on $\mathbb{R}$ whose members have a global minimum. Let $x_1, \ldots, x_n \in \mathbb{R}$ be points, let $a_1, \ldots, a_n \geq 0$ be coefficients of which at least one is positive, let $p \geq 1$ and $q > 0$ be exponents, and let

$$f(x) = \left(\sum_{i=1}^{n} a_i \mid x - x_i \mid^p \right)^{q/p}. \tag{5}$$

Including the limit case by letting p tend to infinity, we get

$$f(x) = (\max\{a_1 \mid x - x_1 \mid, \ldots, a_n \mid x - x_n \mid\})^q. \tag{6}$$

This limit is a consequence of the transition from the p-norm to *max*-norm as is well known. The above functions are continuous and satisfy $\lim_{|x| \to \infty} f(x) = \infty$, so they have a global

minimum. The related functions $g = f^{1/q}$ are convex. The minimum points of f and g coincide because a power function with a positive exponent is increasing on the interval of nonnegative numbers. When $q \geq 1$, the functions in (5) and (6) are convex as the compositions of increasing convex and convex functions ($f = h \circ g$, where $h(x) = x^q$ for $x \geq 0$). If $p > 1$ and $q > 1$, the above functions are strictly convex.

Let $I^* \subseteq I \subseteq \mathbb{R}$ be intervals with the nonempty interior, and let $f : I \to \mathbb{R}$ be a convex function. Then f is continuous on the interior of I, and each its local minimum is global. As for the minimum, if $x^* \in I^*$ is a point so that $f(x^*)$ is a minimum on I^*, then $f(x^*)$ is minimum on I.

Let $c \in \mathbb{R}$ be a coefficient, let $p > 1$ be an exponent, and let $h(x) = |x - c|^p$. The function h is strictly convex, and differentiable at each point $x \in \mathbb{R}$ with the derivative

$$h'(x) = \begin{cases} p\dfrac{|x-c|^p}{x-c} & \text{if} \quad x \neq c \\ 0 & \text{if} \quad x = c \end{cases}.$$

The derivative of the convex function $h(x) = |x - c|$ is included in first line of the above equation with $p = 1$.

We are discussing global minimum points of the functions in equations (5) and (6). The interval which includes the points x_i comes into play. If $x_{(1)} = \min\{x_1, \ldots, x_n\}$ and $x_{(n)} = \max\{x_1, \ldots, x_n\}$, then the closed interval $[x_{(1)}, x_{(n)}]$ contains the global minimum points of the observed functions. Further, it all depends on the exponent p.

A strict global minimum point exists if $p > 1$.

Lemma 2.1. *Let $x_1, \ldots, x_n$ be points of $\mathbb{R}$, let $a_1, \ldots, a_n \geq 0$ be coefficients such that $a = \sum_{i=1}^n a_i > 0$, let $p > 1$ and $q > 0$ be exponents, and let*

$$f(x) = \left(\sum_{i=1}^n a_i \, | x - x_i |^p \right)^q .$$

Then a strict global minimum point of f exists in the interval $[x_{(1)}, x_{(n)}]$.

Proof. We observe the strictly convex function

$$g(x) = (f(x))^{1/q} = \sum_{i=1}^n a_i \, | x - x_i |^p .$$

Using the fact that at least one of the coefficients a_i is positive, and applying the derivative

$$g'(x) = p \sum_{i=1}^n a_i \frac{| x - x_i |^p}{x - x_i}$$

outside the interval $[x_{(1)}, x_{(n)}]$, it follows that $g'(x) < 0$ if $x \in (-\infty, x_{(1)})$, and $g'(x) > 0$ if $x \in (x_{(n)}, +\infty)$. The strictly convex function g decreases on $(-\infty, x_{(1)})$ and increases on $(x_{(n)}, +\infty)$, and so it reaches a global minimum at a unique point of the remaining part $[x_{(1)}, x_{(n)}]$. The same is true for the function f. □

Lemma 2.1 also applies to the function f in (6).

The weighted mean appears in the case $p = 2$.

Lemma 2.2. *Let $x_1, \ldots, x_n$ be points of $\mathbb{R}$, let $a_1, \ldots, a_n \geq 0$ be coefficients such that $a = \sum_{i=1}^n a_i > 0$, let $q > 0$ be an exponent, and let*

$$f(x) = \left(\sum_{i=1}^n a_i \, | x - x_i |^2 \right)^q .$$

Then a strict global minimum point of f exists as the weighted mean of the points x_i respecting the weights $w_i = a_i / a$.

Proof. Using the sums

$$b = \sum_{i=1}^n a_i x_i \text{ and } c = \sum_{i=1}^n a_i x_i^2$$

as the coefficients in the presentation

$$g(x) = (f(x))^{1/q} = a\left(x - \frac{b}{a} \right)^2 + \frac{ac - b^2}{a},$$

we obtain a unique minimum point of g and f as

$$\bar{x} = \frac{b}{a} = \frac{1}{a}\sum_{i=1}^{n} a_i x_i = \sum_{i=1}^{n} w_i x_i,$$

representing the weighted mean of the points x_i respecting the weights w_i. □

The weighted medians occur in the case $p = 1$.

Lemma 2.3. *Let $x_1 < \ldots < x_n$ be strictly ordered points of $\mathbb{R}$, let $a_1, \ldots, a_n \geq 0$ be coefficients such that $a = \sum_{i=1}^{n} a_i > 0$, let $q > 0$ be an exponent, and let*

$$f(x) = \left(\sum_{i=1}^{n} a_i \, | x - x_i | \right)^q .$$

If the point x_k exists as a weighted median of the points x_i respecting the weights $w_i = a_i / a$, then x_k is a strict global minimum point of f.

If the points x_k and x_l exist as a lower and upper weighted median, then each element of $[x_k, x_l]$ is a global minimum point of f.

Proof. We include weights w_i through the function

$$g(x) = \frac{1}{a}(f(x))^{1/q} = \sum_{i=1}^{n} w_i \, | x - x_i |,$$

which is convex and so continuous on $\mathbb{R}$, and differentiable on $\mathbb{R} \setminus \{x_1, \ldots, x_n\}$ with the derivative

$$g'(x) = \sum_{i=1}^{n} w_i \frac{| x - x_i |}{x - x_i}.$$

Obviously, $g'(x) = -\sum_{i=1}^{n} w_i = -1$ if $x < x_1$, and $g'(x) = \sum_{i=1}^{n} w_i = 1$ if $x > x_n$. Let δ be a positive number so that for each point x_k the interval $(x_k - \delta, x_k + \delta)$ does not contain any point x_i other than x_k.

The derivative of the function g around a point x_k stands as

$$g'(x) = \begin{cases} \sum_{i=1}^{k-1} w_i - \sum_{i=k}^{n} w_i & \text{if} \quad x \in (x_k - \delta, x_k) \\ \sum_{i=1}^{k} w_i - \sum_{i=k+1}^{n} w_i & \text{if} \quad x \in (x_k, x_k + \delta) \end{cases}.$$

Suppose that x_k is a weighted median. Applying the conditions in formula (3) to the above derivative, we obtain that $g'(x) < 0$ if $x \in (x_k - \delta, x_k)$, and similarly that $g'(x) > 0$ if $x \in (x_k, x_k + \delta)$. Since g is continuous, x_k is a strict minimum point on $(x_k - \delta_k, x_k + \delta_k)$. Since g is convex, x_k is also a strict minimum point on $\mathbb{R}$. Thus, x_k is a strict global minimum point of the functions g and f.

The derivative of the function g around points x_k and x_l, where $l \geq k+1$ and $w_{k+1} = \ldots = w_{l-1} = 0$ if $l \geq k+2$, stands as

$$g'(x) = \begin{cases} \sum_{i=1}^{k-1} w_i - w_k - \sum_{i=l}^{n} w_i & \text{if} \quad x \in (x_k - \delta, x_k) \\ \sum_{i=1}^{k} w_i - \sum_{i=l}^{n} w_i & \text{if} \quad x \in (x_k, x_l) \\ \sum_{i=1}^{k} w_i + w_l - \sum_{i=l+1}^{n} w_i & \text{if} \quad x \in (x_l, x_l + \delta) \end{cases}.$$

Suppose that x_k and x_l are a lower and upper weighted median. Applying the conditions in formula (4) to the above derivative, we obtain that $g'(x) < 0$ if $x \in (x_k - \delta, x_k)$, $g'(x) = 0$ if $x \in (x_k, x_l)$, and $g'(x) > 0$ if $x \in (x_l, x_l + \delta)$. Each element of $[x_k, x_l]$ is a minimum point of g on $(x_k - \delta, x_l + \delta)$, and consequently on $\mathbb{R}$. Thus, each such element is a global minimum point of g and f. □

Remark 2.4. *If at least two of the points x_i are distinct, the functions used in the above lemmas are positive. Using $q < 0$, we have a global maximum point instead of global minimum point.*

Example 2.5. *Find a global maximum value of the function*

$$f(x) = (| x+5 | + 4 | x | + 3 | x-6 | + 8 | x-7 |)^{-5}.$$

According to Lemma 2.3, we need to examine the weighted medians of the points

$$x_1 = -5 < x_2 = 0 < x_3 = 6 < x_4 = 7$$

respecting the weights

$$w_1 = \frac{1}{16}, w_2 = \frac{4}{16}, w_3 = \frac{3}{16}, w_4 = \frac{8}{16}.$$

Using equation (4), we find that the points

$$x_3 = 6 \text{ and } x_4 = 7$$

are a lower and upper weighted median. Relying on Lemma 2.3 and Remark 2.4, we can take any point $x^* \in [6,7]$ to get the global maximum value

$$f(x^*) = f(6) = 43^{-5}.$$

Three algorithms for the weighted median problem are presented in [1]. Improved performances of the weighted median filter for the image processing are presented in [2]. Problems relating to the global minimum of convex functions can be found in [3]. Algorithms for calculating extremum points of convex functions are presented in [5]. Optimization problems are discussed in [4].

3. Medians in higher dimensions

Basic norms on the space $\mathbb{R}^m$ are p-norms generated by real numbers $p \geq 1$. The p-norm of a point $T = (x_1, \ldots, x_m) \in \mathbb{R}^m$ is

$$\| T \|_p = \left(\sum_{i=1}^{m} | x_i |^p \right)^{1/p}.$$

Let $T_1, \ldots, T_n \in \mathbb{R}^m$ be points, let $a_1, \ldots, a_n \geq 0$ be coefficients of which at least one is positive, let $p \geq 1$ and $q > 0$ be exponents, and let

$$f(T) = \left(\sum_{i=1}^{n} a_i \| T - T_i \|_p^p \right)^{q/p}.$$

The above functions are continuous and satisfy $\lim_{\|T\| \to \infty} f(T) = \infty$ for every norm on $\mathbb{R}^m$, thus each one of them attains a global minimum value.

Let $A = (a_1, \ldots, a_m)$ and $B = (b_1, \ldots, b_m)$ be points in $\mathbb{R}^m$, and let $\preceq$ be the partial order relation of points in $\mathbb{R}^m$ stated by

$$A \preceq B \text{ if and only if } a_1 \leq b_1, \ldots, a_m \leq b_m.$$

The above relation generates the closed interval between A and B in the form of the m-fold Cartesian product of the closed intervals $[a_j, b_j]$,

$$\preceq A, B \succeq = [a_1, b_1] \times \ldots \times [a_m, b_m].$$

In the next theorem, we will also use the strict partial order relation of points in $\mathbb{R}^m$ by means of

$$A \prec B \text{ if and only if } a_1 < b_1, \ldots, a_m < b_m.$$

Employing the partial and strict partial order relation, we can generalize Lemma 2.3. The case $p = 1$ for multivariate functions also refers to weighted medians.

Theorem 3.1. *Let $T_1 \prec \ldots \prec T_n$ be strictly ordered points of $\mathbb{R}^m$, let $a_1, \ldots, a_n \geq 0$ be coefficients such that $a = \sum_{i=1}^{n} a_i > 0$, let $q > 0$ be an exponent, and let*

$$f(T) = \left(\sum_{i=1}^{n} a_i \| T - T_i \|_1 \right)^q.$$

If the point T_k exists as a weighted median of the points T_i respecting the weights $w_i = a_i / a$, then T_k is a strict global minimum point of f.

If the points T_k and T_l exist as a lower and upper weighted median, then each element of $\preceq T_k, T_l \succeq$ is a global minimum point of f.

Proof. We consider the function $g = (1/a) f^{1/q}$ in the form of

$$g(x_1, \ldots, x_m) = \sum_{j=1}^{m} g_j(x_j), \qquad (6)$$

where

$$g_j(x) = \sum_{i=1}^{n} w_i | x - x_{ij} |.$$

Since $T_1 \prec \ldots \prec T_n$, the points x_{ij} satisfy the strict order $x_{1j} < \ldots < x_{nj}$ for every $j = 1, \ldots, m$. So, we have the following two convenient cases.

The point x_{kj} is a weighted median of the points x_{ij} respecting the weights w_i. Then x_{kj} is a strict global minimum point of g_j by Lemma 2.3. This applies to each index j. Thus the point T_k is a weighted median of the points T_i respecting the weights w_i, and T_k is a strict global minimum point of g by equation (6).

The points x_{kj} and x_{lj} are a lower and upper weighted median. Then each element of $[x_{kj}, x_{lj}]$ is a global minimum point of g_j by Lemma 2.3. It refers to each j. Thus the points T_k and T_l are a lower and upper weighted median, and each element of

$$[x_{k1}, x_{l1}] \times \cdots \times [x_{km}, x_{lm}] = \preceq T_k, T_l \succeq$$

is a global minimum point of g by formula (6). □

Remark 3.2. *If at least two of the points T_i are distinct, then using $q < 0$ in the above theorem, we have a global maximum point instead of global minimum point.*

Example 3.3. *Find a global minimum value of the function*

$$f(x,y) = (5(|x+2|+|y|) + 2(|x-3|+|y-1|) + 3(|x-4|+|y-2|))^{3/2}.$$

According to Theorem 3.1, we need to examine the weighted medians of the points

$$T_1 = (-2,0) \prec T_2 = (3,1) \prec T_3 = (4,2)$$

respecting the weights

$$w_1 = \frac{5}{10}, w_2 = \frac{2}{10}, w_3 = \frac{3}{10}.$$

Using equation (4), we find that the points

$$T_1 = (-2,0) \text{ and } T_2 = (3,1)$$

are a lower and upper weighted median. Relying on Theorem 3.3, we can take any point $T^* \in \preceq T_1, T_2 \succeq = [-2,3] \times [0,1]$ to get the global minimum value

$$f(T^*) = f(-2,0) = 36^{3/2} = 216.$$

4. Conclusion

In the last decades, weighted median algorithms and different filters are widely used in the science, engineering and economics. Therefore, any clarification or simplification relating to the medians is very useful.

5. References

[1] C. Gurwitz, Weighted median algorithms for L_1 approximation, *BIT Numerical Mathematics*, **30** (1990), 301--310.

[2] J. Kaur, M. Garg, An improved weighted median filter for the image processing application, *IJSR International Journal of Science and Research*, **2** (2013), 2319--7064.

[3] C. P. Niculescu, L. E. Persson, *Convex Functions and Their Applications*, Springer Science+Business Media New York, 2006.

[4] M. R. Osborne, *Finite Algorithms in Optimization and Data Analysis*, John Wiley & Sons New York, 1985.

[5] G. A. Watson, *Approximation Theory and Numerical Methods*, John Wiley & Sons New York, 1980.

OVERDETERMINED SYSTEMS OF LINEAR EQUATIONS

Zlatko Pavić*, Vedran Novoselac and Zvonimir Kovačev[student]

Mechanical Engineering Faculty in Slavonski Brod, J. J. Strossmayer University of Osijek, Croatia
Corresponding author e-mail: zpavic@sfsb.hr

Abstract

The paper offers a fundamental overview of the theory relating to overdetermined systems of linear equations. Relying on the theory of projections, we examine the nature of the set of optimal solutions of the given overdetermined system. The paper also provides a brief functional approach to the above problem by utilizing p -norms.

Keywords: overdetermined system, optimal solution, orthogonal projection, convexity

1. Introduction

We consider a system of m linear equations with n unknowns $x_1,\ldots,x_n$ written as

$$\begin{matrix} a_{11}x_1+ & \ldots & +a_{1n}x_n=b_1 \\ \vdots & \ddots & \vdots \\ a_{m1}x_1+ & \ldots & +a_{mn}x_n=b_m \end{matrix}. \quad (1)$$

The matrix form of the above system is

$$Ax=b \quad (2)$$

where

$$A=\begin{bmatrix} a_{11} & \ldots & a_{1n} \\ \vdots & \ddots & \vdots \\ a_{m1} & \ldots & a_{mn} \end{bmatrix}, x=\begin{bmatrix} x_1 \\ \vdots \\ x_n \end{bmatrix}, b=\begin{bmatrix} b_1 \\ \vdots \\ b_m \end{bmatrix}. \quad (3)$$

We identify the matrix A with a linear operator from $\mathbb{R}^n$ to $\mathbb{R}^m$, the column matrix x with a vector of $\mathbb{R}^n$, and the column matrices Ax and b with vectors of $\mathbb{R}^m$.

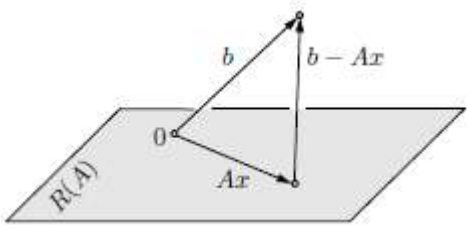

Figure 1. *Inconsistent system* $Ax=b$

If the vector b is not contained in the image $R(A)$ of the operator A, then the system in equation (2) has no solution. Such a system is said to be inconsistent, and it is illustrated in Figure 1. A system of linear equations is said to be overdetermined if there are more equations than unknowns. The overdetermined system with linearly independent equations is inconsistent.

In order to study the inconsistent system $Ax=b$, we need a norm on $\mathbb{R}^m$. If we have some norm, then we require vectors $x^*\in\mathbb{R}^n$ which satisfy

$$\| b-Ax^* \| = \min_{x\in\mathbb{R}^n} \| b-Ax \|. \quad (4)$$

Each vector $x^*\in\mathbb{R}^n$ which meets the condition in formula (4) is called an optimal solution of the observed system respecting the given norm.

The general problem of least absolute deviations was discussed in [1]. Several algorithms for solving the approximation problem were presented in [5].

2. Projections onto closed convex sets

Throughout the section, we use a real vector space $\mathbb{V}$ and its subset V. A brief overview of the theory of projections will be presented.

Let $u,v\in\mathbb{V}$ be vectors, and let $\kappa,\lambda\in\mathbb{R}$ be coefficients. Then the linear combination $\kappa u+\lambda v$ is said to be affine (convex) if we have that $\lambda=1-\kappa$ $(0\le\lambda=1-\kappa\le 1)$. A set $V\subseteq\mathbb{V}$ is said to be affine (convex) if it contains all binomial affine (convex) combinations of its vectors.

Let $\| \|$ be a norm on the space $\mathbb{V}$. The distance of a vector $b\in\mathbb{V}$ from a nonempty set $V\subseteq\mathbb{V}$ is the number

$$d(b,V)=\inf_{v\in V}\| b-v \|. \quad (5)$$

If there is a vector $b^*\in V$ such that $d(b,V)=\| b-b^* \|$, then it is usually called a projection of b onto V or minimal distance vector. The projections are located on the sphere S centered at b with radius $r=d(b,V)$. If the projection b^* is unique, then it is called the orthogonal projection or nearest vector.

Lemma 2.1. (Projections) *Let $\mathbb{V}$ be a real normed space, let $V \subseteq \mathbb{V}$ be a nonempty closed (convex) set, and let $b \in \mathbb{V}$ be a vector.*

Then the set $V_b \subseteq V$ of projections of b onto V is a closed (convex) set including the empty set.

Proof. We have to assume that $V_b \neq \emptyset$. If V is closed, we employ a sequence $(b_n^*)_n$ of vectors $b_n^* \in V_b$ converging to some vector $b^* \in V$. Since $\| b - b_n^* \| = d(b,V)$, it follows that $\| b - b^* \| = d(b,V)$, and therefore $b^* \in V_b$. Thus, V_b is closed.

If V is convex , we take a convex combination $\lambda_1 b_1^* + \lambda_2 b_2^*$ of vectors $b_1^*, b_2^* \in V_b$. By utilizing the convexity of V, and the triangle inequality of $\| \ \|$, it follows that

$$\| b - (\lambda_1 b_1^* + \lambda_2 b_2^*) \| = d(b,V),$$

and therefore $\lambda_1 b_1^* + \lambda_2 b_2^* \in V_b$. This indicates that V_b is convex. □

A norm on $\mathbb{V}$ is said to be strictly convex if the equality $\| u \| = \| v \| = 1$ for $u \neq v$ implies the strict inequality $\| u/2 + v/2 \| < 1$. Consequently, the related implication applies to any sphere in $\mathbb{V}$.

Corollary 2.2. *Let $\mathbb{V}$ be a real normed space, let $V \subseteq \mathbb{V}$ be a finite-dimensional subspace, and let $b \in \mathbb{V}$ be a vector.*

Then the set $V_b \subseteq V$ of projections of b onto V is a nonempty closed convex set. If the space norm is strictly convex, then V_b is a singleton.

Proof. We pick a vector $v \in V$, and the ball B centered at b with radius $r = \| b - v \|$. We put $d = d(b,V)$, and take a sequence $(v_n)_n$ of vectors $v_n \in V \cap B$ such that

$$d \leq \| b - v_n \| \leq d + 1/n. \qquad (6)$$

Since the set $V \cap B$ is compact in the subspace V, the sequence $(v_n)_n$ has a subsequence which converges to some vector $b^* \in V \cap B$. Then the converges to some vector $b^* \in V \cap B$. Then the related subsequence of norms in formula (6) converges to d. Since $\| b - b^* \| = d$, the vector b^* is a projection of b onto V. Thus the set V_b is nonempty, and by Lemma 2.1 it is closed and convex. Suppose that the norm is strictly convex, and take $b_1^*, b_2^* \in V_b$. Since V_b is convex, the midpoint $b_1^*/2 + b_2^*/2 \in V_b$, and so $\| b - b_1^* \| = \| b - b_1^* \| = \| b - (b_1^*/2 + b_1^*/2) \| = d$. Since the norm is strictly convex, it follows that $b_1^* = b_2^*$. □

An inner product on the space $\mathbb{V}$ generates the norm by means of $\| v \| = \sqrt{\langle v, v \rangle}$. Such norm satisfies the parallelogram law

$$\| u + v \|^2 + \| u - v \|^2 = 2 \| u \|^2 + 2 \| v \|^2 .$$

A norm on the space $\mathbb{V}$ satisfying the above parallelogram law generates the inner product by means of

$$\langle u, v \rangle = \frac{1}{4} (\| u + v \|^2 - \| u - v \|^2).$$

Theorem 2.3. (Orthogonal projection) *Let $\mathbb{V}$ be a real Hilbet space, let $V \subseteq \mathbb{V}$ be a nonempty closed convex set, and let $b \in \mathbb{V}$ be a vector.*

Then there is the orthogonal projection b^* of b onto V.

Proof. Each sequence $(v_n)_n$ of vectors $v_n \in V \cap B$ that satisfy formula (6) is a Cauchy sequence converging to the unique vector $b^* \in V$. The proof is based on the parallelogram law of the generated norm and convexity of V. □

Vectors x and y belonging to an inner product space are said to be orthogonal if $\langle x, y \rangle = 0$. In Theorem 2.3, the vectors $b - b^*$ and b^* are not necessarily orthogonal.

Corollary 2.4. *Let $\mathbb{V}$ be a real Hilbert space, let $V \subseteq \mathbb{V}$ be a finite-dimensional subspace, let $b \in \mathbb{V}$ be a vector, and let b^* be its orthogonal projection onto V.*

Then the vector $b-b^*$ is orthogonal on each vector of the subspace V.

In Corollary 2.4, for each vector $v \in V$ the zero inner product $\langle v, b-b^* \rangle = 0$ implies the equality

$$\langle v, b \rangle = \langle v, b^* \rangle. \quad (7)$$

3. Sets of optimal solutions

Let $A: \mathbb{R}^n \to \mathbb{R}^m$ be a linear operator where $n < m$, and let $b \in \mathbb{R}^m$ be a vector. Our objective is the equation $Ax = b$ with unknown vectors $x \in \mathbb{R}^n$. If $b \in R(A)$, then the set of solutions of the above equation is the preimage of b written as

$$A^{(-1)}(b) = \{x \in \mathbb{R}^n : Ax = b\}.$$

If $b \notin R(A)$, the equation $Ax = b$ is inconsistent. To include both cases, using a norm $\| \ \|$ on $\mathbb{R}^m$, we consider a more general equation

$$\| b - Ax \| = d(b, R(A)), \quad (8)$$

which is reduced to $Ax = b$ if $b \in R(A)$. Solutions of the above equation are also called optimal solutions of the equation $Ax = b$ respecting the given norm.

Corollary 2.2 ensures the existence of optimal solutions as follows.

Theorem 3.1. *Let $A: \mathbb{R}^n \to \mathbb{R}^m$ be a linear operator where $n < m$, let $\| \ \|$ be a norm on $\mathbb{R}^m$, and let $b \in \mathbb{R}^m$ be a vector.*

Then the set $X \subseteq \mathbb{R}^n$ of solutions of the equation in (8) is nonempty, closed respecting any norm on $\mathbb{R}^n$, and convex. It can be presented by the union

$$X = \bigcup_{b^* \in R(A)_b} A^{(-1)}(b^*). \quad (9)$$

Proof. By putting $\mathbb{V} = \mathbb{R}^m$ and $V = R(A)$, Theorem 3.1 fits into Corollary 2.2, and so it follows that the set $R(A)_b$ of projections of b onto $R(A)$ is nonempty. Each projection $b^* \in R(A)_b$ generates the affine set $A^{(-1)}(b^*)$ of solutions $x^* \in \mathbb{R}^n$ satisfying $Ax^* = b^*$, and so the set X is nonempty. Containing all solutions, X is the union of all $A^{(-1)}(b^*)$ where $b^* \in R(A)_b$.

The set X is closed respecting any norm on $\mathbb{R}^n$ because the operator A is continuous respecting any pair of norms on $\mathbb{R}^n$ and $\mathbb{R}^m$.

To prove that the set X is convex, we take a convex combination $\kappa x^* + \lambda y^*$ of solutions $x^*, y^* \in X$. Using the norm triangle inequality and $\| b - Ax^* \| = \| b - Ay^* \| = d(b, R(A))$, we can prove that

$$\| b - A(\kappa x^* + \lambda y^*) \| \ \leq \ d(b, R(A)).$$

Since $d(b, R(A))$ is minimal, it follows that $\| b - A(\kappa x^* + \lambda y^*) \| = d(b, R(A))$, which shows that the combination $\kappa x^* + \lambda y^*$ belongs to X. □

By using norms on spaces $\mathbb{R}^m$ and $\mathbb{R}^n$ in Theorem 3.1, the sets $R(A)_b \subseteq \mathbb{R}^m$ and $X \subseteq \mathbb{R}^n$ are nonempty, closed and convex. The set $R(A)_b$ is still bounded because it is on the sphere S centered at b with radius $r = d(b, R(A))$.

If the norm on $\mathbb{R}^m$ in Theorem 3.1 is strictly convex, then the projection b^* is unique, and consequently $X = A^{(-1)}(b^*)$. By using an inner product on $\mathbb{R}^m$, the members of X can be expressed explicitly.

Let $\mathbb{V}$ be an inner product space, let A be a matrix consisting of columns $a_1, \ldots, a_n \in \mathbb{V}$, and let C be a matrix consisting of columns $c_1, \ldots, c_m \in \mathbb{V}$. Their Gram product $\langle A, C \rangle$ is defined as the $n \times m$ matrix with the inner product $\langle a_i, c_j \rangle$ at the place (i, j). The matrix $\langle A, A \rangle$, called the Gram matrix of A, is invertible if and only if the columns of A are linearly independent.

We have the following practical application of Corollary 2.4.

Lemma 3.2. *Let $A: \mathbb{R}^n \to \mathbb{R}^m$ be a linear operator where $n < m$, let $\langle , \rangle$ be an inner product on $\mathbb{R}^m$, let $b \in \mathbb{R}^m$ be a vector, and let b^* be the orthogonal projection of b onto $R(A)$.*

Then the set $X \subseteq \mathbb{R}^n$ *of solutions of the equation in (8) can be presented by the preimage of* b^**, so* $X = A^{(-1)}(b^*)$*. If the columns of* A *are linearly independent, then* X *contains only the vector*

$$x^* = \langle A, A\rangle^{-1}\langle A, b\rangle. \qquad (10)$$

Proof. In this case, the orthogonal projection b^* is unique by Theorem 2.3, and therefore the union in formula (9) is reduced to the set $A^{(-1)}(b^*)$.

In order to apply Corollary 2.4, we put $\mathbb{V} = \mathbb{R}^m$ and $V = R(A)$. Let a_i be the columns of A. Using the equation $Ax = b^*$ in the vector form

$$a_1x_1 + \ldots + a_nx_n = b^*,$$

taking the inner product with each a_i, and applying the equalities $\langle a_i, b^*\rangle = \langle a_i, b\rangle$ by formula (7), we get the quadratic system

$$\begin{matrix} \langle a_1, a_1\rangle x_1 + & \ldots & +\langle a_1, a_n\rangle x_n = \langle a_1, b\rangle \\ \vdots & \ddots & \vdots \\ \langle a_n, a_1\rangle x_1 + & \ldots & +\langle a_n, a_n\rangle x_n = \langle a_n, b\rangle \end{matrix}. \qquad (11)$$

If a_i are linearly independent, then utilizing the matrix form $\langle A, A\rangle x = \langle A, b\rangle$, and the invertibility of the Gram matrix $\langle A, A\rangle$, we obtain the unique solution of the above system as $x = x^* = \langle A, A\rangle^{-1}\langle A, b\rangle$. □

Using the Euclidean inner product obtained from 2-norm, formula (10) takes the form

$$x^* = (A^{\mathsf{T}}A)^{-1}A^{\mathsf{T}}b. \qquad (12)$$

The matrix $A^+ = (A^{\mathsf{T}}A)^{-1}A^{\mathsf{T}}$ is often referred to the Moore-Penrose inverse of A, see the presentation of linear optimization problems in [2].

Lemma 3.2 can be extended to the case of linear dependence of vectors a_i.

Theorem 3.3. *Let the assumptions of Lemma 3.2 be fulfilled. Let the columns of* A *be such that columns* $a_1, \ldots, a_k$ *are linearly independent and columns* $a_{k+1}, \ldots, a_n$ *depend on them, let*

$$b_{(k)} = b - a_{k+1}x_{k+1} - \ldots - a_nx_n,$$

and let $A_{(k)}$ be the matrix consisting of columns $a_1, \ldots, a_k$.

Then

$$x^*_{(k)} = \langle A_{(k)}, A_{(k)}\rangle^{-1}\langle A_{(k)}, b_{(k)}\rangle. \qquad (13)$$

Proof. Since the projection $b^*_{(k)} = b^* - a_{k+1}x_{k+1} - \ldots - a_nx_n$ is orthogonal on the image space $R(A_{(k)})$, we can apply Lemma 3.2 to $A_{(k)}$ and $b_{(k)}$, and so obtain formula (13). □

4. Using convex functions

Let V be a convex set in a real vector space. A function $f : V \to \mathbb{R}$ is said to be convex if the inequality

$$f(\kappa u + \lambda v) \le \kappa f(u) + \lambda f(v) \qquad (14)$$

holds for all convex combinations $\kappa u + \lambda v$ of points $u, v \in V$. Given the importance of functions in mathematics in general, we are presenting the inconsistent equation problem by using functionals. A convenient functional approach enables Theorem 3.1 which yields the following.

Corollary 4.1. *Let* $A : \mathbb{R}^n \to \mathbb{R}^m$ *be a linear operator where* $n < m$*, let* $\| \ \|$ *be a norm on* $\mathbb{R}^m$*, let* $b \in \mathbb{R}^m$ *be a point, and let* $f : \mathbb{R}^n \to \mathbb{R}$ *be the function defined by*

$$f(x) = \| b - Ax \|. \qquad (15)$$

Then f *is convex and has the global minimum.*

Proof. The convexity of f is a consequence of the linearity of A and convexity of $\| \ \|$. Using a projection b^* of b onto $R(A)$, the function f attains the global minimum $f(x^*) = \| b - b^* \|$ at each point x^* of the set X in formula (9). □

Let $m \ge 2$, and let $v = (v_1, \ldots, v_m) \in \mathbb{R}^m$ be a point. In applications we use p-norms defined for $p \ge 1$ by

$$\| v \|_p = \left(\sum_{i=1}^{m} | v_i |^p \right)^{\frac{1}{p}},$$

and their limit case the *max*-norm as

$$\| v \|_\infty = \max_{1 \le i \le m} | v_i |.$$

If A, x and b are as in formula (3), then respecting the above norms the function f in formula (15) takes the forms

$$f_p(x) = \| b - Ax \|_p = \left(\sum_{i=1}^{m} | b_i - \sum_{j=1}^{n} a_{ij} x_j |^p \right)^{\frac{1}{p}}$$

and

$$f_\infty(x) = \| b - Ax \|_\infty = \max_{1 \le i \le m} | b_i - \sum_{j=1}^{n} a_{ij} x_j |.$$

The conditions that ensure the existence and uniqueness of the global minimum point of a convex functional can be found in [3]. Some algorithms for calculating extremum points of convex functionals are presented in [6]. Optimization problems concerning convex functionals are discussed in [4].

5. Examples

Example 5.1. *Using the usual inner product generated by* 2*-norm, find the optimal solutions of the overdetermined system*

$$\begin{array}{rcrcrcl} 3x_1 & + & 2x_2 & + & x_3 & = & 20 \\ -x_1 & - & 2x_2 & + & x_3 & = & 1 \\ x_1 & + & 3x_2 & - & 2x_3 & = & 0. \\ x_1 & + & x_2 & & & = & 10 \\ 3x_1 & & & + & 3x_3 & = & -8 \end{array} \qquad (16)$$

Emphasizing the vector equation form $a_1 x_1 + a_2 x_2 + a_3 x_3 = b$ of the given system, we have

$$\begin{bmatrix} 3 \\ -1 \\ 1 \\ 1 \\ 3 \end{bmatrix} x_1 + \begin{bmatrix} 2 \\ -2 \\ 3 \\ 1 \\ 0 \end{bmatrix} x_2 + \begin{bmatrix} 1 \\ 1 \\ -2 \\ 0 \\ 3 \end{bmatrix} x_3 = \begin{bmatrix} 20 \\ 1 \\ 0 \\ 10 \\ -8 \end{bmatrix}. \qquad (17)$$

The calculation of inner products

$$\begin{array}{llll} \langle a_1, a_1 \rangle = 21, & \langle a_1, a_2 \rangle = 12, & \langle a_1, a_3 \rangle = 9, & \langle a_1, b \rangle = 45 \\ \langle a_2, a_1 \rangle = 12, & \langle a_2, a_2 \rangle = 18, & \langle a_2, a_3 \rangle = -6, & \langle a_2, b \rangle = 48 \\ \langle a_3, a_1 \rangle = 9, & \langle a_3, a_2 \rangle = -6, & \langle a_3, a_3 \rangle = 15, & \langle a_3, b \rangle = -3 \end{array}$$

and application of formula (11), give the system

$$\begin{array}{rcrcrcl} 21x_1 & + & 12x_2 & + & 9x_3 & = & 45 \\ 12x_1 & + & 18x_2 & - & 6x_3 & = & 48. \\ 9x_1 & - & 6x_2 & + & 15x_3 & = & -3 \end{array}$$

By applying the Gauss elimination method or some related method, we get the solutions of the above system as triples containing a real parameter t,

$$x_1 = x_1^* = 1 - t, x_2 = x_2^* = 2 + t, x_3 = x_3^* = t.$$

So, the optimal solutions of the given system in formula (16) are vectors of the line in $\mathbb{R}^3$ presented by the vector-parametric equation

$$x^* = x^*(t) = \begin{bmatrix} 1 - t \\ 2 + t \\ t \end{bmatrix}, \qquad (18)$$

and the orthogonal projection of b onto $R(A)$ is the vector

$$b^* = \begin{bmatrix} 3 \\ -1 \\ 1 \\ 1 \\ 3 \end{bmatrix} x_1^* + \begin{bmatrix} 2 \\ -2 \\ 3 \\ 1 \\ 0 \end{bmatrix} x_2^* + \begin{bmatrix} 1 \\ 1 \\ -2 \\ 0 \\ 3 \end{bmatrix} x_3^* = \begin{bmatrix} 7 \\ -5 \\ 7 \\ 3 \\ 3 \end{bmatrix}.$$

Since $a_3 = a_1 - a_2$, and a_1 and a_2 are linearly independent, it is appropriate to point out the vector equation form $a_1 x_1 + a_2 x_2 = b - a_3 x_3$ of the given system as

$$\begin{bmatrix} 3 \\ -1 \\ 1 \\ 1 \\ 3 \end{bmatrix} x_1 + \begin{bmatrix} 2 \\ -2 \\ 3 \\ 1 \\ 0 \end{bmatrix} x_2 = \begin{bmatrix} 20 - x_3 \\ 1 - x_3 \\ 2x_3 \\ 10 \\ -8 - 3x_3 \end{bmatrix}. \qquad (19)$$

The calculation of matrices

$$A_{(2)}^{\mathrm{T}}A_{(2)} = 3\begin{bmatrix} 7 & 4 \\ 4 & 6 \end{bmatrix}, (A_{(2)}^{\mathrm{T}}A_{(2)})^{-1} = \frac{1}{78}\begin{bmatrix} 6 & -4 \\ -4 & 7 \end{bmatrix}$$

and

$$A_{(2)}^{\mathrm{T}}b_{(2)} = 3\begin{bmatrix} 15-3x_3 \\ 16+2x_3 \end{bmatrix},$$

and application of formula (12) in the form of

$$x_{(2)}^{*} = (A_{(2)}^{\mathrm{T}}A_{(2)})^{-1}A_{(2)}^{\mathrm{T}}b_{(2)},$$

yield the optimal solutions

$$\begin{bmatrix} x_1^* \\ x_2^* \end{bmatrix} = \begin{bmatrix} 1-x_3^* \\ 2+x_3^* \end{bmatrix},$$

which can be presented as in formula (18).

Example 5.2. *Using three basic functions f_1, f_2 and f_∞, find the optimal solutions of the overdetermined system*

$$\begin{array}{rcl} x_1 & = & 1 \\ 3x_1 + x_2 & = & 0. \\ x_1 + x_2 & = & 4 \end{array} \qquad (20)$$

Using the function

$$f_1(x_1, x_2) = |x_1 - 1| + |3x_1 + x_2| + |x_1 + x_2 - 4|,$$

and its presentation $f_1(x_1, x_2) = x_1 + 5$ on the triangle with vertices $(-2, 6)$, $(1, -3)$ and $(1, 3)$, we can conclude that $x^* = (-2, 6)$ is the unique minimum point, and the global minimum is

$$f_1(-2, 6) = 3.$$

Using the function

$$f_2(x_1, x_2) = \sqrt{(x_1 - 1)^2 + (3x_1 + x_2)^2 + (x_1 + x_2 - 4)^2},$$

and applying the differential calculus, we find that $x^* = (-1, 4)$ is the unique minimum point, and so the global minimum is

$$f_2(-1, 4) = \sqrt{6}.$$

Using the function

$$f_\infty(x_1, x_2) = \max\{|x_1 - 1|, |3x_1 + x_2|, |x_1 + x_2 - 4|\},$$

and removing the absolute values, we obtain that $x^* = (-1/2, 3)$ is the unique minimum point, and thus the global minimum is

$$f_\infty\left(-\frac{1}{2}, 3\right) = \frac{3}{2}.$$

6. Conclusion

If we use the Euclidean norm (2-norm) in finding the optimal solutions of the overdetermined system, then it is most appropriate to utilize the prepared formula (12). In other cases, when we solve the overdetermined system respecting the norm which is not Euclidean, it is more convenient to utilize the convex functions from the collection $f_p(x)$ or the function $f_\infty(x)$.

7. References

[1] P. Bloomfield, W. Steiger, *Least Absolute Deviations: Theory, Applications and Algorithms*, Birkhauser Basel, 1983.

[2] M. Fiedler, J. Nedoma, J. Ramik, J. Rohn, K. Zimmermann, *Linear Optimization Problems with Inexact Data*, Springer-Verlag US, 2006.

[3] C. P. Niculescu, L. E. Persson, *Convex Functions and Their Applications*, Springer Science+Business Media New York, 2006.

[4] M. R. Osborne, *Finite Algorithms in Optimization and Data Analysis*, John Wiley & Sons New York, 1985.

[5] R. W. Owens, V. P. Sreedharan, Algorithms for solving overdetermined systems of linear equations in the l_p-metric, $0 < p < 1$, *J. Approx. Theory*, **24** (1978), 1-17.

[6] G. A. Watson, *Approximation Theory and Numerical Methods*, John Wiley & Sons New York, 1980.

OPTIMAL NUMBER OF CLUSTERS PROVIDED BY k-MEANS AND E-M ALGORITHM

Vedran Novoselac* and Zlatko Pavić

Mechanical Engineering Faculty in Slavonski Brod, J. J. Strossmayer University of Osijek, Croatia
**Corresponding author e-mail: vnovosel@sfsb.hr*

Abstract

The paper considers the problem of determining the optimal number of clusters in data set by grouping index. The problem of clustering are provided with k-means and E-M (Expectation Maximization) algorithm. In addition to well-known indexes that are frequently used, two new indexes are presented. New indexes are based on the orthogonal distances from data to the line which represent corresponding cluster in the partition obtained with mentioned algorithms.

Keywords: k-means, E-M, grouping index

1. Introduction

The paper considers the problem of partitioned a set of data $\mathcal{A} = \{a_i \in \mathcal{R}^n : i = 1,\ldots,m\} \subset \mathcal{R}^n$ into k nonempty disjoint subsets $\pi_1,\ldots,\pi_k$, $1 \le k \le m$, such that $\bigcup_{i=1}^{k} \pi_i = \mathcal{A}$. The partition will be denoted by $\Pi(\mathcal{A}) = \{\pi_1,\ldots,\pi_k\}$. The elements of partition Π are called clusters and the set of all such partitions are denoted by $\mathcal{P}(\mathcal{A},k)$. For this purpose k-means and E-M algorithms are described [1, 2, 3, 6, 8]. Calculation of the various indexes on final partition indicates the quality of separateness and compactness of clusters. Some of the most popular indexes that are frequently used are Davies-Bouldin, Dunn, Calinski-Haradsz, and Simplify Silhouette Width Criterion [2, 6, 7, 9]. In addition to these indexes two new indexes Orthogonal Distances Criterion (ODC) and Width Ortogonal Distances Criterion (WODC) are presented. Indexes ODC and WODC are based on line which is determined by eigenvector of corresponding largest eigenvalue of covariance matrix and mean of observed cluster. The optimal number of clusters of data set $\mathcal{A}$ are provided with observation on mentioned indexes.

2. Grouping algorithms

This section presents the standard k-means and E-M algorithm. Mentioned algorithms have very broad application and they are often closely modified to the related issue [4,5].

2.1. k-means algorithm

Let $d(x,y) = \|x-y\|_p$, $p \ge 1$, be a metric (in paper we use Euclidean norm, i.e. $p = 2$). In the sense of the given metric center c_i of corresponding cluster π_i is defined as

$$c_i = \underset{c \in \mathcal{R}^n}{\operatorname{argmin}} \sum_{a \in \pi_i} d(a,c). \qquad (1)$$

Data $a \in \mathcal{A}$ is attached to cluster π_i if is closest to the center c_i in comparison with the distances from the centers of other clusters. In that sense objective function $F : \mathcal{P}(\mathcal{A},k) \to \mathcal{R}$ is defined as

$$F(\Pi) = \sum_{i=1}^{k} \sum_{a \in \pi_i} d(a,c_i), \quad \Pi \in \mathcal{P}(\mathcal{A},k). \qquad (2)$$

Thus defined stopping criterion of k-means algorithm due to the so-called threshold $\varepsilon > 0$. Stoppage criterion is reached if absolute value of the difference between the objective function of iteration step does not exceed defined threshold ε. Thus, the k-means algorithm can be written as follows:

ALGORITHM 1. (k-means)

STEP 0.
Input number of clusters k, data set $\mathcal{A}$, stoppage criterion $\varepsilon > 0$, and initial centers $c_1^0,\ldots,c_k^0$. Set step of the algorithm $s = 0$;

STEP 1.
Apply the principle of minimum distance to determine the initial partition $\Pi^s = \{\pi_1^s,\ldots,\pi_k^s\}$, with an initial clusters

$$\pi_i^s = \{a \in \mathcal{A} : d(a,c_i^s) \le d(a,c_j^s),\ j = 1,\ldots,k\},$$

for every $i = 1,\ldots,k$;

STEP 2.

Form a new centroids c_i^{s+1}, $i=1,\ldots,k$, which are obtained by solving minimization problems

$$c_i^{s+1} = \underset{c\in\mathcal{R}^n}{\operatorname{argmin}} \sum_{a\in\pi_i^s} d(a,c);$$

Create a new partition $\Pi^{s+1} = \{\pi_1^{s+1},\ldots,\pi_k^{s+1}\}$ with clusters

$$\pi_i^{s+1} = \{a \in \mathcal{A} : d(a,c_i^{s+1}) \le d(a,c_j^{s+1}),\ j=1,\ldots,k\},$$

for every $i=1,\ldots,k$;

STEP 3.

If $|F(\Pi^s) - F(\Pi^{s+1})| \le \varepsilon$ then **STOP**, else $s = s+1$ and go to **STEP 2.**

2.2. E-M algorithm

E-M algorithm is based on the principle of soft grouping, where the boundaries between clusters are not solid. Specifically, it is a probabilistic grouping that each element of the reference data set determines the probability of belonging to each cluster. E-M algorithm is generally based on the Gaussian mixture model. Gaussian mixture model approximates the data as a linear combination of k density

$$p(x) = \sum_{i=1}^{k} w_i\, f_i(x \mid \theta_i), \qquad (3)$$

where x is n-dimensional vector, and weights w_i, $i = 1,2,\ldots,k$ respectively represent the percentage of data belonging to a cluster π_i, $i = 1,2,\ldots,k$, what imply $\sum_{i=1}^{k} w_i = 1$. Parameter $\theta_i = (\mu_i, \Sigma_i)$ of density function $f_i(x|\theta_i)$ in Gaussian mixture model is presented with expectation μ_i and covariance matrix Σ_i determining the density function for the normal (Gaussian) distribution, i.e.

$$f_i(x \mid \theta_i) = \frac{1}{\sqrt{(2\pi)^l \mid \Sigma_i \mid}} \exp\left(-\frac{1}{2}(x-\mu_i)^T \Sigma_i^{-1} (x-\mu_i)\right), \qquad (4)$$

Quality of Gaussian mixture model presented with parameters $\Phi = \{(w_i, \mu_i, \Sigma_i) : i = 1,\ldots,k\}$ is measured with log-likelihood

$$L(\Phi) = \sum_{x\in S} \log\left(\sum_{i=1}^{k} w_i\, f_i(x \mid \mu_i, \Sigma_i)\right). \qquad (5)$$

The process is repeated until the log-likelihood of the mixture model at the previous iteration is sufficiently close to the log-likelihood of the current model. The algorithm proceeds as follows for Gaussian mixture model:

ALGORITHM 2. (E-M)

STEP 0.

Initialization of parameters $\Phi^0 = \{(w_i^0, \mu_i^0, \Sigma_i^0) : i = 1,\ldots,k\}$ (zero partition), $s = 0$, and stopage criterion $\varepsilon > 0$ (set by user or at random).

STEP 1. (E step)

For every $a \in \mathcal{A}$ calculate π_i cluster probability as

$$w_i^s(a) = \frac{w_i^s\, f_i(a \mid \mu_i^s, \Sigma_i^s)}{\sum_{n=1}^{k} w_n^s\, f_n(a \mid \mu_n^s, \Sigma_n^s)}, \quad i = 1,\ldots,k.$$

STEP 2. (M step)

Calculation of new parameters for Gaussian mixture model for every $i = 1,2,\ldots,k$:

$$w_i^{s+1} = \sum_{a\in\mathcal{A}} w_i^s(a),$$

$$\mu_i^{s+1} = \frac{\sum_{a\in\mathcal{A}} w_i^s(a)\, a}{\sum_{a\in\mathcal{A}} w_i^s(a)},$$

$$\Sigma_i^{s+1} = \frac{\sum_{a\in\mathcal{A}} w_i^s(a)(a-\mu_i^{s+1})(a-\mu_i^{s+1})^T}{\sum_{a\in\mathcal{A}} w_i^s(a)}.$$

STEP 3.

If $|L(\Phi^s) - L(\Phi^{s+1})| \le \varepsilon$ then **STOP**, else $s = s+1$ and go to **STEP 1.**

3. Grouping indexes

In order to measure the compactness and separateness of k optimal partitions one of the most common indexes are used: DB (Davies-Bouldin), D (Dunn), CH (Calinski-Harabasz), SSC (Simplify Silhouette Width Criterion). In addition to these , we construct two new indexes ODC (Orthogonal Distances Criterion) and WODC (Width Orthogonal Distances Criterion). They are based on the sum of the orthogonal distance to the line which is passing through the centroid and is determined by the eigenvector of the largest eigenvalue of covariance matrix of observed cluster. Next figure

present such a lines of the case when set $\mathcal{A}$ are contained of the two clusters.

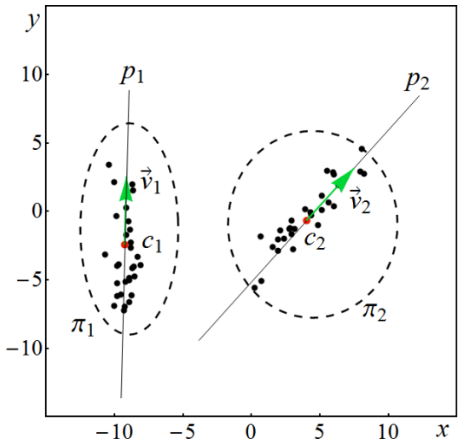

Figure 1. Index construction

Below we present a detailed definition of the aforementioned indexes:

a) Davies-Bouldin index

$$DB = \frac{1}{k}\sum_{i=1}^{k} R_i, \tag{6}$$

where

$$R_i = \max_{i \neq j} R_{ij}, \quad R_{ij} = \frac{r_i + r_j}{D_{ij}}, \quad D_{ij} = d(c_i, c_j),$$

$$r_i = \frac{1}{m_i}\sum_{a \in \pi_i} d(a, c_i).$$

More compact and better separated clusters will result smaller DB index.

b) Dunn index

$$D = \min_{1 \le i < j \le k} \left(\frac{D(\pi_i, \pi_j)}{\max_{1 \le s \le k} diam\pi_s} \right), \tag{7}$$

where

$$D(\pi_i, \pi_j) = \min_{a \in \pi_i, b \in \pi_j} d(a, b),$$

$$diam\pi_s = \max_{a,b \in \pi_s} d(a, b).$$

More compact and better separated clusters will result smaller D index.

c) Chalinski-Harabasz index

$$CH = \frac{(m-k)\mathcal{G}(\Pi)}{(k-1)\mathcal{F}(\Pi)}, \tag{8}$$

where $\mathcal{F}, \mathcal{G} : \mathcal{P}(\mathcal{A}, k) \to \mathcal{R}$ are functions defined as:

$$\mathcal{F}(\Pi) = \sum_{i=1}^{k}\sum_{x \in \pi_i} \|c_i - x\|_2^2, \quad \mathcal{G}(\Pi) = \sum_{i=1}^{k} m_i \|c_i - c\|_2^2,$$

$$c_i = \frac{1}{m_i}\sum_{a \in \pi_i} a, \quad c = \frac{1}{m}\sum_{a \in \mathcal{A}} a.$$

More compact and better separated clusters will result larger DB index.

d) Simplify Silhouette Width Criterion

$$SSC = \frac{1}{m}\sum_{a \in \mathcal{A}} \frac{\beta_{ai} - \alpha_{ai}}{\max\{\alpha_{ai}, \beta_{ai}\}}, \tag{9}$$

where for all $a \in \pi_i \cap \mathcal{A}$ follows that $\alpha_{ai} = d(a, c_i), \quad \beta_{ai} = \min_{j \neq i} d(a, c_j).$

e) Orthogonal Distances Criterion

$$ODC = \sum_{i=1}^{k} D_i, \tag{10}$$

where

$$D_i = \sum_{a \in \pi_i} d(a, p_i).$$

$d(a, p_i)$ present orthogonal distance from a to the line p_i which is determined by centroid c_i and eigenvector of corresponding largest eigenvalue. More compact and better separated clusters will result smaller ODC index.

f) Width Orthogonal Distances Criterion

$$WODC = \sum_{i=1}^{k} W_i, \tag{11}$$

where

$$W_i = \frac{1}{d_i}\sum_{a \in \pi_i} d(a, p_i), \quad d_i = \min_{\substack{j=1,\ldots,k \\ j \neq i}} d(c_i, c_j).$$ More compact and better separated clusters will result smaller WODC index.

4. Experimental results

In this chapter we examine data sets $\mathcal{A} \subset \mathcal{R}^2$ on implementing problem of determining k optimal partition obtained by k-means and E-M algorithm. The problem of finding an optimal partition of the set $\mathcal{A}$ can be reduced to the global optimization problem of objective function of k-means and E-M. In our case we run observed grouping algorithms for many different initial parameters and choose the solution with the best quality. The experimental data were generated using Gaussian random variable, i.e. $X \sim \mathcal{N}(\mu, \Sigma)$. The figure below shows illustrative examples of such functions density. In Figure 2(a) is present case with expectation $\mu = (0,0)$, and identity covariance matrix $\Sigma = I$. Figure 2(b) present case with $\mu = (0,0)$ and covariance matrix $\Sigma = \begin{bmatrix} 1.1 & 0.3 \\ 0.3 & 1.9 \end{bmatrix}$.

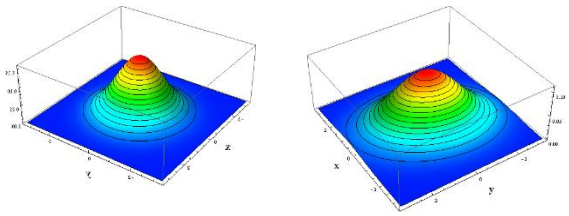

(a) (b)

Figure2 . PDF of Gaussian distribution

In the paper we also generated data with the extended model of the Gaussian distribution defined as

$$X \sim \mathcal{N}(\rho A + (1-\rho)B; \Sigma), \qquad (12)$$

where $A, B \in \mathcal{R}^n$ and ρ is uniformly distributed random variable within the interval $[0,1]$, i.e. $\rho \sim \mathcal{U}([0,1])$. Such data are distributed in a way that the expectation of the Gaussian distribution is uniformly distributed along the $\overline{AB}$. The density function of such defined random variable is given as

$$f(x \mid A, B, \Sigma) = \int_0^1 f(x \mid \rho A + (1-\rho)B, \Sigma)\mathrm{d}\rho. \qquad (13)$$

The Figure 3 below shows illustrative examples of such extended Gaussian PDF, where $A = (0,0)$, $B = (5,5)$, and identity covariance matrix $\Sigma = I$ are taken into the calculation of (13).

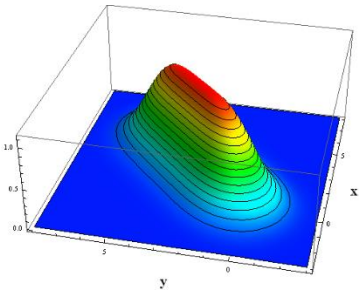

Figure 3. PDF of extended Gaussian distribution

The following examples illustrate the calculation of optimal number of clusters of data set $\mathcal{A} = \bigcup_{i=1}^{N} \mathcal{A}_i$, where every set $\mathcal{A}_i$ is generated with Gaussian random variable or extended Gaussian random variable defined by (12). To determinate the k optimal partition we have apply 100 randomly initializations of k-means and E-M algorithm respectively. Among the all randomly generated algorithms we presente those one with the best solution, i.e. best observed indexs value.

Example 1. ***1*** *The set of data $\mathcal{A}$ is generated by the Gaussian random variable which is presented in Figure 4. The Figure 5 shows the movement of the indexes of the k optimal partition.*

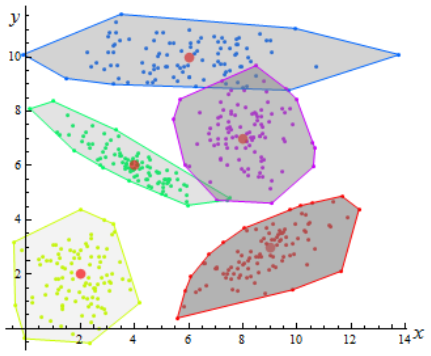

Figure 4. Data set $\mathcal{A}$

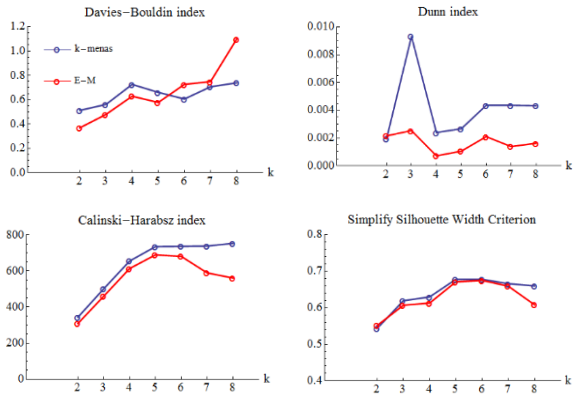

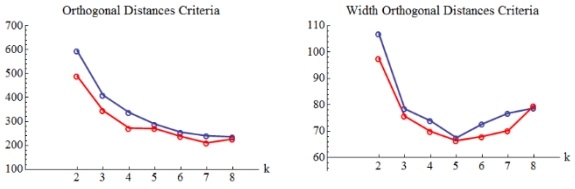

Figure 5. Indexes results

Example 2 *The set of data $\mathcal{A}$ is generated by the extended Gaussian random variable which is presented in Figure 6. The Figure 7 shows the movement of the indexes of the k optimal partition.*

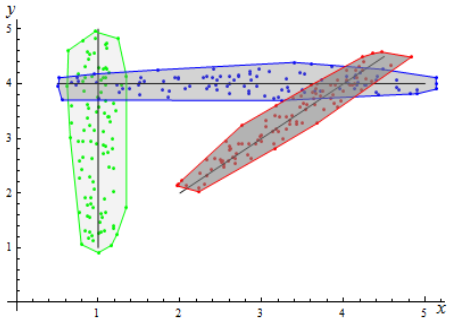

Figure 6. Data set $\mathcal{A}$

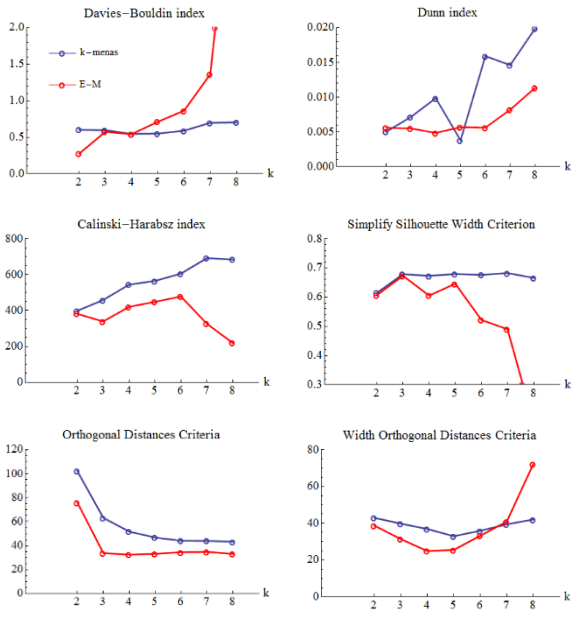

Figure 7. Indexes results

Example 3. ***2*** *The next set of data are generated by combination of Gaussian random variable and extended Gaussian random variable which is presented in Figure 6. The Figure 7 shows the movement of the indexes of the k optimal partition.*

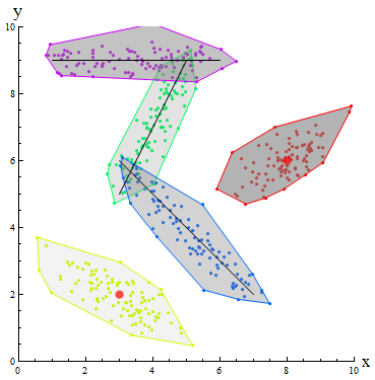

Figure 8. Data set $\mathcal{A}$

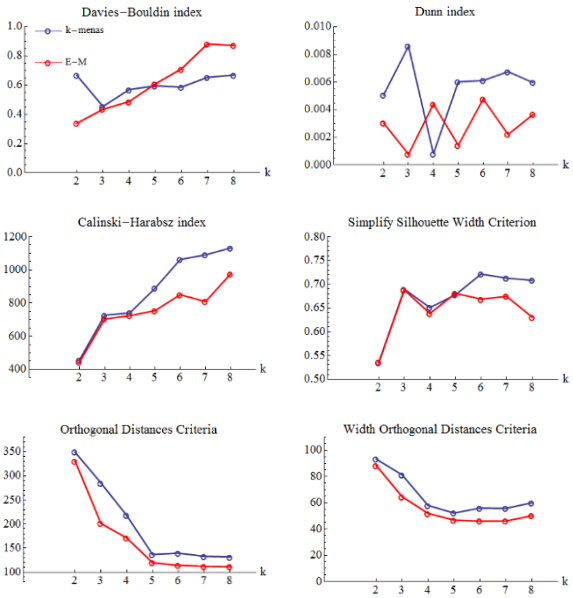

Figure 9. Indexes results

5. Conclusion

Problem of determination of the optimal numbers of clusters in observed data present a problem which we have solved by the investigation of the grouping indexes. Among the common used indexes we have construct two new indexes which shows good properties of finding the optimal number of clusters. Experimental results shows that the mentioned problem depends on many facts and indexes do not clearly shows unique optimal number. This shows that the problem must be precisely studied in order to finde optimal number of cluster what is present in the papper.

6. References

[1] P. S. Bradley, U. M. Fayyad, C. A. Reina, *Scaling EM (Expectation-Maximization) Clustering to Large Databases*, Microsoft Research, 1999.

[2] G. Gan, C. Ma, J. Wu, *Data Clustering, Theory, Algorithms and Applications*, SIAM, 2007.

[3] A. Kak, *Expectation-Maximization Algorithm for Clustering Multidimensional Numerical Data*, An RVL Tutorial Presentation, Summer 2012, Purdue University, 2013..

[4] T. Marošević, R. Scitovski, *Multiple ellipse fitting by center-based clustering*, Croatian Operational Research Review. 6(2015), 1; 43-53.

[5] V. Novoselac and Z. Pavić, *Outlier detection in experimental dana using a modified expectation maximization algorithm*, Proceedings of 6th International Scientific and Expert Conference of the International TEAM Society, Kecskemet, 2014, 112-115.

[6] K. Sabo, R. Scitovski, I. Vazler, *Grupiranje podataka: klasteri*, Osječki matematički list 10(2010), 149-176.

[7] R. Scitovski, S. Scitovski, *A fast partitioning algorithm and its application to earthquake investigation*, Computers and Geosciences, 59, 2013, 124-131.

[8] S. Theodoridis, K. Koutroumbas, *Pattern Recognition, Fourth Edition*, Elsevier, 2009.

[9] Lucas Vendramin, Ricardo J. G. B. Campello, Eduardo R. Hruschka, *On the Comparison of Relative Clustering Validity Criteria* , Proceedings of the SIAM International Conference on Data Mining, SDM 2009, April 30 - May 2, 2009, Sparks, Nevada, USA. SIAM 2009, 733-744.

Comparative analysis of apple quality monitoring methods in computer vision

S. Kukolj [a], J. Mastilović [b], Ž. Kevrešan [c], G. Ostojić [d], S. Stankovski [e]

[a] Faculty of Technical Sciences, University of Novi Sad, Trg Dositeja Obradovića 6, 21000 Novi Sad, Serbia, sandra.kukolj@rt-rk.com

[b] Institute of Food Technology, University of Novi Sad, Bulevar Cara Lazara 1, 21000 Novi Sad, Serbia, jasna.mastilovic@fins.uns.ac.rs

[c] Institute of Food Technology, University of Novi Sad, Bulevar Cara Lazara 1, 21000 Novi Sad, Serbia, zarko.kevresan@fins.uns.ac.rs

[d] Faculty of Technical Sciences, University of Novi Sad, Trg Dositeja Obradovića 6, 21000 Novi Sad, Serbia, goca@uns.ac.rs

[e] Faculty of Technical Sciences, University of Novi Sad, Trg Dositeja Obradovića 6, 21000 Novi Sad, Serbia, stevan@uns.ac.rs

Abstract

Under controlled atmosphere conditions (ultra low oxygen-ULO), texture and colour as parameters characterizing fruit ripening, disease development and maturity stages are changed and thus should be permanently monitored. Monitoring of apple properties during the storage in ULO chambers is a challenge since opening of chambers represents a hazard regarding controlled atmosphere composition as well as for safety of operators. Image processing method represents one of the possibilities for automatic monitoring in ultra-low oxygen chambers. Utilization of digital photographs and their analysis for identification and prediction of changes on the surface of fresh and stored apples was investigated. Various fruit's characteristics and influence factors were analysed. This survey analyses methods applied on both NIR and visual images, which employ image segmentation and feature extraction. The possibilities of NIR and visual images utilization for prediction of apple skin defects occurrence is also briefly analysed. Possibilities for early identifying of apple skin decay symptoms based on NIR and visual images were discussed in several methodologies.

Keywords: Advanced technology and Technics in Agriculture, image analysis, apple ripening monitoring, NIR images, visible spectrum images.

1. INTRODUCTION

There is a constant need in finding a low-cost methodology that would predict fruit ripening stages, considering that the maturity of fruit affects the quality factors of the fruit. Fruits are prone to changing colour and texture, and eventually decay. Therefore, characteristics of raw food depend on their maturity and storage conditions, like temperature, humidity, storage duration, fungal infections and volatile substances. Further difficulties can be caused by the same chromaticity of the found defect as of the fruit skin, as well as the need to correctly identify foreign material such as stems, leaves and dirt and not confuse them with other fruit skin blemishes. Yet another difficulty is caused by poorly chosen light sources that can result in glares on images, and therefore sample illumination needed for computer vision systems must be appropriate.

The illumination in these systems depends on the sample's geometry. For example, apples are often illuminated by two halogen lights set at 45° and on the opposite sides of the system.

Image acquisition is done using a high-resolution camera, and its model solely depends on the needs for a particular application. After image acquisition (conducted in a previously determined suitable illumination environment), a data set of images is obtained for testing and processing.

Besides images in the visual spectrum, special attention is brought to processing of near-infrared (NIR) images. NIR spectroscopy is based on selecting optimal wavelengths that correlate best with the subjected fruit.

Having all this in mind, there are a lot of influential factors and numerous analysis techniques. Some of the texture analysis techniques are statistical methods, structural methods and transform-based models.

This paper is an overview of image analysis related to fruit quality assessment using machine vision systems and spectral analysis, and presents some of the mostly used technologies and their applications.

2. INFLUENCE FACTORS

Disorders and diseases commonly detected as defects on apples are rot, bitter pit, scab and blotch, but defects can also be mechanical damages like bruises and lesions made accidently. Some factors that have influence on apple fruits are briefly described, as they have a major impact on further decisions related to system's architecture and methods that would be appropriate.

2. 1. Contamination

Fruit skin can be contaminated by fecal material which can have pathogens like E. coli. Kim et al. [1] applied multispectral imaging 450–851 nm to detect fecal with thin and thick layer on apples with different green and red colorations. This was somehow successful for thick patches. Apple coloration caused problems with thin layer. Kim et al. [2] studied also fluorescence spectral information. They identified four optimal bands (450, 530, 685, and 735 nm) for fecal detection and suggested the use of a simple ratio.

2.2. Maturity

Maturity or fruit ripeness affects the quality and taste of the fruit. Tanaka and Kojima [3] studied the growth stages and maturity of Japanese pear fruit using the sugar concentration as an indicator. Pear juice from different maturity stages produced different spectra, the absorption bands of which were related to carbohydrate. Multiple linear regression models were applied to determine the content of sucrose, fructose, sorbitol, and glucose sugars with 3–7 wavelength variables. Sirisomboon et al. [4] used NIR with principal component analysis (PCA) to classify tomatoes. The model provided a prediction for maturity.

2.3. Storage

Veraverbeke et al. [5] utilized NIR transmission spectra to solutions of single wax components and extracted apple wax. The wax was collected from apples with different parameters: apple cultivar (Jonagold, Jonagored, and Elshof), picking data (early, commercial, and late), storage time (0, 4, or 8 months in controlled atmosphere), and shelf life periods (0, 1, and 2 weeks). They applied canonical discriminant analysis on the first derivative of spectra. The proposed NIR technique could identify cultivar and storage duration but not very well the picking date or shelf life period. It seems that storage time and cultivars are related to differences in the number of aliphatic chains, like alkanes and esters, and the presence of α-farnesene.

3. DEFECT DETECTION AND CLASSIFICATION

Various image processing techniques with the aim of fruit defect detection have some kind of methodology of apple fruit part segmentation and its classification. The first step of a basic approach of defect (or disease) detection is data

set preparation. After preparing and testing the data set of apple fruit images, parts from the tested image with defects are segmented, and then features characteristic to the tested subject on images are extracted. These features are mostly color and texture. The final step is classification of extracted defects using classifiers.

3.1. Segmentation

The basis of segmentation is in identifying regions of interest from images by simplifying and/or changing the representation of an image in order to get a more meaningful and easier image to analyze.

3.2. Feature extraction

Feature vectors are considered to be color, texture, morphology and structure of fruits.

Color is the most valuable property for human for recognition. Conversion into HSI (hue, saturation, and intensity) color space is needed, since the RGB (red, green and blue) color space is influenced by the angle and light of the image. The color features utilized as a part of the fruit classification or fruit diseases identification are HSV (hue, saturation, and value) Histogram, L*a*b, RGB, YUV, Global Color Histogram, Color Coherence Vector, mean of three color array, Dominant color method, color difference histogram.

Morphology is used on the entire set of images. Eroding images from the dataset, boundaries are acquired for each fruit image from the database.

Texture feature identification techniques use modelling textures as two-dimensional deviation of gray level.

3.3. Classifiers

Classifiers are used for classifying images based on their features. Available classifiers are K-Nearest Neighbours (k-NN), Support Vector Machine (SVM), Artificial Neural Network (ANN) and Random Forest Tree Classifier [6].

Classification techniques may be supervised and unsupervised, which are based on predefined classification schemes classifying entire pixels.

4. METHODOLOGIES AND ALGORITHMS

Methodologies describe different techniques for specific aims in both pre-harvest and postharvest image processing. Each methodology is slightly different and just by differently combining existing algorithms, results can be satisfying. Algorithms used for different operations on images of apple fruits are PCA (Principal Component Analysis), LDA (Linear Discriminant Analysis), neural networks and other techniques (e.g. fuzzy algorithms).

In computer vision systems, NIR reflectance is proved best with optimized wavelengths between 400 and 1800nm [7], having in mind that multispectral images consist of a few spectral channels (a few wavelengths), while hyperspectral images have a continuous range of wavelengths.

Apple scab detection using differences in spectral responses at 450, 675 and 686 nm with a 6nm bandwidth provided an excellent method independent of apple cultivar and color [8]. The asymmetric second difference method and PCA gave very similar results for disease detection, bruises, fungal contamination and soil contamination on apples. A neural network using up to 200 neurons was used to detect diseases on apples using entropy, energy, local homogeneity and inertia as image parameters. This study achieved an 89% success rate on the detection of damaged apples [9]. Apple defect inspection using automatic NIR vision system was developed for using a monochrome CCD (charge-coupled device) camera attached with a 700 nm long-pass filter. The inspection procedure consisted of four steps: blob extraction, feature extraction, rule base construction and recognition [10]. Also, a NIR and MIR (mid-infrared) dual-camera vision system was used for quality inspection on refrigerated apples [11].

An adaptive approach for the identification of fruit diseases is done. K-Means clustering technique is utilized for defect segmentation, followed by features extraction and classification using a Multi-class Support Vector Machine [12]. Their accuracy was up to 93%.

A NIR hyperspectral imaging bruise detection technique is improved using both MNF (minimum noise fraction transform) and PC (principal component transform) methods in order to get the best results [13]. The observed spectral region was between 900 and 1700nm. Results were obtained with a detection rate of 88.1% and classification was obtained with 94% correctly classified bruises.

Bitter pit lesions, a disorder developed during storage, are identified in a hyperspectral NIR imaging system [14]. After pre-processing steps were done, a discriminant PLS (partial least squares) analysis was carried out. The conclusion was that this system is capable of detecting bitter pit even before visual symptoms occur. A calibration model was developed to predict bitter pit in apple as a validation.

A hyperspectral imaging system with a spectral range 0f 400-1000nm was used for detecting chilling injuries in apples. BPNN (Back-Propagation Neural Networks) technique was used and ANN (Artificial Neural Network) models were developed for wavelength selection, firmness prediction and classification of apples. The third model has achieved an accuracy of 98.4% and 100% in distinguishing normal from injured apples.

An algorithm for feature extraction called SURF (speed up robust feature) is applied and is used as a local descriptor and blob detector [15]. The architecture of the proposed system is presented in figure 1. This approach brings an accurate diagnosis of fruit diseases.

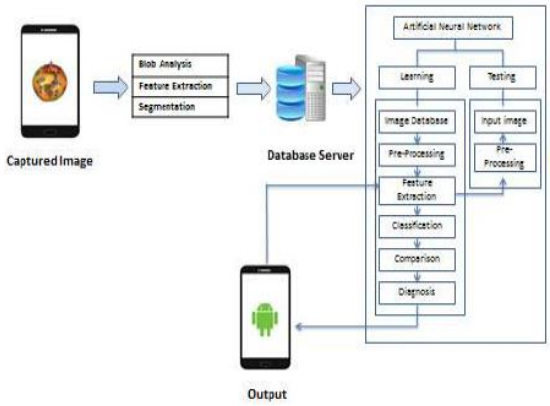

Fig. 1. System architecture for feature extraction

5. CONCLUSIONS

The cost of any system for computer vision for apple quality monitoring has to be affordable, having in mind its benefit, i.e. it should relate to its capacity to predict the disorder. Besides of an appropriate system setup, there are numerous methods for defect detection or their prediction. For instance, prediction can be achieved accelerating the fruit's maturity, but this can be difficult to achieve due to various factors that influence the outcome. A combination of visible bands gives a much lower detection level than combinations of wavebands in the NIR, therefore some of the existing methodologies are evaluated using NIR, as a composition of a large set of overtones and combination bands.

6. REFERENCES

[1] M. Kim, A. Lefcourt, K. Chao, Y. Chen, I. Kim, D. Chan, "Multispectral detection of fecal contamination on apples based on hyperspectral imagery: part I application of visible and nearinfrared reflectance imaging," Transactions of the ASABE, vol.45, no. 6, pp. 2027–2037, 2002.

[2] M. Kim, A. Lefcourt, Y. Chen, I. Kim, D. Chan, K. Chao, "Multispectral detection of fecal contamination on apples based on hyperspectral imagery: part II application of hyperspectral fluorescence imaging," Transactions of the American Society of Agricultural Engineers, vol. 45, no. 6, pp. 2039–2047, 2002.

[3] M. Tanaka, T. Kojima, “Near-infrared monitoring of the growth period of Japanese pear fruit based on constituent sugar concentrations,” Journal of Agricultural and Food Chemistry, vol. 44, no. 8, pp. 2272–2277, 1996.

[4] P. Sirisomboon, M. Tanaka, T. Kojima, P. Williams, “Nondestructive estimation of maturity and textural properties on tomato “Momotaro” by nearinfrared spectroscopy,” Journal of Food Engineering, vol. 112, no. 3, pp. 218–226, 2012.

[5] E. A. Veraverbeke, J. Lammertyn, B. M. Nicola¨ı, J. Irudayaraj, “Spectroscopic evaluation of the surface quality of apple, ”Journal of Agricultural and Food Chemistry, vol. 53, no. 4, pp.1046–1051, 2005.

[6] U. Solanki, U. K. Jaliya, D. G. Thakore,”A Survey on Detection of Disease and Fruit Grading”, International Journal of Innovative and Emerging Research in Engineering Volume 2, Issue 2, 2015.

[7] P.Williams, D. Sobering, “Comparison of commercial near infrared transmittance and reflectance instruments for analysis of whole grains and seeds,” Journal Near Infrared Spectroscopy,vol. 1, no. 1, pp. 25–32, 1993.

[8] P.M. Mehl, Y-R.Chen, M.S. Kim, D.E. Chan, “Development of hyperspectral imaging technique for the detection of apple surface defects and contaminations”, J. Food Eng. 2004, 61, 67-81

[9] D. Unay, B. Gosselin, “Apple defect detection and quality classification with MLP- Neural networks”, Proceedings of PRORISC 2002, Veldhoven: The Netherlands, 2002.

[10] Z. Wen, Y. Tao, “Building a rule-based machine-vision system for defect inspection on apple sorting and packing lines”, Exp. Syst. Appl. 1999, 16, 307-313

[11] X. Cheng, Y. Tao, Y.R. Chen, Y. Luo, “NIR/MIR dual sensor machine vision system for online apple stem-end/calyx recognition”, Trans. ASAE 2003, 46, 551–558

[12] S. R. Dubey, GLA University Mathura, A. S. Jalal, “Adapted Approach for Fruit Disease Identification using Images”, arxiv.org/pdf/1405.4930, 2014

[13] R. Lu, “Detection of Bruises on Apples Using Near-Infrared Hyperspectral Imaging”, American Society of Agricultural Engineers (2003), 0001-2351

[14] B. M. Nicolai, E. Lotze, A. Peirs, N. Scheerlinck, K. Theron, “Non-descrutive measurement of bitter pit in apple fruit using NIR hyperspectral imaging”, Postharvest Biology and Technology 40 (2006), 0925-5214

[15] A. Awate, D. Deshmankar, G. Amrutkar, U. Bagul, S. Sonavane, “Fruit Disease Detection using Color, Texture Analysis and ANN”, IEEE 2015, 978-1-4673-7910-6/15

Ambrosia artemisiifolia allelochemicals and relationship to pollen allergy with air

V.J. Vojnich, A. Hüvely, J. Pető, E. Pölös

Pallasz Athéné University, Mészöly Gyula Square 1-3, 6000, Kecskemét, vojnich.viktor@kfk.kefo.hu

Abstract

Common ragweed (*Ambrosia artemisiifolia*) has become the most widespread weed in Hungary. It causes a significant economic damage, and it causes pollen allergy affecting 20% of the country's population. Therefore its reduction has become a major task. An environmental-friendly method has been developed for its destruction by bioherbicids. This bioherbicide contains allelochemical retardants. Allelochemicals are active chemical inhibition ingredients between plants (allelopathy). This method was applied in the urban areas in Kecskemét, Hungary.

Keywords: Ambrosia artemisiifolia, allelochemical, pollen allergy, air pollution, Kecskemét

1. INTRODUCTION

Common ragweed originates from North America. The temperate zone is its home. It appeared in Hungary in the 1920s appeared, and until the 1940s it was only found in South Transdanubia. After 1945, it spreads rapidly, especially along roadsides and railway embankments. Aggressive, extremely allergenic weed, since the average individual are capable of producing up to 8 billion pollen grain during 2-3 months. Hungary is considered to be Europe's most ragweed infected country. About 20-25% of the country's total population is suffering from pollen allergy of ragweed [1].

Despite strict regulatory measures against it, and grants for its elimination, ecological, biological and technological research is being done in Hungary its importance and area has not decreased. The ecological and human health problems caused by *Ambrosia artemisiifolia* are well documented and data are available from many years [2].

It's widespredness can be traced back to several reasons like it's biological characteristics (e.g. high adaptability, intensive regeneration, effective reproductive strategy, allelopathy, etc.), or technological mistakes, the fragmentation of crop fields, soil factors like soil acidification, improper fertilization, and climate change [3].

Methods for the control of common ragweed are difficult to improve, as there are still uncharted areas of the research of its biological distinctiveness. Since the Indian tribes used it as medicinal plant in its original habitat (its tea is used for local bleedings and gastric diseases, the leaves are used externally on inflamed wounds) it is extensively studied now as a medicinal plant too. In Hungary the plant's judgment is just not as simple as that. The regulatory board opinion is that it is an aggressive and noxious weed, which must be eradicated, but others think it is a useful medicinal plant with soil protecting capabilities.

2. METHODS AND MATERIALS USED FOR RESEARCH

Around 200 hectares of public land has to be weed controlled in Kecskemét according to the 2014 data. 20-30% of this area is infected by ragweed (Fig. 1.) [4].

Fig. 1. Common ragweed

The Aerobiological Network of the National Public Health Service was created in 1992, and was expanded continuously with three more stations. There are 19 monitoring stations (in Pest - OKI, Budapest, Pécs, Debrecen, Győr, Miskolc, Szekszárd, Zalaegerszeg, Békéscsaba, Kecskemét, Szolnok, Nyíregyháza, Veszprém, Salgótarján, Eger, Mosdós, Szeged, Szombathely, Tatabanya), which collect, analyze and evaluate data concerning atmospheric allergens. The employees the Aerobiological Network monitor the atmospheric pollen and spore concentration of 32 species and 3 funguses [5].

Pollen traps are arranged in these stations which suck the air through the reverse wind direction opening. The air particles then stick on the film (2 cm wide tape) attached to a drum in the trap that is smeared with vaseline. Both pollens and mould spores could adhere. The drum rotation speed is 2 mm / hour, so it is able to do one complete rotation in 7 days that is capable of capturing pollens seven day. The pollen traps are placed at least 15 meters high on top of the buildings so that a wall or other surface does not shield the wind conditions. Pollens, adhering on the ribbon of pollen traps, are mailed weekly to the National Environmental Health Lab of the National Public Health Institute, where microscopes help identify and count the various plants pollen (Fig. 2.) [5].

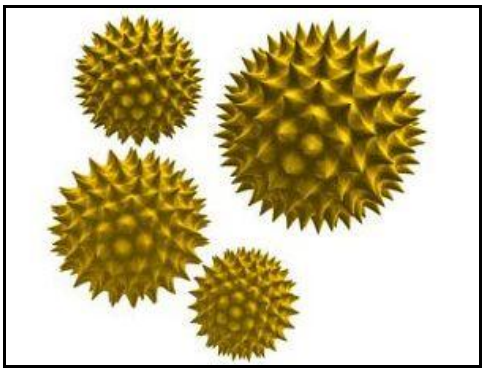

Figure 2. Pollen of common ragweed

This network has been providing statistical information since 1996 about 32 regularly monitored atmospheric allergens including ragweed. The Aerobiological Network of the National Public Health Service operates pollen traps in Kecskemét, Békéscsaba and Szeged in the Southern Plains region. From these traps, sampling drums are sent to the Aerobiological Network on a weekly basis. As the National Public Health Service has no jurisdiction in matters relating to official ragweed control, local governments should work with the sub regional institutions to ensure that they are able to accomplish their programs. For this reason, the National Public Health Service made an agreement with, Kecskemét - Kunszentmiklósi Lajosmizse small regional municipalities, under which they carry out ragweed control related tasks [6].

The weed survey and weed control trials took place in the area in front of Kecskemét Bolyai High School. The test site area is 600 m^2. The weed survey took place on 15 July 2015 before the flowering period of ragweed using Braun-Blanquet's estimation method. A-D values were

taken into account (Annex 2), which estimate the analytical marks of the site during recordings. The A-D levels can be determined with a five-point ordinal scale. Abundance (A) and density (D) are suitable to characterization of species occurring in the sampling site.

At that time, ragweed was in a 15-leaf phenological stage and had an average height of 20 cm. The weed control experiment was directed mainly against *Ambrosia artemisiifolia*. Disinfestations' was carried out in a biologic way. A bioherbicide has been used which contains biological agent (in this case, herbal medication). This effect of the bioherbicide is based on that it contains allelochemicals that inhibit growth, development and germination. The bioherbicide was sprayed over by knapsack sprayer.

3. RESULTS AND ACHIEVEMENTS

The experiments fields were occurring in plants shown in Table 1.

Table 1. Plant list

Plant name	Coated (%)	A-D value
Ambrosia artemisiifolia	30	3
Lactuca serriola	20	2
Conyza canadensis	10	1-2
Chenopodium album	10	1-2
Cynodon dactylon	5	1
Melandrium album	5	1
Tribulus terrestris	5	1

The values of sanitary limits of air contamination were shown in Table 2.

Table 2. Sanitary limits of air contamination

Air contamination	**Sanitary imit ($\mu g/m^3$)**
ozone (O_3)	120
particulate dust (PM_{10})	50
sulphur-dioxide (SO2)	250
nitrogen-dioxide (NO_2)	100
carbon-monoxide (CO)	10.000

We were measured the common ragweed concentration period between August 8th and September 19th 2015 (Fig. 3. and Fig. 4.).

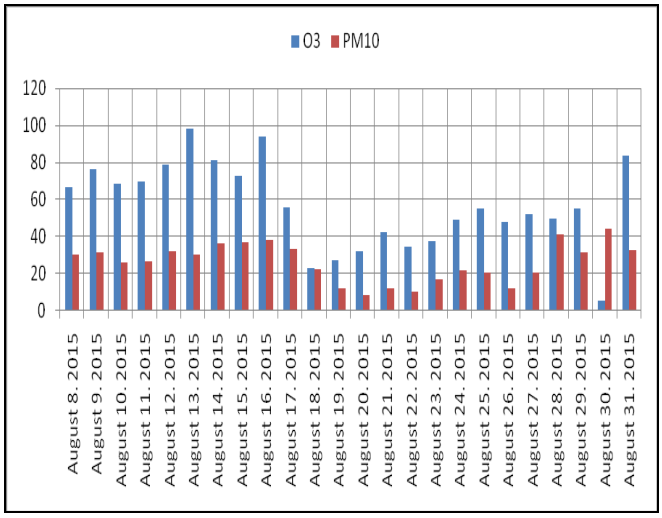

Fig. 3. Concentrations of ragweed pollen in August 2015

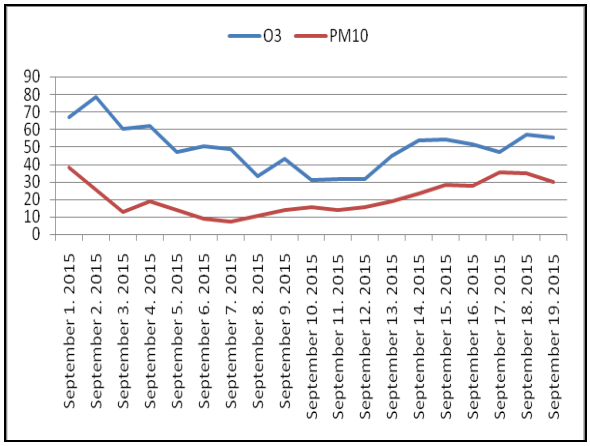

Fig. 4. Concentrations of ragweed pollen in September 2015

4. CONCLUSIONS

Common ragweed (*Ambrosia artemisiifolia*) has become the most widespread weed in Hungary. It causes a significant economic damage, and it causes pollen allergy affecting 20% of the country's population. Therefore its reduction has become a major task. An environmental-friendly method has been developed for its destruction by bioherbicides. This bioherbicid contains allochemical retardants. Allelochemicals are active chemical inhibition ingredients between plants (allelopathy). This method has been applied in the urban areas in the city of Kecskemét, Hungary.

During the high (31-100 parts/m^3) and very high (101- parts/m^3) concentrations of ragweed pollen (period between August 8th 2015 and September 19th 2015), the ozone concentration in the air exceeded health limit (120 mg/m^3) on seven occasions, which significantly worsened the symptoms of pollen allergy patients. One particular group of starting pollutants is the nitrogen oxides, originating from vehicles exhaust emissions. From these nitrogen-oxides, with the effect of solar radiation, ozone (O_3) arises [8].

Particulate (**PM_{10}**) concentrations during the high and very high ragweed pollen production times (from August 08. till September 19.2015.) exceeded the health limit (**50 µg/m^3**) on thirteen occasions, which is very dangerous, since it is potentially harmful even in the lowest concentrations.

The main sources of particulate are the exhaust gases and coal burning. These have an effect of increasing the rate of respiratory diseases (for example asthma and chronic bronchitis diseases), including pollen allergy as well [8].

In 2015 at the Pulmonary Care Institute in Kecskemét, almost 80% (3220 people) of the 4033 patients registered with pollen allergy produced allergic symptoms for ragweed pollen as well. Compared to 2014, the number of registered pollen allergy patients increased by 222.

Common causes of the high production of ragweed pollen are (among others) the steady increase of CO_2 in the atmosphere - and global warming.

The examinations of researchers in Vienna confirmed that high concentration of ozone in the air increases the plants' (such as ragweed) allergen content as well. The main reason for this is that high proportion of ozone charged species' protein essence strongly reacts with immunoglobulin-E antibodies, which play a significant role in the formation of the allergy. Nitrogen oxides (**NO_x**) destroy the exterior protective covering of ragweed pollens, therefore resulting the irritate effect in respiratory tracts [7].

5. ACKNOWLEDGEMENTS

This work was supported by the Kecskemét College, Faculty of Horticulture in Kecskemét. Thanks for Evelin Fekete for common ragweed measurements.

6. REFERENCES

[1] Gy. Kröel-Dulay, A. Csecserits, K. Szitár, E. Molnár, R. Szabó, Z. Botta-Dukát, A parlagfű mint egészséget veszélyeztető özöngyom elterjedésének ökológiai vonatkozásai. Magyar Tudomány, 172(6) p.658. (2011).

[2] L. Szentey, Á. Tóth, I. Dancza, Közös érdekünk, a parlagfűmentes Magyarország. Növény- és Talajvédelmi Központi Szolgálat, pp.3-27. (2004).

[3] R. Novák, A parlagfű és egyéb allergén gyomnövények bemutatása. NÉBIH NTAI, p. 6. (2013).

[4] http://keol.hu/kecskemet/bombahir-kecskemeti-kutatas-menti-meg-a-vilagot-a-parlagfutol, last access 03/11/2015

[5] http://www.webbeteg.hu/cikkek/allergia/16236/igy-keszul-a-pollenjelentes, last access 18/02/2016

[6] www.csmkh.hu/beszamolok/item/download/2623, last access 18/02/2016

[7] http://www.egeszsegkalauz.hu/allergias-betegsegek/az-ozon-es-az-allergiakelto-hatas-mit-varhatunk, last access 14/03/2016

[8] http://www.muszeroldal.hu/assistance/legszennyezo_anyagok_hatasa.pdf, last access 18/06/2005

Weed control of potato with herbicide containing the active substance metribuzin

V.J. Vojnich, J. Pető, A. Hüvely, E. Pölös, A. Palkovics, J. Ágoston

Pallasz Athéné University, Mészöly Gyula Square 1-3, 6000, Kecskemét, Hungary
vojnich.viktor@kfk.kefo.hu

Abstract

The potato (*Solanum tuberosum*) is a major food in Europe. In our experiment we studied the Balatoni rózsa cultivar. This type is a high-quality potato and has high resistance of Potato virus Y (PVY), Potato virus A (PVA), Potato virus X (PVX) and Potato leaf roll virus (PLRV). The cultivar Balatoni rózsa has some less desirable qualities, for example because the sparse foliage the sand gets hot and burns the base of the plant, causing the death of the shoot. During the experiment, the active substance metribuzin herbicide was employed.

Keywords: Plant protection, Potato (*Solanum tuberosum*), Balatoni rózsa, herbicide, Sencor 600 SC

1. INTRODUCTION

Potato originates from Middle- and South America, from high altitude (mountain) regions, like Mexico, Chile, Peru and Bolivia [1]. It arrived to Europe in the 17th century as an ornamental plant. The tuber became a foodstuff at the end of 17th and the beginning of 18th century, after this it spread quickly. It arrived to Hungary about a half century later, than in Western Europe, and became a crop later [2].

Potato is produced on 23 000 hectare in Hungary. In May, June and July we do not have enough indigenous potatoes for the market, so yields are significantly lesser than the ecologically capabilities of the country. With proper irrigation 45 t/ha yield can be achieved compared to the 20-25 t/ha average [3].

The magnitude of the tuber yield is defined by the dry weight produced during the growing season and the growth type of the variety. There are two main growth types: 1. short growing season with early and fast tuber growth with medium canopy and high harvest index (dry weight of tuber divided by total produced dry weight) with moderate yield.; 2. long growing season with lush foliage, later tuber set, but because of these a larger yield.

For a large crop a large canopy a good water and nutrient availability and optimal (not too high) temperatures are necessary. The optimum of photosynthesis is 20-25 °C daytime and 10-12 °C at night, the optimal daily average is 15-19 °C. Under favorable temperatures the respiration loss is 20-25%, but can be remarkably higher under high temperatures. The fresh yield potential is 100 t/ha [4, 5].

Traits of Balatoni rózsa cultivar: Hungarian national registration: 2007; Parentage: 87.3143 x Kuroda; Crop type: early; Tuber traits: Regular, oval shape, dark pinkish-red skin and eyes with a yellow tuber flesh color, with shallow eye depth. Dry matter content: medium (19-20%) Foliage: with strong stems, matte, green leaves. Inflorescence: Medium filled, soft violet; Cooking type: B, fairly firm, not floury. General utilization, mainly for boiled with good to excellent taste;

Growing and storage specifications: High yield potential, 8-10 tubers per plant. Early maturation, but with long dormancy, with good storage ability. Stress tolerance and shape keeping is excellent. Recommended for forcing, open field cultivation in foil and summer planted potato cultivation. Resistance: Very highly resistant (immune) to Potato viruses Y, X, A. Has a high field resistance against PLRV. Has a medium susceptibility for canopy infection of *Phytophthora infestans*. Resistant to patotype 1 of *Synchytrium endobioticum*, common scab, and *Globodera rostochiensis* race 1 and 4 [6].

2. METHODS AND MATERIALS USED FOR RESEARCH

The trail was carried out in Nyírbátor (Szabolcs-Szatmár-Bereg county) on an open field. The fore crop was watermelon with high infestation of *Echinochloa crus-galli* and *Ambrosia artemisiifolia*. The planting material is 3rd generation of certified Balatoni rózsa cultivar, hand graded, and planting size tubers. It is known, that this cultivar is sensitive to the active ingredient metribuzin, but the sensitivity to different doses were not investigated. On the trial field we used Sencor 600 SC, which has metribuzin as active ingredient [7]. The liquid herbicide is registered for potato, tomato, soybean and asparagus crops.

Characterization of Sencor 600 SC herbicide: Active ingredient: 600 g/l metribuzin; Distribution category in Hungary: II. Packing: 1 liter, 5 liter; Dose: 0.55-0.9 l/ha, 250-300 liter spraying volume. For metribuzin sensitive crops use 0.8 l/ha as pre-emergent treatment, for post emergent treatment till 15-20 cm plant height use 0.35 ml/ha [8].

It is necessary to present in details assumptions of study to such an extent manner that a reader could repeat that work if he/she was going to confirm achieved results. This information should be given in as short as possible version.

Sencor 600 SC has a very good efficiency for most dicot and monocot weeds, has a wide range of efficiency in killing weeds, and is selective. Sencor is also effective against hard-to-kill weeds like: *Abutilon theophrasti, Amaranthaceae, Ambrosia artemisiifolia, Atriplex spp., Chenopodium album, Datura stramonium, Stellaria media, Helianthus annuus, Matricaria chamomilla, Sinapis arvensis, Portulaca oleracea, Xanthium spinosum, Veroniceae, Echinochloa crus-galli, Digitaria sanguinalis*.

Biological effectiveness: Sencor 600 SC's active ingredient, metribuzin, is taken up by weeds through roots and foliage. It is blocking the photosynthesis. The symptoms manifest early, the growth stops, the leaves turn yellow, and then they die.

The ridges were made on 24th of April 2015; the planting took place on the 4th of May. The trial had 4 treatments in 4 repetitions; the trial had a randomized complete block arrangement (Figure 1.).

Fig.1. The potato grew in open field.

The treatments are as follows: 1. untreated control, 2. 0.3 l/ha, 3. 0.6 l/ha, 4. 0.9 l/ha Sencor 600 SC. A plot had a total area of 10 m^2; the whole trial had a total area of 160 m^2. The statistical analysis was preformed with SPSS v19 software [9]. The mean differences were regarded as significant at the 0.05 level.

3. RESULTS AND ACHIEVEMENTS

The trial was harvested on 11th of November 2015. On the 1st Figure we can see the weight results of the trial in kg per plot.

We measured the control and three treatments area. The minimum and maximum mass can be found in Table 1. The maximum weight was found in the 0.6 l/ha Sencor 600 SC treatment (number 3), the minimum was among the control and 0.9 l/ha Sencor 600 SC treatment (number 4).

Table 1. Tukey-HSD test of food potato (Solanum tuberosum). Values of the three treatments were measured in 2015 (Parameter: potato weight, kg).

Treatments	N	Mean (kg/ha)	Std. Dev.	Std. Error	Mini-mum (kg)	Maxi-mum (kg)
1. control	4	7,650	2.475	1.237	5.0	10.0
2. 0.3 l/ha Sencor 600 SC	4	13,850	0.700	0.350	13.0	14.6
3. 0.6 l/ha Sencor 600 SC	4	13,100	2.706	1.353	11.0	17.0
4. 0.9 l/ha Sencor 600 SC	4	8,850	2.516	1.258	6.2	11.0

The number 2 and number 3 treatments were significant (Table 2), but the number 4 was not.

Table 2. Tukey-HSD test of food potato (Solanum tuberosum). Values of the three treatments were measured in 2015 (Parameter: potato weight, kg).
**The mean difference is significant at the 0.05 level.*
n.s. = not significant

Treatment (A)	Treatment (B)	Average difference between treatments (A-B)	Std. Dev.	Signi-ficance
1. control	2. 0.3 l/ha Sencor 600 SC	-6.2000*	1.591	0.010
	3. 0.6 l/ha Sencor 600 SC	-5.4500*	1.591	0.023
	4. 0.9 l/ha Sencor 600 SC	-1.2000 n.s.	1.591	0.873

The average mass homogeneity is shown in Table 3.

Table 3. Tukey-HSD test of food potato (Solanum tuberosum). Means for groups in homogeneous subsets are displayed.
a. Uses Harmonic Mean Sample Size = 4.000

Treatments		Subset for alpha = 0.05			
		N	1	2	3
Tukey HSD[a]	Control	4	7,650		
	0.9 l/ha Sencor 600 SC	4	8,850	8,850	
	0.6 l/ha Sencor 600 SC	4		13,100	13,100
	0.3 l/ha Sencor 600 SC	4			13,850
	Significant		0.873	0.083	0.964

The total weight of potato tubers are shown in Table 4. The highest was treatment 3 (0.6 l/ha Sencor 600 SC), while the lowest were treatment 4 and the untreated control.

Table 4. Tukey-HSD test of total potato (Solanum tuberosum). Values of the three treatments were measured in 2015 (Parameter: potato weight).

Treatments	N	Mean (kg/ha)	Std. Dev.	Std. Error	Mini-mum (kg)	Maxi-mum (kg)
1. control	4	18,050	2.821	1.410	14.4	21.0
2. 0.3 l/ha Sencor 600 SC	4	21,750	2.235	1.117	19.8	24.0
3. 0.6 l/ha Sencor 600 SC	4	21,200	2.898	1.449	18.4	25.0
4. 0.9 l/ha Sencor 600 SC	4	19,250	2.886	1.443	15.4	22.0

The significances levels for the whole trial are shown in Table 5. None of the treatments were significant compared to the untreated control.

Table 5. Tukey-HSD test of total potato (Solanum tuberosum). Values of the three treatments were measured in 2015 (Parameter: potato weight).
**The mean difference is significant at the 0.05 level.*
n.s. = not significant

Treatment (A)	Treatment (B)	Average difference between treatments (A-B)	Std. Dev.	Signi-ficance
1. control	2. 0.3 l/ha Sencor 600 SC	-3.7000 n.s.	1.926	0.270
	3. 0.6 l/ha Sencor 600 SC	-3.1500 n.s.	1.926	0.397
	4. 0.9 l/ha Sencor 600 SC	-1.2000 n.s.	1.926	0.923

The detailed results of the harvest (total, food, little) are shown in Table 6.

Table 6. Values of control and three treatments of potato were measured in 2015. (Parameter: potato weight, kg).

Treatments		Repetitions				Total
1. control		I.	II.	III.	IV.	
	food	9.5	10	5	6.1	30.6
	little	4.9	9.3	16	11.4	41.6
	total	14.4	19.3	21	17.5	**72.2**
2. 0.3 l/ha Sencor 600 SC		I.	II.	III.	IV.	
	food	13	14.6	14.2	13.6	55.4
	little	6.8	8.2	10.2	6.4	31.6
	total	19.8	22.8	24.4	20	**87.0**
3. 0.6 l/ha Sencor 600 SC		I.	II.	III.	IV.	
	food	11	11.6	12.8	17	52.4
	little	8.6	6.8	9	8	32.4
	total	19.6	18.4	21.8	25	**84.8**
4. 0.9 l/ha Sencor 600 SC		I.	II.	III.	IV.	
	food	11	7.2	6.2	11	35.4
	little	4.4	11.6	11.8	9.8	41.6
	total	15.4	18.8	22	20.8	**77.0**
Total		**69.2**	**79.3**	**89.2**	**83.3**	321

The weight differences between treatments are shown on Figure 2.

Fig.2. The control and the three treatments potato (2015).

4. CONCLUSIONS

On Figure 2 we can see, that different treatments of the herbicide containing metribuzin as active ingredient on potato cultivar Balatoni rózsa had differences on the crop. The dose of Sencor 600 SC is inversely

proportional to the number of tubers produced. The higher the dose the smaller the number and the size of potatoes harvested. This is why the crop of treatment 4 (0.9 l/ha Sencor 600 SC) and the untreated was nearly the same.

Treatment 3 (0.6 l/ha Sencor 600 SC) has the highest yield. This could happen, because the herbicide was less toxic to the potato cultivar Balatoni rózsa, but was still effective against some hard-to-kill weeds in the early stage of growth. Both the edible size (52.4 kg), and the total (84.8 kg) potato production was the second highest on the treatment with 0.6 l/ha Sencor 600 SC.

Treatment 2 (0.3 l/ha Sencor 600 SC) had the highest weight of edible (55.4 kg) and total (87.0 kg) tubers.

The treatment with 0.9 l/ha Sencor 600 SC (treatment 4) had also high tuber production, and the herbicide was most effective here, so the plot was weed free longest here. So the potato could grow in the poisoned environment longer.

The plots untreated were the weediest, and the cleanest were treatment 4. As we increased the dose from 0.3-0.6-0.9 l/ha so as the weed covered area got smaller.

5. REFERENCES

[1] J. Antal, Plant growing 2. Root and tuber crops. Mezőgazda Kiadó, Budapest, (2005).

[2] Gy. Czimber, Plant taxonomy. Agriculture botany, Mezőgazda Kiadó, Budapest, (2001), pp. 325-329.

[3] A. Kosztolányi, Situation of domestic potato growing in Hungary. Agrofórum, (2007a), 18(10):52-54.

[4] J. Kruppa, The effects of weather on potatoes and irrigation significance. Agrofórum, (2007b), 18(10):60.

[5] S. Hoffmann, Industrial and forage crop cultivation. TÁMOP-4.1.2-08/1/A-2009-0010 project, Development of curricula. (2011).

[6] Potato Research Centre, Pannon University, Agricultural Science Centre. http://www.burgonyakutatas.hu, last access 13/06/2016

[7] Z. Ocskó, Plant protection products, crop-raising materials I., Ministry of Agriculture, Budapest, (2015).

[8] NÉBIH, Sencor herbicide spray. Budapest, (2014).

[9] L. Huzsvai, Biometric methods in SPSS. Textbook. University of Debrecen, Faculty of Agriculture, Debrecen, (2004), pp. 65-66.

Economic evaluation of different technologies of corn growing in Hungary

Á. Ferencz, Zs. Deák, V.J. Vojnich

Pallasz Athéné University, Mészöly Gyula Square 1-3, 6000, Kecskemét, Hungary
vojnich.viktor@kfk.kefo.hu

Abstract

In our study we examined the crop production of three agricultural enterprises that apply various fertilizing technologies through describing the innovative crop production technology and the operational steps. The first company provides the appropriate nutrients by fertilizing; the second, a private enterprise, delivers manure under the crops every three years, applying fertilizer only during the years in between. The third, a family farm, uses a fertilization technique where nutritional requirements are provided by bacteria and organic bio-manure. In our work we analyzed the costs, revenues, income and efficiency indicators of the production technologies. The companies examined employ the most advanced production technology thus the results of our analysis can provide important answers for corn-farmers. The corn-growing businesses rely heavily on state aid, therefore when examining the effectiveness of these enterprises this should also be taken into account. The economic evaluation of maize production in addition is supported by fundamental profitability indicators. With the right bacteria and bacterial-manure soil conditions can be maintained and improved which will protect the plants during years of drought. Based on several years of data, we have found that using bacterial-manure production technology better results can be achieved than with traditional production methods. In the long-term bacterial-fertilization produces the best yields with the best economic results.

Keywords: economic evaluation, best practice, environmental protection

1. INTRODUCTION

The elimination of the rotation and drying out of land is an important issue. During soil rotation the soil is exposed to several stress effects such as obstruction of soil ventilation and moisture movement caused by the plow [1]. The nutrient supply should be complemented by bacterial fertilizers and soil and a plant conditioning products [2,3]. This material is produced completely organically, in particular, containing animal and vegetable oils, herbal extracts, trace elements and essences. It generally also contains some algae [4]. Bacterial manures are easily digestible carbon-hydrate resources for useful soil micro-organisms [5]. As a result of treatment bacteria native to our area rapidly proliferate in the soil to assist and accelerate favorable demolition processes [6].

A significant accumulation and activity of useful bacteria brings about faster organic material degradation and formation of organic colloids which results in the improvement of soil fertility. The application of an ensemble of live bacterial strains bred for specific purposes enhances soil life, increases the set of nutrients that can be utilized, supports better absorption of fertilizers and improves soil structure thus increasing its fertility and strength. It can be freely stated that organic manure would be the most appropriate fertilization technique [7]. Its availability, however, is limited because the appropriate amount cannot always be provided. The use of bacterial manure is an important tool for replacement of fertilization. However, their impact must be investigated not only technically

but also economically [8]. This study provides answers to these questions.

2. METHODS AND MATERIALS USED FOR RESEARCH

2.1. Production technology of the enterprises

The corporation owns a large site and several agricultural machines. In 2015, they have conducted plant production on 400 hectares. The private enterprise produces corn on an area of 20 acres out of 60-acre farm. The farm uses organic fertilizers every 3 years and fertilizers in the interim years. The family farm grew maize on 48 acres of its 200 acres of land in 2015. They have been managing the farm without chemical fertilizers for five years. They utilize bacterial fertilizers, bacterial suspension and algae to improve soil conditions.

2.2. Methods

2.2.1. Cost of production technology

The soil work in maize production has been implemented in the same way at all three of the enterprises. While two companies begin with plowing, the third omits plowing using easing operation instead resulting in lower costs. The cost of working the soil consists of fuel charges, trucker wages and overhead burdens and amortization. A soil job, calculated with a consumption of 15 liters per hectare, comes to 20 Euros in material costs. Worker's salary is set by the businesses 5 Euro per hectare while depreciation was uniformly determined as 10 Euros. The costs of the application of different fertilization are shown in Table 1.

Table 1. The costs of nutrient application per hectare of maize production (2015)

Operation	Labor cost	Fuel cost	Amorti-zation	Total
Organic Fertilization	23.5 €	0 €	0 €	23.5 €
Nitrosol application	1.5 €	7 €	3.5 €	12 €
Fertilizing	2.5 €	8.5 €	4.5 €	15.5 €

The cost differences that occur are already readily observable as regardless of the amounts spent these differ considerably for the individual technology variants. For all three of the firm's seedbed preparation and planting, plant protection, row cultivation could be calculated almost in the same manner (Table 2.).

Table 2. The operational costs of maize production per hectare (2015)

Operation	Labor cost	Fuel cost	Amorti-zation	Total
Seedbed preparation	2 €	7 €	4 €	13 €
Sowing	3 €	10 €	5 €	18 €
Plant protection	2 €	9.5 €	4.5 €	16 €
Tillage	2 €	10 €	5 €	17 €

Harvesting costs are different in the three experimental enterprises, since in two of the farms corn harvesting is outsourced while the corporation has its own harvesting machines resulting in less expenditure (Table 3.).

Table 3. The costs harvesting per hectare (2015)

Operation	Labor cost	Fuel cost	Amorti-zation	Total
Harvesting through outsourcing				67 €
Harvesting w/ own combine	3 €	10 €	5 €	18 €

2.2.2. Profitability of corn growing

In determining revenue at all three businesses yield per year was multiplied by the average selling price. Both the yields and the purchase prices differ significantly from year to year. The results from technologies used at the companies were studied in two ways. In the traditional case expenses incurred during the production were extracted from revenues. In the other case income included area based subsidies, and in the case of the enterprise that used bacterial fertilizers the value of the so-called Carbon-

subsidies was also included. Carbon-subsidy is granted for those that are willing to use technology with algae treatment and without soil tillage.

3. RESULTS AND ACHIEVEMENTS

3.1. Costs of corn growing

Cost of corn growing for the corporation is presented in Table 4. while it's structure can be seen in Figure 1.

Table 4. Cost of maize growing per hectare, Corporation (2015)

Operation	Labor cost	Fuel cost	Amorti-zation	Total
All machine work cost	24 €	110 €	50 €	184 €
Material Cost				
Seeds	160 €		Total: 450 €/ha	
Pesticides	143 €			
Fertilizers	147 €			
Total cost per ha: 634 €				

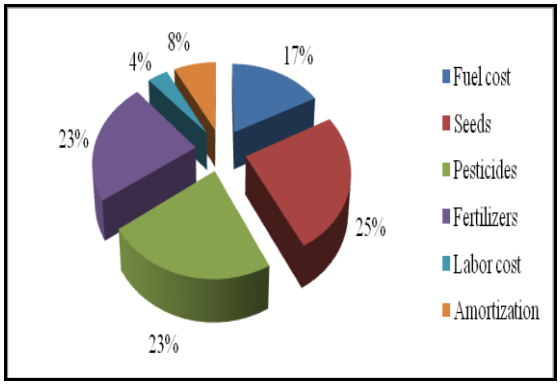

Fig. 1. Cost structure of maize production, Corporation

Cost of corn growing for the private enterprise is presented in Table 5. while it's structure can be seen in Figure 2.

Table 5. Cost of maize growing per hectare, Private Enterprise (2015)

Operation	Labor cost	Fuel cost	Amorti-zation	Total
All machine work cost	85 €	80 €	37 €	197 €
Material Costs				
Seeds	167 €		Total: 408 €/ha	
Pesticides	101 €			
Fertilizers	140 €			
Total cost per ha: 605 €				

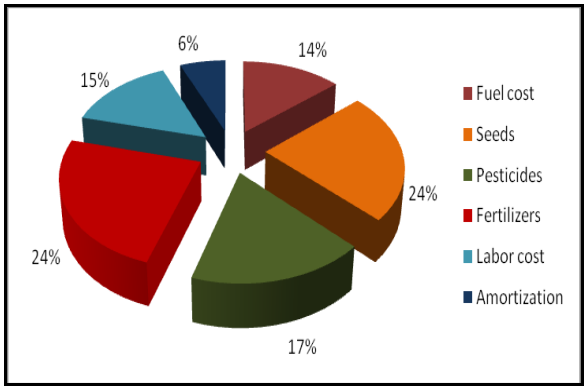

Fig. 2. Cost structure of maize production, Private Enterprise

Cost of corn growing for the family farm is presented in Table 6. while it's structure can be seen in Figure 3.

Table 6. Cost of maize growing per hectare, Family Farm (2015)

Operation	Labor cost	Fuel cost	Amorti-zation	Total:
All machine work cost	84.5 €	77.5 €	35 €	197 €
Material Costs				
Seeds	154 €		Total: 463 €/ha	
Pesticides	75 €			
Fertilizers	140 €			
Nitrosol	23.5 €			
Amalgerol	23.5 €			
Alga	23.5 €			
Phylazonit	23.5 €			
Total cost per ha: 660 €				

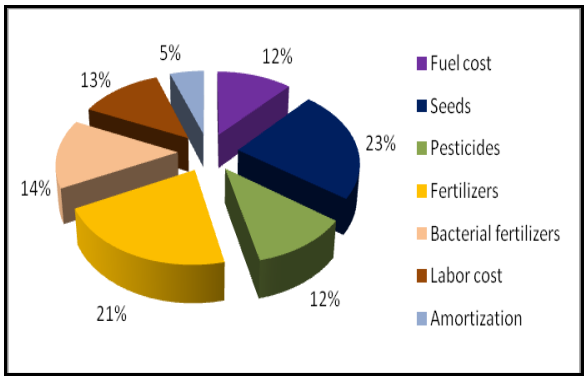

Fig. 3. Cost structure of maize production, Family Farm

3.2. Revenues and income of corn growing

Table 7. presents average yield, selling price and revenues achieved for the various producers.

Table 7. Revenues (2015)

Producer	Avg. Yield	Selling price	Revenue/ Ha
Corporation	6.53 t	153.5 €/t	1001 €
Private Enterprise	6.01 t	153.5 €/t	922 €
Family Farm	7.01 t	153.5 €/t	1075 €

It can be concluded that the use of bacterial manure yields a surplus of 0.5-1 tons which is reflected in sales.

Table 8. and Figure 4. illustrate the differences in businesses' income with and without subsidies. The best income is achieved by the family farm, significantly outperforming the other two companies. The sole proprietor with less effort realized less profit as the active ingredients in organic fertilizers applied the first year were used up and could not be made up by fertilization alone.

Table 8. Income per hectare (2015)

Producer	Revenue + subsidies	Total Cost	Income	Income with subsidy
Corporation	1230 €	634 €	367 €	596 €
Private Enterprise	1150 €	605 €	317 €	574 €
Family Farm	1300 €	660 €	415 €	640 €
Family Farm w/ carbon subsidy	1350 €	660 €	465 €	690 €

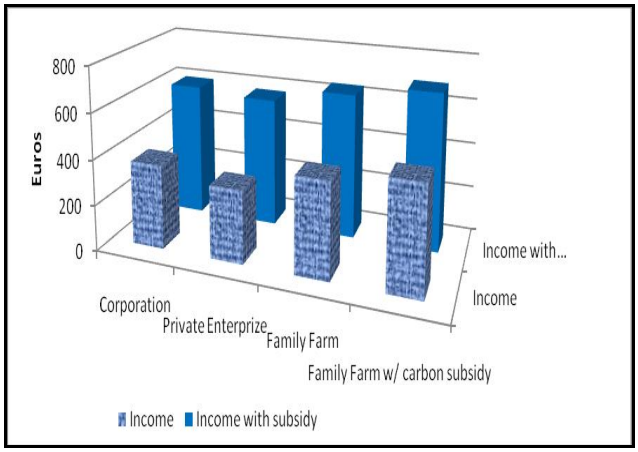

Fig. 4. Income per hectare (2015)

Table 9. shows the profitability of maize cultivation with and without subsidies.

Table 9. Profitability of maize production

Producer	Profitability w/o subsidy	Profitability w/ subsidy	Profitability w/ Carbon subsidy
Corporation	58 %	94 %	
Private Enterprise	53 %	90 %	
Family Farm	63 %	96 %	104 %

4. CONCLUSIONS

By abandoning chemical fertilizers we can protect and rest our soil. With the right bacteria and bacterial fertilizers soil conditions can be maintained and improved which means that in drought years our plants are protected from a biotic stress. Research was carried out in the selected companies for three years as data from one year is not sufficient to draw reliable conclusions. Through examination of the three years data it can be ascertained in an exact manner that favorable results can be achieved with bacterial fertilizer production technology versus traditional cultivation.

Beneficial effects materialize in lower production costs, higher average yield and thus higher income levels which carbon support can make even more productive [9]. It can be concluded that subsidies significantly improve profitability of Hungarian corn production. Carbon subsidy improved profitability by 8% which is a considerable achievement that even supporters of traditional production should contemplate.

5. REFERENCES

[1] M. Birkás, Környezetkímélő és energiatakarékos talajművelés. Akaprint Kiadó, Budapest, (2002).

[2] A. Hüvely, E. Hoyk, J. Pető, I. Cserni, The effects of different NPK nutrients doses of red pepper's yield and vegetative parts in pots. Review on Agriculture and Rural Development 2 (2): pp. 583-586. (2013).

[3] J. Pető, A. Hüvely, E. Pölös, I. Cserni, Leaf macronutrient composition of grapes in south plain hungarian vineyards. Review on Agriculture and Rural Development 3:(1) pp. 250-255. (2014).

[4] S. Balázsy, T. Bartók, Sz. Benedek, B. Bíró, Zs. Keresztes, S. Máté, Á. Szécsi, T. Zászlós, A beforgatott jövő, talajbiológiai és baktériumtrágyázási ismeretek mindenkinek. Imi- Print nyomda, Budapest, (2012).

[5] www.cheminova.hu (2014): Cheminova Magyarország KEuro

[6] www.phylazonit.hu (2012): Phylazonit Tele Élettel

[7] P. Pepó, Tartalékok a kukorica agrotechnikájában. Agrofórum, 23:(47) pp. 5-11. (2012).

[8] I. R. Kőszegi, Young farmers' sustainability perspective in Hungary. Annals of the Polish Association of Agricultural and Agribusiness Economics 16:(5) pp. 119-127. (2014).

[9] I. R. Kőszegi, F. Baglyas, Trade-off analysis in a wine market research in Hungary. Review on Agriculture and Rural Development 2:(1) pp. 120-125. (2013).

Effect of nitrogen on the growth and ingredients of celery

J. Pető, A. Hüvely, V. J. Vojnich, I. Cserni

Department of Horticulture, Faculty of Horticulture and Rural Development, Pallasz Athéné University, Kecskemét, Mészöly Gy. tér 1-3. 6000, peto.judit@kfk.kefo.hu

Abstract

In our experiments we used large (0.30 m^2 surface) flow lysimeter pots in the internal study garden of our faculty, in 2013 and 2014. In our series of experiments celery (Apium graveolens convar. rapaceum) test plants were used Applying six different manure doses in four replications, crop mass and nutrient contents were followed by standard analytical methods. After N_{60}, N_{120}, N_{180} fertilizer treatments tuber weight increased to more than half of the total plant weight (57-58% of total weight). However, there were no statistically significant differences among treatments. The highest yield was reached after manure treatment. . Laboratory tests were made in our laboratory (Soil and Plant Testing Laboratory of Faculty of Horticulture). The analytical tests showed increased N content in the tuber with higher nitrogen fertilizer treatment. Potassium levels tended to decrease however. Changes in the other macro- and microelement (K, Na, Ca, Mg, Zn, Cu, Fe, Mn, B) concentrations were also shown.

Keywords: celery, N fertilizer, manure, crop weight, macro and microelements.

1. INTRODUCTION

One of the relatively poorly studied vegetable plants is celery, though its use is diverse. It occurs in the daily feeding of the population, in fresh or dried form, as a component of soups, seasonings and condiment mixes. Its presence in foods is often not conscious for the consumers. It is worth to pay attention to the cultivation, increase of the nutritional values of ingredients and maintaining of its beneficial properties during preparing technologies of consumption.

During the production of vegetables and other areas of the horticultural production it is becoming increasingly clear that farmers and researchers would take into account the criteria of high crop quality, and beside this at least the maintaining or improving the environmental conditions, as well. In sandy soils, the use of very high doses of nitrogen fertilizer often occurs. Occasional over-watering or large amounts of biomass left on the fields at the end of the growing season may contribute to the increase of leaking water and the undesirable load of the environment.

The celeriac cultivation in our country is mostly done by raising seedlings. In field conditions rooting of celery is difficult, especially if the soil moisture in the first period of the growing season is low. Therefore medium heavy loam soil - with good water-holding capacity - is the most suitable for growing. The quantity and the quality of the crop is effected by the amount of irrigation and the salinity of the soil and the irrigation water as well [1]. Celery was shown very sensitive to nutrient disorders and a wide variety of quality problems that can often be caused by nutrient deficiencies, excesses or imbalances [2].

In our study celery test plants were used in lysimeter type pots filled with loose sandy soils common in our region [3]. Plant growth, nutrient content and the relationships of them were also observed.

2. METHODS AND MATERIALS USED FOR RESEARCH

2.1. Plant growing and treatments

Our nitrogen fertilization experiment was carried out in the research garden of the Faculty of Horticulture and Rural Development. We used large (0.30 m^2 surface) flow lyzimeter pots. Plant pots were filled with sandy soil which is typical in the research garden and our region too. The bottoms of the plant pots were open, and they had a sinkhole and a deflector, to avoid stagnant water.

Our investigation was carried out in the growing season of 2013 and 2014. Seedlings were transplanted in 4-5 leaf stage with 5 plants/pot crop density. We made six N treatments, with four repetitions in every treatment.

Nitrogen fertilizer treatments were used as follows:

1st treatment – Control: normal field growing without any fertilization.

2nd treatment – Cropcare control $N_{60} : P_{60} : K_{120}$, N, P_2O_5, K_2O kg/ha inorganic fertilizer.

3rd treatment – Cropcare $N_{60} : P_{60} : K_{120}$, N, P_2O_5, K_2O kg/ha + 60 kg/ha N fertilizer (two times 30-30 kg/ha in growing season.

4th treatment – Cropcare $N_{60} : P_{60} : K_{120}$, N, P_2O_5, K_2O kg/ha + 120 kg/ha N fertilizer (distributed four times 30-30-30-30 kg/ha in growing season.

5th treatment – Cropcare $N_{60} : P_{60} : K_{120}$, N, P_2O_5, K_2O kg/ha + 180 kg/ha N fertilizer (distributed six times 30-30-30-30-30-30 kg/ha in growing season.

6th treatment – Cropcare $N_{60} : P_{60} : K_{120}$, N, P_2O_5, K_2O kg/ha + barn manure appropriated to 240 kg/ha N fertilizer.

During the growing season plant pots were kept weed free by mechanical methods, drip irrigation method was used according to the needs of the plant. The harvest was made at the end of the growing season, reaching the marketable state of the development of the tubers. Tuber samples were cleaned and washed, and taken to the laboratory.

2.2. Analytical methods and statistics

Analytical testing methods were made in the Soil and Plant Testing Laboratory of Faculty of Horticulture and Rural Development (Pallasz Athéné University, Kecskemét) Standard analytical methods were used. As part of the investigations we measured the amount of wet yield. Celery tubers were shred and dried, than they were homogenized and digested by wet destruction. We determined the total organic amount of nitrogen by Kjeldahl-nitrogen method. Phosphorus, potassium, calcium, magnesium, sodium and microelement (Zn, Cu, Fe, Mn, B) content of the tuber samples were analyzed by optical emission spectrometer (ICP-OES method).

Vitamin C content was measured in fresh tubers after extraction and titration.

Statistically significant differences (SD <5%) and correlation coefficients (Pearson's r value) were estimated in the estimation of the effects of different treatments.

3. RESULTS AND ACHIEVEMENTS

There were no statistically significant differences in total crop mass and tuber crop masses between the levels found in the two consecutive years. Total crop mass/pot levels increased after nitrogen fertilization as shown in Figure 1. Changes seemed to be significant (5%) after treatment 3.

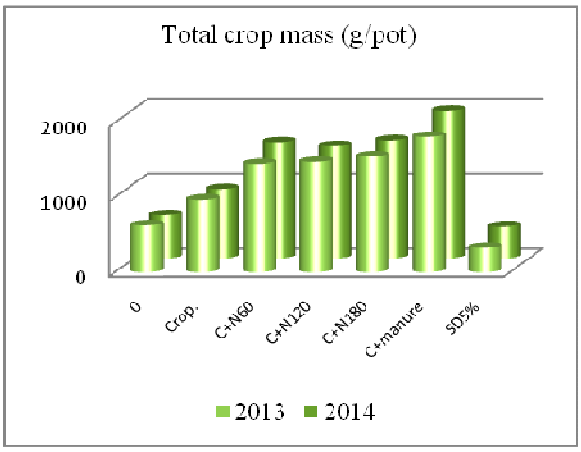

Fig. 1. Changes in total crop mass in pots after N fertilizer treatment 1-6

Changes in tuber mass are shown in Figure 2.

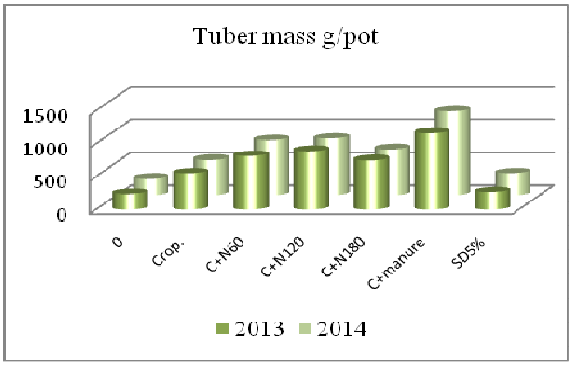

Fig. 2. Changes in tuber mass in pots after N fertilizer treatment 1-6

Best results were achieved after manure treatment. Total crop mass reached 1900 vs. 600 g/pot on average (6th treatment vs.1st treatment). It was the case regarding tuber mass as well; manure significantly increased tuber mass (1220 vs. 240 g/pot, 6th vs.1st treatment).

Nitrogen fertilizer use increased the ratio of tuber to total biomass (Table 1). Without any N fertilizer (absolute control) tuber represented about one third of the biomass. This ratio increased in treatment 2-5 into about 50% on average (changes among various N treatments were not significant); and reached two-thirds ratio after barn manure treatment.

Besides the results of the yield tests it seems very important to determine how the N-fertilizer treatments could affect the changes of the macro and micro elements in tuber. Tuber nitrogen content changed parallel with the applied N fertilizer amount (Table 2.). Phosphorus, magnesium and sodium levels decreased, whereas potassium and calcium concentrations remained constant. Among microelements, copper, manganese and boron levels moderately decreased, whereas iron content increased significantly, especially in the case of manure (r=0.8288, <2%). There was a strong negative correlation between N fertilizer doses and Zn concentration in tuber (r= 0.7534, <5%).

We tested vitamin C content in tuber in each treatment group. The results are shown in Figure 3. Vitamin C levels increased, especially after manure treatment.

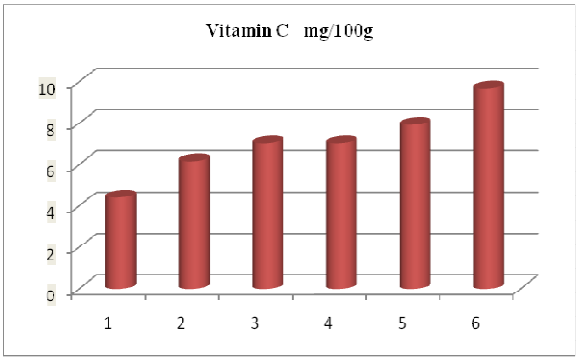

Fig. 3. Changes in vitamin C content in tuber after N fertilizer treatment 1-6

Table 1. Ratio of tuber mass to total biomass (%) after different nitrogen treatments (1-6).

Treatment / Year	1. N_0	2-3-4-5. *Crop.* + N_{0-180}	6. *Crop. + manure* N_{240}
2013	38	56	64
2014	35	55	65

Table 2. Average concentration of the main macro- and microelements in the tuber after treatment 1-6.

		Treatment					
Parameter	*Unit*	1	2	3	4	5	6
N	*m/m %*	1.04	0.94	0.95	1.13	1.34	1.84
P	*m/m %*	0.47	0.41	0.43	0.35	0.33	0.35
K	*m/m %*	0.98	1.59	1.72	1.35	1.25	1.50
Ca	*m/m %*	0.24	0.26	0.26	0.23	0.26	0.22
Mg	*m/m %*	0.13	0.09	0.09	0.11	0.08	0.08
Na	*mg/kg*	0.48	0.22	0.14	0.22	0.26	0.07
Fe	*mg/kg*	25.2	23.5	25.4	33.2	28.4	33.3
Mn	*mg/kg*	23.9	19.3	19.2	21.5	19.6	16.7
Zn	*mg/kg*	19.8	17.0	16.7	17.5	16.7	14.7
Cu	*mg/kg*	7.66	6.88	7.49	6.84	7.78	5.25
B	*mg/kg*	17.5	22.7	23.9	20.0	19.4	18.9
Mo	*mg/kg*	<0.50	<0.50	<0.50	<0.50	<0.50	<0.50

4. CONCLUSIONS

Optimizing of vegetable growing technology including fertilization is important from both economical and environmental points of view [4].

As shown in our study, the results of celery growing in two consecutive years did not differ significantly. We showed that N fertilizer treatments enhanced total crop mass, and tuber N content, which is in accordance with the findings of other studies [5, 6]. However, as a new result, tuber mass seemed to stay independent of the applied N dose (2-5th treatment). The use of starter NPK fertilizer (Cropcare) at the beginning of the growing season in our sandy soil, may contribute to this effect. The phenomenon was probably due to the potassium content of Cropcare.

Tuber mass was the most significantly increased by manure (1220 vs. 240 g/pot). The ratio of tuber weight to total crop mass was the highest after treatment 6, as well (65%).

We showed that tuber nitrogen content increased parallel with increasing N fertilizer amount.

N treatments were in relation with changes of main and micro nutrients. Enhanced amount of N fertilizer increased iron content and decreased concentration of zinc in tuber significantly.

Vitamin C content in tuber proportionally increased with N fertilizer. This may call attention for the more beneficial effects and increasing antioxidant capacity of celery after N treatment [7, 8].

As celeriac is a relatively poorly studied vegetable but widely used in our life, we are on continuing our examinations. Further studies would be made in tuber and green leaves of celery as well, to examine the relationships between nutrients and internal components in various growing technologies.

5. ACKNOWLEDGEMENTS

The authors wish to thank to our colleagues in the testing laboratory for the expert technical assistance.

6. REFERENCES

[1] S. De Pascale; A. Maggio; C. Ruggiero; G. Barbieri. Growth, water relations, and ion content of field-grown celery [Apium graveolens L. var. dulce (Mill.) Pers.] under saline irrigation. Journal of the American Society for Horticultural Science 128(1) (2003). pp.136-143.

[2] Y Li; T. Wang; J. Li; Y. Ao. Effect of phosphorus on celery growth and nutrient uptake under different calcium and magnesium levels in substrate culture. Horticultural Science 37(3) (2010). pp. 99-108.

[3] I. Cserni; A. Kovács; Sné Zana; Bné J. Pető. The migration of elements (N,P,K) in sandy soil III. Alps-Adria Scientific Workshop (2004) pp. 30-34.

[4] A. M. Evers; E. Ketoja; M. Hägg; S. Plaami; U. Häkkinen; R. Pessala. Decreased nitrogen rates and irrigation effect on celery yield and internal quality. Plant Foods for Human Nutrition 51(3) (1997). pp. 173-186.

[5] A. M. Evers. The influence of fertilization and environment on some nutritionally important quality criteria in vegetables – a review of research in the Nordic countries. Agriculture Science of Finland 3 (1994). pp. 177–188.

[6] G. Martignon; D. Casarotti; A. Venezia; F. Malorgio. Nitrate accumulation in celery as affected by growing system and N content in the nutrient solution. International Symposium on New Cultivation Systems in Greenhouse 361 (1993). pp. 583-589.

[7] G. Duthie; F. Campbell; C. Bestwick; S. Stephen; W. Russell. Antioxidant effectiveness of vegetable powders on the lipid and protein oxidative stability of cooked Turkey meat patties: Implications for health. Nutrients 5(4) (2013). pp. 1241-1252.

[8] J. Leclerc; M. L. Miller; E. Joliet; G. Rocquelin. Vitamin and Mineral Contents of Carrot and Celeriac Grown under Mineral or Organic Fertilization. Biology in Agriculture and Horticulture 7 (1991). pp. 339–348.

Familiarity of Honey Products in Slavonski Brod

M. Zetić [a], K. Mirosavljević [b,*], T. Benković-Lačić [b]

[a] graduate of College of Slavonski Brod, Ulica dr. Mile Budaka 1, HR-35000 Slavonski Brod, Croatia, zmatea18@gmail.com

[b] College of Slavonski Brod, Ulica dr. Mile Budaka 1, HR-35000 Slavonski Brod, Croatia, krunoslav.mirosavljevic@gmail.com ; tblacic@vusb.hr

Abstract

Honey is a dense, sweet, viscous, liquid or crystallized product that is produced by collecting nectar from honey plants. After collecting nectar, honeybees deposit nectar in the honeycombs. Honey consists from the sugars (comprising glucose, fructose, sucrose and maltose), proteins, amino acids, enzymes, organic acids, pollen, minerals, vitamins and other substances. There are various types of honey and the most popular types in Croatia are flower honey, acacia honey, chestnut honey, honey from rapeseed, buckwheat honey, meadow honey and so on. A survey conducted in Slavonski Brod (Croatia) found that half the population of Slavonski Brod consume honey and honey products often and they are generally satisfied with the consumption of those products. The most famous type of honey that examinees recognized were the acacia honey and flower honey. Other honey products commonly consumed included liqueurs, propolis and pollen.

Keywords: Biotechnology in agricultural environment; Honey; Honey products; Survey; Slavonski Brod.

1. INTRODUCTION

Honey is a dense, sweet, viscous, liquid or crystallized natural product produced by honeybees. It is produced by collecting pollen of different species in the hives. Honey is used on daily basis for health and food benefits and many types of liqueurs, schnapps, spreads etc. are produced of it. Its medicinal properties make it useful for treatments of colds, flu, healing wounds and other diseases/disorders as well as in prevention of many diseases. It can be consumed in tea, in various sauces or as an independent product. Honey consists mainly from the sugars **(**comprising glucose, fructose, sucrose and maltose**)**, but proteins, amino acids, enzymes, organic acids, pollen, minerals, vitamins and other substances are also significantly present [1].

Bees get their raw materials from natural nectar and honeydew from which they make honey. Nectar is a sweet juice that is produced by nectar glands of honey plants. Nectar attracts bees that pollinate the flowers and each plant species has a specific nectar.

Honeydew is sweet juice excreted by aphids on the tree leaves. The bees have to visit 15 million flowers to create one kilogram of honey. Bees take nectar into honey bladder that is separated from the digestive system. Nectar of honey in the bladder is enriched by ferments for the decomposition of complex sugars into simple sugars. Processed nectar is then delivered into the hive for the further processing and storage in the honeycomb. Finally, honey is produced by reducing the water content of the nectar to 15-20 % in honeycombs [2].

There are various types of honey and the most popular types in Croatia are flower honey, acacia honey, chestnut honey, honey from rapeseed, buckwheat honey, meadow honey and others [3].

There are also various preparations of honey products. The well-known honey products are pollen, propolis, royal jelly, beeswax, creamy honey, various dairy products based on honey with additives and various creams.

Quality control of honey and honey products usually include organoleptic testing, physical, chemical and biological analysis and pollen analysis [4,5,6,7].

The aim of this paper is to show how much the inhabitants of Slavonski Brod (Croatia) consume honey and honey products. The work will show how many residents know about the healing properties of honey, its consumption properties and purposes as well as the ways of its acquisition for common use.

2. METHODS AND MATERIALS USED FOR RESEARCH

The survey (poll) used in preparation of this work included 13 questions:

1. Age
2. Sex
3. Do you consume honey?
4. How often do you consume honey?
5. Are you satisfied with frequency of your consumption of honey? If not, state your reason for insufficient consumption of honey.
6. Which type of honey are you familiar with?
7. Which type of honey do you usually consume?
8. How do you usually consume honey?
9. What is the deciding factor in process of buying the honey?
10. Where do you usually buy the honey?
11. What is your first association on word "honey"?
12. Are you familiar with health benefits of honey?
13. Do you consume other honey products (pollen, propolis, royal jelly)? If you do, state which products.

The survey was conducted in centre of the City of Slavonski Brod (sixth largest city, situated in the eastern part of Croatia) on 100 examinees. 63 of them were female and 37 male persons. Most of them (31%) belonged to the age group of 45 years to 60 years, 25% to the age group of 35 years to 45 years, 19% had less than 25 years, 15% of examinees had 25 years to 35 years and only 10% belonged to the age group over 60 years.

3. RESULTS AND ACHIEVEMENTS

All 100 examinees answered that they consumed honey (question 3).

3.1. How often do you consume honey?

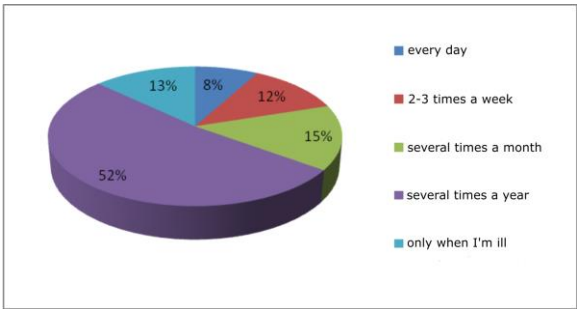

Fig. 1. Results of survey on question "How often do you consume honey?"

The results of survey on question "How often do you consume honey?" show that around the half of the people in Slavonski Brod consume honey only several times a year (52%). Only 8% of examinees consume it every day, which is quite a low ratio if well-known benefits of honey consumption are taken into account.

3.2. Are you satisfied with frequency of your consumption of honey?

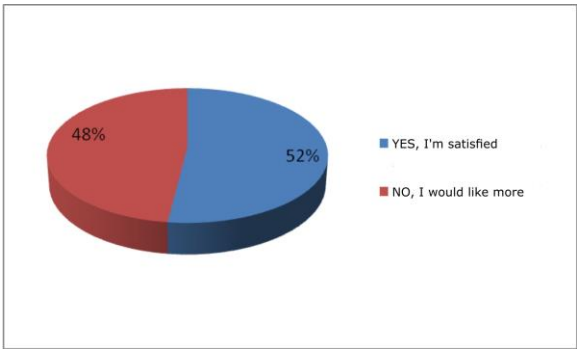

Fig. 2. Results of survey on question "Are you satisfied with frequency of your consumption of honey?"

About the similar number of examinees responded "YES" (52%) and "NO" (48%) on question "Are you satisfied with frequency of your consumption of honey?". Those 48% who answered "NO" were asked to say the reasons for insufficient consumption of honey. 26% stated that lack of habit is the main reason for that and 22% declared high price of honey as the main reason for insufficient consumption of honey.

3.3. Which type of honey are you familiar with?

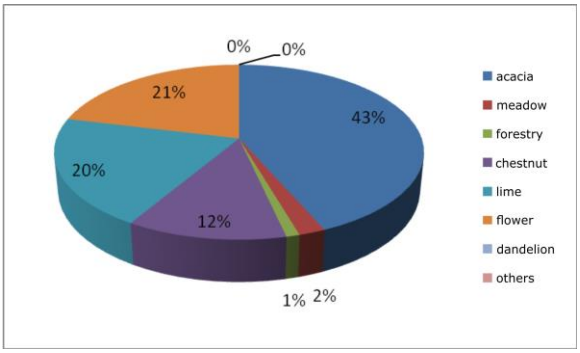

Fig. 3. Results of survey on question "Which type of honey are you familiar with?"

From the results of conducted survey it seems that population of Slavonski Brod is the most familiar with acacia honey (43%), followed by floral (21%), lime (20%), chestnut (12%), meadows (2%) and forestry honey (1%). Dandelion honey is not recognized at all (0%) and no other types of honey are specified in answers of examinees.

3.4. Which type of honey do you usually consume?

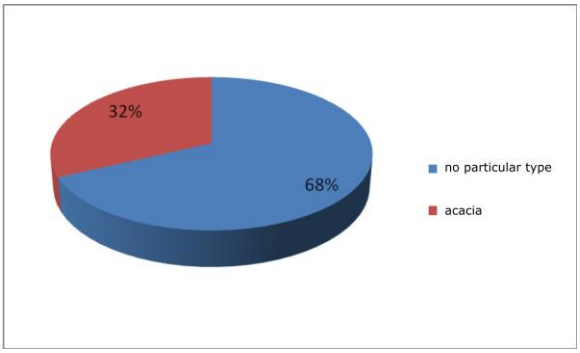

Fig. 4. Results of survey on question "Which type of honey do you usually consume?"

Figure 4 shows that 68% of examinees declared that they did not have favourite type of honey and the other 32% named acacia honey as their favourite one. This is in accordance with previous findings that acacia honey is the most recognisable type of honey in Slavonski Brod (results from section 3.3) and one of the most popular honeys in Croatia as well [3].

3.5. How do you usually consume honey?

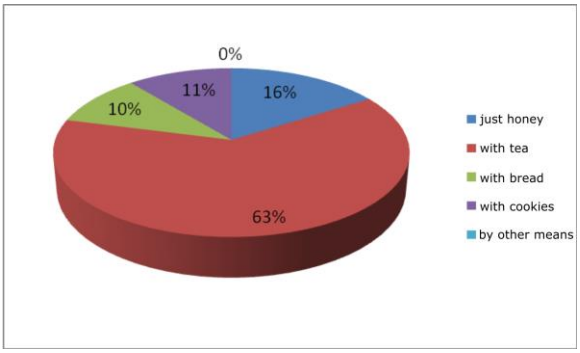

Fig. 5. Results of survey on question "How do you usually consume honey?"

Consumption of honey with tea is the most popular way of honey consumption in Slavonski Brod. About 2/3 of people in survey (63%) answered that they used honey with tea. 16% of examinees eat honey with spoon and about equal number of people consume it with bread and with or within cookies (10% and 11%, respectively). No other ways of consumption are mentioned.

3.6. What is the deciding factor in process of buying the honey?

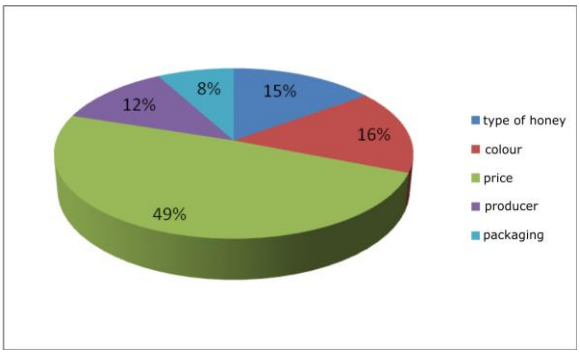

Fig. 6. Results of survey on question "What is the deciding factor in process of buying the honey?"

About half of examinees (49%) stated that the price of honey is the deciding factor in process of buying the honey. This finding is very significant and expected to some extent because of the economy crisis still present in Croatia. The usual price of the honey is about 7.5 euro per kilogram. The other half of examinees answered that colour is their deciding factor during the buying of honey (16%), followed by type of honey (15%), producer of honey (12%) and 8% of people are mainly guided by the packaging of the honey they intend to buy.

3.7. Where do you usually buy the honey?

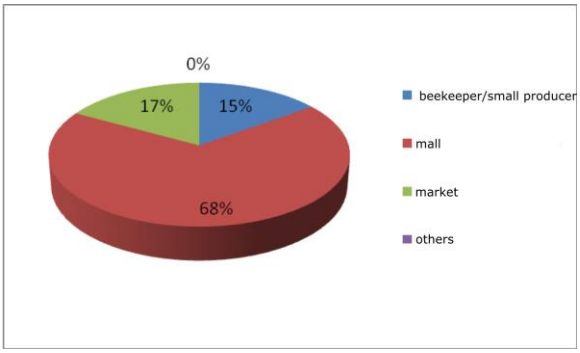

Fig. 7. Results of survey on question "Where do you usually buy the honey?"

Majority of people buy the honey in malls (big supermarkets). About 17% buy it in market and only 15 % buy the honey directly from small producers (beekeepers). This finding possibly reveals some reasons for high price of the honey, which the examinees in conducted survey recognised as the deciding factor in process of buying the honey (results from section 3.6).

3.8. What is your first association on word "honey"?

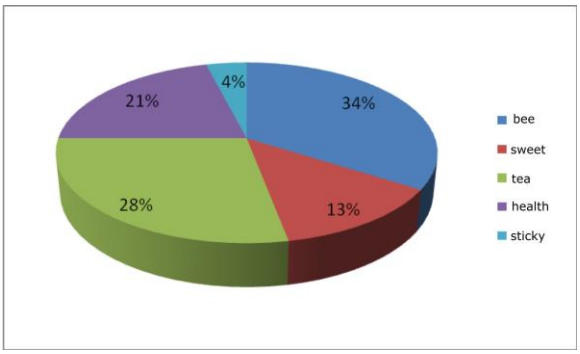

Fig. 8. Results of survey on question "What is your first association on word "honey"?"

The answers on question "What is your first association on word "honey"?" revealed many items associated with honey. Bees are frontrunners for 34% of the surveyed people in Slavonski Brod, tea for 28% of them, health for 21% and sweet taste for 13%. Small ratio of people associate honey with its sticky properties (4%).

3.9. Are you familiar with health benefits of honey?

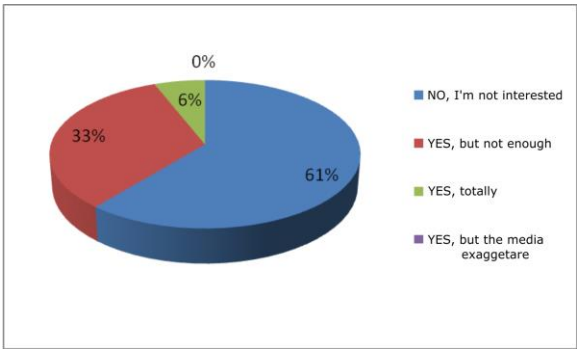

Fig. 9. Results of survey on question "Are you familiar with health benefits of honey?"

The conducted survey surprisingly revealed that 61% of people were not familiar with health benefits of honey and that they were not interested in it. Only 6% think that they are totally aware of health benefits of honey and the rest of examinees (31%) consider themselves partially aware of it. No one thinks the media exaggerate with this issue, which could open the door for further education processes and activities in this area.

3.10. Do you consume other honey products (pollen, propolis, royal jelly)?

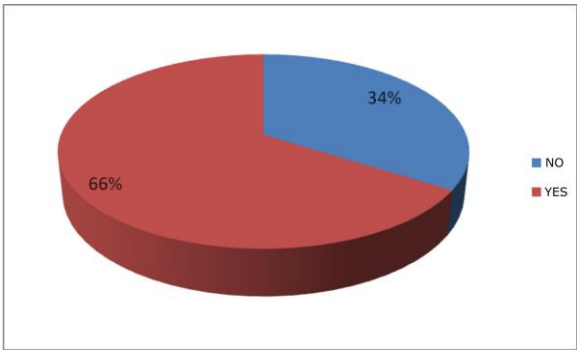

Fig. 10. Results of survey on question "Do you consume other honey products (pollen, propolis, royal jelly)?"

Figure 10 shows that about 2/3 of examinees in conducted survey in area of Slavonski Brod declared that they sometimes consumed other honey products, such as pollen, propolis and liqueurs.

Asked about those honey products, they mentioned liqueurs (24%), propolis (22%) and pollen (20%) in similar shares, as shown in Figure 11.

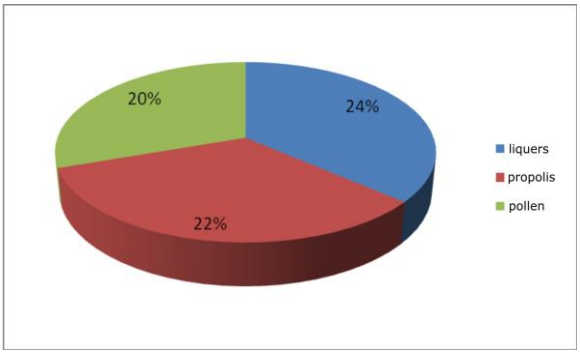

Fig. 11. Types of honey products consumed in Slavonski Brod

4. CONCLUSIONS

From the results of the survey, it can be concluded that inhabitants of Slavonski Brod often consume honey, but most of them only a few times a year. More than half of examinees are satisfied with their consumption of honey. The rest of the surveyed people that do not consume honey so often cited primarily high price, and then the lack of habit as the main reasons for that.

Acacia honey is the most familiar and most consumed among the surveyed people, then it follows floral, linden, chestnut, meadow and forest honey. Honey is the most commonly consumed in tea, but at least with cookies and bread. Examinees declared the price as the deciding factor when buying honey. Due to the high price of honey, consumption is reduced to a minimum. Honey is the most frequently purchased in big supermarkets (malls).

Despite the frequent information about honey as a healthy product, most of the persons are not interested in the impact of honey on the health, and they believe that they are not sufficiently informed about the honey and its medicinal properties. Various liqueurs, propolis and pollen are the most common final products prepared from honey that are consumed. The vast majority of people are not well informed about how honey has an impact on health and that its consumption can prevent a variety of diseases, and that honey can be a healthy substitute to medicines (drugs) that are regularly consumed on daily basis.

5. ACKNOWLEDGEMENTS

The authors express their sincere gratitude to prof. Valentina Obradović for her efforts, help and supervision in preparation and conduction of survey.

6. REFERENCES

[1] Z. Laktić; D. Šekulja, Modern beekeeping (in Croatian), Globus, Zagreb, (2008).

[2] V. Mujović, The gifts of nature and bees to our health (in Serbian), Podgorica, (2006).

[3] F. Velagić, Bee products for healthy and sick people (in Croatian), Harfo-Graf, Tuzla, (2004).

[4] Honey origin control (in Croatian) http://med-zdravlje.blogspot.hr/2011/12/kontrola-podrijetla-meda.html, (last access 07/09/2015)

[5] Food products quality control (in Serbian) http://www.vpps.edu.rs/Literatura/Kontrola_kvaliteta_pp/KKPP_Predavanje_04.pdf, (last access 07/09/2015)

[6] J. Belčić; J. Katalinić; D. Loc; S. Lončarević; L. Peradin; S. Šimić; I. Tomašec, Beekeeping (in Croatian), Znanje, Zagreb, (1977).

[7] B. Mihajlović, Medical treatments by bee products (in Serbian), Partenon, Beograd, (2007).

Financial analysis – indicator of business success

M. Vretenar Cobović [a], M. Cobović [b], A. Kulaš Mirosavljević [c]

[a] College of Slavonski Brod, Dr. Mile Budaka 1, 35 000 Slavonski Brod, Croatia, maja.vretenar@vusb.hr

[b] College of Slavonski Brod, Dr. Mile Budaka 1, 35 000 Slavonski Brod, Croatia, mirko.cobovic@vusb.hr

[c] College of Slavonski Brod, Dr. Mile Budaka 1, 35 000 Slavonski Brod, Croatia, anita.kulas@vusb.hr

Abstract

Financial analysis transforms the financial reports in the information essential for decision-making and enterprise management. Analysis of financial reports performed by various instruments and procedures, which are generally unbundling and comparing the results. The authors analyzed the basic financial reports of enterprise Kraš d.d. in the period from 2013 to 2015. They use a series of scientific research methods (methods of analysis, comparison, induction, deduction, description, classification etc.) as well as certain statistical and mathematical methods. The calculation of the chain index positions of the balance sheet, profit and loss account, and cash flow report, authors assessed the financial position of companies in the market and its further development. The aim of this paper is on the basis of the conducted horizontal financial analysis to calculate the financial indicators of enterprises and rank them according to certain parameters. Based on the calculation of financial indicators it is possible to recognize the positive and negative aspects of the business enterprise and give recommendations for the success of future business.

Keywords: financial analysis, financial reports, financial indicators, enterprise, business success

1. INTRODUCTION

Financial analysis is important instrument which financial manager is used to making decisions related to the operation of enterprises. In the process of analyzing financial reports, it is possible to use the whole range of different procedures, which are based on the parse and comparing [1, pp. 227].

Comparative financial reports that are required for the implementation of horizontal analysis can be considered in the context of the comparisons. Conversely, structural financial reports that are required for the implementation of the vertical analysis can be considered in the context of parsing.

Analysis of the financial reports which allows comparison of data over a longer period of time to detect trends and dynamics of changes of certain balance positions is called horizontal analysis [1, pp. 228]. Under vertical analysis implies is usually comparing financial data in one year [1, pp. 230].

2. FINANCIAL REPORTS AND FINANCIAL INDICATORS

For a successful business enterprise, it is necessary to appropriate information basis. A significant portion of such information occurs in accounting and is written in the financial statements. The aim of financial reporting is to inform interested users about the financial situation of the enterprises and the success of the business. This information is contained in the series of the financial statements of which the basic are:

1. Balance sheet - shows the status of asset, liabilities and capital on a certain day;
2. Profit and loss account - provides information on the enterprise success, and on revenues, expenditures and business results;
3. Cash flow report - allows management assessment of the success of cash management as well as the assessment of future cash flows;
4. Notes to financial reports - are used to explain the data from the financial reports.

2.1. The division of financial indicators

The indicator is rational or relational number, which implies that one economic size is placed in relation to other economic size. Financial indicators are the main carriers of information and the basis for the management of the company and its development.

These indicators is possible to divided into several groups:
1. Liquidity ratios - measures the ability of enterprises in the context of the ability to pay due short-term liabilities;
2. Leverage ratios - a reflection of the structure of liabilities and show how assets financed by own capital (equity), and the amount of assets financed by foreign capital (liabilities);
3. Activity ratios - show how to efficiently use the resources of enterprises in the business process;
4. Economical ratios - measures the ratio of revenues and expenses and indicate how the revenue realized per unit of expenses;
5. Profitability ratios - measures return on invested capital;
6. Investibility ratios - show the success of investments in shares.

3. ANALYSIS OF FINANCIAL REPORTS OF ENTERPRISE KRAŠ D.D.

Kraš d.d. is one of the leading food industry in the Republic of Croatia with a long tradition in the production of chocolate and other sweets. Table 1 shows the chain index for the individual positions of the balance sheet of enterprise Kraš d.d. in the period from 2013 to 2015.

Table 1. Chain index for the individual positions of the balance sheet

Term	Ci 2013	Ci 2014	Ci 2015
A) Long-term assets	92,97	98,10	94,22
B) Short-term assets	89,43	91,19	110,26
C) Prepaid expenses of the future period and deferred income	96,02	103,95	104,56
D) Total assets	**92,21**	**95,23**	**101,81**
A) Capital and liabilities	96,80	101,06	99,39
B) Long-term liabilities	85,16	70,23	116,98
C) Short-term liabilities	87,76	100,71	101,65
D) Deferred settlement of charges and income deferred to future period	81,73	56,97	82,97
E) Total capital and liabilities	**92,21**	**95,23**	**101,81**

Source: author's calculations based on the financial reports of enterprise Kraš d.d.

In Table 1, with the assistance of 'chain index are presented individual position of assets and liabilities of the balance sheet in the current year compared to the previous year within the observed period. Observing the data in the table it is possible to see decrease of long-term assets in 2015 compared to 2014 for 5.78%, while the short-term assets recorded an increase of 10.26%. Total assets during the the whole observed period had pronounced increasing trend.

On the liabilities side of the balance sheet has also come some changes. Capital and liabilities in 2015 compared to 2014 recorded a slight decrease of 0.61%, while the long-term and short-term liabilities recorded a slightly higher trend of growth. But despite that, it is possible to conclude that the enterprise during the observed period operated successfully.

Table 2 shows the chain index for the individual positions of profit and loss account of enterprise Kraš d.d. in the period from 2013 to 2015.

Table 2. Chain index for the individual positions of profit and loss account

Term	Ci 2013	Ci 2014	Ci 2015
A) Operating income	91,40	98,04	102,48
B) Operating expenses	93,47	97,26	102,09
C) Financial income	70,85	42,88	107,52
D) Financial expenses	84,50	69,80	74,01
E) Total income	90,96	97,10	102,45
F) Total expenses	93,17	96,42	101,57
G) Profit or loss for the period	91,57	98,77	99,15

Source: author's calculations based on the financial reports of enterprise Kraš d.d.

Based on the data in the table it is possible to observe constant growth in operating income in the observed period. Financial income recorded a decreasing trend in 2014 compared to 2013, but after that begin to increase. Total income recorded a constant increasing trend within observed period, and the highest were recorded in 2015, as well as enterprise profit.

Analyzing the operating, financial and total expenses of the enterprise, it is possible to observe equal trend to their increase or decrease as in operating, financial and total income of the enterprise.

Table 3 shows the chain index for the individual positions of cash flow report of enterprise Kraš d.d. in the period from 2013 to 2015.

Table 3. Chain index for the individual positions of cash flow report

Term	Ci 2013	Ci 2014	Ci 2015
A) Cash and cash equivalents at beginning of the year	**92,15**	**93,80**	**81,10**
B) Increase of cash and cash equivalents	-	-	82,11
C) Decrease of cash and cash equivalents	93,25	91,27	-
D) Cash and cash equivalents at end of the year	**80,17**	**81,10**	**95,17**

Source: author's calculations based on the financial reports of enterprise Kraš d.d.

Based on the data in the table it is possible to observe a decrease of cash and cash equivalents at the end of the year in 2013 and 2014 compared to cash and cash equivalents at the beginning of the observed years. In 2015, this trend has stopped and the money at the end of the year under review was recorded increase in relation to the initial period in 2015. Moreover, analyzing cash flow report of enterprise Kraš d.d. it is possible to observe an increase of cash and cash equivalents from operating activities during the observed period, while cash flow from financing and investing activities recorded a decreasing trend in the period from 2013 to 2015. Table 4 shows the calculations of liquidity ratios of enterprise Kraš d.d.

Table 4. Liquidity ratios

Term	2013	rank	2014	rank	2015	rank
Cash ratio	0,12	1	0,09	2	0,12	1
Quick ratio	0,17	1	0,09	3	0,12	2
Coefficient of financial stability	0,77	1	0,75	2	0,64	3

Source: author's calculations based on the financial reports of enterprise Kraš d.d.

According to the data in the table it is possible to observe decrease in the cash ratio and quick ratio in 2014 compared to 2013. But, in 2015 these ratios again recorded increasing trend. A preferred value of these indicators should be 1, based on which it is possible to conclude that the enterprise has significant difficulties with liquidity, but despite that it is a financially stable enterprise. This confirms the coefficient of financial stability, which should be less than 1, because of part of long-term resources should finance short-term assets. If greater than 1, it means that the long-term assets funded by short-term liabilities, ie. that there is a deficit of working capital, which in the case of enterprise Kraš d.d. does not exist. Liquidity ratios of enterprise are also shown in the chart 1.

Chart 1. Liquidity ratios

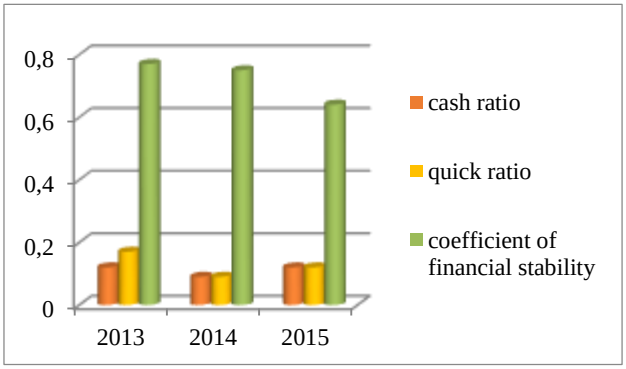

Source: author

Table 5 shows the calculations of leverage ratios of enterprise Kraš d.d.

Table 5. Leverage ratios

Term	2013	rank	2014	rank	2015	rank
Debt ratio	0,46	2	0,48	1	0,46	2
Coefficient of own funding	0,45	2	0,47	1	0,47	1

Source: author's calculations based on the financial reports of enterprise Kraš d.d.

According to the data in the table it is evident that debt ratio and coefficient of own funding in 2014 compared to 2013 increased slightly. But, in 2015 in accordance with the assigned range, again decreasing. The coefficient of own funding in 2014, increasing from 0.45 to 0.47, and retains the same value in 2015. According to the leverage ratios Kraš d.d. is not debt enterprise. For the debt ratio is preferable to be as low as possible, and a maximum amount can be 1. This ratio in the observed period did not exceed the amount of 0.5. Leverage ratios of enterprise are also shown in the chart 2.

Chart 2. Leverage ratios

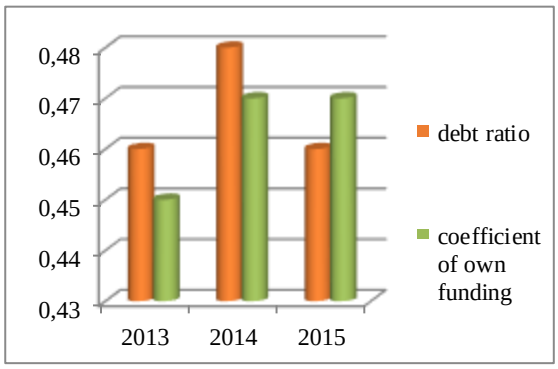

Source: author

Table 6 shows the calculations of economical ratios of enterprise Kraš d.d.

Table 6. Economical ratios

Term	2013	rank	2014	rank	2015	rank
Economical of total business	1,01	2	1,01	2	1,02	1
Economical of financing	0,50	1	0,19	3	0,28	2

Source: author's calculations based on the financial reports of enterprise Kraš d.d.

Economical ratios are calculated based on profit and loss account and it is advisable to be as large as possible. According to the data in the table enterprise Kraš d.d. has successfully ratios of the total business of the economical of financing. Ratios of economical of total business in 2013 and 2014 are equal, while in 2015 recorded a slight increase. Ratios of economical of financing in 2014 decreased from 0.50 to 0.19, as compared to 2013. But in 2015 again increase, which greatly affected the entire business enterprise. Economical ratios of enterprise are also shown in the chart 3.

Chart 3. Economical ratios

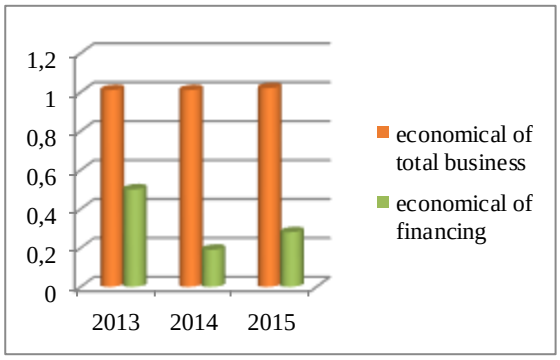

Source: author

4. CONCLUSIONS

Financial reports and their analysis are one of core activities for successful business enterprise. With the assistance of certain calculations it was made the analysis of financial reports and financial indicators of enterprise Kraš d.d. and thereby fortified its financial position in the market.

Despite the decline of certain positions within the balance sheet of enterprise (decrease of long-term assets, capital) and profit and loss account (decrease of financial income) enterprise remains financially stable and one of the leading producers of sweet products in the Republic of Croatia.

The impact of the financial crisis on business enterprise it is possible to observe on the basis of calculation of liquidity ratios that show negative trends.

But, despite of that, the coefficient of financial stability also as leverage and economical ratios confirmed a very good market position of enterprise and its financial success.

5. REFERENCES

[1] L. Žager; K. Žager, Analysis of financial reports (in Croatian). Masmedia, Zagreb, (2008).

[2] J. C. Van Horne; J. M. Wachowicz, Basics of financial management (in Croatian). Mate, Zagreb, (2002).

[3] B. Matić, Monetary economy (in Croatian). Ekonomski fakultet u Osijeku, Osijek, (2011).

[4] M. Vretenar Cobović; M. Cobović; K. Bratanić, Business Analysis of Croatian Banks During the Financial Crisis. 5th International Scientific and Expert Conference TEAM 2013, (2013), pp. 161-164

[5] B. Matić; H. Serdarušić; M. Vretenar Cobović, Economic Circumstances and Personal Finance Management. Interdisciplinary Management Research X, (2014), pp. 557-564

[6] Financial reports of enterprise Kraš d.d., http://www.kras.hr/hr/kako_poslujemo, last access 13/06/2016

The impact of the economic crisis on youth leaving Croatia

S. Knežević [a], L. Duspara[b], D. Drašković [c]

[a] College of Slavonski Brod, Dr. Mile Budaka 1, 35000, Croatia, sanja.knezevic@vusb.hr

[b] College of Slavonski Brod, Dr. Mile Budaka 1, 35000, Croatia, lena.duspara@vusb.hr

[c] student of College of Slavonski Brod, deadraskovic@gmail.com

Abstract

The global economic crisis has caused disruptions in the labour market in most European countries, including Croatia. Unfavourable economic conditions in Croatia in recent years have forced an increasing number of young people to seek better perspectives abroad. Unemployment is one of the main factors. The drama of unemployment particularly affects young people. Youth unemployment is a growing problem with long-term consequences for individuals, communities, the economy and society, and in early working life can have long-term consequences in the lifelong perspective of young people. In Croatia, there is a noticeable tendency of brain drain. Talented and educated young people go abroad, because of greater opportunities and country loses population and deepens demographic crisis. Highly educated persons are particularly great loss for the country because in their education has been invested and they can the most contribute to economic development. The aim of this paper is to show how the economic crisis has affected the youth in Croatia, with special emphasis on unemployment. Based on the processing and analysis of collected data paper will show the current situation of young people in Croatia and their perspective for the future.

Keywords: economic crisis, unemployment of young people, labour market, Croatia

1. INTRODUCTION

The global financial crisis has caused disruptions in the labour market that have led to an increase in the unemployment rate in most European countries, including Croatia. During a crisis young people are particularly vulnerable group, looking for employment in the labour market, which already offers little employment opportunities facing with the individuals who have more experience.

Besides, young people in Croatia are faced with socio-economic problems, meaning concretely low standard of living, lack of life perspectives and unemployment. The crisis is also a place to discover new possibilities. It is an opportunity for innovative and productive employment of human resources. Most important is try to create conditions that enable profitable, productive and worthily employment or people. The key challenge is to increase employee productivity, but also the activity of the population.

2. PROBLEMS AND POTENTIALS OF YOUTH IN THE LABOUR MARKET

The entire social events are reflected in the world of young people to the extent that can be said that the young people are credible indicators of all social events. The relatively unfavourable economic conditions in the Croatia in recent decades forced a certain number of young people to seek better prospects abroad. The most important reasons for relocation and displacement are economic nature. Due to the

economic crisis that has affected Croatia and most developed countries, it reduces the employment opportunities and the higher living standard. So far, the EU Member States applied a wide range of policies and measures in an effort to solve problems, create jobs and greater professional opportunities for young people. "These policies and measures include: enabling work experience, improving the relationship between education and work, guarantee for young people, support for finding a job, promoting entrepreneurship, and lifelong career guidance."[1]

The guidelines provided by the National Employment Policy served in creating the first program of active employment policy. „The program contains measures: 1.co-financing employment of young people without work experience, 2.Co-financing introduction into work or training, 3.Co-financing professional training, retraining and additional training for known and unknown employer, 4.Co-financing employment of demobilized Croatian veterans, children and spouses of the missing and the dead, 5.Co-financing employment of women less than 45 years of age and men over 50 years of age, 6.Co-financing the employment of persons with disabilities."[2, p.56]

„Two-thirds of young people tend to educate in educational institutions in Croatia, while for overseas as well as for the private sector, decided to one third. Croatia despite an increase in national and international mobility of students, and the creation of new institutions of higher education in the country, is still a country of low mobility. The European Union implements programs such as "Europe 2020", aimed at increasing the number of highly educated from 32% to 40%, and reduce early school leaving from 14% to less than 10%."[2, p.58] Despite all of the above the greatest problem of youth is unemployment. „The young generation in Croatia is extremely affected by the economic crisis, especially due to high unemployment, which is in the last twenty years above 30%."[3] Faced with such unfavourable trends, young people often accept jobs outside their profession. However young people should be the largest potential of the country.

Some of the measures to support active employment of young Croatian Employment Service are: package of measures for young people- young and creative. "The measures are aimed at raising the competence and preparation of young people for employment, and in particular to strengthen the involvement of young people in entrepreneurship" [4]

Measures of the package includes: "With half - half of the first work - support for the employment of young people without work experience; Fifty-fifty - aid for employment; Your initiative - your workplace - support for self-employment; Your initiative - your workplace green economy - Support for self-employment; Together we are stronger - aid for employment manager of the cooperative; Work and after the summer - aid for employment in tourism; Work and after vocational training - aid for employment; I'm learning on the job - support for training of newly employed persons; Knowledge is worth -education unemployed; Young people learn to work - programs of education and training of unemployed young people and for the known employer; Learning to entrepreneurs; Training in the Workplace; Training on the job - training for a known employer; Programs literacy of young people - the education of unemployed; Work and internship and transport, - vocational training for work without employment; Municipal public works can co-financed employment in municipal public works; Work for the community and ourselves - are / were financed employment in public work; Help yourself and others' - employment through individual projects of public works; Youth for Youth - helpers in the classroom - public works for young people; Youth for EU - co-workers at EU projects in the NGO sector and social partner organizations - public works for young people; Young people in the community - a mini public works for young people; Employment in social entrepreneurship - financing of employment in public works in the social companies; Support transformation and deinstitutionalization of social care and support social inclusion; Run community - recruiting volunteer coordinator through the public works; The coordinators of community service."[4]

3. YOUTH UNEMPLOYMENT – THE BIGGEST PROBLEM OF YOUTH IN CROATIA

Unemployment is one of the most significant problems faced by the country, and is particularly worrying unemployment of young people who are significant human capital of the economy and society. The trends pointed to an

increase of the population of young people who never manages to find a satisfactory job or any paid work. Unemployment in Croatia is a result of lack of structural changes in the economy.

"The destruction of workplaces in the liquidation and bankruptcy of a large number of companies has not been followed by opening of a sufficient number of new jobs in the private sector. Relatively high wages and salaries, institutional flexibility and the general mismatch between supply and demand appear to be major obstacles to the dynamic labour market performance."[5, str.47] The following figure shows the number of unemployed in the last five years.

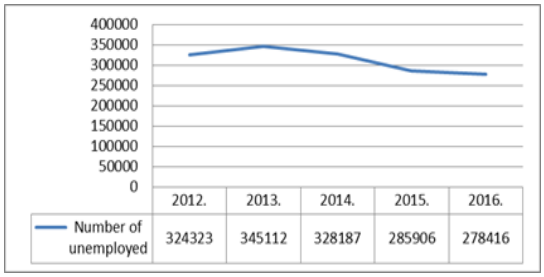

Fig.1 The number of unemployed persons for the period 2012 - 2016 [4]

The figure shows that the number of unemployed reached its peak level in 2013, unemployment reduction occurred in 2015, while seeing an increased number of unemployed again in 2016, although the data for 2016 are available only up to March. Despite the reduction phases of and rising unemployment, it is certainly a great number of unemployed.

According to Eurostat Croatia is still at the top of the youth unemployment among the EU a country. "At the end of 2015 youth unemployment rate was 45 percent."[6] The following table shows the number of unemployed by age.

Table 1 Unemployed by age from 2012 to 2016[4]

Age	2012	2013	2014	2015	2016
15-19	17186	18140	16683	14814	11812
20-24	44875	47619	42593	34910	32615
25-29	45445	47441	43207	35001	32385
30-34	37031	39361	36513	30615	28090
35-39	32146	35013	33440	28940	27223
40-44	31009	23949	31106	27409	26227
45-49	33204	35584	33900	29664	27891
50-54	36553	37653	36380	32541	31602
55-59	35057	37708	39303	36334	35005
60-	11816	13644	15061	15678	16347

Table shows that considering the age, especially are vulnerable young people from 20 to 29 years. Unless mentioned it is noticeable unemployment of age groups from 55 to 59 years. The data for 2016 are available only up to March but it is still noticeable negative trend. Croatia is in terms of youth unemployment at the bottom of the European scale, together with Greece and Spain. The following figure shows the structure of unemployed persons by level of education.

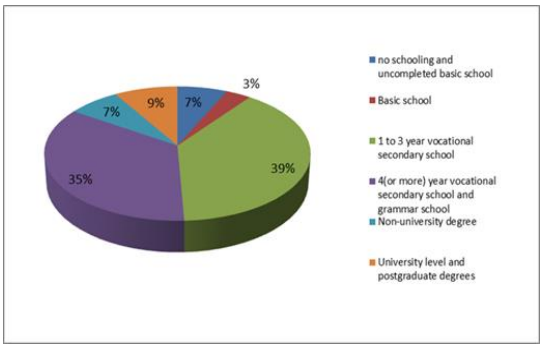

Fig.2 Structure of unemployed persons, by educational background, end of March 2016[4]

The figure shows that in educational structure of the unemployed are the most numerous people with secondary vocational school lasting up to 3 years followed by persons with secondary vocational school for a period of 4 years. The smallest number of unemployed is persons with basic school. People who finished university cover 9% of unemployed. The following figure shows the unemployed highly educated persons.

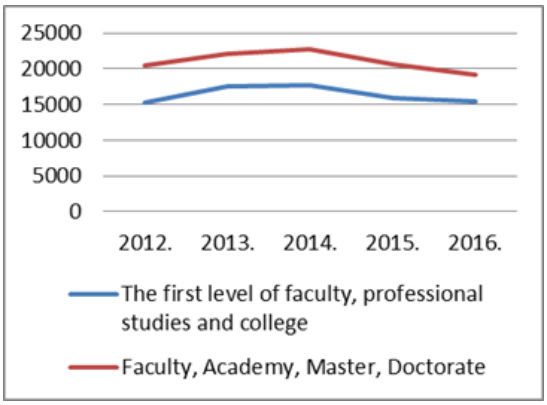

Fig.3 Unemployed highly educated from 2010 to 2014 [author according to 4]

The figure shows that from 2012 to 2014 there was a significant increase in the number of unemployed persons with college or university degrees. From 2014 to 2016 is slowly decreasing, but still high. The data for 2016 are

available only up to March. “Even 71.3% of young people believe that their profession is not adequately appreciated in society.”[7] This is one of the reasons why highly educated leaving Croatia.

4. THE FUTURE OF YOUTH IN THE LABOUR MARKET IN CROATIA

Current situation in the Republic of Croatia shows relatively poor indicators, young people face difficulties in finding any job, even harder to work according to their qualifications. It is extremely low percentage of young people who've been able to provide a safe job or indefinite contract. “Almost every other young person is unemployed, and 60% of them have a salary below average.”[7]

The country is trying with its measures such as vocational training, various co-financing, and incentives for youth employment to help young people and provide them with employment and to remain in Croatia. With these programs should be involved and additionally focus on youth unemployment, because it will further deepen the crisis also increase the possibilities of political and social unrest.

Despite predictions that the measures of the Croatian Employment Service and measures at EU level such as ‘Youth Guarantee’ enable greater competitiveness to its customers, its own measures do not help to create new jobs. The lack of education and early school leaving remain biggest problem. High unemployment and youth leaving the country have negative consequences not only on the national demographics and economy, but also to criminal behaviour and delinquency.

“According to estimates by the European Commission which are stated in the Report of the aging population in Europe, for the period up to 2060, if the negative trends continue, Croatia will lose the population of 600,000 inhabitants, which will mostly affect the youngest age cohort (0-14).”[8] Therefore, there is a justified fear for the future of young people and for the entire society.

5. CONCLUSION

Youth unemployment is a growing problem with long-term consequences for the Croatian economy and the overall situation in the country. Getting acquainted with the possibilities of working life of young people, vocational guidance; are key ingredients to support young people to find a job.

The generation of young people is facing record levels of unemployment despite high levels of qualifications and years of education. Although Croatia offers a number of measures for employment, youth unemployment is high. These measures do not create permanent jobs.

If it continues the negative trend of growth of youth employment, the European Union and thereby Croatia, could face the long-term economic, political and social consequences. There is no time to wait, and resolving youth unemployment should be as soon as possible to access.

6. REFERENCES

[1] European lifelong guidance policy network, http://www.elgpn.eu/publications/browsebylanguage/croatian/HR_youth_unemployment_concept_note_web.pdf, last access 25/05/2016

[2] V. Frančević, V. Puljiz, The work in Croatia against challenges of the future, Faculty of Law in Zagreb, Zagreb, (2009).

[3] J.Ilišin et al, Young people in times of crisis, Institute for social research in Zagreb, Zagreb 2013

[4] Croatian Employment Service (e.g. in Croatian, Hrvatski zavod za zapošljavanje), http://www.hzz.hr, last access 15/06/2016

[5] P. Tomašić, Unemployment in transition in Croatia, Christian presents, Zagreb, (2010).

[6] Index.hr, http://www.index.hr/vijesti/clanak/porazni-podaci-nezaposlenost-mladih-u-hrvatskoj-preko-45-posto/866838.aspx, last access 17/06/2016

[7] Centre for Education, Counselling and Research, http://www.cesi.hr/hr/kakva-je-buducnost-mladih-u-hrvatskoj/, last access 20/06/2016

[8] Policy for youth: sustainable future of young people in Croatia, https://www.orah.hr/files/Programski_stavovi_310515/Politika_za_mlade_ORaH.pdf , last access 18/06/2016

Youth Entrepreneurship

L. Duspara [a], S. Knežević [a] , D. Veraja [b]

[a] College of Slavonski Brod, Ul.Dr. Mile Budaka 1, 35000 Slavonski Brod, Croatia, lena.duspara@vusb.hr; sanja.knezevic@vusb.hr

[b] former student of College of Slavonski Brod, Ul.Dr. Mile Budaka 1, 35000 Slavonski Brod, Croatia

Abstract

Today, entrepreneurship is considered an important factor overall social progress. It brings major benefits to society by fostering economic growth, creating new products and technologies, as well as increasing efficiency in the use of resources. Entrepreneurship today is important not only because it helps businesses to better meet personal needs, but also because of the economic contribution of the new venture. It brings major benefits to society by fostering economic growth and creating new products and technologies. Emigration of young and educated people from the country is specific consequence of high unemployment, but good way to keep them is certainly encouraging youth entrepreneurship. In this paper is explained the importance of entrepreneurial skills and knowledge to run the company, as well as the opportunities that are available to young people entering the business world. Evaluation of opportunities is the most critical element of the entrepreneurial process, because it allows the entrepreneur to estimate returns whether a product or service required returns given the required resources. Young entrepreneurs are the drivers of the national economy and that's why in them must be constantly invest and encourage their creativity in order to achieve prosperity of the economy and the country. Education and training for entrepreneurship are most important in creating enterprising individual, a successful entrepreneur and a successful economy and ultimately successful country. European Union countries are very long ago declared entrepreneurship as one of the key competences, which should be systematically incorporated into all levels of education.

Keywords: Entrepreneurship, entrepreneurial process, strategy, young entrepreneurs, incentives, entrepreneurial incubators.

1. INTRODUCION

Business plays an important role in the overall social progress, and society brings great benefits by creating new products and fostering economic growth. The entrepreneur is creative person with a new idea, runs a business activity, assumes the risk and creates innovation. There are different reasons why people start new ventures; some are doing it in order to achieve financial prosperity, others to create new employment after losing their job, and the third just to create something new and interesting. Entrepreneurship is a very good chance of survival in an environment prone to uncertainty.

The aim of this paper is to research youth entrepreneurship, which is important today, probably more than ever before. It is known that young people are affected by high unemployment and very often leave their country in search for work. Promotion of entrepreneurship among young people is very important, in order to stop this negative trend and encourage the entrepreneurial mind-set of the population. It is important to explore the ways in which young people can easily start their own business and secure a livelihood, but also the progression and survival in the business world.

The paper starts by defining the fundamental business concepts, whose understanding is necessary to know if it is thinking about starting of business. Also, will be explained entrepreneurial process, development of youth entrepreneurship, role of entrepreneurial education and so on. Before starting of business, young entrepreneurs have to make a good analysis of the environment. The last part of the article talks about risk of unemployment, but also the opportunities that are available to young

people, as well as incentives and assistance in starting their own businesses.

2. IMPORTANCE OF YOUTH ENTREPRENEURSHIP

Today, entrepreneurship is considered as an important factor overall social progress. It brings major benefits to society by: „fostering economic growth, creating new products and technologies, as well as increasing efficiency in the use of resources."[1] The term enterprise includes the launch of a change in production and business. Entrepreneurship is a continual process of creating new values uniting unique combination of resources in order to exploit market opportunities.

2.1. Entrepreneurial process

The entrepreneurial process is the exploitation of opportunities and further work on its construction and development. It's more than just solving the problem, because the entrepreneur has to find assess and develop an opportunity transcending forces which oppose the creation of something new. The process has four phases: identification and assessment of opportunities that develop a business plan, with identification of necessary resources. Although these phases follow one after the other, neither one of them is not engaged in isolation, as none is completely finished without a comprehensive vision of all phases of the enterprise. For example, to successfully identify and assess opportunity, the entrepreneur must have in mind the type of work which eventually wants to deal with.

2.2. Development of youth entrepreneurship

Entrepreneurship is base of the market economy. Small and medium enterprises account for about 97% of the economy of most countries of the European Union, they are also the generators of the national economy. Education and training for entrepreneurship are assumption for creating individual enterprising, successful entrepreneur and successful economy and ultimately successful country. "European Union countries are very long ago declared entrepreneurship as one of the key competences, which should be systematically incorporated into all levels of education". [2]

2.3. The role of entrepreneurship education in Croatia

Entrepreneurship education has never been so important in terms of subjects and academic research like today. Number of colleges and universities that offer at least one course in entrepreneurship increases every year. Many universities in Europe have well-established programs in entrepreneurship. There are also some unique entrepreneurial programs, such as graduate programs of entrepreneurial science and technology enterprises. But, very small number of universities is involved in the actual process of creating a company, where universities, teachers and students share sales and profits from the new venture.

Education plays a major role in the education of entrepreneurs. Many entrepreneurs cited the need for education in the area of strategic planning, management, communication, finance and marketing. A wider range of knowledge allows entrepreneurs wider network to generate opportunities and adaptation to new situations. A quality system of higher education, science and economy are able to develop and deploy innovative technologies, which are based on the competence of human resources, such as creativity, intellectual curiosity, knowledge and motivation.

Croatia is characterized as a land of economic and social transition, with insufficiently supportive environment and without a continuous tradition in entrepreneurship. Nevertheless, the number of entrepreneurs is growing from year to year. Some processes speed up the accession to the European Union, but each process needs some time for exercising. Keeping up with all the intensive development of the competitiveness of national economies is possible through "an effective national learning strategy for young people about entrepreneurship, but it is also an indispensable factor of stability in the development and survival of the national economy". [3]

Entrepreneurial learning is best presented in the national strategy document - Strategy for Entrepreneurial Learning "Enterprising Croatia"

for the period from 2010 to 2014. The strategy was a response to the many questions and problems faced by the Republic of Croatia. Aim is accepting of entrepreneurship as national, social, economic and educational activities". The Strategy provides a system and dynamics of introducing entrepreneurship in all of educational levels, starting from pre-school up to the level of higher education.

2.4. Youth unemployment

According to official data of the Central Bureau of Statistics, "merges unemployment in the Republic of Croatia in March this year amounted to 17.2%" [4], which means that at present there are around 260,000 unemployed persons.

According to the Croatian Chamber of Commerce, in March this year was 21.4 million EU citizens were unemployed, and the unemployment rate was 8.8%. The biggest shift in the absolute difference in the rate last year was recorded by a member of the group with the highest rates: Croatia, Cyprus and Spain, with the exception of Bulgaria and Slovakia. Croatia in March, measures the level of 14.9% and is on the third place according to the amount of the unemployment rate, immediately after Greece (24.4%) and Spain (20.4%). The lowest rates are Germany, Czech Republic and Malta.

In addition to the general rate of unemployment, Croatia has the third highest rate of youth unemployment, which in March of this year amounted 39%. It means that 57,000 people younger than 25 years did not have a job, 19,000 more than in March 2008. Croatian labour market indicators are among the worst in the EU; it needs a more dynamic recovery than most Member States in order to join the EU average.

2.5. Young Croats in relation to young Europeans

Due to high unemployment, technological and economic backwardness and the general social standards situation of young people in Croatia can hardly be compared with the social situation of young people in highly developed European countries. Young people hit a high unemployment rate and are employed mainly in jobs of short duration. Knowledge should encourage change and create new business projects that will solve their problem of employment and economic problems.

The observed differences in the representation of certain skills; for young people from Croatian is most important a good education, communication skills, and knowledge of foreign languages and professional competence. Young Europeans priority is knowledge of foreign languages and information technology, and then a good general education, and communication skills. The cause of these differences probably are differences between the labour market in Croatia and other states of the European Union, in which greater emphasis is placed on the additional skills and learning processes, rather than on the basic requirements, such as professional competence. Further differences are evident in the fact that young Croats are more extent than other Europeans perceive the importance of good looks and completion of internship incentives for young entrepreneurs

Lending that through its regular programs offered by commercial banks young entrepreneurs generally cannot be realized, due to relatively high interest rates. In order to facilitate young entrepreneurs, start a business, institutions have developed programs to facilitate obtaining loans from commercial banks. The Ministry of Business and Trade (MINPO) and wishes to encourage entrepreneurship among young people by allowing them more favourable borrowing that is particularly difficult in the beginning. [5]

3.1. HBOR loan program for young entrepreneurs

Croatian Bank for Reconstruction and Development (HBOR) under the "Youth Entrepreneurship", encourages the creation and development of economic entities that are owned by Croatian citizens in the age group up to the age of 30 and to create conditions for successful business young.

Entrepreneurs' borrowers can be companies, dealers, and individuals owning a private business, cooperatives and institutions in which [6]:

• one or more persons in the age group up to 30 years has at least 51% of the capital or the

persons in the age group up to 30 years of age and registered owners

• people in the age group up to 30 years of life leads Management.

It is important to note that the founder of the business is obliged, in the established business entity, after the realization of the investment to be active and keep busy on responsible workplace.

3.2. Micro loans

MINPO (The Ministry of Business and Trade) encourage young entrepreneurs through other programs, so the Croatian Agency for Small Business, Innovation and Investments (HAMAG BICRO) offers the possibility of micro-lending. [7]

HAMAG BICRO micro crediting began as a pilot project in 2013., the program is intended for start-ups operating less than 24 months. Micro loans provide fast and efficient source of finance. The collateral for these loans are reduced in practice, on debentures of companies and owners without mortgages and other instruments.

The minimum amount of loan that is offered to entrepreneurs is 10,000 HRK, and the highest 120,000 HRK, with a repayment period of 5 years, with included the start of six months. Fixed interest rate for these loans is only 0.99% per year.

3.3. Business incubators

Business incubators are places that bring together entrepreneurs who just started to do business. The term business incubator includes space with required computer infrastructure, use of shared administrative services and expert advice for the beginner entrepreneurs. Requirements for the development of space relate to the possibilities of teamwork, lectures by experts and workshops, which make flexible space that, must follow the requirements of the user.

The main point is that the entrepreneur-beginner can for free or very convenient to use the space for a certain period in order to develop their business ideas. Therefore, entrepreneurial star-up incubators have a function test ideas and possibilities of their technical development and placement on the market. The main goal is to run the business of young entrepreneurs.

3. CONCLUSIONS

Entrepreneurship is one of the core competencies that should be systematically incorporated into all levels of education, because it is the premise of creating enterprising. Emigration of young and educated people from the country is a result of high unemployment, from the standpoint of development has far-reaching implications for the entire society. A large number of unemployed youth is ready to leave the country in search of business, which suggests a need for more dynamic economic recovery.

4. REFERENCES

[1] M. Karić, Ekonomika poduzeća, 2. izdanje, Ekonomski fakultet u Osijeku, Osijek (2009.):

[2] V. Tafra, Učenje i osposobljavanje za poduzetništvo i obrazovni sustav – strategijski pristup, Učenje za poduzetništvo, 6/12., str. 16-21 (2013.):

[3] Državni zavod za statistiku, podaci o broju nezaposlenih, http://www.dzs.hr/Hrv/system/first_results.htm, last access 28/4/2016

[4] Hrvatska gospodarska komora - HGK: Stope nezaposlenosti, https://www.hgk.hr/sektor-centar/centar-makroekonomija/najvise-stope-nezaposlenosti , Last access 29/4/2016

[5] Hrvatske agencija za malo gospodarstvo, inovacije i investicije, http://www.hamagbicro.hr/, last access 4/5/ 2016

[6] Hrvatska banka za obnovu i razvitak: Poduzetništvo mladih, http://www.hbor.hr/novo-poduzetnistvo-mladih, last access 4/5/ 2016

[7] Hrvatske agencija za malo gospodarstvo, inovacije i investicije, http://www.hamagbicro.hr/hamag-bicro-i-hbor-svojim-programima-olaksavaju-mladim-poduzetnicima-ulazak-u-poduzetnistvo/, last access 4/5/2016

Emotional intelligence in business

A. Kulaš Mirosavljević [a], M. Rubil [b], M. Vretenar Cobović [c]

[a] College of Slavonski Brod, Dr. Mile Budaka 1, 35000 Slavonski Brod, Croatia, anita.kulas@vusb.hr

[b] Ex student of College of Slavonski Brod, 35000 Slavonski Brod, Croatia, rubilmarija@gmail.com

[c] College of Slavonski Brod, Dr. Mile Budaka 1, 35000 Slavonski Brod, Croatia, maja.vretenarcobovic@vusb.hr

Abstract

Emotional intelligence is "something" that is in every man intangible. It affects how the man manages his own behavior, how he handles social complex situations, and how he makes personal decisions that achieve positive results. Emotional intelligence is a fundamental element of human behavior that differs from intellect. It is not known link between IQ and emotional intelligence. Someone's emotional intelligence cannot be predicted based on how much someone is smart.

Emotional intelligence refers to the ability to recognize our own feelings and the feelings of others, to motivate ourselves and manage our own emotions and manage relationships. Emotional intelligence consists of four basic skills that belong to the two primary competencies: personal and social competence. Ability to manage emotions and openness to them, enable individual easier adaptation to different situations and relationships.

People with high emotional intelligence can manage their emotional state and thus achieve the objectives which have a certain value for them.

Management of emotions is vitally area where someone may be more or less successful, and has a unique set of skills.

The aim of this study is to more closely examine how emotions affect the quality of work of individuals, groups and organizations, as the organization is to be emotionally intelligent, and how such action helps to business success.

Keywords: emotional intelligence, motivation, empathy, competences

1. INTRODUCTION

Management of emotions is a vitally area in which someone can be more or less successful and has unique set of skills.

Changes in the business world also reflect on the organizations that have to change their features in order to survive and prosper. All these changes increase the value of emotional intelligence.

The value of people who motivate themselves, show initiative, have an inner desire to surpass themselves are sufficiently optimistic in stressful situations. Empathy skills become more important because of the need for higher customer service quality. The skills of emotional intelligence are important for successful work.

More and more companies realize that the encouraging development of emotional intelligence is a key component of the management of each organization. Companies are no longer compete only with its products, but also with the interpersonal skills of their employees.

2. THE EMOTIONAL INTELLIGENCE

In order to have a successful interpersonal relationship with people, you need to have the ability to empathize.

Empathy means to feel and to understand what others feel without to say it. They show their feelings through their facial expressions,

tone of voice and other nonverbal cues, and is based on self-awareness and self-control.

In order to encourage people to work effectively, you should expect the best from them, even if they immediately don't show it. You need to tell them the problem and seek a solution from them.

The negative impact on the work can be prejudice someone against someone or something. Thus they increase emotional power, but reduce the results of the work and incapacitate them, creating discomfort and emotional distance.

Accepting diversity and appreciation of the unique mode of different people can contribute a lot to the progress and improvement of the quality of work.

Emotional intelligence refers to the ability to recognize our own feelings and the feelings of others. Five basic emotional and social competencies are:

1. Self-awareness: to know how you feel at any given time and according to these preferences to manage your decisions; to evaluate realistically your own abilities and have a well-grounded sense of self-confidence
2. Self-control: to cope with your emotions when you have a problem; be conscientious and delayed satisfaction in order to achieve the target
3. Motivation: to use your own deepest preferences in order to be encouraged and guided to your targets, to take the initiative and to be spired to improve and persevere when you faced by failures and disappointments
4. Empathy: to feel what people feel, to be able to take their views and cultivate personal relationships
5. Social skills: to deal with emotions in relationships and accurately read social situations and networks; to be capable of interacting; to use these skills to convince and lead, negotiate and resolve conflicts and achieve cooperation and team work [1, p. 301].

3. THE EMOTIONAL INTELLIEGENCE AS A KEY OF BUSINESS SUCCESS

When the work place is intellectually more demanding then it is necessary to have higher emotional intelligence.

Intelligence quotient (IQ) has a minor role in determination of success among the people of high intelligence that is needed for the navigation of the most demanding areas.

In the specialization programs such as business administration emotional intelligence is more important to achieve a successful position leader than IQ. While in occupations such as engineering, law or medical professional selection is based solely on intellectual abilities.

Top-workers possess synergy of emotional intelligence and cognitive skills. The same skills can make people very successful in various occupations, but certain occupations require specific skills. Competences of the person who climbs on the ladder of social success can be changed. In the large organizations, senior members of the management need a higher level of political consciousness than those on the lower leadership positions.

High IQ and technical expertise can paradoxically act on people who seem promising, but nevertheless fail. Their technical skills are often the reason why they get a managerial position. But when they get to higher positions, their technical skills turned into a disadvantage. Arrogance has encouraged some of them to offend colleagues and act superior, while others humiliate subordinates even those technically more skilled.

This is the Peter Principle in action. People progress to the level of their incompetence. Why? Because when someone progresses because of its expertise and found on a new level, where the majority of the duties is related to the work with people, not on technical skills, it will fail. This would mean that the business world is full of bad leaders. Peter Principle explains well why there are so many rough, insensitive and otherwise interpersonally incompetent persons set to high positions in organizations around the world. The error is to assume that a person who has a special technical expert must have leadership skills.

More than two-thirds of managers of human resources, about 71%, say that their emotional intelligence is more important than IQ. 59% of them say that they would not employ a person with a low level of emotional intelligence and high IQ [2].

Emotionally mature manager is the person who supervises its feelings and also controls them, rational acts under stress, submitted failures and disappointments. The most desirable skills for manager are communication skills, interpersonal skills and mastery of oneself [3].

4. THE EMOTIONAL INTELLIEGENCE IN MANAGERIAL WORK

Emotional competence is especially important for leader, whose role is to get others to work effectively and efficiently.

Interpersonal inability of leader reduces work performance. It wastes time, creates dissatisfaction, motivation and dedication decline, and occur hostility and dispiritedness. The extent to which a leader is transformational, is measured first, in terms of his influence on the followers [4].

Flexible planning is an important ability during frequent changes that occur in everyday life. On that way, people can easily observe wider picture of possible solutions.

Tasks that require creativity are solving with better organization and using the information collected by the person ago. It is important that people have confidence in their abilities for thus they will longer work on a problem.

Emotions are using to increase the motivation of someone to perform different tasks. People who have a positive attitude towards life, create relationships that feel comfortable with themselves.

5. THE EMOTIONAL INTELLIEGENT ORGANIZATION

The organization is like an organism, it is born, grows, matures, and dies at the end. Companies have lifespan.

If the future can be inferred on the basis of the past, for about forty years two-thirds of the company from the list of Fortune 500 will no longer exist.

Most likely will survive only flexible. Elements of effective organization contain also a healthy dose of emotional intelligence.

Emotional intelligent organizations must harmonize difference between declared values and work values. Decisive and confident in decision-making in the corporation bring out certain values of the organization, of its spirit and mission.

Declaration on the mission of the organization performs an emotional function. It articulates a shared sense of goodness that allows us to realize what it is worth the effort. Working in a company that measures its success not only to get profit, raises morale and energy among people.

Realization of common values demands emotional self-awareness across the organization. As each person describes its profile of strengths and weaknesses in different areas of its competence, the same applies to organizations.

One of the most overlooked signs of the vitality of the organization can be seen in the typical emotional state of employees.

The overall level of emotional intelligence in the organization determines the degree in which it realize the intellectual capital of the organization and thus its overall success. The ability to increase intellectual capital is in alignment of cooperation of people in whose minds are knowledge and expertise. The essential competencies and technical skills that make the company competitive depend on the relations of people who work in the community.

The increase of IQ of small workgroups depends on the effective cooperation of people in the group. That is also applied to organization as a whole. Emotional, social and political awareness can increase or reduce what the organization is capable to do. Collective intelligence suffers if the people in the organization cannot work well together, if they have lack of initiative, association or other emotional competence.

This need for undisturbed coordination of widely available knowledge and technical

expertise lead some corporations to create a new position of the Director for Learning, whose job is to direct the knowledge, information and technical expertise into database. Organizations that have such directors for learning should spread their duty to maximize collective emotional intelligence.

Despite the fact that the most organizations do not conduct tests of emotional intelligence of employees, however, they tend to make the emotionally intelligent organization [1, p. 284, 296].

6. HOW TO MEASURE THE EMOTIONAL INTELLIGENCE

Anyone can have an opinion about its own emotional intelligence and the effect on those around it.

"Standardized" test goes beyond self-assessment and provides an objective picture and policy measures based on scientific principles. This can be invaluable in the construction of emotionally intelligent organization [1, p. 309]. Standardized test can identify areas that will contribute to organizational development. It provides a metric for evaluation progress in the development of emotional intelligence, the individual and the organization. It also provides an objective measure of emotional intelligence on many different levels that are comparable with their personal (subjective) ratings. Test provides insight into the blind spots that can affect an individual's ability in everyday interpersonal relationships.

The first famous test of emotional intelligence is the Multifactor Emotional Intelligence Scale (called: MEIS). It is consisted of 12 measures of ability emotional intelligence, placed in four broad areas of competence: 1) detecting emotions, 2) assimilation of emotion in thinking, 3) understanding emotions and 4) management of emotions.

Some of the tests of emotional intelligence, which are implemented in organizations are: Mayer-Salovey-Caruso Emotional Intelligence Test, The Genos Emotional Intelligence Inventory, Judgement Index, The Myers Briggs Type Indicator.

7. CONCLUSIONS

Today people live in a time when the prospects for the future increasingly depending on how someone manages itself and how it manages its emotions.

In business, no matter what the business role is, the emotional elements play a major role. The good news is that the emotional intelligence can be learn. Today each of us can add these skills to its warehouse tools for survival at a time when the stability of the job sounds like an impossible option.

The elements of emotional intelligence at the individual level can be identified, evaluated and improved. At the group level, this means to adjust interpersonal dynamics so that group works harmoniously. At the organizational level, this means to renew hierarchical order so that the emotional intelligence becomes a priority in recruitment, training, development, performance assessment and promotions.

As the work changes, human skills can help a person not only to compete with others, but also to nurture the ability to work is a pleasure, even joy and happiness.

8. ACKNOWLEDGEMENTS

This paper grew out of final paper.

9. REFERENCES

[1] D. Goleman, Emocionalna inteligencija u poslu, Denona, Zagreb, (2015).

[2] K. Madden, Why whiners don't win at work, http://edition.cnn.com/2011/09/19/living/whiners-at-work-wb/index.html?hpt=ibu_r1, last access 1/8/2015

[3] D. Sambol, Emocionalna inteligencija i poslovna izvrsnost, http://www.poslovni-savjetnik.com/sites/default/files/dir_management/PS%2037-%20emocionalna%20inteligencija.pdf, last access 1/8/2015

[4] Transformational leadership, https://en.wikipedia.org/wiki/Transformational_leadership, last access 30/8/2016

Importance of managing communication process in crisis situations

J. Jukic [a], I. Blazevic [b], M. Tokic [c], M. Stanic [d]

[a] College of Slavonski Brod, Dr. Mile Budaka 1, 35000 Slavonski Brod, Croatia, josip.jukic@vusb.hr

[b] College of Slavonski Brod, Dr. Mile Budaka 1, 35000 Slavonski Brod, Croatia, ivona.blazevic1@gmail.com

[c] College of Slavonski Brod, Dr. Mile Budaka 1, 35000 Slavonski Brod, Croatia, marijatokic.vusb@gmail.com

[d] College of Slavonski Brod, Dr. Mile Budaka 1, 35000 Slavonski Brod, Croatia, milan.stanic@vusb.hr

Abstract

The crisis is every internal and external event which interferes with the normal operations of the organization, and, if it is inadequately managed, very easily destroys the hard-earned reputation and business of the organization. Crisis situations are an integral part of the environment in which the organization operates. Communication in crisis is one of the most important items for any organization, company and institution. Upon the occurrence of crisis situation, stakeholders who are affected by it have a strong need for timely information. Business partners, employees, suppliers, customers and others are interested how crisis occurred, how company will deal with it and in which direction will business go when crisis situation finishes. Crisis communication is of great importance for every company, as well as the preparation for crisis situations, their management and crisis planning.

This paper defines meaning of managing communication process in crisis situations and analyzes the concept of communication. Emphasis is placed on the analysis of the communication plan before, during and after a crisis situation, there are located areas on which should be concentrated while learning from crisis. The authors used the following scientific methods of research: methods of analysis, comparison, induction, deduction, description and classification, as well as the specific methods used for the analysis and ranking of certain parameters.

Keywords: management, communication processes, communication plan, crisis situations

1. INTRODUCTION

Economic crisis is a challenge for self-knowledge, which is the first step out of the crisis. Management must leave many of their own views and beliefs in order to open new possibilities. Instead of changing themselves and the company, management is trying to change the environment of enterprises. Another way of reacting on crisis is tapping in, unwillingness to take the next development step, firmly adhesion to the current way of doing business, although there is the increasing visibility of the inefficiency of the aforementioned mode. Management is trying to circumvent the crisis as well as all the fundamental questions asked. Although, the crisis is always an opportunity and positive step forward in building of harmonious business. Economic crisis is nothing but an expression of the fundamental disharmony within the enterprise and between enterprises and the environment, and way out of the crisis is the establishment of a new, internal and external dynamic harmony. Acceptance of a

business crisis and questioning its message - these are the true beginnings of reversal, converting crisis into opportunity.

2. CONCEPT OF COMMUNICATION

Communication that runs through all the functions of this process is an essential for successful performance of management process. The time that managers spend on communication and individual functions can be seen from the following table.

Table 1. The time that managers spend on individual functions [1]

Management functions	% of total time
Planning	13
Organizing	14
Human Resource Management	11
Guidance	13
Controlling	12
The mediation processes	
Decision making	11
Communications	15
Influencing	11
	100

Of all the functions shown in Table 1. the highest percentage has the process of communicating which emphasizes the importance of communication in management. The process of communication, due to the time spent, could be named as a new function management. The second place occupies the process of organizing, and then the functions of planning and guidance, so half of this functions and processes can be called the basis of the functioning of the management. Communication is a very important part of the business, organization and management system. Transmission of messages, exchange and information processing, issuing and receiving of orders between the structures of the organization, contacts with business partners and etc. - all of this makes the communication system work, without which the organization could not operate. Therefore, business communication can be realized in two ways:

- it involves all employees of the organization - within the organization;
- it involves only some employees of the organization - outside the organization.

Looking through the time, communication is becoming increasingly easier and more convenient, barriers and problems have disappeared and emerged with the development of society and technology, as well as the overall communication changed from day to day. For a modern society is often said to be based on information, it is massive, network structured and global. Changes in the human environment are changing the way human functioning and character of social life. Numerous studies of all branches of science point to the presence of new elements and new structure of the environment that come as a new "social quality". Human communication is experiencing revolutionary changes. Hence the new age brings new problems in communication. Modern problems of communication are shown in Figure 1.

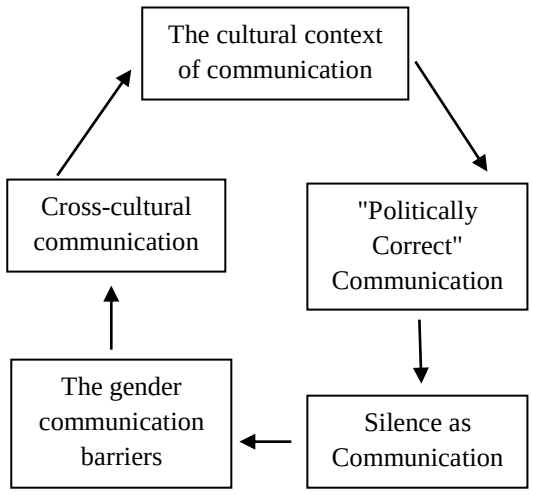

Fig. 1. Contemporary problems of communication [2]

Poor communication in most cases lead to lower success in the performance of duties or to establishment of bad relationships with co-workers. Distorted communication, as it can exclude a person from family and partners, it can also hinder employees in its work in the organization, which can lead to rejection, retirement, helplessness, etc. If the obstacles are not realized on time, poor communication can lead to permanently damaged relations within the organization. Some of the obstacles in communication occur predominantly or exclusively on an individual level, and to some generally occurs due the organizational structure. Since the overcoming the crisis is something necessarily, and since there is always the fear and uncertainty of what will new situation turns into, the task of communication is emphasizing the positive aspects of the situation, and the task of crisis management and the administration is emphasizing the opportunities arising from the reversal.

3. THE IMPORTANCE OF COMMUNICATION IN CRISIS

Crisis communication can be defined as a system for the collection, processing and separation of the information required to deal with a crisis [3]. The importance of crisis communication in institutions is essential for business today. No organization, no matter how financially successful, reputable, is not immune to the crisis. Professional approach to a crisis situation can improve the reputation of the organization, but also, bad approach can return the organization to the bottom. In this case, it takes months and years to recover the public trust. Crises have one characteristic that is unpleasant for all participants in the business, and that is that they are always unannounced, sudden and unexpected. Although the crisis always surprise the organizations, for them it is quite normal, an integral part of the environment in which the organization operates. The crisis for the organization represents the stimulation for restoration, improvement and transformation of enterprises, as well as an opportunity for management to change the way of thinking in the company. Crisis communication can be a major tool for crisis management in the state and in private business, as well as in non-profit organizations. When an emergency situation occurs, it is vitally important how the crisis affected organization is prepared to manage the crisis and successfully communicate in crisis conditions.

The crisis is marked by two facts: first, its indications are quite early, and another, these hints no one notices. If timely detected, the crisis can be avoided. In the second case, the crisis is simply there. In the first step is important to have communion of first and second levels management and the company owners. But also open and frank discussion, in which top management is ready to listen to other level associates, is novelty and operates highly motivating. Transparent conception of reversal and communication plan is jointly developed in the second step, of course, if there is enough knowledge and enough experts. In practice, however, this is often not the case; in particular in crisis first and second level management is so preoccupied with the daily work that does not have the time to review the company distress nor to think and develop the concept of the future position of the company. Instead, the management takes care of timely delivery and attracting new customers. Although these are important tasks, it neglects the construction of vital concepts of business reversal. In such situations, it makes sense hiring outside experts or consultants to observe what management, which is in that business for years and that led the company into crisis, for a long time do not see. Certain levels of communication in a crisis can be displayed by the model in four stages. These steps are not strictly separated from each other but they overlapping and interdependently complementing each other.

Table 2. Model of communication in crisis [4]

Increase the level of familiarity	Inform the press	Reassure	Better mutual understanding
content: partial or complete information about the product / company	**content:** press preparation of information with a high content of truth	**content:** information and assurance of the public about the attitudes of businesses and prepare for changes	**content:** dialogue as a way of communication of companies and public
target: acquaint	**target:** information published in the press	**target:** scientifically based model of persuasion	**target:** excellent communication on a scientific basis for better mutual understanding
channel: unilateral information with insufficient knowledge about recipients of information	**channel:** unilateral information with analysis of the benefits from information for the recipients	**channel:** asymmetric two-way communication with feedback through the public test results	**channel:** symmetrical two-way communication with feedback through the test results to the public
stage 1	**stage 2**	**stage 3**	**stage 4**

The model has a general importance and as the communication is getting more important, the role of this model is higher. Strive to achieve the fourth degree of communication, without previous degrees and without delay, is the main goal of communication in crisis. In this way the confidence among businesses and the public is growing.

Guiding principle of successful communication in a crisis is: work target-oriented and inform about it. Communication and action are closely connected. Crisis management and administration must run the entire company, so communication must match reality. The main goal of good communication is to create a trust towards associates, owners, financial institutions, customers and suppliers. Such a relationship of trust does not exclude unpleasant measures. Conflict situations can not always be avoided, but differences in opinion must be reckoned with.

4. COMMUNICATION PLAN IN A CRISIS SITUATION

Within the organization, it is always good to have a crisis response team armed with plans for the contingencies. If it comes to crisis, team will be able to deal with the crisis before it inflicts too much damage. The only thing that matters is that the team recognize the crisis and act on time.

Communications planning before the crisis can be defined as:

• forecasting and identification of potential crises

• creating crisis communication group and training their members

• recognition the public involved in a crisis situation

• devising a communication strategy

• determination and establishment of effective communication channels for the public involved and for reducing company's reputation

• testing and adjustment of the communication plan

• spokesman determination and training

• preparing of crisis communications center

• preparing list for the potential crisis and main informations about the company [2].

In a crisis situation, the first 24 hours after the beginning of the crisis are the most important.

They determine the direction in which crisis situation will continue to unwind. The crisis is a danger, but above all it is a challenge and an opportunity for a new beginning. A proactive and reactive approach, is an important decision for any organization in crisis. The plan for crisis communication must exist, it must contain all the relevant data for overcoming the crisis in which the organization found itself. The most important for the successful management of crisis communication is to control the crisis, and the organization can achieve it if fulfills three basic conditions: if there is complete information about the event, if it is prepared in advance to a crisis situation and if communicates proactively. Signs that indicate that the crisis has ended are: employees are returned to their regular activities; customers and suppliers have shown confidence necessary for a successful business; sales, income and other measures of business success have stabilized again. Management must determine what the crisis has acted at and what not. It must be determined which parts of the plan were done well, but the most important is to determine whether the organization timely revealed the crisis and understood its meaning.

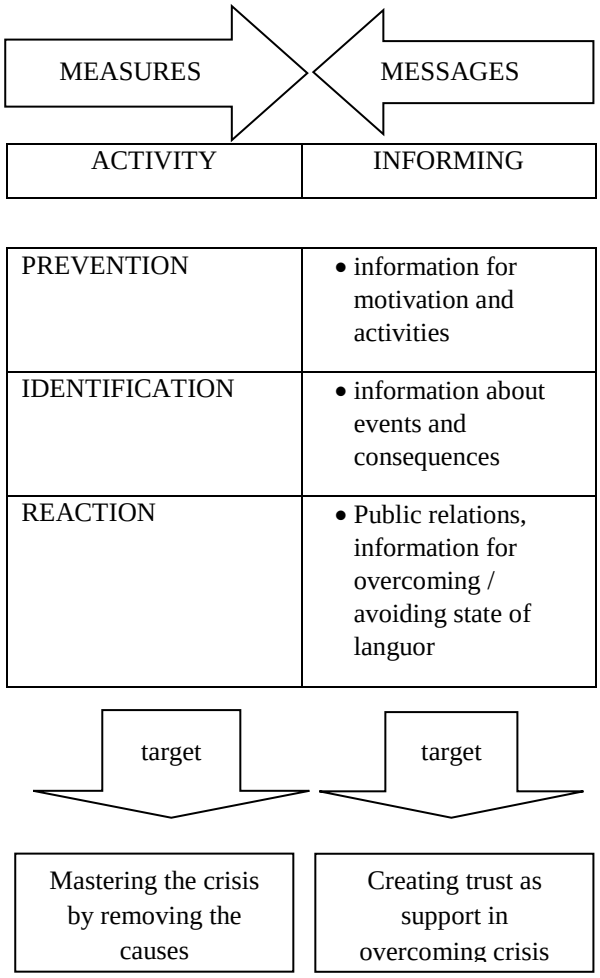

Fig. 2. Dependence of crisis management and communication in crisis [4]

5. THE PROCESS OF LEARNING FROM THE CRISIS

Learning from the crisis is concentrated on two areas. One area is an information level, as learning always involves the collection and processing of information. On the other hand learning leads to undertaking certain measures and activities, therefore the organizational level is the second area of learning. Organizational measures, as learning from the crisis, are derived from the cognition of the information level. The close relationship between crisis management and communication in crisis presents the Figure 2.

The foundation of good crisis management is the harmony of measures and messages, action and information. The aim of action is successfully pursuit of the business, crisis identification and removal of its causes, principally by effective prevention. The messages are intended to inform, they complementing activity and create confidence. The trust is created on the ability and desire to master the crisis and measures to create it. The mutual dependence of action and information is an important aspect of crisis management and should not be neglected. The process of overcoming the crisis is a common task for the entire company. Crisis management must always re-explain the concept of overcoming the crisis and continuously offer assistance.

Most of the companies after the crisis ends operates in the same manner as before crisis, whereby ignores its own mistakes that led to the crisis. Therefore, it is very important to conduct an analysis of the crisis immediately, upon the crisis period, not later than one month, as new tasks would not draw away attention from the learning process from the crisis. Learning from the crisis thus becomes a preventive instrument to prevent a new crisis, and if future crises can not be avoided, it will last shorter, and its effects will be less devastating.
In the business world today, a competitor may also be one of your customers, suppliers, distributors, or investors. One entity may play many roles. So, destroying a competitor could mean harming oneself [6]. There is another view that the company should never get out of the crisis. Management should generate and intensify crisis situations. and that the business in crisis is their normal way of doing business. That's why many managers will find their company flies from one crisis to another and that the business in crisis is their normal way of doing business [7].

6. CONCLUSIONS

For the successful conduct of the communication process in crisis situations the most important is the art of controlling the crisis, and to achieve this, information about the event should be accurate, and the organization should be prepared in advance and communicate proactively. Conversely, poor management of crisis situations and bad crisis communication creates enormous material and immaterial damage to organization. Usually it is impossible to predict every single crisis, but despite this, there are ways for each company to be prepare to it. There is simply no unified communication process which would be valid for all circumstances. Therefore, companies need to act preventively, also in terms of planning communications in a crisis. The successful management of information coming from different sources is of great importance, because only successful communication helps in combating the crisis.

7. REFERENCES

[1] P. Sikavica, F. Bahtijarević-Šiber, Management: Theory of management and big empirical research in Croatia (Menadžment: Teorija menadžmenta i veliko empirijsko istraživanje u Hrvatskoj), Masmedia d.o.o., (2004), pp. 79

[2] P.S. Robbins, A.T. Judge, Organizational behavior, (Organizacijsko ponašanje), 12. edition, Mate d.o.o., Zagreb, (2009), pp. 386-389

[3] B. Skoko, The manual for Understanding Public Relations (Priručnik za razumijevanje odnosa s javnošću), Millenuim promotion, (2006).

[4] N. Osmanagić Bedenik, Crisis as opportunity (Kriza kao šansa), Zagreb, (2007), pp. 237-240

[5] B. Novak, Crisis communication and issue management, (Krizno komuniciranje i upravljanje opasnostima), Bionoza Press, Zagreb, (2001), pp. 134

[6] P. Kotler, J.A. Caslione, Chaotics: The Business of Managing and Marketing in The Age of Turbulence, (Kaotika: upravljanje i marketing u turbulentnim vremenima), Zagreb School of Economics and Management, (2009), pp. 167

[7] D. Sučević, Crisis management (Krizni menadžment), Lider, Zagreb, (2010), pp. 152

Diversification as growth strategy for small enterprises

A. Katolik Kovačević [a], V. Vučemilović [b], M. Škoro [c]

[a] College of Slavonski Brod, Dr. Mile Budaka 1, 35000 Slavonski Brod, Croatia, andreja.katolik@vusb.hr

[b] College for Management in Tourism and Informatics in Virovitica, Matije Gupca 78, 33000 Virovitica, vesna.vucemilovic@yahoo.com

[c] Auto-klub "Našice", V. Lisinskog 59, 31500 Našice, milena.skoro@gmail.com

Abstract

Diversification is one of the growth strategies that can be very demanding and implementation includes risks especially for small and medium enterprises. It can be related to business activities in present scope of business operations where company is using synergy or it can mean entering in completely new businesses. Companies are using diversification as growth strategy to reduce risks in present business operations, expand range of products and services, develop competitive advantage and preserve or increase number of employees.

The aim of this paper is to emphasize problems related to diversification as growth strategy for small enterprises which is even more risky because of limited resources meaning financial, material and human resources. Top managers' determination to accept involved risks can be an important issue in process of selecting and implementing diversification as growth strategy. Managers in small enterprises often avoid investments in new businesses and focus on everyday activities which on a long run actually means just surviving.

Practical part of this paper is covering case study related to one small Automobile Association. It is non-profit association with business activities related to basic operation which is technical inspection of vehicles. Trough diversification this small enterprise aims to give full service to potential and present customers. They also as non-profit association have objective of preserving present number of employees and increase their number in future.

Keywords: diversification, growth strategies, small enterprises

1. INTRODUCTION

Important strategic decision of each and every company is commitment to growth and development. The aim of this paper is to prove that entrepreneur's way of thinking and development trough growth can be implemented in every company regardless of ownership and organizational structure. Small and medium enterprises are regarded as driving force of every country's economic development. Same is in Republic Croatia which is coming out from a long period of recession. It is obvious that entrepreneur's way of thinking and behavior, together with education of existing entrepreneurs is becoming more and more important.

Our case study is covering one small Automobile Association which is non-profit association. That is specific legal form of small enterprise whit also untypical ownership structure. Authors' intension is to give contribution to small entrepreneurship

development on demanding market in competition with large companies, trough diversification as one of the most demanding strategies. Diversification strategy can be way of sustaining the business or developing the bigger company.

Automobile Associations in Republic Croatia are non-profit associations governed by their members trough managerial or supervisory boards and association's secretary. Automobile Associations according to size are regarded as small enterprises and they usually have shortage in recourses. Nevertheless, great number of them are developing growth strategies in achieving goal of satisfying their present and potential costumers trough improving and developing range of services for their members. The most common way of expanding present business activities is horizontal growth on new services related to main business activity as source of financial resources and way of keeping present customers. Nevertheless, growth strategies are still not governed controlled and systematically in small enterprises. Because of that, this paper aims to present diversification as growth strategy whit specific characteristics when is implemented in small enterprises.

«Strategy is result of creative and innovative companies' effort.» [1] There is great number of different classifications in theory. One of them is emphasized by Buble at al. (1997.) which differentiates corporate strategy, strategic business units' strategy and functions strategy. «Growth strategies serve to realize new business elements combinations. (…) New combinations meaning developing and introducing new products, new production methods or entering new markets » [1]. We can resume that every growth strategy results with introducing new products, new methods or new markets. Different authors by that mean strategic decision for growth as companies' long term commitment. Thomas (1998.) says that growth strategies include significantly more «implementation goals» [2]. According to Thomas, growth can be gained through focusing organizations resources on current products, distribution system and/or consumers; diversification on related or nonrelated products, markets and/or technologies and alliances with other organizations in purpose of risk reduction.

Diversification as a strategy is usually presented on large companies because it is considered to be growth strategy for big corporations. There is not much empirical and theoretical material covering diversification as growth strategy for small enterprises. In spite of that, small enterprises often use diversification in their business activities. Facing competition, small enterprises often change business activities frequently, without long term plan and strategic consideration.

This paper aims to identify concept which will be acceptable and applicable in small enterprises. It also tries to enhance empirical base for diversification effects evaluation in small enterprises.

2. METHODS AND MATERIALS USED FOR RESEARCH

This paper is written by using case-study methodology which is often used for different business situations simulation. Information used in this paper are primary and secondary data. Primary data are collected through interviews of relevant persons for the topic of this paper. Secondary data used in paper are statistical data, legal acts etc. Case study is part of paper which analyses problem in specific small business. Conclusions based on analysis lead to evaluation of different alternative solutions.

3. DIVERSIFICATION

Diversification strategy Ansoff defines as creation of new products for new markets and emphasizes higher risk involved in this strategy compared to other growth strategies. Nevertheless, it is possible to achieve success with high return on equity or potentially high profit [3]. Term «diversification» can have many meanings. Porter (1986.) term «diversification»

uses in at least six meanings: research and development diversification, functional diversification, product diversification, customers' diversification, international diversification and financial diversification [4]. Author of this division regards as diversification, change in any stated element of a company.

Diversification can be differentiated related to existing range of products. According to Meler it can be concentric diversification, horizontal diversification and conglomerate diversification. Concentric diversification means that new product has direct relation to existing range of products, horizontal diversification means that new product is indirectly related to existing range of products and conglomerate diversification means that new product is not related in any way what so ever, to existing range of products [5]. Byars at al. (1996.) majority of diversification strategies classify in linked diversification and conglomerate diversification [6]. Linked diversification are those when diversification is linked in a sort of way with existing companies' business operations but clearly distinguished from it. Conglomerate diversification is when company diversify business operations in areas which have no link on present scope of companies' business operations.

Diversification goal is according to Thomas (1988.) allowing company to enroll lines of business operations which are in a certain degree different from current business operations and through that making more successful business operation as a whole [2]. Meler states that more goals can be achieved through diversification of present range of products with new products and services. This goals are completing range of products, fully satisfying consumer needs, increasing competitive advantage, higher profitability, decreasing sales risks, better usage of total capacity etc. [5].

No meter diversification being risky growth strategy, there is a high number of companies implementing this particular growth strategy. Companies find motive for diversification in many areas such as decline in their main business operation due to recession or escape from much stronger competitors. Buble at al. reasons for diversification find in need to reinvest profits and conclude that this strategy is often motivated with desire to build powerful position or make the most of synergy effects such as better use of material or human resources [1].

According to Byars at al. diversification is when company enters in business operations clearly differentiated from its current business operations [6]. There are many reasons for selecting this strategy. The most common one is risk dispersion which has to reduce companies' dependency on particular product or service. Second reason for diversification is management attitude towards diversification as attractive strategy compared to other growth strategies. Third reason is management perception regarding entering new business as a challenge and last one is related to achieving balance between seasonal or cyclic fluctuations in demand for product or service.

3.1. Small enterprises diversification

Product life cycle is shortening because of new technologies, new materials, changes in consumers taste and consumption itself. Companies are forced to constantly develop new products and replace old ones to satisfy market demands. Small enterprises are even more sensitive on product changes because of limitations regarding resources as basic condition for growth. Because of flexible and entrepreneur behavior they often enter market niche or face low price strategy from competition. They usually have solvency problems and much stronger competitors on the market. While loss of products for big corporation means potential reduction of share prices, for small enterprise it can mean bankrupt. Facing market reduction in current business operations small enterprise can only focus on new markets or pull out from the market.

Zook and Allen emphasize that successful diversification strategy develops when company expands its stabile basic business operation on predictable and same way – on linked markets where it can distinguish itself [7].

Diversification is one of the most explored business areas. Conclusions made by economic analysts state that it is often hard to achieve successful diversification. Entering new markets is always risky decision, and unsuccessful diversifications are more often than successful ones. Some unsuccessful diversifications are caused by too ambitious business enterprises and some are caused because the lack of basic competencies needed for focusing on new product development and new markets.

Sandvig and Coakley analyzed nine companies [8]. They came to conclusion that diversification creates value only when diversification results are higher than entering barriers on new markets and when market ensures high profits. Authors say that from experience of thousands small enterprises which tried diversification on new markets can be learned a lot. Diversification on new markets is complex question with great deal of risk involved. Nevertheless, companies today have no choice but to face it. Entering new markets involves uncertainty and potential crises in present business activities.

To reduce the risk involved in implementation of diversification as growth strategy, Zook and Allen give advices for «taking moves» according to precisely established moves [7]. For generating high growth further advices are crucial: not to jeopardize basic business operation, deciding move should be taken only if leading position is expected, only one possibility at once should be selected and only one variable at a time should be changed. These advices they justify by fact that only small percentage of successful diversification strategies are implemented and even 75% are unsuccessful.

4. CASE STUDY

Croatian Automobile Association is established in 1906. As national drivers association by name «First Croatian Automobile Club». In year 1910. by Bans Regulation Club became responsible for running drivers' tests and vehicles inspection. Since year 1911. Club started developing sport activities and in year 1912. Club gets approval for opening a driving school and publishing.

Automobile Association from our case study is established in 1954. At that time Automobile Associations were holders of various activities related to the improvement of traffic safety, motor sports, and the development of traffic-technical culture.

During the time of general progress, number of automobiles was increasing and road construction was intensified, which lead to necessity of organizing service which will take care of travel safety and comfort. That was beginning of SPI service (Help and information service) which was established in year 1963. Within Automobile Associations there are several activities such as driving schools, servicing, points for giving drivers help and advices, publishing road maps and paper for members. In a seventies Croatian Automobile Association is regarded to be powerful organization with wide range of business activities. It consists of 125 Automobile Associations with more than 74.000 members. During that period was established Traffic Information Center and cooperation with international Automobile Associations is being intensified. In seventies and eighties Automobile Associations are getting stronger because of taking over drivers tests and possession of stations for technical inspection of vehicles. During the war in Croatia business activities stagnate and number of members decreases on almost 40.000. Road traffic also decreased significantly and association changes name in Croatian Automobile Association (HAK). In year 2015. it includes 75 Automobile Associations and almost 170.000 members.

Croatian Automobile Association becomes association with main task to protect interests of

drivers and other participants in traffic, proposing measures for improving traffic policies especially in part of road traffic security and environmental protection from negative traffic influence. There are big differences among Automobile Associations, therefore Croatian Automobile Association recognizes two types according to number of members and material base. According to that criteria there are primary and local Automobile Associations. There are 24 primary Automobile Associations with 80% of total members and 51 local Automobile Association counting 20% of total members.

Automobile Association in our case study is fifty years old association with goals congruent with global policy and directed towards drivers interests. Association is being financed mostly by providing services. In 2015. 99,2% of all income comes from services and only 0,8% from membership fee. Automobile Association was expanding range of services provided to drivers during the years. Today range of services provided through association is driving school, station for technical inspection of vehicles (STP), repairs and maintenance of vehicles, help and information service, issuing documents and materials for members such as international driving licenses and licenses for driving others vehicles abroad. As we can see, this Automobile Association majority of business operations base on public authorities under supervision of organizations such as Croatian Automobile Association, Croatian Centre for Vehicles and Ministry of Internal Affairs.

The aim of this analysis is to appraise resources in association, prove or eliminate potential for growth and suggest solution. Implementation of suggested solution should as a result have new range of services, steady income, preservation or increase of current number of employees and risk dispersion through establishing strategic business centers.

Key problems of Automobile Association are legal status, decrease in demand for driving school services, lack of entrepreneurs behavior, insufficient range of services provided for vehicle owners and low level of utilization regarding funds provided for reinvestment.

Association first of all has to make reorganization. Driving school is a segment which becomes obstacle for growth. This working places reduction can be neutralized through creation of new working places and retraining.

Therefore is crucial that management focuses on diversification in similar areas of business operations. Driving school should be organized as independent business unit with finances of they own. In that way association will gain strong financial potential for growth. At the same time driving school employees should retrain or educate for new possible jobs.

Present strength which association gains from market position of station for technical inspection of vehicles, will probably not be for a long period of time. Therefore is important to develop new services to ensure steady income.

Trough analysis of four different strategies Automobile Associations management decided to implement diversification of services as growth strategy. As possible ideas for new suggested business operations are self-service carwash, workshop for LPG (liquefied petroleum gas) gas installations in cars and LPG gas station for charging cars.

Association has no experience with none of quoted business operations. Therefore, research of business environment and detailed analysis before entering the market are of great importance. Because of investment, association can face many risks including insolvency, so starting new business operations should be gradual. It would be of great importance to make analysis of costs and benefits involved in new business operations.

5. CONCLUSIONS

This paper describes case study related to Automobile Association which is non-profit association whose management became aware

of problems in internal business organization. One business activity is well positioned on the market without competition and with solid and safe income. Nevertheless, it is not enough for successful and profitable business in total. For several years association finances business activities that are not profitable. Associations Board of managers in spite of fact that is changeable and delegated outside the association, has clear and whole image about the associations' business activities. They came to conclusion that working capital should be managed more rationally and profit has to be reinvested in new businesses. Automobile Associations' representatives are responsible to members of association which is founded for satisfying driver's needs. Therefore strategic activities must be focused on introducing new services for satisfying needs of vehicles owners.

There was real risk of working places reduction in not profitable business activities. Management decided to eliminate that risk by retraining them for new businesses.

By using several scientific methods in case study associations main strengths and opportunities were identified and new strategy was created which connects the most favorable elements from internal and external environment. Trough diversification as growth strategy association is creating new services. Experience in finance management guaranties that investment will be handled carefully without bringing into danger other associations business activity. In that way Automobile Association, registered sixty years ago for driver's needs, will trough diversification create new services for drivers and gain direct and indirect benefits for business operations in total. Association will through implementing this strategy solve several problems and gain significant advantages on the market. It will reorganize business operations, preserve positive environment within the organization, keep at least same number of working places and expand range of services for vehicle owners which will have positive impact on the number of associations' members. Implementation of new strategy will also confirm that associations' management is running business effectively and that they adopted entrepreneurs' way of thinking.

6. REFERENCES

[1] M.Buble i dr., Strategijski management, Ekonomski fakultet, Split, (1997.), pp. 155.

[2] J. G. Thomas, Strategic Management: Concepts, Practice, and Cases, Harper&Row, Publishers, New York, (1988.) pp. 200.

[3] Ansoff, J, Corporate Strategy, McGraw-Hill, New York (1965.)

[4] M. E. Porter, Note on Diversification as a Strategy, Harvard Business Scholl, 9-382-129, (1986.) pp. 1-9.

[5] M. Meler, Marketing, Ekonomski fakultet u Osijeku, Osijek (1999.) pp. 201-207.

[6] L. L. Byars; L. V. Rue, S. A. Zahra, Strategy in a Changing Environment, IRWIN, Boston, Chapter 5, (1996.) pp. 105-121.

[7] C. Zook; J. Allen, Growth Outside the Core, Harvard Business Review, Product 5518, (2003.) pp. 1-11.

[8] J. C. Sandvig; L. Coakley, Best Practices in Small Firm Diversification, Business Horizons (1988.) pp. 33-39.

Company size and employee training: Case of Vojvodina Manufacturing Industry

B. Lalić [a], M. Delić [b], N. Tasić [c], U. Marjanović [d], N. Cvetković [e], J. Muškinja [f]

[a] University of Novi Sad, Faculty of technical sciences, Trg Dositeja Obradovića 6, 21000 Novi Sad, Serbia, blalic@uns.ac.rs

[b] University of Novi Sad, Faculty of technical sciences, Trg Dositeja Obradovića 6, 21000 Novi Sad, Serbia, delic@uns.ac.rs

[c] University of Novi Sad, Faculty of technical sciences, Trg Dositeja Obradovića 6, 21000 Novi Sad, Serbia, nemanja.tasic@uns.ac.rs

[d] University of Novi Sad, Faculty of technical sciences, Trg Dositeja Obradovića 6, 21000 Novi Sad, Serbia, umarjano@uns.ac.rs

[e] University of Novi Sad, Faculty of technical sciences, Trg Dositeja Obradovića 6, 21000 Novi Sad, Serbia, nela_cvetkovic@yahoo.com

[f] University of Novi Sad, Faculty of technical sciences, Trg Dositeja Obradovića 6, 21000 Novi Sad, Serbia, jmuskinja@uns.ac.rs

Abstract

In order to enhance their competitiveness and market position, companies recognize the benefits of investing in human capital, expecting improved job motivation, productivity, innovation potential and similar. However, not all of the firms have the same approach when it comes to this topic, and practices may differ depending on many factors, among which one is the size of a company. This paper investigates the relationship between company size and planned intensity (duration) of training per employee during one-year time span. The data was collected through the European Manufacturing Survey (EMS) in 2015. The results are presented using descriptive statistics and they show that, despite the initial assumption, there is no significant relationship between the company size and the intensity of employee training in case of manufacturing firms in Vojvodina. Furthermore, positive trend in employee training and development is noticed within SMEs participating in this research.

Keywords: Employee training, employee development, Company Size

1. INTRODUCTION

Investing in employee training and improvement of their skills are considered to be one of the main engines of growth of any company. This is directly related to the fact that in today's trend of globalization, intensive competition and rapid changes in modern business environments, human resources become one of the key factors for their survival [1]. According to [2], augmented labour is seen as the key input in production and therefore,

every investment in human resources directly meliorates productivity.

Researchers suggest that there is notable difference in employee training practices and other human resource development activities undertaken by businesses of different sizes [3]. In literature, there is evidence demonstrating that larger production companies are willing to invest more resources in training, due to the complexity and need for higher capital investments in their processes [5], [6] and sheer economy of scale [7]. Nonetheless, the increase of the awareness of SMEs regarding the importance of training has been noticed. In their research (barriers), authors have identified that, when it comes to the managers of SMEs, as the main benefits of investing in workers' skills improvement they perceive possibility for profit increase, better productivity and improved general performances. However, it was observed that manufacturing SMEs are mostly neglecting job training, since 46% per cent of respondents claiming not to invest in employee trainings were from manufacturing sector.

So far, in literature there are few represented studies on this topic, mostly covering developed countries like United States and Australia [8], [9]. However very few studies are available when it comes to the situation in developing countries, wherefore we recognize the need for paper dealing with this topic in the territory of Autonomous Province Vojvodina (APV).

The aim of this paper is to present the state of employee training practices in manufacturing companies in APV and to examine if there is relationship between the intensity of employee training and the size of a company. Based on literature preview, our assumption is that the results will reveal that large companies are providing more days of training to their employees than micro and SMEs.

2. EMPLOYEE TRAINING

According to human capital theories, employee training can be explained as an investment in human capital with the aim to enhance work skills, productivity and motivation [10].

Progressively, management is recognizing the valuable benefits of employee training, emphasising the positive effects on increased job satisfaction and improved product or service quality [1], contributing to the elevated organizational competitiveness [1], [11] and especially to the job motivation. According to [12], motivation is directly associated with work performance, commitment of employees to an organization, and capability to adapt to changes. Related to that, authors [13], pointed out that training enables to the employees to prepare for changes and make changes permanent in an organization, since business environment is ever-changing. Finally, rapid development of new technologies and process innovations require continues learning by workers [4].

There are certain factors influencing the decision whether company should invest in the training of employees [4], when, and in what way benefits might be the best way exploited. Business strategy represents the factor which determines the need for training, based on the analyses of existing skills inside the organization and gap between those, and skills required in order to accomplish strategic goals. Likewise, the tendency towards innovations influences the decision about employee training, since it is necessary for provision of adaptability to workers, needed to cope with innovations. Finally, important factor is the level of trust between managers and employees in the firm (analysing firm training).

Although most of the companies, especially large ones, acknowledge the significance of employee trainings, there are still some firms with a lack of incentives to invest in the skills of their workers, caused by the fear they could leave the organization and use those skills for other employers [1].

3. RESEARCH METHODOLOGY

The data was collected through European Manufacturing Survey (EMS), covering results from the year 2015 in the territory of APV, where Faculty of Technical Sciences in Novi

Sad had conducted the EMS survey in coordination with Fraunhofer ISI from Germany. To the extent of our knowledge, so far there are no recent studies directly addressing this perspective on the presented topic in APV, thus making this interesting on a small scale. EMS investigates technological and non-technological innovation in European industry, focusing on technology diffusion and organizational innovation [14]. The data was collected from manufacturing companies having at least 20 employees. Total population of 600 companies in APV meets above mentioned criteria. In order to obtain representative sample, 334 companies evenly distributed across all manufacturing sectors and in all districts of APV were contacted. Total number of companies that participated in this research is 123, representing a response rate of 36.8%.

Section 5 of the survey is devoted to employee education, qualification and training. First and most important question for this research is related to the number of days within a year that workers spend on training. Other questions comprising this section concern the following topics:

- Specific trainings;
- Interdisciplinary trainings;
- Self learning or e-learning;
- Knowledge transfer and job rotation;
- Professionals gatherings;
- Continuous learning programs;

4. RESULTS

First, the plan of manufacturing firms regarding the duration of employee training was analyzed. Results are shown in Table 1.

As presented in table 1, most of the companies (38,2%) plan the duration of education and training no longer than 5 days per worker during one year. Following, 18,7% of companies are planning to engage their workers in training for 6 to 10 days per year. Finally, 20,3% of firms responded to plan more than 10 days of education and training during one year per worker.

Table 1. Number of days (out of one year) planned for training per worker

	Number of companies	Percentage
No more than 5 days of training	47	38,2
6 to 10 days	23	18,7
More than 10 days	25	20,3

Since the size of a company plays an important role in the employee training practices of an organization, the size of the firms that had been participating in EMS is presented in table 2.

Company size is defined by the number of employees, where companies with up to 10 employees are classified as Micro and up to 50 employees as Small companies. Medium companies are the ones with up to 250 employees and Large with more than 250 employees (interdependences).

Table 2. Number of companies based on the size

	Companies	Percentage
Micro	5	4.1
Small	69	56.1
Medium	34	27.6
Large	15	12.2
Total	123	100

Table 2 demonstrates that highest share of companies (56.1%) is classified as small enterprises, 27.6% as medium enterprises (27.6%), 12.2% as large and 4.1% as micro manufacturing firms in APV.

In order to investigate possible relationship between company size and planned intensity (overall duration) of training per worker, comparative analysis was conducted. The results are presented in table 3.

Within micro companies, half of the respondents plan up to 5 days of training per worker, while the other half plan to ensure more than 10 days of training. 43% of small

companies have indicated to plan up to 5 days of training per worker in the following year, 29% have chosen to provide 6 to 10 days of training, and 28% of small companies have answered to plan over 10 days of training.

Table 3. Percentage of different-sized companies opting for different duration of employees training per year

	Micro	Small	Medium	Large
No more that 5 days of training	50%	43%	54%	78%
6 -10 days	50%	29%	17%	22%
More than 10 days	0%	28%	29%	0%

Concerning medium companies, 54% of them intend to provide up to 5 days of training per one employee, 17% between 6 and 10 days, while 29% of medium firms stated to plan over 10 days of employee training. Finally, majority of large companies (78%) tend to have training for a period no longer than 5 days per worker during the year and 22% have stated that training per worker will include more than 10 days during one year.

5. DISCUSSION

Results indicate that, regardless of the size of a company, majority of them tends to have up to 5 days of training during one year per worker. Considering that opting for this duration of employee training is not specific for the certain size of an organization, it can be said that it is influenced by business climate and state of economy where investing in workforce is not yet an integral part of business strategy.

On the other hand, the surprising results are the tendency of SMEs to engage their employees in training activities more intensively than in the case of large companies, which is opposite to our expectations and assumptions. One of the possible explanations for this could be the increased competitiveness motive [11] within SMEs. Although disposing with less resources than large companies, which represents notable obstacle for investing in training and human capital development, SMEs are suitable for inter-organizational partnerships and associations (such as clusters), where one of the main field of action is mutual education and training provision.

The other extreme case is a lack of large firms stating to plan overall more than 10 days in one year per employee.

6. CONCLUSIONS

Employee training, as an investment in human capital, is seen as the key input for work skills investment, productivity and motivation, which further indirectly influences many other business aspects.

Considering literature review, which has given evidences about training practices in large companies and SMEs, the assumption in this paper was that there will be clear relationship between the intensity (total duration) of employee training and the size of a company. However, the results have not shown an obvious linkage. This indicates that, although in many cases the size of an organization has been the key factor, that is not exclusive factor, but one of many other parameters, such as organizational culture, specific industry, organizational maturity, economic development and similar.

What is encouraging is the result that SMEs tend to provide higher number of days of training than large companies, which could elevate their human reassurance capital and help them grow. Large companies are less flexible and adaptive. Comparing the results with the ones from developed countries like United States and Australia, it is possible to see that large companies there have more structured training programme, as well as the higher number of training days than the ones in APV. Once more, this can be credited to the state of economy where working in a large company in transitional economy gives people security, while working in a large company in developed

countries gives workers a chance to improve their skills and knowledge base. Further research could be directed towards examination of how companies plan their education and training programme, is it a systematic strategic approach or an opportunity and project based approach. Another interesting approach would be to investigate if there is some influence on training intensity depending on the industry instead of the size of a company.

7. ACKNOWLEDGEMENTS

The authors would like to thank Faculty of technical sciences and Fraunhofer ISI institute for conducting European Manufacturing Survey thus providing very important data available for researchers.

8. REFERENCES

[1] Chatzimouratidis, I. Theotokas, and I. Lagoudis, "Decision support systems for human resource training and development", *International Journal of Human Resources Management*, vol. 23, no.4, pp. 662-692, 2012.

[2] F. Sepulveda, "Training and Productivity: evidence for USE manufacturing industries". *Oxford Economics papers*, vol. 62, pp. 504-528, 2010.

[3] K. Padachi, S.-L. Bhiwajee, "Barriers to employee training in small and medium enterprises", European Journal of Training and Development, vol. 40., no. 4, 2014.

[4] D. Acemoglu and J.-S. Pischke, "Beyond Becker: Training in imperfect labour markets," *Econ. J.*, vol. 109, no. 453, pp. 112–142, 1999.

[5] K. R. Troske, "Evidence on the Employer Size-Wage Premium from Worker-Establishment Matched Data," *Rev. Econ. Stat.*, vol. 81, no. 1, pp. 15–26, 1999.

[6] D. A. Black, B. J. Noel, Z. Wang, D. A. Black, B. J. Noel, and Z. Wang, "On-the-Job Training, Establishment Size, and Firm Size: Evidence for Economies of Scale in the Production of Human Capital," vol. 66, no. 1, pp. 82–100, 1999.

[7] C. J. Waddoups, "Firm Size and Work-Related Training: New Evidence on Incidence, Intensity, and Training Type from Australia," *J. Labor Res.*, vol. 32, no. 4, pp. 390–413, 2011.

[8] C. Brown and J. Medoff, "The Employer Size Wage Effect," *J. Polit. Econ.*, vol. 97, pp. 1027–1059, 1989.

[9] T. Lallemand and F. Rycx, "Employer Size and the Structure of Wages: A Critical Survey," *Reflets Perspect. la vie économique*, vol. XLVI, no. 2, p. 75, 2007.

[10] G. Becker, 1975. Human Capital, second ed. Columbia University Press, New York.

[11] H.-Y. Cheung. A.-L. Chan. "Increasing the competitive positions of countries through employee training", *International Journal of Manpower*, vol. 33, no. 2, 2012.

[12] C. Vithessonthi, and M. Schwaninger, " Job motivation and self-confidence for learning and development as predictors of support for change", *Journal of Organizational Transformation and Social Change*, Vol. 5 No. 2, pp. 141-57., 2008.

[13] L.A. Kappelman, L.A. and T.C. Richards, " Training, empowerment, and creating a culture for change", *Empowerment in Organizations*, Vol. 4 No. 3, pp. 26-9., 1996/

[14] EMS Project Overview, "EMS Project Overview," 2016. [Online]. Available: http://www.isi.fraunhofer.de/isi-en/i/projekte/fems.php.

Is Economy of Vojvodina ready for joining EU ?

I. Beker[a], D. Sevic[a], S. Milisavljevic[a], V. Radlovacki[a], M. Delic[a], N. Brkljac[a]

[a] University of Novi Sad, Faculty of Technical Sciences, Trg Dositeja Obradovica 6, 21000 Novi Sad, Vojvodina, Serbia, beker@uns.ac.rs

Abstract

This study is aimed to assess the organisational competitiveness, and readiness of Serbian economy to compete in the open market of EU. The concept of organisational competitiveness is discussed and viewed through the implementation of Lean practices. To assess the maturity of Lean, over 200 organisations from various industries of northern province of Serbia were included into the survey design. The questionnaire was used as a research instrument. For the research purposes of ensuring higher response rate, this study is based on a Dillman' approach. Emphasizing the Social Exchange Theory, the results have yielded a 30% response rate. The study shows the absence and lack of awareness about key Lean drivers. Such shortcomings might negatively impact the competitiveness of Serbian economy, due to the fact that most of EU companies are heavily oriented towards the implementation of key Lean concepts.

Keywords: Competitiveness, Lean, Serbia, survey.

1. INTRODUCTION

Republic of Serbia started the process of accession to the European Union, by initiating a Stabilisation and Association Agreement (on 7 November 2007.) and in December 2013 the Council of the European Union approved opening negotiations on Serbia's accession in January 2014. If work hard, Serbia is expected to become member of EU in some 5 years. Then, Serbian economy will become a part of huge market, without possibilities of using administrative measures to protect its enterprises. That will be moment of truth and we will get answer to the question Is Economy of Serbia ready for joining EU? This paper aims to assess readiness of enterprises in northern part of Serbia – region of Vojvodina.

This study was conducted with the aim to reveal the real position of our organizations in terms of competitiveness and to indicate direction of action in order to improve their competitiveness and increase the chance of survival in the circumstances of more severe competition than it is now.

To our knowledge, there was no similar research conducted in Serbia previously.

2. LITERATURE REVIEW

Today, it is not enough to acquire new machines and production systems, to be competitive. Besides that, organization must adopt / implement contemporary management concepts like "…restructuring, (investments, divestments, mergers and acquisitions and the creation of groups of companies), TQM (Total Quality Management), kaizen, benchmarking, outsourcing, reengineering (business process reengineering), Lean Management, TBM (Time Based Management), Six Sigma, TOC (Theory of Constraints), controlling, knowledge management, organizations: virtual, fractal, network, flexible, intelligent, learning, as well as quality management…"[1]. Automotive industry, due to success of Toyota, generally

accepted lean management as a precondition for survival on the market, and after that, lean management penetrated all of the other areas of economy and human operations in general. So, our focus in this research was on the level of implementation of contemporary management concepts, specifically lean management, in enterprises of Vojvodina.

Once, Lord Kelvin said "If you cannot measure it, you cannot improve it"[2]. Also, words that are attributed to lord Kelvin addresses the core of our problem: "When you can measure what you are speaking about, and express it in numbers, you know something about it; but when you cannot express it in numbers, your knowledge is of a meagre and unsatisfactory kind; it may be the beginning of knowledge, but you have scarcely in your thoughts advanced to the state of science."[3].

This means that in order to improve competitiveness of our enterprises, it is necessary to establish what starting point is: where is Serbian economy in comparison with potential competition from EU today. We have to find way to measure assumed gap between competitiveness of our and EU enterprises. Convenient situation is that we have results of similar research done in EU by Allied Consultants Europe [4] about level of implementation of lean in European industry.

As a measurement instrument, questionnaire was used, and as a method for collecting data, we have used Dillman's approach [5]. Reason for this is our previous experience with questionnaires and Serbian enterprises. In the year 2015, we have participated in EMS - European Manufacturing Survey [6] conducted by Fraunhofer Institute for Systems and Innovation Research, Germany, and in that study we followed Dillman's approach and achieved over 30% response rate.

3. METHOD OF RESEARCH

For this research, it was necessary to develop a questionnaire as a tool for data collection. After creating the first version of the questionnaire, we have conducted validation within the academic community. Ten professors from the Faculty of Technical Sciences analysed the questions from the questionnaire, and they simulated answering these questions. For all questions that were unclear, ambiguous, or in any way caused problem to give unambiguous answer, they suggested an improvement. After analysis of suggestions, questionnaire was modified and pre-test on small sample of business organizations was conducted. The 30 organizations was contacted (organizations that are known that have already adopted some of the modern management concepts and that are expected to have a deep understanding of the problems which are the focus, as well as understand all terms used in the questions. From 30 organizations contacted, 11 gave suggestions for improvement, which were accepted. In this way, final form of questionnaire was obtained. Questionnaire has

Part A: General data
Part B: Process improvement activities
Part C: Achieved results
Part D: Change management
Part E: Future ambitions
Part F: Level of implementation

This questionnaire was made available in three versions, to make it possible for every organization to use the version that best suits them. The first version was a word document (if the organization does not have Internet access but would like to complete the questionnaire electronically), the second version represented the printed version questionnaire (if the organization does not have Internet access and would like to complete the questionnaire by hand) and the third version of the questionnaire was set up on the Internet (address of the questionnaire is https://www.surveymonkey.com/r/SpremnostprivredeV) for organizations that have access to the Internet and want to complete an electronic form.

The next step was to contact the regional chambers of commerce and making arrangements about a promotional lecture that should present the aim of the project to economic organizations as well as modern management concepts and results achieved by organization from developed economies that was due to these management concepts. Another goal of these contacts was to compile a list of organizations that gravitate to certain regional chamber of commerce, which could be an important participant in this study.

Next important thing was to calculate limit of the sample representativeness. According to Statistical Office of the Republic of Serbia, and

their report Enterprises in the Republic of Serbia by size, in 2014 [7], Vojvodina had 130 large organizations, 583 medium and 21094 small organizations. Having in mind that each group has to be represented in the sample, it is calculated that sample has to be at least 211, to be representative. As this is taken into account, and our decision to use Dillman's approach, we expected to achieve response rate of 30%, so our sample had to be at least 704 organizations.

After these introductory steps, 707 organizations were selected and contacted by telephone, in order to obtain their agreement to send electronic invitations to participate in the research. Of all organizations contacted, 516 organizations agreed to participate in the research. Further work on data collection has proceeded as follows. To each organization which agreed to participate in the research was sent a regular or electronic mail (depending on their preferences) with a physical questionnaire or link to the questionnaire which was located on the Internet. If the organization has not completed questionnaires within one week, first reminder of the research was sent to them, and if they had not completed the questionnaire for the next 2 weeks, second reminder of the research was sent to them. If organization even then has not completed questionnaires, it was considered that they changed their mind and decided not to participate in the study. Finally 217 completed (answered) questionnaires were collected, which is slightly higher than lower limit for sample to be representative - that is 211 organizations.

4. ANALYSIS OF RESPONDS

By analysing data collected in the first part of the questionnaire (Part A), it can be concluded that there is no statistically significant difference between the representation of the organizations that participated in the survey and data of Statistical Office of the Republic of Serbia, Working Paper - Enterprises in the Republic of Serbia by size, year 2014 [7]. In other words, organizations that participated in the survey, by their geographical distribution, size, production activities, nature and origin of the initial capital are fully reflecting actual structure of the organization from the territory of AP Vojvodina.

The second part of the questionnaire (Part B) refers to the activities that organizations want to implement in order to progress. This part of the questionnaire is supposed to show how seriously our organizations take its situation, and market laws and the conditions in which they operate, and both on the basis of that perceptions to define development plans and activities that are part of these plans.

It is not a rare situation that development and improvement plans in our organizations are just a wish-list and a reflection of the knowledge what would have been able to improve. Also, contact persons from organizations sometimes simply wish to present themselves in a positive – better way. In these situations it is better to inspect the report of implementation of the previous development and improvement plans, and on that basis to conclude how intensively the organization development is. Unfortunately, due to the questionnaire that allowed such subjectivity, it was not always possible to distinguish between subjective and objective answers. Therefore, when interpreting the results of this part of the questionnaire, this should be kept in mind.

All results obtained under this set of questions surpass the results obtained from a similar survey of organizations from the European Union for more than one point. Anyone who has had insight into organizations business performance which are from developed, economically strong countries can easily conclude how illogical it is, and this can only be attributed to subjectivity of respondents.

In addition to this illogicality, there was another one in the actual data. The average grade of the whole set (both the organizations that have or have not implemented some of the modern management concepts) compared to the score of only those organizations that have implemented some of the modern management concepts, are very close - they differ by 0.2 on average which is very small difference. Even on an issue (B.09 Competencies development, Staff training) occurs difference in favour of the whole sample, against organizations that have implemented some of the modern management concepts. It is hard to find any book or journal article about lean, WCM or Agile, that do not mention importance of training and competence development of staff. It is clear that this situation is possible only when the respondents do not understand the essence of the question or are excessively subjective.

To overcome these problems, it is necessary to carry out future research in a manner that will diminish subjectivity and provide as realistic as possible image of the current situation, since only on the basis of reliable image of the actual situation could be defined actions that will have a chance to ensure real improvement and development of our organizations.

In Part C of the questionnaire (achieved results) analysis can be separated into two directions, the answers from organizations that have implemented some of the advanced concepts of management, and from organizations that have not implemented these concepts, with the result that the first part includes integrated responses of organizations that have implemented contemporary concepts of management and those that have not.

The results of this part indicate that organizations that have implemented some of the modern management concepts are slightly better than other organizations, but it is not clear the extent of the respondent's subjectivity had an impact on this, or is there a really small difference between them. Researcher's opinion is that it was a subjectivity and an unwillingness to criticize or negatively comment on their own organization. Unfortunately, only objective and impartial evaluation of business results could provide a valid answer.

Part D (change management) of the questionnaire indicated the serious problems that most organizations have when it comes to any kind of systematic action in direction of development and improvement, and the only conclusion that can be drawn from this is that organizations do not have sufficient knowledge and awareness to take some of the more complex activities in that direction.

Furthermore an additional problem is being caused by needed time that elapses from the moment of action until the moment when they can identify the beneficial consequences of such action. Is it a lack of patience by owners / managers of most organizations or because of lack of consistency in the definition and monitoring of key performance indicators or the systems that will allow this monitoring, the questionnaire did not provide the basis for reaching such a conclusion.

Presented research results in Part D suggest that the respondents, i.e. tested organization in a number of cases do not have clearly established mechanism or method by which they are planning and predicting the effects of the achievement of planned improvements. Statistics suggests on this conclusion and shows a lot of unrealistic expectations and evaluations of the respondents. In some cases the respondents, i.e. organizations expressed the opinion that there is no need for improvement, although it is known that the survival of the organization in the market largely depends on such improvements. On the contrary, in some areas evaluation of respondents are bordering wishes, and not realistic considerations. This attitudes marginality and polarity points to the obvious lack of a systematic approach to identify improvement through clearly defined mechanisms, as well as the absence of a methodical approach regarding considered problem. Primarily, this refers to the identification of key factors on the basis of data from the process and the environment, as well as the analysis of such data using recognized analytical methods. In other words, the key shortcoming is lack of evidence-based decision-making by managerial structure, in terms of identifying key areas of improvement in organizational business performance. Further, based on the results, it is possible to express doubts in existence of any short-and long-term objectives and eventually improvement strategies. In conclusion, considering that a large number of organizations from the EU has some kind of mentioned mechanisms and methods, it can be said that local organizations are not competitive. Furthermore, the absence of a clear idea what local organizations should seek in terms of improving business performance raises concerns about the existence of development vision. Such a situation could have a negative impact on employees in these organizations, and in some way on local community in which the organization exists and operates.

The dynamic environment in which organizations operate imposes the need for continuous planning of all activities with a focus on those activities that need to establish specific improvements in the future. It is easy to conclude from the questionnaire that organizations realize the importance of planning their activities for a longer period in the future, but at the same time suggests that in organizations there is insufficient awareness of the potential opportunities for improvement as

well as the modern trends that would ensure improvements could be realized.

Typical for Part E group of questions: Activities for improvement over the next two years, is that there is a fairly consistent view within organizations in terms of essential and non-essential activities that can be implemented. It can be concluded that as activities are largely irrelevant was highlighted those that are less known to managers in organizations and with which did not have the opportunity to meet in the previous operation, such as the operation according to the "pull" system or a system for performance management, visual project management, SMED - tool exchange time and organizing directed to the effective and efficient production process. It is important to note that despite the fact that listed activities are considered less important for improving business in the future, organizations show a fairly high readiness for their implementation, which supports the thesis that the organization are declaratively ready to change even when improvement scope are largely unknown, as well as that in the coming period further efforts are needed, primarily through the specifically aimed training, to help them get closer and explain the benefits of these activities.

On the other hand the activities that are present for a long time in business organizations and which are "adopted" in the economic environment was positively evaluated. Thus reduction of 8 wastes was rated as the most significant, because the word "waste" highly indicates on something that has to be removed. At the same time it can be concluded that awareness of importance of employees training is at high level which is the result of changes in operations that have occurred in the past, and is directly linked to the importance of developing leadership qualities in all management positions, which is also evaluated as extremely significant. Quality assurance is also adopted concept and therefore evaluated as a very significant, followed by continuous improvement, visually cleanliness of working area and need for standardization of working methods. It is important to mention that each of these activities with high significance evaluation is followed by a high degree of readiness to implement in the coming period of two years.

The general impression is that there is an awareness of the need for planning, there is readiness for implementation of activities on that improvement, but also a certain lack of knowledge and capacity to implement these activities in a greater extent, which could be resolved by insisting on more training and more involvement of experts in certain fields.

Of the 32 organizations that declared that they have implemented some of the modern management concepts, not all organizations gave answers to the questions and it is unclear why it was so. In fact, from 10 to 12 organizations, out of the 32, did not reply to some questions, and it makes up about 30% or about 1/3 of these organisations.

The answers indicate that our organization were successfully overcome the basic tools of modern management concepts. For questions pertaining to these tools, it happened that neither organization has not made answer "1" neither the answer "2" (i.e. questions related to 5S - order and cleanliness maintenance, low level of work in progress. In other questions there was no answer "1", also the questions with the worst evaluation were rare and they are mostly related to more advanced or more complex objectives or tools (e.g. SMED, reducing the number of suppliers to a small value in order to develop much closer strategic partnership with them).

Data from this part of the questionnaire indicate that organizations that have implemented some of the modern management concepts are mostly successful organization, according to the indicators that were included in this study. The bad news is that there are very few, far below the average in developed but also developing economies (Asia, South America and even Africa). It would be good that those although few organizations popularize this approach and publish their own (successful) results and also help their suppliers to follow the same path.

5. CONCLUSION

The general conclusion of the entire research would be that good organizations from region of Vojvodina could cope with competition from developed countries, with a small extra effort and development, but unfortunately there are very few of these organizations. Most organizations would not "survive" a direct confrontation on the market with organizations from developed economies. It is very likely that

some of these organizations (few of them) would be taken over by more developed organizations, while a number of these organizations would simply perish. This might not seem a big deal, since in the territory of AP Vojvodina would operate successful organizations (organizations from the European Union who will come to this area), but the problem is that these organizations would come from one specific reason: to make extra profit due to cheaper labour. Proof of this is part of the questionnaire related to general information on organizations, where it is evident that our organizations founded with foreign capital have only slightly higher salaries than our organizations, and not close to salaries that these organizations have in their home countries. In the case that Serbia standard rises and that the labour stop to be the cheapest in the region, that organizations would relocate their production facilities to other countries (which would have cheaper labour), and on our territory would not remain even those organizations that are previously existed. This is a very bad scenario and therefore it is necessary to make the maximum effort to avoid it and to find a way to improve the competitiveness of our organizations

Having in mind difficulties Serbia had in the last quarter of the century, one can understand why its managers developed appreciation for some specific skills (like resourcefulness, intensive utilisation of the private connections etc.) and not for knowledge. But that time has passed. For that reason, first step must be promotion of the knowledge at the state level and strong support of education of already employed persons/managers, regarding new management concepts and its practical implementation. Education of all management levels in enterprises must be corroborated by government, as well as supported financially. Also it can be encouraged and carried out by potential business partner / buyer from developed countries, especially by knowledge transfer through mutual projects / cooperation.

After this phase, it is expected that positive results would be achieved and the crucial step in that moment would be dissemination of those results. When everyone becomes aware of those positive results, “snow ball” effect will assume control and the continuation of the process will be ensured.

6. ACKNOWLEDGEMENTS

The study was carried out within the Project Preparedness of economy of Vojvodina for competition with economy of EU (in Serbian), financed by the Provincial secretariat for Science and Technological Development of Autonomous Province of Vojvodina, Republic of Serbia. Report of the project was published as [8].

7. REFERENCES

[1] E. Wojnickasycz and P. Walentynowicz, “The Application of New Management Concepts to Stimulate Cooperation Between Universities and Business,” *Przedsiębiorstwo we współczesnej Gospod. - Teor. i Prakt.*, no. 3, pp. 57–69, 2013.

[2] B. Atkin and A. Brooks, *Total Facilities Management*, vol. 53, no. 9. Wiley-Blackwell, 2009.

[3] D. Hubbard, *How to measure anything*. John Wiley & Sons, Inc., 2014.

[4] Allied Consultants Europe, “Operational and Lean Management Survey 2008,” 2008.

[5] D. A. Dillman, J. D. Smyth, and M. C. Leah, *Internet, phone, mail, and mixed-mode surveys: the tailored design method*. John Wiley & Sons, Inc., 2014.

[6] “European Manufacturing Survey.” [Online]. Available: http://www.isi.fraunhofer.de/isi-en/i/projekte/fems.php. [Accessed: 14-Sep-2016].

[7] “Enterprises in the Republic of Serbia by size, in 2014,” 2015. [Online]. Available: http://pod2.stat.gov.rs/ObjavljenePublikacije/G2015/pdf/G201510090.pdf. [Accessed: 14-Sep-2016].

[8] I. Beker, D. Sevic, S. Milisavljevic, V. Radlovacki, M. Delic, and N. Brkljac, *Preparedness of economy of Vojvodina for competition with economy of EU (in Serbian)*. University of Novi Sad, Faculty of Technical Sciences, 2016.

SPONSORS

The FIRST WELDING, Inc. is a research and development – manufacturing, certification – consulting company acting in the field of modern technologies of welding, cutting and heat treatment of materials.

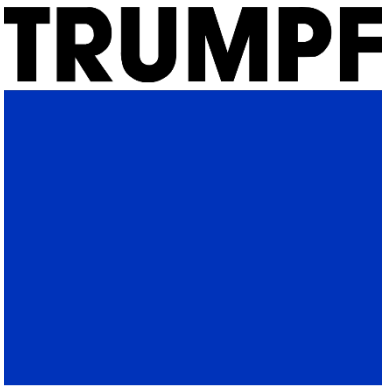

The high-technology company TRUMPF provides manufacturing solutions in the fields of machine tools, lasers and electronics. These are used in the manufacture of the most diverse products, from vehicles, building technology and mobile devices to state-of-theart power and data storage.

As world market leader for robot welding and technological leader worldwide for arc- and resistance spot-welding the Division Perfect Welding has a mastery of the entire spectrum: MMA, TIG, MIG/MAG, plasma and LaserHybrid.

Company Ecoplin scored Ltd. is a family company that has over 20 years of rich experience in the field of liquefied petroleum gas. The main activity of the company is engaged since its establishment: M 71.200 Technical testing and analysis.